LEABHARLANN CHOLÁISTE NA TRÍONÓIDE, BAILE ÁTHA CLIATH | TRINITY COLLEGE LIBRARY DUBLIN
Ollscoil Átha Cliath | The University of Dublin

Terms and Conditions of Use of Digitised Theses from Trinity College Library Dublin

Copyright statement

All material supplied by Trinity College Library is protected by copyright (under the Copyright and Related Rights Act, 2000 as amended) and other relevant Intellectual Property Rights. By accessing and using a Digitised Thesis from Trinity College Library you acknowledge that all Intellectual Property Rights in any Works supplied are the sole and exclusive property of the copyright and/or other IPR holder. Specific copyright holders may not be explicitly identified. Use of materials from other sources within a thesis should not be construed as a claim over them.

A non-exclusive, non-transferable licence is hereby granted to those using or reproducing, in whole or in part, the material for valid purposes, providing the copyright owners are acknowledged using the normal conventions. Where specific permission to use material is required, this is identified and such permission must be sought from the copyright holder or agency cited.

Liability statement

By using a Digitised Thesis, I accept that Trinity College Dublin bears no legal responsibility for the accuracy, legality or comprehensiveness of materials contained within the thesis, and that Trinity College Dublin accepts no liability for indirect, consequential, or incidental, damages or losses arising from use of the thesis for whatever reason. Information located in a thesis may be subject to specific use constraints, details of which may not be explicitly described. It is the responsibility of potential and actual users to be aware of such constraints and to abide by them. By making use of material from a digitised thesis, you accept these copyright and disclaimer provisions. Where it is brought to the attention of Trinity College Library that there may be a breach of copyright or other restraint, it is the policy to withdraw or take down access to a thesis while the issue is being resolved.

Access Agreement

By using a Digitised Thesis from Trinity College Library you are bound by the following Terms & Conditions. Please read them carefully.

I have read and I understand the following statement: All material supplied via a Digitised Thesis from Trinity College Library is protected by copyright and other intellectual property rights, and duplication or sale of all or part of any of a thesis is not permitted, except that material may be duplicated by you for your research use or for educational purposes in electronic or print form providing the copyright owners are acknowledged using the normal conventions. You must obtain permission for any other use. Electronic or print copies may not be offered, whether for sale or otherwise to anyone. This copy has been supplied on the understanding that it is copyright material and that no quotation from the thesis may be published without proper acknowledgement.

The Design, Synthesis, and Evaluation of the Azetidin-2-one Ring as a Scaffold for Novel Combretastatin A4 Analogues

Thomas F. Greene B.Sc. (Hons)

A thesis presented to the University of Dublin
for the degree of
Doctor of Philosophy in Pharmaceutical Chemistry

Based on research carried out under the supervision of
Prof. Mary J. Meegan
B.Sc., Ph.D., (N.U.I.), M.A.
at the School of Pharmacy and Pharmaceutical Sciences
Trinity College Dublin

2009

TRINITY COLLEGE
10 AUG 2009
LIBRARY DUBLIN
THESIS
8842

This thesis has not been presented as an exercise
for a degree at any other university.
The work described except where duly acknowledged,
was carried out by me entirely.

I agree that the library may lend or copy
this thesis upon request.

Thomas F. Greene

Abstract

Combretastatin A-4 (CA4) is a natural product first isolated from the Combretum caffrum South African willow tree by Pettit and co-workers. CA4 has proved to be a potent antimitotic agent, with a mechanism of action subsequently elucidated to be that of a tubulin binding agent at the colchicine site. Currently, a water soluble phosphate ester prodrug (CA4P) has shown promise as a vascular targeting agent (VTA) in clinical trials. Our work describes the use of the four-membered azetidin-2-one (β-lactam) ring as scaffold for CA-4 analogues in an effort to gain access to novel agents that possess the potent anticancer activity of CA4 while minimising the problems traditionally associated with CA4 such as stability and water solubility.

Initial efforts focussed on the synthesis of a structurally focussed library of β-lactam/CA4 analogues with the aim of identifying promising substitution patterns at the 4-position of the β-lactam ring which mimics the substituted aryl "B" ring of CA4. This library was screened for activity against the MCF7 breast cancer cell line, with the most potent analogues being selected for further optimisation at the 2 and 3-positions of the β-lactam ring. As a result of this process it was found that the biochemical activity of the analogues could be modulated by the substituents attached at the 3-position. This led to the identification of a number of highly optimised analogues that displayed comparable biochemical activity against the MCF7 cell line to that of CA4. One notable analogue proved more potent than CA4 both against the MCF7 cell line and in tubulin polymerisation assays. A number of analogues were submitted to the NCI for screening against the NCI 60 cell line panel and displayed activity comparable to or exceeding that of CA4.

The stability of the newly synthesised analogues was determined by HPLC at a variety of pHs and in human blood plasma.

Molecular modelling studies were undertaken to establish a working structure activity relationship (SAR) for the newly synthesised analogues. The ligands used for the study were obtained from a number of sources including XRD crystal structures, energy minimised models from Macromodel and MOE, and conformers generated from Omega. The ligands were docked into the colchicine site in the crystal structure of tubulin deposited in the PDB by using FRED, and the results visualised in PyMol and MOE. A QSAR was carried out using the auto QSAR function in MOE.

Acknowledgements

The most exciting phrase to hear in science, the one that heralds new discoveries, is not "Eureka!" but "that's funny...."
Isaac Asimoz

Mistakes are the portals of discovery
James Joyce

A special word of thanks goes to Prof. Mary J. Meegan for her help and guidance over the course of this research project.

I am grateful to the Centre for Synthesis and Chemical Biology (CSCB) and the Higher Education Authority (HEA) for funding, and to Trinity College Dublin for a Postgraduate Award and a Continuing Postgraduate Award.

My thanks also go to Dr. Daniela Zsisterer, School of Biochemistry, TCD, for her input into the biological evaluation of my compounds and to her research group Sandra, Seema, and Lisa for their practical advice and the use of their lab space.

I am grateful to Dr. John O'Brien and Dr. Manuel Ruether for their excellent work on the NMR spectroscopy of my compounds, and to Dr. Martin Feeney for the HRMS data. I am especially thankful to Dr. Tom McCabe for his tireless work in preparing, mounting and carrying out the structure determination of my compounds by XRD and his advice in all things XRD.

A thank you goes to the technicians in the School of Pharmacy especially Ray Keevney for his help and advice with HPLC. Thanks to Orla Woods for giving me some of her time and advice for the tubulin polymerisation assay and Dr. John Walsh for the use of his plate reader.

There have been a number of postgrads and postdocs who have had an input in some shape or form into this thesis so a special thanks goes to the older recruits such as Stephen, Irene, Juan, Mike, Gerry, Niall, Joanne, Kinga, Jason, Ciaran, Andy, Denise, Jenny, and Cormac. A very special word of thanks goes to Dr. Miriam Carr for her expert help in showing me the ropes in biochemistry and in the lab. Her patience with me is nothing compared to the patience she has as a long suffering follower of Limerick hurling. To the newer postgrads Niamh, Ruchika, Jun, and Yvonne, thanks for your help and remember that everyone gets to the end of the thesis, and at least wait a few days before stealing all my glassware (especially you Yvonne).

A very special thanks goes to my family especially my brother Noel for his expert opinions on everything and my parents Tom and Mai for their help and support over the years. I'm saving my last thank you for my long suffering girlfriend Niamh. She has been with me every step of the way during this thesis, always there to lend a helping hand, never failing to cheer me up, and always being supportive and loving. Thank you.

Table of Contents **Page No.**

List of Figures iii
List of Tables viii
List of Schemes x
List of Abbreviations xiii

Chapter 1

1.1 Cancer – an overview 2
1.2 Cancer on the molecular level 3
1.3 Current cancer therapy 8
1.4 Tubulin/microtubules as a target 12
1.5 The combretastatins 23
1.6 Novel combretastatin analogues 39
1.7 The β-lactam ring as a scaffold in bioactive compounds 48
1.8 Aims 66

Chapter 2

2.1 Introduction 69
2.2 Synthesis of imines 71
2.3 β-lactam formation by the Staundinger reaction 78
2.4 Transformation of β-lactams 99
2.5 Further optimisation 117

Chapter 3

3.1 Introduction 137
3.2 Modification of the Staundinger reaction 138
3.3 Addition reactions to 3-unsubstituted β-lactams 149
3.4 Transformations of 3-vinyl β-lactams 168

Chapter 4

4.1 Introduction 187
4.2 Materials and methods used 191
4.3 Results from library evaluation 196
4.4 The role of the carbonyl group at C_2 on the β-lactam ring 206
4.5 Chlorambucil coupled analogues 209
4.6 The role of the trimethoxy phenyl ring in antiproliferative activity 211
4.7 Hydroxy and nitrogen containing modification of ring "B" 212
4.8 Ring "B" azide substituted CA4 analogues 213
4.9 Optimisation of the 3" and 4" substitutions required at ring "B" 214
4.10 Optimisation of the 3-position substitutions 216

4.11 Transformations of the 3-vinyl β-lactams 222
4.12 Tubulin polymerisation assay 225
4.13 HPLC stability studies 230
4.14 Molecular modelling studies 240
4.15 The NCI 60 cell line panel 278

Chapter 5

5.1 Materials and methods 287
5.2 Synthesis of imines 289
5.3 Synthesis of hydroxy containing imines 294
5.4 Synthesis of β-lactams 300
5.5 Synthesis of silyl ether protected β-lactams 307
5.6 Oxidation of Sulphur 311
5.7 Reduction of nitro derivatives 313
5.8 Chlorambucil coupling 314
5.9 Sulphurisation of the β-lactam carbonyl 316
5.10 DIBAL-H reductions 317
5.11 Dearylated analogues 318
5.12 Combretastatin A1 analogues 322
5.13 Nitrated isovanillin derivatives 327
5.14 Azide analogues 342
5.15 3''' and 4''' aryl ring substitutions 345
5.16 3-Position analogues 351
5.17 Phthalimido route to 3-NH_2 β-lactams 354
5.18 Substituted acid formation 357
5.19 Formation of β-lactams by the Reformatsky reaction 359
5.20 Reaction of 3-unsubstituted β-lactams 361
5.21 Oxidation of the hydroxy group 365
5.22 OsO_4 Mediated transformation 368
5.23 Ethylidene compounds 369
5.24 Synthesis of 3-vinyl amino containing compounds 371
5.25 Further 3-vinyl compounds 373
5.26 XRD studies 375
5.27 Biochemical testing 376
5.28 Stability studies 379

References **382**

Appendices

List of Figures **Page No.**

Fig 1.1	Physiological cell cycle	**4**
Fig 1.2	Examples of chemotherapy agents	**9**
Fig 1.3	High resolution XRD image of the tubulin with the stathmin like domain of RB3	**12**
Fig 1.4	Progressive organisation of tubulin into the mitotic spindle	**13**
Fig 1.5	Stages of the mitotic cycle with/without the addition of antimitotic drugs	**14**
Fig 1.6	Structures for the vinca alkaloids with vindoline and catharanthine	**16**
Fig 1.7	Position of the vinca site on tubulin as determined by XRD	**16**
Fig 1.8	Structures for various natural products binding at the *vinca* domain	**17**
Fig 1.9	Structures of clinically important taxoids	**18**
Fig 1.10	The location of the Taxol site on tubulin	**19**
Fig 1.11	Structures for various natural products binding at the taxoid domain of tubulin	**19**
Fig 1.12	Structure of colchicine	**20**
Fig 1.13	DAMA colchicine derivative and its position in the colchicine site as determined by XRD	**21**
Fig 1.14	Illustration of the straight and curved conformations of β-tubulin	**21**
Fig 1.15	Natural product (-) combretastatin	**23**
Fig 1.16	Unnamed members of the combretastatin B-series	**25**
Fig 1.17	Single member of the combretastatin C-series	**26**
Fig 1.18	Members of the combretastatin D-series	**26**
Fig 1.19	Members of the unnamed phenanthrene combretastatin	**27**
Fig 1.20	Overview of the antivascular effects of CA4 on tumour blood vessels	**29**
Fig 1.21	Representation of Z and (E) isomers of CA4	**30**
Fig 1.22	Metabolism of CA1 and CA4 in MAC29 tumour homogenate	**32**
Fig 1.23	Various prodrugs of combretastatin	**33**
Fig 1.24	MRI showing antivascular effects of CA4	**38**
Fig 1.25	Effects of CA4P, cisplatin, 5-fluorouracil and radiation on growth of CaNT tumours	**38**
Fig 1.26	CA4 structure and areas for modifications	**39**
Fig 1.27	Natural product antimitotic agents all containing the trimethoxy subunit	**40**
Fig 1.28	Various ring systems replacing the B ring	**43**
Fig 1.29	Modifications to the olefin bridge of CA4	**44**
Fig 1.30	Heterocycles for the replacement of the olefin bridge	**46**
Fig 1.31	Selection of β-lactam antibiotics	**48**
Fig 1.32	Key structures in the development of Ezetimibe	**49**
Fig 1.33	β-lactam based protease inhibitors	**50**
Fig 1.34	Anticancer β-lactams	**52**
Fig 1.35	Antimalarial β-lactams	**52**
Fig 1.36	Use of the β-lactam ring as a synthon in Taxol semisynthesis	**53**

Fig 2.1	Use of the β-lactam ring as a scaffold for CA4	**69**
Fig 2.2	Retrosynthesis of the desired β-lactam analogues	**70**
Fig 2.3	*E and Z isomers of imines*	**72**
Fig 2.4	^{1}H NMR spectrum for compound **204**	**74**
Fig 2.5	^{1}H spectrum for compound **208**	**77**
Fig 1.31	Important β-lactam containing medicinal products displaying the importance of stereoselectivity in β-lactam forming reactions	**80**
Fig 2.6	Chiral oxazolidinylacetyl chloride for use as a precursor to a chiral ketene in the Staundinger reaction	**81**
Fig 2.7	^{1}H NMR spectrum for **256b** *trans* isomer	**92**
Fig 2.8	^{1}H spectrum for **256a** *cis* isomer	**92**
Fig 2.9	Structure of 256b as determined by XRD illustrating the trans geometry of the β-lactam ring and the presence of a pair of enantiomers	**94**
Fig 2.10	^{1}H NMR spectrum for **263**	**101**
Fig 2.11(a)	^{1}H NMR spectrum for **262**	**101**
Fig 2.11(b)	^{1}H spectrum for **262** highlighting the two sets of signals obtained	**102**
Fig 2.12	Structure of **262** as determined by XRD	**102**
Fig 2.13	^{1}H spectrum collected for **264a** & **264b**	**104**
Fig 2.14	Mass spectrum of **264a**	**105**
Fig 2.15	^{13}C spectra (blue), DEPT 90 (red) and DEPT 135 (green) for compound **265**	**108**
Fig 2.16	Selection of thioamides as medicinal products	**112**
Fig 2.17	CA1 and proposed β-lactam analogue **278**	**117**
Fig 2.18	^{1}H NMR spectrum of **280**	**117**
Fig 2.19	Comparison of ^{13}C spectra of **281** & **282**	**120**
Fig 2.20	Possible aryl azide photoaffinity probes	**129**
Fig 2.21	Photoactivation of arylazide photolabel	**129**
Fig 2.22	Investigating the role of the substituted aryl ring at C_4	**132**
Fig 3.1	Summary of the structural features identified for compounds **256** & **264** necessary for activity	**137**
Fig 3.2	^{1}H spectrum of **344** with a close up of δ3.6 to δ5.9 illustrating the trans stereochemistry of H_3 & H_4	**142**
Fig 3.3	HSQC experiment for **344**	**143**
Fig 3.4	3-Bromo substituted β-lactams as an intermediate in synthesis	**144**
Fig 3.4	^{1}H NMR spectrum for **379**	**156**
Fig 3.5	^{13}C NMR spectrum for **379**	**157**
Fig 3.6	^{1}H NMR spectrum for **393** illustrating the presence of diastereomers and a closer image of the area δ3.1-6.2ppm	**160**
Fig 3.7	HSQC spectrum for **393**	**161**
Fig 3.8	^{13}C DEPT NMR spectrum for **393**	**161**

Fig 3.9	HPLC chromatogram showing the separation of the diastereomers of **393**	**163**
Fig 3.10	Illustration of the stereoisomers present in compound **393**	**164**
Fig 3.11	IR spectrum for **395** showing two carbonyl peaks	**167**
Fig 3.12	Possible transformations of **343** to be examined	**168**
Fig 3.13	^{1}H NMR spectrum of **398**	**173**
Fig 3.14	HSQC spectrum of **398**	**174**
Fig 3.15	E and Z isomers of **397**	**176**
Fig 3.16	^{1}H NMR spectrum for **397**	**177**
Fig 3.17	Single isomer of **397**	**178**
Fig 3.18	^{1}H NMR spectra for **410**	**181**
Fig 3.19	^{1}H NMR spectrum for **399**	**182**
Fig 3.20	Investigating the introduction 3-vinyl group in combination with other substitution patterns in C_4 aryl ring	**184**
Fig 4.1	Effect of CA4 on the organisation of the cytoskeleton network in HUVEC cells	**188**
Fig 4.2	Surviving fraction of tumour 18-24 hours after treatment with various doses of CA4P	**189**
Fig 4.3	MCF-7 cells at 20X magnification	**192**
Fig 4.4	Enzymatic conversion of tetrazolium salt to formazan for the detection of LDH released from dead cells	**194**
Fig 4.5	Ezymatic cleavage of MTT by dehydrogenase enzymes in the mitochondria of metabolically active cells	**195**
Fig 4.6	Effect of placement of the trimethoxy phenyl ring on the potency of selected analogues reported by Sun	**197**
Fig 4.7	Compound **72**	**198**
Fig 4.8	Selected amino containing combretastatin analogues	**201**
Fig 4.9	Illustration of various hydroxy containing combretastatins and their corresponding β-lactam analogues	**205**
Fig 4.10	Antiproliferative and cytotoxicity dose response curves for **256b**	**207**
Fig 4.11	Antiproliferative and cytotoxicity dose response curves for **343**	**218**
Fig 4.12	Antiproliferative and cytotoxicity dose response curves for **380**	**219**
Fig 4.13	Antiproliferative and cytotoxicity data for selected analogues from Carr	**220**
Fig 4.14	Tubulin polymerisation assay for compound **343** at 10μM, 5μM, and 1μM with DMSO, Taxol (10μM), and CA4 (10μM) controls	**226**
Fig 4.15	Tubulin polymerisation assay for compounds **255** (10μM), **250b** (10μM), **343** (10μM) with DMSO, Taxol (10μM), CA4 (10μM) controls	**227**
Fig 4.16	Compound **256** selected as a model compound for the stability study	**230**
Fig 4.17	Linear response test for **256**	**232**
Fig 4.18	Degradation curve for **256** at ph 4.0	**233**
Fig 4.19	Degradation curve of **256** at pH 7.5	**234**

Fig 4.20	Degradation curve of **256** at pH 10.0	**234**
Fig 4.21	Chromatograph obtained from incubation of CA4 with rat (top) and human (bottom) liver microsomes	**236**
Fig 4.22	Structures for metabolites of CA4	**238**
Fig 4.23	Degradation of compound **256** in human blood plasma	**239**
Fig 4.24	Comparison of energy minimised model and XRD structure of **256**	**242**
Fig 4.25	Comparison of the XRD structures of **256** and CA4P	**242**
Fig 4.26	Comparison of *MOE* energy minimised model and XRD structure for **256**	**243**
Fig 4.27	DAMA colchicine ligand (**20**) in the colchicine site of tubulin as determined by XRD	**244**
Fig 4.28	Tubulin hetereodimer on a stathmin like domain as determined by XRD	**244**
Fig 4.29	Representation of the DAMA colchicine ligand with the T7 loop and H8 helix of β-tubulin	**245**
Fig 4.30	Procedure developed for validating the use of FRED in docking	**248**
Fig 4.31	Validation of docking protocol	**249**
Fig 4.32	Finalised procedure for docking of energy minimised compounds	**250**
Fig 4.33	CA4 E and Z isomers	**252**
Fig 4.34	Docked solution of *Z*-CA4 with the original DAMA colchicine (**20**)	**252**
Fig 4.35	Docked solution of Z-CA4 and *E*-CA4 with the original DAMA colchicine ligand	**253**
Fig 4.36	Protein-ligand interactions for *cis* and *trans* bromine compounds **248**	**254**
Fig 4.37	Docked solution of trans 3hydroxy (**256a**) and cis 3hydroxy (**256b**) with DAMA colchicine (**20**)	**255**
Fig 4.38	Docked solution of *trans* 3hydroxy (**256**) and *trans* 3amino (**264**) with DAMA colchicine (**20**)	**256**
Fig 4.39	Protein-ligand interactions for the trans isomer of **256**	**256**
Fig 4.40	Enlarged view of the trans isomer of **256** docked in the colchicine site along with DAMA colchicine	**257**
Fig 4.41	Protein-ligand interactions for the azetidine **272** and the thione **267**	**258**
Fig 4.42	Docked solution of DAMA colchicine (**20**), sulfoxide (**262**) (purple), and sulphone (**263**)	**259**
Fig 4.43	Ligand-protein interactions for the sulfoxide **262** and the sulfone **263**	**259**
Fig 4.44	Docked solution of the azide compound (**319**) with hydrogen bonding between the ligand and residues Val α181 and Lys β352	**261**
Fig 4.45	Pose adopted by the DAMA colchicine ligand (**20**), 2-amino CA4 analogue (**73**) and the 2-amino compound (**305**)	**262**
Fig 4.46	Docked solution for **256** of 3S 4S enantiomer and 3R 4R enantiomer along with DAMA colchicine (red) (**20**) clearly showing the different poses adopted in the pocket by both enantiomers	**263**
Fig 4.47	Docked solution of **256** trans isomer, phthalimido (**191**) (turquoise), trimethoxy (**361**) and DAMA colchicine (**20**)	**264**

Fig 4.48	Docked solution of **342** alongside **256b** for comparison	**265**
Fig 4.49	Docked solutions for the dichloro (**340**), Reformatsky (**380**), **256** and DAMA colchicine	**266**
Fig 4.50	Docked solutions for **256**, chloro (**339**) and phenyl (**341**)	**267**
Fig 4.51	Protein-ligand interactions for the ethylidene compound (**397**) and the diol (**398**)	**268**
Fig 4.52	Docked solutions for isopropnyl (**344**), vinyl (**343**) and DAMA colchicine (**20**)	**269**
Fig 4.53	Protein-ligand interactions for the vinyl compound (**343**)	**270**
Fig 4.54	Docked solution for the vinyl compound (**343**)	**271**
Fig 4.55	Docked solutions of **343**, **391**, **388** and colchicine (red) (**20**)	**272**
Fig 4.56	Docked solutions for **399**, **264** and DAMA colchicine (**20**)	**273**
Fig 4.57	Docked solutions for **245**, **412** and DAMA colchicine (**20**)	**274**
Fig 4.58	Top ranked QSAR model obtained	**276**
Fig 4.59	Second ranked QSAR model obtained	**277**
Fig 4.60	Structure of NCI-175636	**282**

List of Tables **Page No.**

Table 1.1	Phases in the mitotic cycle	**5**
Table 1.2	Classes of chemotherapy agents	**10**
Table 1.3	Structures and biochemical data for the combretastatin A series	**24**
Table 1.4	Structures and biochemical data for the combretastatin B series	**25**
Table 1.5	Biochemical data for A ring modified combretastatins	**41**
Table 1.6	Biochemical data for B ring modified combretastatins	**42**
Table 1.7	Biochemical data for B ring modified combretastatins containing nitrogen	**43**
Table 1.8	Potency values and antitubulin effects for bridge modified analogues	**45**
Table 1.9	Summary of biochemical data for selected heterocycles	**47**
Table 2.1	Yields, IR, and melting points for imines	**73**
Table 2.2	Yield, IR, and melting points for silyl ether benzaldehydes and silyl ether imines	**76**
Table 2.3	Model reaction used for the investigation of the role of the ketene in the stereochemical outcome of the Staundinger reaction	**84**
Table 2.4	Yields and spectroscopic data for compounds **244-255**	**89**
Table 2.5	Yields and spectroscopic data for compounds	**91**
Table 2.6	Monitoring of triphosgene activated β-lactam forming reaction by ^{1}H NMR	**97**
Table 2.7	Yields and spectroscopic data for compounds **262** & **263**	**102**
Table 2.8	Yields and spectroscopic data for compounds **264a** & **264b**	**104**
Table 2.9	Yield and spectroscopic data for **265** & **266**	**108**
Table 2.10	Yield and spectroscopic data for compounds **267** & **272**	**114**
Table 2.11	Yield and spectroscopic data for **273** & **276**	**116**
Table 2.12	Spectroscopic and yield data for the benzaldehyde (**280**) and the corresponding imine (**281**)	**123**
Table 2.13	Yields, melting points and spectroscopic data for **292-301**	**126**
Table 2.14	Yields, melting points and spectroscopic data for N-containing β-lactams **302-307**	**128**
Table 2.15	Yield and spectroscopic data for azide compounds **316-319**	**131**
Table 2.16	Yields, melting points, and spectroscopic data for imines (**320-323**) and β-lactams **324-329**	**134**
Table 3.1	Effect of β-lactam substituent at the 3-position upon cytotoxicity in selected cell lines	**138**
Table 3.2	IR, melting point and yield data for 3-substituent analogues	**140**
Table 3.3	Melting point, yield, and IR data for **355**	**147**
Table 3.4	Effect of extra charge of zinc upon yield of **379**	**154**
Table 3.5	Yield, melting point, and IR data for compounds **388-393**	**162**

Table 3.6	Melting point, yield, and IR data for compounds **412** & **413**	**185**
Table 4.1	Antiprolifferative and cytotoxic data for compounds **244**, **246**, **250**, **253**, **255**	**196**
Table 4.2	Antiproliferative and cytotoxicity data for the halogenated compounds	**199**
Table 4.3	Antiproliferative and cytotoxicity data for nitrogen-containing compounds	**200**
Table 4.4	Antiproliferative and cytotoxicity data for thio methyl compounds	**202**
Table 4.5	Antiproliferative and cytotoxicity data for naphthyl containing compounds	**203**
Table 4.6	Antiproliferative and cytotoxicity data for hydroxy containing compounds	**204**
Table 4.7	Antiproliferative and cytotoxicity data for modified C_2 compounds **272** & **267**	**206**
Table 4.8	Antiproliferative and cytotoxicity data for chlorambucil analogues	**209**
Table 4.9	Antiproliferative and cytotoxicity data *p*-methoxy β-lactam **276**	**211**
Table 4.10	Antiproliferative and cytotoxicity data for various N-containing compounds	**212**
Table 4.11	Antiproliferative and cytotoxicity data for azide analogue	**213**
Table 4.12	Antiproliferative and cytotoxicity data for compounds bearing substituents at C_3'' and C_4'' of the C_4 aryl ring	**214**
Table 4.13	Antiproliferative and cytotoxicity data for various C_3 substituted β-lactams	**216**
Table 4.14	Antiproliferative and cytotoxicity data for various compounds obtained from **73**	**221**
Table 4.15	Antiproliferative and cytoxicity data for compounds **397** & **398**	**222**
Table 4.16	Antiproliferative and cytoxicity data for compounds **410** & **399**	**223**
Table 4.17	Antiproliferative and cytotoxicity data for compounds **412** & **413**	**224**
Table 4.18	Fold inhibition data for compound **343** compared to CA4	**228**
Table 4.19	Calculated half lives for **256** in pH buffers	**233**
Table 4.20	Descriptor values for set of β-lactam compounds used to test the QSAR model obtained	**277**
Table 4.21	Summary of NCI 60 cell line screening results for compounds **256**, **264**, **342** & **341**	**280**

List of Schemes

		Page No.
Scheme 1.1	Synthesis of CA4 via the Wittig reaction	34
Scheme 1.2	Suzuki route to CA4	35
Scheme 1.3	Perkin route to CA4	36
Scheme 1.4	Conversion of CA4 to CA4P	36
Scheme 1.5	Transformation of CA4 to a furazan fixed ring analogue	47
Scheme 1.6	Staundinger reaction for formation of the β-lactam ring	54
Scheme 1.7	Reformatsky reaction	54
Scheme 1.8	Formation of β-lactam ring by electrochemical cyclisation	55
Scheme 1.9	Cycloaddition of a isocyanate and an alkene	56
Scheme 1.10	Mannich type reaction	56
Scheme 1.11	Pd catalysed cycloaddition	57
Scheme 1.12	Photochemical cyclisation	57
Scheme 1.13	Cyclisation of ferrocene containing imines	58
Scheme 1.14	Lactone route to β-lactams	58
Scheme 1.15	Copper and manganese catalysed reactions	59
Scheme 1.16	Examples of free radical cyclisations to form the β-lactam ring	60
Scheme 1.17	Free radical cyclisation initiated by Ni/acetic acid	61
Scheme 1.18	Formation of β-lactams from β-enaminoketoesters	62
Scheme 1.19	Lithium enolate-imine route	63
Scheme 1.20	Condensation of lithium ester enolates	64
Scheme 1.21	Polymer supported ester-enolate reaction	65
Scheme 2.1	Synthesis of imines via condensation of an appropiatley substituted benzaldehyde and 3,4,5-trimethoxyaniline	71
Scheme 2.2	Acid catalysed formation of imines	72
Scheme 2.3	Formation of silyl ether protected imines	75
Scheme 2.4	Proposed mechanism for the Staundinger Reaction	79
Scheme 2.5	Asymmetric synthesis of the β-lactam ring by induction from a chiral imine	80
Scheme 2.6	Intramolecular SN_2 type mechanism for the Staundinger reaction	82
Scheme 2.7	Stereochemical outcome based on approach of imine to ketene	83
Scheme 2.8	Stereochemical outcome based upon isomerisation of intermediate	83
Scheme 2.9	Model reaction used for the investigation of the role of the ketene in the stereochemical outcome of the Staundinger reaction	84
Scheme 2.10	Isomerisation of zwitterionic intermediate leading to stereodivergent outcome	84
Scheme 2.11	Original ketene isolated by Staundinger	86
Scheme 2.12	Thermal Wolff rearrangement of diazo ketones	87
Scheme 2.13	Photochemical rearrangement of diazo ketones	87

Scheme 2.14	Staundinger reaction favouring production of *cis* isomer	**88**
Scheme 2.15	*t*BAF cleavage of silyl ethers	**90**
Scheme 2.16	Triphosgene acid activation for generation of ketenes	**95**
Scheme 2.17	Mukaiyama dehydration of carboxylic acid to yield a ketene	**96**
Scheme 2.18	Triphosgene acid activation reaction	**96**
Scheme 2.19	Microwave induced formation of **245**	**98**
Scheme 2.20	Oxidation of thio methyl analogue to corresponding sulfoxide and sulfone	**99**
Scheme 2.21	Mechanism for the oxidation of sulphur methyl group by mCPBA	**101**
Scheme 2.22	Reduction of nitro group of compounds **251a** & **251b**	**103**
Scheme 2.23	Chlorambucil coupling to **256** & **251**	**106**
Scheme 2.24	Mechanism for the EDCL/DMAP coupling of chlorambucil to β-lactam 256	**107**
Scheme 2.25	Thionation of the carbonyl in **256a** by Lawesson's Reagent	**110**
Scheme 2.26	Mechanism for the thionation of the β-lactam carbonyl group	**111**
Scheme 2.27	DIBALH reduction of the β-lactam carbonyl functional group	**113**
Scheme 2.28	Atempted CAN dearylation of **277**	**115**
Scheme 2.29	CAN removal of p-methoxy phenyl	**116**
Scheme 2.30	Proposed mechanism for selective BCl_3 demethylation at the 2 and 3 positions	**118**
Scheme 2.31	Routes towards the protected imines **282** & **283**	**119**
Scheme 2.32	Attempted diol protection using TMS	**120**
Scheme 2.33	Alternative protecting groups used unsuccessfully	**121**
Scheme 2.34	Attempted synthesis of CA1 type β-lactam using the mono-protected imine **282**	**122**
Scheme 2.35	Synthesis of nitrated imines **296** & **297**	**124**
Scheme 2.36	Nitration of isovanillin at the 5-position	**125**
Scheme 2.37	Synthesis of N-containing β-lactams	**127**
Scheme 2.38	Formation of 4-azido β-lactam	**130**
Scheme 2.39	Synthesis of β-lactams **324-329**	**133**
Scheme 2.40	Reduction of nitro containing β-lactams to amino β-lactams (**327-329**)	**134**
Scheme 3.1	Synthesis of β-lactams **339-344** with varying C_3 substituents via the Staundinger reaction	**139**
Scheme 3.2	Attempted synthesis of 3-bromo analogue	**144**
Scheme 3.3	Attempted synthesis of 3-amino substituted β-lactam **356**	**146**
Scheme 3.4	Mechanism for the cleavage of the phthalimido group by methylhydrazine	**147**
Scheme 3.5	Substituted acid formation as a means of incorporating structural diversity at C_3	**148**
Scheme 3.6	Reformatsky reaction of Gilman and Speeter	**149**
Scheme 3.7	Substituted bromo acetates leading to diastereomeric products	**150**
Scheme 3.8	Two possible mechanisms underlying the Reformatsky reaction	**150**

Scheme 3.9	Use of the Reformatsky reaction to synthesize monocyclic intermediates in carbapenam synthesis	**152**
Scheme 3.10	Reformatsky reaction for the formation of 3-unsubstituted β-lactam **380**	**154**
Scheme 3.11	LDA mediated addition of carbonyl reagents to **379**	**158**
Scheme 3.12	Oxidation of C_5 alcohol group in β-lactams	**165**
Scheme 3.13	Synthetic routes for introduction of acyl group at C_5 of β-lactam **395**	**166**
Scheme 3.14	Epoxides as key intermediates for 3-substituted β-lactams	**169**
Scheme 3.15	Prilezheav reaction for the attempted synthesis of **405** as used by Burke	**170**
Scheme 3.16	Prilezheav reaction for the attempted synthesis of **407**	**171**
Scheme 3.17	Proposed mechanism of mCPBA epoxidation of **337**	**171**
Scheme 3.18	OsO_4 hydroxylation of the 3-vinyl β-lactam	**172**
Scheme 3.19	Synthetic routes to the 3-ethylidene product	**175**
Scheme 3.20	Mitsunobu reaction for the dehydration of alcohols	**176**
Scheme 3.21	Mitsunobu dehydration of alcohol	**177**
Scheme 3.22	Synthesis of 3-N containing compounds **410** & **399**	**180**
Scheme 3.23	Synthesis of 3-vinyl substituted β-lactams	**185**

Abbreviations

CA1	combretastatin A1
CA1P	combretastatin A1 phosphate
CA4	combretastatin A4
CA4P	combretastatin A4 phosphate
CAI	cholesterol absorption inhibitor
CAN	acetonitrile
CAN	cerric ammonium nitrate
CASP	caspase
Cdk	cyclin Dependent Kinase
CTMS	chlorotrimethylsilane
Cys	cysteine
DAB10	10-deacetylbaccatin
DBU	diazobicyclo-undecene
DCC	dicyclohexylcarbodiimide
DCE	dichloroethane
DCE-MRI	dynamic contrast medium enhanced magnetic resonance imaging
DCM	dichloromethane
DEPT	distortionless enhancement by polarization transfer
DHT	dihydroxytestosterone
DIBALH	diisobutlyaluminium hydride
DIPEA	diisopropylethylamine
DMF	dimethylformamide
DMSO	dimethylsulfoxide
EpoA	epothilone A
EpoB	epothilone B
EtOH	ethanol
GTP	guanosine triphosphate
HB	halichondrin B
HPLC	high performance liquid chromatography
HPLC-MS	high performance liquid chromatography mass spectrometry
HPV	human papilloma virus
HSQC	heteronuclear single quantum coherence
HUVECs	human umbilical vein endothelial cells
Hz	Hertz
IC50	half maximal inhibitory concentration
IGF	insulin like growth factor
IR	infrared
LDA	lithium diamine

LDH	lactate dehydrogenase
LHRH	luteinising hormone-releasing hormone
Lys	lysine
mCPBA	meta-chloroperbenzoic acid
MDR	multidrug resistance
MDRP	multidrug resistant protein
MEME	modified Eagle's minimum essential media
MeOH	methanol
MMP	matrixmetalloproteinases
MORE	microwave induced organic reaction enhancement
MP	melting point
MPF	maturation Promoting Factor
MRI	magnetic resonance imaging
MT	microtubules
MTD	maximum tolerated dose
MTT	dimethylthiazol-diphenyltetrazolium bromide
nBuLi	n-butyl lithium
NCI	national cancer institute
NMR	nuclear magnetic resonance
NPC1L1	Niemann-Pick C1 like 1
PBS	phosphate buffered saline
PCC	pyridinium chlorochromate
PET	positron emission topography
PPh3	triphenyl phosphine
PSA	prostate specific antigen
SARMs	selective androgen receptor modulators
SERMs	selective estrogen receptor modulators
TB	tuberculosis
tBAF	tert-butylammonium fluoride
tBDMSCl	tert-butyldimethylsilylchloride
TEA	triethylamine
THF	tetrahydrofuran
TMS	trimethylsilyl
Val	valine
VEGF	vascular endothelial growth factor
VTA	vascular targeting agent
XRD	X-ray diffraction
μV	microwave

Chapter 1

Introduction

1.1 Cancer – An Overview

The term cancer refers not to a single disease but rather to a catalogue of over 100 pathological conditions. The common thread between these conditions is the presence of abnormal cells that are no longer governed by the normal regulatory circuits present in normal cells. The breakdown of these regulatory processes results in the cells developing the ability to: (1) grow indefinitely "*cell immortalisation*"; (2) become growth factor independent "*transformation*""; and (3) invade normal tissue "*metastasis*". As the cells continue to rapidly divide, they group together to form a tumour (a neoplasm). The cells that make up the tumour and consequently the tumour itself can be divided into two main types – benign and malignant. A benign tumour is the less serious condition of the two. Once the tumour grows beyond 1 mm in size, it needs to develop a vascular system for the delivery of nutrients and the removal of waste products[1]. This facilitates the further growth of the tumour, but crucially the benign tumour is not capable of invading normal tissue (metastasis) and so the tumour cells remain encapsulated within the tumour. Intervention may be needed if the size of the tumour affects the functioning of surrounding tissue[2].

On the other hand, a malignant tumour will invade surrounding tissue and spread to other parts of the body to form new foci of malignacy. This "spread" is referred to as metastasis and leads to the formation of secondary tumours at some distance to the primary tumour. Malignant tumours present a serious problem since they invade surrounding tissue and prevent normal functioning of affected organs and tissues.

In Ireland there are approximately 20,500 cancers diagnosed per year, with 7,600 resulting deaths[3]. For women, breast cancer is the most common form accounting for 28% of cases, and is also the leading cause of cancer related mortality in women (18%). In men prostate cancer is the most common form making up 20% of the total numbers of cases, but lung cancer is the leading cause of cancer related death (24%).

1.2 Cancer on the Molecular Level

Cancer encompasses a range of conditions, but on the molecular level six hallmarks have been identified that are present in most if not all tumour cells[4].

- A self sufficiency in growth signals
- Ability to ignore anti-growth signals
- Ability to bypass the process of apoptosis in the cell cycle
- A limitless replication mechanism
- Angiogenesis (ability to form a vascular supply to the tumour)
- Ability to undergo and promote metastasis

At its most fundamental level cancer is caused by the failure of the cellular mechanisms that control the proliferation of healthy cells. This failure allows the cell to achieve the six crucial features outlined above. As such, it is useful to contrast the mechanisms at work in controlling proliferation in a normal cell, and how these mechanisms are bypassed in the cancer cell.

1.2.1 The Physiological Cell Cycle

Within a normal cell a carefully choreographed series of events takes place that controls the growth and proliferation of the cell. This sequence of events is referred to as the cell cycle (**fig 1.1**)[5].

Cells which are not in the process of division are in what is referred to as the G_0 phase, which lies outside the cell cycle. The cycle is itself divided into four stages - G_1, S, G_2, and M. G_1 and G_2 are the "gap" phases which lie between the S (synthesis) and M (mitosis) phases.

The S phase is where the synthesis of a copy of the cells existing DNA occurs. Collectively the G_1, G_2, and S phases are referred to as the interphase and represent the period when the cell is involved in normal metabolic activity.

Within the cell cycle, there exist a number of control features that regulate the movement of the cell through the various stages of the cycle. Cyclin Dependent Kinase (Cdk) and Maturation Promoting Factor (MPF) are the major triggers for the progression of the cell through the cycle.

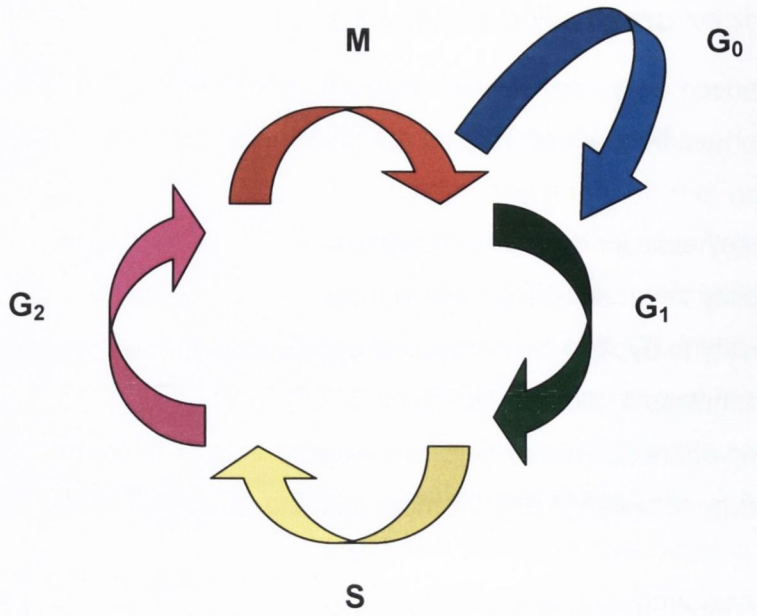

Fig1.1: Physiological cell cycle

There are a number of checkpoints dispersed throughout the cycle to insure that each daughter cell will obtain an accurate copy of the mother cell's DNA. Of particular interest is the p53 protein which is responsible for stopping the cycle upon sensing DNA damage. Either the damage is repaired and the cycle continues as normal, or if the damage is too severe, the cell will enter a process of programmed cell death called apoptosis. The M phase is where the splitting of the cell into two daughter cells occurs. The M phase is further divided into six parts – prophase, prometaphase, metaphase, anaphase, telophase, and cytokinesis (**table 1.1**). The M phase represents a popular target for anticancer agents, including the taxanes, vinca alkaloids, and more recently the combretastatins. These agents work by interfering with the microtubule dynamics that are crucial to the proper functioning of the mitotic spindle and are discussed in greater detail later.

Phase of Mitosis	Characteristic
Prophase	Chromosomes synthesised in the S phase condense into pairs and become visible Mitotic spindle begins to form from microtubules
Prometaphase	Nuclear membrane dissolves Kinetochores with microtubules attached created Chromosomes begin to move across to the middle of the cell
Metaphase	Mitotic spindle align chromosomes to insure correct sharing of chromosomes between daughter cells
Anaphase	The pairs of chromosomes separate and move to opposite ends of the cell using the microtubules
Telophase	New nuclear membrane formed Chromosomes and mitotic spindle disperse in preparation for cytokinesis
Cytokinesis	The daughter cells each with a complete copy of chromsomes split from one another

Table 1.1: Phases in the mitotic cycle

1.2.2 The Hallmarks of Cancer

If the cell cycle can be described as an a means of defending the cell from turning cancerous, then the six hallmarks of cancer represents the traits that a cell must develop to bypass the physiological cell cycle and turn cancerous.

1.2.2.1 Self Sufficiency in Growth Signals

Cells require growth signals to switch from a quiescent state to a proliferating state. Cancer cells have the ability to become autonomous of the growth signals in the cell cycle. The most obvious mechanism available to the cancer cell is to develop a method of producing its own growth factors independently of the cell cycle. The cancer cell can also over express growth factor receptors (e.g. Her2 in breast cancer) which lead to the cell becoming more sensitive to normal levels of growth factor. The third method available to the cell is to alter its cell machinery to become more sensitive to signals from growth factor receptors.

1.2.2.2 Ignoring Anti-growth Signals

In the physiological cell cycle there also exists a number of anti-growth signals that are used by the cell to switch from a proliferating state to a quiescent state. These

signals lead the cell to enter the G_0 phase of the cell cycle or else to start on the path to cell death. Cancer cells develop the ability to disrupt these signals.

1.2.2.3 Bypassing Apoptosis

Apoptosis is a major barrier to a cell turning cancerous. The cell has safeguards to sense that the normal cell cycle has gone awry. This leads to the triggering of apoptosis which is the programmed death of the cell. Cancer cells can bypass this pathway by either turning off the apoptotic signals (such as mutating p53), or by overwhelming the apoptotic signals with anti-apoptotic signals (switching on IGF-2 genes)

1.2.2.4 Replication

Even with achieving the first three hallmarks, a cancer cell cannot go on replicating forever. Telomeres are strands of DNA located at the end of chromosomes that function as a kind of internal clock, becoming shorter with each replication of the cell. As the telomeres shorten, the cells genome becomes unstable and eventually apoptosis is triggered. Cancer cells are able to maintain telomeres usually by using telomerase to replace the short strands of DNA at the end of chromosomes. This allows the cell to maintain a stable genome and avoid apoptosis through countless replications.

1.2.2.5 Angiogenesis

In order for a cancer tumour to grow beyond a few millimetres in diameter, it needs to develop its own vasculature. Such vasculature is required to disperse the nutrients and oxygen needed for further growth through out the tumour. Angiogenesis is required to develop such vasculature. This angiogenesis is controlled by both initiating and inhibiting signals. The cancer cell learns to tip the balance in favour of the initiating signals such as vascular endothelial growth factor (VEGF).

1.2.2.6 Metastasis

The final hallmark of cancer is the ability of the primary tumour to migrate to distant parts of the body and to initiate secondary tumours. This represents the most lethal aspect of cancer. Through the process of angiogenesis the tumour has access to the circulatory system. For metastasis to occur the tumour cells must have the ability to break off from the primary tumour, migrate through the stromo, enter and survive in the bloodstream while they migrate to a secondary site, penetrate the blood vessel walls at the secondary site, migrate into surrounding tissue, and proliferate until

a critical mass is reached that allows it to generate its own vasculature and hence a secondary tumour.

Although the example given above describes metastasis through the circulatory system, the tumour can also spread through the lymphatic system or through body cavities.

1.2.3 Possible Causes of Cancer

The underlying cause of the switch between a normally functioning cell and a cancer cell has been the subject of much study. At the heart of the cancer cell is a genetic mutation or mutations, which leads to its ability to bypass normal regulation. These mutations can be induced, spontaneous, or inherited[6].

Spontaneous mutations result from random errors that occur during the replication of DNA. The human body goes through 10^{16} cell divisions during its lifetime. The rate of spontaneous mutations is estimated at 10^{-6} mutations per gene per cell division[2]. If this error is not sensed and repaired by the cell, then the mutation can be passed onto daughter cells. Correct replication of DNA is no guarantee of success. Failure to pass the replicated material equally into each of the two daughter cells will lead to the formation of aneuploid cells. The presence of an incomplete set of genes has obvious implications for cell regulation.

Induced mutations stem from exposure to some external factor. Foremost in the popular mind set are the exposure to radiation and carcinogenic chemicals which are capable of causing mutations in the cell. There are also more insidious means by which mutations can be induced. The metabolism of food in the body can lead to the formation of free oxygen radicals which are in themselves mutagenic. Viruses can also be associated with cancer such as the papilloma virus and cervical cancer, the Epstein-Barr virus[7] and lymphoma, and Hepatitis-B and liver cancer[8]. These viruses are capable of inserting their own genes into host DNA thereby disrupting normal function of key genes involved in cell regulation. Genotyping of the various forms of cancer has led to the identification of a number of mutations that can be passed from one generation to the next leading to an increased cancer risk. In breast cancer these include BRCA1 and BRCA2[9]. It is generally accepted that the occurrence of cancer is the apex of a series of genetic mutations, evidence of which is provided by the correlation between age and incidence of cancer[10].

1.3 Current Cancer Therapy

Cancer treatment has long been based upon the three pillars of surgery, chemotherapy, and radiotherapy. In Ireland, approximately 60% of patients who have been diagnosed with a cancer receive surgery, 20% radiotherapy, and 15% chemotherapy (these figures include patients who receive more than one form of treatment)[11]. About one quarter of all patient receives a combination therapy and another one quarter of patients receive no treatment. Treatment regimes have evolved to encompass all three interventions, however only the use of chemotherapy is dealt with here. **Fig 1.2** and **table 1.2** illustrate some clinically important chemotherapy agents.

1.3.1 Overview of current chemotherapy agents

1.3.1.1 Early Agents

This group includes the nitrogen mustards such as mechlorethamine (**1**) and folate antagonists such as methotrexate (**2**), and have been in use since the 1940's. The nitrogen mustards are alkylating agents that induce DNA damage in cells by reacting with the nitrogen atoms of the heterocyclic bases of DNA. Such severe damage leads the cells to undergo apoptosis. Other alkylating agents are chlorambucil (**3**) and cisplatin (**4**). Folate antagonists such as methotrexate (**2**) are antimetabolites. In the case of methotrexate, it works by blocking the action of the enzyme dihydrofolate reductase which is crucial in folic acid biosynthesis. These early agents are not cancer cell specific but rather target all rapidly growing cells within the body, leading to toxic side effects. Intercalating agents such as daunorubicin (**5**) block DNA replication by occupying the space between base pairs of the strands of DNA

1.3.1.2 Hormone Therapy

The principle hormonal treatments available are Selective Estrogen receptor Modulators (SERMs) and Selective Androgen Receptor Modulators (SARMs).[12] [13] Their basic principle is to prevent the hormone signals that contribute to cancer cell growth. Tamoxifen (**6**) was the first SERM to be widely used[14]. SERMs mechanism of action lies in their binding to the estrogen receptor and thereby inducing a conformational change. Its major drawback is that it has an estrogenic effect in endometrial tissue. The next generation of SERMs such as raloxifene (**7**) do not display this estrogenic effect[15]. SARMs such as flutamide (**8**) work by binding preferentially to androgen receptors on the cancer cell thereby blocking the binding of

testosterone and dihydroxytestosterone (DHT). Other important hormone based therapies include luteinising hormone-releasing hormone (LHRH) agonists which are used in the treatment of prostate cancer. These include peptides such as leuprolide, goserelin, and buserelin.

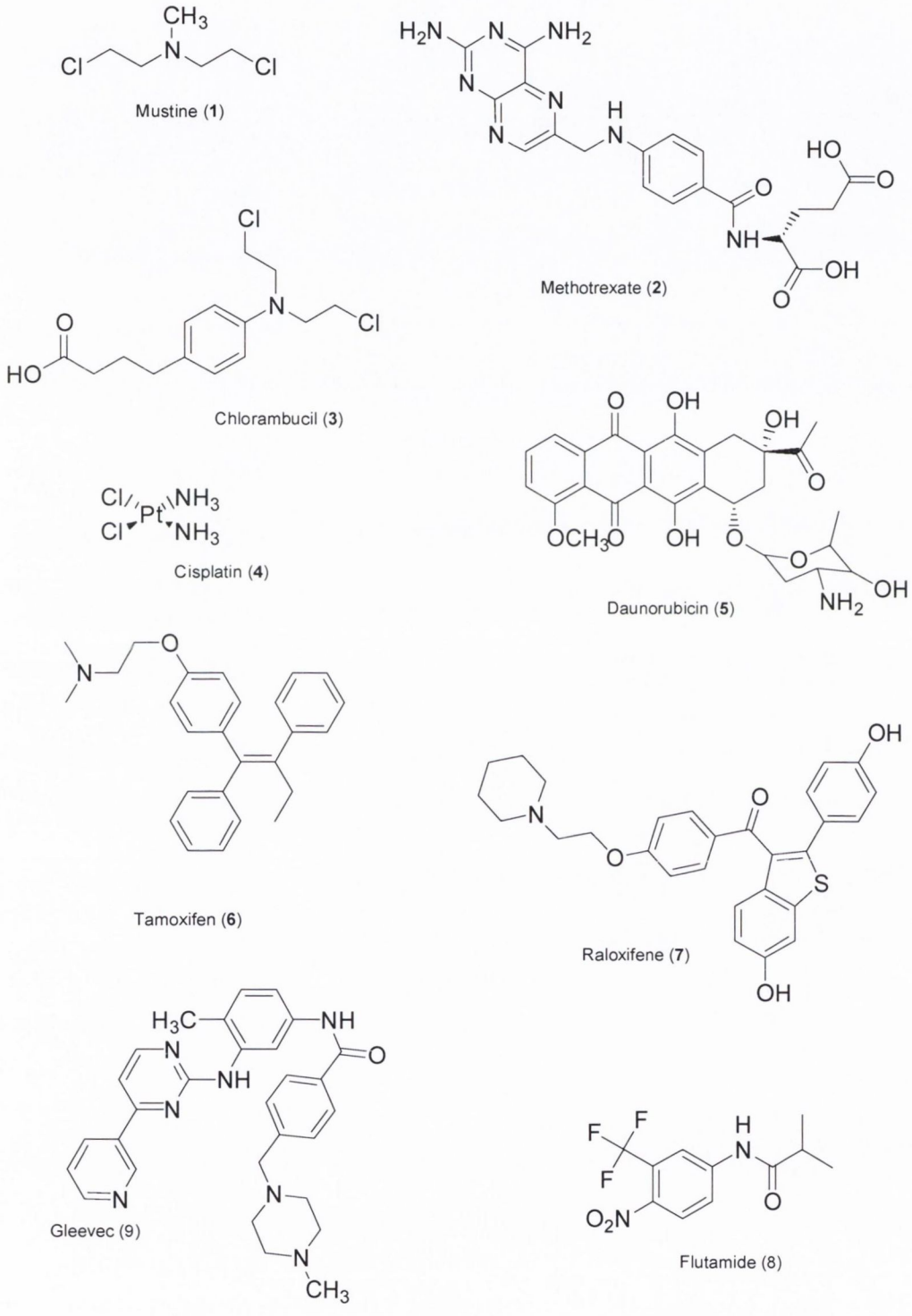

Fig 1.2 Examples of chemotherapy agents

Therapy	Description	Examples
Alkylating Agents	Interferes with DNA replication by reacting with DNA base pairs	Chlorambucil (**3**), Cisplatin (**4**) etc. Alkylating agents carry with them severe side effects including the development of secondary cancers
Intercalating Agents	Interferes with DNA replication by occupying the space between the DNA double helix	Daunorubicin (**5**), Epirubicin, Mitoxatrone etc. Also carry with them many toxic side effects
Antimetabolites	Block normal metabolism in the cell by mimicking natural metabolites	Methotrexate (**2**), 6-Mercaptopurine, 5-Fluorouracil etc. Development of resistance and toxic side effects are major issues
Tubulin/Microtubule Targeting Agents	Targets microtubule structures in the cell which are crucial to cell division	A particularly important class including the vinca alkaloids, the taxanes and the combretastatins which are currently in development
Hormone Therapy	Interferes with the cancers cells' response to hormones	SERMS such as Tamoxifen (**6**), Raloxifene (**7**) etc. Hormone therapy particlarly useful for cancers of the breast, ovaries, and prostate
Specific Inhibitors	Targets a cancer specific pathway in the cell	Kinase inhibitors such as Gleevec (**9**). A relatively new area including entities with much higher molecular weights than traditional pharmaceuticals such as proteins
Antibody Therapy	Uses antibodies to target cancer cell specific receptors	Monoclonal antibodies such as Herceptin.
Vaccines	"Primes" the immune system to seek out and destroy cancer cells	Cervical cancer vaccines are about to enter clinical use.

Table1.2 Classes of chemotherapy agents

1.3.1.3 Biological Agents

Biological agents are a rapidly emerging area in cancer treatment. This group makes use of high molecular weight agents such as proteins, antibodies, vaccines etc. Examples include Herceptin, a monoclonal antibody which targets human epidermal growth factor receptors on the cancer cell surface. These HER2/neu receptors are

overexpressed in about 30% of breast cancers. Gardasil is a vaccine against human papillomavirus. It is effective against a number of types of HPV causing around 70% of cervical cancer cases.

1.3.1.4 Tubulin/Microtubule Targeting Agents

A particularly important class of agents is those which act through a variety of targets on microtubules or on the tubulin protein that forms microtubules. These agents are classed according to the site on tubulin that they target namely the vinca, taxol, and colchicine sites. Agents that bind at the first two sites are already in widespread use for a variety of cancers (paclitaxel was first approved for the treatment of ovarian cancer, the vinca alkaloids have been used in the treatment of haematological cancers for three decades)[16] while the colchicine site is of enormous interest for the development of new treatments. Before the discussion of these agents, it is useful to gain an insight into the role of tubulin in the cell.

1.4 Tubulin/Microtubules as a Target

Due to its role in cell mitosis, tubulin (or microtubules which are polymerised tubulin) presents an interesting target from which to develop novel anti-cancer agents. Already two different classes of agents, the vinca alkaloids and the taxanes, are in widespread clinical use[16]. Their mechanism of action lies within their ability to disrupt microtubule dynamics (by binding at the vinca site and taxane site respectively). A third class that targets the colchicine site is in current clinical development, of which the combretastatins show the greatest promise. To better understand the mechanism of action of each different class of agents, it is necessary to examine the structural features of tubulin/microtubules.

1.4.1 Structural Features of Tubulin/Microtubules

Tubulin exists in the cell as a heterodimer made up of sub-units of α-tubulin and β-tubulin (**fig 1.3**). Ravelli has determined the crystal structure of tubulin sourced from bovine brain tissue stablised on a stathmin like domain.[17] One end of the microtubule has the β-dimer facing the solvent and is referred to as the (+) end. Conversely the other end has the α-dimer facing the solvent and is referred to as the (-) end. In this form it is referred to as soluble tubulin. In the cell, soluble tubulin is organised into progressively more complicated structures, ultimately forming the mitotic spindle.

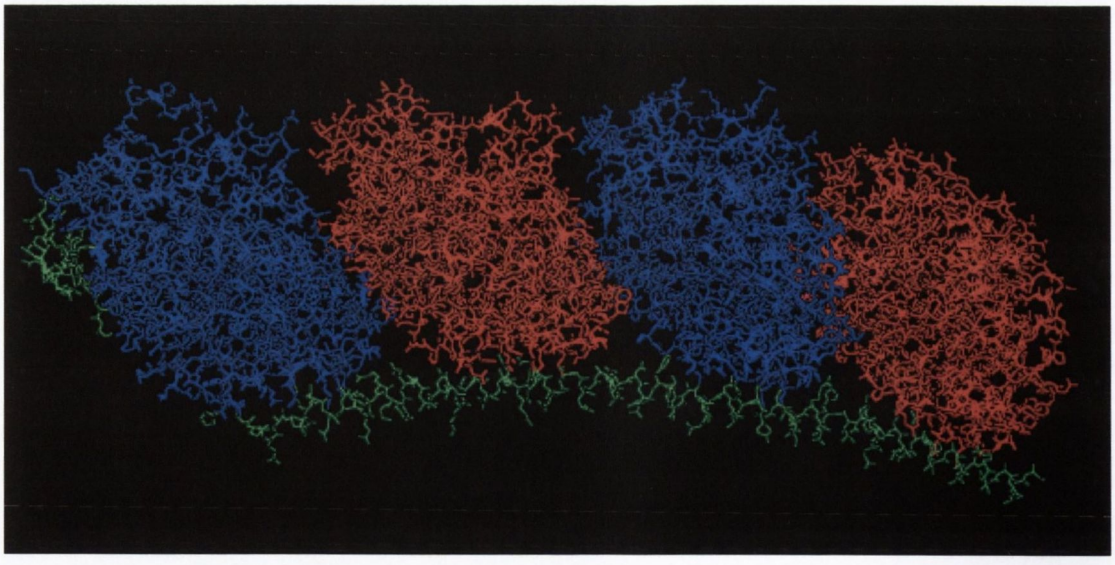

Fig 1.3: High resolution XRD image of the tubulin with the stathmin like domain of RB3 (green). Alpha unit in blue, beta unit in red (Ravelli et al)[17]

Soluble tubulin undergoes a polymerisation reaction to form structures known as protofilaments. In turn, 13 protofilaments go to forming a microtubule which

resembles a hollow tube in shape. These tubes are approximately 24nm in diameter and can be several micrometers long (**fig 1.4**).[18] [19] Microtubules make up the mitotic spindle which is a crucial part of the mitotic apparatus in the cell.

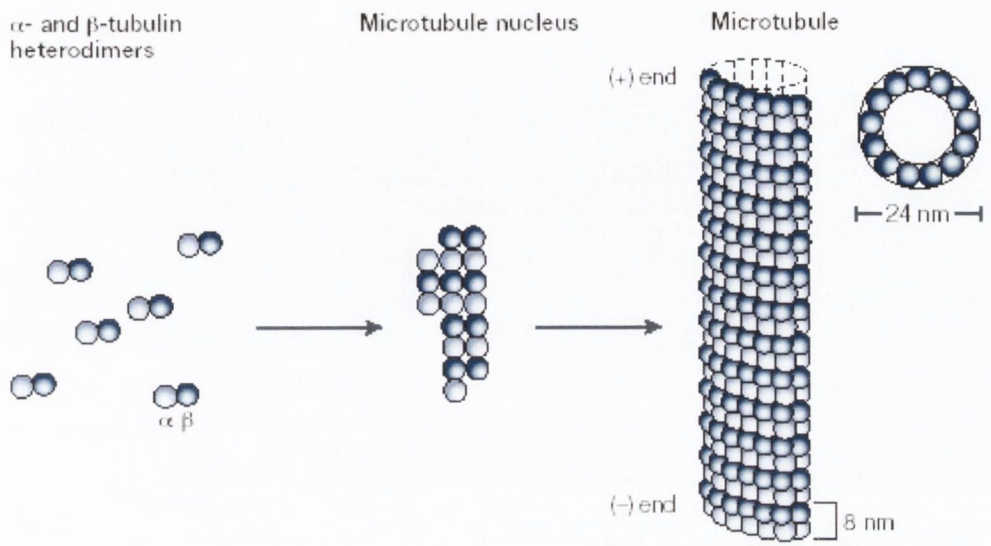

Fig 1.4: Progressive organisation of tubulin into the mitotic spindle[26]

1.4.2 Microtubule Dynamics

The polymerisation reaction of tubulin is in a constant state of flux. Soluble tubulin undergoes polymerisation, while at the same time the microtubule structures are undergoing depolymerisation to replenish the pool of soluble tubulin within the cell. Therefore soluble tubulin and microtubules are in dynamic equilibrium[20]. GTP is thought to play an important role in this dynamic equilibrium. GTP is capable of binding to the ends of the tubulin heterodimer. It is the hydrolysis of GTP from the β-tubulin end at the same moment that the tubulin heterodimer becomes polymerised to the microtubule end that provides the energy for the polymerisation process. GTP bound at both ends of the microtubule is referred to as a GTP cap. The presence of this cap significantly stabilizes the microtubule allowing for rapid lengthening (rescue) of the microtubule. Conversely, the loss of the GTP cap results in the microtubule being destabilised resulting in shortening of the microtubule.

Within this dynamic equilibrium there are two distinct patterns that emerge. The first is referred to as threadmilling [21] [22]. This involves the microtubule growing at one end through a polymerisation reaction, while shortening at the other end through a depolymerisation reaction. The net effect on the length of the microtubule is nil. The second process is dynamic instability[23] [24]. Here each end goes through periods of rapid polymerisation or of depolymerisation and can also experience a period of

quiescence. Each end experiences these periods to a different extent leading to changes in microtubule length. This dynamic equilibrium plays a crucial role in the proper functioning of microtubules especially in their role in the mitotic spindle.

1.4.3 Tubulin/Microtubules in the Cell

Tubulin plays a crucial role in a number of cellular mechanisms including transport, signalling, structural rigidity and cell mitosis[25]. It is its role in cell mitosis and structural rigidity which is of interest from a cancer therapy point of view (**fig 1.5**). During the metaphase of mitosis, tubulin polymerises to form microtubule fibres that radiate out from the two centrosomes at opposite ends of the cell (referred to as the mitotic spindle). The cell's chromosomes attach themselves to these fibres. In the anaphase the mitotic spindle pulls the two halves of each chromosome apart and guides each half to opposite sides of the cell.

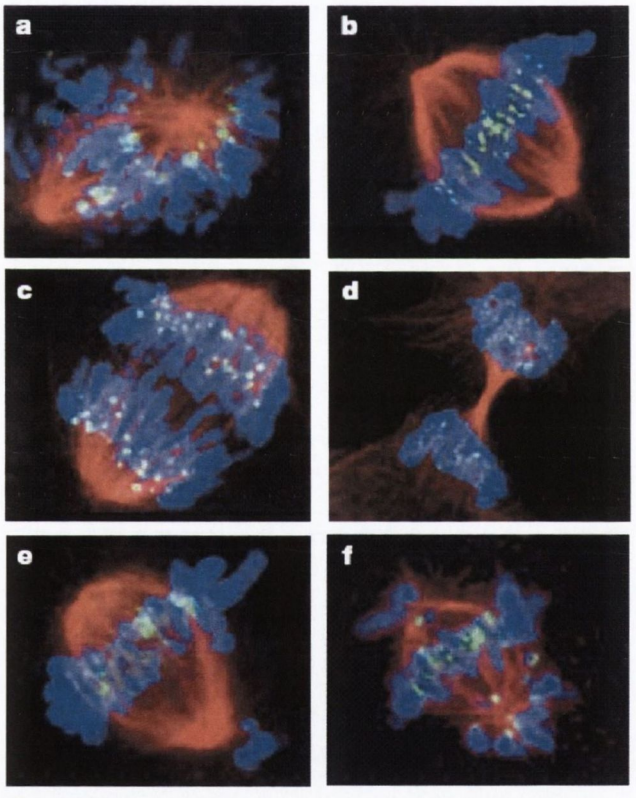

Fig 1.5: Stages of the mitotic cycle with/without the addition of antimitotic drugs. (a) prometaphase (b) metaphase (c) anaphase (d) telophase (e) treated with 10nM paclitaxel resulting in some chromosomes not migrating along the microtubules (f) treated with 50 nM vinflunine which again disrupts the microtubules. Microtubules are shown in red and chromosome are in blue. (Jordan & Wilson [26])

1.4.4 Current Tubulin/Microtubule Targeting Agents

An excellent review of tubulin/microtubules as a target for anticancer drugs is presented by Jordan and Wilson[26]. As mentioned above there are three main families of agents classified by the site that each agent binds to on tubulin. These agents are now discussed in further detail.

1.4.4.1 The Vinca Site

Vinblastine (**10**) and vincristine (**11**) were the first two bis indole alkaloids isolated from the Madagascar periwinkle (*Catharanthus rosea*) by Eli Lilly in the 1960's as part of a screening program to discover novel diabetic treatments (illustrated in **fig 1.6**). The periwinkle had use in folklore as a treatment for diabetes and so was screened[27]. The plant extracts depressed bone marrow and white blood cell counts in rats, which hinted at the anticancer properties of the extracts. Both vinblastine and vincristine are obtained from the dried leaves of the plant. Vinblastine is more abundant (0.01%) compared to vincristine (0.0003%), and vinblastine can be converted to vincristine by oxidation of the indolinyl N-methyl group[28]. In the clinic vinblastine is used in the treatment of Hodgkins lymphoma, non-small cell lung cancer, breast cancer, and testicular cancer. Vincristine is commonly use for non-Hodgkins lymphoma, some leukaemias, and kidney cancer. The major side effects of the vinca alkaloids include myeleosuppression and neuropathy.

The mechanism by which the vinca alkaloids were inhibiting cell proliferation was found to be by interfering with the polymerisation of tubulin into microtubules[29]. Vinblastine binds reversibly at the vinca site in β-tubulin[30 31], and the effect of the binding was found to be dose dependent. At higher concentrations the microtubules depolymerise and the mitotic spindle is destroyed. At lower (sub micromolar) levels the dynamics of tubulin polymerisation are disrupted leading to blockage of mitosis and ultimately apoptosis. Jordan[32] indicates that this effect is observed due to the suppression of microtubule dynamics, rather than tubulin depolymerisation. It has also been noted that vinblastine can bind at the growing microtubule (+) end, resulting in the suppression of the dynamic instability of the end especially at low concentrations. The suppression of this dynamic instability has obvious knock on effects for the assembly and proper functioning of microtubules [33 34]. Gigant *et al* has determined the nature of the vinca site by XRD at 4.1A resolution (**fig 1.7**)[35]. The site is at the interdimer interface of the heterodimer, buried into the protein to about 80%. Vinblastine interacts with both protein dimers through its catharanthine and vindoline moieties. The position of the site correlates very well with previous work that identified a number of key residues involved in the vinca site by photochemically crosslinking protein residues with an anthranilate–vinblastine analogue[36]. Upon the binding of the photolabelled vinblastine to tubulin a noticeable increase in fluorescence intensity was recorded. The site was further localised by denaturing the protein, followed by separation and sequencing on the protein fragments displaying fluorescence. Two fluorescent sequences were obtained in this way, one each from the α and β subunits, which is good evidence for the vinca site lying at the interface of α-β tubulin. Gigant proposes

that the bound vinca alkaloid induces a conformational change in the tubulin protein that prevents the formation of important stabilising lateral contacts between dimers during polymerisation.

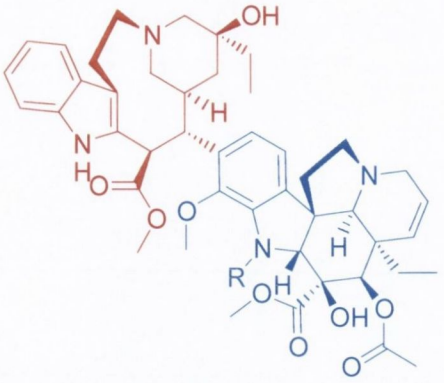

R= CH_3 Vinblastine (**10**)
R= CHO Vincristine (**11**)

Fig 1.6 Structures for the vinca alkaloids with the vindoline highlighted in red and the catharanthine highlighted in blue

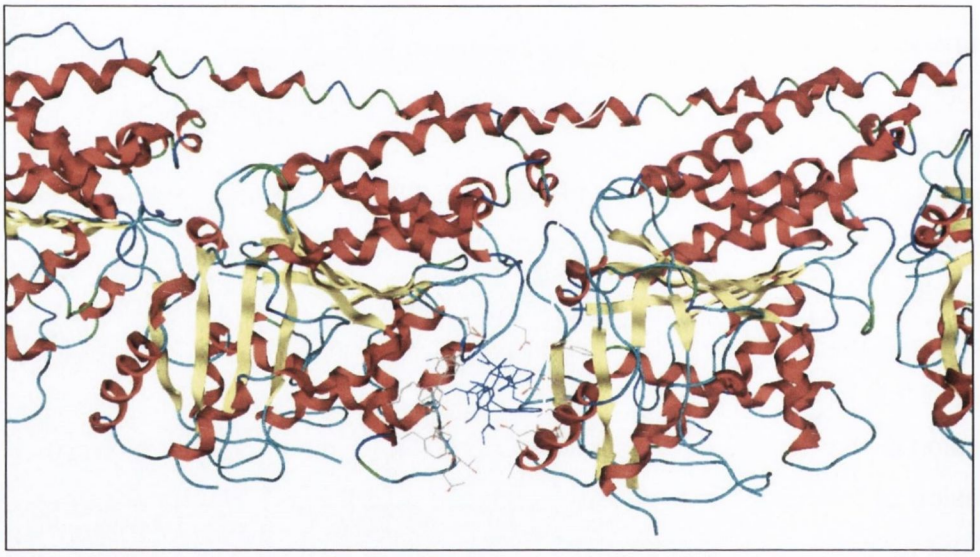

Fig 1.7 Position of the vinca site on tubulin as determined by XRD[35]. The site is located at the interdimer interface.

A number of other natural products (illustrated in **fig 1.8**) have been shown to bind at the vinca site of tubulin such as the cryptophycins (**12**)[37],halichondrins[38], and dolastatins (**13**)[39]. Cryptophycin has been shown to destroy microtubules in vascular smooth muscle cells and inhibit the binding of vinblastine to tubulin[40]. Halichondrin B (HB) has been shown to induce tubulin aggregates and prevent the binding of vinblastine to tubulin, both of which indicate that HB is acting through the vinca site on tubulin[41]. Dolastatin 10 and 15 have both been shown to inhibit the assembly of microtubules in the cell and inhibit the binding of the vinca alkaloids however Hamel *et al* has shown that the binding site may only be near the vinca site[38].

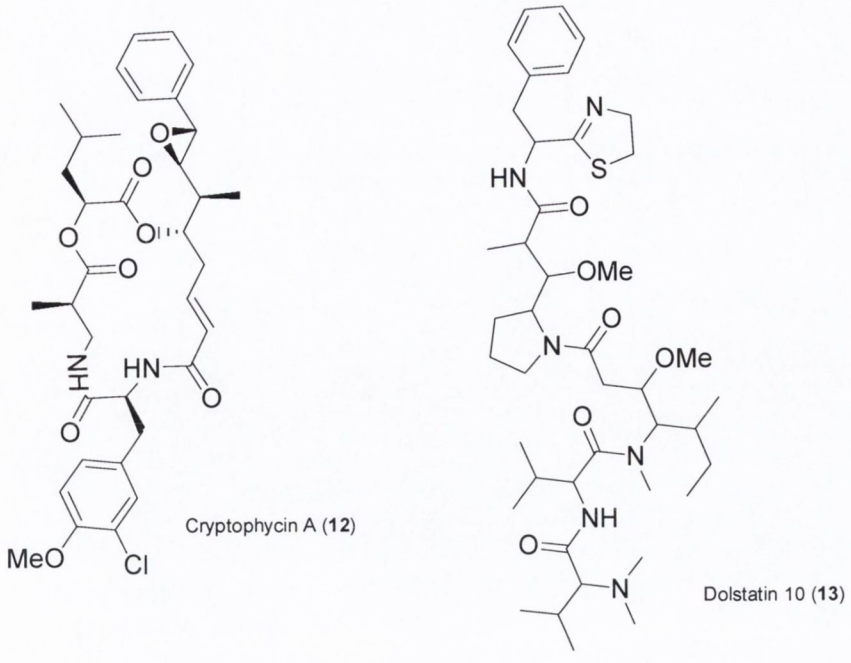

Fig 1.8 Structures for various natural products binding at the *vinca* domain

1.4.4.2 The Taxane Site

Paclitaxel (Taxol) (**14**), was first isolated as part of a NCI screening program from the bark and needles of the Pacific yew tree (*Taxus brevifolia)* in the 1960's. Its structure was first published in 1971 by Wall, Wani, and McPhail (**fig 1.9**).[42] Paclitaxel was not approved for use in the clinic until 1995. A number of factors contributed to this delay between discovery and clinical use such as the low yield in its isolation from natural sources, solubility, problems with formulations, and the need to produce sufficient quantities of the compound. The issue of supply was solved by employing a semisynthetic route using a related *genus* Taxus baccata (European Yew) as a source for 10-deacetylbaccatin (DAB10) which provides the paclitaxel core. DAB10 can be isolated in 0.1% yield compared to 0.004% yield for taxol from the Pacific yew tree[43]. The European yew is also more sustainable that the Pacific yew. More recently plant cell fermentation has been used as a source of taxol[44]. The specific cell line can be grown in aqueous media and the taxol product isolated from the media. The total synthesis of taxol has been described[45 46] with an overall yield of 2%, although the plant cell fermentation technique remains the most cost effective route to taxol.

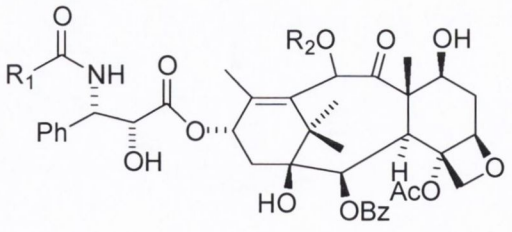

R_1= -C_6H_5, R_2= Ac **Taxol (14)**
R_1= O-(tButyl), R_2= H **Taxotere (15)**

Fig 1.9 Structures of clinically important taxoids

Schiff[47] demonstrated that paclitaxel had a mechanism of action different from that of the vinca alkoloids in that it promoted polymerisation of tubulin. At high concentrations (stoichiometric) it stabilises the microtubules and increases the polymerisation of soluble tubulin into microtubules both of which lead to an increase in microtubule mass.[48] At lower concentrations, paclitaxel can decrease the dynamic instability of microtubules without increasing tubulin polymerisation. This leads to mitotic arrest at these lower concentrations since the dynamic instability of the microtubule is crucial to the proper functioning of the mitotic spindle[49]. Rather than bind with soluble tubulin, paclitaxel binds instead with the polymerised tubulin that makes up the wall of the microtubule fibre, with the binding site located on the inside of the microtubule. The paclitaxel gains access to the site on the inside of the microtubule by diffusing through small holes in the microtubule. The actual binding site is well documented with a crystal structure of the site available.[50] The taxol site is located in the β-subunit (**fig 1.10**) surrounded by helix H1, H6, H7, stand B7, and loop M. The M loop is regarded as being essential for the binding of the taxane ring.

There are a number of other compounds acting through the taxane site including epothilones (**16**)[51], discodermolide (**17**)[52], and eleutherobin (**18**)[53] (**fig 1.11**). Epothilones A and B (EpoA, EpoB) occupy the same site as taxol but adopt different ligand-protein contacts[51]. EpoB and semisnthetic derivatives thereof are in clinical trails (Phase 2) with Novartis (EPO906) and Bristol Meyers Squibb (BMS-247550). Discodermolide was found to be equally as potent as taxol in the MCF7 cell line with an IC_{50} value of 2.4nM compared to 2.1nM for taxol[52]. It was also found that discodermolide could displace taxol from tubulin and vice-versa[54]. Discodermolide is the subject of an ongoing clinical trial (XAA296A), where it has been found to be well tolerated in patients. Studies to find the optimum dosing schedule are ongoing.

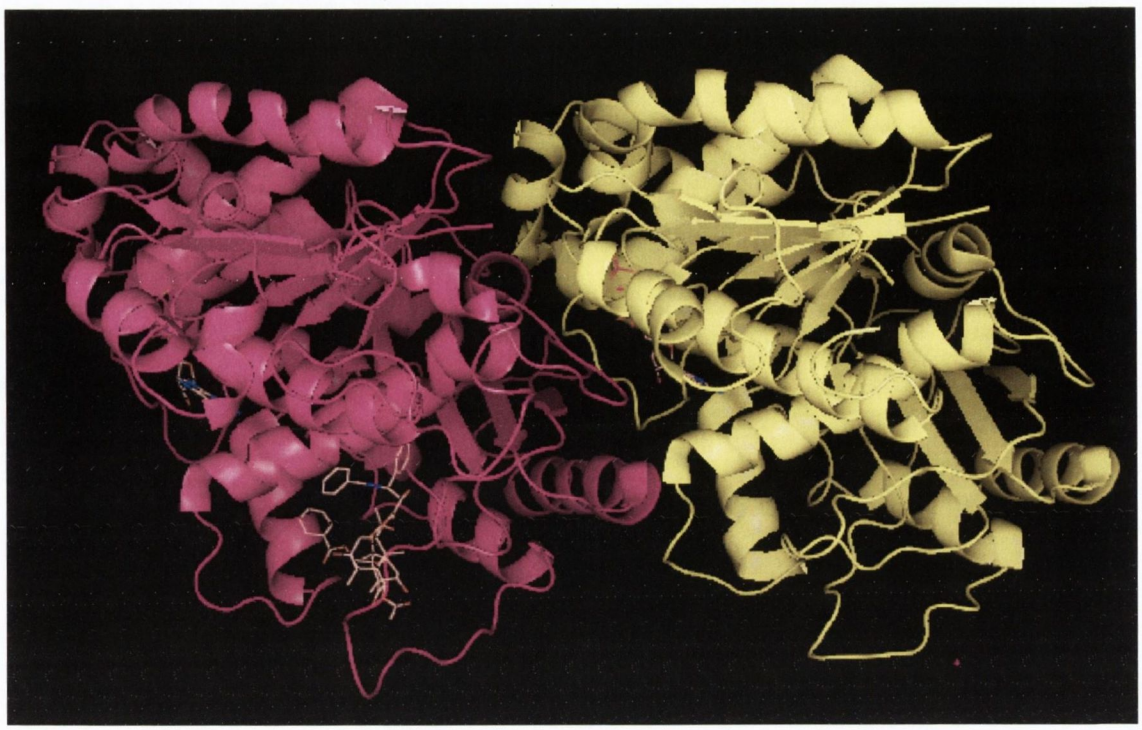

Fig 1.10 The location of the Taxol site on tubulin.[50] The site is in the β-subunit (pink).

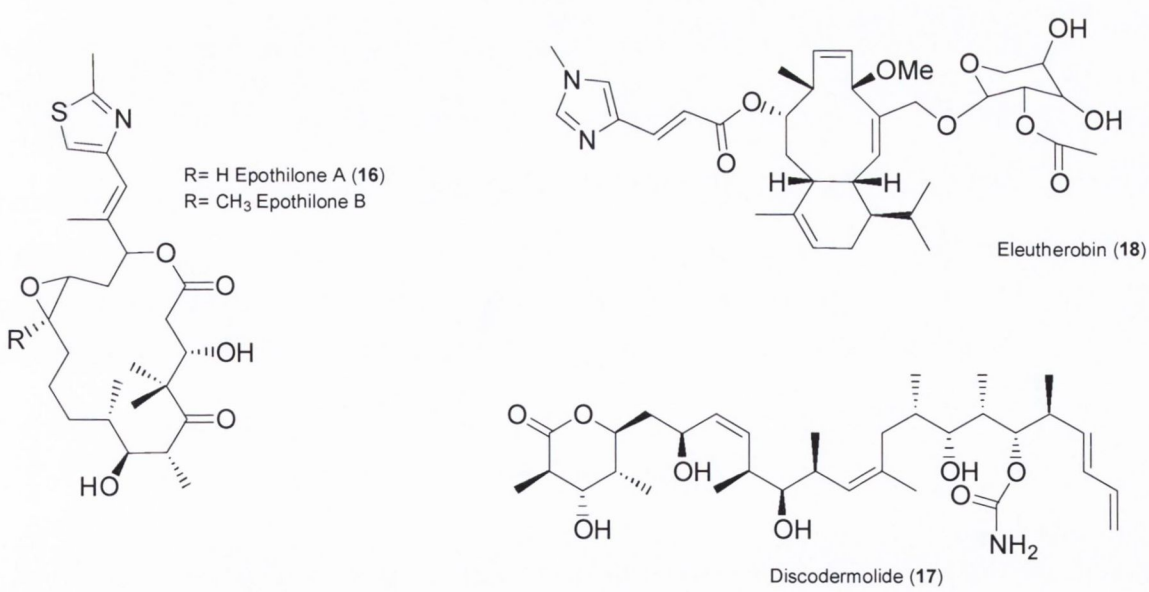

Fig 1.11 Structures for various natural products binding at the taxoid domain of tubulin

1.4.4.3 The Colchicine Site

Of the natural products that act on tubulin discussed thus far, colchicine (**19**) (**fig 1.12**) was the first to be isolated in 1928. In common with the vinca alkaloids, colchicine was shown to depolymerise tubulin at high concentrations and stabilize microtubule dynamics at low concentrations, thereby acting as an antimitotic agent.[55] [56] [57] [58] It has also been shown that colchicine can have vascular effects, inducing haemorrhagic necrosis within 8 hours of treatment[59]. Colchicine has not entered clinical use for the treatment of neoplasms due to its toxicity, but it has been used for the treatment of gout since the 1930's[60]. The exact mechanism by which it relieves gout is unknown. To minimise side effects, low doses (500μg) must be used.

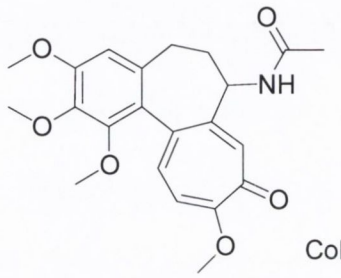

Colchicine (**19**)

Fig 1.12 Structure of colchicine

A crystal structure of a derivative of colchicine bound in tubulin is available from which the position of the colchicine site has been clearly determined (**fig 1.13**).[17] The site is mainly buried in the β-tubulin subunit, but it does maintain some interactions with the α-subunit. The major components of the site are strands S8 and S9, loop T7, and helixes H8 and H9 of β-tubulin, and loop T5 of α-tubulin. The position of colchicine as determined by XRD correlates well with previous experiments that highlighted the important role of Val β318 and Cys β241 in the site. It was found that in the case where the methoxy groups of colchicine were replaced with more reactive groups, crosslinking with Cys β241 was observed.[61] It has also been shown that tubulin which lacks the Val β318 residue becomes insensitive to colchicine.[62]

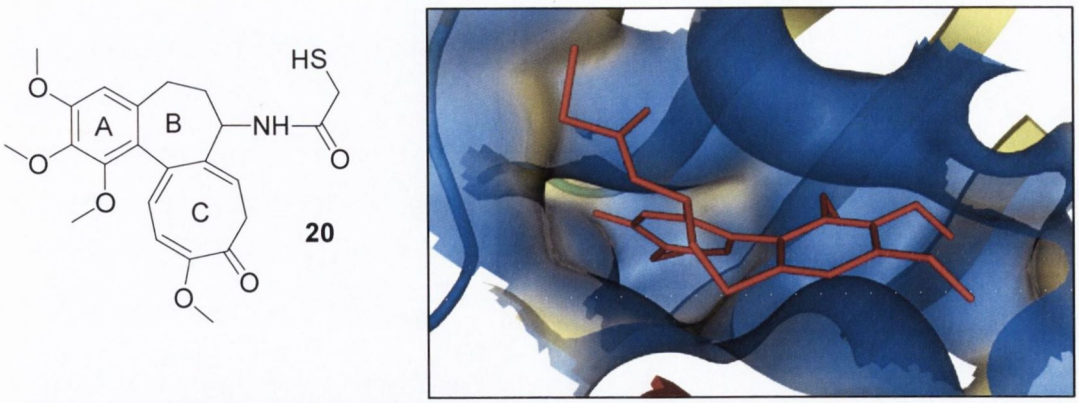

Fig 1.13 DAMA colchicine derivative (**20**) (left) and its position in the colchicine site as determined by XRD (Ravevlli[17]). The α-subunit is not shown for clarity.

By comparing the structure of tubulin both with and without bound colchicine (**fig 1.14**), Ravelli was able to propose a reasonable mechanism by which colchicine disrupts tubulin polymerisation[17]. At the onset of polymerisation α and β tubulin adopt a straight chain conformation which maximises favourable interactions all along the polymerising protofilaments. Bound colchicine induces a conformational change in tubulin so that the straight chain conformation can no longer be adopted with an obvious knock on effect on tubulin polymerisation. Colchicine prevents the α-subunit of tubulin from adopting its preferred position for polymerisation by steric hindrance between colchicine and residues Asn α101 and Val α181 of the α-subunit. The colchicine also forces the T7 loop and H8 helix and Lys β352 side chains to interfere with the α-subunit.

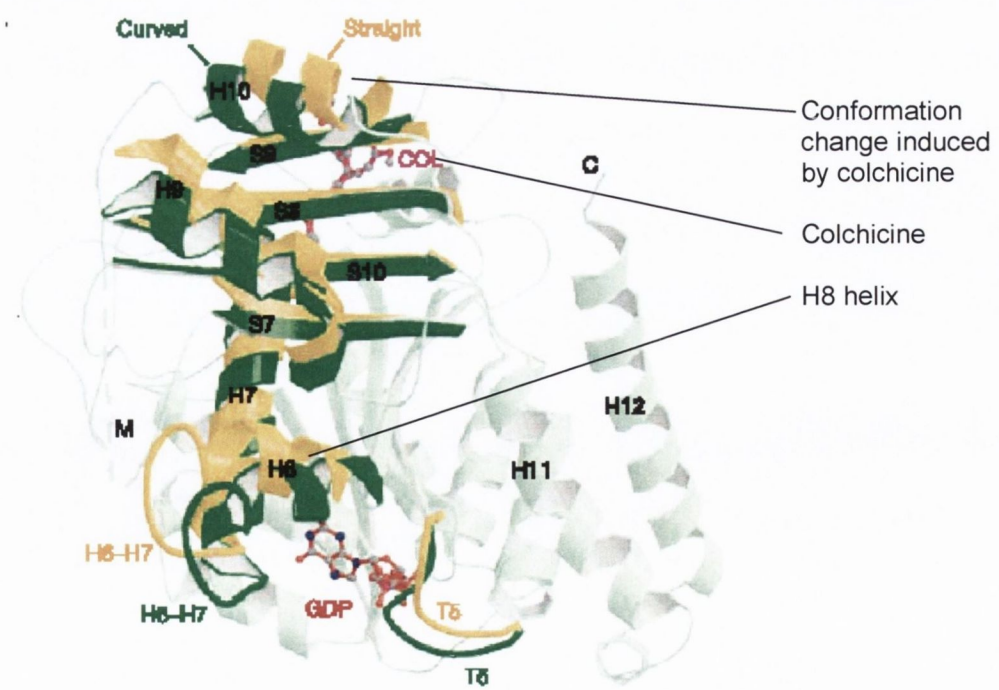

Fig 1.14 Illustration of the straight (yellow) and curved (green) conformations of β-tubulin. (taken from Ravelli *et al* [17])

The binding of colchicine to tubulin appears to involve a number of steps that are described in detail by Skoufias[63]. Skoufias examined the binding of a radiolabeled colchicine to bovine tubulin. There is an initial rapid formation of a reversible complex. This complex goes on to slowly form a poorly-reversible final equilibrium complex where the tubulin protein has undergone conformational changes. Skoufias also notes that this conformational change may be detrimental to the further polymerisation of the tubulin. Colchicine has the ability to inhibit tubulin polymerisation at very low (substoichiometric) concentrations. This is most likely due to the incorporation of tubulin-colchicine complex into the ends of the polymerisation microtubule, resulting in the disruption of polymerisation dynamics.

As an anticancer agent colchicine has not found use in the clinic mainly due to its toxicity and narrow therapeutic window. It is only in recent years that the colchicine site has been further exploited as a target for design of chemotherapeutic agents. In particular a number of compounds based on the combretastatin family of natural products have displayed promising results in clinical trials. This particular group of natural products is dealt with in more detail in **section 1.5**.

1.5 The Combretastatins

To date the most promising tubulin inhibitor acting through the colchicine site is a natural product belonging to a series of compounds collectively known as the combretastatins.

1.5.1 Discovery

The starting point for the discovery of the combretastatins came from a natural product screen carried out by the NCI in the 1970's. As part of the screen, extracts from the South African bush willow tree (*Combretum caffrum)* were found to be active against murine lymphocytic leukaemia (P-388).[64] Subsequent work by Pettit led to the characterisation of a number of active compounds contained within the extracts.[65 66 67]

1.5.2 Structure

The first product isolated was designated (-) combretastatin (**21**) (**fig 1.15**)[68], however the subsequent discovery of numerous other active compounds in the extract led to the combretastatins being divided into four groups according to their structures, labelled A-D. The A-series comprises the diaryl stilbenes, the B-series the diaryl ethylenes, the C-series the quinones, and the D-series the macrocyclic lactones. There is also a fifth group of unnamed compounds that share a common phenanthracene structure[69].

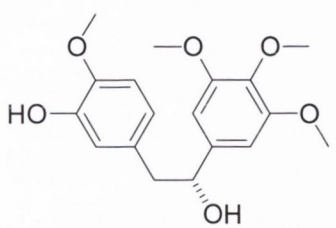

(-) Combretastatin (**21**)

Fig 1.15 The natural product (-) combretastatin

(-) Combretastatin was found to be cytotoxic in the the murine leukaemia cell line L210 with an IC_{50} value of 50nM. It was also found to be an effective tubulin polymerisation inhibitor with an IC_{50} value of 5-7.5μM.

1.5.2.1 Combretastatin A-series

The combretastatin A-series (CA1[65], CA2[70], CA3 & CA4[67], CA5 & CA6[71]) (**22-27**) is characterised by the presence of two aromatic rings, with varying substituents attached by an unsaturated carbon double bond in the *cis* conformation. This carbon double bond is referred to as the bridge between the two ring systems. It is important to note that CA1 (**22**) and CA4 (**24**) both contain a trimethoxy substituted aryl ring in common with colchicine. The "A" series has been tested for antiproliferative activity in the NCI panel of 60 cell lines. CA1 and CA4 represent the two most promising leads with mean IC_{50} values in the panel of 32nM and 3nM respectively[72] which compares favourably to other agents such as taxol (IC_{50} 1.1nM)[73] with CA4 particularly effective against lung and colon cancers. Both also have excellent antitubulin activity with IC_{50} values for inhibition of tubulin polymerisation of 1.9μM and 1.2μM respectively.[74] The excellent *in vitro* results for CA1 and CA4 has led to interest in their development as novel anticancer agents. The antiproliferative and antitubulin data for compounds (**22-27**) are shown in **table 1.3**.

Clearly CA4 and CA1 have potential as antiproliferative agents in their own right, but the observation that treatment of proliferating human umbilical vein endothelial cells (HUVEC) with 1μM CA4 results in morphological changes and detachment of cells from each other, hinted that CA4 may be able to disrupt tumour vasculature.

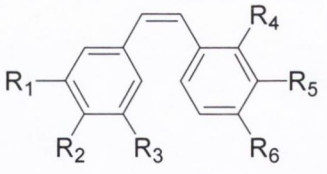

22-26

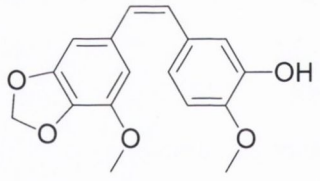

CA2 (**27**)

Entry	Name	R_1	R_2	R_3	R_4	R_5	R_6	Tubulin Polymerisation (μM)	L210 (μM)
22	CA1	OMe	OMe	OMe	OH	OH	OMe	1.2	0.6
23	CA3	OH	OMe	OMe	H	OH	OMe	4-5	0.026
24	CA4	OMe	OMe	OMe	H	OH	OMe	1.9	0.0034
25	CA5	OH	OMe	OMe	H	OMe	OMe	75-100	2
26	CA6	OH	OMe	OMe	OMe	OMe	H	>100	30
27	CA2							4-5	0.027

Table 1.3 Structures and biochemical data for the combretastatin A series. The biochemical data was taken from *Anticancer Agents from natural Products*[75]

1.5.2.2 Combretastatin B-series

The combretastatin B-series (CB1, CB2, CB3, CB4) (**28-31**) is similar to the A-series with the notable exception that the aromatic rings are bridged with a saturated carbon carbon bond. Again the trimethoxy substituted aryl ring appears for two of the members (CB1 and CB3). The biochemical data for compounds **28-31** are illustrated in **table 1.4** for the murine leukaemia cell line L210 and for tubulin polymerisation inhibition.

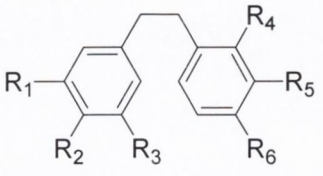

Entry	Name	R_1	R_2	R_3	R_4	R_5	R_6	Tubulin Polymerisation (IC_{50}) (μM)	L210 (IC_{50}) (μM)
28	CB1	OMe	OMe	OMe	OH	OH	OMe	4-5	3
29	CB2	OH	OMe	OMe	H	OH	OMe	40	3
30	CB3	OMe	OMe	OMe	H	OH	OH	>100	3
31	CB4	OMe	H	OMe	H	OH	OH	25-30	1
32	-							>100	4
33	-							10-15	1
34	-							>100	50

Table 1.4 Structures and biochemical data for the combretastatin B series. The biochemical data was taken from *Anticancer Agents from natural Products*[75]

There are also three structurally similar compounds in the series that have not been named (**32-43**) illustrated in **fig 1.16**.

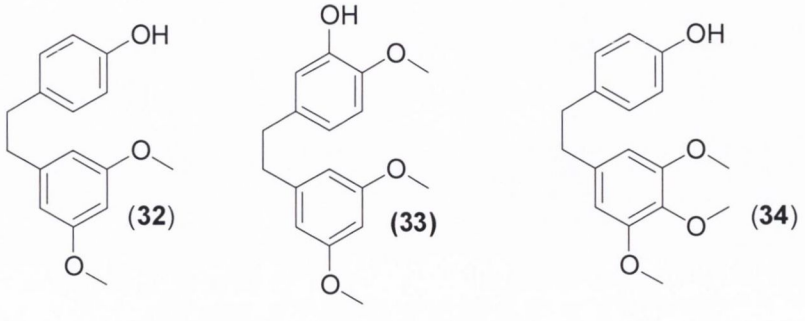

Fig 1.16 Unnamed members of the combretastatin B-series

1.5.2.3 Combretastatin C-series

The C-series (CC1) (**35**) marks a departure from the structures seen in the first two series and only contains a single member (**fig 1.17**). The carbon bond bridge has been replaced with a third ring system, and there is a distinctive quinine structure present. **35** is about 1000 times less active in the P388 leukemia cell line.

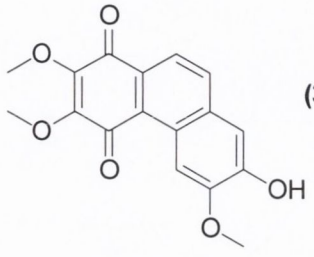

(35)

Fig 1.17 The single member of the combretastatin C-series

1.5.2.4 Combretastatin D-series

The D-series (CD1[76] & CD2[77]) (**36** & **37**) is made up of two macrocyclic structures (**fig 1.18**). As was the case with the C-series, neither of the D-series display potencies approaching that of CA4. In the P388 leukemia cell line IC_{50} values of 3.3μM and 5.2μM were obtained compared to 0.0034μM for CA4.

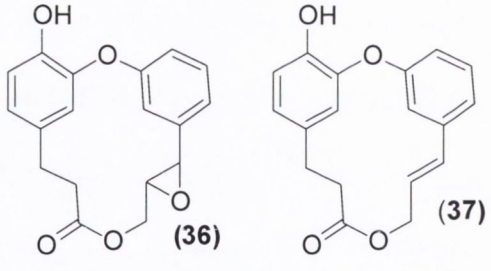

(36) **(37)**

Fig 1.18 The members of the combretastatin D-series

1.5.2.5 Phenanthrene Series

There are four members (**38-41**) of the phenanthrene type combretastatins (**fig 1.19**). These compounds remain as yet unnamed. All four members display poor antitubulin effects with IC_{50} for inhibition of tubulin polymerisation of greater than 100μM, and consequently have poor potencies in the P388 leukemia cell line.

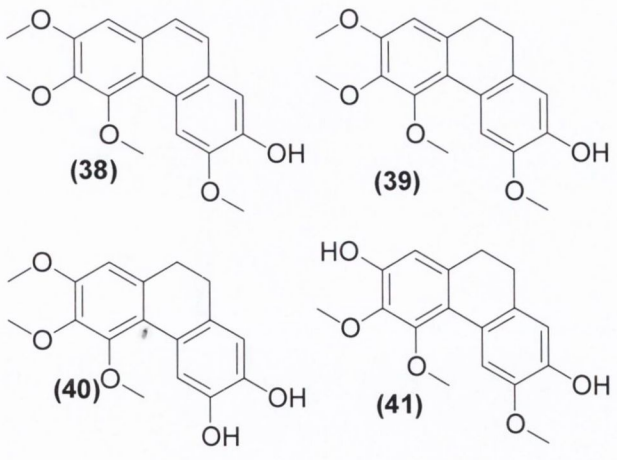

Fig 1.19 The members of the unnamed phenanthrene combretastatin.

1.5.3 Binding at the Colchicine Site

The mechanism of action of CA-4 was subsequently elucidated to be that of tubulin dynamics disruptor binding at the colchicine site. Hamel *et al* [65] demonstrated that CA4 can inhibit the binding of radiolabelled colchicine to tubulin by over 97% where in comparison podophyllotoxin only inhibited binding by 89%. In contrast to colchicine where the binding to tubulin occurs via an initial slow step, CA4 was found to bind much quicker to tubulin. It was also found that CA4 dissociates from the tubulin complex much faster than colchicine. The half lives for the CA4-tubulin and colchicine-tubulin complexes were found to be 3.6 minutes and 405 minutes. It has been suggested that this difference in binding to tubulin gives rise to the differences observed in the toxicity of CA4 compared to colchicine[78].

1.5.4 CA4 as a Vascular Targeting Agent

Section 1.2.2.5 outlined the role that angiogenesis plays in cancer pathology. A well developed vascular system is needed for any tumour to grow beyond a few millimetres in size. Up to this threshold, the tumour can obtain the nutrients and oxygen it requires through diffusion from the surrounding tissue.[1] The importance of tumour vasculature is evident from the direct relationship between the over expression vascular endothelial growth factor (VEGF) and poor patient prognosis. So high levels of VEGF leads to the formation of dense tumour vasculature which in turn leads to high levels of morbidity and mortality in patients.

This observation has led to interest in developing therapies that target tumour vasculature. Such therapies can be grouped into those that prevent development of

vasculature (antiangiogenesis) and those that shutdown the tumour vasculature once it has been formed (vasculature targeting agents). CA4 and CA1 have shown enormous promise as vasculature targeting agents (VTAs). Griggs[79] *et al* and Tozer[80] *et al* both present excellent reviews of this area.

1.5.4.1 Characteristics of Tumour Vasculature

Tumour vasculature differs from physiological vasculature in a number of important respects which allows CA4 to selectively target the tumour vasculature while leaving physiological vasculature unscathed.

The vascular walls of the tumour are immature, poorly developed and lacking the smooth muscle that is characteristic of normal vasculature. The endothelial cells making up the walls are irregularly shaped, and the connections between individual cells are weak. They rely upon tubulin rather than actin to lend structural rigidity to the blood vessel walls. These poorly formed walls are very permeable which leads to the tumour being particularly susceptible to infiltration by low molecular weight anticancer agents.[81] Increased permeability of tumour vasculature also increases the interstitial pressure within the tumour.

The tumour vasculature is highly branched and irregular. Higher than normal pressure is needed to maintain blood flow through such a chaotic network. Blood flow rates within in the centre of the tumour are particulary slow, and often the flow has been deoxygenated by the time it reaches the centre of the tumour leading to hypoxic zones within the tumour.[82] As a result the centre of the tumour is very sensitive to even small changes in blood flow[83].

1.5.4.2 Effects of CA4 on Tumour Vasculature

CA4 has antiproliferative activity in the low nanomolar range against a variety of cancer cell lines, however it is its ability to shutdown tumour vasculature *in vivo* which is of particular interest. *In vivo* experiments in the P22 carcinosarcoma rat tumour model has demonstrated a 100 fold reduction in tumour blood flow within the first minutes after a single dose of 100mg/kg of CA4 and maintained up to 6 hours later[84]. Importantly no major reduction in blood supply to the heart, kidney and small intestine were noted with only a minor reduction to the skin, brain, and spleen. Even at a lower dose of 30mg/kg vascular effects in the tumour were are noticed. Galbraith used dynamic contrast medium enhanced magnetic resonance imaging (DCE-MRI) to demonstrate the vascular effects of CA4 both in rats and humans. Gadolinium diethylenetriamine pentaacetic acid was used as the contrast agent which allows for the monitoring of blood flow in tissues by MRI.

This vascular shutdown is believed to result from the changes in the endothelial cells brought about by the administration of CA4[85]. CA4 disrupts the microtubules within the endothelial cells. In the absence of microtubules the actin cytoskeleton is overwhelmed in its task of maintaining cell shape. The endothelial cells are observed to undergo morphological changes – they become more rounded in shape and form blebs on the vessel wall. Blebbing restricts the blood flow through the vessel and also increases vascular permeability. The slowing of blood flow leads to red blood cells clumping together, increasing the viscosity of the blood, and leading to a further reduction in blood flow. Increased permeability leads to leakage from the vessels, increasing interstitial pressure, which results in a further constriction of the vessel. Through these proposed mechanisms, vascular shutdown is brought about. The antivascular effects of CA4 on tumour blood vessels is illustrated in **fig 1.20** as presented by Tozer *et al.*[86]

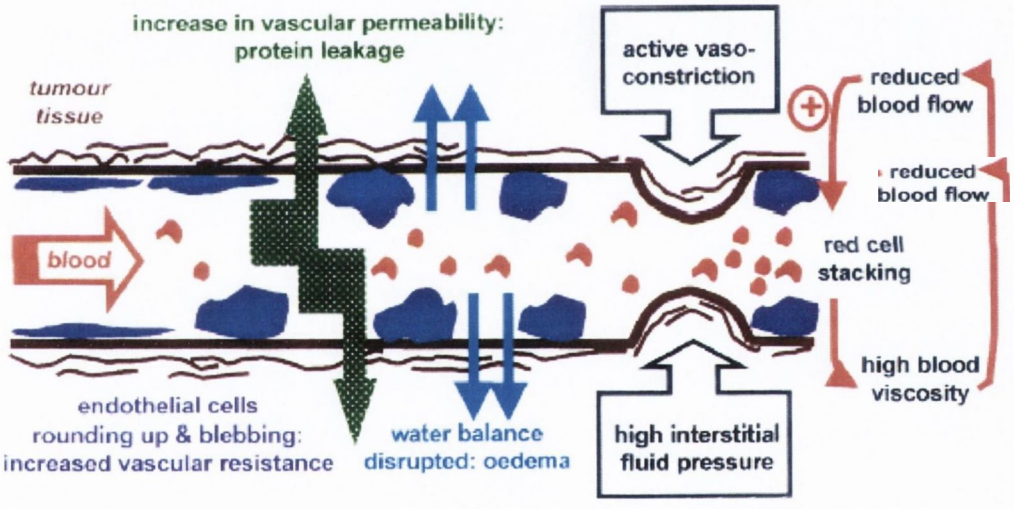

Fig 1.20 Overview of the antivascular effects of CA4 on tumour blood vessels Tozer *et al* [86]

Other antimitotic agents such as the vinca alkoloids and colchicine can also bring about vascular shutdown in tumours but not at the low concentrations observed for the combretastatins[65]. It is proposed that the reversible binding of CA4 to tubulin compared to the binding of colchicine allows for CA4 to exact a vascular effect at a concentration much lower than the maximum tolerated dose. For instance CA4 has a drug dissociation half life from tubulin of 3.6 minutes compared to 405 minutes for colchicine.[65]

1.5.5 CA4 as an Effective Therapeutic Agent

Despite its excellent *in vitro* activity against cancer cell lines and its *in vivo* activity as a VTA, there are a number of barriers to CA4 in current development. The stereochemistry around the carbon carbon double bond is of vital importance to activity [69 87 88]. CA4 can exist as both *E* and *Z* isomers (**fig 1.21**). The *Z* isomer is by far the more active of the two, but the *E* isomer is the more thermodynamically stable. The *Z* compound will ultimately convert to the energetically more favourable *E* isomer over a short period of time. The conversion is catalysed by light and by protic solvents. The storage conditions needed to guarantee an isomerically pure form would be difficult. A number of fixed ring analogues have been synthesised to restrict the *E/Z* isomerisation of CA4 and are discussed in greater detail in section **1.6**. The second hurdle faced by CA4 is its poor water solubility[89 90], in fact CA4 is water insoluble, and this decreases its bioavailability.

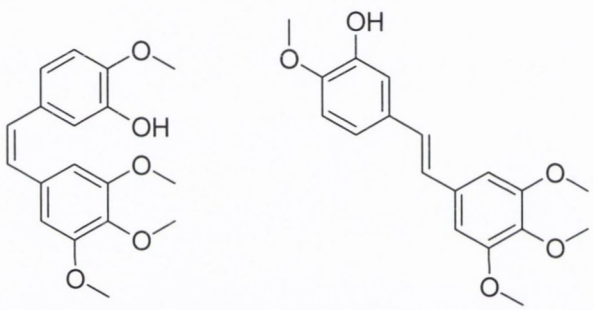

Fig 1.21 Representation of Z (left) and (E) isomers of CA4

Despite these challenges, CA4 is an attractive lead compound as a vascular targeting agent. It has a wide enough therapeutic window (a dose of 100mg/m^2 typically represents 20% of the MTD) between the effective dose and the maximum tolerated dose (MTD) when compared to other compounds in the same class such as colchicine[91]. By targeting the tumour blood supply, it may be a valuable agent against multidrug resistant (MDR) cancers. MDR cancers arise from the cancer cell adopting a number of different approaches to limit the effect of chemotherapeutic agents on the cell. These include altered binding sites, enzymatic deactivation, altered metabolism, decreased permability, and increased efflux of the agent. In terms of providing a target for blocking resistance, the efflux mechanism is the most important, particularly inhibition of P-glycoprotein and the multidrug resistance protein (MDRP). Excellent reviews of the area are available[92]. VTAs are a promising treatment for MDR cancers because the shutdown of tumour vasculature will induce hypoxia and necrosis in the tumour regardless of the presence of MDR cancer cells. Since CA4 is expected to act

on the endothelial cells of vasculature rather than directly on the tumour cells, resistance is less likely to emerge[93].

1.5.5.1 Water Soluble Prodrugs

A major hurdle to the clinical use of the combretastatins is the poor water solubility. A number a prodrugs have been prepared. These include the obvious choice of converting the free hydroxy to the corresponding sodium (**42**) and potassium salts (**43**), as well as a succinic acid prodrug ester (**44**) (**fig 1.23**).[94] The most promising prodrugs are those using the dipotassium and disodium phosphate moiety (**45** & **46**). Of these the disodium phosphate prodrug of CA4 (called CA4P) (**46**) is of particular interest and is undergoing a number of clinical trials as a combination therapy with other well established chemotherapies and radiotherapy.[95 96 97] The solubility of this salt has been reported as *circa* 20mg/mL in distilled water.[98] In a similar way a disodium phosphate prodrug of CA1 (**47**) has also been synthesised and is undergoing further investigation.[99] *In vivo* it is expected that these phosphate prodrugs undergo rapid hydrolysis by phosphatases to yield CA4.[99] Kirwan *et al* [100] carried out a study on the metabolism of CA4P and CA1P *in vivo* in mice by HPLC-MS. They determined that both prodrugs were dephosphorylated rapidly in tumour homogenate (MAC29), but more slowly in blood and blood plasma. In blood plasma both prodrugs were dephosphorylated at a rate of approximately 30ng/g/min. In whole blood the same rate was maintained for CA1P but increased to 133ng/g/min for CA4P. The half life for CA4P was found to be 1.38 hours and 0.72 hours in plasma and tumour respectively while for CA4 half lives of 0.35 hours and 9.62 hours in plasma/tumour were observed. The group also carried out an interesting analysis of the metabolism of CA1 and CA4 in tumour homogenate the results of which are shown in **fig 1.22**. This clearly shows that the CA4 is more stable in the tumour but may also be due to CA1 being covalently bound to tubulin in such a way that it cannot be extracted from the homogenate. There is growing evidence that CA1P outperforms CA4P in retarding tumour growth.[101 102] Kirwan concludes that this may be due to the metabolism of CA1 to yield a reactive intermediate.

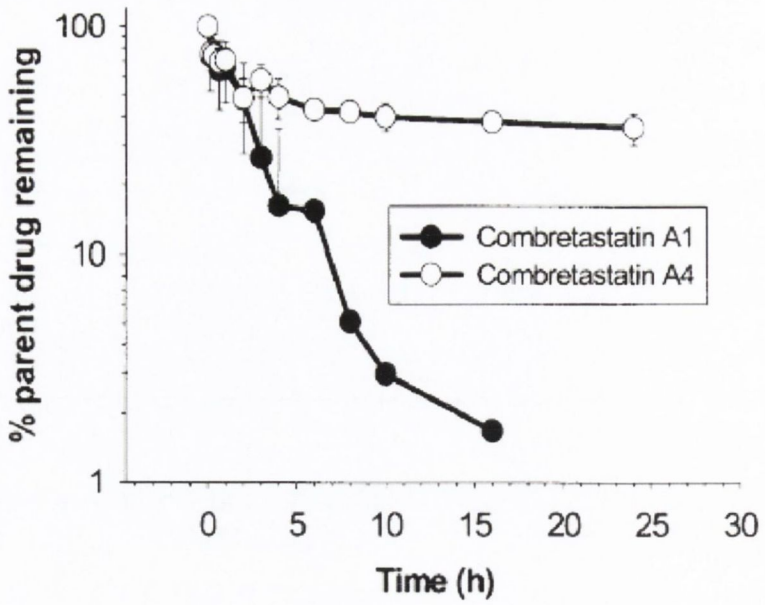

Fig 1.22 Metabolism of CA1 and CA4 in MAC29 tumour homegenate

CA4P has been shown to depolymerise microtubules in human umbilical vein endothelial cells (HUVECs) *in vitro*.[103] Such an observation hints that CA4P is itself capable of binding at the colchicine site of tubulin and interfering with microtubule dynamics, however it is unlikely that CA4P remains intact *in vivo* for long enough to be taken up by proliferating cells.

Aventis Pharma have developed a novel serinamide hydrochloride prodrug (AVE8062) (**48**) (**fig 1.23**). The basis for this prodrug is an analogue of CA4 where the 3-hydroxy group has been replaced with that of a 3-amino group, from which a serine hydrochloride salt can be synthesised [104]. The prodrug is converted back to its parent compound by cleavage of the amide bond by aminopeptidases. The substitution of the hydroxy group with an amino group has been recognized as an important analogue of CA4 that retains similar biological activity to CA4.[105] [106] [107] **48** was found to have a solubility of 14.7mg/mL in phosphate buffered saline compared to 0.11mg/mL for CA4.

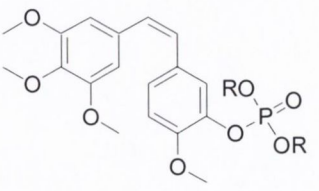

R = Na (**46**)
R = K (**45**)

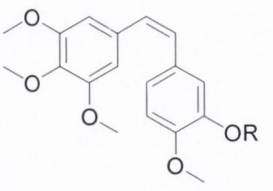

R = Na (**42**)
R = K (**43**)
R = $COCH_2CH_2CO_2H$ (**44**)

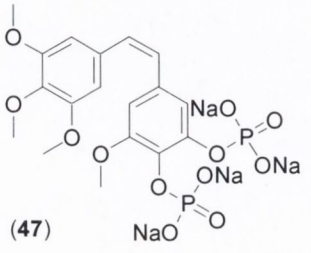

(**47**)

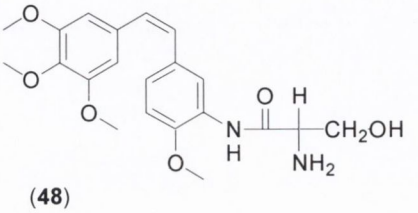

(**48**)

Fig 1.23 Various prodrugs of combretastatin

1.5.5.2 Synthesis of CA4 and its prodrugs

The synthesis of CA4 and its conversion to the phosphate ester prodrug CA4P is described in **scheme 1.1**. The key step in the reaction is the Wittig reaction between the phosphonium bromide (**49**) and trimethoxybenzaldehyde (**50**), which is a route first described by Pettit[71]. The Wittig reaction results in the formation of both *Z* and *E* isomers with the biologically less active *E* isomer being favoured. The separation of the two isomers is difficult and the overall yield for the *Z* isomer is only 19%.

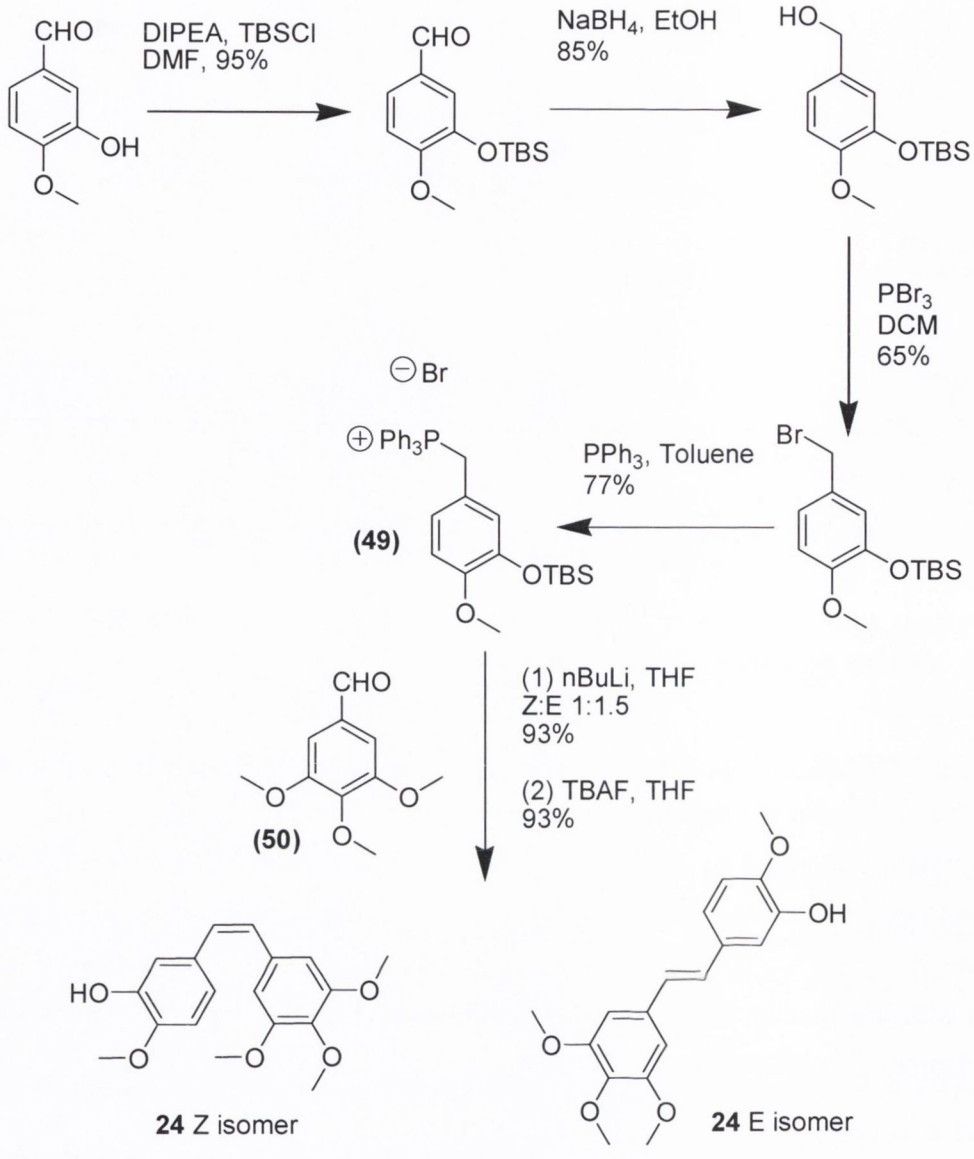

Scheme 1.1 Synthesis of CA4 via the Wittig reaction as described by Pettit[71]

Gaukroger *et al* [108] has described the use of a Suzuki cross coupling in the synthesis of CA4 (**scheme 1.2**). The first step is the Corey-Fuchs Wittig like bromination of protected isovanillin (**51**), followed by a stereoselective reduction of the deprotected brominated product (**52**) using tributyltin hydride to yield the *Z* vinyl bromide (**53**). A Suzuki coupling between the bromide (**53**) and boronic acid (**54**) resulted in the isolation of the desired *Z* isomer in 70% yield. The overall yield for this reaction from the isovanillin starting material was 16%.

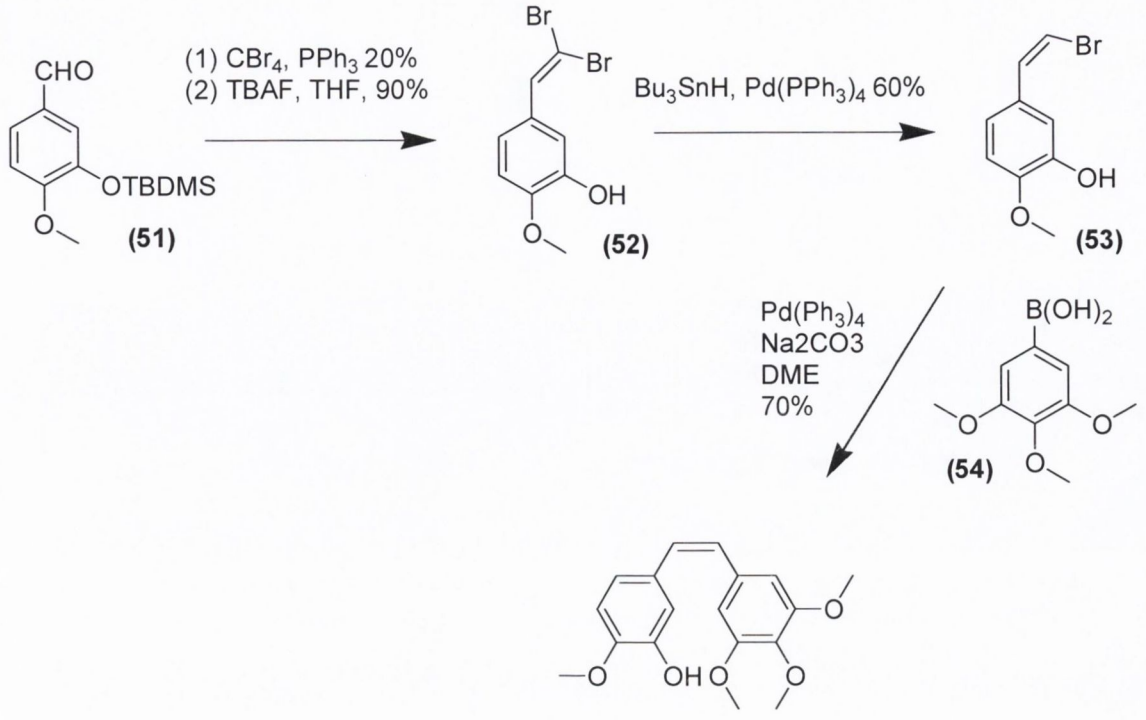

24 Z isomer

Scheme 1.2 Suzuki route to CA4

Although the Suzuki route described above did increase the stereoselectivity of the reaction, the overall yield remained poor. Gaukroger[108] also examined the use of the Perkin reaction in the synthesis of CA4 (**scheme 1.3**). Initially a cinnamic acid (**57**) was formed from the Perkin condensation of isovanillin (**55**) and trimethoxyphenyl (**56**) acetic acid. Decarboxylation of this intermediate afforded the desired *Z* CA4 in 42% overall yield.

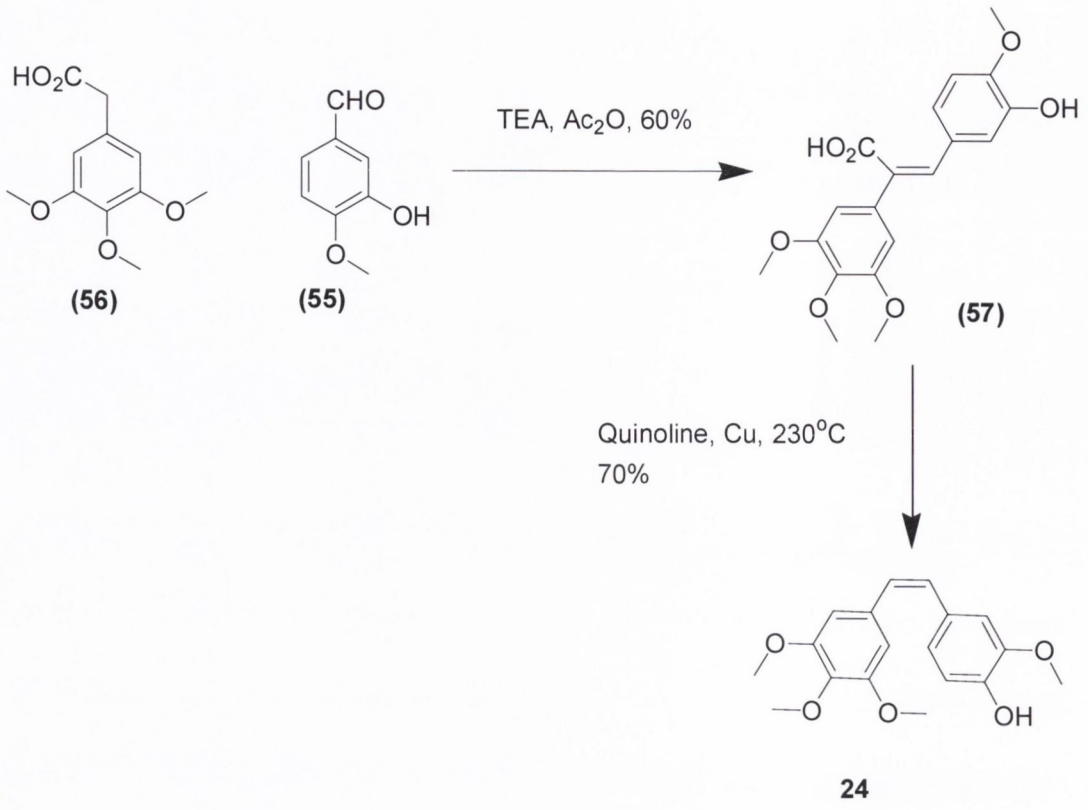

Scheme 1.3 Perkin route to CA4

CA4 can be converted in two steps to CA4P in high yield as described by Pettit[109] (**scheme 1.4**). A dibenzyl phosphate ester (**58**) is initially formed which is then debenzylated with sodium iodide/chlorotrimethylsilane. Treatment with sodium methoxide gives CA4P.

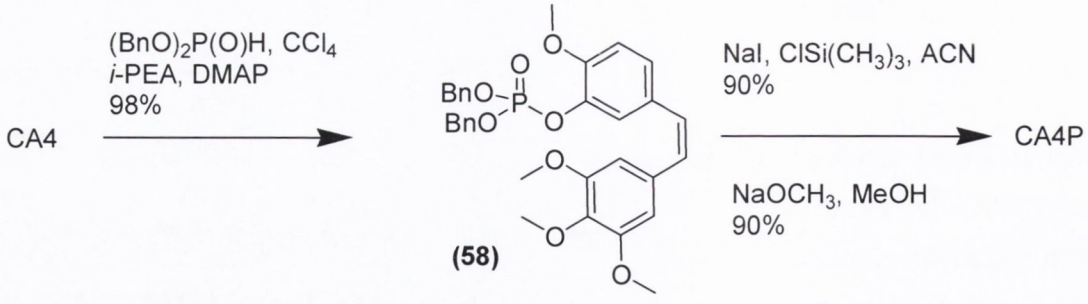

Scheme 1.4 Conversion of CA4 to CA4P

1.5.5.3 Combination Therapy

As outlined above CA4 shows promise as a VTA. Functional MRI[110] studies have revealed that while CA4 is capable of shutting down tumour blood flow and inducing hypoxia and consequently cell death in the centre of the tumour, a thin rim of viable cells remain on the periphery of the tumour **(fig 1.24)**. The tumour rim is often the best vascularised and oxygenated part of the tumour which may explain its

insensitivity to CA4. The existence of such a rim explains the observation that CA4 is not as effective at achieving retardation of tumour growth as might be expected [93] **(fig 1.25)**.

In more traditional cancer therapies, the outside of the tumour often proves the most vulnerable to damage while the center of the tumour remains untouched. Therefore it was theorised that the use of CA4 in combination with a traditional chemotherapy or radiotherapy might yield improved outcomes for patients over the use of a single therapy.

The effects of combination therapy have been well demonstrated for a number of chemotherapy agents[111] as well as for radiation[97]. The combination of CA4P with cisplatin or taxol appears to have potential as effective regimes[112]. Due to the ability of CA4P to modify blood flow within the tumour, the use of a properly timed combination therapy may allow for the trapping of a chemotherapy agent within in the tumour with obvious implications for tumour survival. CA4P is capable of increasing the radiation damage seen in animal tumour models. The timing of the CA4P dose is critical. CA4P given before the radiation dose leads to tumour hypoxia and a subsequent reduction of proliferating cells which leads to a less effective radiation dose. A CA4P dose after radiation can impact radiation resistant cells. The combination of CA4P and radiation may prove particularly useful in the treatment of large tumours, where the CA4P can target the centre of the tumour and the radiation can deal with the viable rim left at the surface of the tumour.

A number of clinical trials involving such combination therapies are in progress. The most promising of these trials include: CA4P in combination with Taxol/Carboplatin in the treatment of anaplastic thyroid cancer (NCT00507429); CA4P in combination with cisplatin, doxorubucin, and radiation in the treatment of anaplastic thyroid cancer (NCT00077103); and CA4P in combination with the monoclonal antibody Avastin (NCT00395434) for the treatment of solid tumours.

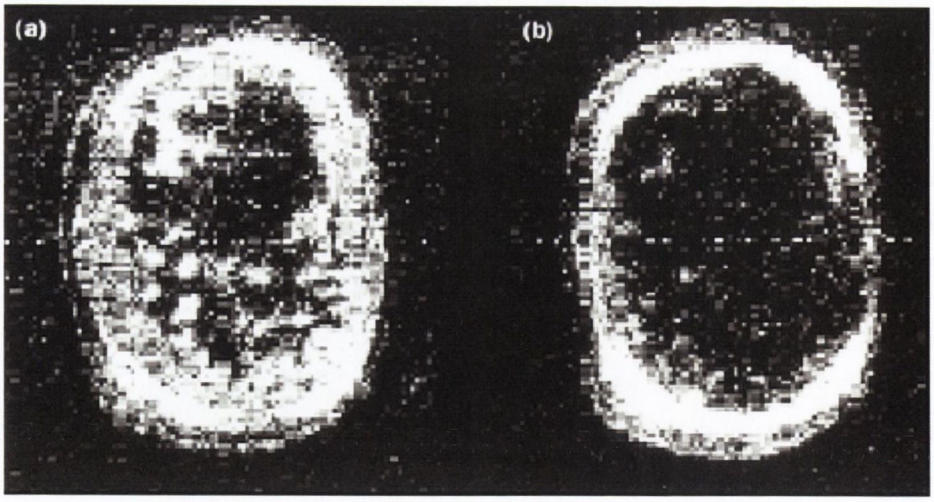

Fig 1.24 MRI showing antivascular effects of CA4. White areas mark the distribution of a contrast-enhancing agent which indicates areas of blood flow. (a) is before and (b) is 160 minutes after treatment with 100mg/kg of CA4[122].

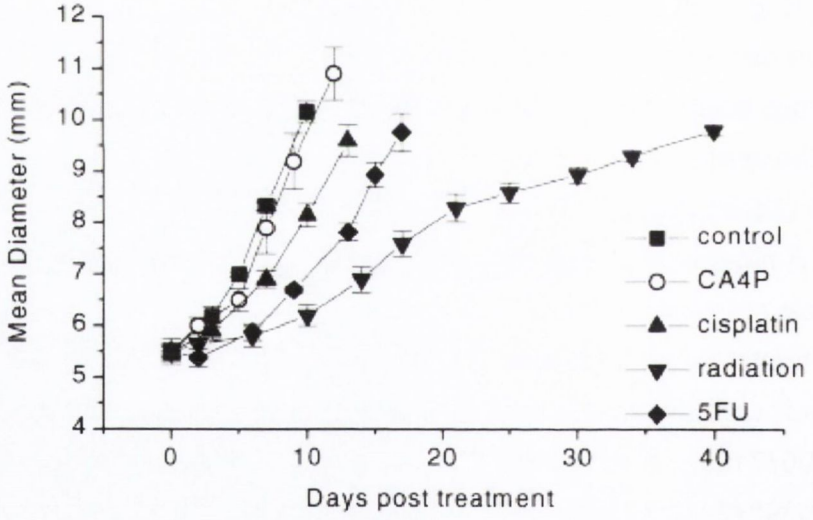

Fig 1.25 Effects of CA4P (500mg/kg), cisplatin (5mg/kg), 5-fluorouracil (125mg/kg), and radiation (20Gy) on growth of CaNT tumours (Chaplin *et al* [95])

1.6 Novel Combretastatin Analogues

A number of potential antiproliferative agents based upon CA4 have been synthesised to date, with the goal of improving pharmacokinetic properties, potency, stability etc. These analogues can be broadly divided into three groups depending upon where the structure has been modified – the "A" ring, the "B"ring, and the ethene bridge as illustrated in **fig 1.26** where the possible sites in CA4 for structural modification are highlighted. Relative potency compared to CA4 is used to describe the biochemical effects of these analogues. This allows for the direct comparison of analogues that have been tested across a number of laboratories over a period of many years. Excellent reviews on the medicinal chemistry of CA4 are available[113 114]

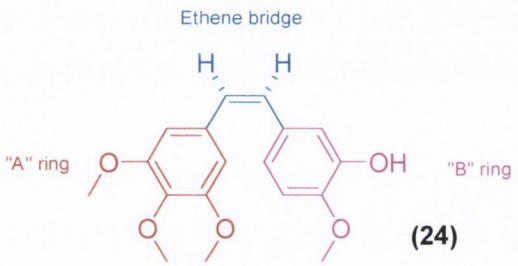

(24)

Fig 1.26 CA4 structure and areas for modifications

1.6.1 Key Structural Features in CA4

Compared to other cytotoxic compounds, CA4 has a relatively simple structure but it does possess a number of structural features that are essential to the potency of CA4.

The geometry about the bridge is vital to activity. Upon the conversion from the *Z* to the *E* isomer there is a drastic decrease in activity.[39] Unfortunately this isomerisation occurs readily and is catalysed by exposure to light.[115 116] Many of the analogues in literature have replaced the ethene bridge with a variety of linkers with the intent of remedying these issues and restricting isomerisation. **Section 1.6.4** provides an overview of the literature dealing with the modification/replacement of the ethene bridge.

The "A" ring which contains the 3,4,5-trimethoxy moiety is also deemed necessary for activity although there are a number of analogues that have modifications to the "A" ring that display activity approaching that of CA4. The 3,4,5-trimethoxy substitution pattern is conserved in a number of other members of the combretastatins as well as appearing in colchicine and in general the "A" ring is

considered sacrosanct in terms of incorporating modifications. **Section 1.6.2** presents an overview of the literature dealing with modifications of the "A" ring.

The majority of analogues incorporate changes onto the "B" ring of the molecule and is discussed in detail in **section 1.6.3**. Many of these modifications result in a decrease in activity, but there are exceptional cases where activities approaching or exceeding that of CA4 are observed.

1.6.2 Modifications to the A-Ring

The 3,4,5-trimethoxy pattern present in ring A of CA4 is conserved in a number of other antimitotic agents such as colchicine(**19**), steganacin (**59**), and podophyllotoxin (**60**) (**fig 1.27**). Evidence of the crucial role of this subunit is presented in many studies.[117 118 119] Indeed the replacement of the 3-methoxy with a 3-hydroxy group as seen in CA3 leads to a decrease in cytotoxicity. More recently the absolute necessity of this subunit has been called into question. Gaukroger *et al* [120] proposed that this particular subunit is an artefact arising from Shikimic acid (**61**) which is a biosynthetic precursor of these antimitotic natural products. A number of CA4 analogues have been synthesised to investigate the role of the trimethoxy subunit. The ubiquitous nature of the 3,4,5- trimethoxy subunit may only be a consequence of biosynthetic origin, rather than representing a highly optimised pharmacophore. To test this hypothesis a number of substitution patterns have been incorporated onto the A ring of CA4.

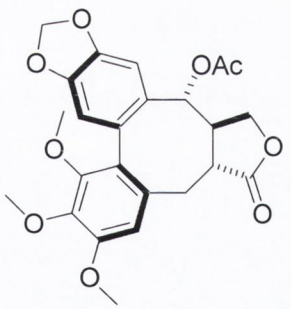

Steganacin (**59**)

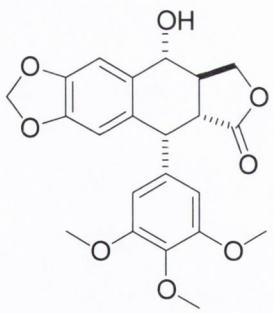

Podophyllotoxin (**60**)

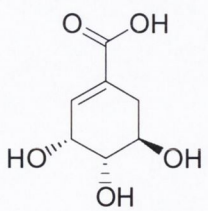

Shikimic acid (**61**)

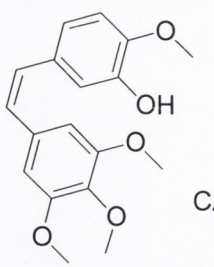

CA4 (**24**)

Fig 1.27 Natural product antimitotic agents (**59**, **60**, **24**) all containing the trimethoxy subunit possibly due to Shikimic acid (**61**) as a precursor.

Replacement of the 3,4,5 methoxy groups of CA4 ring A with ethoxy groups (**62**) leads to a decrease in activity (**table 1.5**).[120] This would indicate that steric factors may be involved in modulating biochemical activity. The trimethyl (**63**) analogues also resulted in a loss of cytotoxicity, however it was noted that inhibition of microtubule assembly was maintained. From the point of view of developing a VTA antitubulin activity may be more important than cytotoxic effects. Work by Pettit *et al* involved the replacement of the methoxy groups with fluorine. Of particular note was an analogue with a fluoro at the 3-position (**64**) which displayed both similar cytotoxicity and antitubulin effects to that of CA4[121]. The replacement of the fluorine with bromine (**65**) or chlorine (**66**) led to a loss of activity in the cell line but antitubulin activity was maintained (data presented in **table 1.5**).

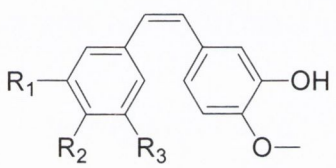

Entry	R_1	R_2	R_3	Potency Value	Tubulin Inhibition (μM)
62	OEt	OEt	OEt	18 (K562)	nd
63	Me	Me	Me	20 (K562)	nd
64	F	OMe	OMe	<6 (P388)	1.5
65	Br	OMe	OMe	8 (P388)	1.6
66	Cl	OMe	OMe	7 (P388)	1.5

Table 1.5 Biochemical data for A ring modified combretastatins (**62-66**). The potency value represents the activity of the test compound with reference to CA4

1.6.3 Modifications to the B-Ring

Many of the combretastatin analogues synthesised thus far involve modifications to the B ring. Biochemical activity for a selection of these compounds (**67-72**) is presented in **table 1.6**). These of course include the water soluble prodrugs discussed above. To begin with the substitution of either the 3-hydroxy or the 4-methoxy with other groups can be examined. It has been established that the 4-methoxy group is essential while the 3-hydroxy is not.[117] Replacing the methoxy with a bulkier group such as an ethoxy leads to a reduction in activity and likewise for the replacement of the oxygen atom with that of sulphur[122]. Interestingly incorporating a dimethylamino group into the C_4 position leads to a significant loss of cytotoxicity while antitubulin activity remains unaffected (**72**)[123]. This indicates that cytotoxicity and antitubulin activity may be divorced from one another. As such a large number of groups have been incorporated into the 3-position. It is expected that the presence of

a halogen group would yield an analogue less susceptible to metabolism, thereby increasing half life. Both the fluoro (**68**)[124] and the bromo (**69**)[125] analogues show decreased activity compared to that of CA4 but the fluoro compound does retain some activity. Kong *et al* made use of a boronic acid analogue (**70**) in an effort to increase the water solubility of CA4.[126] A detailed molecular modelling study was carried out that indicated that the boronic acid was a suitable mimic of the 3-hydroxy group displaying greater tubulin polymerisation inhibition and cytotoxicity to that of CA4. It displayed an IC_{50} value of 17nM against the MCF7 breast cancer cell line compared to 32nM for CA4. The modelling study showed that one of the hydroxy groups of the boronic acid adopts a similar position to the hydroxy group of CA4. The remaining hydroxy group of the boronic acid forms a hydrogen bond with the Thrα179 of the protein which is not present in the docked solution of CA4 which may explain the enhanced activity of (**70**) over CA4. The introduction of a 3-NH_2 group (**71**) is noteworthy since it increases slightly the potency of the analogue[106]. The NH_2 group is also amenable to the conversion to a water soluble prodrug (AVE8062) (**section 1.5.1.1**).

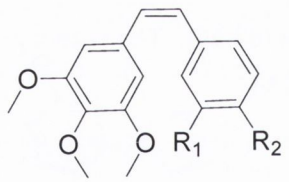

Entry	R1	R2	Potency Value	Tubulin Inhibition (μM)
67	H	OMe	1.16	2.5
68	F	OMe	1.3(K562)	nd
69	Br	OMe	62 (P388)	nd
70	$B(OH)_2$	OMe	0.53 (MCF7)	1.5
71	NH_2	OMe	2.4 (Colon 26)	2.6
72	H	$N(CH_3)_2$	890 (A549)	3.4

Table 1.6 Biochemical data for B ring modified combretastatins (**67-72**). The potency value represents the activity of the test compound with reference to CA4

A number of the naturally occurring combretastatins have substituents at the 2, 5, and 6 positions (which are free on CA4) most notably CA1 (**22**). Monk *et al* introduced an amino group at these positions leading to two analogues with similar antitubulin effects to that of CA4 (data presented for compounds **73, 74** in **table 1.7**)[74].

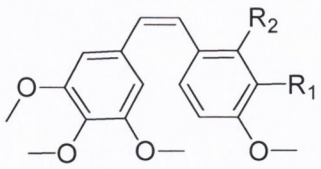

Entry	R_1	R_2	Potency Value	Tubulin Inhibition (μM)
73	OH	NH_2	1.25nM (MHEC5-T)	2.5
74	H	NH_2	1.4nM (MHEC5-T)	2.0

Table 1.7 Biochemical data for B ring modified combretastatins containing nitrogen

There are a number of cases where the "B" ring has been replaced entirely by a heterocyclic/aromatic ring. Maya *et al* [127] demonstrated that the 1-naphthyl (**75**) and 2-naphthyl rings (**76**) can replace the "B" ring (**fig 1.28**). **76** displayed reasonable activity with IC_{50} values across a range of cell lines approaching that of CA4. In the case of the pyridine ring, the position of the nitrogen atom influences the biochemical activity of the analogue.[128] **77** displays a very promising potency factor of 3.3 and an IC_{50} value of 2.0μM for inhibition of tubulin polymerisation.

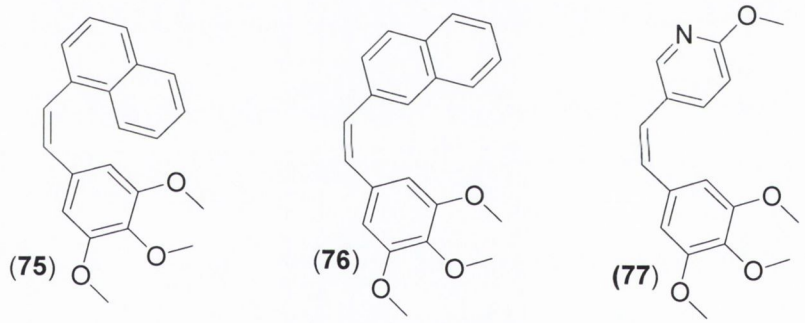

Fig 1.28 Various ring systems replacing the B ring

1.6.4 Modifications to the Bridge

A range of CA4 analogues with modifications to the ethene bridge have been synthesised. Conversion of the bridge from the *Z* to *E* isomer results in a loss of activity[76]. Thus there has been enormous interest in modifying the bridge to overcome the issue of this isomerisation and preserving the orientation of the rings. The two main areas of interest are to modify the olefinic bridge (**fig 1.29** compounds **79-90**) or else the replacement of the bridge with a ring system to effectively lock in the desired stereochemistry. The biochemical activity for compounds **79-90** including antitubulin effects is presented in **table 1.8**.

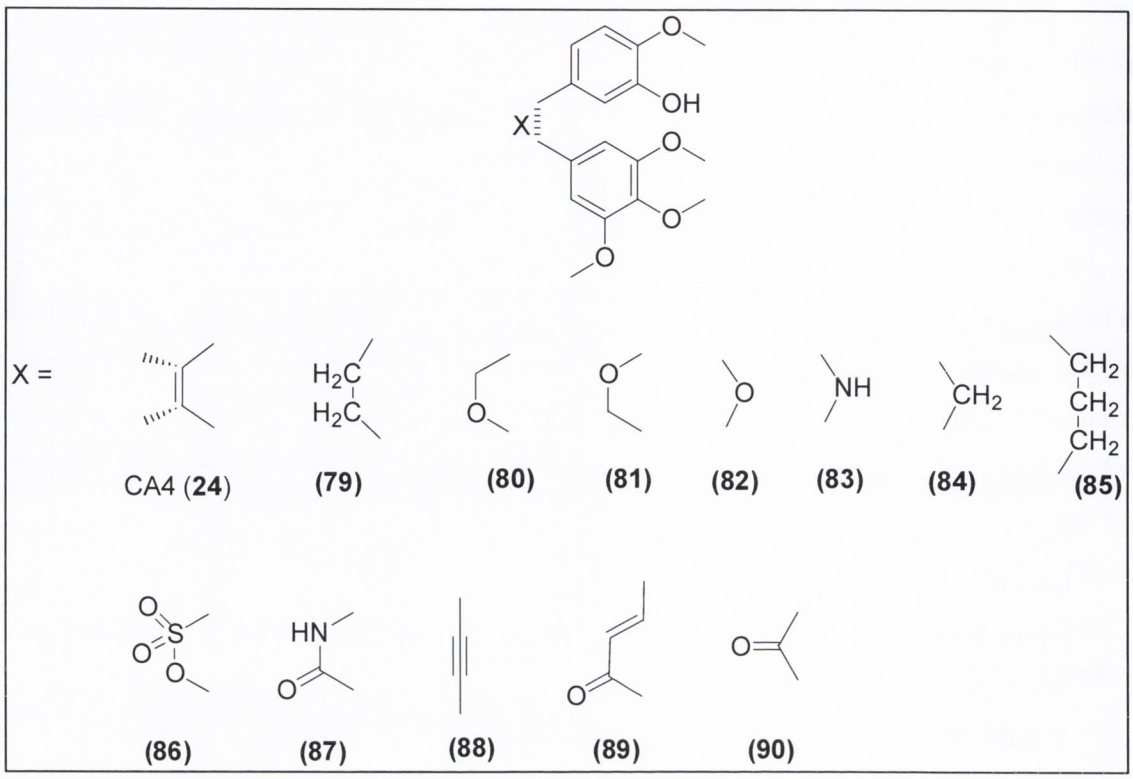

Fig 1.29 Modifications to the olefin bridge of CA4

Hydrogenation of the double bond to give **79** results in a drastic loss in potency but some antitubulin activity is maintained leading to the synthesis of analogues exploring the role of the bridge in activity. The introduction of a triple bond bridge (**88**) also decreases potency. Replacement of either of the carbons of the bridge with an oxygen or nitrogen atom led to a decrease in antitubulin activity. The potency factors could not be calculated for these compounds since no values for CA4 are reported in the paper. The shortening of the bridge to a single carbon (**84**) or the lengthening to a three carbon bridge (**85**) led to a decrease in potency although **84** still had reasonable antitubulin activity. This is not unexpected since the natural product phenstatin (**90**) maintains biochemical activity despite its shortened bridge. Both **80** and **81** show poor antitubulin activity indicating that not only is the length of the bridge important but also its composition. This is also observed for compounds **82** and **83**. In contrast to these observations, **86**, **87**, and **89** all display low nanomolar activities approaching that of CA4. Despite the variety on modifications to the bridge that have been carried out, none of the resulting products display activity matching or exceeding that of CA4. It may be possible then that the spatial arrangement of the biphenyl system is optimised for activity when joined by the olefin bridge. It is also clear that further modification of the bridge may yield promising CA4 analogues.

Compound Number	Potency Value	Tubulin polymerisation inhibition (μM)	Reference
24	1	1.2	74
79	1.2×10^4	3.3	123
80	No values for CA4 were determined	3.5	129
81		22.5	
82		16.3	
83		>100	
84	3	4-5	130
85	140	10/15	
86	No CA4 values	5μM	123
87		nd	131
88	2.1×10^3	nd	113
89	4.3	nd	132
90	8.25	1.0	133

Table 1.8 Potency values and antitubulin effects for bridge modified analogues

Of particular interest is the replacement of the ethylene bridge of CA4 with a heterocyclic system (**fig 1.29**). Incorporating a ring system (very often five membered) into the analogues provided a possible means of "locking in" the desired conformation of *Z* CA4 as well as providing a route to analogues with more "druggable" characteristics. Oxazole[66] (**91**), imidazoles (**92**), thiophene (**93**), dihydro thiophenes[134], indoles (**94**), dioxolane[135] (**95**), tetrazoles (**96**), thiozoles[136] (**97**), and furazans[137] (**98**) have all been used as restricting scaffolds (**fig 1.30**). Promising results from some of these compounds led to the synthesis of three, five, and six membered ring analogues all of which displayed poor activity. The four membered β-lactam ring was also used and appeared to maintain activity. These β-lactam analogues form the basis of this thesis and are discussed in detail in **section 1.7**. A number[138 139 140] of these five membered ring analogues display biochemical activities comparable to that of CA4 in terms of cytotoxicity, inhibition of tubulin polymerisation (**table 1.9**) and competitive binding at the colchicine site. Tron has reported the synthesis of combretastatin-furazan analogues that display *in vitro* activity surpassing that of CA4. The starting point for the synthesis was CA4 (**24**) formed via the Perkin reaction (**scheme 1.5**). The phenol group was protected via a silyl ether before the double bond was hydroxylated

using the Sharpless dihydroxylation reagent to give the diol (**99**), which is then oxidised to the diketone (**100**). The ketone (**100**) was transformed to the corresponding oxime (**101**). The use of excess hydroxylamine and pyridine coupled with heating to 90°C for three days resulted in only the *anti* isomer being formed. The ring closure of the neighbouring oximes was carried out with Mitsunobu conditions to give the furazan (**98**). Attempts to establish a SAR for this diverse set of compounds has proved difficult. It has been generally noted that bulky groups attached to the heterocycle decrease biochemical activity and that switching the position of the rings also leads to a drop in activity, indicating that the orientation of the heterocycle with respect to the two aromatic rings is important for activity[142].

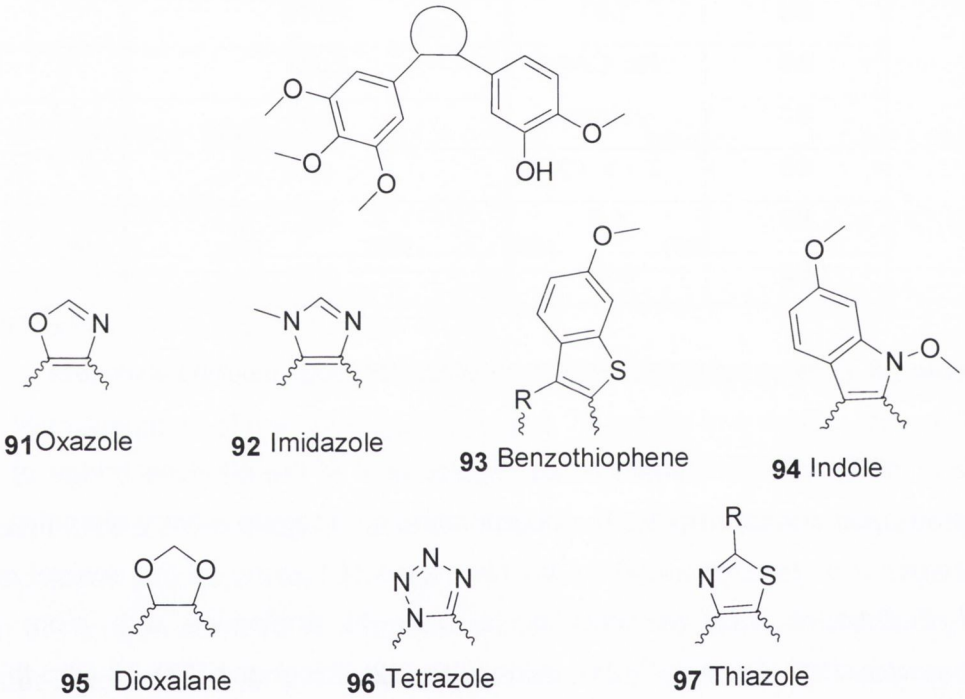

Fig 1.30 Heterocycles for the replacement of the olefin bridge

Compound Number	R	IC_{50} (nM)	Tubulin Polymerisation (μM)
91		2.2nM	0.92
92		8.5 (human large lung NCI-60)	0.68
93	(C=O)	58nM (L1210 murine leukaemia)	1.3
94		>1μM (B16 melanoma)	nd
95		>1000nM (B16)	nd
96		7.2 Human colon 26)	2
97	NH_2	57.5 (Human colon HCT116)	1
	CH_3	2040 (Human colon HCT116)	2
	$NHNH_2$	21.1 (Human colon HCT116)	3

Table 1.9 Summary of biochemical data for selected heterocycles

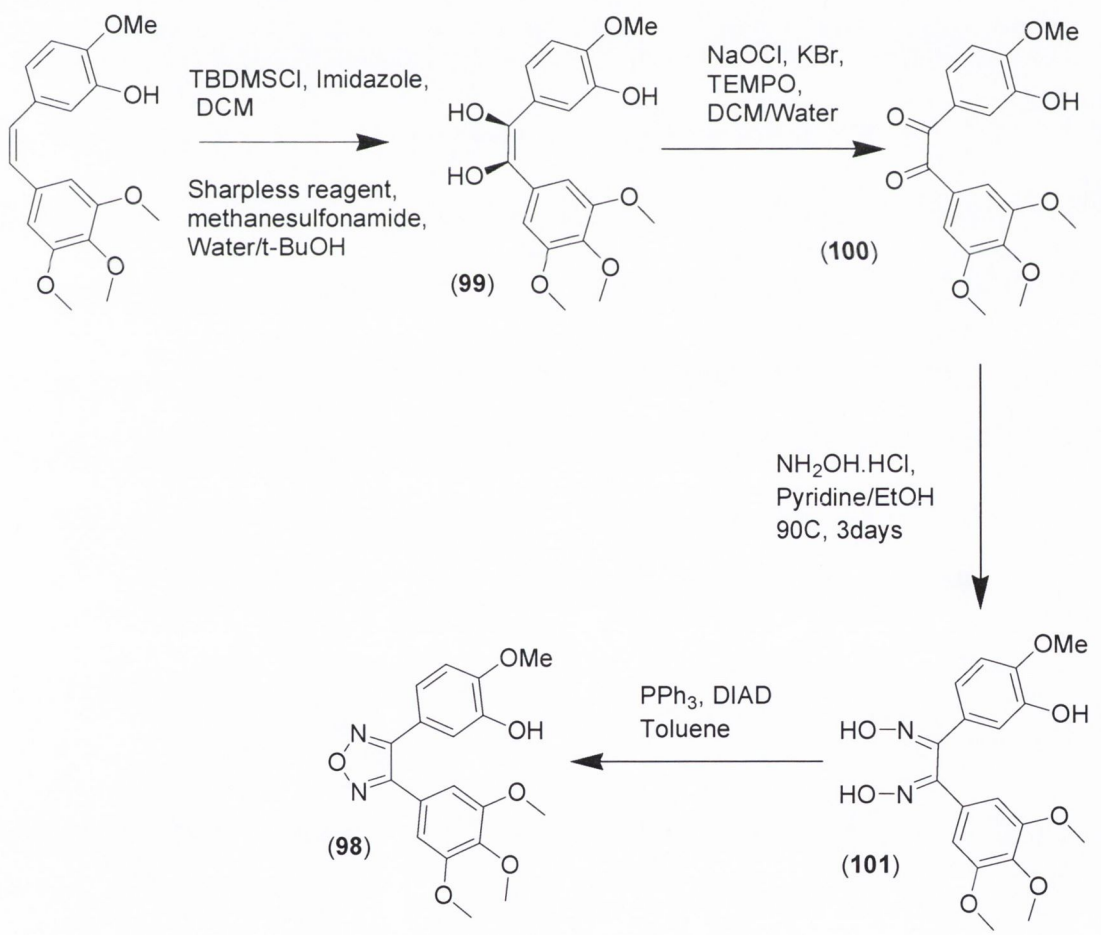

Scheme 1.5 Transformation of CA4 to a furazan fixed ring analogue

1.7 The β-Lactam Ring as a Scaffold in Bioactive Compounds

1.7.1 β-Lactams as Bioactive Compounds

The β-lactam ring is a feature of many bioactive compounds[143]. Of course the ring plays a central role in the antibiotic properties of the β-lactam antibiotics, but also finds use in diverse areas such as cholesterol absorption inhibitors and as substrates for a variety of enzymes. The β-lactam ring can also serve as a synthon in the synthesis of a number of compounds including taxol, acting as a chiral building block.

1.7.1.1Antimicrobial Agents

The β-lactam ring forms the core of a number of classes of antibiotics such as penams(**102**), cephems(**103**), penems(**104**), carbopenems(**105**), monobactams(**106**), trinems(**107**) and nocardicin (**108**) (illustrated in **fig 1.31**) . The prevalence of resistant strains of bacteria has led to a constant interest in the chemistry surrounding the β-lactam ring, in an effort to develop new antibiotics with improved therapeutic properties.

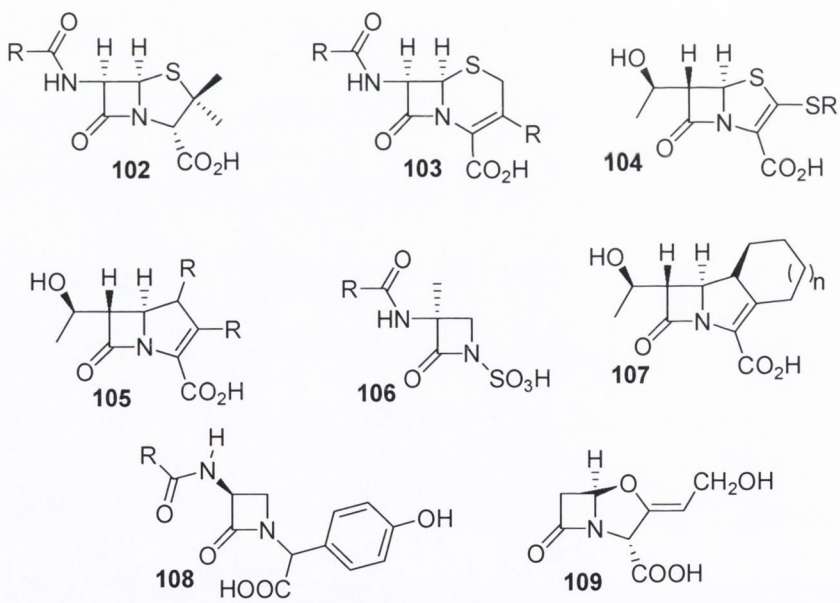

Fig 1.31 Selection of β-lactam antibiotics

The typical mode of action for these β-lactam based antibiotics is by inhibiting the peptidase enzyme responsible for cell wall synthesis in bacteria cells. Specifically the β-lactam ring acylates a serine residue within the active site of the enzyme. β-lactams also find use as inhibitors of β-lactmases (for example clavulanic acid (**109**) which contains the oxapenam structure).

1.7.1.2Cholesterol Absorption Inhibitors

Ezetimibe (**110**) is a cholesterol absorption inhibitor (CAI) which contains a β-lactam core (**fig 1.32**).[144] [145] Once ingested it localises in the small intestine where it acts as a selective inhibitor of cholesterol from dietary sources. Ezetimibe was discovered as part of a development program initiated by Schering Plough[146]. The initial starting point for the investigation was SA 58035 (**111**) which was a known acyl-CoA cholesterol acyltransferase (ACAT) inhibitor. The initial lead compounds took the form of the amide **112**. In an attempt to identify the active conformation of these lead compounds, β-lactam analogues of the form **113** were synthesised. Ezetimibe was the result of a prolonged optimisation and SAR process originating from **113**. Ezetimibe proved to be a very potent CAI but a weak ACAT inhibitor. Ezetimibe is thought to inhibit Niemann-Pick C1 like 1 (NPC1L1) protein which is thought to be crucial to the absorption of cholesterol from dietary sources[147].

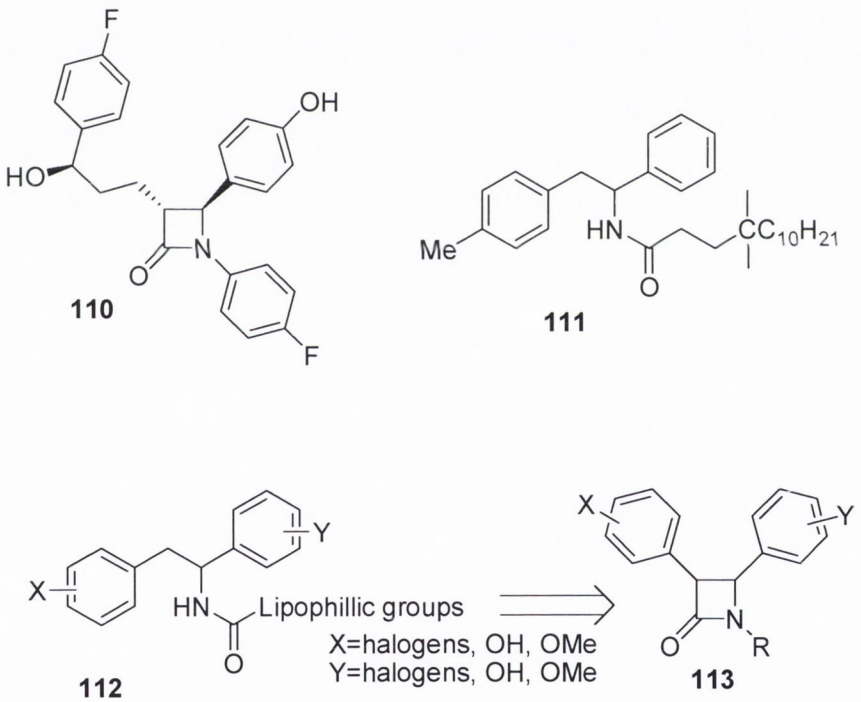

Fig 1.32 Key structures in the development of Ezetimibe

1.7.1.3 Protease inhibitors

β-Lactams can serve as inhibitors of a number of enzymes including serine proteases, and cysteine proteases. They also serve as substrates for peptidases and β-lactamases as mentioned. Serine proteases are involved in a number of physiological processes and include elastase, prostate specific antigen, matrix metalloproteinases (MMP) and thrombin. Their typical role in the body is to cleave/hydrolyse the polypeptide chain of various protein substrates[148] [149]. Serine proteases contain an active site made up of the catalytic triad of serine, histidine, and aspartate. The enzyme functions by the nucleophillic attack on the carbonyl of the substrate by the serine residue of the triad resulting in an acylated intermediate which in turn is cleaved. Many inhibitors of serine proteases function by forming acylated versions of the triad. The results in the inhibitor becoming covalently bound in the active site thereby making the site unavailable its substrate.

The β-lactam ring can serve as a scaffold for inhibitors of proteases. Han[150] synthesised the β-lactam **114** as an inhibitor of thrombin. Thrombin is involved in blood coagulation and is a member of the trypsin family of serine proteases. Prostate specific antigen (PSA) is used as a diagnostic marker for prostate cancer, and possibly stimulates the growth of prostate cancer. The PSA inhibitor **115** has been synthesised making use of the β-lactam ring (**fig 1.33**)[151] to inhibit the acylate the PSA enzyme.

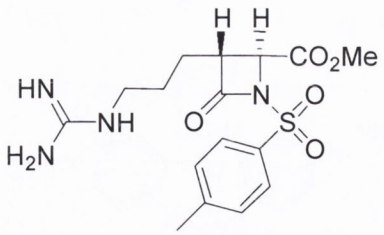

Thrombin inhibitor (**114**)

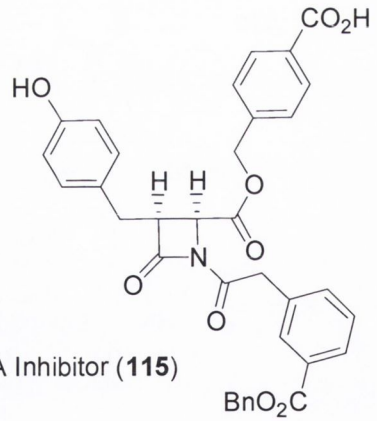

PSA Inhibitor (**115**)

Fig 1.33 β-lactam based protease inhibitors

An excellent review of the role of proteases in cancer biology has been presented by Lopez-Otin[152]. Proteases are known to be involved in a number of steps in cancer progression particularly tumour metastasis[153] and have become a popular target for the development of novel chemotherapies[149]. While the role of proteases in cancer progression is well known, there are also a number of proteases that are involved in antitumour processes in the cancer cell such as caspases which are part of the cells apoptic machinery. It has been found that a number of caspases (such as

CASP8) are mutated in cancer cells in an effort to bypass the cell's apoptotic pathway[154]. Clearly then the inhibition of proteases as a cancer therapy is a double edged sword since proteases have both cancer promoting and cancer suppressing qualities. The classic case of this dual function is the matrix metalloproteinases (MMPs). MMPs promote metastasis by degrading the extracellular matrix around the cancer cell[155]. In contrast MMP8 has antitumour properties. Overexpression of MMP8 in breast cancer cells leads to a reduction in the cells metastatic potential[156]. Because of this dual function of MMPs, MMP inhibitors have displayed poor results in clinical trials[157]. As a result other proteases such as the cysteine cathepsins are now the subject of interest. Joyce *et al* has shown that cysteine cathepsin is associated with increased angiogenic vasculature and increased invasion of surrounding tissue in a pancreatic cancer model[158]. The β-lactam ring may prove useful as a scaffold for the design of future protease inhibitors

1.7.1.4Anticancer agents

It has been shown by Smith *et al* that apoptosis can be induced by a novel β-lactam antibiotic (**116**) (**fig 1.34**)[159]. Treatment of Jurkat T cells with the β-lactam led to DNA damage and inhibition of DNA replication followed by a cascade of biochemical activity including protein kinase activation leading ultimately to S-phase arrest and apoptosis. **116** was evaluated in the MCF7 and MDA-MB-231 breast, PC-3 prostate, and PCI-13 head and neck cancer cell lines, by treating the cells with a single dose of 50μM and comparing the percentage of viable cells remaining after 24 hours to a DMSO control using a MTT assay. It was found that in the breast and head/neck cancer cell lines the numbers of viable cells dropped by 80% compared to the control. For the prostate cancer cell line the figure was 60%.

Banik *et al* has synthesised a number of β-lactams (e.g. **117** & **118**) that display comparable *in vitro* cytotoxicity to that of cisplatin (10.09μM and 9.81μM for **117** and **118** respectively in the MCF7 cell line compared to 10.05 for cisplatin (**fig 1.33**).[160] [161] Banik failed to establish the exact mechanism by which these β-lactams were exerting an anticancer effect but did note that the compounds induced G_2 block in the cell cycle without inducing apoptosis.

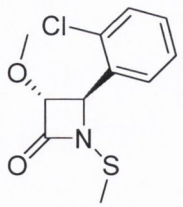

116

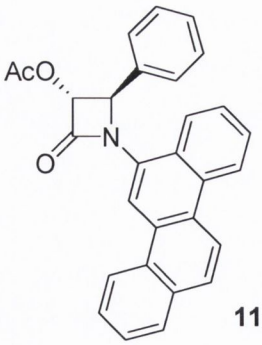

117

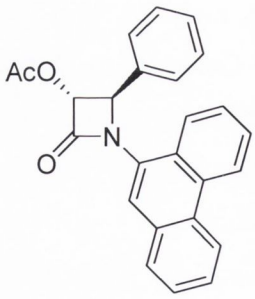

118

Fig 1.34 Anticancer β-lactams

Sun *et al* has demonstrated the use of the β-lactam ring as a scaffold for CA4 analogues.[162] The use of the β-lactam ring as a scaffold for CA4 analogues is discussed in greater detail in Chapter 2.

1.7.1.5 Antimalarial

The development of novel antimalarial agents is of enormous importance considering there are approximately 400 million cases worldwide per year resulting in 2 million deaths.[163] Nivsarkar *et al* outlines the use of bicyclic β-lactams (**119 & 120 fig 1.35**) against both the chloroquine sensitive and resistant malaria parasite *Plasmodium falciparum*[164]. The emergence of resistant strains of the malaria parasite to traditional therapies such as chloroquine led to the exploration of the β-lactams as a scaffold for novel antimalarials. The *in vitro* testing used malarial parsites cultured in human red blood cells. The effect of the test compound on the parasitized cells was monitored by number of mature schizonts in each culture. **119** displayed IC_{50} values of 1.5μM and 1.6μM in the sensitive and resistant strains respectively. **120** displayed IC_{50} values of 1.8μM and 1.8μM in the sensitive and resistant strains respectiviely. This is far less potent than chloroquine (IC_{50} 0.02μM and 0.03μM). The authors comment on the fact that while the compounds synthesised thus far are not as active as chloroquine, the β-lactam ring is amenable to further modification which may provide more active compounds.

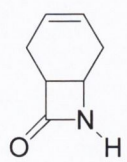

(119)

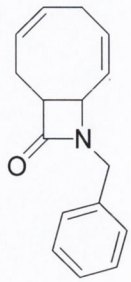

(120)

Fig 1.35 Antimalarial β-lactams

1.7.2 β-Lactams as synthons

The β-lactam containing structures are a particularly important class of biologically active compounds, however owning to their reactivity they have also emerged as important intermediates in the preparation of more complex compounds as outlined by Deshmukh *et al.*[143] Selective ring opening of an enantiomerically pure β-lactam ring provides access to β-amino acids and derivatives thereof.

The best known example of the β-lactam ring as a synthon is provided in the semisynthesis of taxol (see **section 1.4.4.2**). The route involves the coupling of a chiral side chain (**122**) to the natural product 10-deacetyl baccatin, where the side chain is obtained from the nucleophilic ring opening of an enantiomerically pure β-lactam (**121 fig 1.36**)[165].

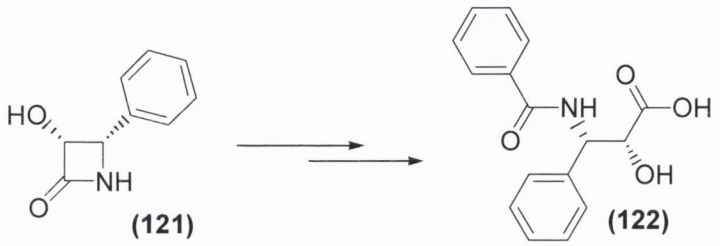

Fig 1.36 The use of the β-lactam ring as a synthon in Taxol semisynthesis

1.7.3 Methods for Synthesis

The initial impetus for the development of methods for the synthesis of the β-lactam ring was the emergence of the β-lactam antibiotics post World War II. However semisynthetic methods dominate the production of β-lactam antibiotics. In more recent years there has been extensive research into the enantio and stereoselective synthesis of the β-lactam ring as required for the total synthesis of carbopenem antibiotics[166]. The β-lactam ring can also serve as a synthon[143] in the synthesis of a number of compounds including taxol as described above.

Gunda[167] presents a review of the common methodologies for β-lactam formation, dividing the methods into groups depending upon the bond(s) in the ring that is formed as a result of the reaction. Singh also presents a review of the synthesis of the β-lactam ring.[166]

1.7.3.1 Cyclisation of β-amino acids

The cyclisation of a β-amino acids is an obvious route towards the β-lactam ring, but has enjoyed little success compared to some other routes. A typical reaction involves the cyclisation of the amino acid by employing a condensation reagent such

as dicyclohexylcarbodiimide (DCC),[168] or 2-chloro-1-methylpyridinium iodide[169] The activation of amino acids by $PhP(O)Cl_2$ has been carried out by Escalante.[170]

1.7.3.2 The Staundinger Reaction

The Staundinger reaction (first reported in 1907) is widely utilised in the synthesis of the β-lactam ring. Palomo *et al* presents a review of this particular reaction concentrating on the asymmetric synthesis.[171] The reaction involves the [2+2] cycloaddition of a ketene to an imine with the ketene typically being formed *in situ* from an acid chloride in the presence of base (**scheme 1.6**). Examples using microwave, thermal, and photochemical methods are reported throughout the literature. The underlying mechanism of the reaction is still the subject of some debate. Of particular interest are the factors affecting the stereochemical outcome of the reaction. It has been noted that the substituents on the reactants, solvent, base used, and the order of addition can all affect the stereochemical outcome of the reaction. The Staundinger reaction provides the basis for the synthesis of a range of β-lactams presented within this thesis and is discussed in detail in Chapter 2.

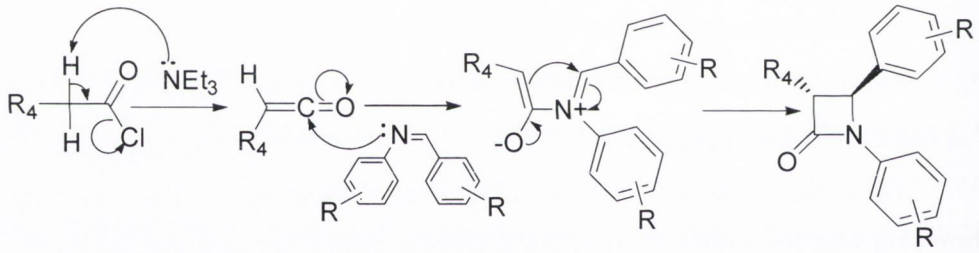

Scheme 1.6 Staundinger reaction for formation of the β-lactam ring

1.7.3.3 The Reformatsky Reaction

The original Reformatsky reaction involved the formation of β-hydroxyesters from α-haloesters and aldehydes or ketones in the presence of zinc[172]. Gliman and Speeter[173] have modified the reaction to yield β-lactams by using imines with α-haloesters as illustrated in **scheme 1.7**. This route remains popular for the synthesis of specific examples required in this thesis and is explored in more detail in Chapter 3.

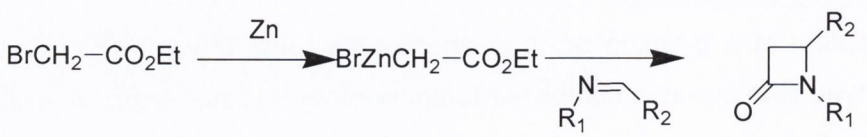

Scheme 1.7 Reformatsky reaction

1.7.3.4 Electrochemical

Feroci *et al* presents the electrochemically cyclisation of bromoamides.[174] The passage of current through the solvent/electrolyte (**scheme 1.8**) leads to the formation of stongly basic intermediates (**123**) which subsequently deprotonates the NH of the bromoamide (**124**). The deprotonated bromoamide undergoes intramolecular cyclisation to form the N-C_4 bond of the β-lactam ring (**125**). The major byproduct of the reaction results from dehalogenation. The paper reports the use of a range of substrates in the reaction leading to yields upwards of 98% in some cases. The reaction yields only the *trans* isomer. The ratio between the desired β-lactam product and the dehalogenated byproduct is dependent upon the number of Faradays per mole supplied, the supporting electrolyte, the type of cell used and the cathode material.

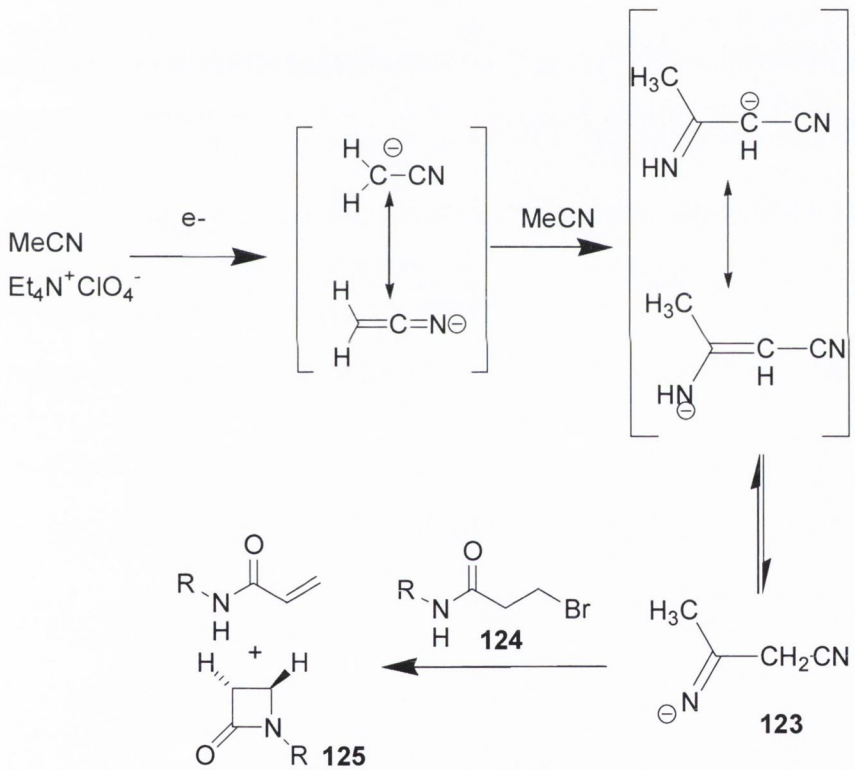

Scheme 1.8 Formation of β-lactam ring by electrochemical cyclisation

1.7.3.5 Isocyanate route

Another example of a [2+2] cycloaddition involves the reaction of an isocyanate with an alkene. Lee[175] *et al* produced N-unsubstituted β-lactams by reacting vinyl sulphide (**126**) and chlorosulfonyl isocyanate (**127**) (**scheme 1.9**). Chlorosulfonyl isocyanate has been shown to react with the alkene group in vinyl esters, vinyl ethers, allenes. Chmielewski *et al*[176] demonstrates the cycloaddition reaction of isocyanates to sugar vinyl ethers. By using a sugar vinyl ether diastereo excesses of 70% were

obtained. Such a sugar containing β-lactam may be useful in increasing in the water solubility of the β-lactam.

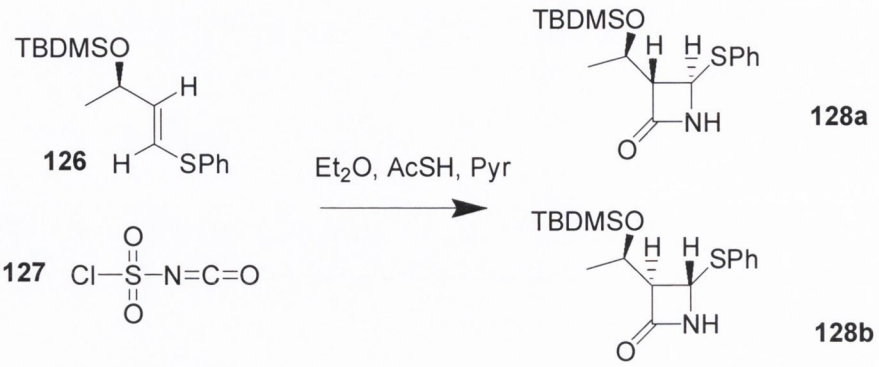

Scheme 1.9 Cycloaddition of a isocyanate and an alkene

1.7.3.6 Mannich type reaction

Takahashi presents a one pot cyclisation of imines (**130**) and silyl enolates (**129**) using a Lewis base catalysis (**scheme 1.10**).[177] The mechanism involves the initial nucleophilic addition of the silyl enolate to the imine resulting in an N-lithiated intermediate that subsequently undergoes cyclisation to yield the β-lactam. It was found that the β-lactam product (**131**) was favoured over the β-amino ester (**132**) when benzyl imines were used. The resulting β-lactams were formed in reasonable to good yield with the *trans* product being favoured. The authors note that the reaction is a practical route to a variety of β-lactams in yields of between 78%-96% and can be carried out in a one pot reaction.

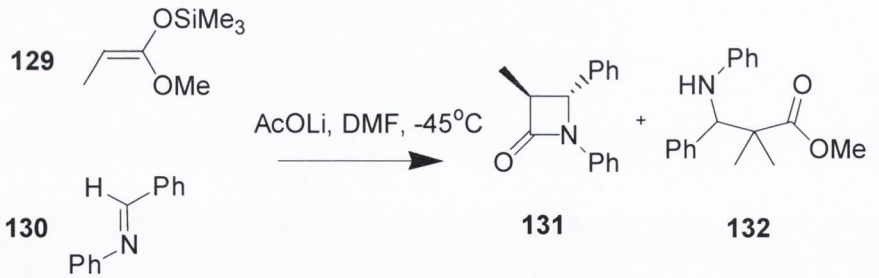

Scheme 1.10 Mannich type reaction

1.7.3.7 Palladium catalysed cycloaddition

A palladium catalysed addition of chiral imines (**133**) to allyl halides (**134**) for the production of chiral β-lactams (**135a-d)** has been reported by Troisi [178] based on a procedure outlined by Tanaka (**scheme 1.11**).[179] The use of an optically pure imine (**133**) starting material results in a steroselective synthesis of **135 a-d** by asymmetric induction. The reactions conditions are not easily obtainable involving 400psi of CO

atmosphere and temperatures of 100°C for 18 hours, but do result in excellent overall yields favouring the formation of the *trans* β-lactam.

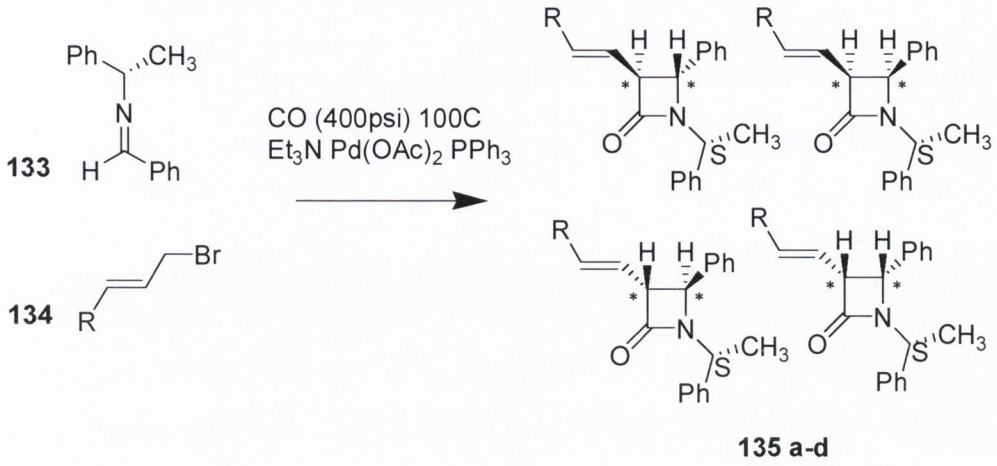

Scheme 1.11 Pd catalysed cycloaddition

1.7.3.8 Photochemical Cyclisation

The photochemical cyclisation of diazoketones and imines has been reported by Lindler.[180] The *trans* selectivity of the reaction may be a consequence of isomerisation induced in the imine by irradiation. The diazoketones are themselves formed from amino acids and serve as an alternative source to acid chlorides for the generation of ketenes. Heckroth *et al* prepared β-lactams **137a**, **137b** photochemically from phenylglyoxamides (**136**) of amino acids.[181] (**scheme 1.12**)

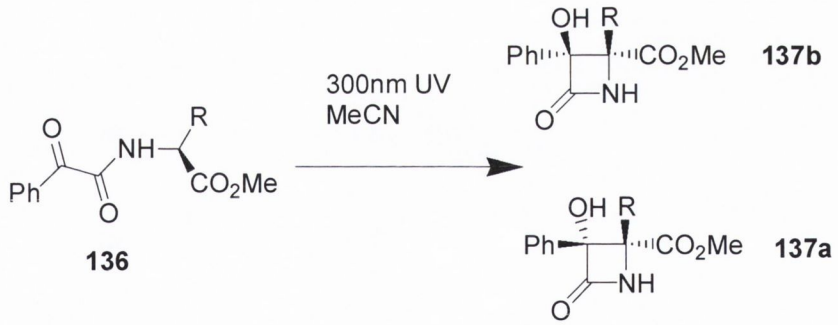

Scheme 1.12 Photochemical cyclisation

Sierra[182] outlines the photochemical cycloaddition reaction of ferrocene containing imines (**138**) and chromium carbonyl-carbene complexes (**139**) (**scheme 1.13**). The authors were interested in the possible antibacterial properties of such compounds as well as using the products as possible electrochemical markers in biological processes and potential use as electrochemical biosensors. The photochemical reactions was carried out using a 450W mercury lamp using a Pyrex filter. The reactants were placed in sealed pressure tube under 90 psi of CO pressure. The typical yield for the reaction was 60%-80% with the *cis* isomer favoured (**140**).

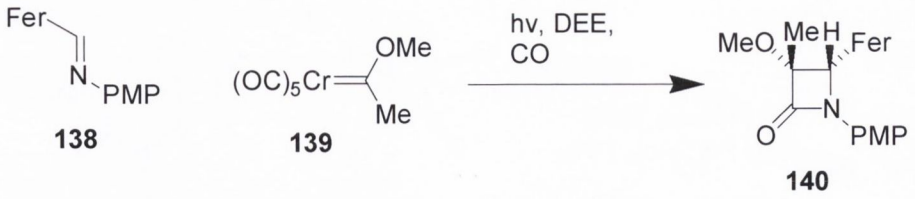

Scheme 1.13 Cyclisation of ferrocene containing imines

1.7.3.9 Lactones

The preparation of β-lactams by the treatment of (S) 3-hydroxy-γ-lactone (**141**) with LDA followed by reaction with imine (**130**) has been outlined by Wu *et al* (**scheme 1.14**).[183] The reaction proceeds through the adducts **143a** and **143b** which undergo cyclisation to yield the β-lactams (**144a** & **144b**). The use of an optically pure lactone (**141**) induces the desired chirality in the β-lactam. Wu notes that the diasteroselectivity of the reaction depends upon the reaction temperature and the base used.

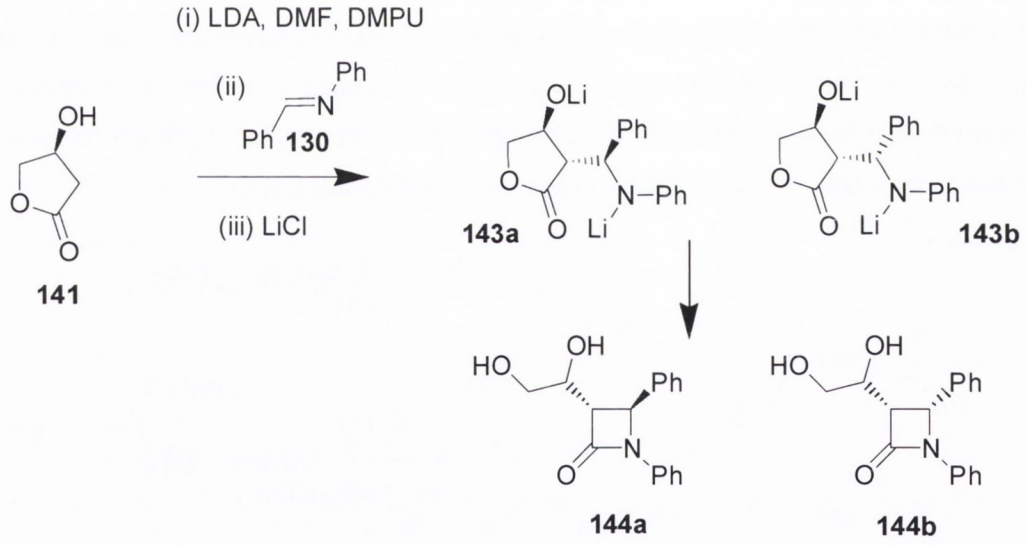

Scheme 1.14 Lactone route to β-lactams

1.7.3.10 Copper & Manganese catalysed cyclisations

The cyclisation of acetamides catalysed by both copper and manganese has been reported to afford lactams.[184] [185] The reaction of Cu(I) phenylacetylides (**145**) and nitrones (**146**) was first reported by Kinusaga (**scheme 1.15**).[186] Recent modifications of the Kinusaga reaction include an asymmetric reaction which has been employed to gain access to optically pure β-lactams (**147**). Fu has reported the use of ferrocene/Cu catalyst to carry out reactions up to 98% ee.[187]

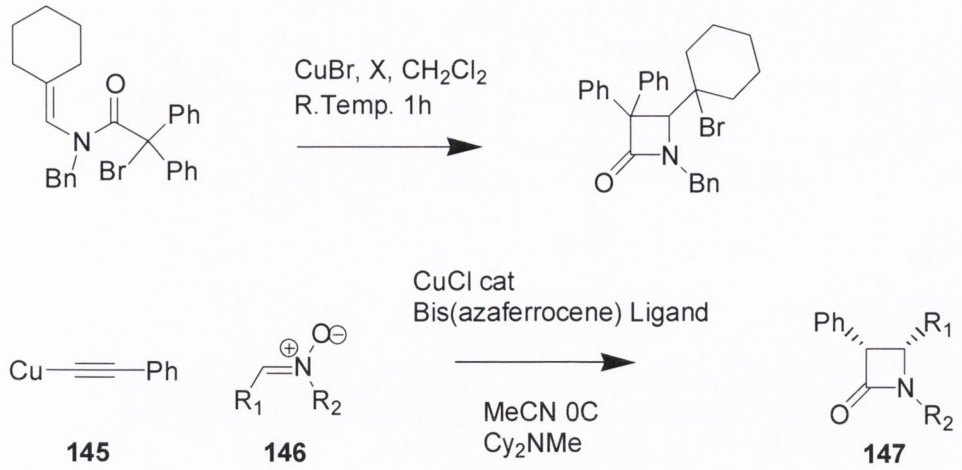

Scheme 1.15 Copper and manganese catalysed reactions

1.7.3.11 Free radical induced cyclisation reaction

Clark, Battlea, and Bridge carried out the radical cyclisation of bromo-enamides (**148**) to afford β-lactams using a tripyridylamine copper(I) halide complex as a mediator (**scheme 1.16**).[188] The authors note that the formation of the β-lactam ring (**149**) is dependent upon the 4-exo rather than the 5-endo reaction pathway being followed. To this end the use of a sterically hindered enamide coupled with a very active atom transfer catalyst leads to the favouring of the 4-exo pathway. Dehalogenation yields the products **150-154**.

Boiteau *et al* generates radicals (**157**) from xanthate derivatives (**156**) of imines (**155**) and lauroyl peroxide.[189] The use of xanthates as a source of free radicals has several advantages including the ease of initiating the reaction by either an organic peroxide or UV light, no use of heavy metals, and a long radical lifetime. The radical cyclisation is a reversible process so once the heterocycle (**158**) is formed, there is a need to "trap" the resulting radical. In the example below allyl acetate (**159**) functions as such a trap. This also provides a means of incorporating structurally diversity onto the β-lactam (**160** and **162**) by the reaction with **161**.

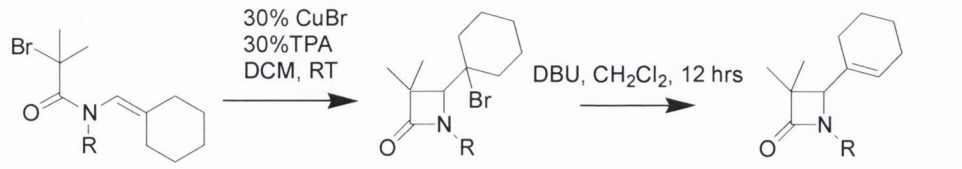

150 R = Bn 96% yield
151 R= PMP 98% yield
152 R = tBu failed
153 R = iBu 98% yield
154 R = o-BrBn 98 %yield

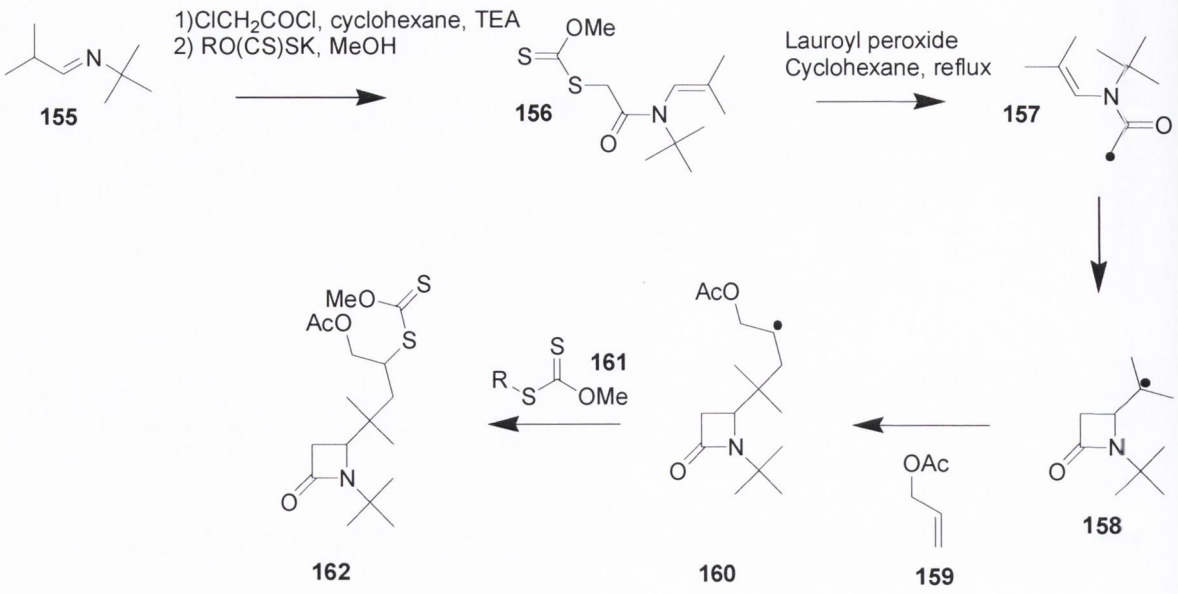

Scheme 1.16 Examples of free radical cyclisations to form the β-lactam ring

There are a number of examples of the use of tin hydrides to form the β-lactam ring by radical cyclisation.[190] The use of tin in such reactions leads to problems with isolation of the product from tin byproducts. Quiclet-Sirea outlines the use of nickel/acetic acid as radical generating system (**scheme 1.17**).[191] The cyclisation is carried out on the allylic sulphide (**164**) which is reacted with nickel/acetic acid to generate the radical **165** which cyclises to form **166**. The fragmentation step is key to transforming the cyclisation step from a reversible to a non-reversible reaction. The resulting β-lactam (**166**) contains both a chlorine at the C_3 of the β-lactam ring and an olefinic side chain, both of which are suitable starting points for further modification.

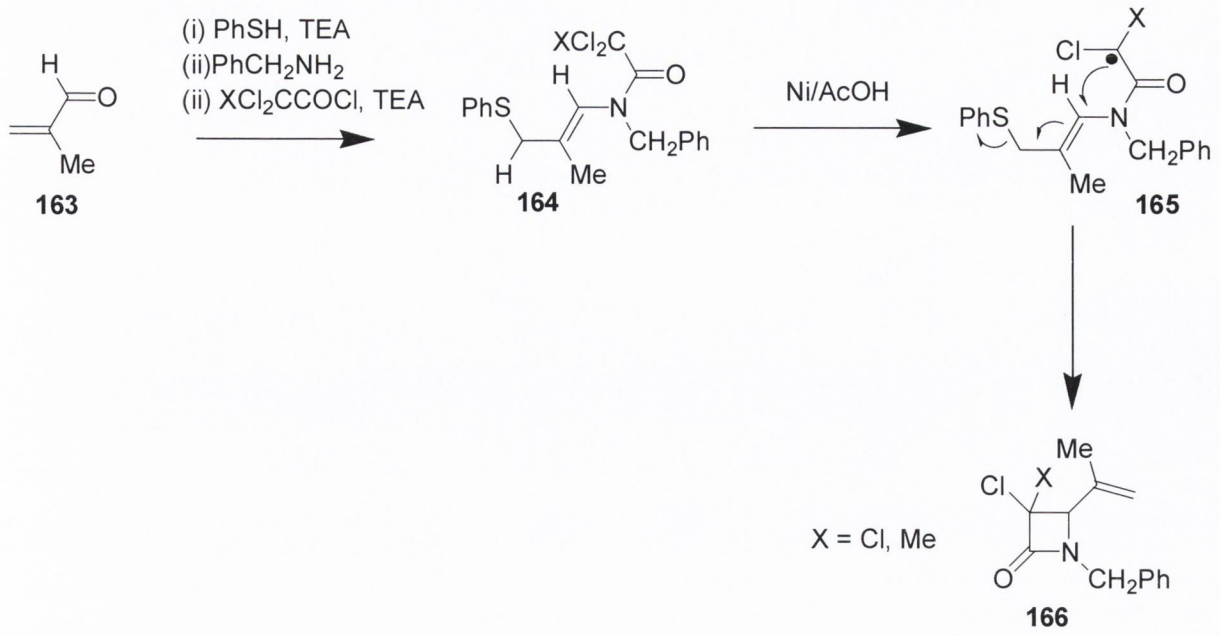

Scheme 1.17 Free radical cyclisation initiated by Ni/acetic acid

1.7.3.12 β-lactams from β-enaminoketoesters

De Risi *et al* presents a route to N-unsubstituted β-lactams (**172a 172b**) from a β-enaminoketoester starting material (**169**) in a multistep synthesis (**scheme 1.18**).[192] The formation of the β-enaminoketoester (**169**) in the first step is based upon the method of Veronese[193]. It involves the metal catalysed addition of either methyl or ethyl cyanoformates (**168**) to the acetoacetate (**167**) to yield the β-enaminoketoester (**169**). The amino group was then protected with a benzyl group to afford **170**. This was followed by the reduction of the carbonyl group (**171**) and protection of the resulting hydroxy group as a silyl ether. The reduction of the carbon double bond was readily achieved by Raney nickel, and also resulted in the cleavage of the benzyl oxy protecting group to give the free amine as a pair of isomers **171a** and **171b** with the **171a** isomer being favoured 9:1. Separation of these isomers was only achieved for the ethyl ester. The final step in the scheme involves a mono protection of the amino group, followed by a Grignard mediated cyclisation to yield the desired β-lactam[194] in a yield of 60-75% depending on the diastereomer.

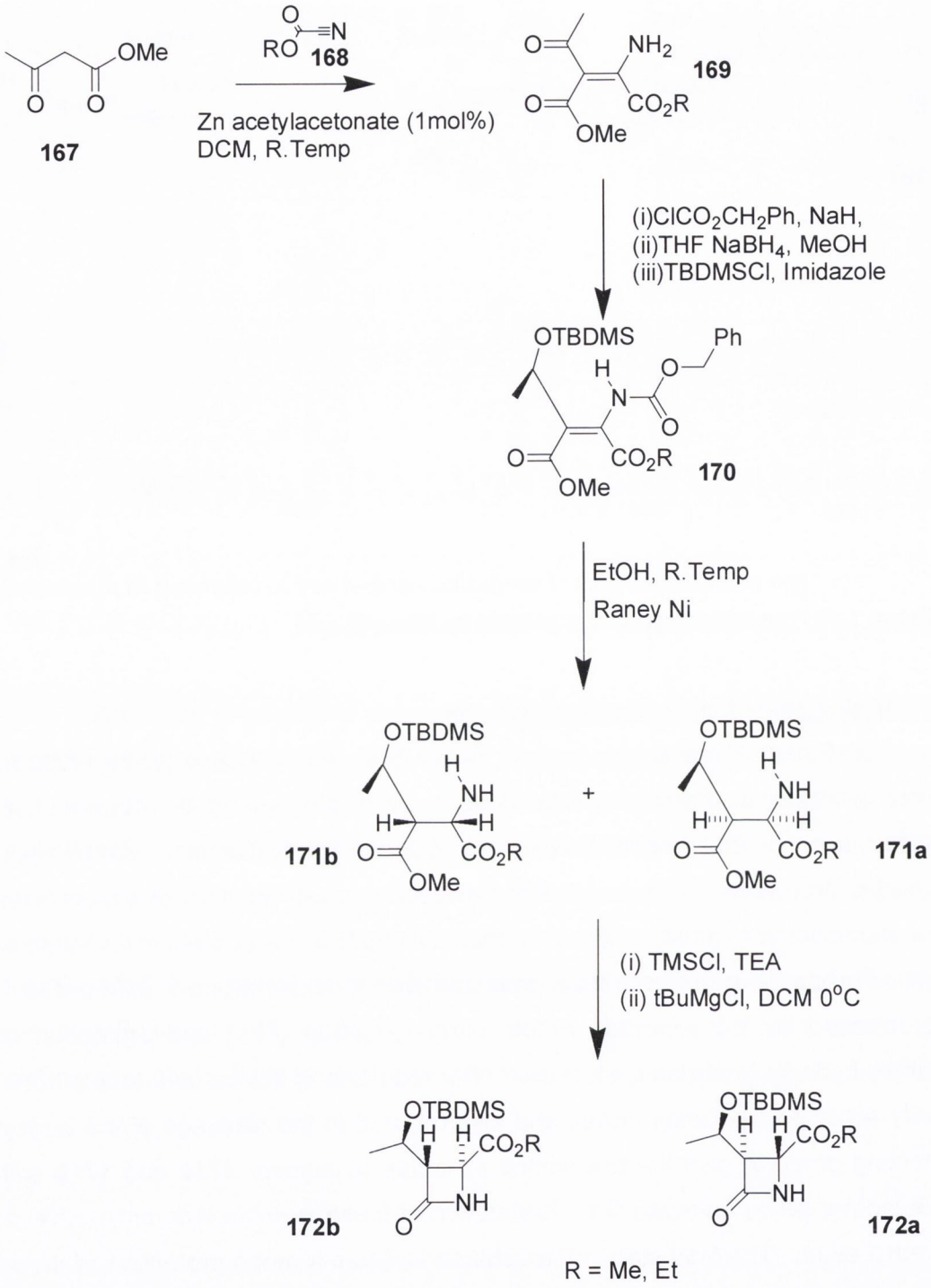

Scheme 1.18 Formation of β-lactams from β-enaminoketoesters

1.7.3.13 Enolate-Imine Synthesis[195]

A number of enolates have been used including lithium, aluminium, tin, zirconium and boron enolates to form the β-lactam ring by reacting with an imine. A review of the subject is provided by Hart.[196] The most obvious use of enolates in the formation of the β-lactam nucleus involves the use of zinc enolates in the Reformatsky reaction. The Reformatsky reaction is restricted to the use of α-bromoesters but lithium

diisopropylamide can be used to generate enolates (**174**) from esters (**173**). The enolate undergoes electrophillic substitution with the imine to yield the intermediate **175**, which cyclises to give the β-lactam (**176**) as a mixture of isomers (**Scheme 1.19**). The lithium enolate route is particularly useful for incorporating heteroatomic, alkyl and aromatic substituents at C_3 whereas the Reformatsky is better suited to cases where an unsubstituted C_3 is desired.

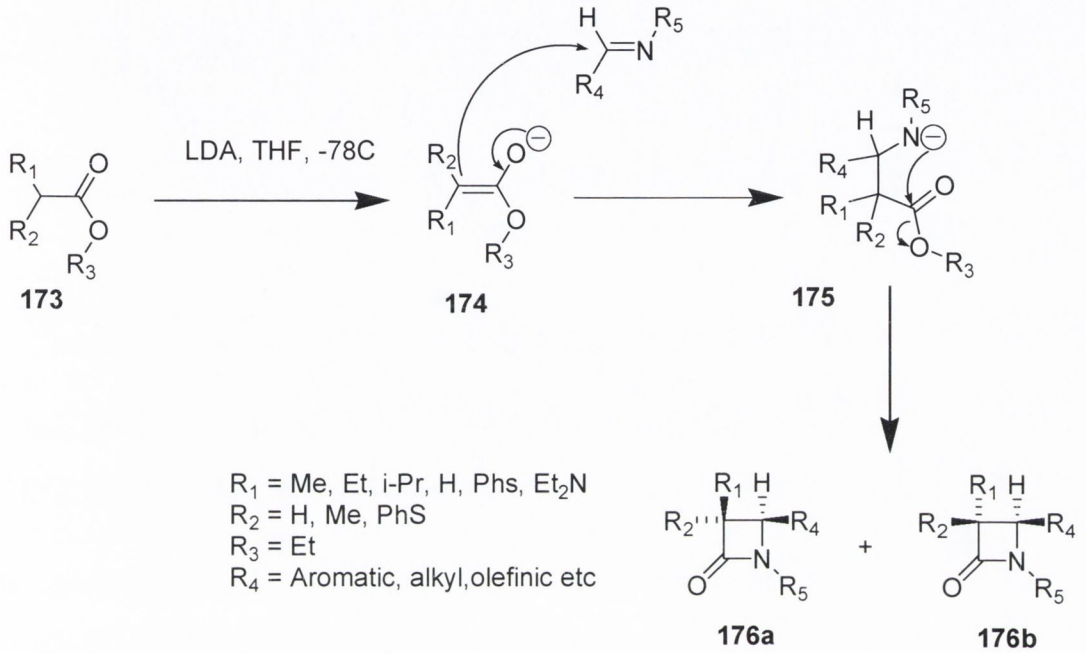

Scheme 1.19 Lithium enolate-imine route

Gluchowski *et al* demonstrates the condensation of lithium ester enolates (**178**) and imines (**scheme 1.20**).[197] The authors note the high diastereoselectivity (favouring *trans*) obtained by the reaction and propose that this is a result of steric factors in the transition state (**179a 179b**) prior to ring closure to yield the products **180a 180b**. They also demonstrate the use of optically pure esters derived from *l* -menthyl for asymmetric induction achieving in one case an *ee* of 60%. The use of lithium enolates from chiral esters has also been reported by other groups[198] [199] with *ee* in excess of 90% reported.

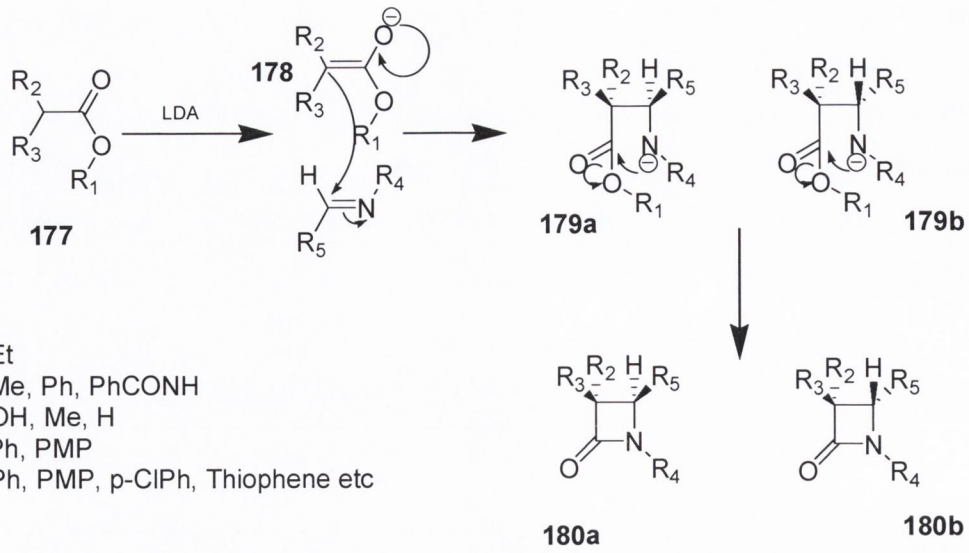

Scheme 1.20 Condensation of lithium ester enolates

1.7.3.14 Solid Phase

Due to the interest in the combinatorial synthesis of β-lactams, methods for solid phase synthesis have been developed. Singh demonstrates the use of a polystyrene resin supported imine in the Staundinger reaction.[200] The imine was synthesised from an appropriate aniline and a resin bound benzaldehyde. The resulting resin bound imine can be easily isolated and purified by washing off any excess reagents. The resin bound imine is subsequently used to form the desired β-lactam under typical Staundinger conditions in excellent yields. It was also shown that the resin bound β-lactam can undergo further chemical transformations and a method for the cleavage of the β-lactam from the resin described. Work by Donati *et al* outlines the use of resin bound Mukaiyama activating agent in the Staundinger reaction.[201] A diverse range of β-lactams were prepared using this resin. At the completion of the reaction, any unreacted imine was removed by reduction with $NaBH_4$ which allowed the β-lactam to be isolated from the reaction in yields between 60% and 80%. The authors do not present any data on the reaction carried out with standard Mukaiyama activiating agent so no comparison in yields could be made.

Schunk[202] makes use of solid phase synthesis in an ester-enolate condensation reaction where an α-substituted amino acid methyl ester is immobilized on resin with a triazene linker (**scheme 1.21**). The initial step involves the diazotation of the amino benzoic acid (**181**) with *t*-butyl nitrite. The reaction of the diaza compound (**182**) with the benzylamine resin (**183**) results in the formation of the triazene linkage (**184**). The carboxylic acid (**184**) was reacted with alanine methyl ester (**185**) by using Mukaiyama's reagent as an acid activating agent to give **186**. The ester enolate-imine cyclisation was subsequently carried out in the solid phase to give **187**, and the β-

lactam product (**188**) cleaved form the resin using TFA. No reaction was carried out using the same reagents without the polymer support so the effect of the polymer support on yield cannot be discussed. However the authors do report that the reaction was used to successfully prepare a number of β-lactams with overall yield ranging from 53% to 71% with purities in excess of 90% achievable after passage of the cleaved β-lactam through a short pad of silica.

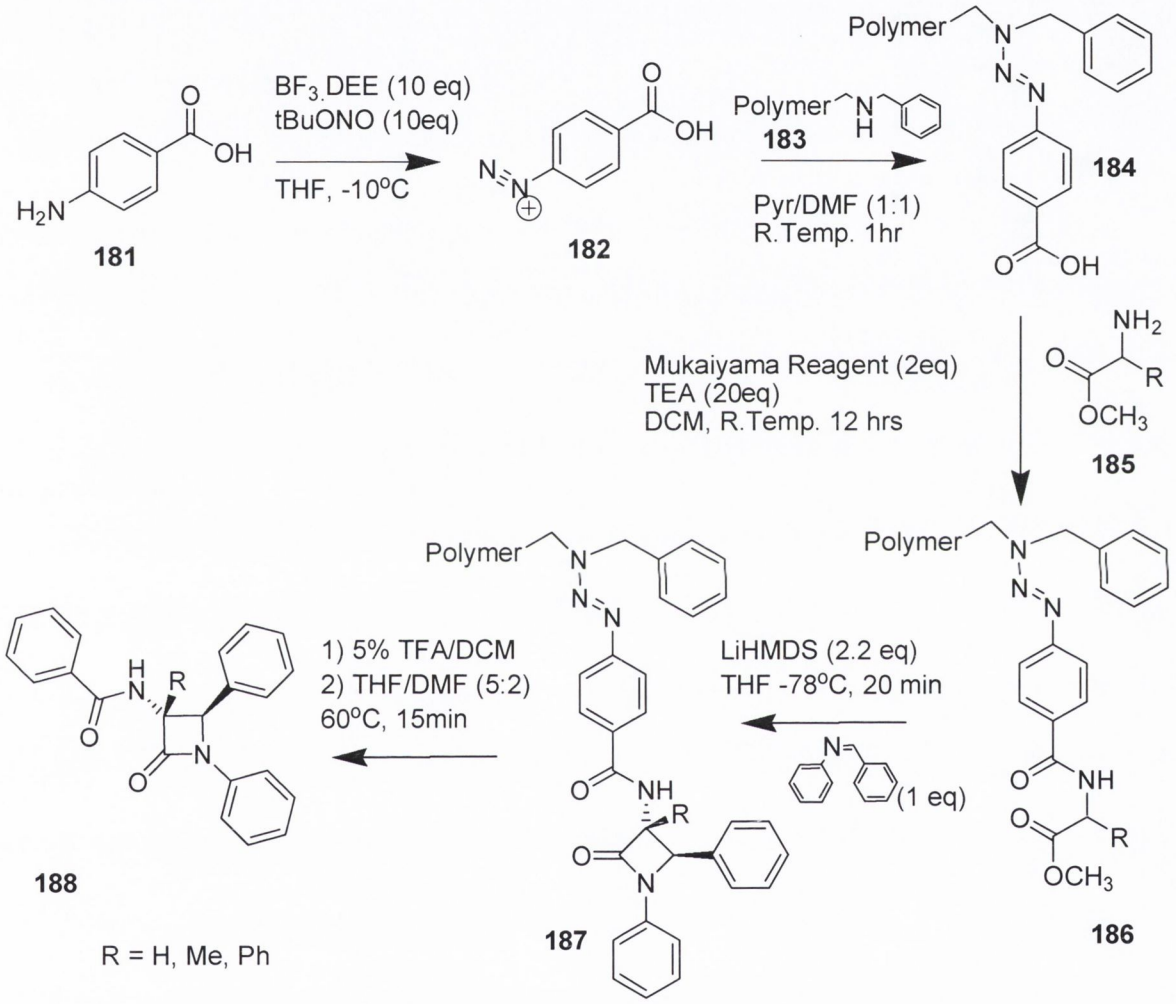

Scheme 1.21 Polymer supported ester-enolate reaction

1.8 Aims

Combretastatin A4 (CA4) has been identified as a promising anticancer agent that selectively targets tumour vasculature. CA4 mechanism of action is by inhibition of tubulin polymerisation by binding at the colchicine site of tubulin. The β-lactam ring has been identified as a suitable scaffold for CA4 from which a variety of novel CA4 analogues can be synthesised. The use of the β-lactam ring may then provide access to analogues of CA4 with improved characteristics. In particular an analogue with increased potency, improved stability, and increased solubility would be useful for further development. To this end the following are the aims of this thesis with the appropriate milestones identified:

A Synthesise a library of structurally focussed β-lactams utilising the Staundinger reaction

I. Identification of promising substitution patterns for the B ring of CA4 from literature
II. Synthesis of appropriately substituted imines
III. Investigation of Staundinger reactions to form a panel of β-lactams varying only in the nature of the substituents at the 4-position

B Evaluate the newly synthesized β-lactams *in vitro*.

I. Evaluation of products in MCF7 human cancer cell line
II. Determination of IC_{50} values for both antiproliferative and cytotoxicity effects

C Upon identification of the most promising substitution patterns at the 4-position, design a second panel with structural modifications at the 2-position.

I. Reduction of the carbonyl group
II. Conversion of the carbonyl group with a thione
III. Examination of changes in structure on *in vitro* activity

D Synthesise a third panel of β-lactams with modifications at the C3-position

I. Examination of the effects of varying the acid/acid chloride used in the Staundinger reaction
II. Formation of 3-unsubstituted analogues formed by Reformatsky reaction
III. Investigation of aldol type reaction of aldehydes to 3-unsubstituted analogues
IV. Examination of effects on *in vitro* activity and optimisation of designed structures

E Further biochemical evaluation of optimized analogues

I. Effect on tubulin polymerization

F Molecular modeling

I. Application of molecular modeling to compounds synthesized for establishment of structure activity relationships

Chapter 2

Synthesis of optimised C4 substituted aryl ring β-lactam analogues of CA4

2.1 Introduction

The use of the β-lactam ring as a scaffold for CA4 analogues has been demonstrated by Sun *et al* and subsequent investigations within this research group[162] [203]. The objectives of this chapter are to:

(1) optimise the substituted aryl ring at C_4 of the β-lactam ring for biochemical activity

(2) investigate the role of substituents on the C_4 aryl ring in biochemical activity

(3) investigate the role of the carbonyl function of the β-lactam ring in biochemical activity.

As illustrated in **fig 2.1** the N_1-C_4 bond of the ring acts as a suitable replacement for the carbon double bond of CA4. Clearly there are still a number of optimisation points available in these β-lactam/CA4 analogues. The aim of the work contained herein is to expand upon this body of previous work, by synthesising and evaluating a range of optimized β-lactam/CA4 analogues. The first library of compounds synthesised concentrated on optimizing region 1 by synthesizing a range of analogues containing promising aromatic substitution patterns identified from literature. This region corresponds to the "B" ring of the parent CA4 compound. As has previously been outlined the "B" ring has been the subject of numerous modifications in the combretastatin series. The most promising substitution patterns identified at this position will be the starting point form which further optimisation of regions 2 and 3 can be carried out.

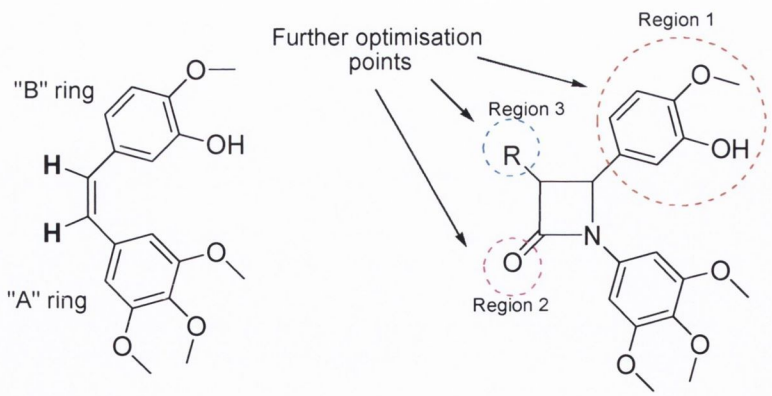

Fig 2.1 The use of the β-lactam ring as a scaffold for CA4

As outlined in Chapter 1 the β-lactam ring plays an important role in a number of different classes of bioactive compounds and as such there are many synthetic routes available for the formation of the β-lactam ring. **Section 1.7.3** presents a review

of the methods available for the synthesis of the β-lactam ring. The choice of route depends upon the structural features desired in the final product. In the initial series of analogues to be synthesised, there is a need to incorporate a diverse range of substituents onto the aromatic ring attached to the 4-position of the β-lactam ring. An obvious retrosynthesis is presented in **fig 2.2** where the β-lactam ring can be formed by the Staundinger reaction between an imine (**189**) and a ketene (**190**). The Staundinger reaction was chosen because of its ease of use, adaptable for use with structurally diverse imines and acid chlorides, and readily available starting materials. A wide variety of substituents can be incorporated onto the 4-position of the ring simply by modifying the aldehyde (**191**) used in the synthesis of the imine.

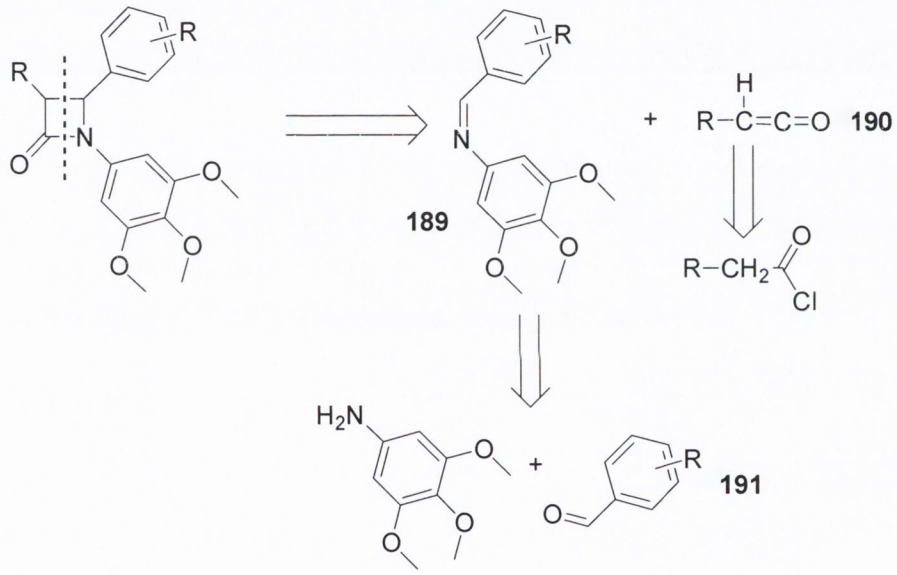

Fig 2.2 Retrosynthesis of the desired β-lactam analogues

2.2 Synthesis of Imines

A series of imines (**192-207**) were formed by the condensation of the appropriately substituted benzaldehyde with 3,4,5-trimethoxyaniline (**scheme 2.1**) under reflux in ethanol. The choice of substitution pattern on the imine was guided by promising substitution patterns identified from literature as discussed in Chapter 1, and included methoxy, hydroxy, and nitro substituents on ring B while maintaining the 3,4,5-trimethoxy substitution pattern on ring A. The imine products (**192-207**) were isolated from the reaction by reduction of the reaction volume followed by cooling to room temperature upon which the imine precipitated out of solution. Where indicated by ^{1}H NMR, impurities were removed by recrystallisation from hot ethanol. For the analogues containing a hydroxy group, poor yields were observed despite increasing the reflux time and the use of a Dean-Stark trap to remove water from the reaction. The addition of a catalytic amount of H_2SO_4 followed by reflux greatly improved yields (**scheme 2.2**). Care was taken to only add a catalytic amount of acid so as not to protonate the amino group of the aniline or hydrolyse the imine and reduce yields.

Data for the IR spectra and yields of the imines (**192-207**) is presented in **table 2.1**. Where applicable the yield without the use of acid catalyst is given in brackets. All of the imines display a characteristic absorption in the IR spectrum at approximately 1590-1640 cm^{-1} indicating the presence of a C=N bond

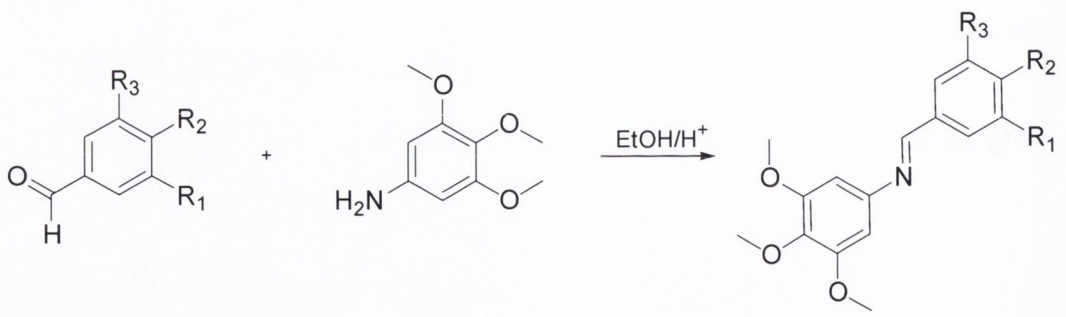

192-207

Scheme 2.1 Synthesis of imines via condensation of an appropiatley substituted benzaldehyde and 3,4,5-trimethoxyaniline

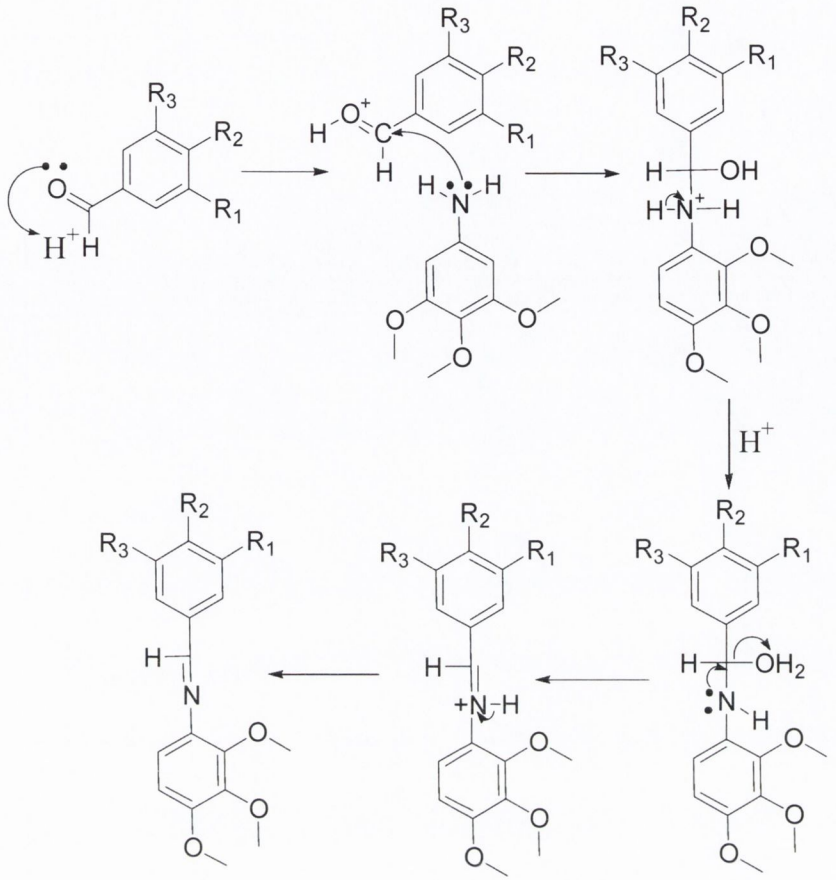

Scheme 2.2 Acid catalysed formation of imines

The imines can exist as *Z* or *E* isomers or as a mixture of both[204]. The role of the stereochemistry of the imine in the Staudinger reaction is discussed in greater in **section 2.3.3.3**. The two isomers are depicted in **fig 2.3**. In all cases in this thesis only a single siomer was observed as evidenced by the appearance of only a single imine signal in the ^{1}H and ^{13}C NMR spectrum. Jennings has shown that there is a distinct difference in the chemical shift of the ^{13}C imine signal for E/Z isomers of imines.[205] It is assumed that since only one isomer is formed in the imine reaction presented in this work, that only the thermodynamically more favourable *E* isomer is present.

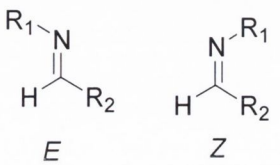

Fig 2.3 E and Z isomers of imines

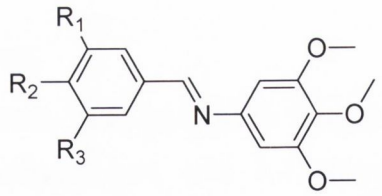

Compound No.	Structure			IR (ν_{max} cm^{-1}) (C=N)	MP (°C)	Yield (%)
	R_1	R_2	R_3			
192	OMe	OMe	OMe	1626	174	75
193	H	OMe	H	1607	114	79
194	$O(CH_2)O$		H	1629	101	68
195	H	SCH_3	H	1628	96	88
196	Br	OMe	H	1585	126	84
197	F	OMe	H	1609	100	84
198	H	CN	H	1580	134	92
199	NO_2	OMe	H	1618	156	94
200	2-Naphthyl			1580	128	94
201	OMe	OMe	H	1626	131	54
202	1-Naphthyl			1584	108	81
203	H	$N(CH_3)_2$	H	1607	83	71
204	OH	OMe	H	1613	134	61 (22)
205	H	OH	H	1624	158	69 (39)
206	OH	OH	H	1645	58	82 (44)
207	OMe	OH	H	1613	140	89 (41)

Table 2.1 Yields, IR, and melting points for imines **192-207**

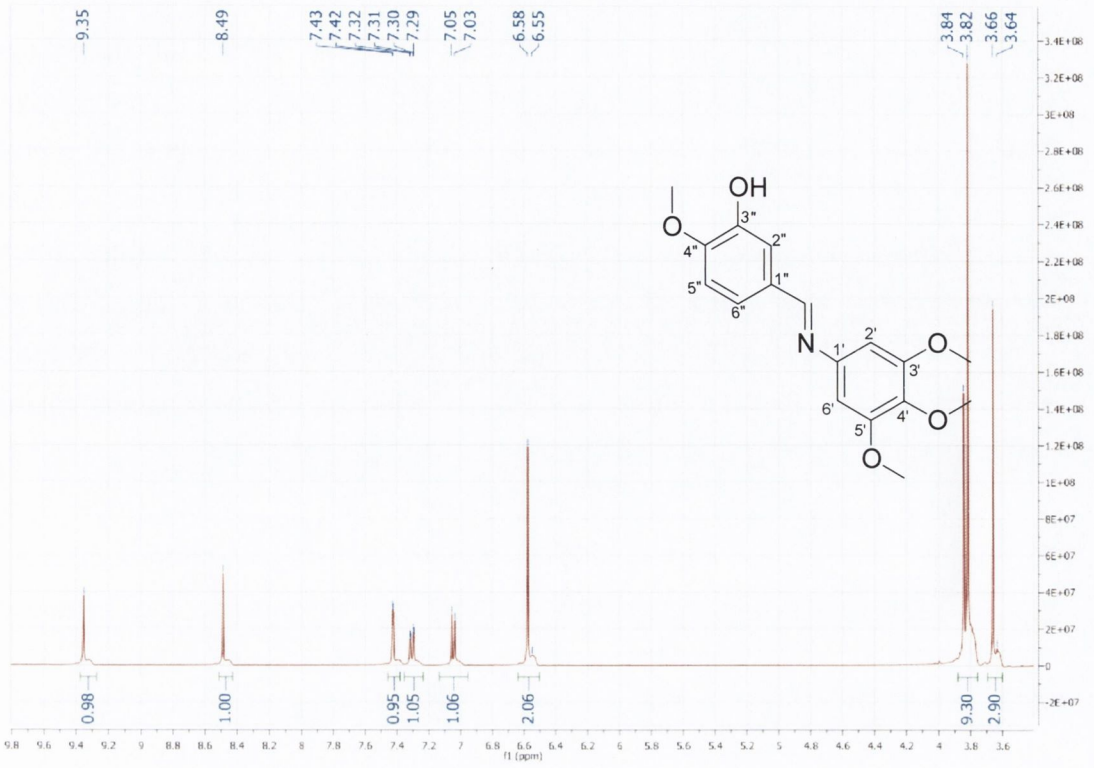

Fig 2.4 ^{1}H NMR spectrum for compound **204**

An example of a typical spectrum obtained for an imine is presented in **fig 2.4**. The signal at δ 8.49 ppm is diagnostic for the imine group proton. The methoxy groups appear close together at δ3.64-3.84. The 2' and 6' protons are equivalent and appear as a singlet at δ6.58. The H_5'' proton appears as a doublet at δ6.95 with a coupling constant of J=8.52Hz. H_2'' is split with H_6'' and so appears as a doublet at δ7.54 with a coupling constant of J=1.48Hz. H_6'' is split into a doublet of doublets by H_2'' and H_5'' with coupling constants of 1.48 Hz and 8.52 Hz. The hydroxy signal appears as a singlet at δ5.72. Further evidence for this signal arising from the hydroxy group is its disappearance upon treatment of the imine with tBDMSCl in the following reaction for the protection of the phenolic group.

2.2.2 Imine Protection

It was necessary to protect imines containing a hydroxy functionality prior to taking part in the Staundinger reaction. The popular *t*-butyldimethylsilyl ether protecting group (*t*BDMS) was chosen because of the ease of achieving the protection reaction and the fact that the β-lactam product is stable under the cleavage conditions required for removal such as treatment with *t*BAF in THF. The silyl ether was formed by the reaction of the phenol with *t*-butyldimethylsilylchloride in dry DCM at room temperature (**scheme 2.3**). The hindered amine base DBU was used in the reaction to aid in the reaction of the silyl chloride with the phenol by dehydrohalagenation of the silyl chloride.

Initially the protection was carried out on the imines **204-207** (route A) to yield the silyl ether protected imines (**208-211**) in 75 -91% yield (**table 2.2**), but it was observed that cleaner silyl ether products (**208-211**) were obtained if the protection was carried out first on the appropriate benzaldehyde (**212-215**) (route B) in yields of 89-97% (**table 2.2**). This yielded silylether protected benzaldehydes (**216-219**) which were in turn were reacted with 3,4,5-trimethoxy aniline to yield the protected imines (**208-211**). The overall yield of the reaction was unaffected by the choice of route. The data for these compounds is displayed in **table 2.2**.

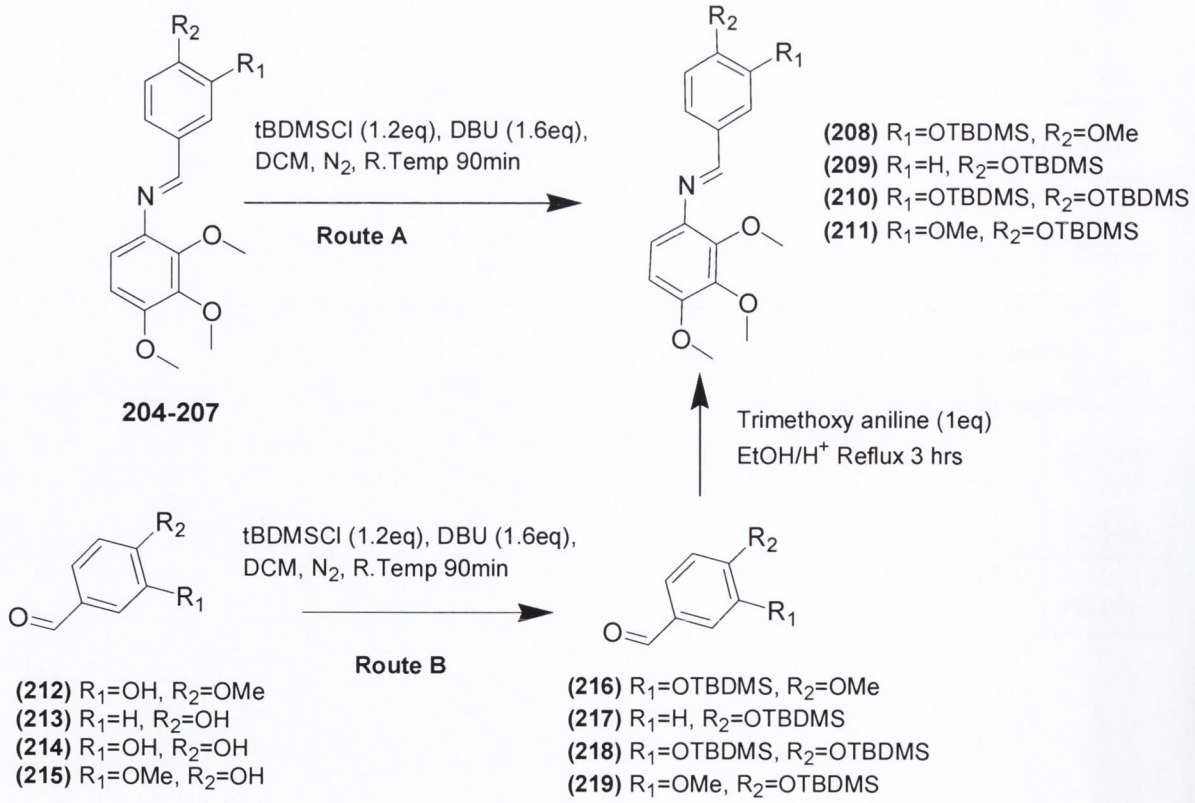

Scheme 2.3 Formation of silyl ether protected imines

Compound No.	Structure		IR (ν_{max} cm^{-1})	MP (°C)	Yield (%)
	R_1	R_2			
216	OTBDMS	OMe	1689	Oil	94
217	H	OTBDMS	1693	97	92
218	OTBDMS	OTBDMS	1694	Oil	89
219	OMe	OTBDMS	1687	Oil	97
208	OTBDMS	OMe	1585	83-87	78
209	H	OTBDMS	1581	Oil	91
210	OTBDMS	OTBDMS	1598	Oil	88
211	OMe	OTBDMS	1574	Oil	75

Table 2.2 Yield, IR, and melting points for silyl ether benzaldehydes (**216-219**) and silyl ether imines (**208-211**)

Fig 2.5 presents an example of the typical ^1H NMR spectrum obtained for a protected imine. The successful addition of the silyl protecting group is apparent from the signals present at δ1.03 ppm and δ0.19 ppm corresponding to the *t*-butyl and dimethyl groups of the silyl ether, and also from the disappearance of the hydroxy signal.

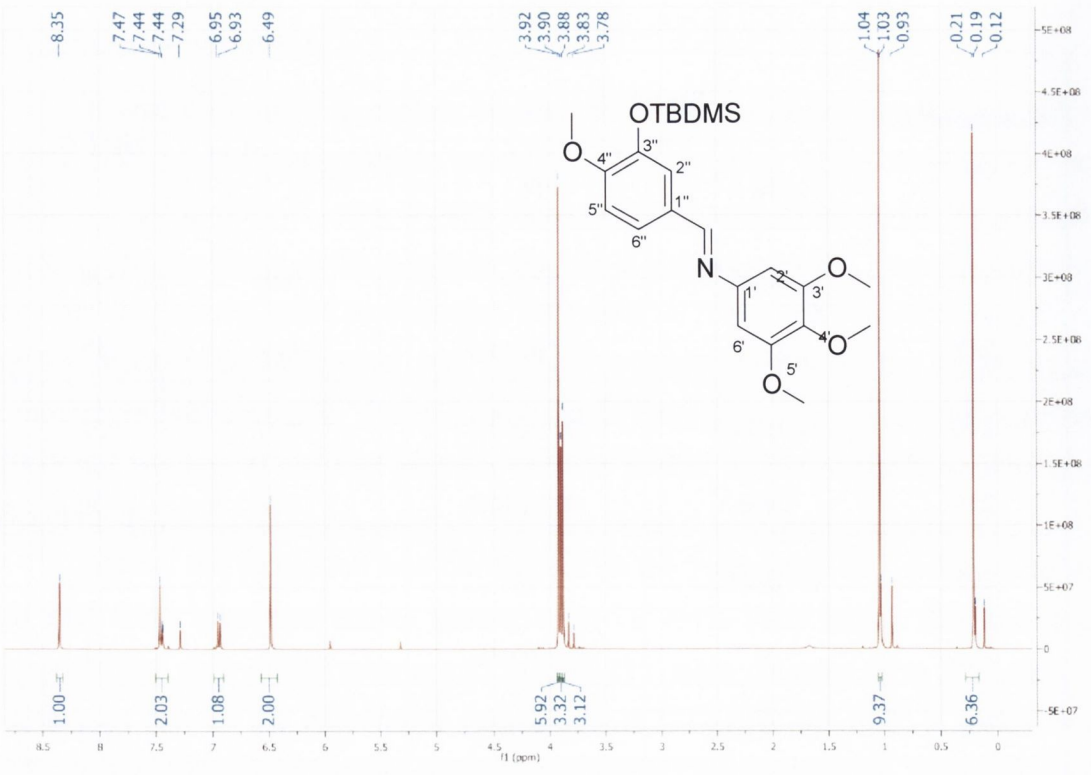

Fig 2.5 ^{1}H spectrum for compound **208**

2.3 β-Lactam Formation by the Staundinger Reaction

Despite being first reported over 100 years ago the Staundinger route remains a popular choice for the synthesis of β-lactams.[170] It provides a direct route to the β-lactam ring utilising standard reaction conditions, but there is still much debate surrounding the mechanism of the reaction particularly in terms of trying to explain the stereochemical outcome of the reaction. Of all the various methods used for β-lactam synthesis, the Staundinger reaction is perhaps the most versatile and therefore most widely used.

2.3.1 Overview of the Staundinger Reaction

The typical Staundinger reaction involves the reaction of a ketene and an imine. Much of the popularity of the reaction is due to the fact that the reagents are easily accessible and/or commercially available. Suitable imines as already outlined can be accessed easily. The ketene can be generated *in situ* usually from an acid chloride and triethylamine.[206] Other sources include the use of a carboxylic acid with an activating agent instead of an acid chloride, or by the rearrangement of a diazoketone.[207] **Section 2.3.4** deals with ketene generation systems in greater detail.

2.3.2 The Mechanism of the Staundinger reaction

In the past the Staundinger reaction has been referred to as a [2+2] cycloadditon, however in more recent times it has come to be considered as a stepwise reaction.[209] The initial step in the reaction is the formation of the ketene by the reaction of an appropriate acid chloride and a base. Work by Lynch *et al* has shown that the ketene is formed prior to the cycloaddition step.[206] The imine then reacts with the ketene to form a zwitterionic intermediate (**220**) which undergoes conrotatory ring closure to yield the β-lactam as *cis*/*trans* isomers (**221a** & **221b**) (**scheme 2.4**). The ring closure of the intermediate is regarded as being key to the stereochemical outcome of the reaction although the exact parameters that dictate the outcome remain obscure. There have been a number of proposals for the factors influencing the stereochemical outcome of the reaction throughout literature including: isomerization of the intermediate[210]; the stereochemistry of the starting imine[211]; substituents on the imine[212]; and the nature of the ketene[213]. The picture is further complicated by the fact

that the reaction conditions also play a role in the stereochemical outcome. Jiao, Liang, and Xu present a very rigorous treatment of the origin of the stereoselectivity in the Staundinger reaction.[214]

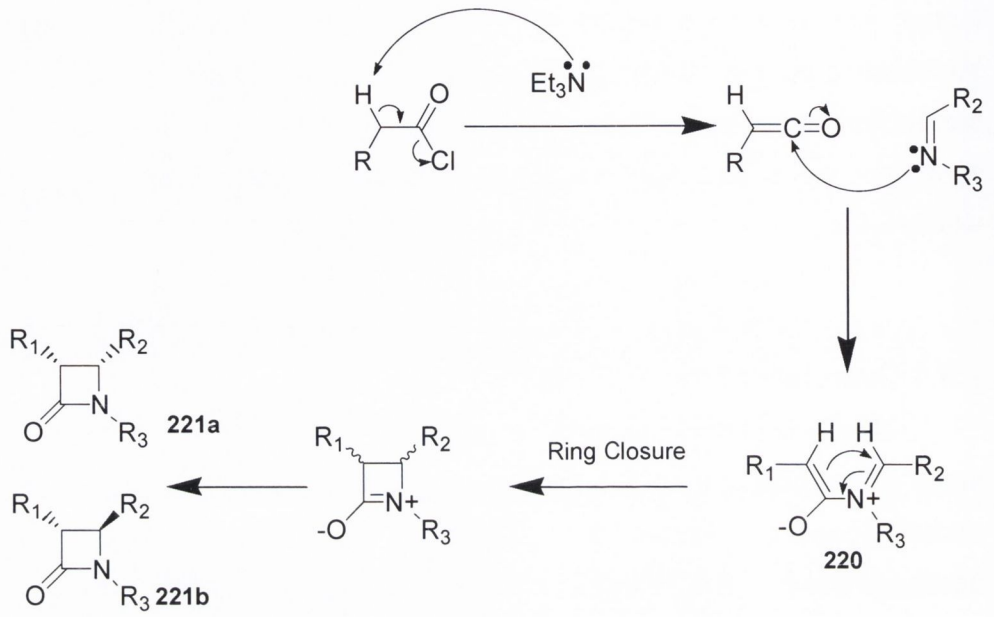

Scheme 2.4 Proposed mechanism for the Staundinger Reaction

2.3.3 Stereochemical outcomes in the Staundinger Reaction

Experimental evidence has shown that the stereochemical outcome (ratio of *cis/trans* diastereomers and generation of racemic/optically pure enantiomers) of the reaction is dependent on the reaction conditions employed and the nature of the reactants[215] [166] [216]. Control of the stereochemistry of the β-lactam ring is vital to the biological activity of a number of important β-lactam containing medicinal compounds (**102-109)** as illustrated in **fig 1.31**, where only a specific diasteromer or enantiomer is active. Rate and order of addition of reagents, acid chloride and imine used, reaction temperature, and solvent all can affect the diastereomeric outcome of the reaction and these factors are discussed in greater detail in **sections 2.3.3.1-2.3.3.5.**

The asymmetric synthesis of β-lactams by the Staundinger reaction is an important route to optically pure β-lactams. Asymmetric induction through either the imine or ketene component of the reaction is possible and is the subject of a thorough review by Palomo *et al*[171]. Chiral imines can be formed from either chiral aldehydes and achiral amines or from chiral amines and achiral aldehydes. For example Bose [217] formed a chiral imine (**222**) from an achiral aldehyde and chiral amine derived from

optically pure *d*-threonine. This imine was successfully used in the Staundinger reaction to give a product **223a** with an *ee* of 90% and **223b** as the minor product (**scheme 2.5**). In the same way chiral aldehydes such as those derived from D-glucose can also be used[218].

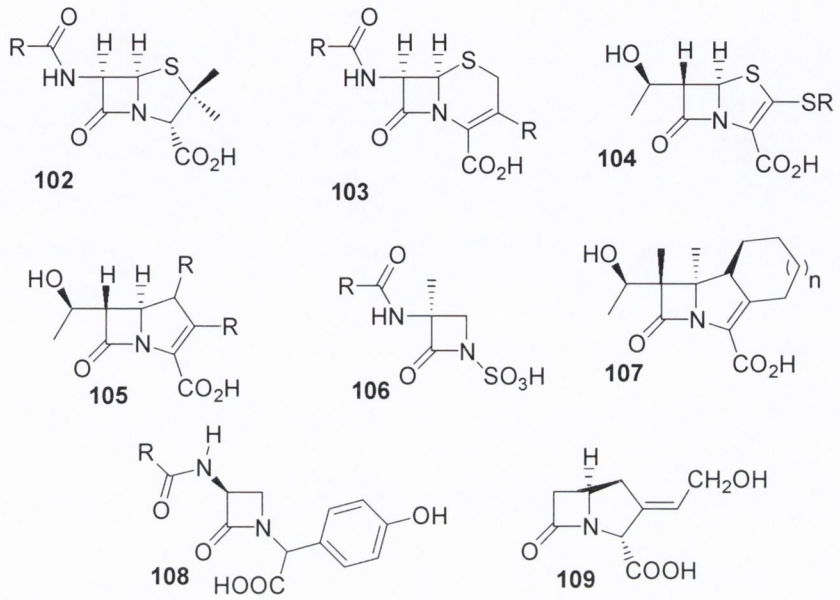

Fig 1.31 Important β-lactam containing medicinal products displaying the importance of stereoselectivity in β-lactam forming reactions.

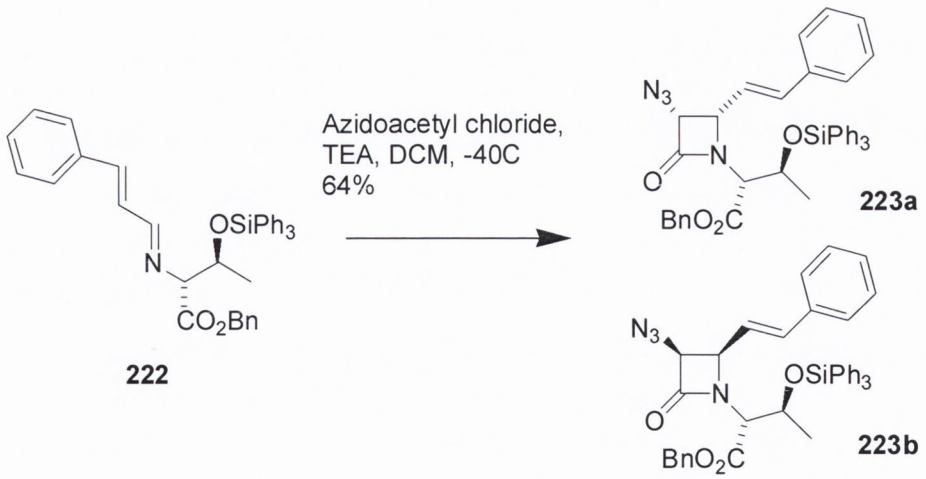

Scheme 2.5 Asymmetric synthesis of the β-lactam ring by induction from a chiral imine

Asymmetric induction from the ketene component has also been described particularly for the synthesis of optically pure 3-amino β-lactams[219]. Ruhlan[220] demonstrated the use of a chiral acid chloride (**224**) in the solid phase synthesis of optically pure β-lactams (**fig 2.7**).

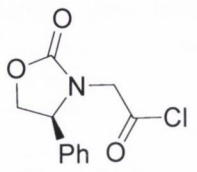

224

Fig 2.6 Chiral oxazolidinylacetyl chloride for use as a precursor to a chiral ketene in the Staundinger reaction

Hodous[221] has employed a 4-(pyrrolidino)pyridine ferrocene chiral catalyst in the Staundinger reaction leading to the synthesis of optically pure β-lactams. Enantiomeric excesses upwards of 90% were recorded for a diversely substituted range of ketenes and imines.

2.3.3.1 Order of addition of the reagents

In general the addition of the acid chloride to a solution of the imine and base heavily favours the production of the *cis* isomer.[222] In contrast the addition of the base to a solution of acid chloride and imine heavily favours the *trans* isomer. Arrieta *et al* attempts to explain the stereochemical outcome by examining the two possible mechanisms associated with each set of reaction conditions with computational methods[223]. The first mechanism is as described in **scheme 2.4** and may be applied to the addition of an acid chloride to a solution of imine and base. The second mechanism (**scheme 2.6**) involves an initial step where the acid chloride and imine react without the presence of a base to form an intermediate (**225**) that ultimately cyclises to **226a** and **226b** *via* an intramolecular SN_2 type mechanism.

For both possible reaction schemes the stereochemistry of the final product is decided by geometry of the intermediate. In the case of **scheme 2.4**, the *E* geometry of the imine and its limited rotation in the intermediate results in the *cis* conformation being favoured. The energy difference between the *cis* and *trans* intermediates was calculated to be of the order of 8 kcal/mol in one example. For **scheme 2.6** there is free rotation around the N_1-C_4 bond which is not present in **scheme 2.4**. In this case the energy difference between the *cis* and *trans* conformations is of the order of 9 kcal/mol in favour of *trans*. These two mechanisms may be used to explain the relationship between the stereochemical outcome and the order of addition of the reagents.

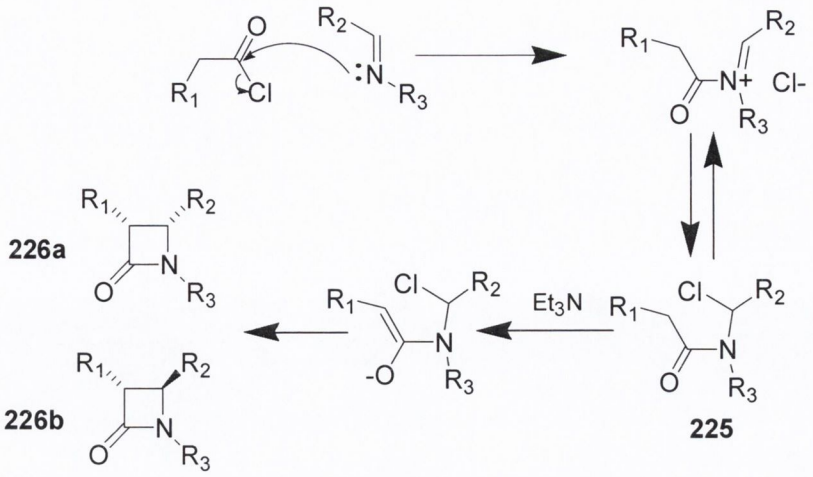

Scheme 2.6 Intramolecular SN_2 type mechanism for the Staundinger reaction

2.3.3.2 Solvent & Reaction Temperature Effects

A number of research groups have observed that solvent plays a role in the stereochemical outcome of the Staundinger reaction.[224] Arrieta *et al* showed that the solvent can affect the energy difference between the zwitterionic intermediates that yield the *cis* and *trans* products. Since the Staundinger reaction is often carried out in refluxing solvent, therefore it may also be possible that temperature may be responsible for the varying stereochemical outcomes observed. It was also proposed that the stereochemical outcome of the reaction was remaining unchanged but that the increase in reflux temperature was converting the product thermochemically to the preferred isomer. The issue of thermochemical isomerisation of the β-lactam products once formed has been shown not to occur.[225]

2.3.3.3 Imine effects

The simplest explanation for the stereochemical outcome may be the stereochemistry of the starting imine, but the majority of Staundinger reactions only involve the use of imines with (E) stereochemistry. The imine could exert an effect by two other means. Firstly the approach of the imine to the ketene may be important (**scheme 2.7**). Secondly the imine may affect the isomerisation of the zwitterionic intermediate prior to ring closure (**scheme 2.8**)

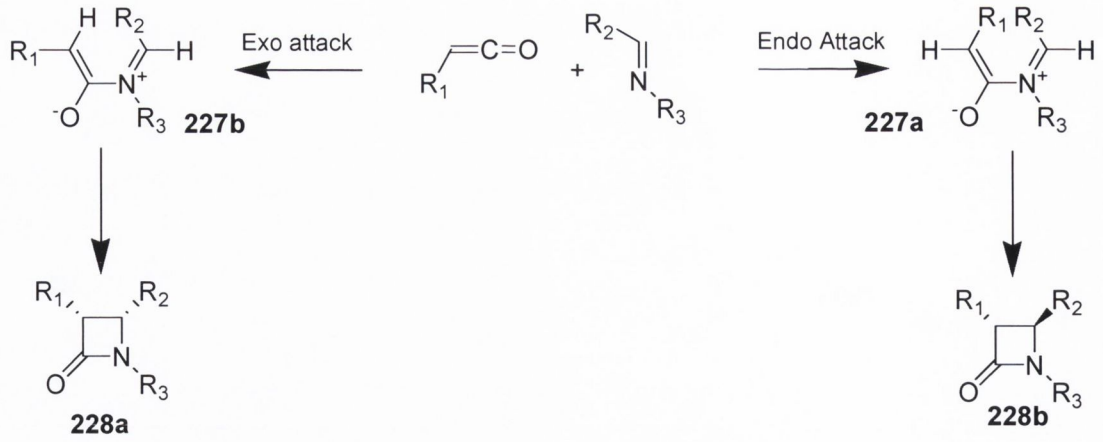

Scheme 2.7 Stereochemical outcome based on approach of imine to ketene

In **scheme 2.7** the ratio of *cis/trans* isomers observed in the β-lactam product (**228a 228b**) could be explained by electronic effects of substituents on the imine affecting its approach to the ketene resulting in favouring **227a** or **227b** as intermediates. Likewise in **scheme 2.8** electronic effects could influence the degree to which the interconversion of the zwitterionic intermediates (**227a** & **227b**) occurs. The stereochemical outcome of the reaction may then arise from the competition between the isomerisation of the intermediate and its ring closure.

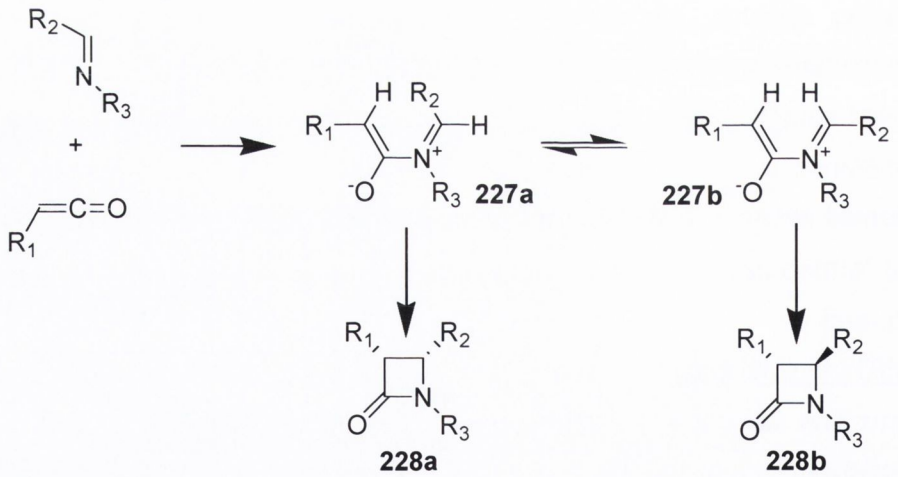

Scheme 2.8 Stereochemical outcome based upon isomerisation of intermediate

2.3.3.4 Ketene Effects

The role of the ketene in the reaction is obviously important since it has been observed that different ketenes reacted with the same imine can lead to radically different stereochemical outcomes. In their paper, Jiao *et al* carried examined the effect of substituents on the ketene on the stereochemical outcome noting that the ratio of *cis/trans* products correlated well with the Hammett constants for the substituents,

with electron donating groups favouring the *cis* isomer and electron withdrawing groups favouring the *trans* isomer (**table 2.3**). **Scheme 2.9** and **table 2.3** presents the data for the model reaction used to investigate the role of the ketene in the stereochemical outcome of the Staundinger reaction.

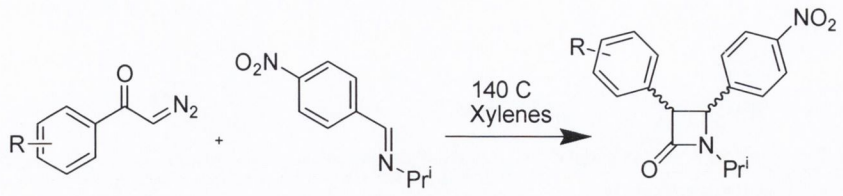

213-236

Scheme 2.9 Model reaction used for the investigation of the role of the ketene in the stereochemical outcome of the Staundinger reaction.

Compound	R	Yield	Cis:Trans
231	*p*-OMe	93	66:34
232	*p*-Me	68	55:45
233	H	52	47:53
234	*p*-Cl	65	40:60
235	*m*-Cl	56	38:62
236	*p*-NO_2	60	27:73

Table 2.3 Model reaction used for the investigation of the role of the ketene in the stereochemical outcome of the Staundinger reaction.

As is the case with the imines, the stereocontrol of the reaction arises from the competition between the isomerisation (k_2 and k_2') of the zwitterionic intermediate and its closure (k_1) (**scheme 2.10**). The rates of these two competing reactions are influenced by the electronic nature of the ketene involved.

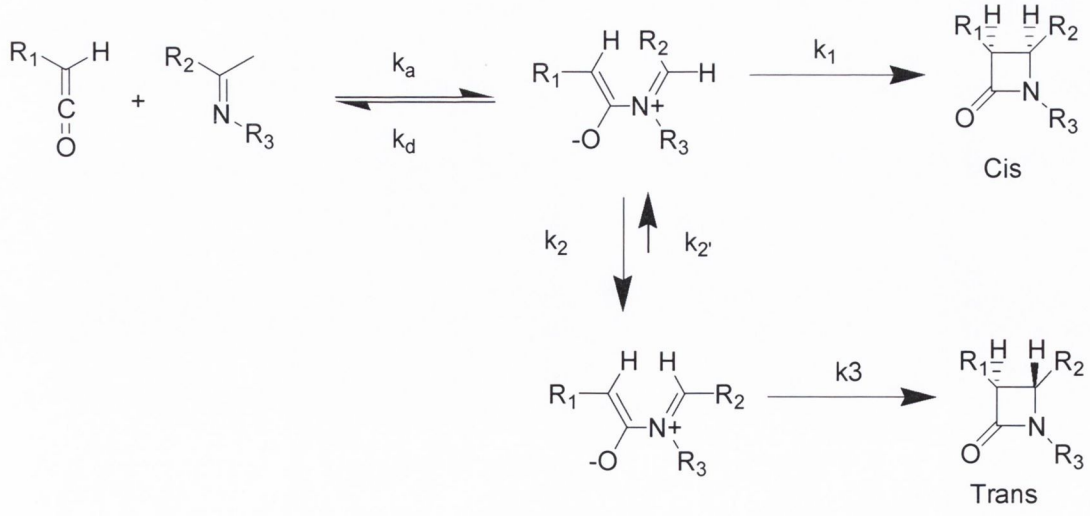

Scheme 2.10 Isomerisation of zwitterionic intermediate leading to stereodivergent outcome

2.3.3.5 The role of the base

The choice of base used in the reaction plays a role in the stereochemical outcome of the reaction. Georg *et al* [226] carried out the Staundinger reaction with phenoxyacetyl acid, substituted aromatic imine, and Mukaiyama's reagent, in the presence of triethylamine/tributylamine/tripropylamine. In all cases the *cis* isomer was favoured but the ratio of *cis:trans* changed from 15:1 for tripropylamine to 3.5:1 for triethylamine. Browne *et al* [224] found that triethylamine and *n*-butyl amine favoured the *trans* (96:4 *trans:cis* and 92:8 *trans:cis* respectively) isomer in the reaction of an acid chloride and aromatic imine, but that the use of pyridine resulted in the almost equal formation of both isomers.

2.3.4 Sources of ketenes

An excellent introduction to ketene chemistry is presented by Tidwell.[227] [228] Ketenes were first prepared by Hermann Staundinger at start of the 20th century by the reaction of an α-halo acid chloride with zinc (**scheme 2.11**) for example the generation of ketene **238** from acid chloride **237**. The ketene is formed by the dehalogenation of **237** by zinc.

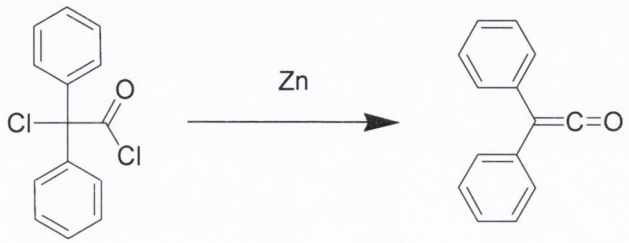

237 **238**

Scheme 2.11 The original ketene isolated by Staundinger

Since their original discovery, many methods for ketene generation have been developed. Ketene dimers can be useful sources of ketenes, but cleavage of the dimer to yield the ketene can necessitate the use of harsh reaction conditions[229]. The most popular methods in the laboratory setting (particularly for the synthesis of the β-lactam ring) involve using carboxylic acids/chlorides or by Wolf rearrangements[230] of diazo ketones[231].

Ketenes may be formed directly from carboxylic acids by dehydration only in cases where the resulting ketene is stablised by electron withdrawing groups[232]. The dehydration may be carried out by using DCC or other suitable dehydrating agents[233]. More often acid activating agents are used, with triphosgene and Mukaiyama's reagent being the two most popular reagents (see **section 2.3.7.1** for further details). A number of ketenes can be formed by the dehydrohalogentaion of an acid chloride and many examples of this particular case are presented within this thesis. Ketenes can generally only be prepared in this manner in cases where the reactivity of the ketene is moderated by the presence of bulky or aryl groups. Dimerisation tends to be the major undesired side reaction in cases where the ketene product is too reactive such as with methyl ketene[234].

The Wolff rearrangement of diazo ketones (**239** & **240**) to produce ketenes such as **241** can be induced thermally, photochemically[236], or by metal catalysis[237]. The thermal rearrangement is particularly useful for diarylketenes, and extensive studies have been made on the substituent effects of this particularly reaction (**scheme**

2.12).[238] The introduction of microwave heating enhanced the yields obtained from the reaction compared to conventional heating[239]. It is suggested that the diazo group interacts with the electromagnetic field of the microwaves resulting in a change in conformation that is more favourable for the rearrangement[240].

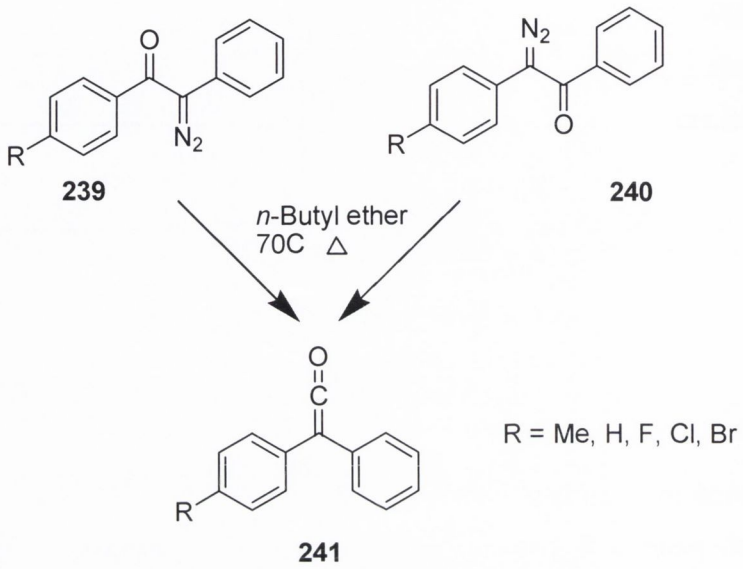

Scheme 2.12 Thermal Wolff rearrangement of diazo ketones

High reaction temperatures (>100°C) are a feature of the thermal decomposition of diazo ketones. Metals such as silver and rhodium have been found to catalyse the decomposition resulting in the use of lower reaction temperatures. The catalytic effects of silver are thought to arise from the formation of silver nanoclusters within the reaction. The photochemical rearrangement of diazo ketones (**242**) has proved useful in the generation of ketenes (**243**) for use in β-lactam formation (**scheme 2.13**).[241]

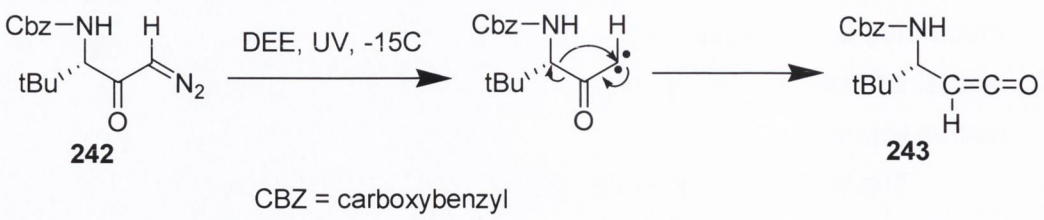

Scheme 2.13 Photochemical rearrangement of diazo ketones

2.3.5 General Synthesis of β-Lactams

In the present work a series of β-lactams (**244-255**) were synthesised from imines (**192-207**) by the method described by Zamboni and Just.[242] The slow addition of a solution of the appropiate acid chloride to a refluxing solution of imine and base should favour the production of the *cis* isomer (**scheme 2.14**). Phenoxyacetyl chloride was selected as a suitable acid chloride from which to synthesise the initial compounds. Cytotoxic β-lactams containing an oxygen atom attached to C_3 in the form of a methoxy of hydroxy group have previously been reported, which was why the phenoxy acetyl chloride was chosen as a starting point. Also the phenoxyacetyl chloride has been previously used in the Staundinger reaction, is commercially available and is easy to handle and store. **Table 2.4** presents the yield and spectroscopic data obtained for products (**244-255**). Where formed the *cis*/*trans* β-lactam isomers were separated by column chromatography on silica.

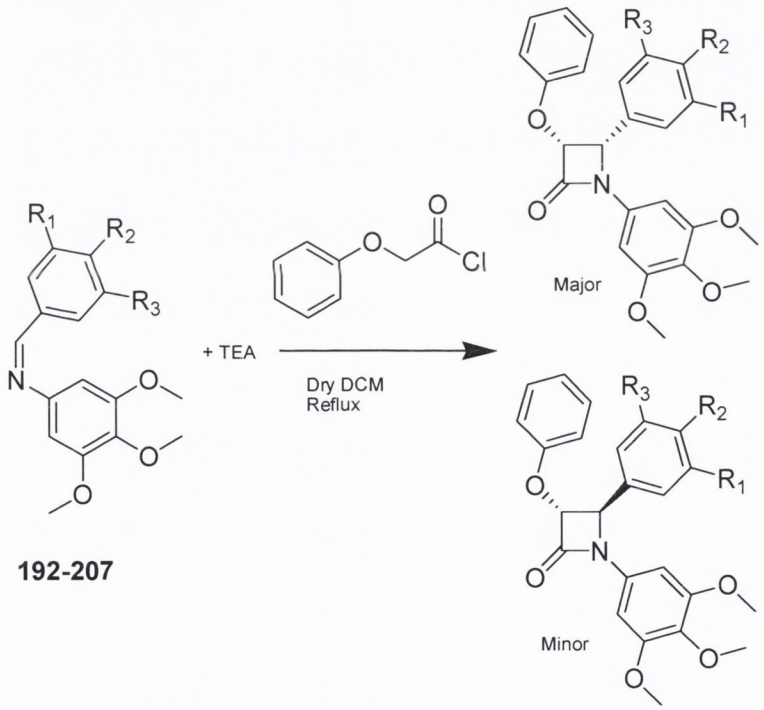

192-207

244-255

Scheme 2.14 Staundinger reaction favouring production of *cis* isomer

Compound No.	Structure			IR (ν_{max} cm^{-1})	MP (°C)	Yield (%)	Isomer
	R_1	R_2	R_3				
244	OMe	OMe	OMe	1762	132-134	32	*Cis*
245a	H	OMe	H	1741	155	33	*Cis*
245b	H	OMe	H	1740	112-114	21	*Trans*
246	$O(CH_2)O$		H	1747	156	71	*Cis*
247	H	SCH_3	H	1744	130	77	*Cis*
248a	Br	OMe	H	1753	158	61	*Cis*
248b	Br	OMe	H	1756	170	31	*Trans*
249	F	OMe	H	1752	120	56	*Cis*
250a	H	CN	H	1765, 2237	174	37	*Cis*
250b	H	CN	H	1760, 2227	162	24	*Trans*
251a	NO_2	OMe	H	1758	136-138	52	*Cis*
251b	NO_2	OMe	H	1753	160	26	*Trans*
252	2-Naphthyl			1746	162	42	*Cis*
253	OMe	OMe	H	1751	152	56	*Cis*
254	1-Naphthyl			1757	182-186	98	*Cis*
255	H	$N(CH_3)_2$	H	1744	166	34	*Cis*

Table 2.4 Yields and spectroscopic data for compounds **244-255**

Compounds (**256-259**) containing the hydroxy functionality were successfully synthesised from their respective silyl ether imines (**208-211**) to give the silyl ether β-lactam, with the *cis* isomer being favoured in the reaction. H_4 and H_3 appear at 5.28ppm and 5.52ppm with a a coupling constant of 4.52 Hz which is typical of the *cis* isomer. For the *trans* isomer H_4 and H_3 appear at 4.89ppm and 5.10ppm with coupling constant of 1.52Hz. For both isomers the formation of the product as the silyl ether protected compound is apparent from both IR and NMR spectroscopy. In the IR spectrum a characteristic absorption is observed at 1729cm^{-1} which is characteristic of the presence of the carbonyl group of the β-lactam. From NMR specetroscopy the presence of the silyl ether is clear from the signals appearing at 0.04ppm and 0.91ppm in the ^{1}H NMR spectrum arising from the dimethyl and *t*-butyl groups of the ether. Likewise in the ^{13}C spectrum, the carbon signals from the silyl ether appear at -4.20ppm 17.88ppm and 23.48ppm. Apart from the silyl ethers of **256a** and **256b** the remaining silyl ethers were not fully characterised due to difficulty in their isolation. Rather the cleavage of the ether was first carried out followed by isolation and characterisation of the phenol products.

Cleavage of the ether was carried out by treatment with *t*-butyl ammonium fluoride (tBAF) to afford the phenolic products **256-259** (**scheme 2.15**). Separation of *cis/trans* isomers formed proved problematic regardless of the separation being carried out on the free hydroxy or on the silyl ether. Compounds **258** and **259** were obtained as an inseparable mixture of *cis/trans* isomers. The yields, spectroscopic data, and melting points for the phenolic products are presented in **table 2.5**. The yields were calculated with respect to the protected imine starting materials.

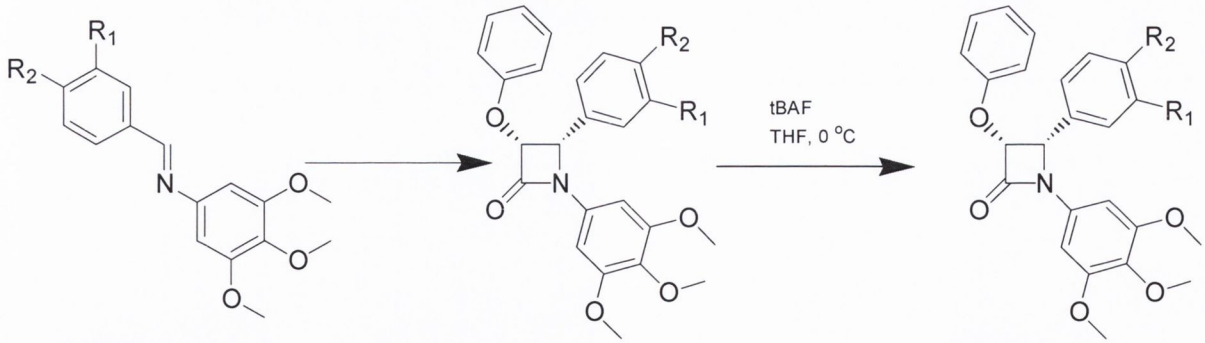

208-211 **256-259**

R_1 = OtBDMS, R_2 = OMe
R_1 = H, R_2 = OtBDMS
R_1 = OMe, R_2 = OtBDMS
R_1 = OtBDMS, R_2 = OtBDMS

Scheme 2.15 *t*BAF cleavage of silyl ethers

Compound No.	Structure		IR (ν_{max} cm^{-1})	MP (°C)	Yield (%)	(Cis:Trans)
	R_1	R_2				
256a	OH	OMe	1739, 3401	176-180	56	Cis
256b	OH	OMe	1737, 3498	162-164	17	Trans
257	H	OH	1741, 3287	142	40	Cis
258	OMe	OH	1757, 3415	158	26	1:2
259	OH	OH	1749, 3426	180-182	57	1:2

Table 2.5 Yields and spectroscopic data for compounds **256-259**

Examples of a typical ^1H NMR spectrum are presented in **Fig 2.7** and **2.8** representative for the *cis* and *trans* isomers of β-lactam **256** synthesised. The presence of a pair of doublets with a coupling constant of J=5.0Hz at δ5.58 and 5.82 is diagnostic for H_4 and H_3 protons respectively of the β-lactam ring. The coupling constants indicate that the β-lactam ring is in the *cis* orientation. Likewise for the *trans* isomer, a pair of doublets is observed at δ5.10 and δ5.35 with a coupling constant of J=2.0Hz.

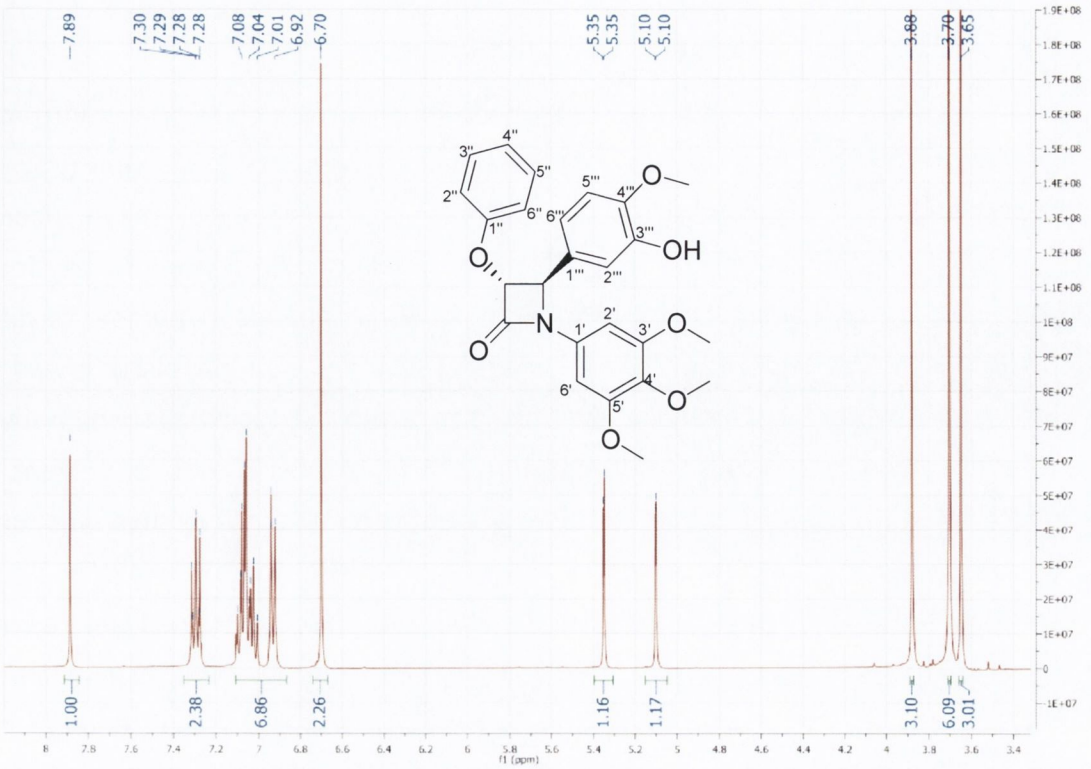

Fig 2.7 ^{1}H NMR spectrum for **256b** *trans* isomer

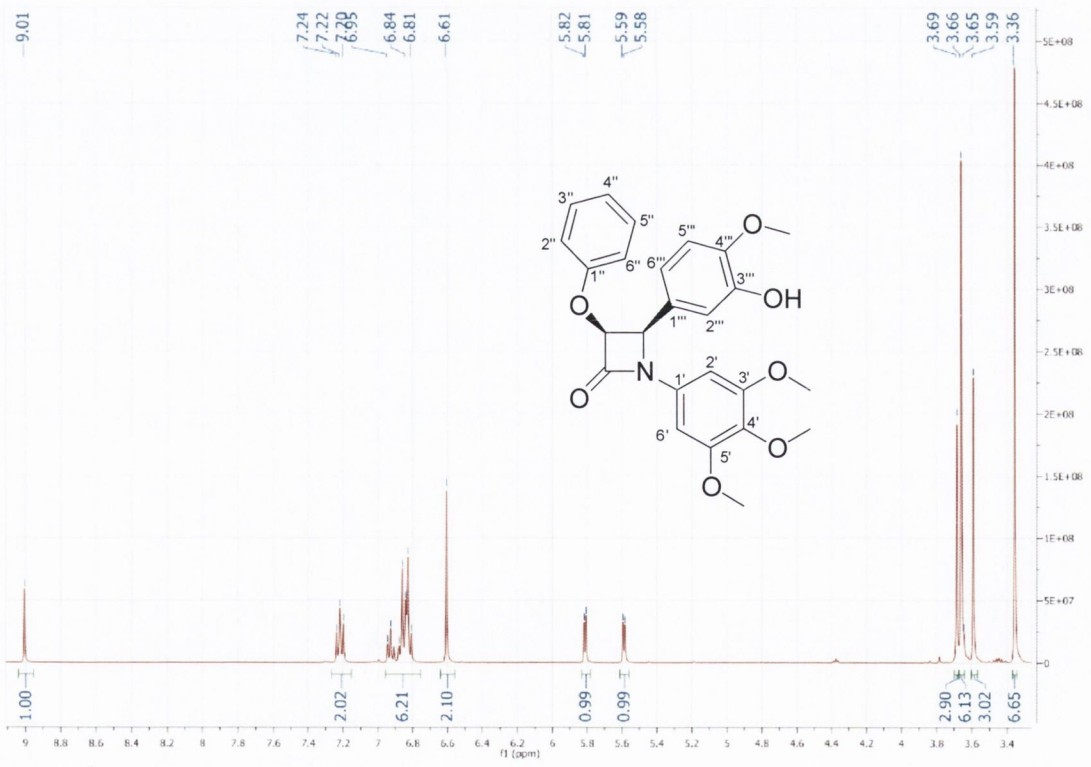

Fig 2.8 ^{1}H spectrum for **256a** *cis* isomer

2.3.6 XRD studies of β-lactam products

In order to determine the absolute stereochemistry of the β-lactam products synthesised in **section 2.3.4** a number of crystals suitable for XRD were grown. An attempt was made at growing crystals for all of the products but with limited success. It was found that the best method for obtaining crystals of high enough quality for XRD was by very slow evaporation of a solution of the compound. A number of different solvents were tried including ethanol, hexane, DCM, and n-propanol but it was found that crystals were only produced when using methanol. A typical procedure involved the preparation of a solution of about 10mg of compound in 2mL of solvent. The solution was placed in a narrow test tube and capped tightly. A pinhole was made in the cap to allow for the slow evaporation of solvent, which was allowed to occur in the dark over a period of approximately two months. The crystals obtained were examined for defects under a microscope before being mounted for analysis. Only compounds **242**, **245b**, **254**, **256b**, **262**, **264b** and **328** yielded crystals of high enough quality suitable for structure determination by XRD. The synthesis of the latter three compounds have yet to be discussed but are none the less illustrated here.

The XRD structures clearly illustrated the presence of *cis/trans* isomerisation and the existence of the products as racemic mixtures. An example of this is presented in **fig 2.9** for **256b**. The enantiomers were assigned as 3S,4S and 3R,4R respectively for the *trans* isomer shown below. For the *cis* isomers, the assignment is 3R,4S and 3S,4R respectively. The coordinates for the XRD structures and their representation as *ORTEP* structures are presented in appendix I. The *ORTEP* structure for **256b** is also presented in **fig 2.9** with the 50% probability ellipsoids shown. Carbon atoms are depicted in white, oxygen atoms in red, and nitrogen atoms in blue.

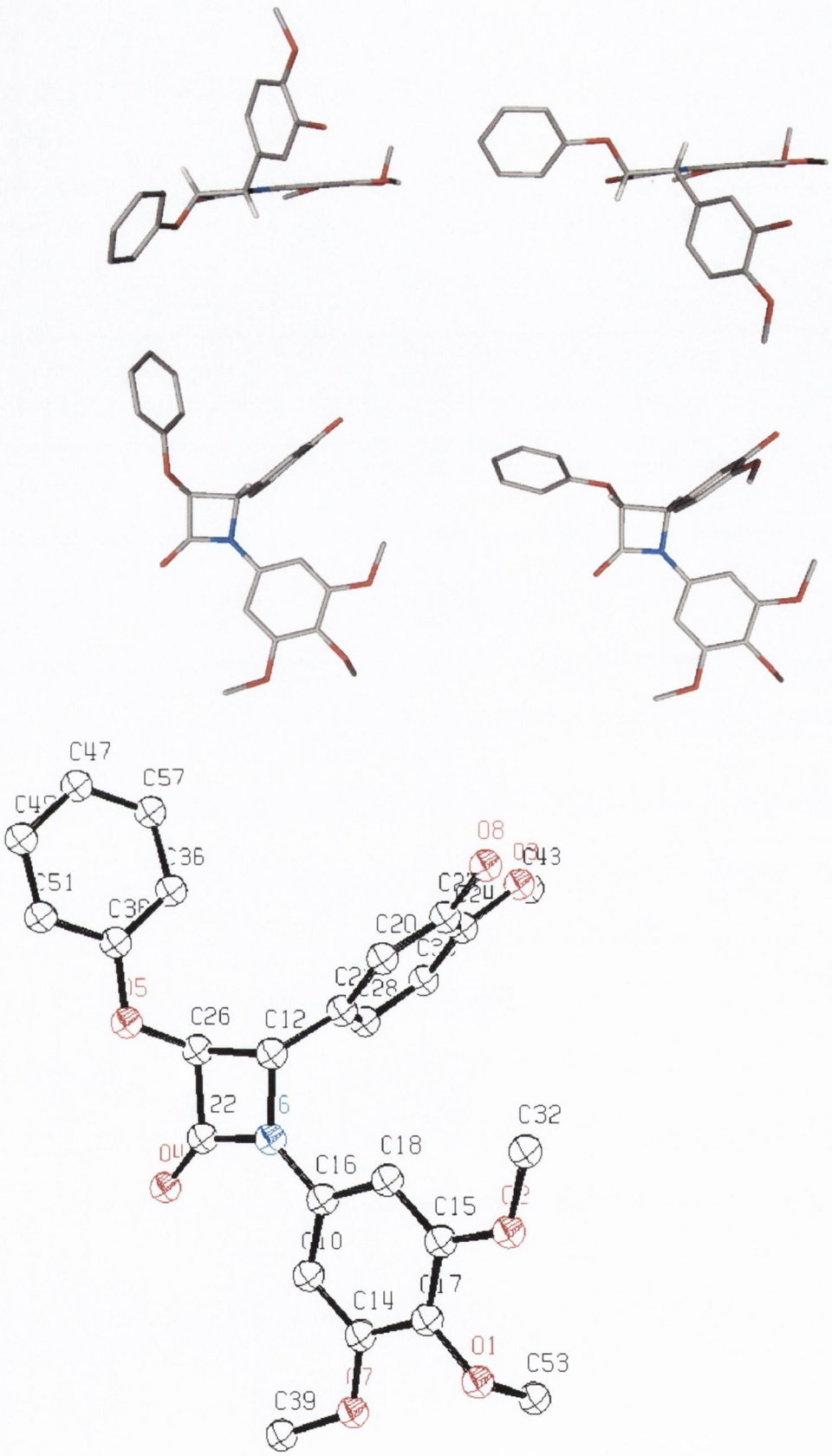

Fig 2.9 Structure of **256b** as determined by XRD illustrating the trans geometry of the β-lactam ring and the presence of a pair of enantiomers

2.3.7 Synthesis of β-Lactams by acid activation and uV irradiation

The Staundinger reaction for β-lactam formation as outlined in **Section 2.3** was modified in an attempt to optimise the reaction conditions for β-lactam formation. While the acid chloride/TEA route is a well known system for generating ketenes, two other methods involving acid activating agents were employed. The effect of microwave irradiation (μV) on the reaction was also examined.

2.3.7.1 Acid activating agents

Both triphosgene **260** and 2-chloro-1-methylpyridinium iodide (Mukaiyama's reagent) **261** are well known acid activating agents for the formation of ketenes from carboxylic acids.[243 244 169 245] The use of an acid activating agent in the Staundinger reaction is attractive especially in cases where the acid chloride may be difficult to handle/prepare or not easily obtainable from commercial sources.

Triphosgene is a safer and easier to handle replacement for phosgene in organic reactions. It decomposes thermally *in situ* to yield phosgene which in turn dehydrates the acid to yield the ketene (**scheme 2.16**).

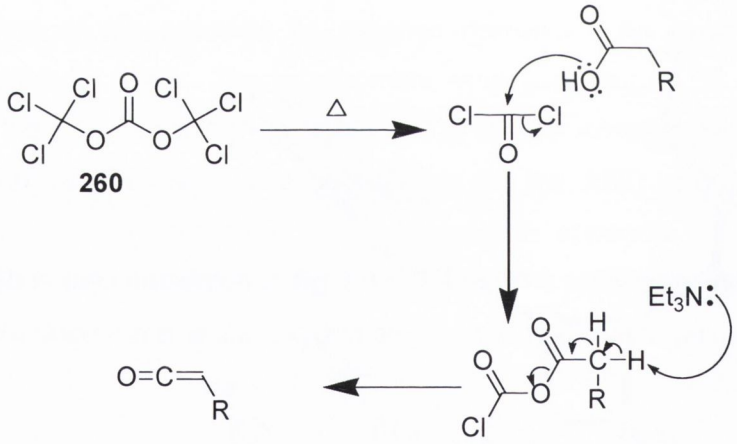

Scheme 2.16 Triphosgene acid activation for generation of ketenes

Mukaiyama's reagent dehydrates carboxylic acids to afford ketenes (**scheme 2.17**).[246] The reagent can be used directly in the reaction or else supported on a polymer as previously discussed in Chapter 1.

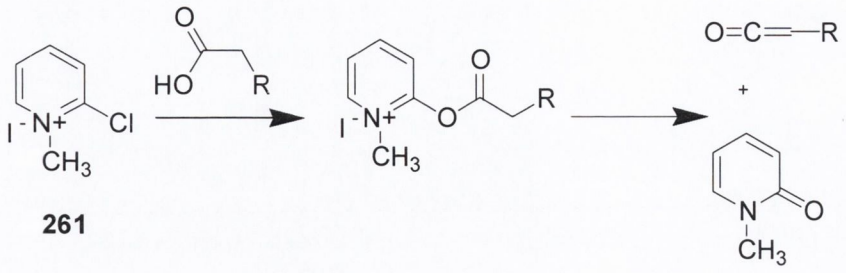

261

Scheme 2.17 Mukaiyama dehydration of carboxylic acid to yield a ketene

Both activating agents were used in the attempted synthesis of **256** from the imine **208** (**scheme 2.18**). The general procedures for both activating agents were similar, with an initial step consisting of allowing the acid and activator to stir prior to the addition of the TEA followed by the addition of a solution of the imine. The formation of product was monitored by ^{1}H NMR. Only the triphosgene reaction yielded the desired β-lactam product with only the *cis* isomer observed in the crude reaction by ^{1}H NMR. The reaction continued to be monitored by NMR during a 5 hour period of reflux followed by stirring at room temperature over night (17 hours) with the results presented in **table 2.6**. The results indicate that the majority of the reaction occurs during the addition of the imine with only minor amounts of product further produced after 1 hour. A final yield after flash chromatography of 53% was recorded which is similar to that observed with the acid chloride.

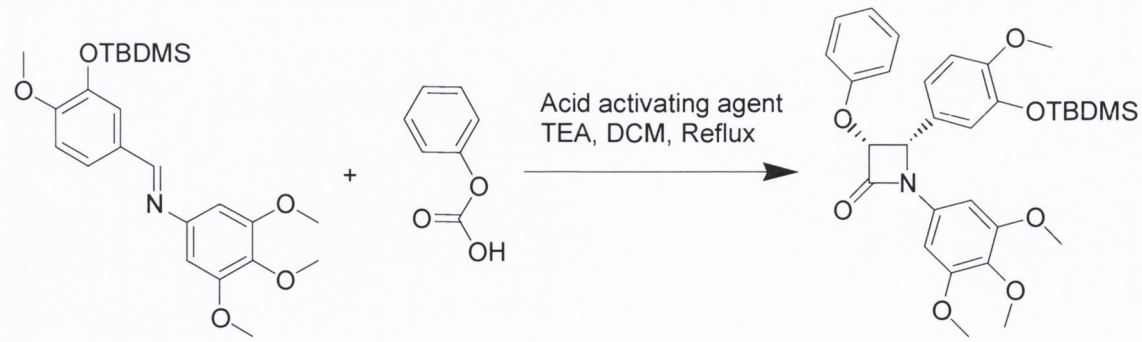

208 **256**

Scheme 2.18 Triphosgene acid activation reaction

Time (after completion of addition of imine)	Product:Starter 208:256	*Cis:Trans*
2 minutes	1:1.11	*Cis only*
1 hour	1:0.98	*Cis only*
5 hours	1:0.94	*Cis only*
Overnight (17 hours)	1:0.92	*Cis only*

Table 2.6 Monitoring of triphosgene activated β-lactam forming reaction by ^{1}H NMR.

2.3.7.2 Microwave assisted reaction

In recent years there has been much interest in the use of microwave technology to enhance chemical reactions. Some of the benefits associated with the use of microwaves include shorter reaction times, cleaner reactions, enhanced selectivities, and elimination of solvents.[247] The effect of microwave irradiation in the synthesis of **245** from the imine **193** and phenoxyacetyl chloride was studied (**scheme 2.19**). Dichloroethane (DCE) replaced dichloromethane (DCM) in the reaction since it is a better absorber of microwave energy. Two sets of reaction conditions were used both of which resembled the thermal conditions used to synthesis (**245**). Firstly the reaction was carried out in one step with all the reagents being added together in a vial and then subjected to microwave irradiation. This resulted in no formation of β-lactam. Secondly, the reaction was carried out as normal except with the replacement of thermal heating with microwave irradiation i.e. addition of acid chloride to a solution of imine and TEA. The reaction was carried out at 40°C (the reflux temperature of DCM) and led to the formation of a 5:1 mixture of *cis:trans* isomers in a yield of 32%. So the reaction appears to possess greater stereoselectivity at 40°C under thermal heating compared to under microwave conditions.

In an effort to further improve the yield, the reaction temperature was increased to 80°C which resulted in an increase in diastereoselectivity (10:1 *cis:trans*) but the yield only increased to 34%. This increase in the diastereoselectivity is surprising since it is thought that higher reaction temperatures should favour the less energetically favourable *trans* isomer as has been reported by Manhas.[248] Despite a variety of conditions being used, the yield of (**245**) was not significantly improved by microwave irradiation. It was interesting to note that the stereoselectivity of the microwave reaction was less than that of the thermal heating reaction. This may be due to the use of dichloroethane instead of dichloromethane in the reaction since solvent is thought to play a role in the stereoselectivity of the reaction as discussed in **section 2.3.3.2**. It

may be that the change in stereoselectivity was brought about by the use of microwave energy. Bose proposes that some of the pathways involved in the cyclisation process (such as isomerisation of the zwitterionic intermediate prior to cyclisation) are accelerated by microwave irradiation leading to stereochemical outcomes that differ from those obtained by convential heating possibly by influencing the transition states involved in the reaction[249].

Due to the greater stereoselectivity of the thermal heating method, further microwave synthesis of β-lactams were not carried out.

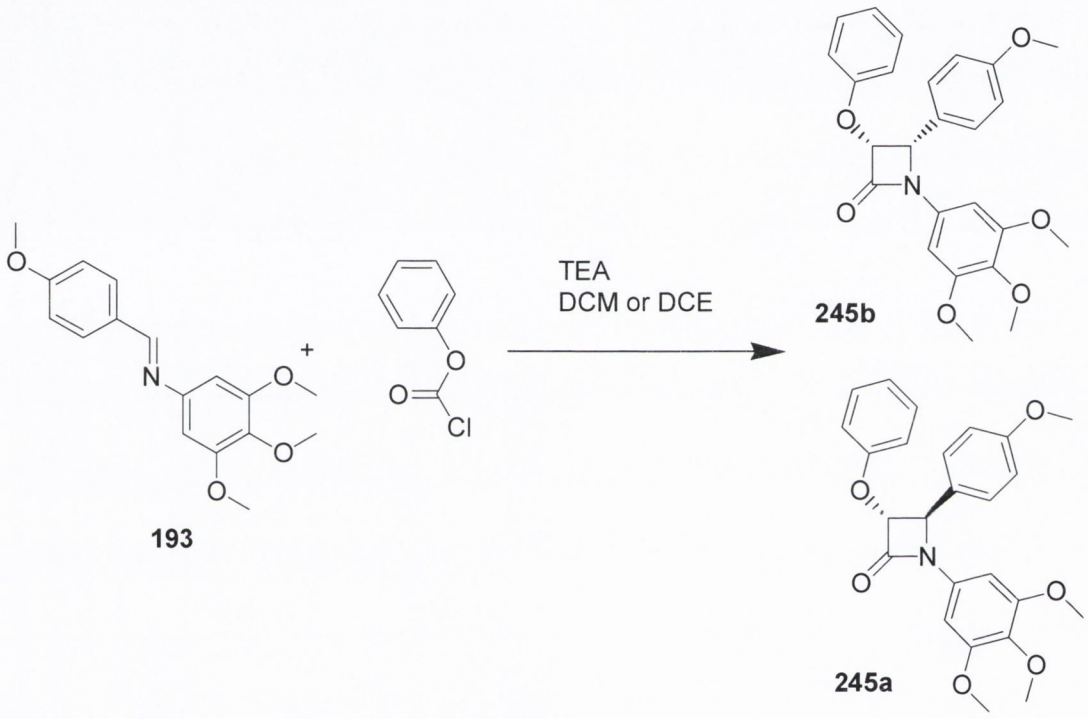

Scheme 2.19 Microwave induced formation of **245**

2.4 Transformation of β-Lactams

2.4.1 MCPBA Oxidations of Sulphur analogues

The 4-methoxy substitution pattern on ring B of is often described as being crucial to the biochemical activity of CA4. The exact relationship between aromatic substitution and activity will be discussed in greater detail in the molecular modelling chapter. To investigate this further, the structurally related thio methyl group was incorporated into the 4-position instead of a methoxy group for compound **247** *m*-Chloroperbenzoic acid (MCPBA) was used to oxidise the sulphur methyl group to the sulfoxide (**262**) and sulfone (**263**). Use of excess of mCPBA led to the formation of the sulfone, while use of one equivalent led to the sulfoxide (**scheme 2.20**).

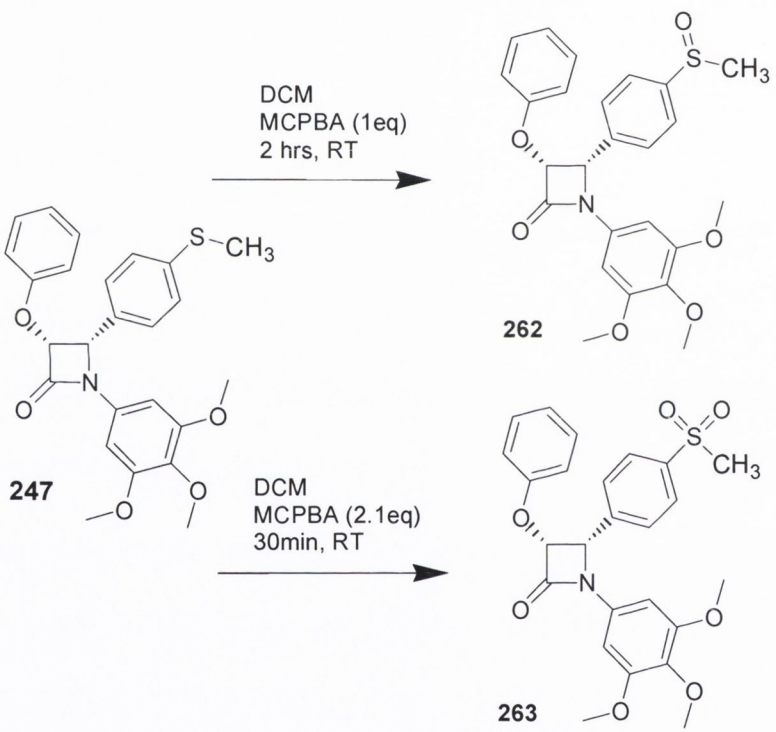

Scheme 2.20 Oxidation of thio methyl analogue to corresponding sulfoxide and sulfone

The mechanism for the oxidation reaction is presented in **scheme 2.21**. Both the sulfoxide and sulfone display S-O stretch in the IR spectrum in the region 1000cm^{-1} to 1300cm^{-1} (**table 2.7**). The ^{1}H NMR spectrum for **263** is presented in **fig 2.10**. The oxidation of the sulphur to the sulphone results in a shifting downfield of the methyl group signal from δβ2.45ppm to δ3.04ppm. The ^{1}H spectrum for the sulphoxide product **262** is shown in **fig 2.11 (a)**. The signals for H_3 and the methyl group appear as overlapping doublets and singlets respectively (**fig 2.11 (b)**). The oxidation of the thiomethyl group to the sulfoxide introduces a new chiral centre into the β-lactam

compound **262**, so the observation of two sets of signals was initially put down to the presence of diastereomers. However if the compound was present as a mixture of diastereomers, then it is surprising that the H_3 rather than H_4 is effected. A second ^1H NMR spectrum was obtained in DMSO, which resulted in a spectrum where only one set of signals was obtained for H_3 and the methyl groups. One possible explanation for these puzzling results is the interaction between the lone pair of electrons on the thio methyl group and H_3.

A crystal of the compound was obtained which was suitable for XRD. The structure of the compound was determined by XRD except for the region around the sulfoxide group which proved difficult to resolve. The partially resolved structure is presented in **fig 2.12**. Carbon atoms are depicted in grey, hydrogen in white, oxygen in red, sulphur in yellow, and nitrogen in blue. It is obvious that the sulfoxide group has not been determined correctly. Further refinement was attempted by substituting one of the oxygens attached to the sulphur atom with chlorine but this did not result in any improvement in refinement. Initially it was thought that the **262** may have degraded during the crystalisation process but HRMS of the crystal confirmed that the compound remained intact. The possibility of the feature being an artifact from the crystallization process cannot be ruled out. It may be possible that the presence of the lone pair of electrons on the sulphur atom is at the heart of the problem, by interacting with the neighbouring oxygen atom. Since the XRD experiment relies upon the dense atomic nucleus to generate the diffraction pattern, it is not a particularly good method for determining the position of electrons. This may also explain the lack of refinement in the region of the sulphur atom.

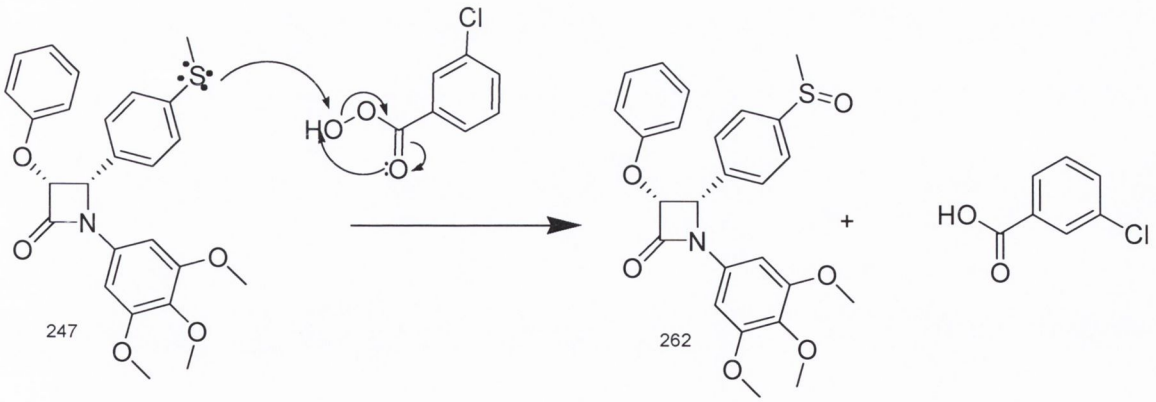

Scheme 2.21 Mechanism for the oxidation of sulphur methyl group by mCPBA

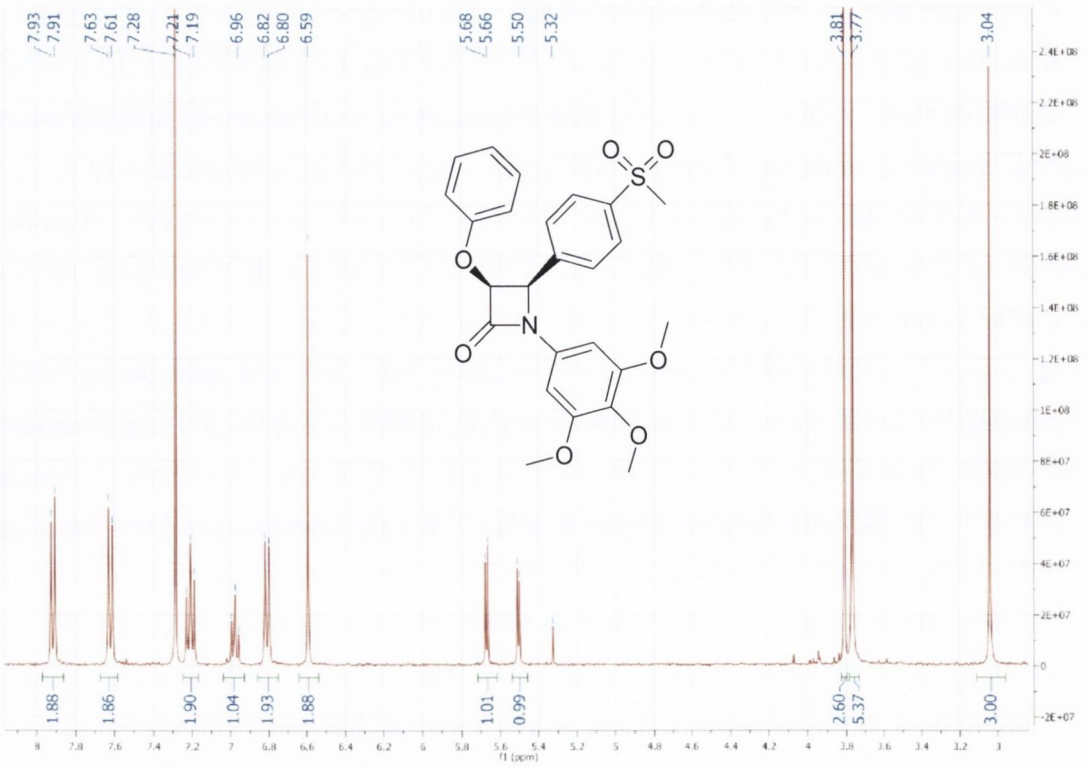

Fig 2.10 ^{1}H NMR spectrum for **263**

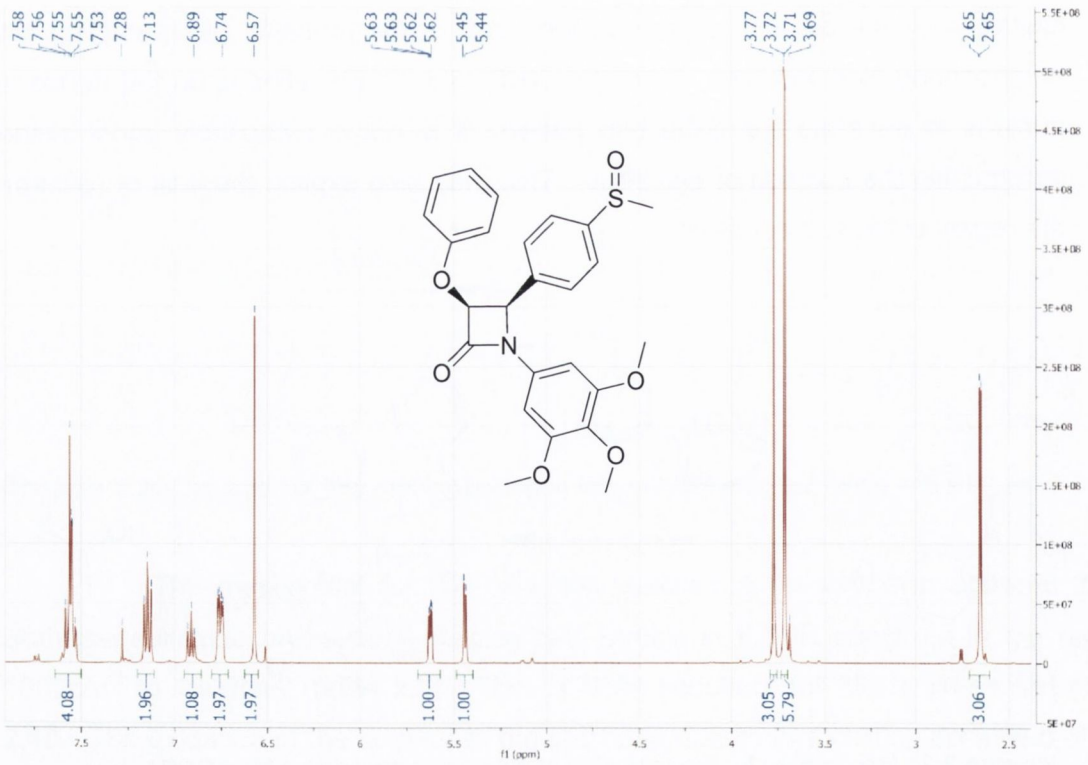

Fig 2.11 (a) ^{1}H NMR spectrum for **262**

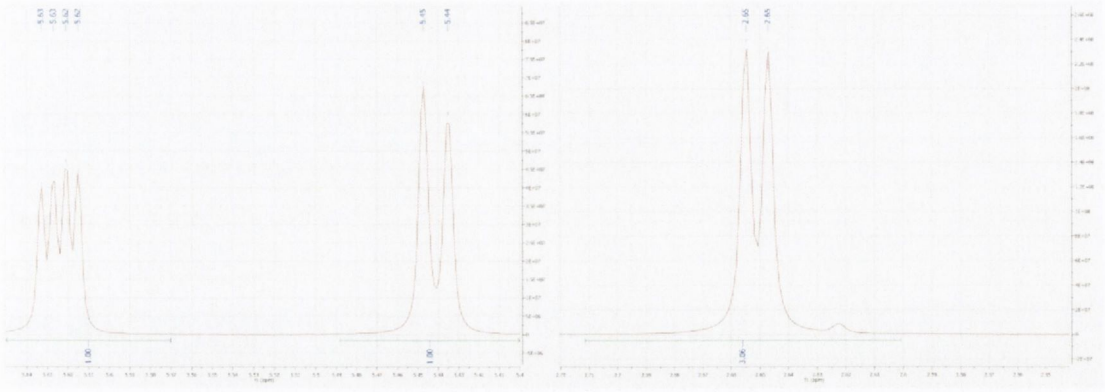

Fig 2.11 (b) ^{1}H spectrum for **262** highlighting the two sets of signals obtained

Compound No.	Structure	IR (γ_{max} cm^{-1})	MP (°C)	Yield (%)
262	Sulfoxide	1749, 1051	156	63
263	Sulfone	1750, 1307, 1221	160-162	66

Table 2.7 Yields and spectroscopic data for compounds **262** & **263**

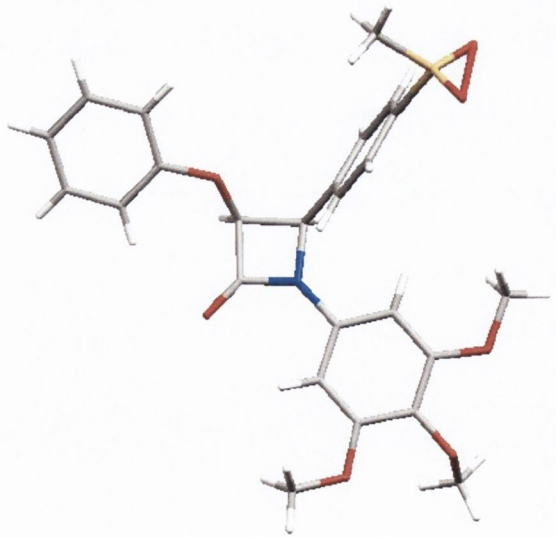

Fig 2.12 Structure of **262** as determined by XRD.

2.4.2 Nitro Group Reduction

The transformation of the nitro group to an amino function in some of the β-lactam products synthesised is attractive for a number of reasons. Analogues of CA4 containing the amino group have demonstrated comparable biochemical activity to phenolic CA4 (see **section 1.6.3**)[106 74]. The amino group is also amenable to conversion to a water soluble prodrug, by conjugation with amino acids and serves as a connection point in coupling reactions[250].

In the present work the nitro containing compound (**251a** & **251b**) were individually reduced to the corresponding *cis* and *trans* amino products (**264a** & **264b**) by using zinc in the presence of acetic acid based on the general method of Sun *et al* (**scheme 2.22**).[162] The reaction proceeded over the course of seven days and was quantitative as monitored by ^{1}H NMR. Both the *cis* and *trans* (**251a** & **251b**) compounds were successfully reduced in separate experiments to the corresponding amino analogues (**264a** & **264b**). It was found that the amino products were difficult to purify by column chromatography but were amenable to further purification by recrystallisation from hot ethanol. The yields and spectroscopic data are presented in **table 2.8**.

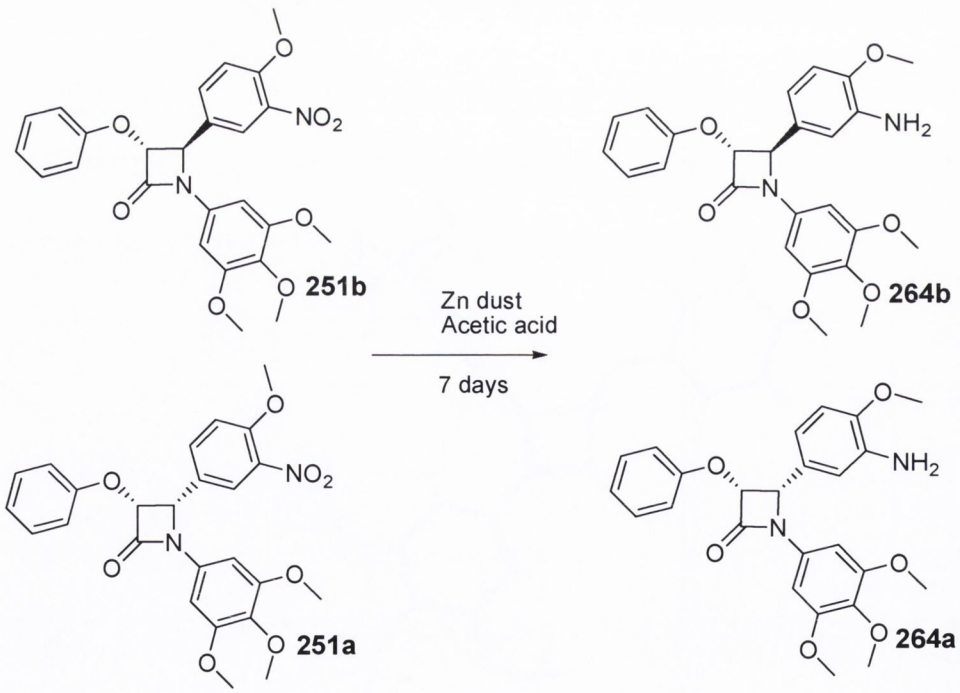

Scheme 2.22 Reduction of nitro group of compounds **251a** and **251b**

Compound No.	IR (γ_{max} cm^{-1})	MP (°C)	Yield (%)
264a	1745, 3368	158	83
264b	1756, 3465	128-130	94

Table 2.8 Yields and spectroscopic data for compounds **264a** and **264b**

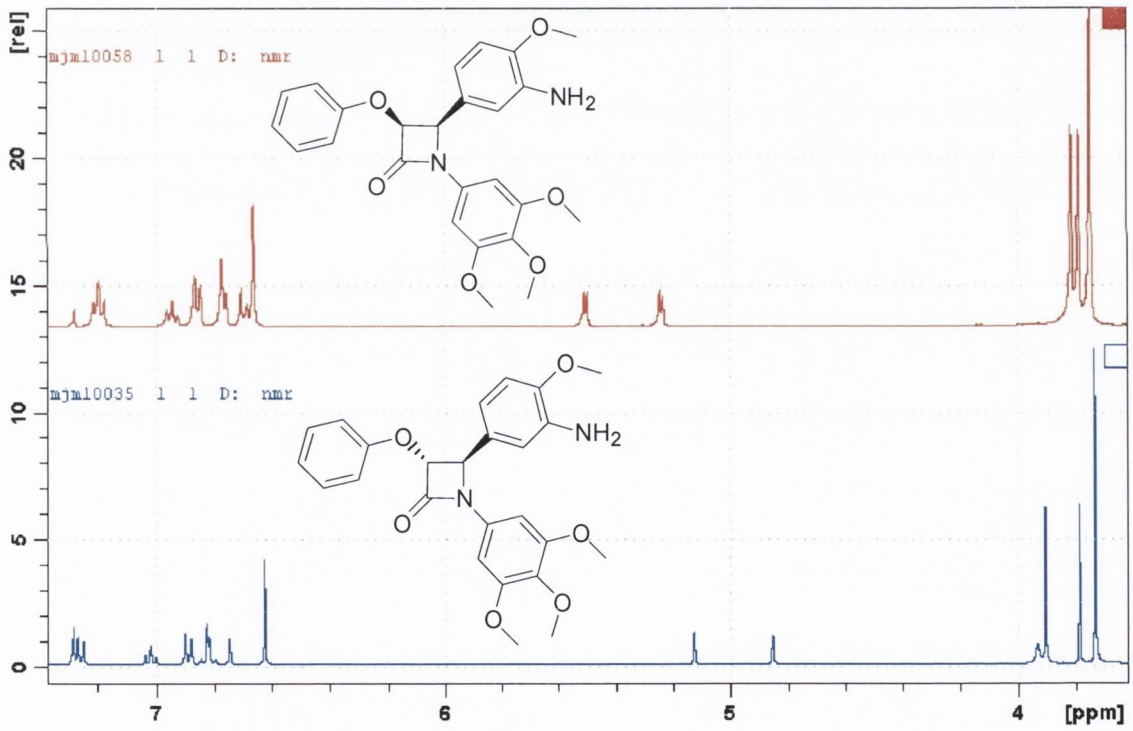

Fig 2.13 ^1H spectrum collected for **264a** (red) and **264b** (blue)

From the IR spectra (**table 2.8**) the reduction of the nitro to the amino group was apparent from the appearance of a broad absorption centered on approximately 2996cm^{-1} and the disappearance of the N-O symmetric stretch at 1350cm^{-1}. In the ^1H NMR spectrum (**fig 2.13**), there is a clear shift upfield in the chemical shifts for the H_3 and H_4 protons of the amino compound compared to the nitro compound. For example

H_3 and H_4 in **251a** appear at δ5.60ppm and δ5.41ppm, and at δ5.49ppm and δ5.23ppm in **264a**. Likewise in the ^{13}C spectrum the signal for C_3''' shifts from δ133.17ppm to δ124.49 upon the reduction of **251a** to **264a** due to the removal of the electron withdrawing effects of the nitro group.

Time of flight electrospray ionisation high resolution mass spectrometry (TOF-ESI-HRMS) was used to further characterise the products obtained from the reaction. For **264a** an ion with (*m/z*) of 473.1720 (4.7ppm) was observed which corresponds to M^++Na. Scission of the C_2-C_3 and N_1-C_4 bonds of the β-lactam ring results in two fragments of (*m/z*) 210.0675 and (*m/z*) 242.1187 as illustrated in **fig 2.14**.

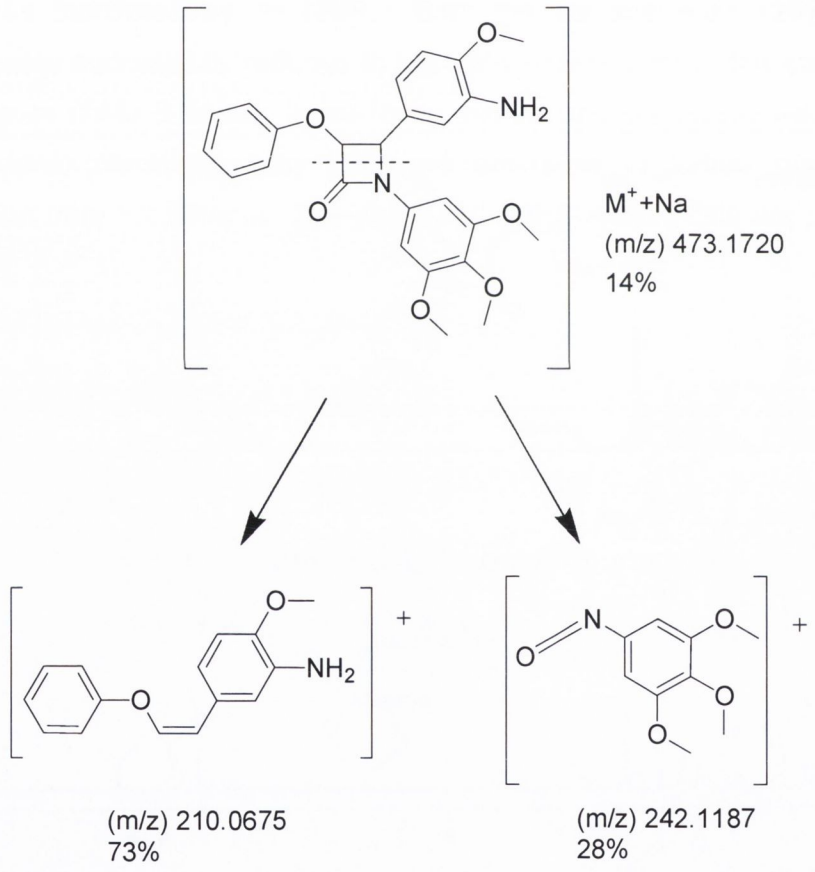

Fig 2.14 Mass spectrum of **264a**

2.4.3 Coupling Reactions

As has been previously discussed in **Section 1.5.5.3**, after exposure to CA4 a viable rim of tumour cells remain around the periphery of the tumour[251]. To overcome this, ongoing clinical trials use a combination of CA4 with either radiotherapy or a well established chemotherapy agent. It may be beneficial then to demonstrate the coupling of our analogues to a traditional alkylating chemotherapy agent such as chlorambucil[252]. Coggiola has previously demonstrated the coupling of combretastatin to the 3-hydroxy group of CA4 through an ester and ether linkages. In the present work chlorambucil was coupled to the hydroxy (**256a**) or amino (**251a**) derivatives through an ester/amide linkage to give **265** and **266** respectively (**scheme 2.23**).

The demonstration of such a coupling may also be useful for the future development of prodrugs of the amino compounds.

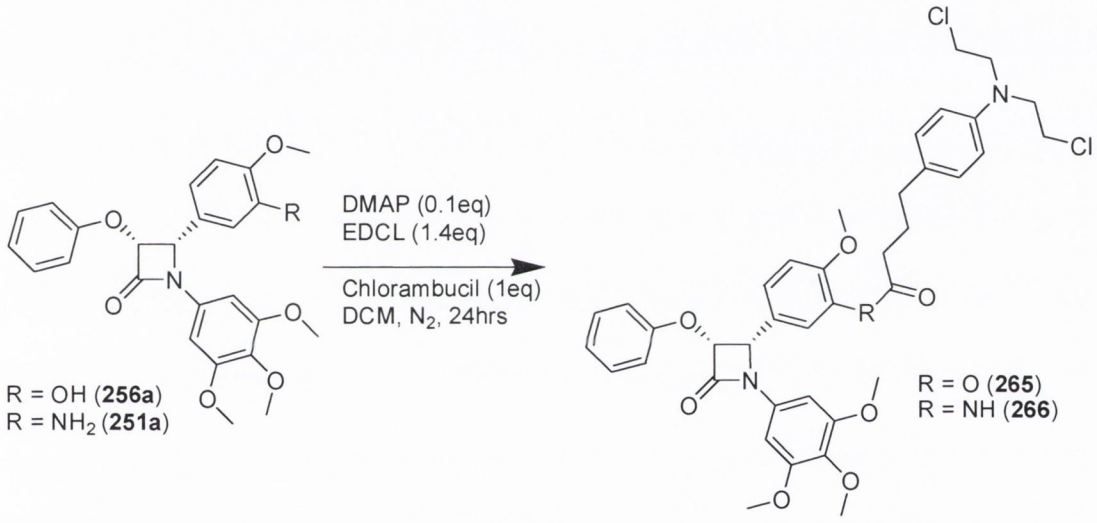

Scheme 2.23 Chlorambucil coupling to **256** & **251**

The coupling was carried out using EDCL/DMAP (**scheme 2.23**). As a carbodiimide EDCL activates the carboxylic acid in a similar manner to DCC (**scheme 2.24**). DMAP is used as a catalyst in the reaction by acting as a stronger nucleophile than the alcohol in the reaction leading to the formation of an amide type intermediate which reacts towards the alcohol. The reaction with chlorambucil occurs in an analogous manner for **251** containing the amino group.

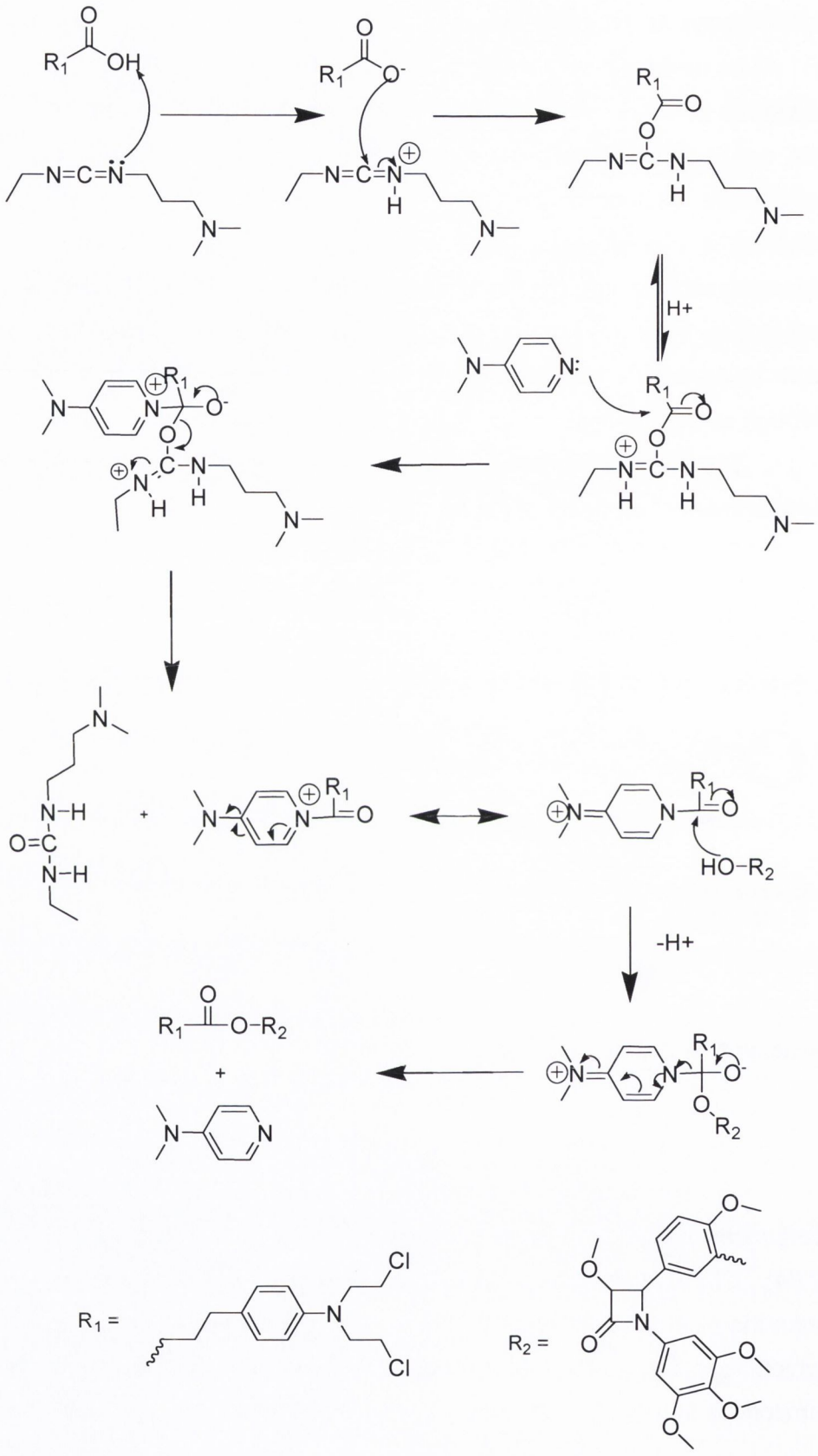

Scheme 2.24 Mechanism for the EDCL/DMAP coupling of chlorambucil to β-lactam **256**

Compound No.	IR (ν_{max} cm^{-1})	Yield (%)
265	1003,1270, 1760	53
266	1686,1755	38

Table 2.9 Yield and spectroscopic data for **265** and **266**

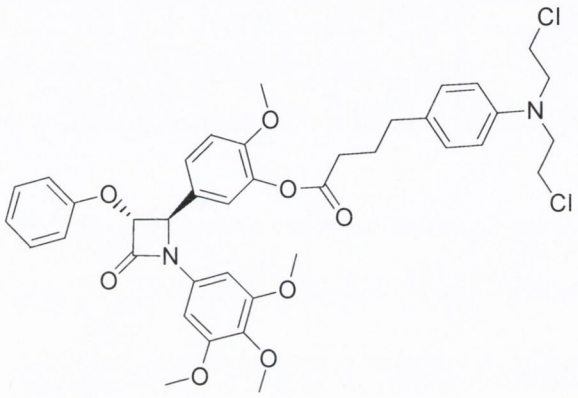

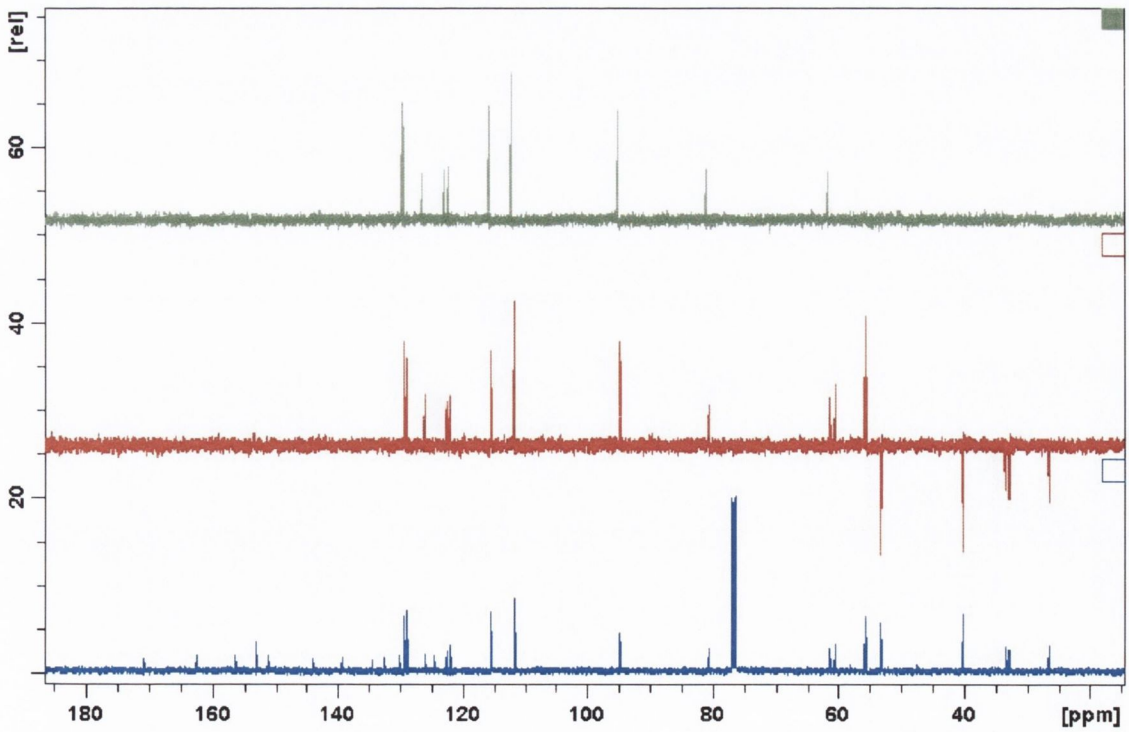

Fig 2.15 ^{13}C spectra (blue), DEPT 90 (red) and DEPT 135 (green) for compound **265**

Both the ester (**265**) and amide (**266**) products were readily characterized by IR (**table 2.9**) and NMR spectroscopy. For the ester **265** the carbonyl of the β-lactam absorption appears at 1760cm^{-1} while that of the ester appears at 1003cm^{-1} and 1270cm^{-1}. For the amide **266** the β-lactam carbonyl absorption appears at 1755cm^{-1} and the amide at 1686cm^{-1}. A DEPT NMR experiment was carried out to unambiguously assign the carbon signals in the ^{13}C spectrum for **265** as illustrated in **fig 2.15**. The DEPT 135 ^{13}C NMR spectrum highlights the presence of CH_2 groups in the system which appear as negative peaks. C_7, C_6, C_8 appear at δ26.42, δ32.77 and δ33.32 and as negative peaks in the DEPT 135 spectrum. C_{11} and C_{12} are equivalent due to symmetry in the molecule and appear as a single signal at δ40.06 and as a negative peak in the DEPT 135 spectrum. C_9 and C_{10} appear as two very close signals at δ53.01 and δ53.14 and also as negative peaks in the DEPT 135 spectrum. The carbons of the methoxy groups appear as a series of signals between δ55.41 and δ60.50 while C_4 and C_3 of the β-lactam ring appear at δ61.29 and δ80.65 respectively. The remaining aromatic signals arise between δ94.81 and δ156.47. The carbonyls of the ester linkage C_5 and the β-lactam ring C_2 are observed at δ162.50 and δ170.75.

2.4.4 Transformation of the Carbonyl Group

The carbonyl group of the β-lactams plays a crucial role in the antibacterial activity of the β-lactam antibiotics. It is also an Achilles heel of sorts in terms of the rings stability under acid/base hydrolysis conditions. In order to examine the effect of the replacement of the carbonyl group on both stability and on the anticancer effects of the newly synthesised analogues, two transformations were carried out on the carbonyl group of these products.

2.4.4.1 Lawesson's Sulphurisation

In the present work the first transformation was the replacement of the oxygen of the carbonyl group of **256a** with the more lipophillic sulphur atom of a thione by using Lawesson's reagent (2,4-bis(4-methoxyphenyl)-1,3,2,4-dithiadiphosphetane 2,4-disulfide). Jesberger *et al* [253] presents an excellent review of the use of Lawesson's reagent for the thionation of a variety of carbonyl compounds. Refluxing the β-lactam **256a** with the reagent in toluene led to the formation of the thione compound **267** in 76% yield (**scheme 2.25**). The disappearance of the carbonyl compound was confirmed by IR spectroscopy. The distinct absorption at 1739cm^{-1} due to the carbonyl disappeared and a new absorption at 1592cm^{-1} due to the newly formed C=S bond appeared. The most obvious effect of the thionation on the ^{1}H NMR spectrum is the shift downfield of the H_3 signal from δ5.53ppm to δ5.78ppm. A slight shift downfield is also observed for H_4 from δ5.29ppm to δ5.32ppm. The extent of the shift downfield is greater in H_3 than H_4 possibly due to its closer position to the newly formed C=S bond.

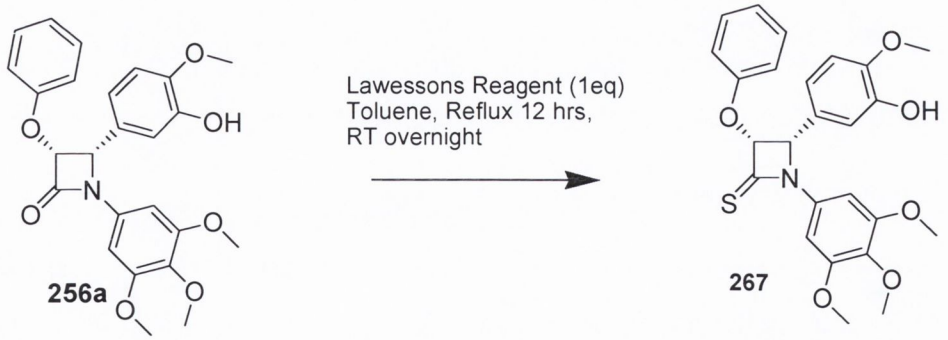

Scheme 2.25 Thionation of the carbonyl in **256a** by Lawesson's Reagent

The proposed mechanism for the reaction is presented in **scheme 2.26**. The thermodynamic driving force for the reaction is the formation of P-O bonds in the products which are stronger than P-S bonds in the reagent.

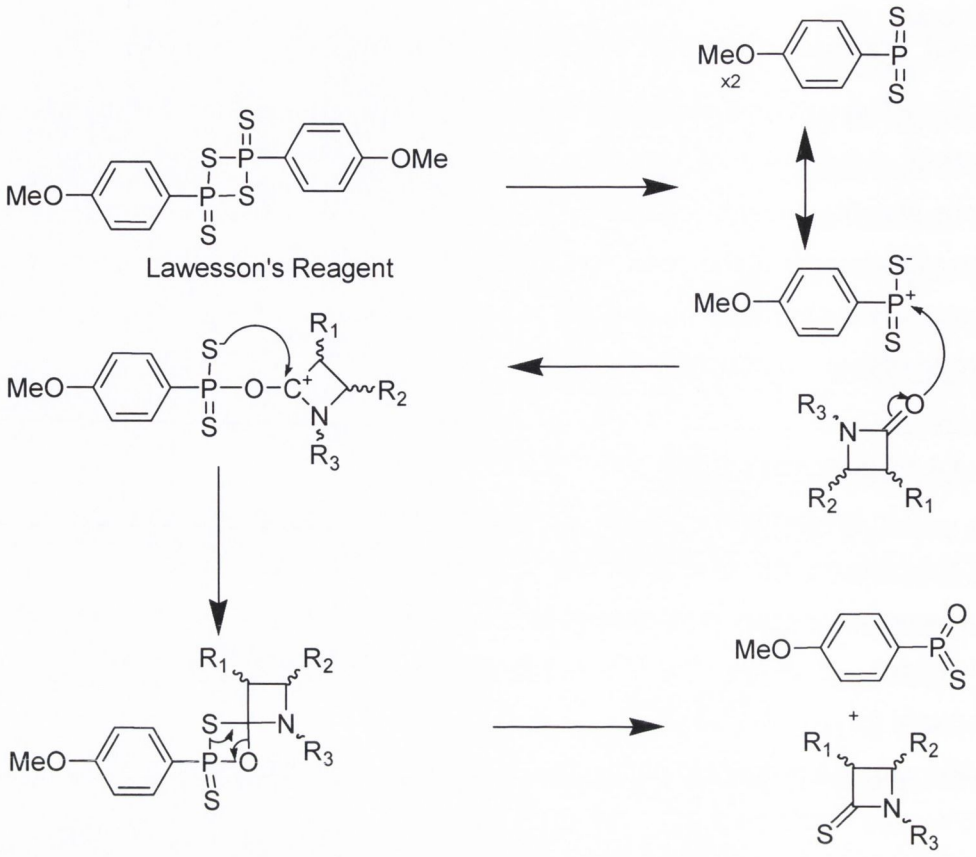

Scheme 2.26 Mechanism for the thionation of the β-lactam carbonyl group by Lawesson's Reagent.

The thionylated product would be expected to have superior stability to nucleophillic hydrolysis than the starting compounds. Cyclic thioamides (**268** & **269**) have found use in the treatment of thyroid disorders by blocking the enzyme thyroid peroxidase (**fig 2.16**). Ethionamide (**270**) has found use for the treatment of TB. Zacharie *et al* [254] used the thioamide group as a replacement for the amide group in the polypeptide **271**. The authors note that the introduction of a thioamide group increases the *in vivo* stability of the compound by removing the degradation pathway of amide cleavage. They also suggest that the replacement of the oxygen atom with the less electronegative sulphur atom may induce conformational changes in the compound, possibly leading to more active compounds.

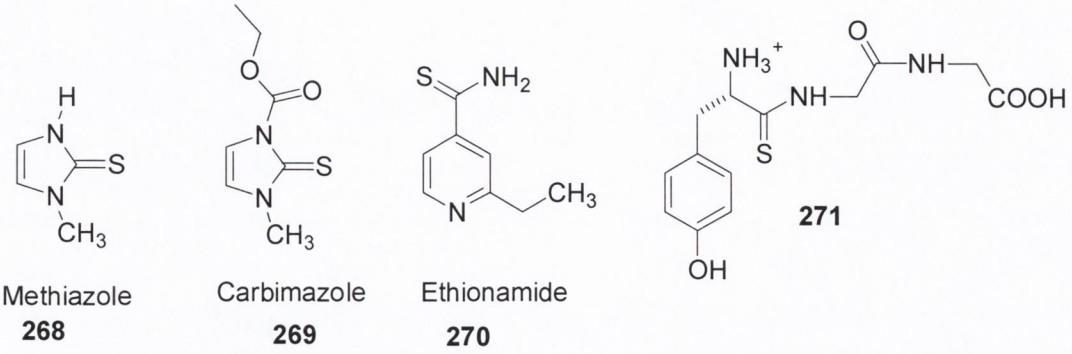

Methiazole **268** Carbimazole **269** Ethionamide **270** **271**

Fig 2.16 Selection of thioamides as medicinal products

2.4.4.2 DIBALH Reduction

The amide bond of the β-lactam is subject to hydrolysis in both acidic and basic media as well as by enzymes such as the β-lactamases. In an effort to increase the stability of the compounds prepared in this thesis the carbonyl group of the β-lactam was reduced to yield an azetidine product. Biochemical evaluation of the azetidine compound should also determine if the carbonyl group has a role to play in activity. Biologically active azetidines have previously been reported[255 256 257], so the azetidine product may display independent biological activity. The carbonyl group in compound **256a** was reduced by reaction with DIBALH to give the resulting azetidine (**272**) in moderate yield (**scheme 2.27**). Purification by column chromatography proved difficult, and only yielded a product approximately 80% pure by HPLC. From IR the reduction of the carbonyl was confirmed from the disappearance of the carbonyl peak at 1739cm^{-1}. The reduction of the carbonyl group can also be confirmed from the ^{1}H NMR spectrum. A series of multiplets integrating for two protons appears at δ4.17ppm and corresponds to the geminal protons of the newly formed CH_2 group. H_3 appears as a series of multiplets shifted slightly upfield to δ5.11 compared to δ5.53ppm in the starting material. The chemical shift for H_4 is also shifted upfield but to a lesser extent from δ5.29ppm in the starting material to δ5.15ppm in the azetidine. H_4 appears as a doublet with a coupling constant of 6.01Hz. The data for azetidine **272** is presented in **table 2.10**. To our knowledge this is the first report use of the azetidine ring as a scaffold for CA4 analogues

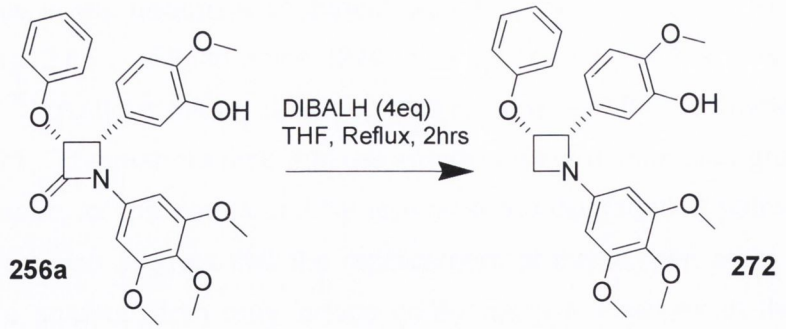

Scheme 2.27 DIBALH reduction of the β-lactam carbonyl functional group

Compound No.	IR (γ_{max} cm^{-1})	MP (°C)	Yield (%)
267	1592, 3336	110	63
272	1508, 1598, 3412	Oil	27

Table 2.10 Yield and spectroscopic data for compounds **267** & **272**

2.4.5 Dearylated Analogues

The presence of the trimethoxy substitution pattern on CA4 is regarded as being crucial to activity[120]. To examine if this structure activity relationship also holds for the newly synthesised β-lactam type analogues, an N-unsubstituted analogue was synthesised (**scheme 2.28**). The classic method for carrying out an N-dearylation for 1,4-diarylated β-lactams is the cerric ammonium nitrate (CAN) dearylation of a *p*-methoxy phenyl group (**scheme 2.29**).

The imine **273** was synthesised by the condensation of *p*-anisidine and isovanillin. The imine was subsequently protected (**274**), and the protected imine used in the synthesis of **275** by the Staundinger reaction. Deprotection of **275** with *t*BAF gave the phenol (**276**). The yield and spectroscopic data for **273** and **276** is presented in **table 2.11**. The dearylation was carried out on **276** according to the procedure laid out by Georg *et al*,[258] however no product (**277**) was recovered. From the ^{1}H spectrum of the crude reaction mixture the starting material had degraded which was surprising since the reaction has been successful on β-lactams bearing other substituents [258 259]. The reaction was also carried out on the protected β-lactam **275** but without success.

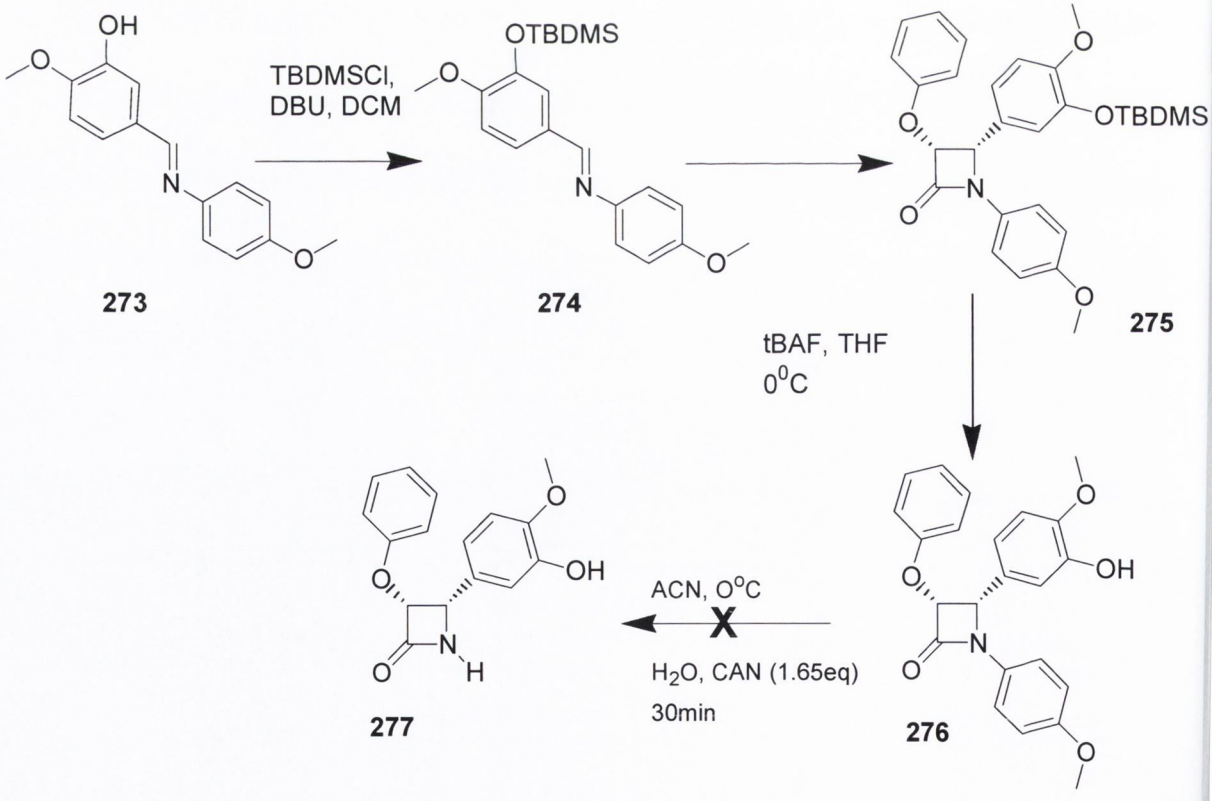

Scheme 2.28 Atempted CAN dearylation of **277**

Compound No.	IR (ν_{max} cm^{-1})	MP (°C)	Yield (%)
273	1576, 3424	112-114	95
276	1743, 3379	136-138	46

Table 2.11 Yield and spectroscopic data for **273** & **276**

Despite the dearylation not being successful, compound **276** is interesting in its own right since it does not contain the 3,4,5-trimethoxy substitution pattern that appears in a number of members of the combretastatin family. Biochemical data for this compound would be useful for proving the necessity of the trimethoxy moiety for antitubulin activity.

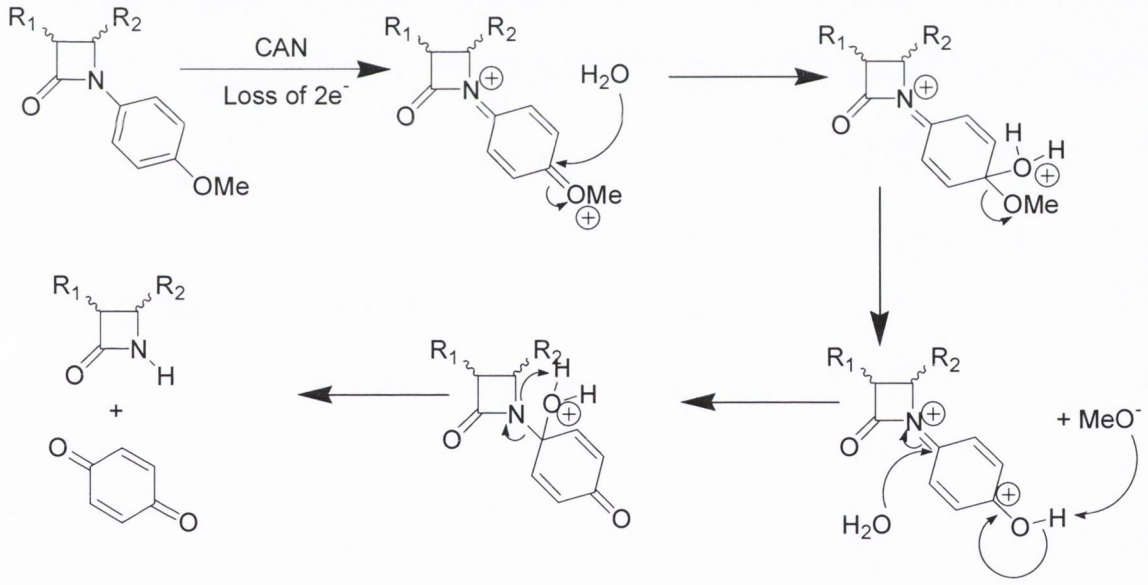

Scheme 2.29 CAN removal of *p*-methoxy phenyl

2.5 Further Optimisation

2.5.1 CA1 Analogues

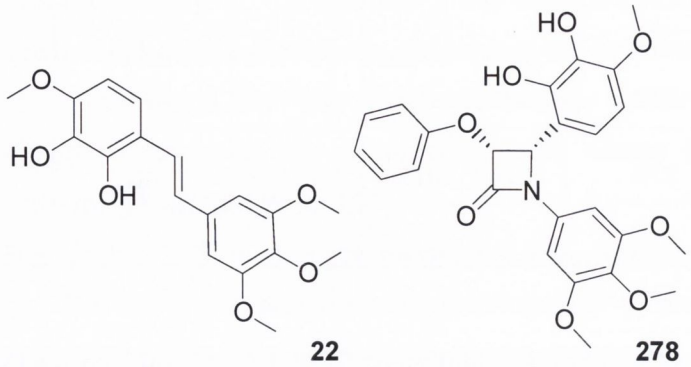

Fig 2.17 CA1 (**22**) and proposed β-lactam analogue **278**

In conjunction with the preparation of analogues based upon the structure of CA4, a CA1 β-lactam containing analogue was also prepared (**278**) (**fig 2.17**). However, difficulty in protecting the diol functionality hindered progress. The desired 2,3-dihydroxy-4-methoxy benzaldehyde **280** was obtained by the BCl_3 demethylation (**scheme 2.30**) of a trimethoxy benzaldehyde (**279**) as described by Kaisalo *et al.*[260] The ^1H NMR spectrum for **280** is depicted in **fig 2.18** and the spectroscopic data is presented in **table 2.12**.

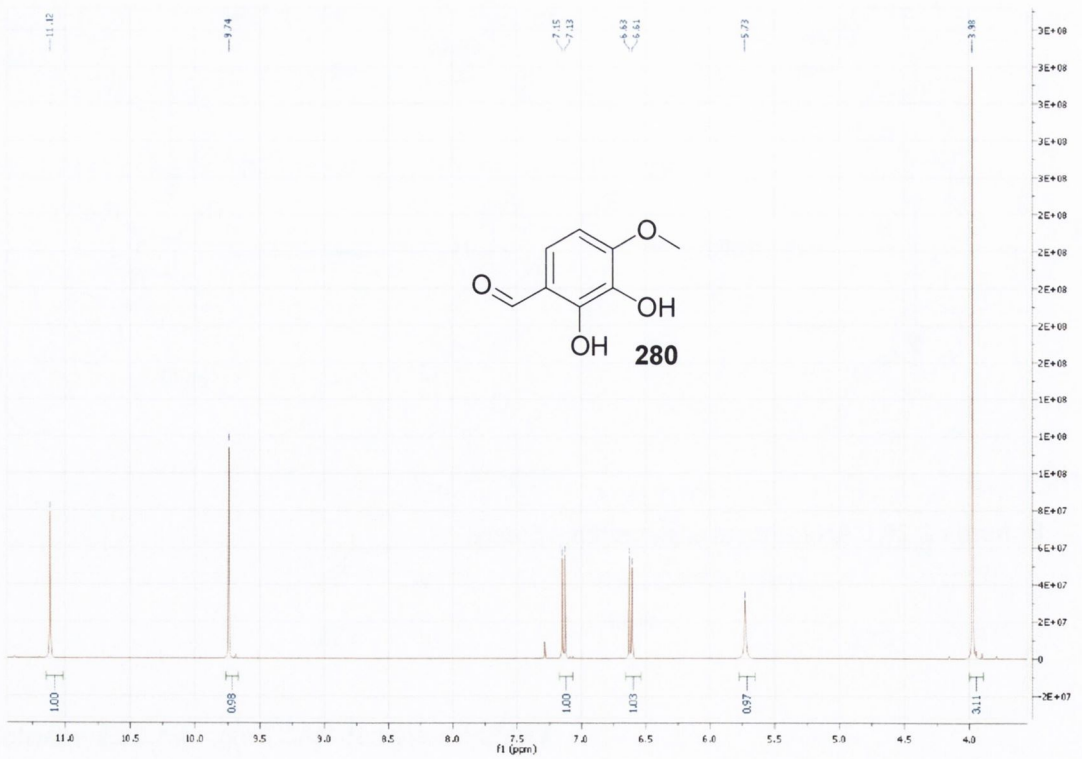

Fig 2.18 ^1H NMR spectrum of **280**

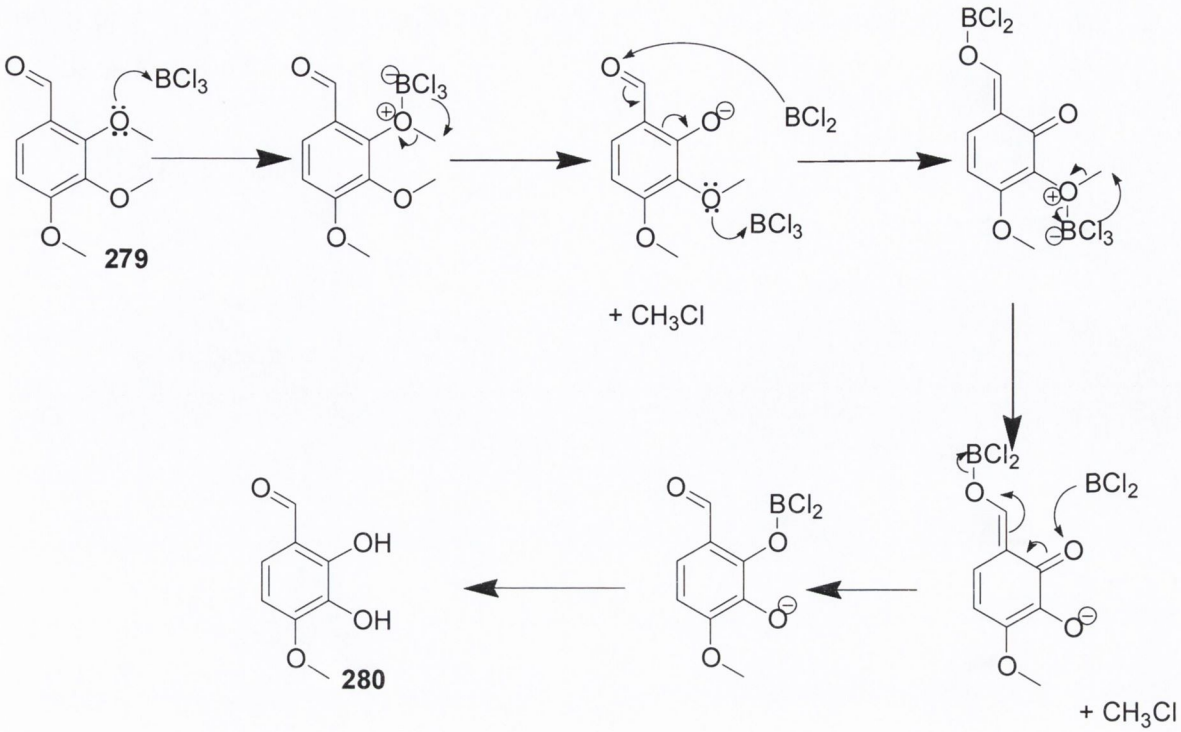

Scheme 2.30 Proposed mechanism for selective BCl_3 demethylation at the 2 and 3 positions

The benzaldehyde (**280**) was reacted with 3,4,5-trimethoxyaniline to form the desired imine **281** in 62% yield (**scheme 2.31**). The imine was treated with tBDMSCl in the presence of DBU in dry DCM as outlined in **Section 2.2.2** but with twice the equivalents of tBDMSCl to form the silyl ether compound. From the ^{1}H NMR spectrum it was apparent that only a single phenol had been successfully protected as a silyl ether leading to the formation of the monoprotected compound (**282**). The position of the silyl ether in the monoprotected imine was determined by inspecting the ^{13}C NMR spectrum, in particular the position of the C_2'' and C_3'' signals in the mono-protected imine versus the phenolic imine (**fig 2.19**). In the phenolic imine C_2'' and C_3'' appear at δ143.10ppm and δ133.04ppm respectively. In the mono-protected product (**282**) the C_2'' signal appears at δ144.34ppm and the C_3'' at δ132.21 indicating that the C_3'' had been protected.

Next the protection step was carried out on the benzaldehyde prior to the imine formation (Route B). Again it was observed that only the phenol at the 3-position was protected (**284**). In effort to drive the reaction to completion the equivalents of tBDMSCl used were once again doubled but without any success. Pettit has carried out the protection of **164** using the same tBDMSCl reagent [261]. Pettit carried out the protection using adding the tBDMSCl into a stirring solution of the benzaldehyde (**280**)

in DMF with diidopropylamine as the base. By applying this procedure to either the benzaldehyde or the imine again only the monoprotected product was obtained.

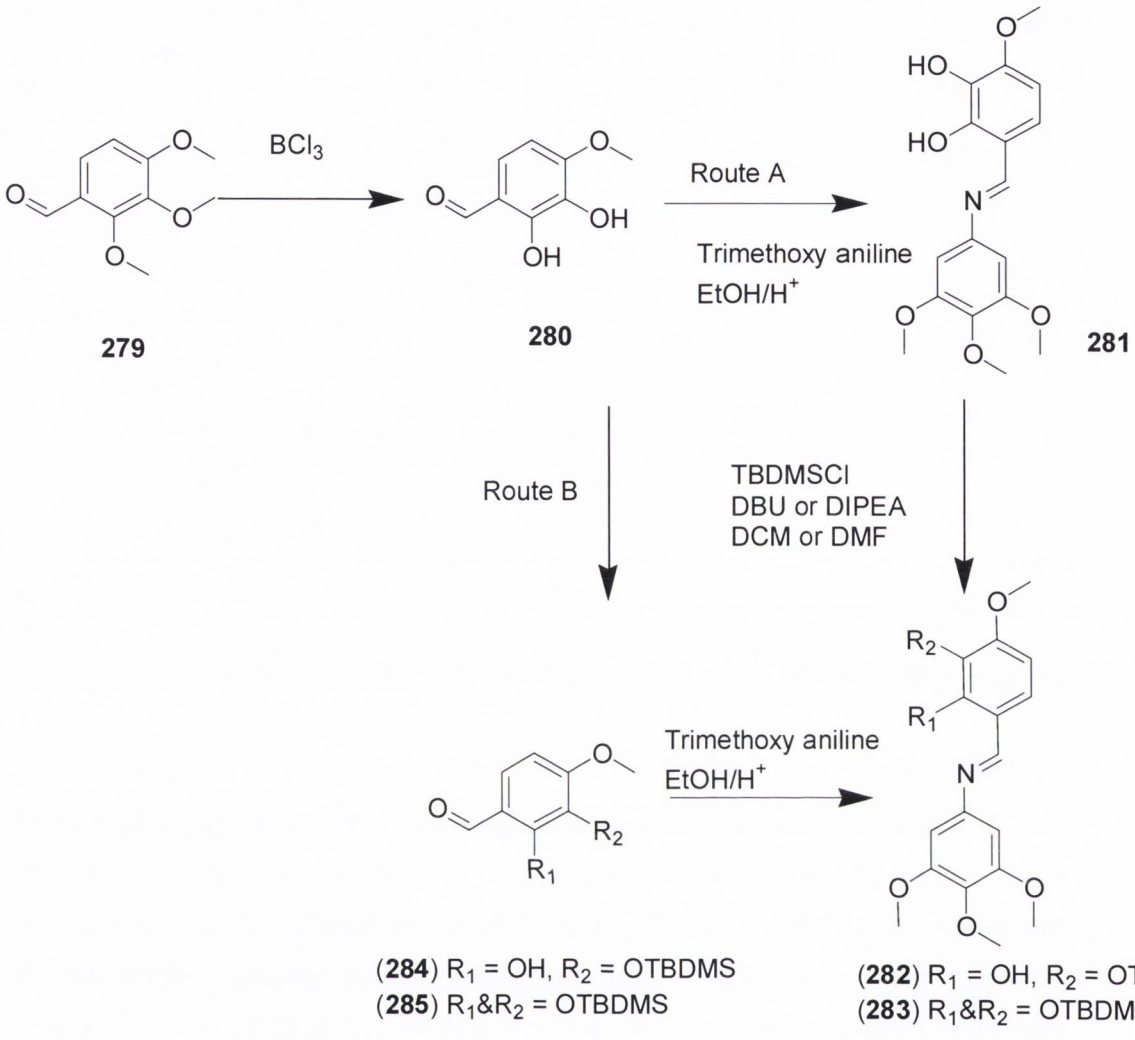

Scheme 2.31 Routes towards the protected imines **282** & **283**

One possible explanation for the silyl ether only being formed for one phenol is the bulkiness of the *t*BDMS group. It is possible that the C_3 phenol is being protected but that the C_2 phenol is prevented from reacting possibly due to steric hindrance from the *t*BDMS group on C_3. This observation led to the attempted protection using the trimethylsilyl (TMS) group on both the benzaldehyde and the imine. Again only the phenol at C_3 was protected successfully (**286** & **287**) (**scheme 2.32**).

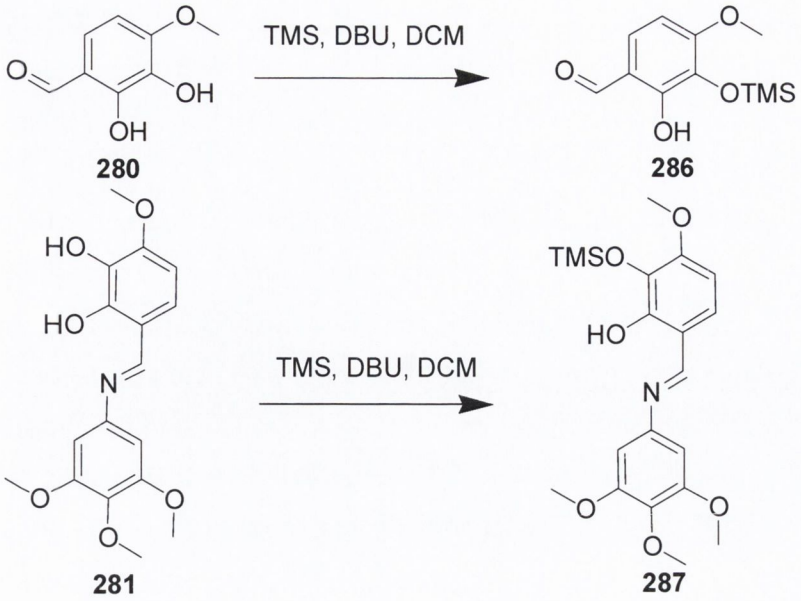

Scheme 2.32 Attempted diol protection using TMS

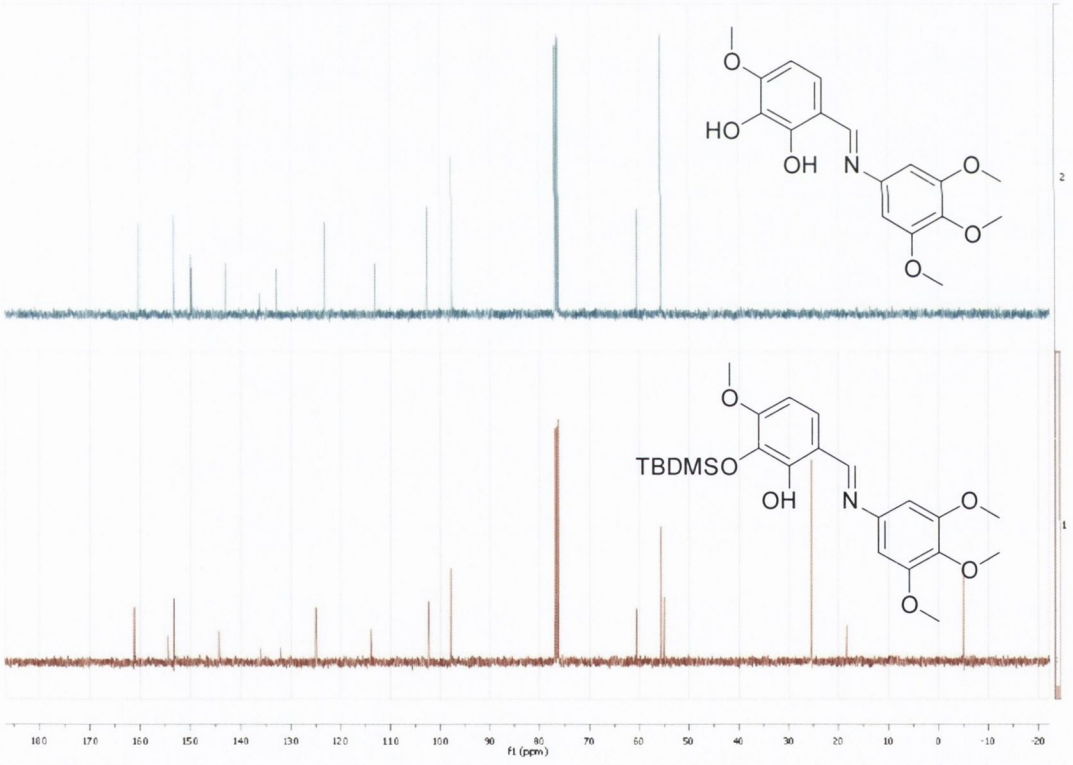

Fig 2.19 Comparison of ^{13}C spectra of **281** & **282**

A number of other functional groups were considered for the diol protection, but the choice is limited by the requirement of having removal conditions in which the β-lactam is stable. Protection with a carbonate or acetal group proved attractive (**scheme 2.33**)[262]. Such cyclic groups are specifically designed for the protection of

diols and both have relatively mild removal conditions. The use of the benzylidene acetal group is particularly attractive since it can be removed by hydrogenolysis, and previous work within our group has demonstrated that the β-lactams are stable under such conditions.

Two methods for the formation of the acetal (**289**) were carried out on the dihydroxy benzaldehyde (**280**). In the first the diol was reacted with benzaldehyde in the presence of $ZnCl_2$, while in the second the diol was reacted with benzaldehyde in DMSO in the presence of H_2SO_4. Both reactions failed. An attempted protection with a cyclic carbonate by the reaction of triphosgene with the diol in DCM in the presence of pyridine to afford **288** was also not successful. Greene notes that higher reaction temperatures are needed to drive the reaction with triphosgene than with phosgene. The failure of the reaction could then be explained by the low reflux temperature of DCM.

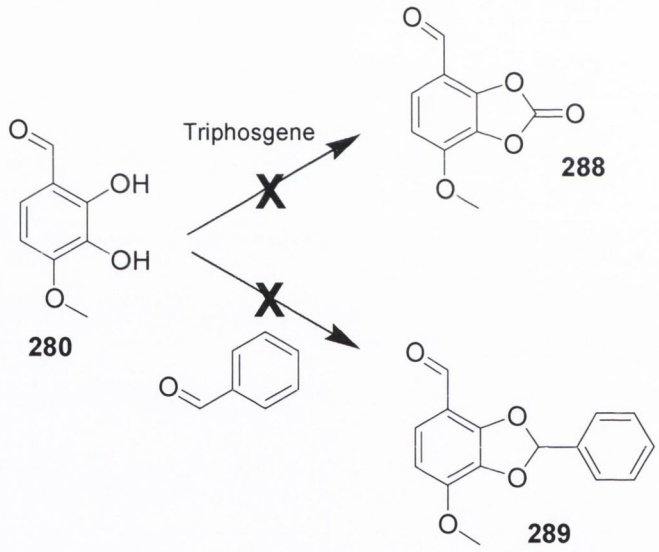

Scheme 2.33 Alternative protecting groups used unsuccessfully

From the difficulty in protecting both phenols it was hoped that the 2-hydroxy group might be sufficiently sterically hindered by the neighbouring tBDMS group to be used in the Staundinger reaction. To this end the Staundinger reaction was carried out on the mono-protected imine (**282**) (**scheme 2.34**). The best outcome for the reaction would be the formation of **290**, where the 2-hydroxy group is protected by default due to steric hindrance from the neighbouring silyl ether. **291** would form in the case where the hydroxy group remains available. While the synthesis of **290** is favoured over **291**,

the ester **291** would still prove useful since the ester may be cleaved to yield the desired CA1 type analogue **278**.

From the ^{1}H NMR of the crude reaction it appeared that a tiny amount (approx. 5% by integration) of β-lactam (**290** or **291**) had formed, although whether it was the free phenol or the ester product was impossible to determine. After subjecting the crude material to column chromatography, none of this material was successfully isolated leading to the conclusion that the material had degraded.

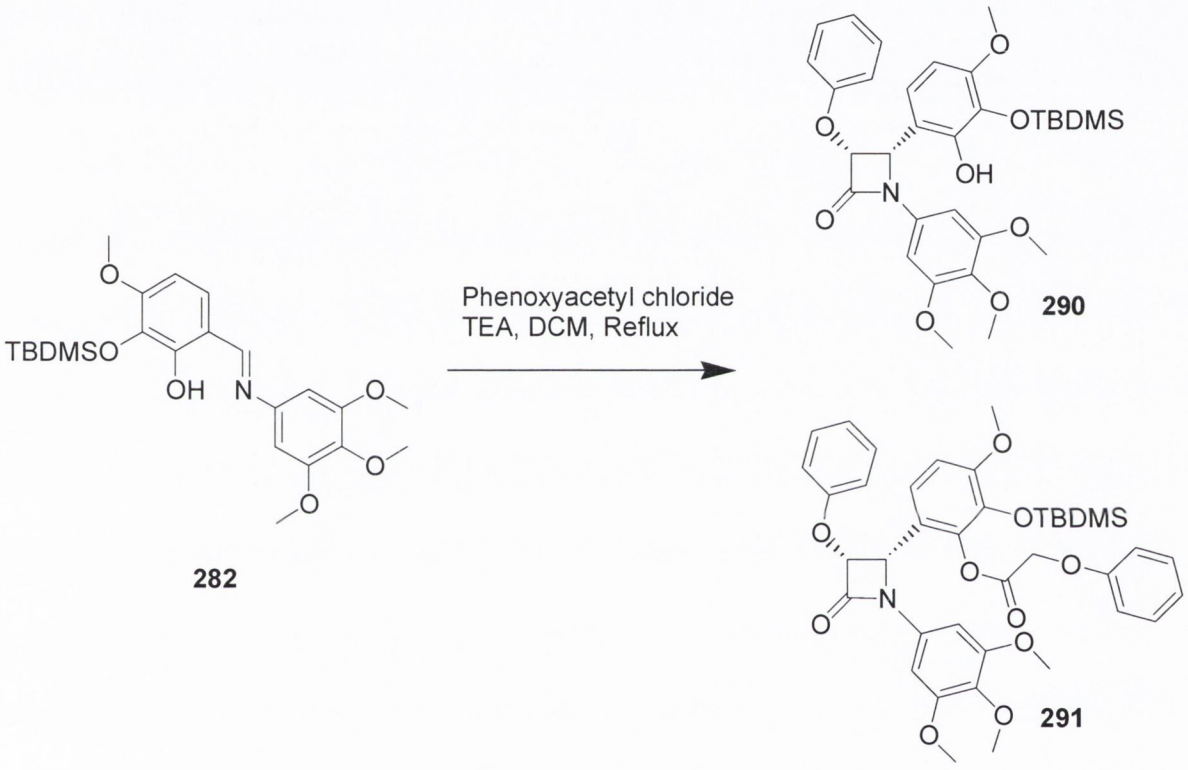

Scheme 2.34 Attempted synthesis of CA1 type β-lactam using the mono-protected imine **282**

Compound No.	IR (ν_{max} cm^{-1})	MP (°C) (Lit.)	Yield (%)
280	1640, 3072	98 (116-117)[263]	67
281	1622, 3270	174	85

Table 2.12 Spectroscopic and yield data for the benzaldehyde (**280**) and the corresponding imine (**281**)

2.5.2 Nitrated Isovanillin Derivatives

Monk *et al* describes a number of stilbene analogues containing amino groups at various positions on the "B" ring of CA4 that possess significant antitubulin activity. To this end in the present work a number of β-lactams were synthesised that incorporate these interesting substitution patterns onto the 4-position of the β-lactam ring. Isovanillin was directly nitrated at the 2 and 6 positions by concentrated nitric acid in acetone to afford products **292** and **293** (**scheme 2.35**). It was observed that the ratio of the two isomers depended both upon the rate of addition of the acid and the reaction temperature. The reaction was optimised to produce both isomers in reasonable amounts (4:1 of 2 isomer: 6 isomer) by the slow addition of the acid at room temperature. It was found that excess of one isomer could be obtained by a selective recrystallisation from hot water, but that it was not possible to completely separate both isomers from one another. Both isomers were converted to the corresponding imines (**294** & **295**) in a one pot reaction. The two resulting imines were separated by recrstallisation followed by conversion to the silyl ether (**296** & **297**).

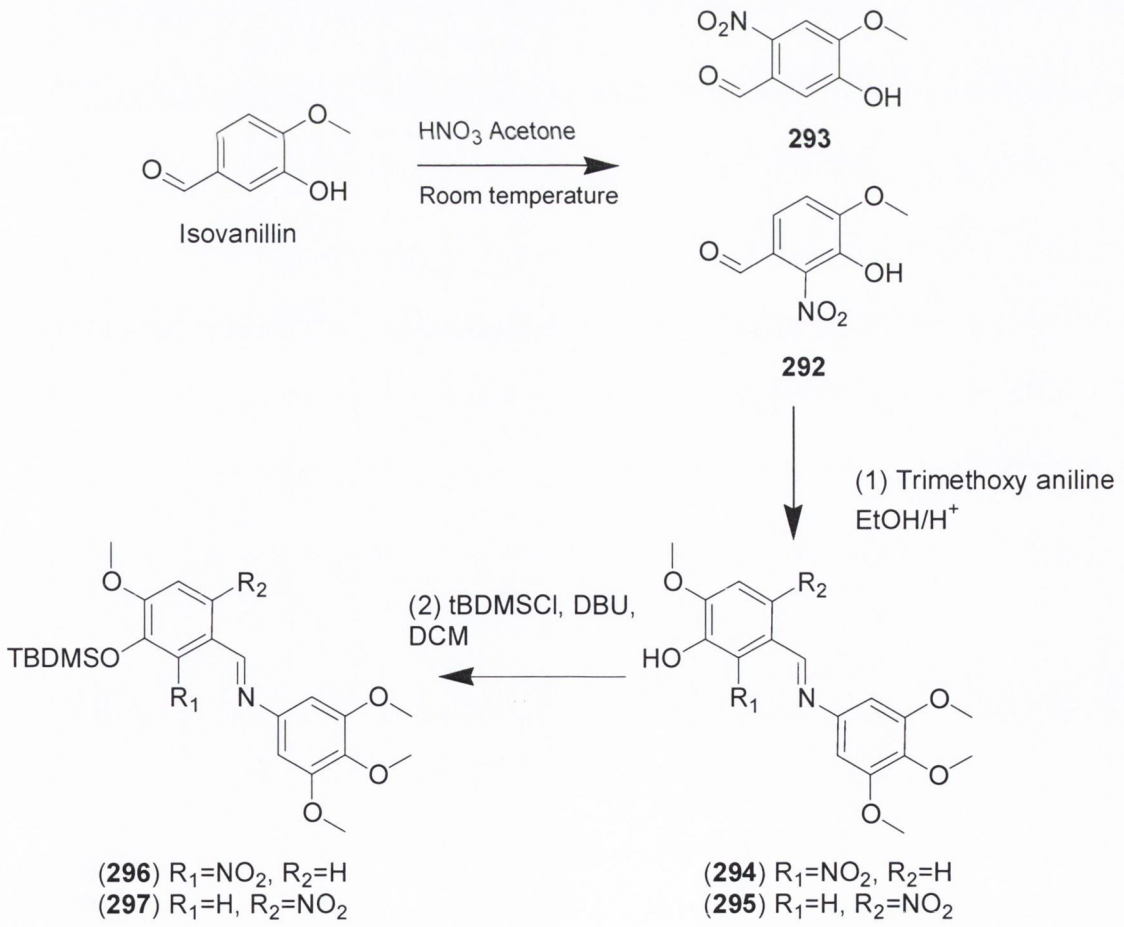

Scheme 2.35 Synthesis of nitrated imines **296** & **297**

The 5-nitro imine (**301**) was obtained in a number of steps as described in **scheme 2.28**. The purpose of the esterification step was to moderate the directing group effect of the hydroxy group by conversion to the ester **298**. The ester (**298**) was nitrated with HNO_3, and the acetate group cleaved with 5% sodium hydroxide to give the 5-nitro benzaldehyde (**300**). The benzaldehyde was converted to the imine (**301**) by condensation with trimethoxy aniline and subsequently the hydroxy group was protected by treatment with tBDMSCl in DCM with DBU to give **302**.

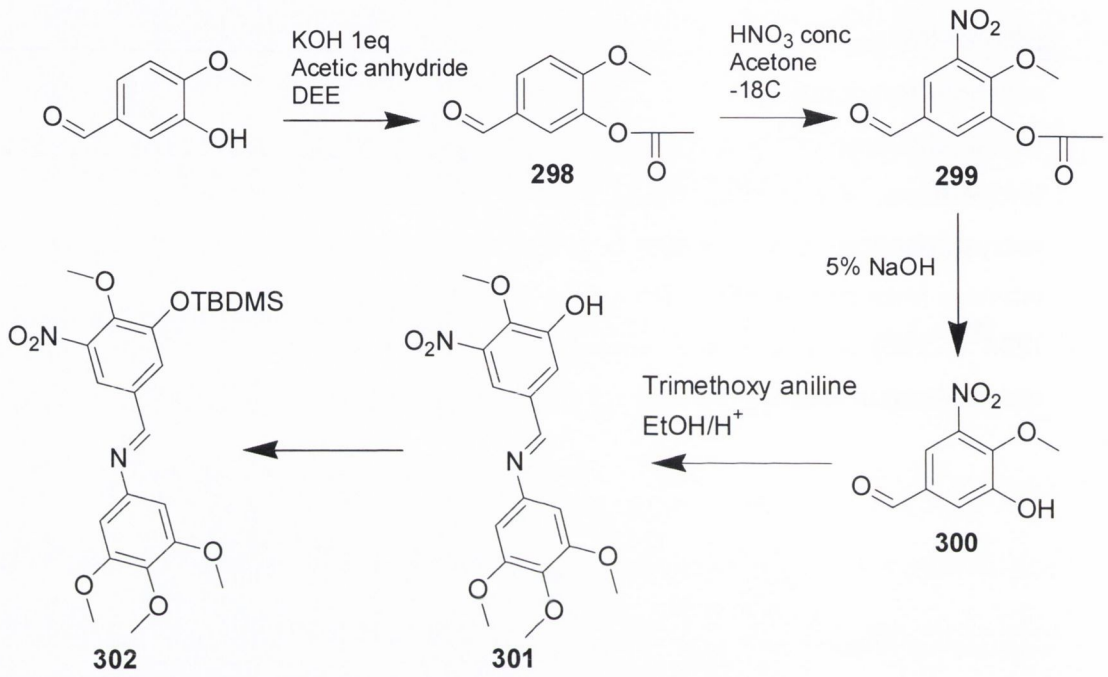

Scheme 2.36 Nitration of isovanillin at the 5-position

The yields, melting points and spectroscopic data for compounds **292-301** are presented in **table 2.13**

Compound No.	IR (γ_{max} cm^{-1})	MP (°C) (Lit. values)	Yield (%)
292	1671, 3326	186 (186-187)[264]	42
293	1694, 3332	142 (165-167)[265]	31
294	1578, 3275	136	23
295	1583, 3428	188	10
298	1684, 1769	73	93
299	1698, 1778	65	82
300	1690, 4415	52-56 (119)[266]	8
301	3420, 1592	105	47

Table 2.13 Yields, melting points and spectroscopic data for **292-301**

From the protected imines (**296, 297, 302**) the corresponding β-lactams (**302-304**) were formed using the same methodology as previously described (**scheme 2.37**). The success of the reaction can be seen for the appearance of the characteristic absorption in the IR spectrum at approximately 1750cm^{-1} from the β-lactam carbonyl. The formation of the β-lactam product is also apparent from the NMR spectra. For example, the 5-nitro compound **304** has two sets of doublets at δ5.36ppm and δ5.61ppm integrating for a single proton each with a coupling constant of 5.04Hz. The signals are assigned to H_4 and H_3 respectively and the coupling constant indicates that it is the *cis* isomer that has been isolated. The methoxy group protons appear as singlets in the area δ3.77-δ3.79 integrating for a total of 12 protons. The broad singlet at δ6.26 was assigned to the hydroxy group. The two equivalent protons H_2' and H_6' appear at δ6.61 as a singlet integrating for two protons. The aromatic protons H_2'' H_6'' and H_4'' appear as multiplets at δ6.82-6.99ppm while the aromatic protons H_2''' H_3'' H_5'' also appear as multiplets at δ7.20-7.30ppm. The aromatic proton H_6''' which is adjacent to the nitro group on the aryl ring appears at δ7.50ppm. The carbons of the β-lactam ring C_4 C_3 appear at δ60.54 and δ80.39ppm while the signal at δ161.96ppm is characteristic of the β-lactam carbonyl. Once the β-lactams were formed and

characterised the nitro groups were reduced by Zn/acetic acid to yield the corresponding amino compounds (**305-307**). The yields melting points and spectroscopic data for these compounds is presented in **table 2.14**.

The success of the reduction of **304** to **307** was apparent from the NMR spectra. The signals for H_4 and H_3 have shifted from δ5.36ppm and δ5.61ppm to δ5.17ppm and δ5.52ppm. The *cis* orientation remained intact as evidenced from the coupling constant of 5.3Hz observed for both sets of douoblets. The reduction of the nitro group to the amino group causes the shift of the H_6''' signal from δ7.50ppm to δ6.39ppm. The H_2''' signal appears at δ6.43ppm and is meta coupled to the H_6''' proton. In the ^{13}C spectrum the C_4 and C_3 signals have shifted from δ60.54ppm and δ80.39ppm to δ60.18ppm and 80.02ppm and the C_6''' has shifted from δ116.09ppm to δ106.98ppm.

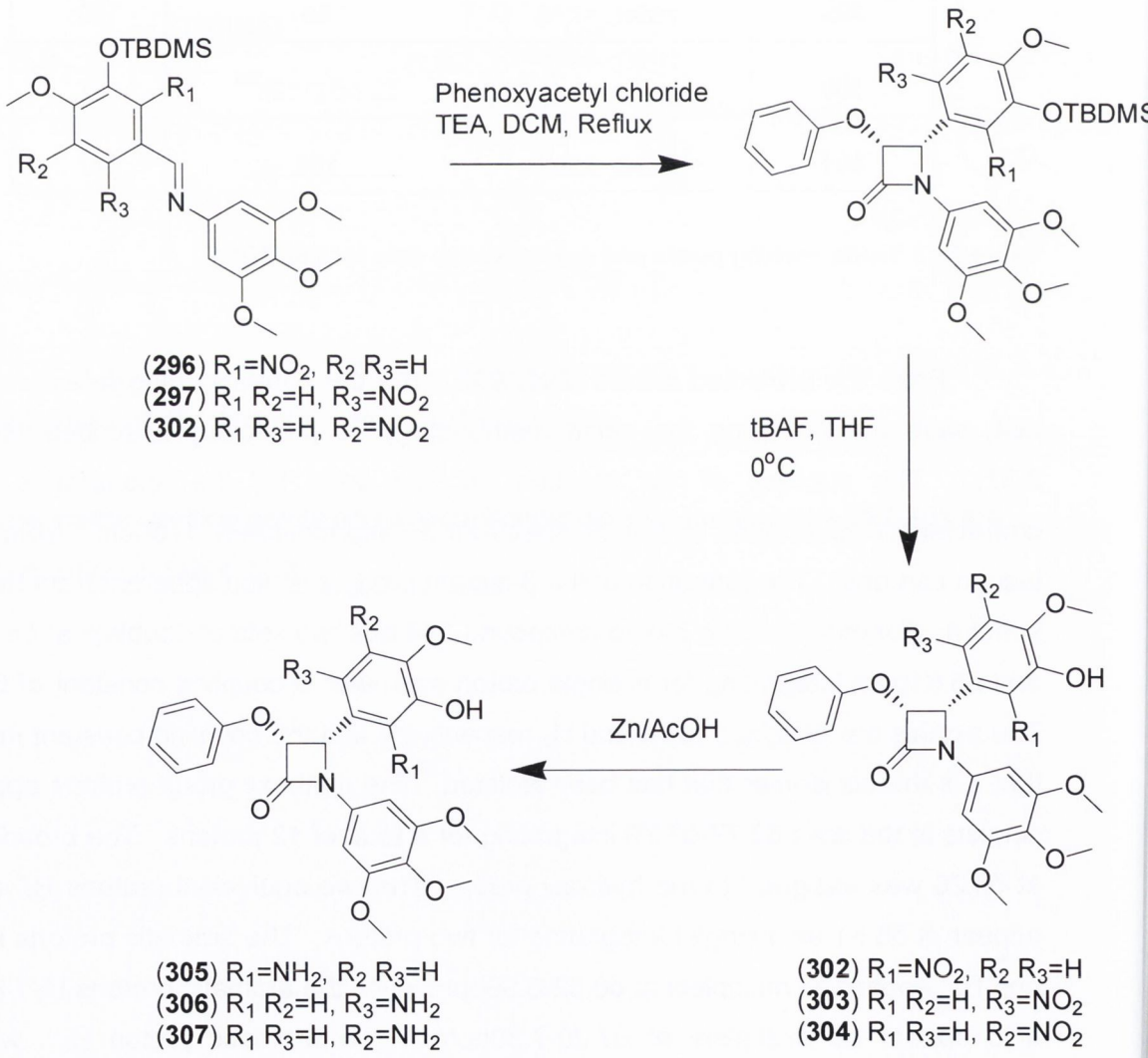

Scheme 2.37 Synthesis of N-containing β-lactams

Compound No.				IR (ν_{max} cm^{-1})	MP (°C)	Yield (%)
	R1	R2	R3			
302	NO_2	H	H	1748, 3274	136	22
303	H	H	NO_2	1757, 3355	188	23
304	H	NO_2	H	1756, 3355	105	39
305	NH_2	H	H	1756, 3359	188	88
306	H	H	NH_2	1756, 3447	210	73
307	H	NH_2	H	1752, 3468	182	91

Table 2.14 Yields, melting points and spectroscopic data for N-containing β-lactams **302** to **307**

2.5.3 Azide Derivatives

The aryl azide group is one of the most commonly employed groups for use as a photoaffinity probe[267]. Spletstoser *et al* describes the use of an aryl azide β-lactam (**308**) to incorporate a photolabel into paclitaxel.[267] Pinney *et al* outlines the incorporation of an azide onto the "B" ring of CA4 instead of the 3-hydroxy and 4-methoxy groups (e.g. **309 310**) (**fig 2.20**).[268] Both groups note that the ideal photolabel should be able to be incorporated into the molecule without affecting the biochemical activity of the molecule of interest. Pinney notes that **310** possesses a similar level of antiproliferative activity compared to that of CA4 thereby making it an ideal photoaffinity probe.

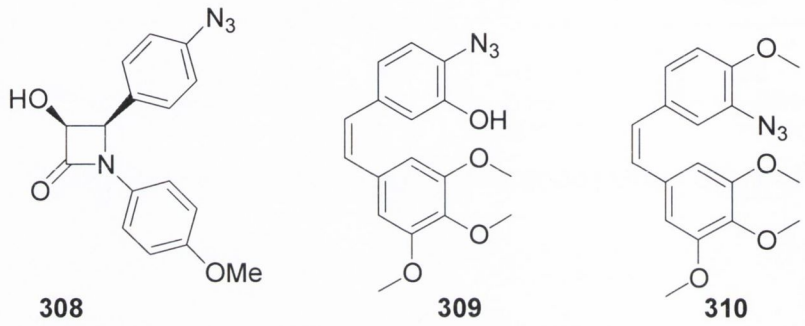

308 **309** **310**

Figure 2.20 Possible aryl azide photoaffinity probes

The azide photolabel (**311**) is activated by irradiation at 280nm which converts the azide to a reactive nitrene compound (**312**). The nitrene compound undergoes ring expansion to the ketenimine compound (**313**) which can react with nucleophiles such as hydroxy and amino groups on nearby residues (**fig 2.21**). The nature of nearby residues has been shown to be a factor in the effectiveness of aryl azide photolabels. Scharz has shown that cysteine residues in particular are strongly favoured by the aryl azide photolabel[269].

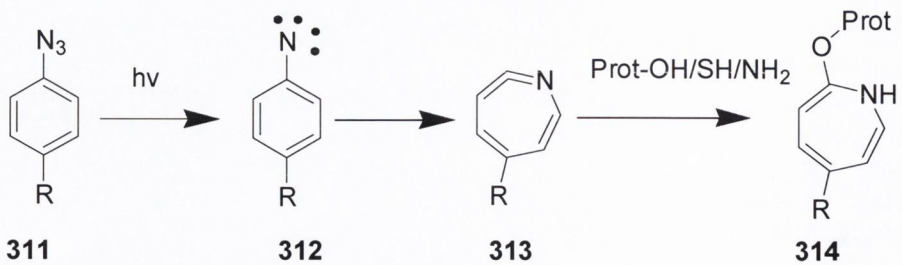

311 **312** **313** **314**

Fig 2.21 Photoactivation of arylazide photolabel

In the present work, initial efforts concentrated on introducing an azide at the 3-position alongside the 4-methoxy of ring B to form a β-lactam analogue similar to **309** & **310**. Both Spletstoser and Pinney make use of the transformation of an amine to an azide using NaN_3 [105]. It is unlikely that an amino β-lactam would prove amenable to such a transformation so the azide functionality was put in place on the benzaldehyde prior to the formation of the β-lactam ring. Spletstoser describes the formation of a 4-azidobenzaldehyde (**317**) to serve as a suitable starting material to form the desired 4-azido imine (**318**). The benzyl alcohol (**315**) was converted to the corresponding diazo compound and the diazo group displaced by treatment with sodium azide to give alcohol (**319**). The alcohol was oxidised using PCC to the aldehyde (**317**) from which the imine (**318**) was formed by condensation with 3,4,5-trimethoxyaniline. The corresponding β-lactam (**319**) was successfully formed from this imine (**scheme 2.38**). The same methodology was applied in the attempted synthesis of a 3-azido-4-methoxy benzaldehyde but without success.

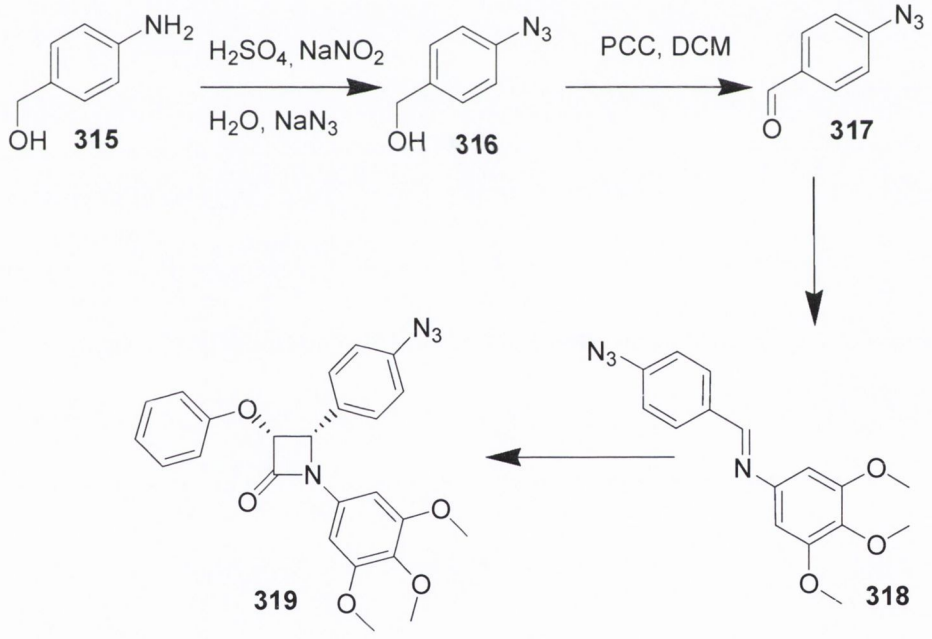

Scheme 2.38 Formation of 4-azido β-lactam

Compound No.	IR (ν_{max} cm^{-1})	Yield (%)
316	2117, 3321	90
317	1694, 2110	78
318	1584, 2120	18
319	1761, 2136	64

Table 2.15 Yield and spectroscopic data for azide compounds **316-319**

Table 2.15 presents the spectroscopic data for compounds **316-319**. The presence of the azide group in these compounds is clear from the absorption observed around 2100cm^{-1}. The ^1H NMR spectrum of **319** showed that only the *cis* product was formed with H_3 appearing at δ5.58ppm and H_4 appearing at δ5.37ppm both with a coupling constant of 4.80Hz. The methoxy groups appear as two singlets at δ3.75ppm and δ3.80ppm integrating for a total of nine hydrogens. H_2' and H_6' appear as a singlet at δ6.61ppm integrating for two hydrogens. H_2'' and H_6'' appear as a doublet with a coupling constant of 7.86Hz at δ6.82. H_4'', H_3''' and H_5''' appear as multiplets integrating for a total of three hydrogens centred on δ6.97ppm. H_3'' and H_5'' appear as a triplet with coupling constants of 8.38Hz and 8.85Hz at δ7.20ppm. H_2''' and H_6''' appear as a doublet at δ7.40ppm with a coupling constant of 8.23Hz

2.5.4 An investigation of the aryl substitution at the 3 and 4-positions

The initial screen for biochemical activity of the β-lactam analogues synthesised thus far indentified two promising substitution patterns of the aromatic ring (**fig 2.22**). In an effort to identify a possible structure activity relationship for these promising compounds, a number of further analogues were synthesised. The most obvious question raised is if either the methoxy, hydroxy, or amino groups on their own are responsible for the biochemical activity of the compounds, or if it is the combination of substituents which are required (**fig 2.22**).

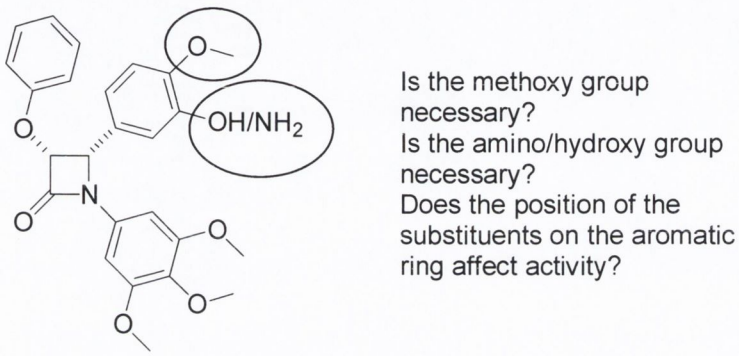

Fig 2.22 Investigating the role of the substituted aryl ring at C_4

The 4-methoxy group in ring B is regarded as being an essential structural feature in CA4. Compounds **245a** and **245b** containing only the 4-methoxy group on the aryl ring at C_4 have already been synthesised earlier in this thesis **section 2.3.5** and should demonstrate if the 4-methoxy group on its own is responsible for activity. To investigate the role of the substituent at the 3-position, **324** and **327** were synthesised containing only the hydroxy or amino group without the 4-methoxy. These compounds should establish if biochemical activity is dependent only on the substituents at the 3-position. Compounds **328** and **329** in combination with the previously synthesised **257** should examine the effect of switching the position of the substituent on biochemical activity.

The imines **320-323** were easily obtained in excellent yields from the condensation of the appropriate benzaldehyde and 3,4,5-trimethoxy aniline. The imine products all displayed the characteristic absorption at approx. 1590cm^{-1} for the C=N bond and displayed a signal for the imine proton at δ8.30ppm in the ^1H NMR spectrum. In the cases where a hydroxy group was present, a protection with tBDMSCl was carried out and the resulting silyl ether was used in the Staundinger reaction without further purification. The silyl ether was cleaved using tBAF in THF at 0°C to give the phenol product. The β-lactams were all obtained in reasonable yields, but only the *cis* isomer was produced (**scheme 2.39**). In keeping with previous observations the H_4

and H_3 signals appear as doublets in the ^1H NMR spectrum with coupling constants characteristic of the *cis* isomer. The reduction of the nitro to the amino group was apparent from both IR and ^1H NMR spectroscopy. In the IR spectrum the characteristic absorption for the amino group is observed in the region of 3360cm^{-1}. In the ^1H spectrum a shift upfield is observed for the H_4 and H_3 protons of the β-lactam ring, in keeping with previous observations for this transformation in this thesis

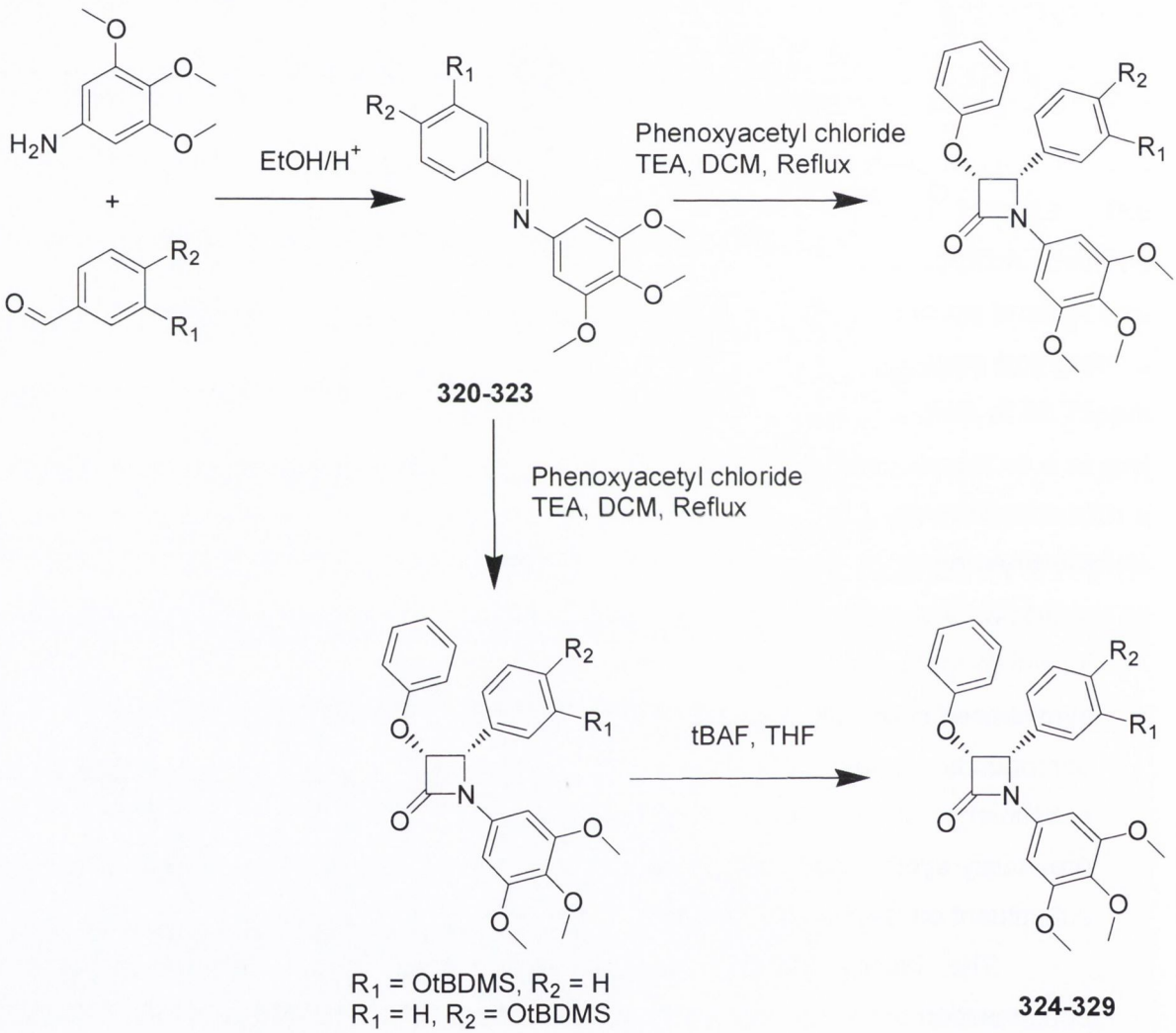

Scheme 2.39 Synthesis of β-lactams **324-329**

The reduction of the nitro compounds to the amino compounds was successfully carried out using zinc in acetic acid and resulted in the amino compounds being isolated in high yields (**scheme 2.40**). The yields, melting points and spectroscopic data for compounds **320-329** are presented in **table 2.16**.

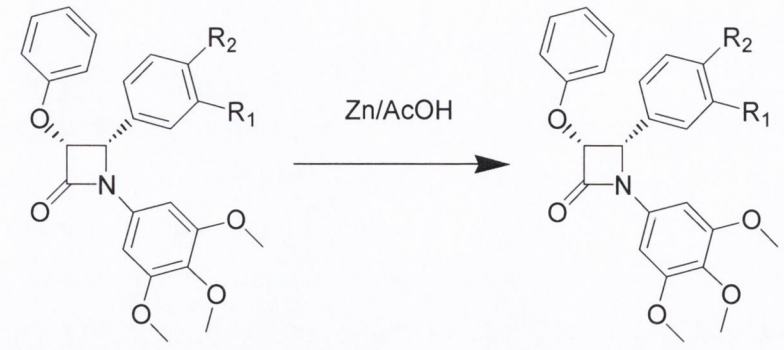

R_1 = H R_2 = NO_2
R_1 = NO_2, R_2 = H

325-326

R_1 = H R_2 = NH_2
R_1 = NH_2, R_2 = H

327-328

Scheme 2.40 Reduction of nitro containing β-lactams to amino β-lactams (**327-329**)

Compound No.	R_1	R_2	IR (ν_{max} cm^{-1})	MP (°C) (Lit values)	Yield (%)
320	**OH**	**H**	1583, 3327	121 (88.8-89.2)[270]	73
321	**NO_2**	**H**	1588	160	93
322	**H**	**NO_2**	1587	158	91
323	**OMe**	**H**	1587	59	88
324	**OH**	**H**	1749, 3380	218-220	43
325	**NO_2**	**H**	1762	170-174	47
326	**H**	**NO_2**	1765	154	39
327	**NH_2**	**H**	1752, 3453	184	87
328	**H**	**NH_2**	1753, 3362	172	79
329	**OMe**	**H**	1749	158	34

Table 2.16 Yields, melting points, and spectroscopic data for imines (**320-323**) and β-lactams **324** to **329**

Conclusions

Chapter 2 presents the synthesis β-lactam containing CA4 analogues. In particular the focus of the chapter was to obtain a series of compounds with the aim of identifying the most promising substitution pattern for the aryl ring at the C_4 position of the β-lactam ring. These compounds were accessed through the Staundinger reaction in reasonable yields and with the *cis* isomer being favoured in all cases. The Staundinger reaction was carried out both by microwave and thermal heating, with the thermal heating method being selected as the favoured method for use in this thesis. Compounds **244-255** are comprised of promising substitution patterns identified from literature. Compounds **256-259** all bear hydroxy substituents on the C_3 aryl ring. Compound **256** is particularly important since it is the direct analogue of CA4. Subsequent to the formation of the β-lactam ring, a number of chemical transformations were carried out on the β-lactam compounds. Notably the reduction of the nitro compound **251** yielded the amino compound **264** which is of interest since a number of amino containing CA4 analogues have displayed exceptional biochemical activity. In an attempt to elucidate the role of the carbonyl group in the biochemical activity of these compounds, the carbonyl group was reduced to yield the corresponding azetidine, and Lawesson's reagent was used for the conversion of the carbonyl to a thione group. Compound **275** was prepared in an effort to access the N-unsubstituted β-lactam **277**, however the dearylation reaction was not successful. Likewise the synthesis of the CA1 analogue **278** was not successful due to difficulty in protecting the diol starting material as a silyl ether. Compounds **302-307** were successfully synthesised and may display similar biochemical activity to the analogous CA4 analogues previously reported. In particular **305-307** are of interest since they contain both hydroxy and amino groups, the presence of which appears to lead to potent compounds such as **256** and **264**. The azide containing compound **319** was synthesised in an attempt to form a photoaffininty probe, but the azide group may also confer biochemical activity on the β-lactam compound in its own right. Compounds **324-329** were synthesised to investigate the positioning of hydroxy, methoxy, and amino substituents on the C_3 aryl ring of the β-lactam.

Chapter 3

Optimisation of the C_3 position of the β-lactam ring for CA4 Analogues

3.1 Introduction

In Chapter 2 the optimisation of the substituents attached to the β-lactam ring at the C_2 and C_4 positions have been discussed. Arising from the biochemical evaluation of these compounds, two promising substitution patterns for the 4-position were identified (**256** & **264**) (**fig 3.1**). It was also observed that the β-lactam carbonyl group at the 2-position appeared necessary for activity and that the *trans* arrangement of the aryl substituents at C_3, C_4 was more active than the *cis* arrangement. Throughout the work discussed in Chapter 2, the phenoxy substituent at C_3 remained unchanged. Having identified two promising substitution patterns for the aryl ring at C_4, the developments discussed in Chapter 3 concentrate on the synthesis of a series of compounds modified at the 3-position in an effort to further optimise biochemical activity. Initially the Staundinger reaction was modified to incorporate a number of possible substituent patterns at C_3. From biochemical evaluation of these compounds, the importance of the substituent at C_3 in modulating biochemical activity became apparent. In an effort to introduce further structural diversity at C_3, a number of analogues were designed which could be synthesised by aldol type addition reaction to C_3 of unsubstituted β-lactams. Further chemical transformations were carried out on the most promising structures identified from biochemical evaluation.

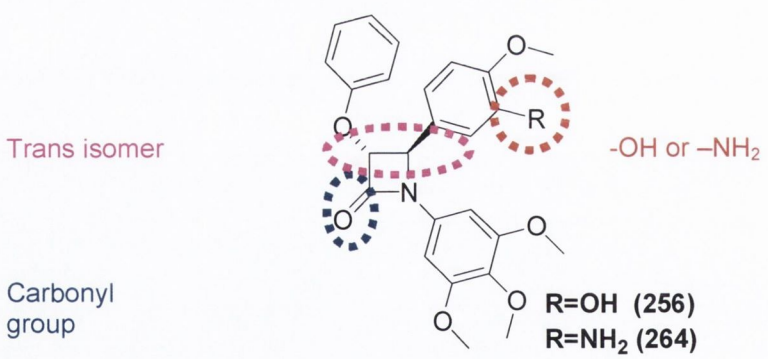

Fig 3.1 Summary of the structural features identified for compounds **256** and **264** in Chapter 2 as being necessary for activity

3.2.1 Modification of the Staundinger Reaction

Evidence that the aryl substituent at the C_3 position has an important role in activity is evident from previous work by Sun.[162] although only three examples of C_3 substitution are given (**330-332**) (**table 3.1**). Interestingly, all of the β-lactams examined by Sun had the *cis* arrangement, and were formed by the Staundinger reaction. Compounds **330-332** also all contain an oxygen atom adjacent to C_3.

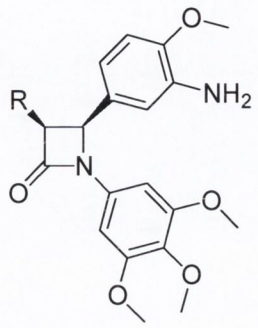

Compound No.	R	Cytotoxicity (IC_{50} nM) in selected cell lines			
		IMR32	NCI-H69	MCF7	CHO-K
330	$OCOCH_3$	73	41	200	509
331	OH	37	25	81	411
332	OMe	>1000	nd	nd	nd

Table 3.1 Effect of β-lactam substituent at the 3-position upon cytotoxicity in selected cell lines

The most obvious means of increasing structural diversity at the C_3 position is provided by changing the nature of the ketene used in the Staundinger reaction. The ease with which these modifications can be made on the β-lactam ring is one major advantage that the β-lactam ring has over other heterocycles that are used as combretastatin scaffolds. In the present work a panel of β-lactam analogues were synthesised using commercially available acids or acid chlorides in a Staundinger reaction or modified Staundinger reaction. It was decided to initially to synthesise β-lactams containing C_4 aryl groups with hydroxy rather than amino compounds for the basis of this library, due to the difficulty encountered earlier in purifiying the amino compounds.

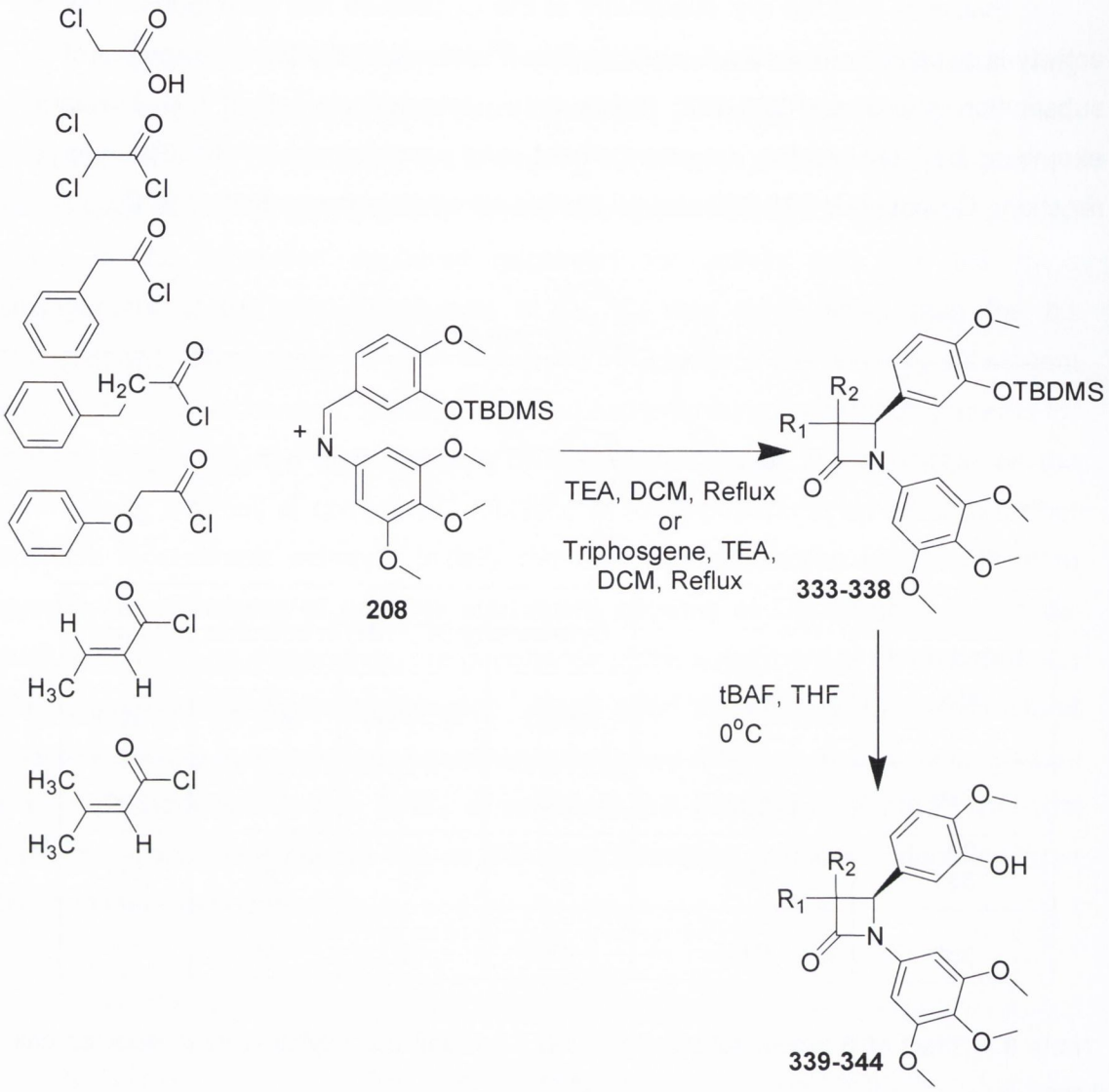

Scheme 3.1 Synthesis of β-lactams **339-344** with varying C_3 substituents via the Staundinger reaction

Scheme 3.1 presents the synthesis of β-lactam analogues (**339-344**) from appropriate acids/acid chlorides. The typical procedure involved the dropwise addition of a solution of acid chloride to a refluxing solution of imine (**208**) and TEA in DCM. Where appropriate triphosgene was used as an acid activating agent as previously described in Chapter 2. The resulting silyl ether β-lactams (**333-338**) were deprotected by treatment with *t*BAF to yield the phenolic β-lactams (**339-334**). The yields and spectroscopic data are presented in **table 3.2**. The products **229-344** contain C_3 substituents that may be confer increased antiproliferative properties on the compounds. They represent a new type of β-lactam containing CA4 analogues

different from the oxygen containing analogues previously reported. Previous work within our group has shown that **341** displays excellent antiproliferative properties and that the C_3 substituent plays an important role in biochemical activity.[203]

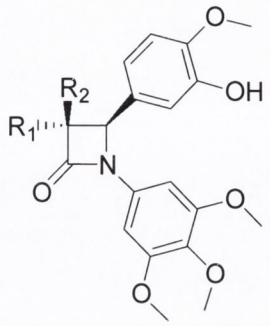

Compound No.	Structure		IR	Yield (%)	Isomer
	R_1	R_2			
339	Cl	H	1770, 3417	34	*Trans*
340	Cl	Cl	1777, 3420	28	*Trans*
341		H	1746, 3418	22	*Trans*
342	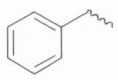	H	1744, 2938, 3346	36	*Trans*
343		H	1732, 3084, 3408	18	*Trans*
344		H	1717, 3197, 3532	22	*Trans*

Table 3.2 IR, melting point and yield data for 3-substituent analogues

All of the analogues were formed using the acid chloride route except **339** which used the triphosgene acid activation route. Interestingly only the *trans* isomer was observed in each reaction which is in complete contrast with the 3:1 *cis*:*trans* mixture observed for **256** where phenoxyacetyl chloride was used. Clearly since the other reaction conditions remained the same, the different stereochemical outcome must be down to ketene effects. Georg [271] has noted that the stereochemical

outcome of the reaction correlates well with the steric demands of the ketene in the zwitterionic intermediate and so has classified ketenes into three distinct groups based upon the steric demands of the ketene substituents. Ketenes with small groups attached form the Bose-Evans group, those with medium sized groups make up the Sheehan group, and finally those with the largest substituents form the Moore ketenes. Each group tends to favour a particular stereochemical outcome in the Staundinger reaction. Bose-Evans ketenes such as formed from phenoxyacetyl chloride tend to favour the production of the *cis* isomer with both dialkyl and diaryl imines[272]. This is in good agreement with the results presented in Chapter 2 for the formation of **256**. The Sheehan ketenes such as formed from crotonyl chloride tend to favour *cis* products when reacted with alkylaryl imines and *trans* products when reacted with diaryl imines[273 274]. Again this is in good agreement with the outcome observed in this thesis for the synthesis of **343** and **344**. Finally the Moore ketenes such as the mono chloro ketene tend to favour *trans* products[272 276] in keeping with the outcomes for **339** & **340**. Jiao[277] et al suggest that the electronic effects of substituents attached to the ketene may play a role in the stereochemical outcome. Jiao notes that the Bose-Evans ketenes contain good electron donating groups, while the Moore ketene contain either weak electron donating groups or electron withdrawing groups. The Sheehan ketenes lie in the middle of these two extremes possibly explaining why the Sheehan ketenes can favour both outcomes in the reaction while the Bose-Evans or Moore ketenes only favour the *cis* and *trans* products respectively.

When evaluated for biochemical activity, the vinyl substituted compound **343** displayed exceptional activity against the MCF7 cell line. For this reason the isopropyl compound **344** was synthesised to investigate if the proton attached to C_5 was amenable to further transformation. The structural assignment of **344** was ambiguous from just the ^1H NMR and ^{13}C NMR spectra (**fig 3.2**) particularly for the assignment of H_3, H_4 and the CH_2 groups, so a HSQC experiment was carried out (**fig 3.3**). The methyl group at C_7 appears as a singlet at δ1.88ppm. The signals at δ3.72 and δ4.72 were assigned to the H_3 and H_4 protons with the H_3 signal overlapping with the signals from the methoxy group. The *trans* stereochemistry of these protons was apparent from the coupling constant of 1.68Hz observed. The corresponding C_3 and C_4 carbons appear at δ60.33 and δ66.83 respectively and are shown to belong to a CH group by the DEPT experiment. The geminal protons of the CH_2 group appear in the ^1H spectrum at δ5.01 and δ5.08 and this carbon appears as a negative signal in the DEPT 90 spectrum at δ114.27ppm. The methoxy groups all appear as singlets in the region δ3.7-δ3.9 integrating for a total of 12 protons. In the

aromatic region there are three signals integrating for 5 protons arising from H_2', H_6', H_2'', H_5'', and H_6''. The broad singlet at δ5.79 has no corresponding carbon signal in the HSQC spectrum and so can be assigned to the hydroxy group.

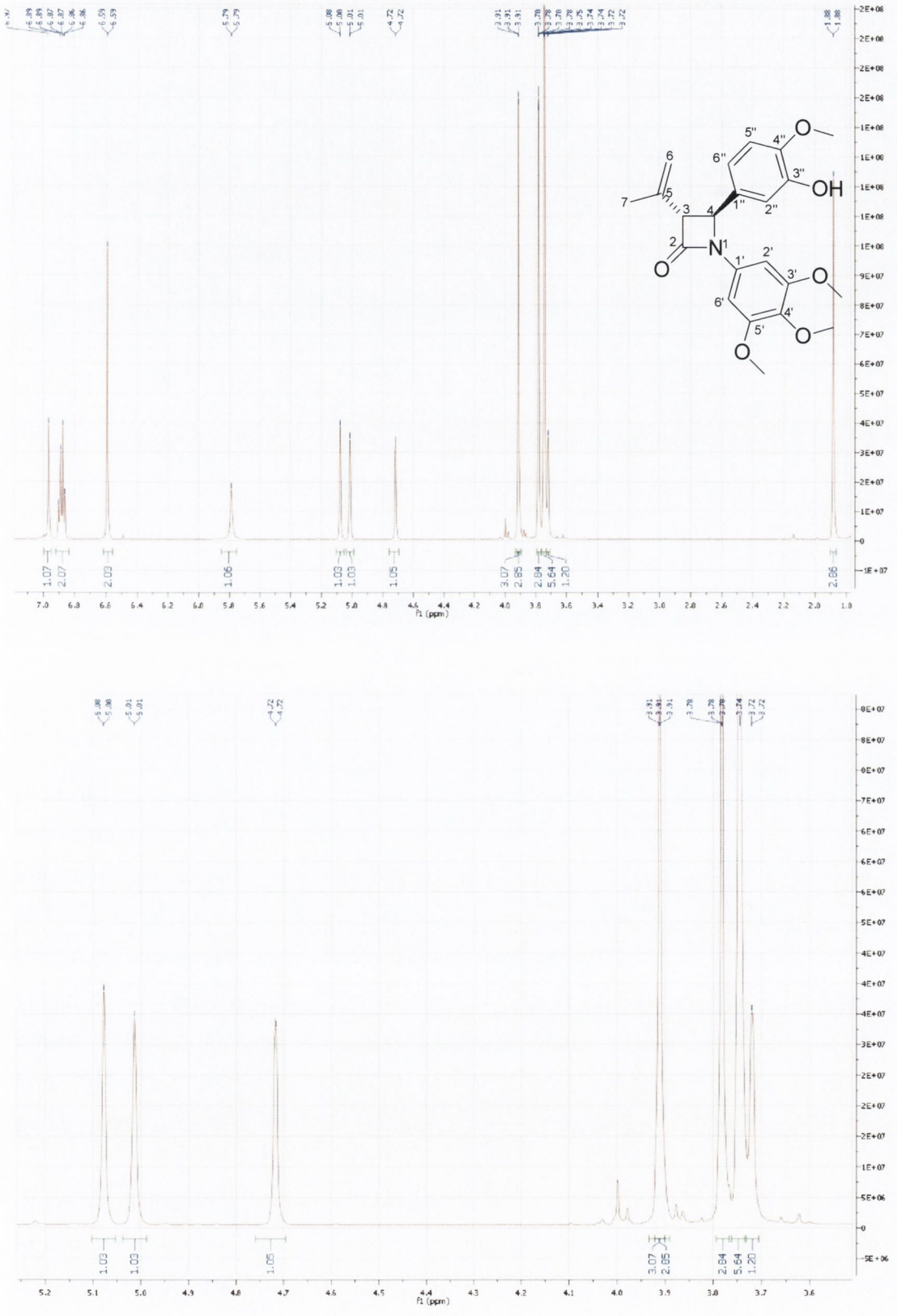

Fig 3.2 ^{1}H spectrum of **344** (top) with a close up of δ3.6 to δ5.9 (bottom) illustrating the trans stereochemistry of H_3 and H_4. Note that H_3 is obscured somewhat by the methoxy peaks.

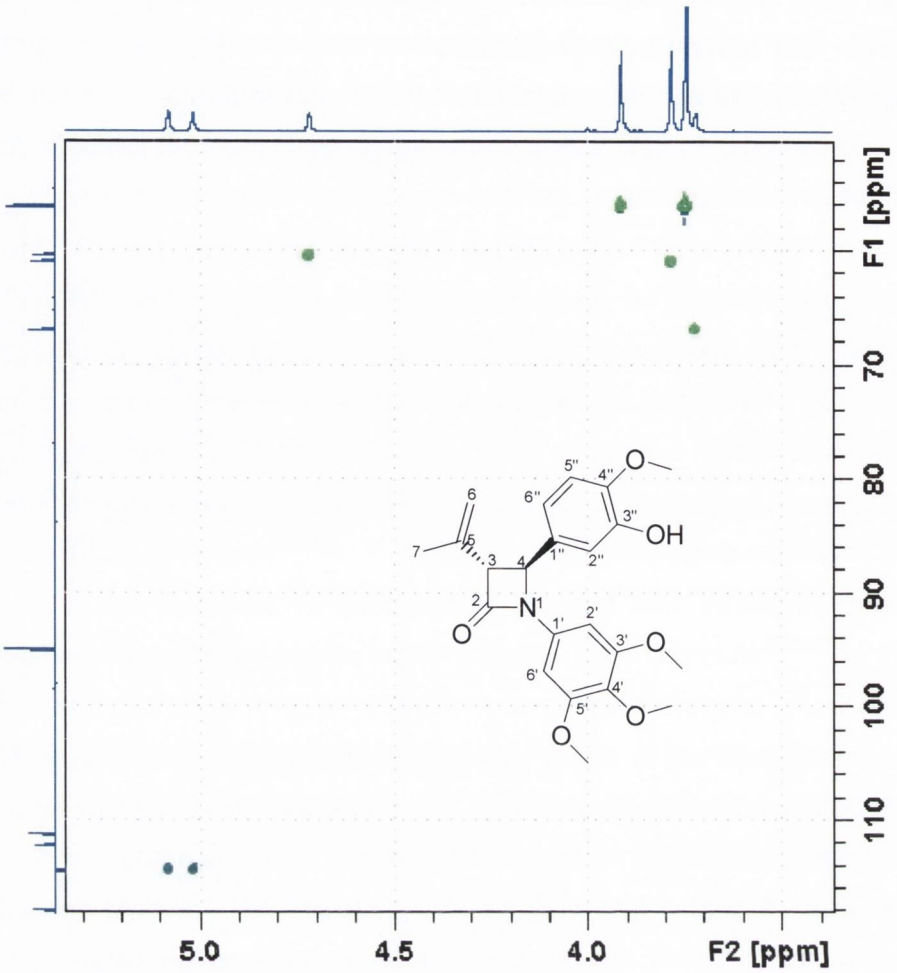

Fig 3.3 HSQC experiment for **344**

The synthesis of a 3-bromo β-lactam (**347**) was attempted using both bromoacetic acid (**346**) and triphosgene acid activating agent and by the Staundinger reaction using bromoacetic chloride (**345**) reacted with the imine **216** without any success (**scheme 3.2**). In both cases no β-lactam product was formed. The formation of 3-bromo β-lactams by the Staundinger reaction has been previously reported[278] although only with a simple diphenyl imine as opposed to the highly substituted imines used in the above reactions. Other possible routes to the 3-bromo β-lactam product include the bromination of a 3-hydroxy β-lactam by CBr_4 and $P(Ph_3)$[279], and the introduction of a 3-bromo substituent from a 3-azido group using KBr[280].

Such a product may be a useful intermediate for the functionalisation of the β-lactam as illustrated in **fig 3.4**. Nucleophilic substitution with sodium azide[281] leads to 3-azido compounds (**348**) which in turn can be converted to the corresponding 3-amino compound (**349**). Magnesium enolates can be formed by halogen-metal exchange between the 3-bromo β-lactam and a methyl Grignard reagent. The

magnesium enolate can in turn react with an appropriate aldehyde to give the hydroxyalkylation product (**350**) [282] [283]. In the case of a 3-bromo penicillin a radical allylation was demonstrated (**351**)[284].

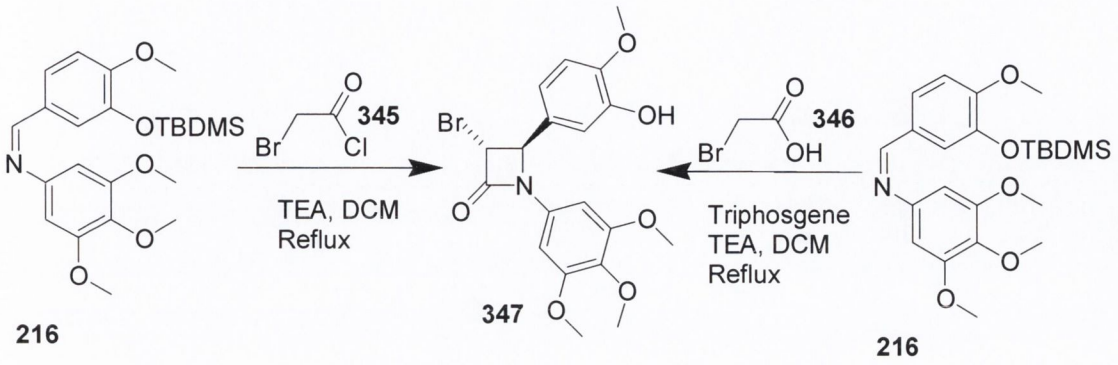

Scheme 3.2 Attempted synthesis of 3-bromo analogue

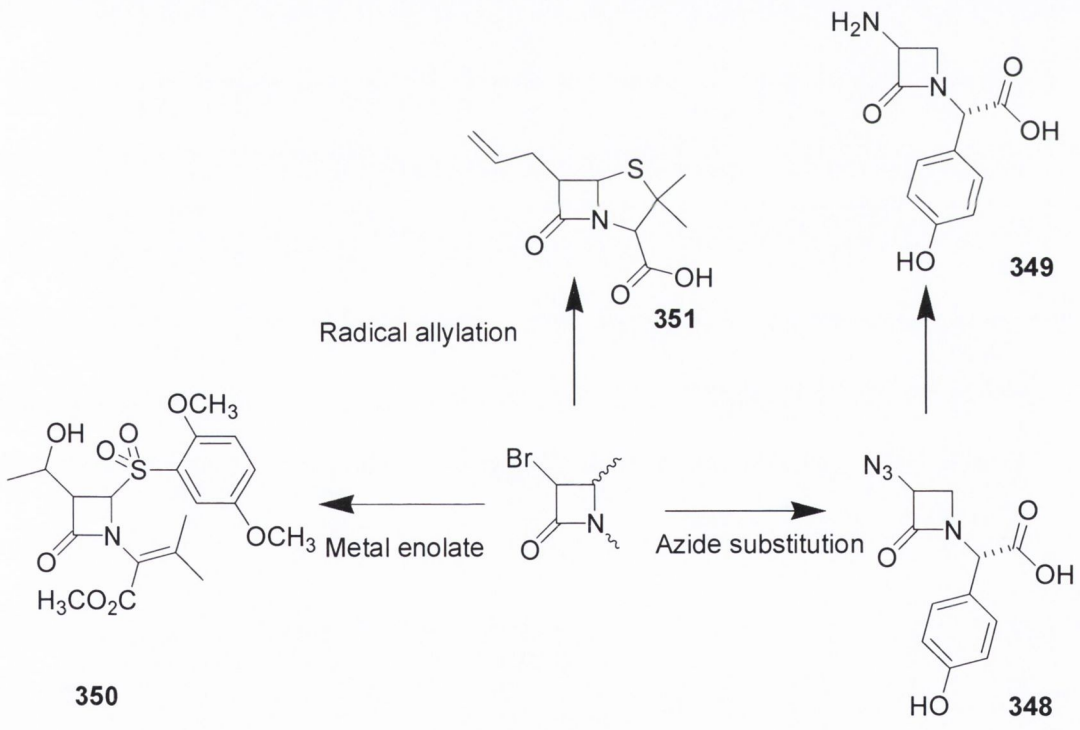

Fig 3.4 3-Bromo substituted β-lactams as an intermediate in synthesis

The products illustrated in **fig 3.4** may be synthesised by other routes. The 3-azido, amino, and vinyl compounds can be produced from the Staundinger reaction by using the appropriate acid chlorides.[166] β-lactam enolates can be generated by other methods as discussed in detail **section 3.3.5**.

3.2.2 3-Phthalimido β-Lactam

The chemistry of the amino group at the 3-position of the β-lactam ring is critical in a number of penicillins, cephalosporinns, and monocyclic β-lactams. A large body of work exists dealing with the synthesis of 3-amino β-lactams and analogues thereof[285] [286] [287]. The use of azidoacetyl chloride in the Staundinger reaction[222] [288] [289] [290] is employed to form a 3-azido intermediate which can be converted to the amino product (**356**). While this route is straightforward there are concerns over the safety of azidoacetic acid/acid chloride[291]. The use of phthalimido acetic acid represents an alternative to the azide route[292]. The phthalimido group effectively functions as a protecting group for the amino group during the β-lactam formation step. The amino group is only revealed upon cleavage of the phthalimido group. This strategy for incorporating an amino group onto the 3-position is popular mainly for the ease with which the phthalimido β-lactam can be formed from the readily available phthalimido acetic acid. For the purposes of this thesis both the 3-amino and 3-phthalimido β-lactams may be of interest in terms of their biochemical activity.

The initial attempt to produce the β-lactam **355** using the acid (**352**) activated with triphosgene failed. The acid **352** was converted to the acid chloride (**353**) using thionyl chloride (**scheme 3.3**). The excess thionyl chloride was removed under high vacuum and the remaining acid chloride was used immediately in the Staundinger reaction without further purification or characterisation. The reaction yielded almost exclusively the *cis* isomer of the β-lactam product **354** with only a trace amount of the *trans* isomer observed in the crude reaction by ^{1}H NMR. This product was subsequently deprotected to yield **355**. The yield, melting point and spectroscopic data for **355** is presented in **table 3.3**.

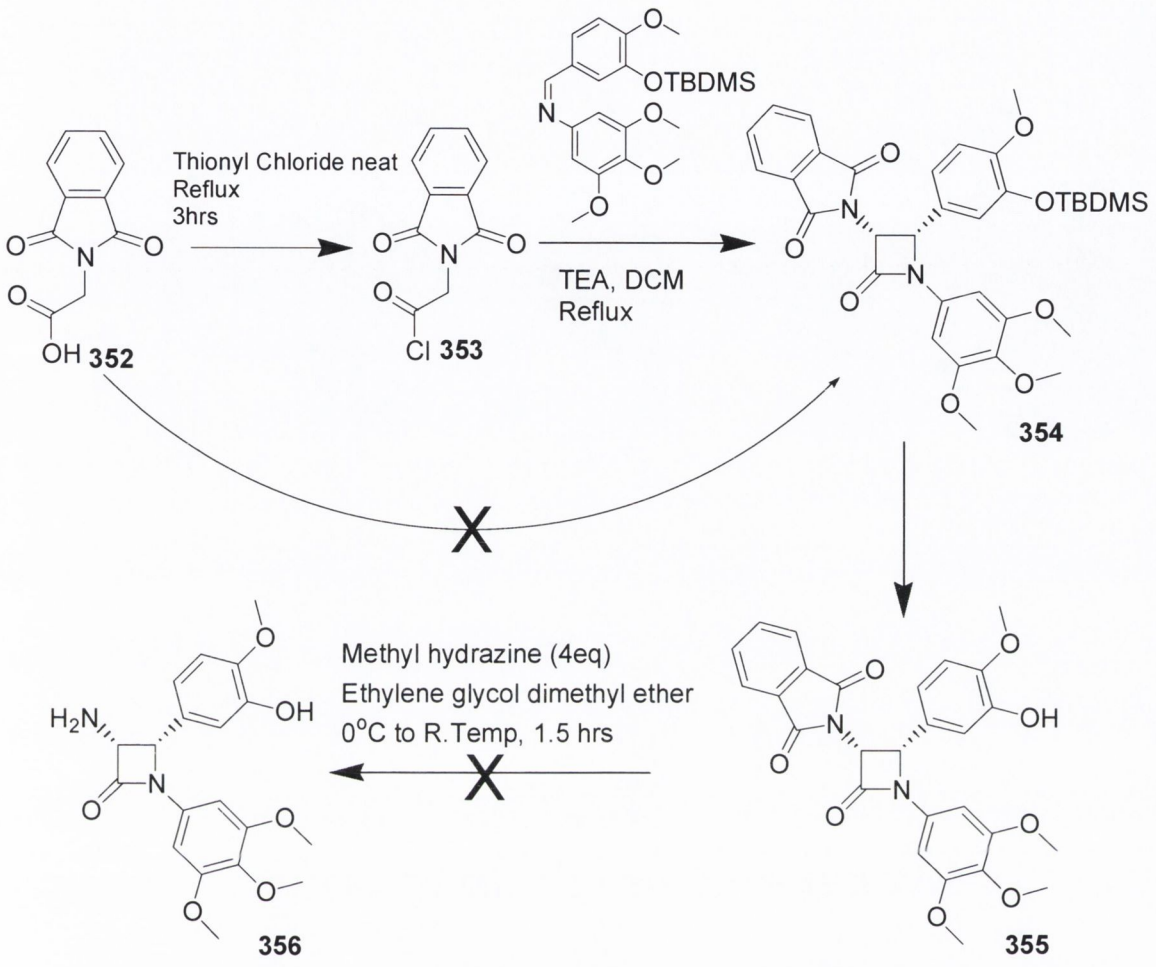

Scheme 3.3 Attempted synthesis of 3-amino substituted β-lactam **356**

The method chosen for the phthalimido cleavage of **355** to yield the amino compound **356** was based on that of Yoshioka *et al* using methyl hydrazine.[293] Barton *et al* has also reported the cleavage of the phthalimido group by methyl hydrazine to yield the 3-amino compounds in yields of 45%.[294] The phthalimido group can be cleaved using hydrolysis however the cleavage proceeds quicker if hydrazine is used. The proposed mechanism for the reaction is presented in **scheme 3.4**. Analysis of the crude material by ^{1}H NMR revealed the destruction of the β-lactam starting material, rather than the failure of the hydrolysis reaction to proceed. A number of other options exist for carrying out the cleavage. For example it has been noted that sodium borohydride in a mixture of 2-propanol, water, and acetic acid at 80°C for 5-8hours can be useful in cases where hydrazine cleavage

has failed.[262] Clearly the β-lactam ring would be subject to acid hydrolysis under such conditions.

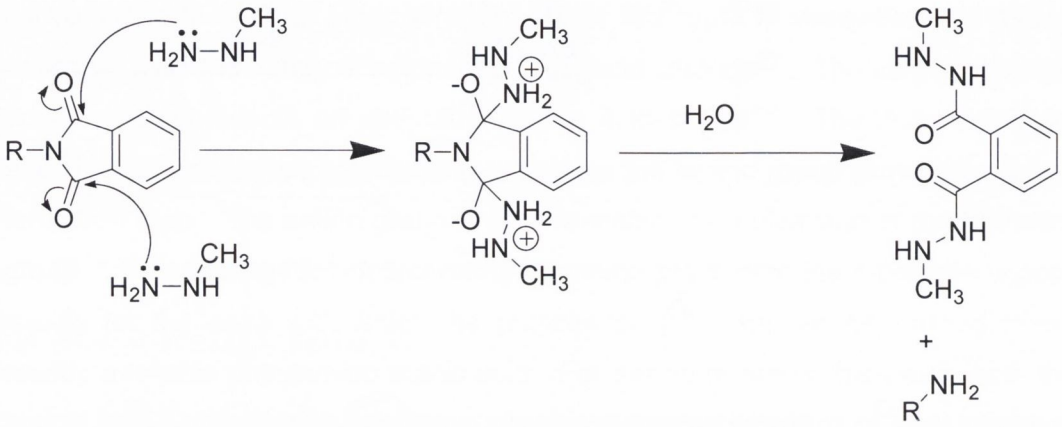

Scheme 3.4 Mechanism for the cleavage of the phthalimido group by methylhydrazine

Compound No.	IR	Yield (%)	Isomer
355	1721, 1762 3423	64	Trans

Table 3.3 Melting point, yield, and IR data for **355**

3.2.3 Substituted Acid formation

As a means of introducing a variety of substituent groups at the C_3 position of the β-lactam product, an appropriately substituted phenol (**357**) was reacted with chloro acetic acid (**358**) in the presence of sodium hydride to yield the 3,4,5-trimethoxyphenoxyacetic acid **359** in 48% yield (**scheme 3.5**). This reaction was carried out primarily to demonstrate a route to incorporating structurally diversity at the 3-position of the β-lactam ring simply by using an appropriately substituted phenol in the reaction and also the trimethoxy subunit is known to be an important structural feature of other members of the combretastatin family. This could then provide an alternative route to the incorporation of the trimethoxy subunit onto the β-lactam ring. The acid was subsequently used successfully in the Staundinger reaction with triphosgene as an acid activating agent to form **360** which contains the 3,4,5-trimethoxyphenoxy fragment at C_3. The silyl ether protecting group was removed to yield the free phenol β-lactam (**361**) in 36% yield.

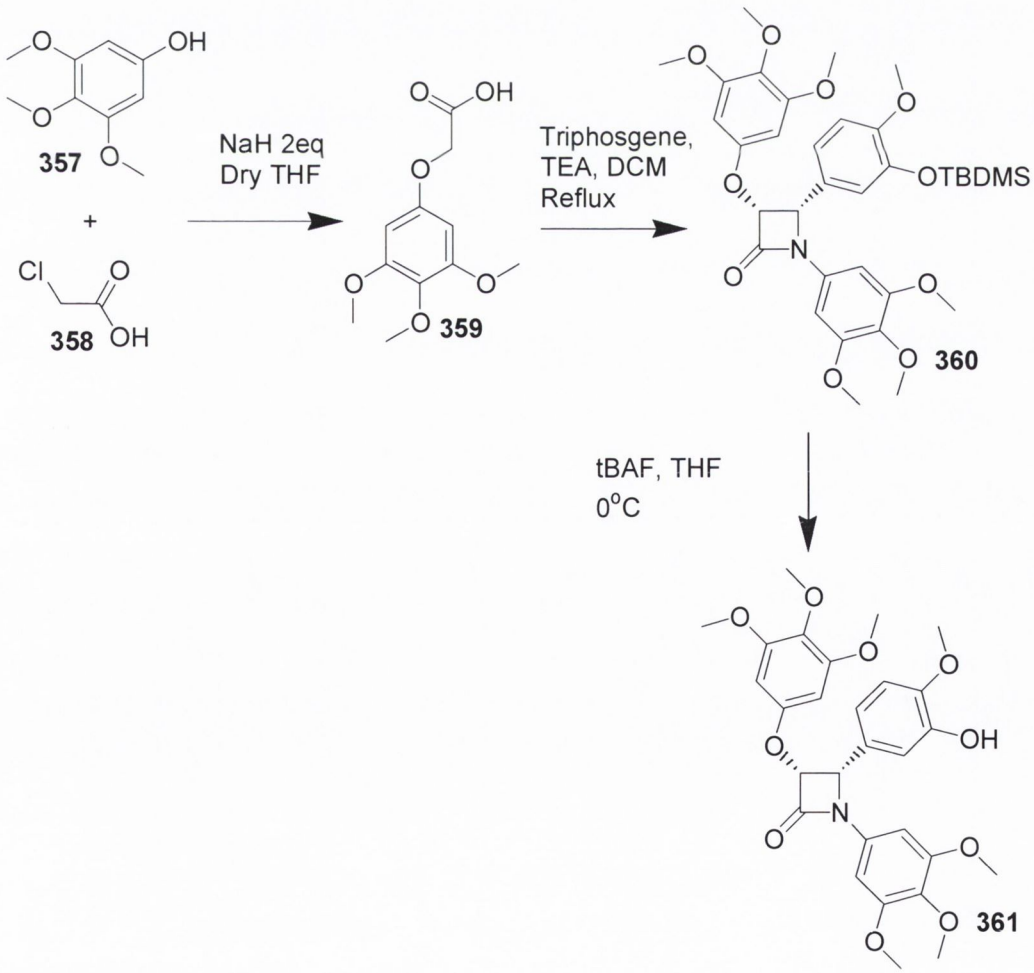

Scheme 3.5 Substituted acid formation as a means of incorporating structural diversity at C_3

3.3 Addition Reactions to 3-Unsubstituted β-Lactams

The previous sections of this chapter have concentrated on the formation of a number of 3-substituted β-lactams through the modification of the Staundinger reaction. As an alternative method for forming 3-substituted β-lactams, the aldol type addition of appropriate aldehydes to a 3-unsubstituted β-lactam was carried out. Due to the exceptional biochemical activity which was observed for **343** a number of vinyl aldehydes were used in this particular reaction to probe the role of the vinyl group.

3.3.1 Formation of 3-Unsubstituted β-lactams

The Reformatsky reaction makes use of a organozinc reagent to form a β-hydroxyester from the carbonyl of a ketone or aldehyde. Hart and Ha have presented an excellent review of this area.[295] The reaction is analogous to the Grignard reaction however the organozinc intermediate is less reactive than a typical Grignard reagent. Gilman and Speeter reported the Reformatsky type reaction to form the β-lactam ring **364** from an α-bromoester **362**, zinc, and an imine **363** as outlined in **scheme 3.6**.

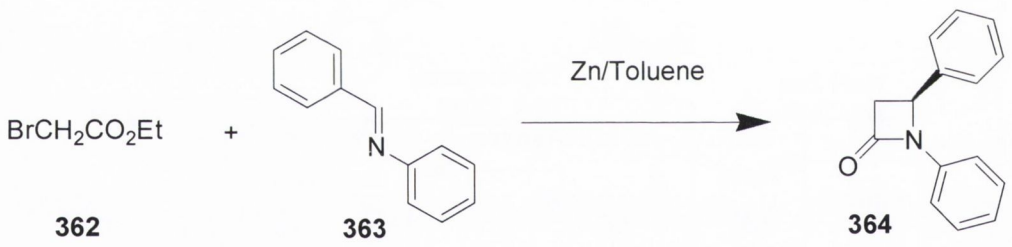

Scheme 3.6 Reformatsky reaction of Gilman and Speeter

The Gilman and Speeter type β-lactam forming reaction has been extended to include a variety of substituted imines resulting in the corresponding 3-unsubstituted β-lactams (**scheme 3.7**). A number of studies on the stereochemical outcome of the reaction involving α-bromo substituted acetates have been carried out. It was observed that the stereochemical outcome of the reaction (**366a** vs. **366b**) was dependent upon the substituent (R_3) attached to the acetate **365** and on the solvent used in the reaction (for an extensive review consult Table II in reference[295]).

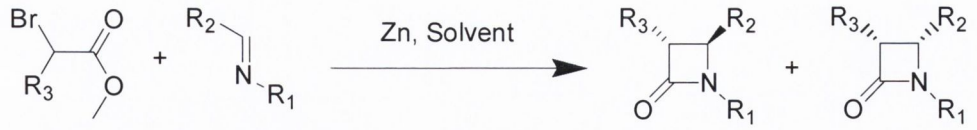

365 **366b Trans** **366a Cis**

R_1 = Ph, PMP, *p*-ClPh, *p*-MePh, *p*-BrPh
R_2 = Ph, PMP,
R_3 = Me, Et, *i*Pr, *t*Bu, Ph

Scheme 3.7 Substituted bromo acetates leading to diastereomeric products

Two proposed mechanisms for the Reformatsky reaction are presented in **scheme 3.8**. Initially the Reformatsky reagent **367** could undergo an elimination to form the ketene **368** which in turn reacts with the imine in a manner similar to the Staundinger reaction. The second option involves the reagent reacting with the imine to give a β-amido ester **369** which in turn undergoes cyclisation to give the desired β-lactam product **370**. A number of studies have been designed to investigate which of these two mechanisms can best explain the outcome of the reaction.

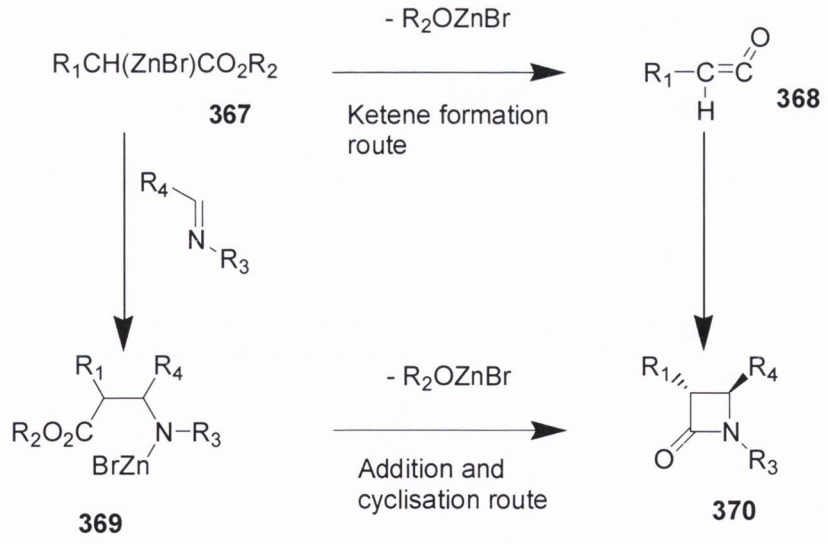

Scheme 3.8 The two possible mechanisms underlying the Reformatsky reaction

The ketene route has fallen out of favour with the observation that the stereochemical outcome of a reaction with the ketene **368** deliberately formed *in situ* differs from that of the Reformatsky reaction[296]. The addition/cyclisation route has gained support from the fact that the addition product **369** can be isolated by

prematurely stopping the reaction.[295] The isolation of **369** would indicate that the addition reaction is relatively fast and it is the cyclisation of the addition product that is the rate limiting step in the reaction.

3.3.2 Reformatsky β-Lactams as Intermediates in Synthesis

The mono-cyclic β-lactams formed as a result of the Reformatsky reaction are key intermediates in a number of antibiotics such as thienamycin carbapenems as outlined by Palomo[172] (**scheme 3.9**). The Reformatsky reaction is used in the first step to synthesise **373** from the imine **372** and the α-bromoacetate **371**. The main advantages of the Reformatsky reaction in such a case is the relative ease with which the appropriately substituted monocyclic β-lactam (**373**) can be synthesised with the all important desired stereochemistry. Ozonolysis of the styrl group in **373** followed by Baeyer-Villiger of the ketone **374** gives the acetoxy **375**. The *p*-methoxyphenyl group is removed by treatment with CAN in acetonitrile/water to give the N-unsubstituted β-lactam **376**. The diazo side chain of **377** was added by the reaction of **376** and the corresponding lithium enolate, followed by cyclisation by carbene insertion to give **378**. The author's note that the key step in the reaction is obtaining the intermediate **373** with the correct stereochemistry intact and in reasonable yield.

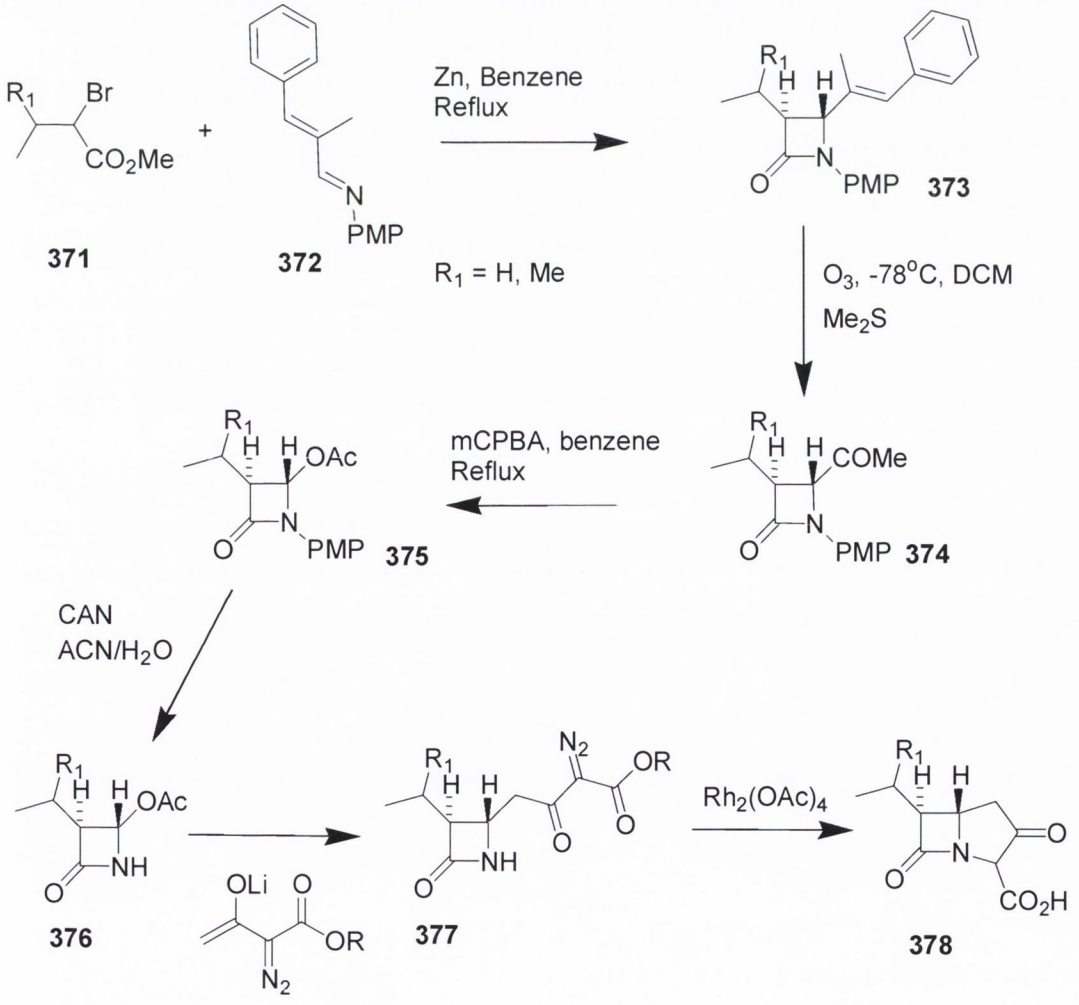

Scheme 3.9 The use of the Reformatsky reaction to synthesize monocyclic intermediates in carbapenam synthesis

3.3.3 Optimised Reformatsky Reaction Conditions

A number of options exist for improving the yield of the Reformatsky reaction. Some reactions employ activated zinc which can be obtained by removing the deactivated oxide layer from the metal by either etching with an acid such as HCl, or by mechanical removal. A particularly popular method uses chlorotrimethylsilane (CTMS) to activate the zinc *in situ*. [297] Ultrasound has been used in the past to promote other reactions involving the use of zinc such as in the Simmons-Smith reaction.[298] The use of ultrasound may aid in the removal of zinc oxide from the surface of the metal thereby forming activated zinc in keeping with the previous observations from Bose[299] and Han[300] that ultrasound can promote the Reformatsky reaction. In recent years, microwave heating has been applied to a number of organic chemistry reactions leading to the development of *Microwave-Induced Organic Reaction Enhancement* (MORE). The use of microwave heating in the Staundinger reaction has been extensively studied, but the application of microwave heating to the Reformatsky reaction for the synthesis of β-lactams has received less attention. [248 301 207]

Carr[203] applied microwave heating to the Reformatsky reaction in an effort to boost the yield of the β-lactam from this type of reaction. It was found that conventional heating to reflux for 8 hours in benzene yielded the product **379** in 46% yield while heating under microwave conditions for 45 minutes boosted the yield to 54%. Both reactions employed CTMS as a zinc activator and it was noted that the product was easier to isolate from the microwave reaction.

3.3.4 Synthesis of 3-Unsubstituted β-Lactams

The β-lactam (**380)** formed *via* the Reformatsky reaction with imine **208** and subsequent deprotection of **379** (**scheme 3.10**). Initially only the 3-hydroxy-4-methoxy product (**380**) was synthesised in the reaction due to difficulties in isolating 3-amino β-lactams. Both the thermal and microwave heating methods were carried out. In keeping with Carr's work, it was found that the microwave method performed better both in terms of yield and a reduction in reaction time. During the course of the synthesis of **379** it was found that the use of extra equivalents of zinc resulted in a further improvement in yield of product β-lactam (**table 3.4**).

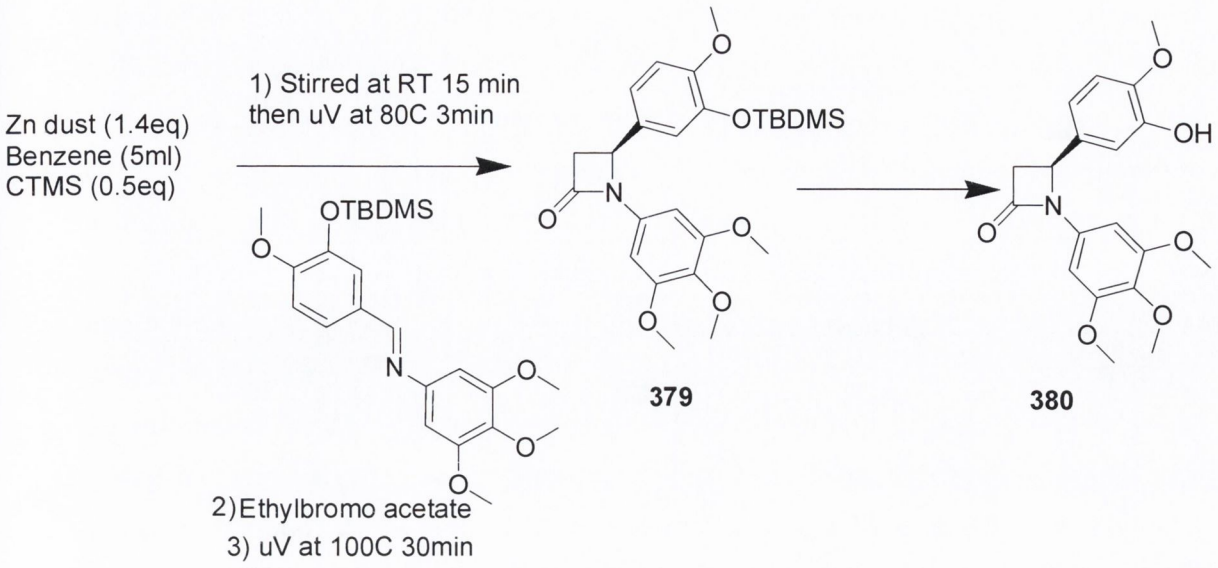

CTMS = Chlorotrimethylsilane

Scheme 3.10 Reformatsky reaction for the formation of 3-unsubstituted β-lactam **380**

Compound No.	No. equivalents of zinc used	Yield (%)
208	1.4	37
208	4.2	77

Table 3.4 Effect of extra charge of zinc upon yield of **379**

In the early development of microwave chemistry, domestic microwave ovens were employed. A typical domestic microwave oven operates at 2.45 GHz, resulting in microwaves having an energy of 0.037kcal/mol which is much less than the energy required to cleave a chemical bond suggesting that microwaves do no affect the reaction by bond cleavage. Microwave heating occurs when polar molecules within the reaction attempt to align themselves with the microwave field[302]. Heating is also observed in samples where ions are present in a similar fashion where the ions attempt to orientate themselves with the microwave field. The main advantage of

such heating is that it takes place directly within the reaction vessel compared to conventional heating where the heat source is external to the vessel. Microwave heating allows the heating process to be carefully controlled since upon removal of the microwave source, heating stops immediately and the reaction begins to cool. In conventional heating the entire reaction vessel must be removed from the heat source and allowed to cool. It is this efficient form of heating that may be responsible for the improved outcomes observed in microwave reactions.

In the use of a domestic microwave, a typical reaction setup involved the use of an open flask containing the reagents placed in the oven along with a large volume of water to act as a heat sink[303]. Temperature control of the reaction could only be achieved by on/off cycling of the oven. Such an arrangement has obvious safety implications. In recent years, microwave reactors that have been specifically designed for chemists have come on to the market. An Initiator™ microwave synthesis system supplied by Biotage was used in this thesis. The Initiator system allows for careful temperature control of the reaction through a combination of modulating the microwave field and cooling of the reaction cavity by compressed air. The system makes use of sealed reaction vials equipped with magnetic stirrers to achieve temperatures up to 250°C and pressures up to 20 bar, conditions which are not attainable with domestic ovens. A number of safety features are built into the system allowing for safe operation at these extreme conditions.

A typical reaction involved an initial step where the zinc and TMS were stirred at room temperature in benzene for 15 minutes prior to heating to 80°C by μV for 3 minutes. The reaction was allowed to cool before the imine (5mmol) and ethylbromoacetate (6mmol) were added and the reaction heated to 100°C for 30 minutes. It was found that the product **379** from the reaction could be easily isolated by recrystallisation from hot ethanol in 77% yield. This product served as the starting material for the addition reactions discussed in the next section. A deprotection reaction was carried out on a small amount of **379** to yield the free hydroxy compound in 49% overall yield compound **380** for testing in the MCF7 cell line.

The ^{1}H and ^{13}C NMR spectra for (**379**) are presented in **fig 3.4** and **3.5**. The two methyl protons of the silyl ether are non equivalent and appear as overlapping singlets at δ0.07ppm and δ0.09ppm integrating for a total of 6 protons. The *t*-butyl protons appears as a singlet at δ0.94ppm integrating for 9 protons. The methoxy protons appear as a series of singlets in the region δ3.71ppm-δ3.81ppm integrating for a total of 12 protons. The 5 protons in the aromatic system appear from δ6.54ppm to δ6.97ppm. The two geminal protons attached to C_3 are non-equivalent and are coupled to both each other and the H_4 proton. They appear as doublets of

doublets centered on δ2.93ppm and δ3.51ppm. Both display a coupling constant of 15.2Hz typical of geminal coupling. The CH_2 group gives rise to the negative signal in the DEPT δ46.03ppm The signal at δ2.93 is also coupled *trans* to H_4 with a J value of 2.5Hz and likewise the signal at δ3.51 is coupled *cis* to H_4 with a J value of 5.5Hz. H_4 appears as a doublet of doublets at δ4.86 coupled to both geminal H_3 protons.

In the IR spectrum of the deprotectd product **380**, the carbonyl and hydroxy groups appear at 1741cm^{-1} and 3443cm^{-1} respectively while the CH_2 absorption appears at 2937cm^{-1}.

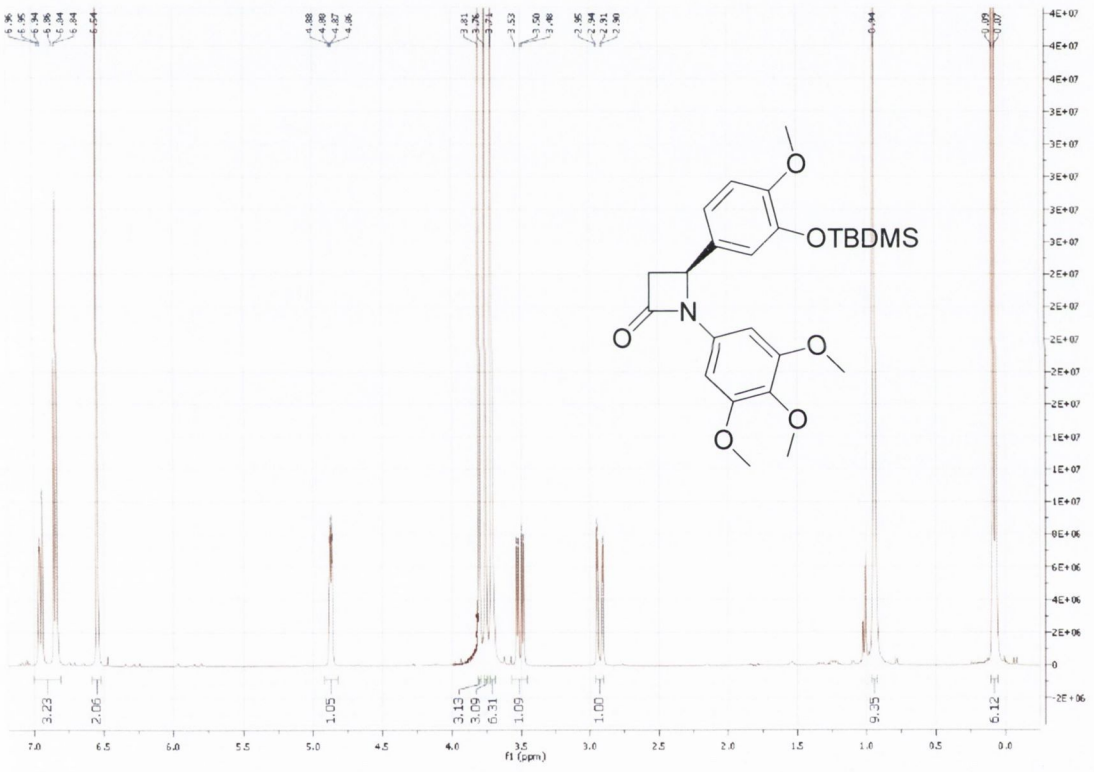

Fig 3.4 ^{1}H NMR spectrum for **379**

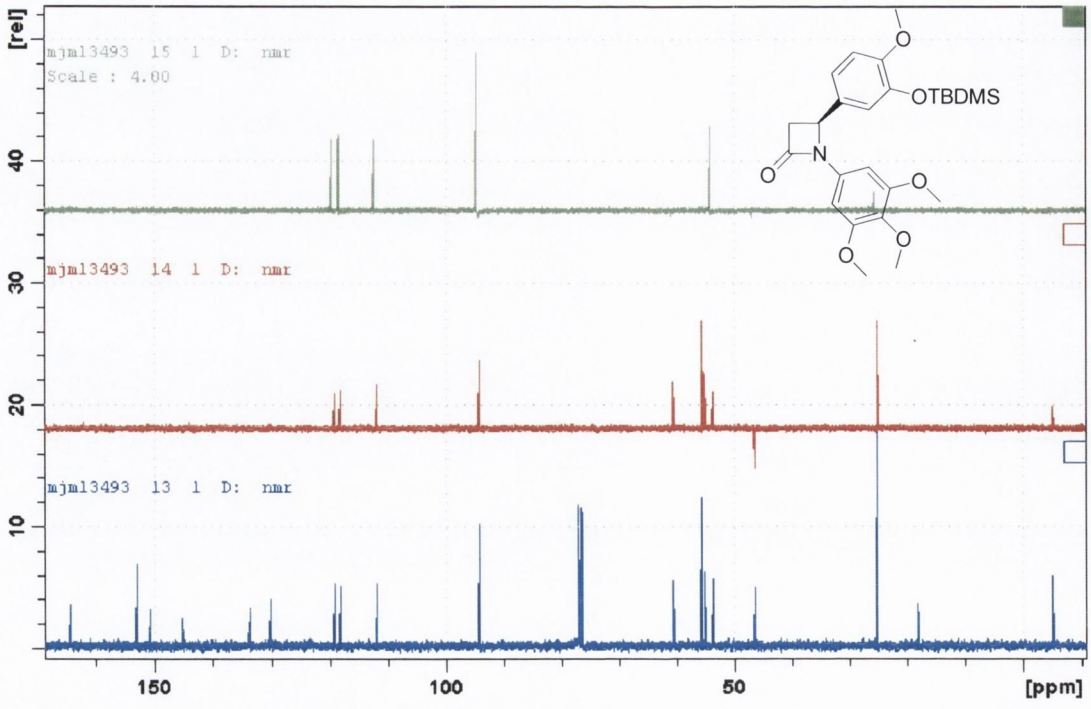

Fig 3.5 ^{13}C NMR spectrum for **379**.

3.3.5 Reaction of 3-unsubstituted β-lactams

The LDA mediated addition of aldehydes or ketones to 3-unsubstituted β-lactams is a well known method for introducing substituents to the C_3 position[304]. By using a strong base such as LDA, it is possible to abstract a single proton from C_3 which in turn can react with a series of aldehydes/ketones to yield an aldol type product. **Scheme 3.11** outlines the reaction of **379** with a series of aldehydes and ketones. The LDA for the reaction can be produced *in situ* by the reaction of diisopropylamine and *n*-butyllithium, or alternatively solutions of LDA in various aprotic solvents are available commercially and the anion **381** is formed in the reaction. The β-lactam ring is itself stable in the LDA solution at -78°C since the reaction is aprotic. Products **382-387** were obtained as the *t*BDMS ether protected compounds which were subsequently deprotected using *t*BAF to yield the phenols (**388-393**) (**table 3.5**)

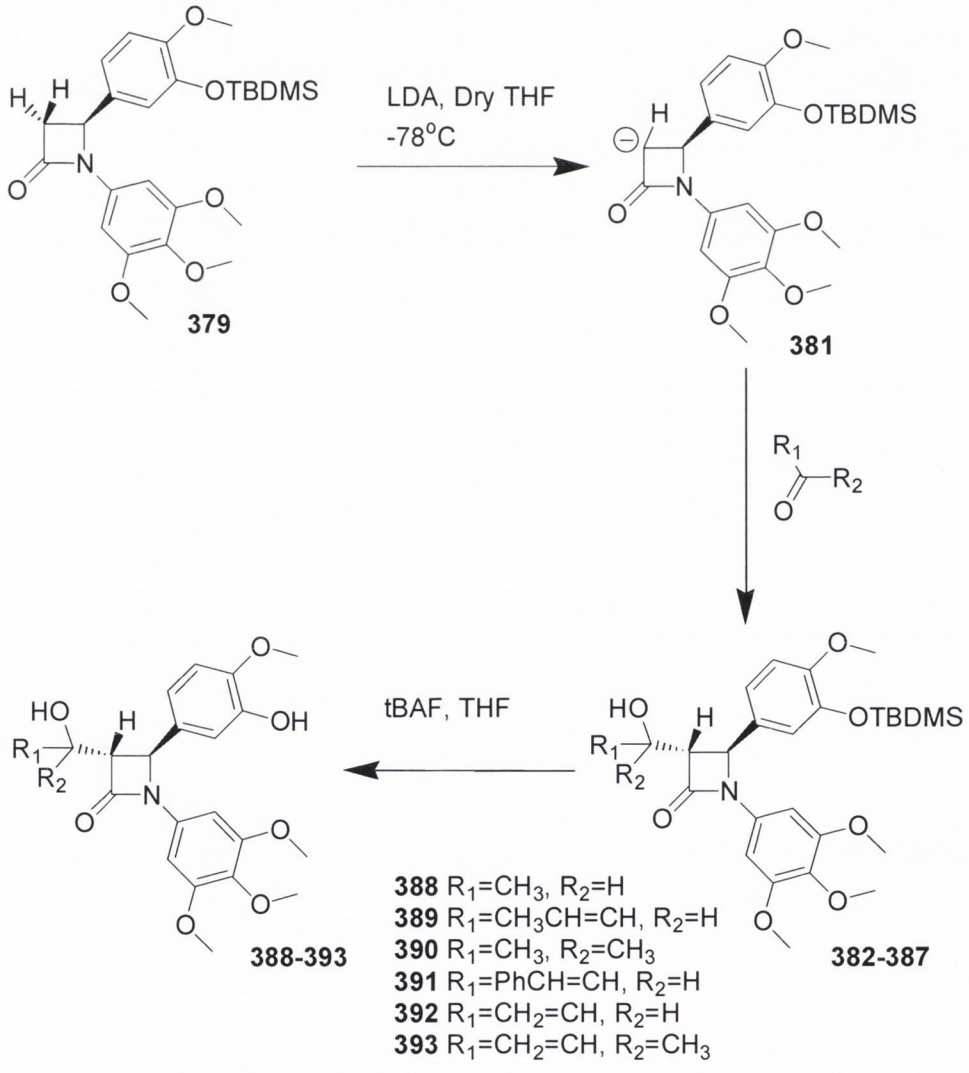

Scheme 3.11 LDA mediated addition of carbonyl reagents to **379**

As proof of concept the first addition involved the reaction of **379** with acetylaldehyde. For the other analogues, a number of vinyl aldehydes were selected due to the exceptional biochemical activity displayed by the 3-vinyl β-lactam **343**. The yields, melting points and spectroscopic data for compounds **388-393** are presented in **table 3.5**. The addition reaction results in the formation of product with three chiral centres at C_3, C_4, and C_5. From the ^1H NMR spectrum the presence of a diastereomeric mixture can be confirmed as illustrated in **Fig 3.6** for compound **393**. In cases where the assignment of the H_3, H_4, and H_5 signals was ambiguous such as with **393**, a HSQC experiment was carried out.

From examination of the ^1H NMR spectrum of compound **393** (**fig 3.6**) it is clearly evident that two sets of diastereomers have been formed in the reaction. The protons of the CH_3 group attached to the chiral C_5 appear as two singlets at δ1.46 and δ1.56. The HSQC spectrum (**fig 3.7**) indicates that these protons are attached to two carbon signals at δ25ppm as is expected for the CH_3 group The H_3 and H_4 signals appear as two sets of doublets centered around δ3.20 and δ4.83 respectively integrating for a total of 1 proton in each case. The coupling constant of approximately 2.4Hz in both cases indicates that they have a *trans* relationship to one another. Both signals are attached to carbon signals at δ70ppm and δ58ppm. The DEPT experiment (**fig 3.8**) indicates that both are CH carbons as is expected for C_3 and C_4. From the both the H_3 and H_4 signals the ratio of diasteromers can be calculated as 1.14:1.00. The methoxy groups appear as a series of overlapping singlets in the region δ3.72 to δ3.89 integrating for a total of 12 protons. The HSQC spectrum shows that these signals are associated to the series of carbons in the range δ55-60ppm. The DEPT spectrum indicates that these carbon signals arise from CH_3 groups. The geminal protons of C_7 are nonequivalent and appear as two sets of multiplets centred on δ5.19 and δ5.39 with each set of signals integrating as a single proton. In the HSQC spectrum both signals interact with a CH_2 carbon at δ110ppm. Two CH_2 signals are observed instead of one due to the presence of two diastereomers. The H_6 proton appears as two sets of multiplets in the region δ5.81-6.14ppm overlapping with a signal from a hydroxy group. The H_6 signals integrate for a total of one proton. The hydroxy signal appears to be made up of two overlapping broad singlets integrating for a total of a single proton. The remaining phenol signal appears as a broad singlet approximately δ1.8ppm

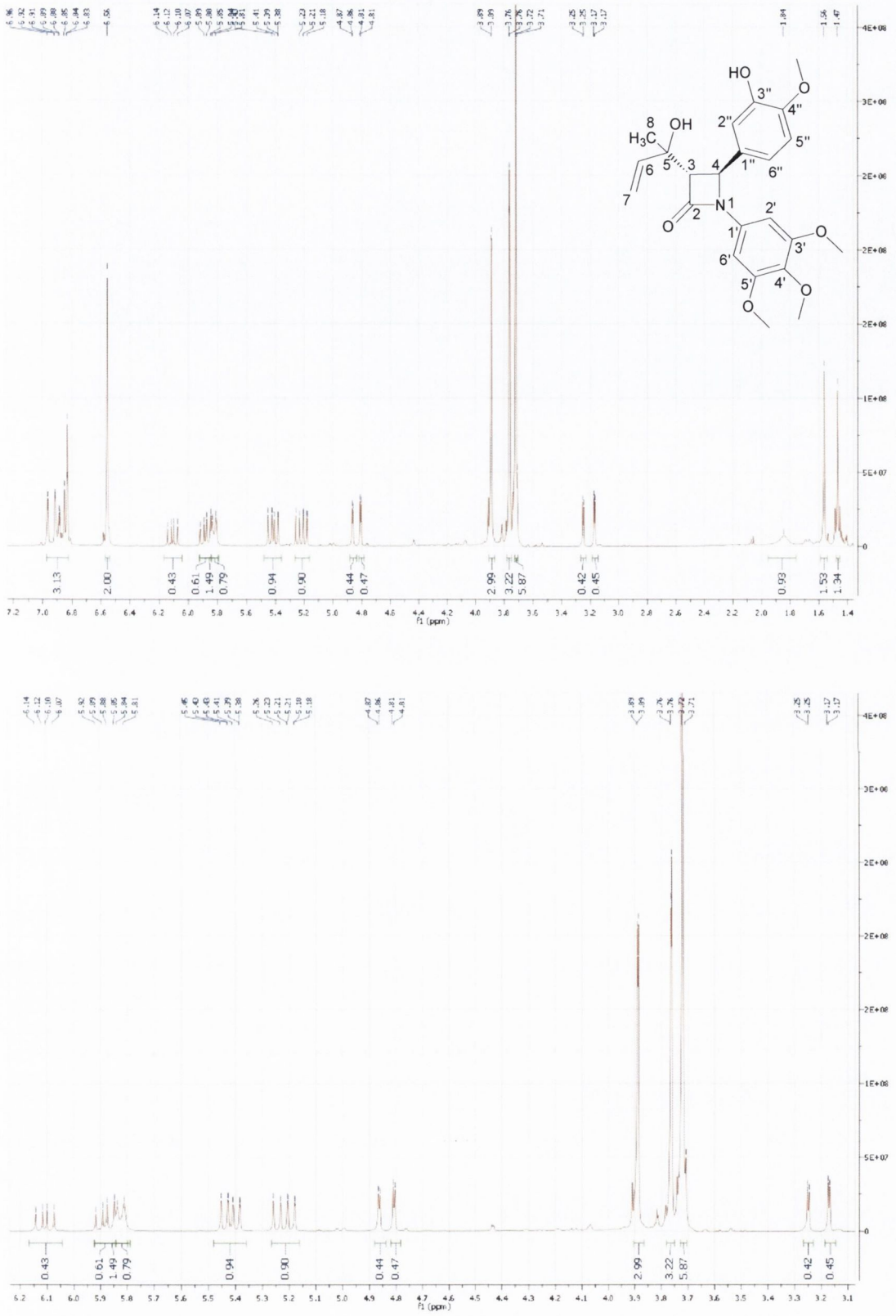

Fig 3.6 ^{1}H NMR spectrum for **393** illustrating the presence of diastereomers (top) and a closer image of the area δ3.1-6.2ppm (bottom).

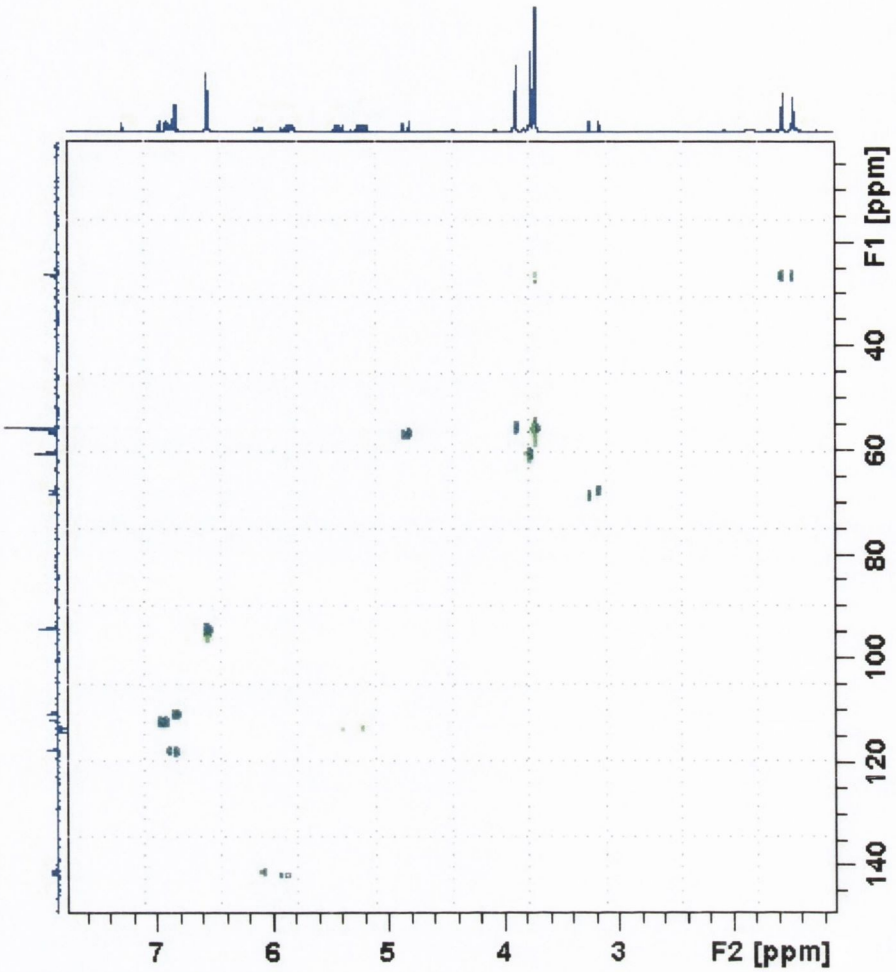

Fig 3.7 HSQC spectrum for **393**

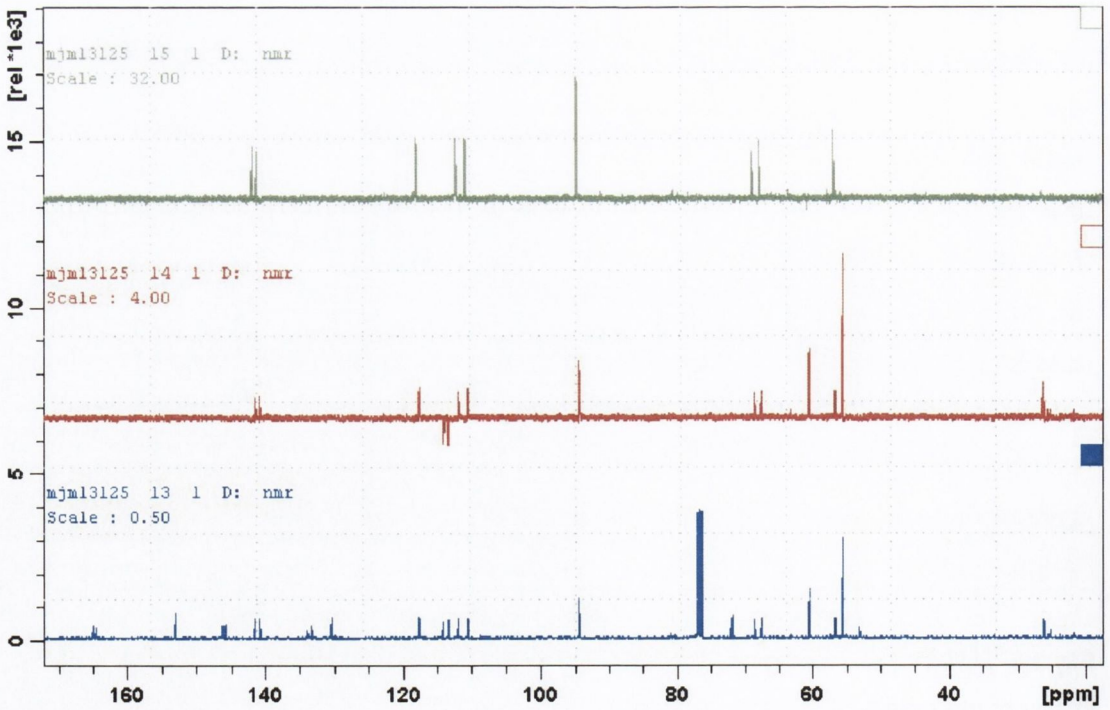

Fig 3.8 ^{13}C DEPT NMR spectrum for **393**

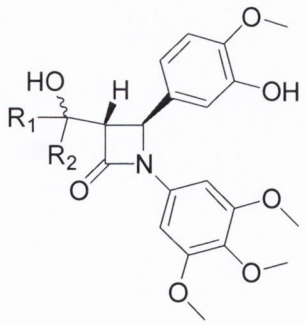

Compound No.	R1	R2	IR	Diastereomer Ratio	Yield (%)
388	CH_3-	H	1732, 3428	2:1	17
389	CH_3CH=CH-	H	1732, 3427	3:2	32
390	CH_3-	CH_3-	1732, 3429		23
391	φ-CH=CH-	H	1732, 3419	2:1	38
392	CH_2=CH-	H	1742, 3323	3:2	22
393	CH_2=CH-	CH_3-	1734, 3433	7:6	18

Table 3.5 Yield, melting point, and IR data for compounds **388-393**

The mixture of diastereomers obtained in the preparation of **388-393** proved impossible to separate by column chromatography, however for compound **393** they were separated into diastereomers by HPLC. A gradient elution using water and acetonitrile with 0.1% TFA added to prevent tailing was used to elute the mixture. The column was equilibrated with 5% water 95% acetonitrile initially. The gradient was made up of 5% water 95% acetonitrile changing to 60% water 40% acetonitrile over the course of 40 minutes. The total run time was set at one hour with the peaks of interest eluting at approximately 31 minutes as shown in **fig 3.9**. The compound was found to be 93% pure by peak area. Since the peaks are not fully resolved, the ratio of diastereomers could only be approximately determined as 61% to 37%. The ^1H NMR spectrum puts the ratio at 53% to 47%. While there are three chiral centres in the molecule, only four isomers are observed that preserve the *trans* arrangement of H_3 and H_4.

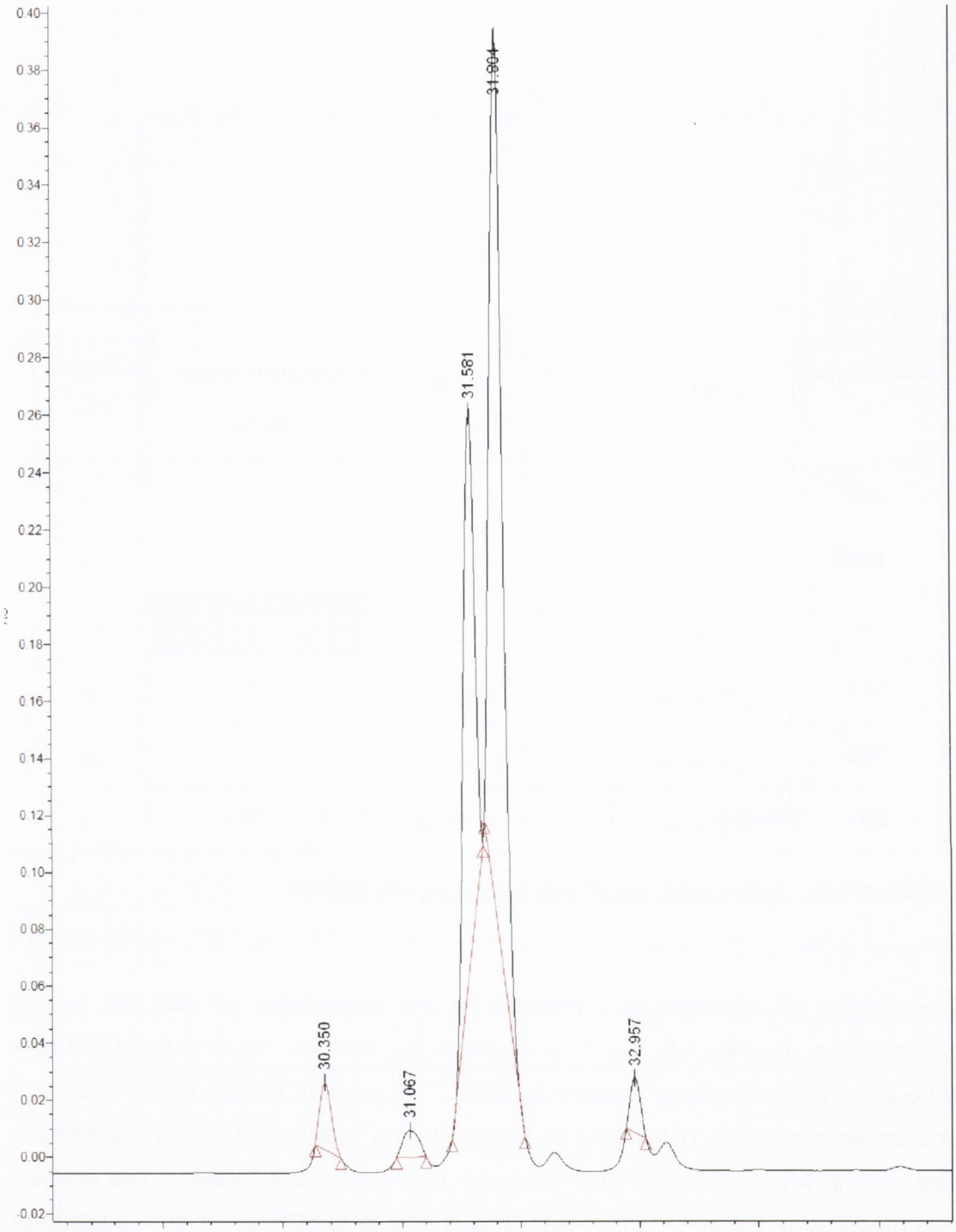

Fig 3.9 HPLC chromatogram showing the separation of the diastereomers of **393**

The four stereoisomers are illustrated in **fig 3.10**. There are two pairs of enantiomers (A and B) for each diastereomer. The HPLC chromatogram in **fig 3.9** clearly shows the presence of these two diastereomers. In turn each diastereomer peak in the chromatogram is composed of a pair of enantiomers. The separation of the racemic mixture into optically pure products was not attempted in this thesis, but is the subject of future investigation within the research group. All of the compounds

presented in this thesis were screened for biochemical activity as racemic mixtures. It is envisaged that the most potent compounds will be subjected to chiral resolution in the future to allow for the activities of the individual enantiomers to be determined. Early indications from molecular modeling studies (discussed in detail in Chapter 4) suggest that differences in activities will be observed.

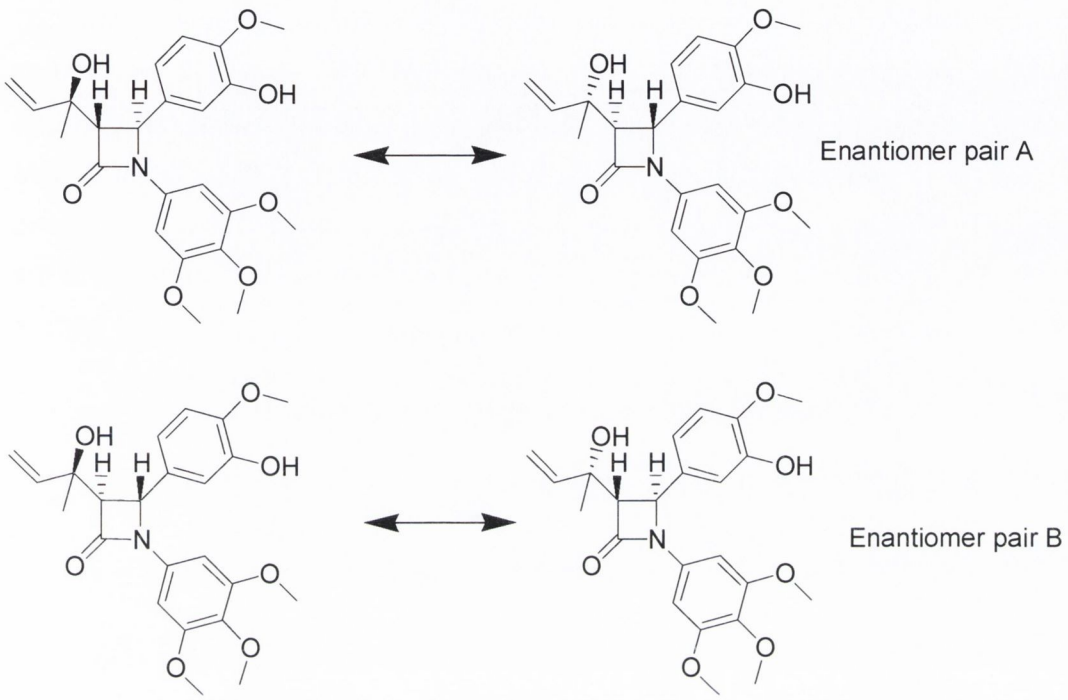

Fig 3.10 Illustration of the stereoisomers present in compound **393**

3.3.6 Oxidation of C_5 Hydroxy Group

To investigate the role of the alcohol group at C_5 in the products **388-393** in biochemical activity the alcohol (**382**) was converted to the corresponding ketone (**395**) (**scheme 3.13**). A number of reagents are available for this oxidation reaction. Chromium (VI) reagents such as PCC, PDC, and Collins reagent (Dipyridine Cr(VI)) are all used widely[305]. The oxidation was initially attempted using the popular PCC oxidizing agent and appeared to be successful however the isolation of the product from the PCC residue proved difficult. Disposal of PCC is somewhat troublesome and PCC is known to be acidic resulting in the possibility of undesired side reactions[305]. Palomo has reported the use of DMSO activated by triphosgene (**scheme 3.12**) as a mild reducing agent[306] which may be a useful alternative in the future. Alternatively a Swern or a Dess-Martin oxidation may be carried out both of which utilize very mild oxidation conditions and avoid the use of heavy metals.[305]

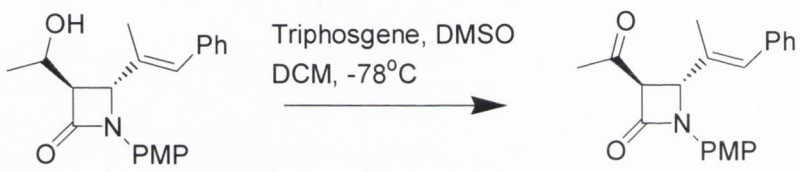

Scheme 3.12 Oxidation of C_5 alcohol group in β-lactams

An alternative route to the desired product **395** was identified where the addition of acetyl chloride to the 3-unsubstituted β-lactam (**379**) at low temperature with LDA gave the desired product (**394**) but only in low yields (11%) with the hydroxy product (**382**) being the major component of the reaction (22%) (**scheme 3.13**).

The IR spectrum for **395** is presented in **fig 3.11**. From the spectrum a carbonyl peak can be seen at 1731cm^{-1} corresponding to the carbonyl of the β-lactam ring. A broad peak at 3434cm^{-1} is assigned to the free phenol. The success of the oxidation of the alcohol to the ketone can be seen from both the ^{1}H and ^{13}C NMR spectra. In the ^{1}H spectrum the H_5 signal is no longer present and the signal for H_3 has shifted downfield from δ3.14ppm to δ4.23ppm. In the ^{13}C NMR spectrum, the carbonyl of C_5 can clearly be seen at δ181.23ppm

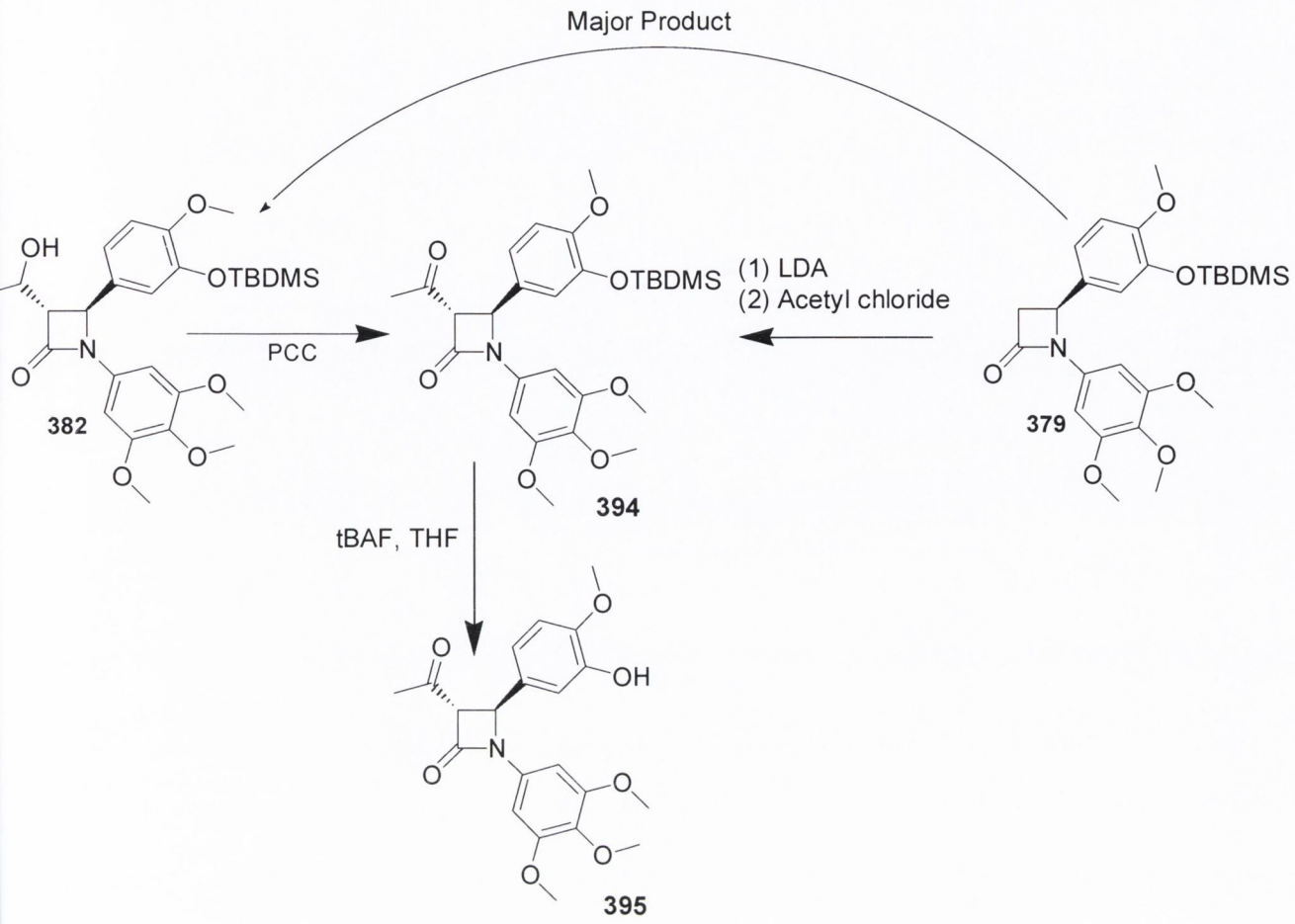

Scheme 3.13 Synthetic routes for introduction of acyl group at C_5 of β-lactam **395**

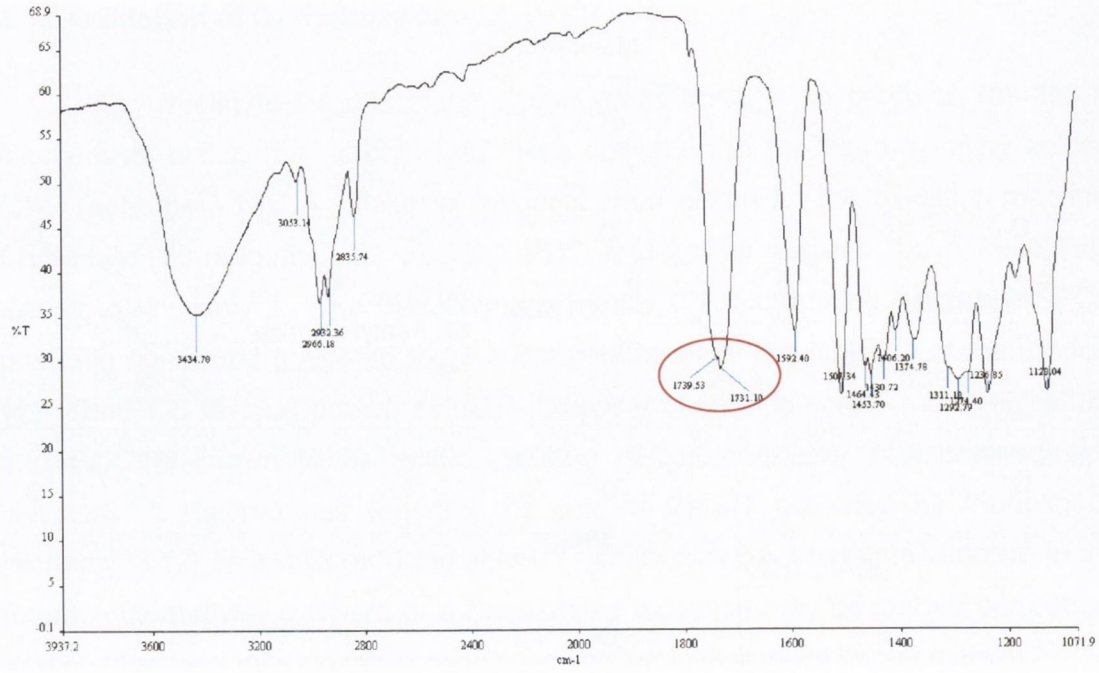

Fig 3.11 IR spectrum for **395** showing two carbonyl peaks (highlighted)

3.4 Transformations of 3-vinyl β-lactams

As previously mentioned compound **343** displays remarkable activity in the MCF7 cell line. To further investigate the role the vinyl group at the 3-position plays in modulating activity a number of chemical transformations were carried out on compound **343**. The conversion of the 3-vinyl group to the epoxide (**396**) was attempted using *m*CPBA. The epoxide group may serve as a useful intermediate for further modifications. The role of the position of the double bond was examined by the synthesis of **397**. The diol **398** was also synthesised by the oxidation of the alkene with OsO_4. Biochemical evaluation of these compounds coupled with a molecular modeling study may aid in understanding the attributes of **343** that result in its exceptional antiproliferative activity. The replacement of the phenolic hydroxy of **343** with an amino group (**399**) was also carried out because the initial screen of compounds indicated that products containing hydroxy and amino substituents on the C_4 aromatic ring are active in antiproliferative assays and this motif is necessary for potent activity.

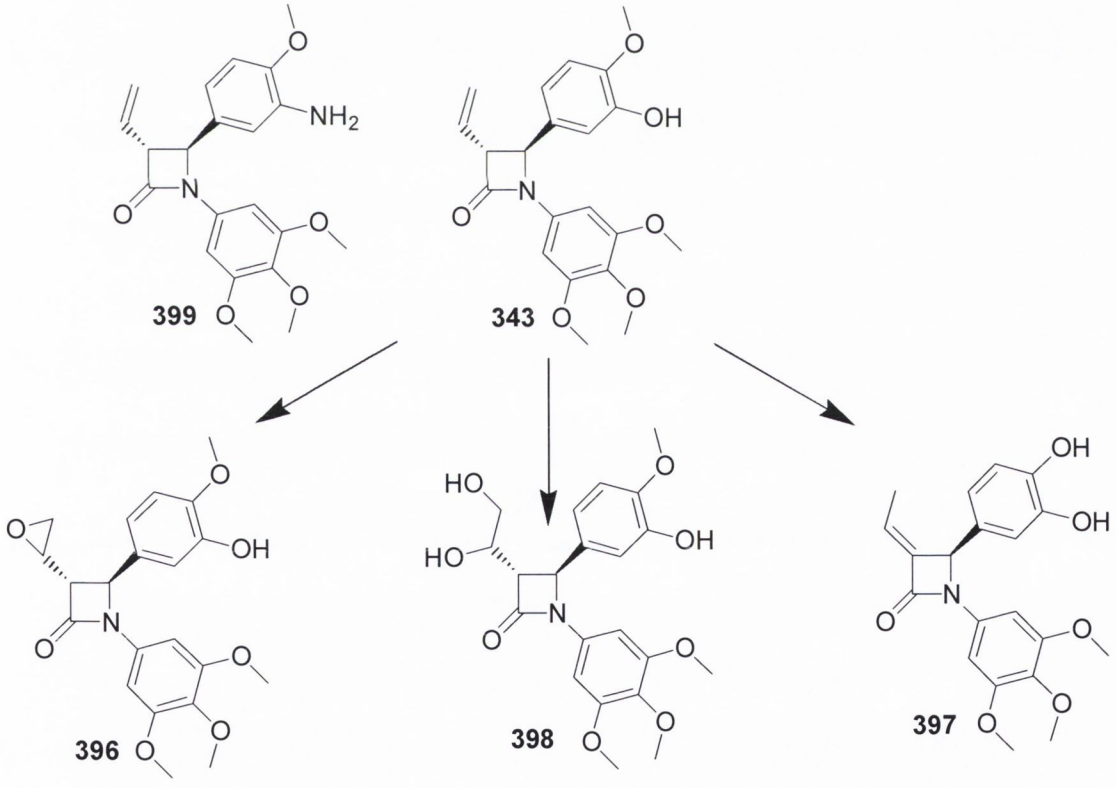

Fig 3.12 Possible transformations of **343** to be examined

3.4.1 Epoxidation Reaction

The epoxidation of the 3-vinyl β-lactam (**343**) is of particular interest since the resulting epoxide (**396**) can serve as a staring point for a further series of chemical transformations. Since the functional group present at the 3-position of the β-lactam is vital to biochemical activity and therefore any method that is capable of introducing diversity to this position is most welcome. Epoxides are subject to ring opening with a large variety of nucleophiles such as alcohols, amines, and cyanide. Asymmetric ring opening can also be performed with chiral reagents or catalysts to yield optically pure products [307] [308] [309]. Cardillo et al made use of epoxide ring opening to form azide and aziridine derivatives and serves as an example of the usefulness of the epoxide functionality (**scheme 3.14**) [310].

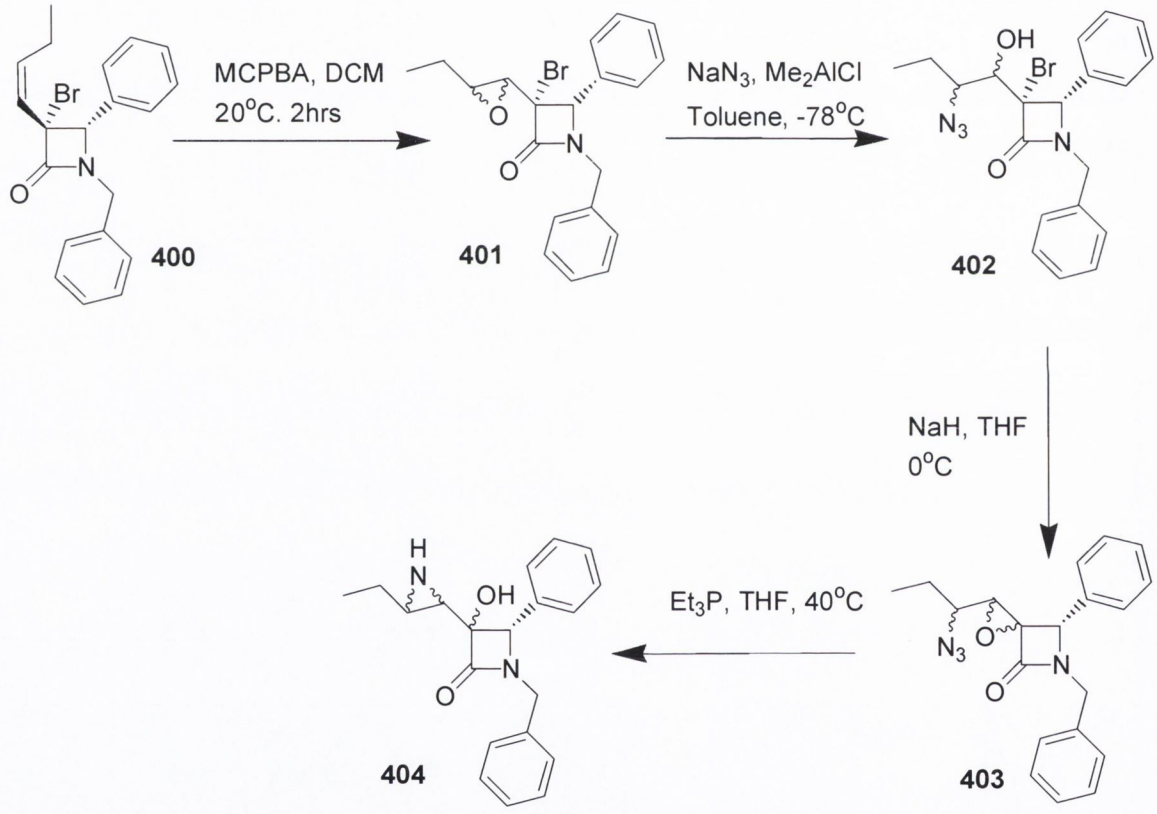

Scheme 3.14 Epoxides as key intermediates for 3-substituted β-lactams (single diastereomer only shown)

The starting material **400** was formed via a Staundinger reaction[311] followed by conversion to the epoxide **401** by mCPBA. 2-Bromoalkenyl chloride treated with TEA led to the desired ketene which in turn was reacted with the appropriately substituted imine to yield **400** in 60% yield The epoxide **401** was formed as a 1:1 mixture of diastereomers which were separable although only one isomer is

illustrated below for clarity. The opening of the epoxide ring was achieved with diethylaluminium azide which was prepared *in situ* with sodium azide and diethylaluminium chloride. The regioselectivity of the reaction is as a result of the azide approaching on the less hindered side of the epoxide. The spiroepoxide **403** was formed upon treatment of **402** with sodium hydride by displacement of the bromine group. The aziridine **404** was formed by the reduction of the azide group of **403** by either triphenyl phosphine or triethylphosphine. The most widely used reaction for the epoxidation of alkenes is the Prilezheav reaction (**scheme 3.15**) involving mCPBA reacting with the electron rich double bond leading to an intermediate which degrades to yield the epoxide. In this case the reaction was carried out by the method presented by Burke[312].

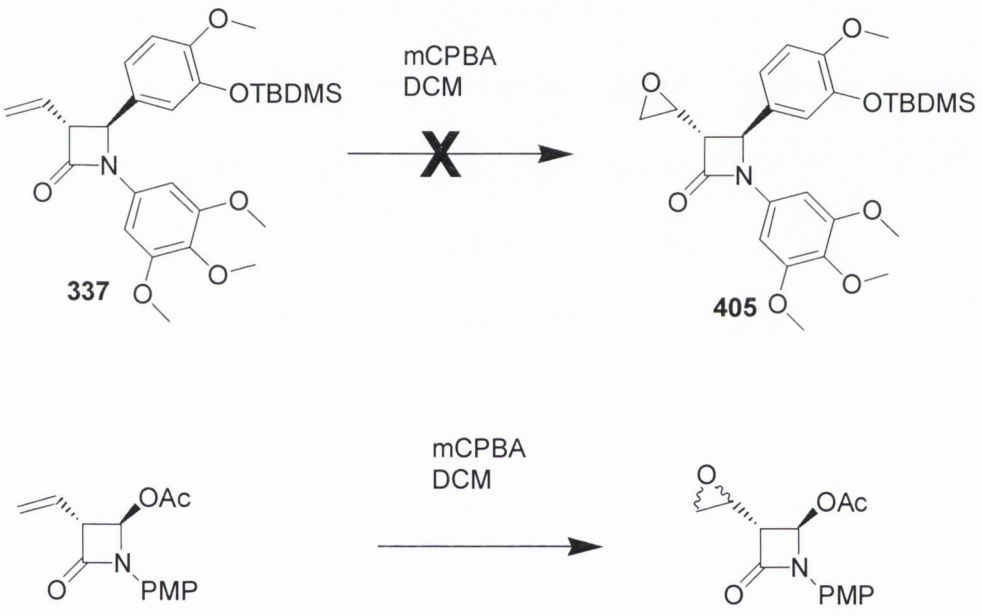

Scheme 3.15 Prilezheav reaction for the attempted synthesis of **405** as used by Burke

An attempt at carrying out the epoxidation in this manner was not successful and resulted only in the degradation of starting material and not formation of **405**. This was surprising since mCPBA was already successfully used in the oxidation of the sulphur methyl compound discussed in Chapter 2. It was thought that the water content of the mCPBA (approx. 40% by mass added for safety regions) may be to blame. A solution of mCPBA was partioned between DCM and saturated brine, followed by drying of the organic layer by $NaSO_4$, to obtain a solution of mCPBA with a greatly reduced water content. The resulting solution also failed to epoxidise the 3-vinyl compound. The reaction was also attempted on an analogue not bearing a 3-

hydroxy group on the aryl ring (**406**) attached to C_4 of the β-lactam ring, but again without success in the formation of **407**. Similar reactions have been carried out by Burke (**scheme 3.15**) in this previous work in this lab and may be useful as antiproliferative compounds.

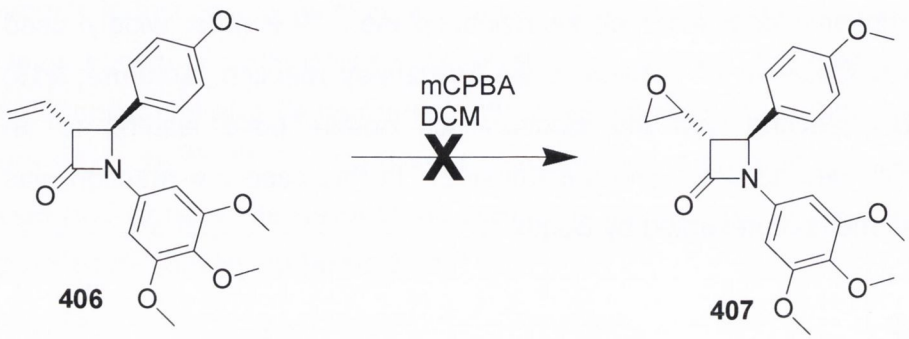

Scheme 3.16 Prilezheav reaction for the attempted synthesis of **407**

A number of other systems are available for epoxidation reactions that may prove useful in future work. These include trifluoroperoxyacetic acid and 3,5-dinitroperoxybenzoic acid which have been noted to be more reactive than mCPBA[313 314]. Epoxidation reactions may also be catalysed by transition metals such as copper, iron, and manganese[315].

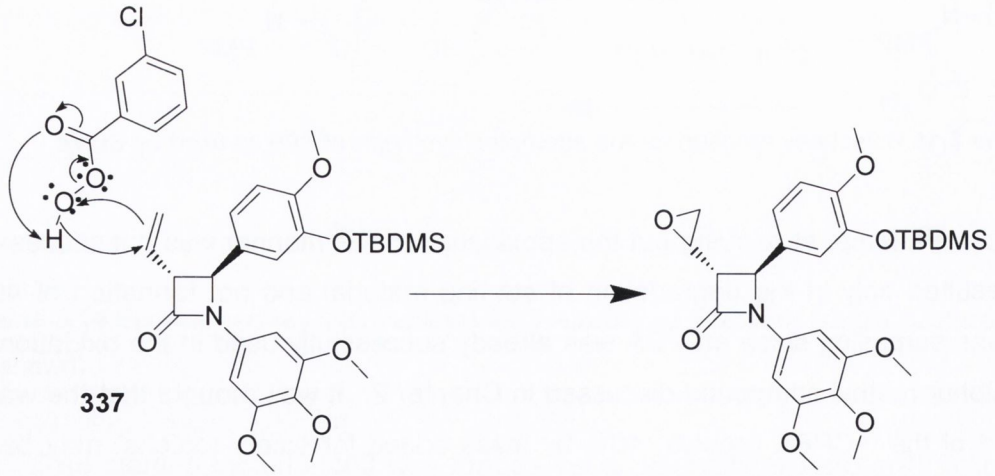

Scheme 3.17 proposed mechanism of mCPBA epoxidation of **337**

3.4.2 OsO_4 Mediated transformation C=C bond

As mentioned above, the introduction of a diol functionality at C_3 was now explored. Since the epoxidation reaction was unsuccessful, an alternative route to this 1,2-diol function (**398**) is outlined in **scheme 3.18** where OsO_4 is used to oxidise the alkene **315** to the desired diol **398** 39% yield.

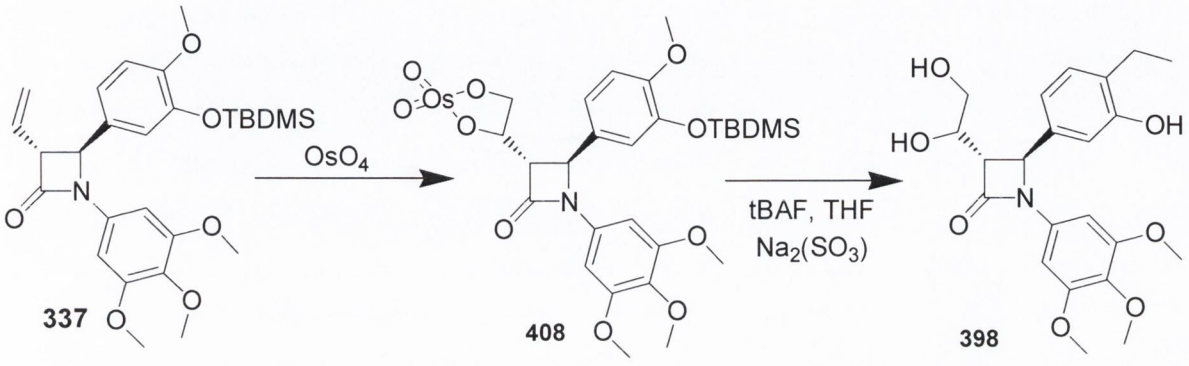

Scheme 3.18 OsO_4 hydroxylation of the 3-vinyl β-lactam

The procedure presented by Neary[316] was followed involving an initial reaction of **315** with OsO_4 to form the intermediate **408**, which is subsequently treated with $Na_2(SO_3)$ and hydrolysed to form the product. From the NMR of the crude material it was apparent that the product was produced as a mixture of diastereomers. Separation of the diasteromers of **398** was attempted by chromatography on a Biotage SP1 flash chromatography system by carrying out a gradient elution from 2% hexane in ethyl acetate to 100% ethyl acetate over the course of 30 column volumes, with no separation of the diastereomers observed.

The ^1H NMR spectrum for **398** is presented in **fig 3.13** and it clearly illustrates the formation of the product as a mixture of diastereomers (**398a** and **398b**). H_3 appears as a pair of double doublets at δ3.16ppm (0.72 protons) and δ3.19ppm (0.29 protons) with coupling constants of 2.42Hz and 5.55Hz. H_4 appears as two separate doublets at δ4.9ppm (0.31 protons) and δ5.0ppm (0.69 protons) again integrating for a total of one proton. H_4 displays a J value of 2.37 Hz which is typical of H_3 and H_4 being *trans* to one another. Both protons interact with carbon signals at δ58ppm and δ63ppm which from the DEPT spectrum are known to be CH carbons. The proton signals of the methoxy groups appear as a series of singlets from δ3.67ppm to δ3.82ppm integrating for a total of twelve protons. From the HSQC spectrum (**fig 3.14**) it is apparent that the geminal protons of C_6 appear somewhat obscured by the

methoxy signals in the ^1H spectrum. The HSQC spectrum clearly indicates that the signal from the second diastereomer is overlapping with the signals for the methoxy groups attached to C_3' and C_5'. When both signals are integrated as a single unit a total of eight protons is obtained. The H_5 proton appears as two sets of quartets at δ4.09 (0.26 protons) and δ4.19 (0.75 protons) with a coupling constant of 5.50Hz The H_5 signal overlaps slightly with a broad singlet centred on δ4.25ppm that the HSQC spectrum confirms arises from a hydroxy group. A second hydroxy peak appears as a broad singlet centered at δ2.7ppm. A third hydroxy signal appears as a set of two broad singlets in the δ6.25-δ6.43ppm region again indicating the presence of diastereomers. The H_2' and H_6' aromatic protons appear as a singlet at δ6.53 integrating for two protons. The remaining aromatic protons H_2'' H_5'' H_6'' appear as multiplets at δ6.77-6.94 integrating for three protons. The IR spectrum of **398** reveals an absorption at 1727cm^{-1} for the carbonyl group and a broad signal at 3454cm^{-1} for the various alcohol groups.

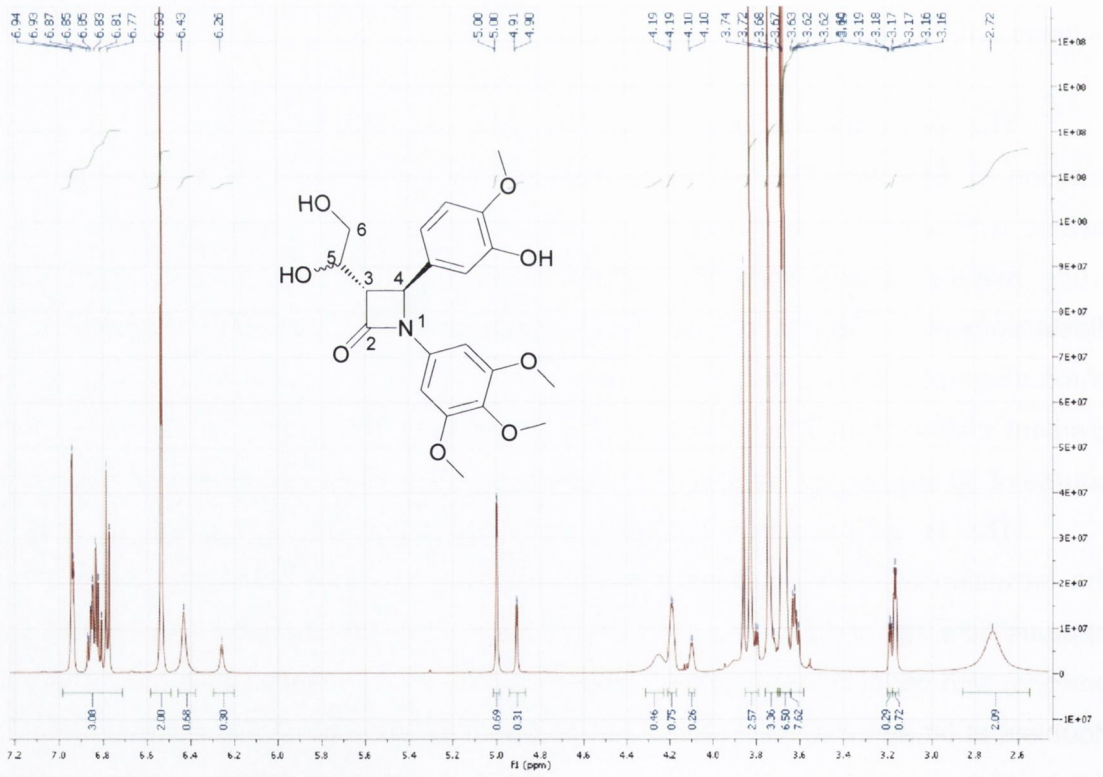

Fig 3.13 ^1H NMR spectrum of **398**.

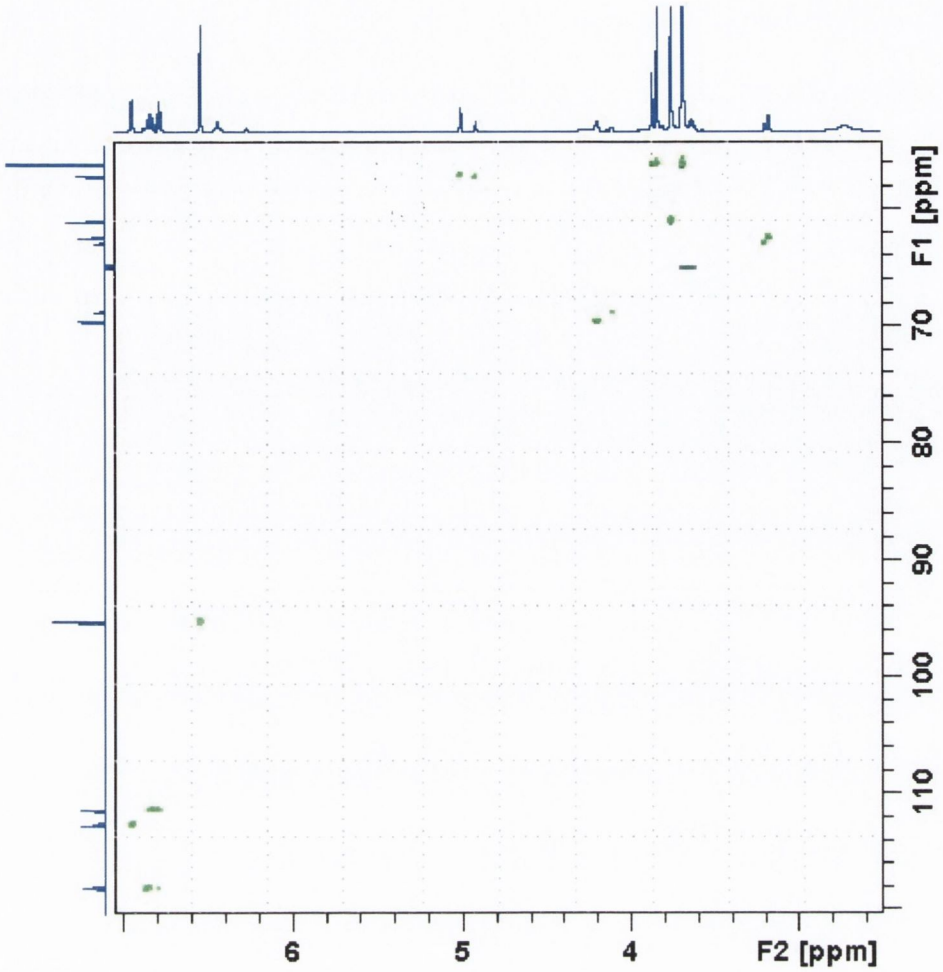

Fig 3.14 HSQC spectrum of **398**

3.4.3 3-Vinyl to 3-Ethylidene tranformation

To further investigate the role of the 3-vinyl substitution pattern in biochemical activity of β-lactams a 3-ethylidene product was formed. The initial route attempted involved the chlorination of the alcohol (**382**) to the alkyl chloride (**408**) using thionyl chloride (**scheme 3.19**). The alkyl chloride can next be dehydrohalogenated with a suitable base such as DBU to yield the desired product. This route is also attractive since the intermediate (**408**) can be screened for biochemical activity and compared to the hydroxy compound.

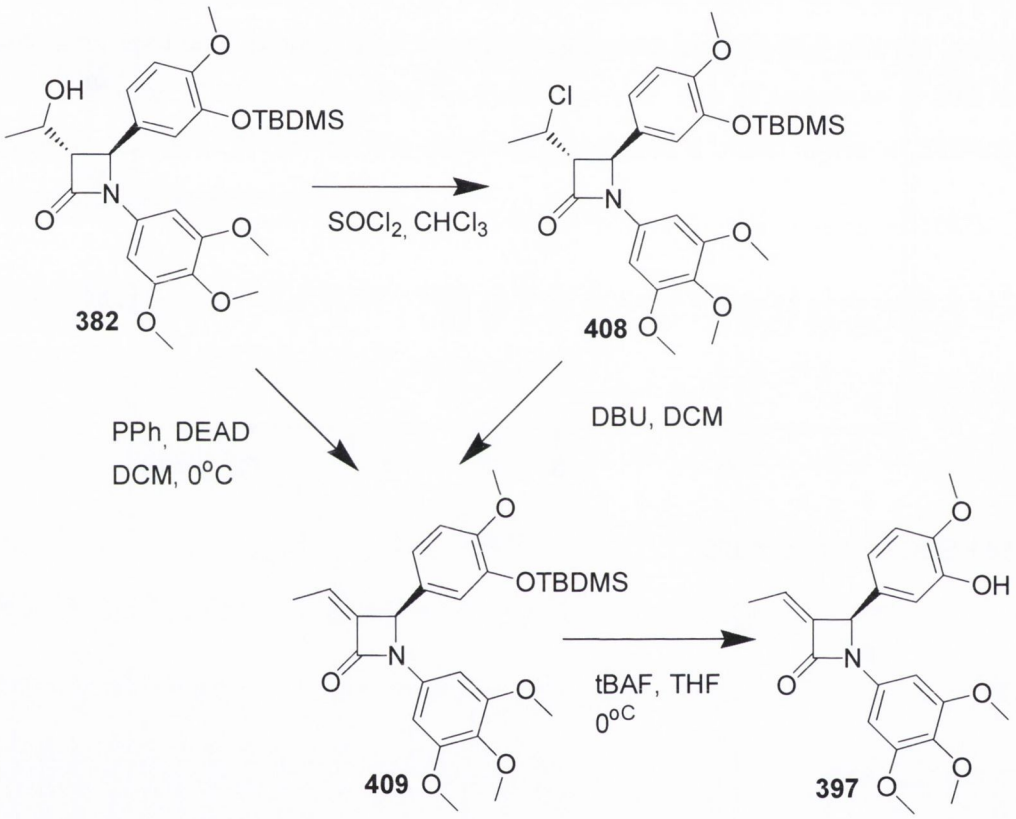

Scheme 3.19 Synthetic routes to the 3-ethylidene product

The procedure of O' Leary[317] was followed for the formation of the alkyl chloride. After two hours of stirring with one equivalent of thionyl chloride in chloroform, TLC and IR both indicated that the chlorination reaction had not gone to completion. A second equivalent of thionyl chloride was added to the reaction and stirring continued for a further two hours. At this stage the ^{1}H NMR of the material indicated that there was no β-lactam in the crude material. This was surprising since the formation of alkyl chlorides of β-lactams is well known. O'Leary reports yields in excess of 70% for the majority of alkyl chlorides formed in this manner however it

was noted that for certain substituents attached to C_5 the yield dropped considerably[316].

A second route to give the 3-ethylidene β-lactams was identified from literature involving the dehydration of the alcohol (**382**) under Mitsunobu conditions to give **409** yield which was subsequently deprotected by treatment with *t*BAF to yield **397** in 63% yield overall . The Peterson olefination of 3-unsubstituted β-lactams has also been reported by Kano[318] as another alternative route to the desired 3-ethylidene β-lactam. The use of the Mitsunobu reaction for the dehydration of alcohols has been described by Solmajer et al[319] in the synthesis of a trinem β-lactamase inhibitor (**scheme 3.20**). In the original paper by Solmajer the Mitsunobu dehydration was carried out on a diastereomerically pure precursor and so only one geometric isomer (*E*) was produced in the reaction. The *E/Z* isomers produced for **397** are illustrated in **fig 3.15**. From **fig 3.16** it can be seen that the product has been formed as a mixture of *Z/E* isomers in a 1:1 ratio only one of which was able to be cleanly isolated **fig 3.17**. The IR spectrum of **397** shows absorptions at 1738cm^{-1} for the carbonyl of the β-lactam ring and at 2935cm^{-1} for CH stretching. An absorption for the hydroxy group appears at 3327cm^{-1}. **Scheme 3.21** outlines the the mechanism for the Mitsunobu dehydration reaction.

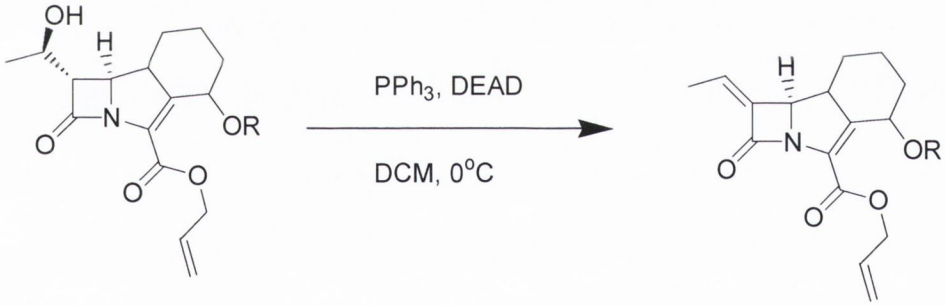

Scheme 3.20 The Mitsunobu reaction for the dehydration of alcohols

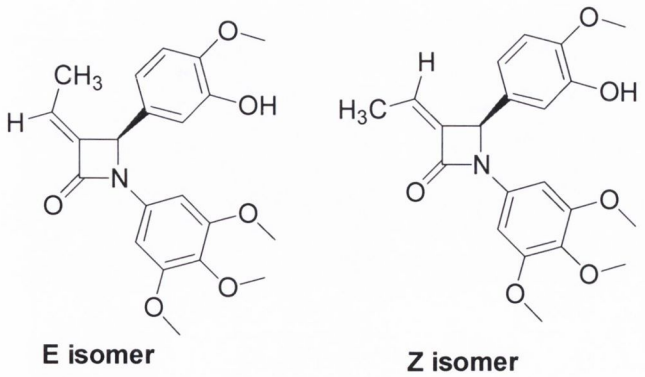

E isomer **Z isomer**

Fig 3.15 *E* and *Z* isomers of **397**

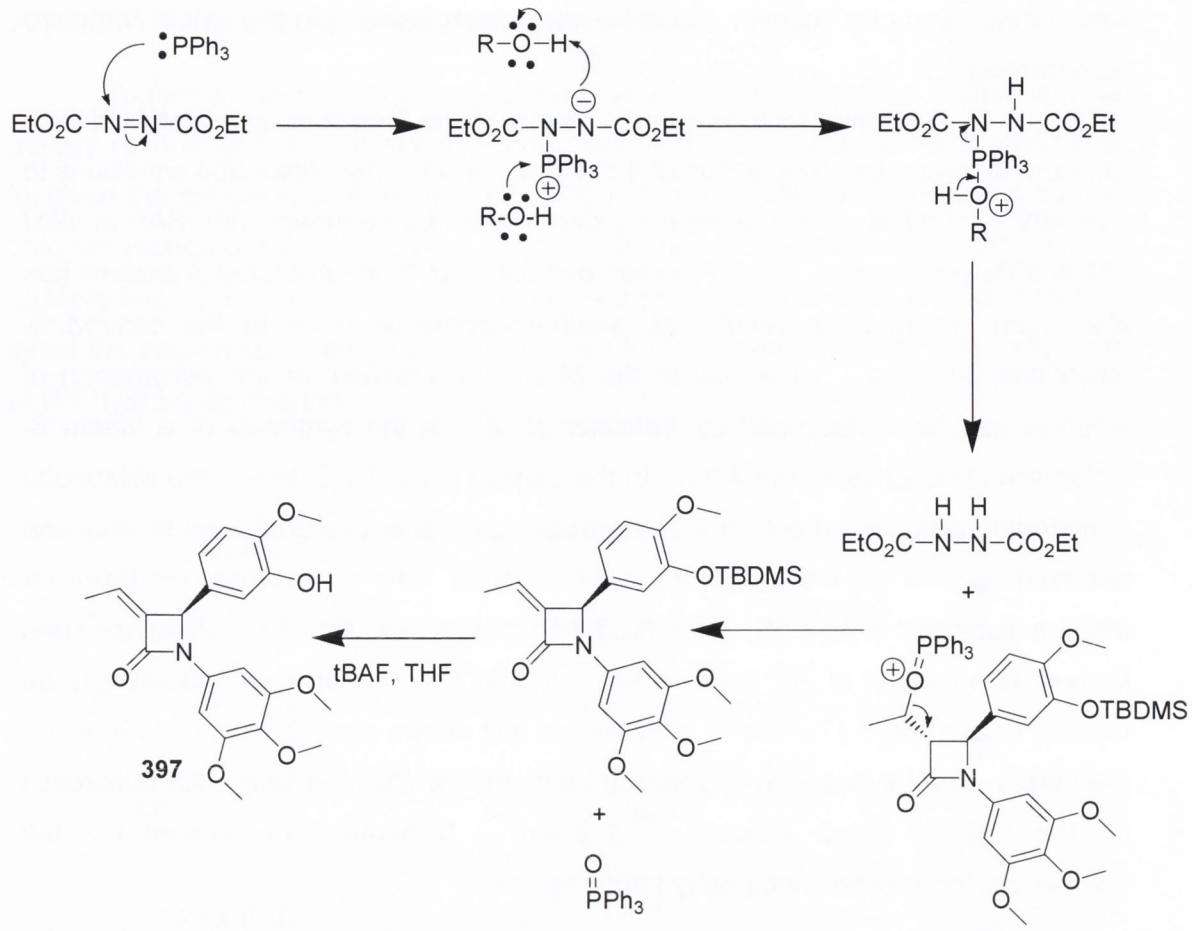

Scheme 3.21 Mitsunobu dehydration of alcohol

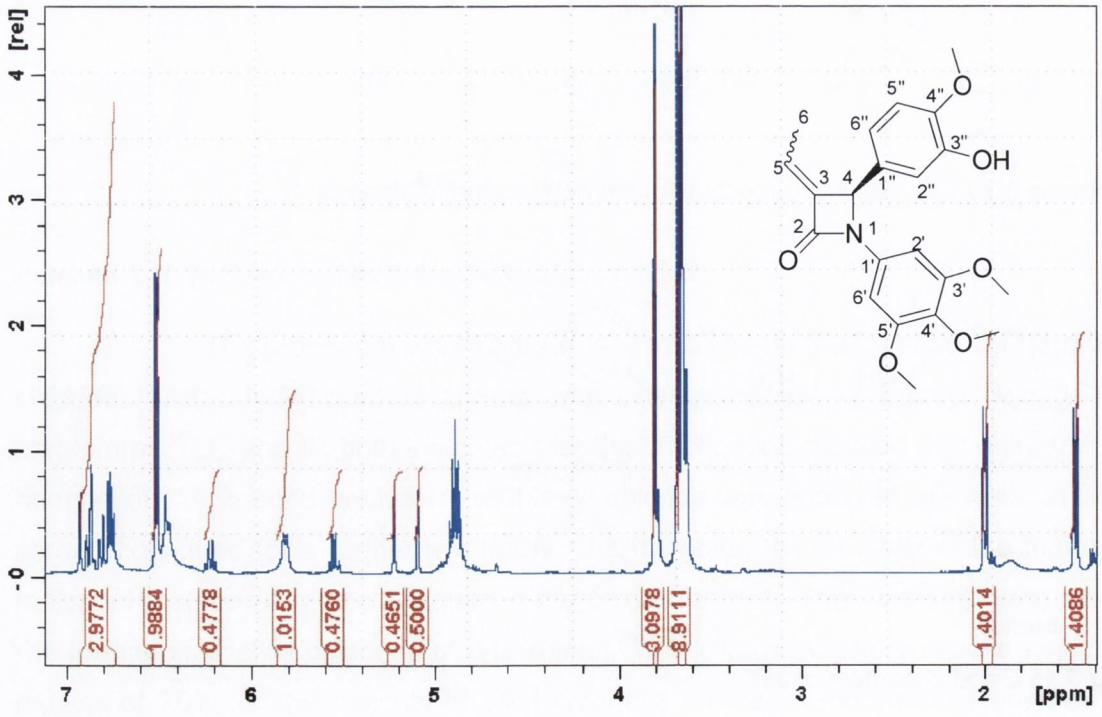

Fig 3.16 ^{1}H NMR spectrum for **397** (crude reaction)

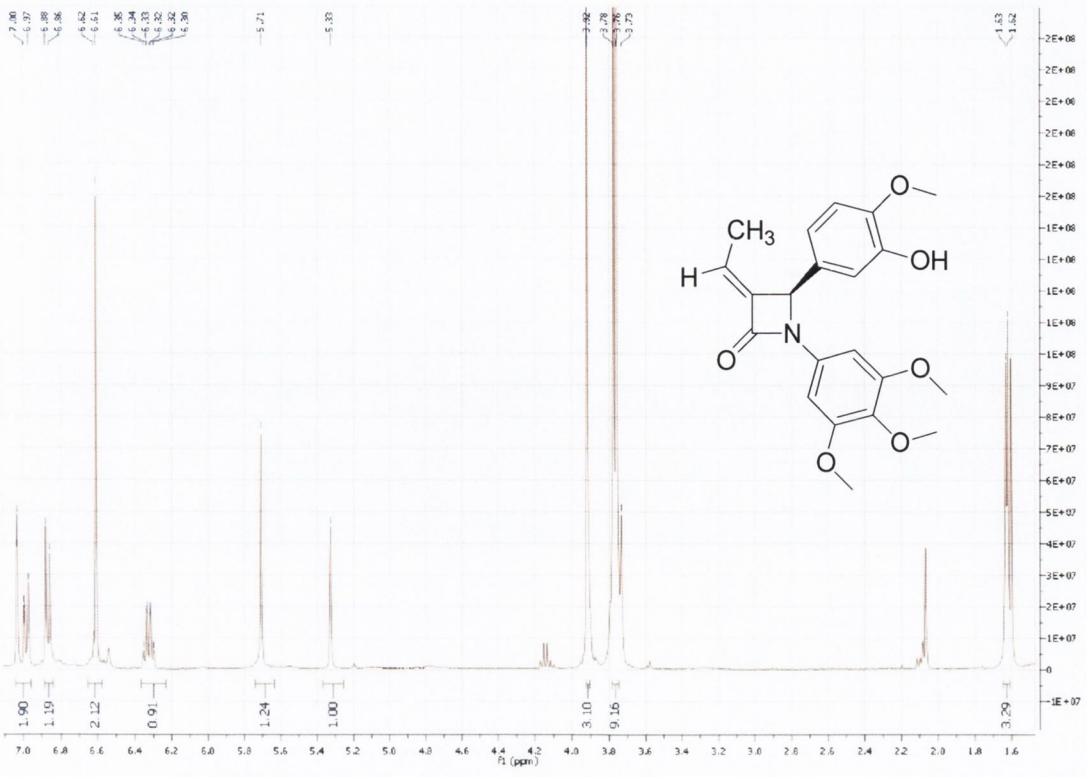

Fig 3.17 single isomer of **397** (*E* isomer)

It is possible to assign the configuration of the isomer isolated by examining the chemical shifts associated with the protons at C_6 and C_5. Fortunately Burke[312] has synthesised a number of similar compounds for which the *Z*/*E* configuration is known and this aids in the identification of the configuration of the product in this case. In the *Z* isomer the C_6 methyl group should be closer to the carbonyl group of the ring than in the corresponding *E* isomer and should be deshielded to a larger extent. By the same reasoning the *E* isomer will have a methyl group that is deshielded to a much lesser extent. This effect is clear to see in **fig 3.16**, where there two separate signals for the methyl protons can be clearly seen at δ1.62ppm and δ2.05ppm. The further downfield signal (δ2.05ppm) is more deshielded and so belongs to the *Z* isomer, and likewise the signal at δ1.62ppm belongs to the *E* isomer. Therefore it is the *E* isomer that has been isolated and illustrated in **fig 3.17** where the methyl group appears as a doublet at δ1.62ppm integrating for a total 3 protons. The H_4 proton appears as a singlet at δ5.71ppm integrating as a single proton, while the hydroxy appears as a singlet at δ5.33ppm. H_5 appears as a multiplet centred on δ6.32ppm and integrating for a single proton. The aromatic region from δ6.61 to δ7.03ppm integrates for a total of 5 protons. The equivalent $H_{2'}$ and $H_{6'}$ protons appear as a singlet integrating for two protons at δ5.71. The signal for $H_{5''}$ appears as a doublet at δ6.86ppm integrating as a single proton with a coupling constant of 8.2Hz due to coupling to $H_{6''}$. $H_{2''}$ appears as a doublet at

δ7.03ppm integrating for a single proton and displaying a coupling constant of 1.96Hz indicating that it is coupled to $H_{6''}$. $H_{6''}$ appears as a doublet of doublets at δ6.99ppm since it is coupled to both $H_{2''}$ and $H_{5''}$ and integrates for a single proton.

3.4.4 Synthesis of 3-Vinyl Azetidin-2-ones: Amino Containing Compounds

All of the analogues synthesised in the previous sections of this work contained a common 3-hydroxy-4-methoxy substituted phenyl ring located at the 4-position. However in Chapter Two it was demonstrated that the 3-amino-4-methoxy phenyl substituent is also of importance. In this section, the 3-amino phenyl pattern and the 3-vinyl pattern identified above as having exceptional biochemical activity, are now combined in a new subgroup of compounds, in order to synthesise an analogue optimized at both the 3 and 4 positions of the β-lactam ring. This was achieved as outlined in **scheme 3.22** involving first the synthesis of (**410**) by the Staundinger reaction, followed by reduction of the nitro group to the 3-amino compound (**399**) by using the zinc/acetic acid reducing conditions previously employed. **410** was obtained in 37% yield by the dropwise addition of a solution of crotonyl chloride into a stirring solution of the imine **199** and TEA in DCM under nitrogen. Only the *trans* isomer was observed in the mixture.

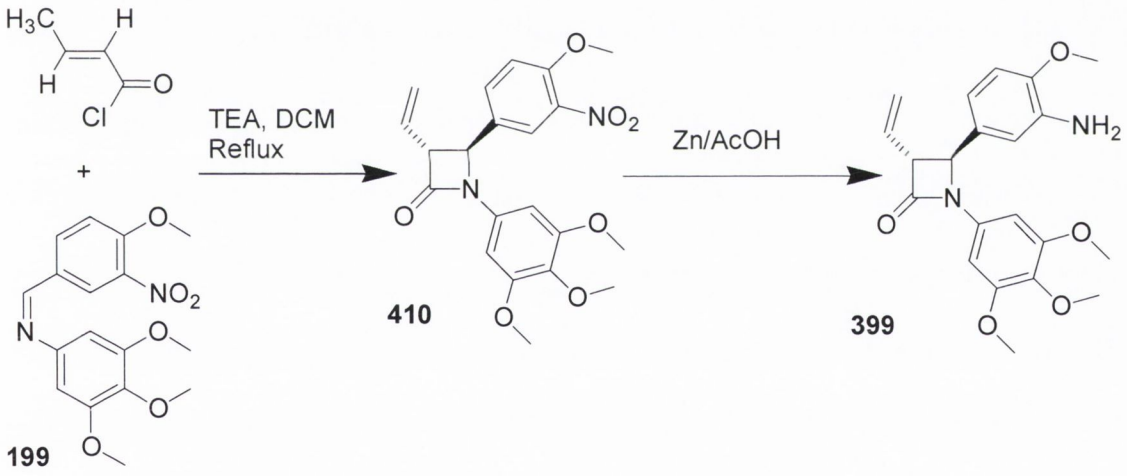

Scheme 3.22 Synthesis of 3-N containing compounds **410** and **399**

The reduction was carried out over the course of seven days at room temperature and was monitored by TLC resulting in the isolation of **399** in 83% yield. **Fig 3.18** and **Fig 3.19** present the ^{1}H NMR spectra for both the nitro and amino compounds (**410** and **399**). The conversion to an amino group is apparent from the shift upfield of a number of signals especially in the aromatic region. The resulting amino compound proved very difficult to fully purify by column chromatography. It was also formed as an oil which ruled out the possibility of purification by recrystallisation commonly used for other β-lactams synthesised in this thesis. Final

purity of only 83% by area in HPLC was achieved and this results in the trace amount of impurities seen in **fig 3.19**. The reduction of the nitro group in **399** was apparent from IR spectroscopy. An absorption band at 1746cm^{-1} assigned to the carbonyl group and at 3470 cm^{-1} assigned to the amino group were observed. In the nitro starting material (**410**) the carbonyl group absorption was observed at 1754cm^{-1}.

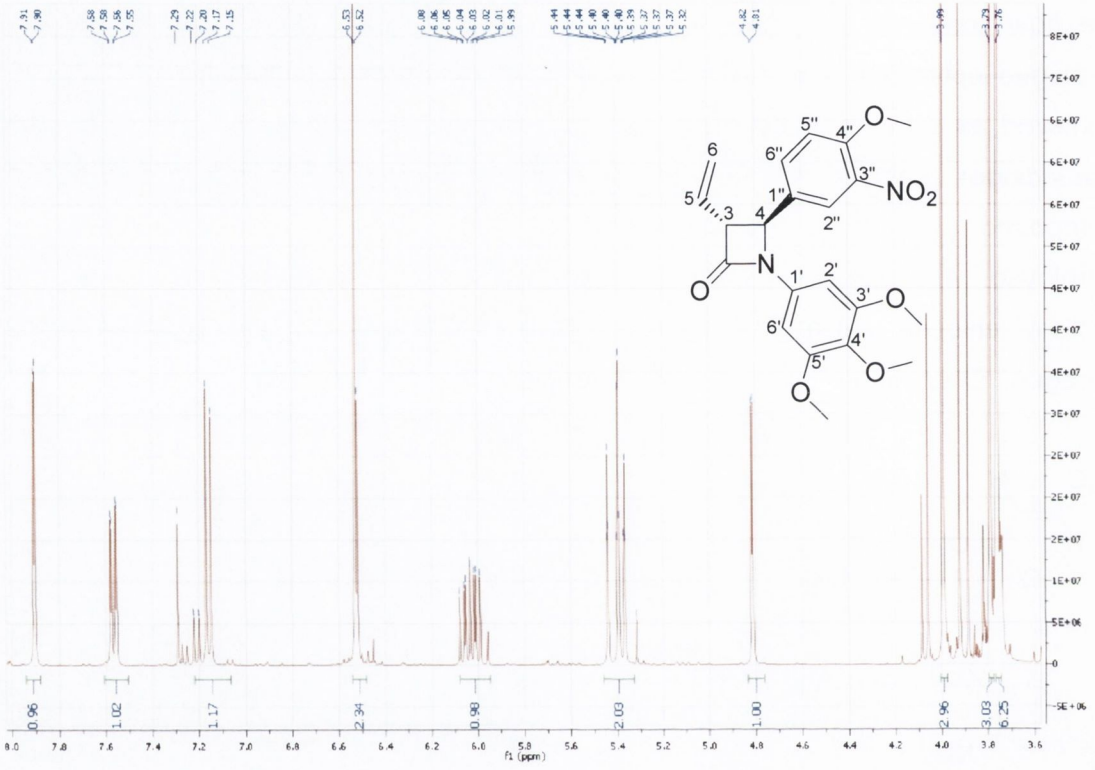

Fig 3.18 ^{1}H NMR spectra for **410**

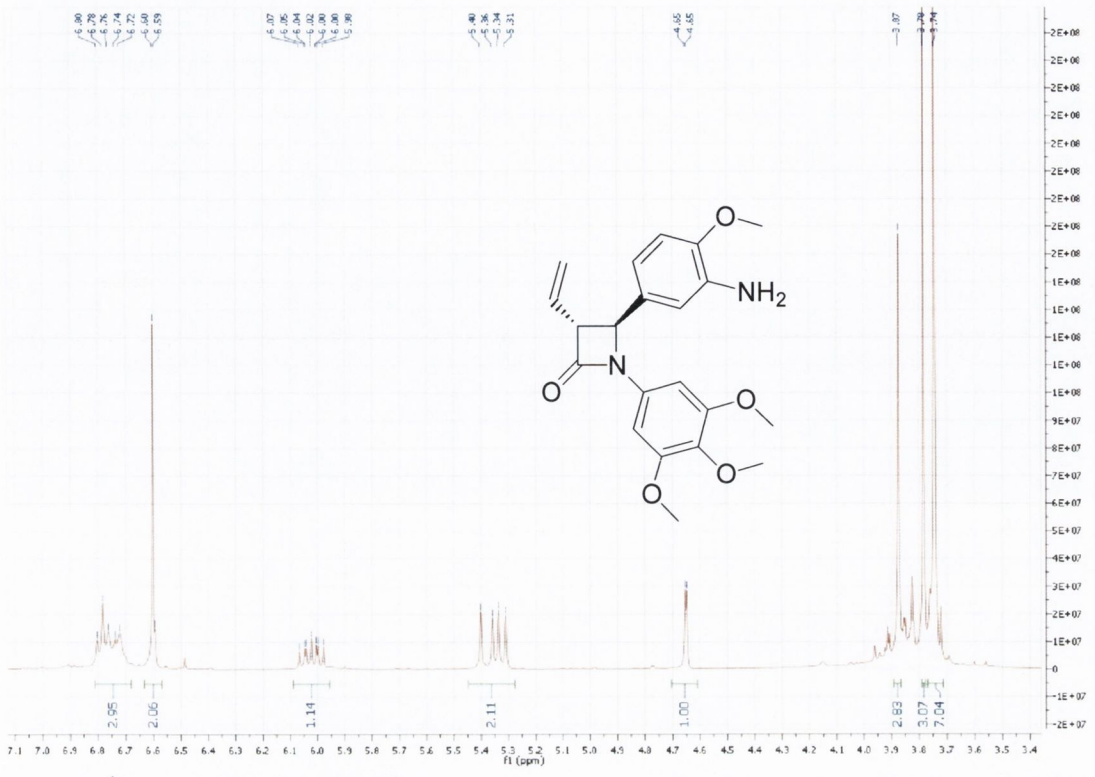

Fig 3.19 ^{1}H NMR spectrum for **399**

For the nitro substituted 3-vinyl β-lactam **410** the ^{1}H NMR spectrum is uncomplicated except for the apparent lack of a signal for H_3. Upon closer examination it can be seen that the large singlet from the methoxy protons of $C_{3'}$ and $C_{5'}$ at δ3.76ppm integrate as seven protons instead of six indicating that the H_3 signal is obscured by these methoxy signals. The remaining methoxy signals appear at δ3.78ppm and δ3.99ppm integrating for three protons each. H_4 appears as a doublet at δ4.81ppm integrating for one proton with a coupling constant of 2.44Hz indicating that it is coupled *trans* to H_3. The protons attached to C_5 and C_6 appear as a series of multiplets centered on δ6.01ppm and δ5.34ppm respectively. In the aromatic region $H_{2'}$ and $H_{6'}$ are equivalent and give rise to the singlet at δ6.51ppm integrating for two protons. $H_{5''}$ appears as a doublet at δ7.15 integrating for a single proton coupled to $H_{6''}$ with a coupling constant of 8.72Hz. $H_{2''}$ also appears as a doublet at δ7.90 integrating for a single proton and is coupled to $H_{6''}$ with a coupling constant of 2.28Hz. $H_{6''}$ appears as double doublets centered on δ7.56 and integrating for one proton.

In the ^{1}H NMR spectrum for the amino product **399**, the conversion of the nitro to the amino group is apparent from the shift upfield of signals from the aromatic protons compared to **410**. This shift is more obvious for signals arising from groups

close to $C_{3''}$. For the methoxy group attached to $C_{4''}$ there is an obvious shift from δ3.99ppm to δ3.87ppm. Likewise for the three aromatic protons $H_{2''}$ $H_{5''}$ and $H_{6''}$ which previously displayed chemical shifts greater than δ7.0ppm but as a result of the reduction now all occur as a series of multiplets integrating for three protons centered on δ6.76ppm.

3.4.5 The Role of the 3-Vinyl Group in other Compounds

In preliminary biochemical studies it was demonstrated that the introduction of the 3-vinyl substituent for compounds **343** and **399** led to a marked improvement in antiproliferative activity. The question that arises from this observation is whether the presence of both substitution patterns in the same compound (ie 3-vinyl and 3-hydroxy/amino phenyl) has a synergistic effect in terms of biochemical activity. To this end the 3-vinyl group was incorporated into two compounds **245b** and **250b** that had previously displayed only average biochemical activity in the MCF7 cell line (**fig 3.20**).

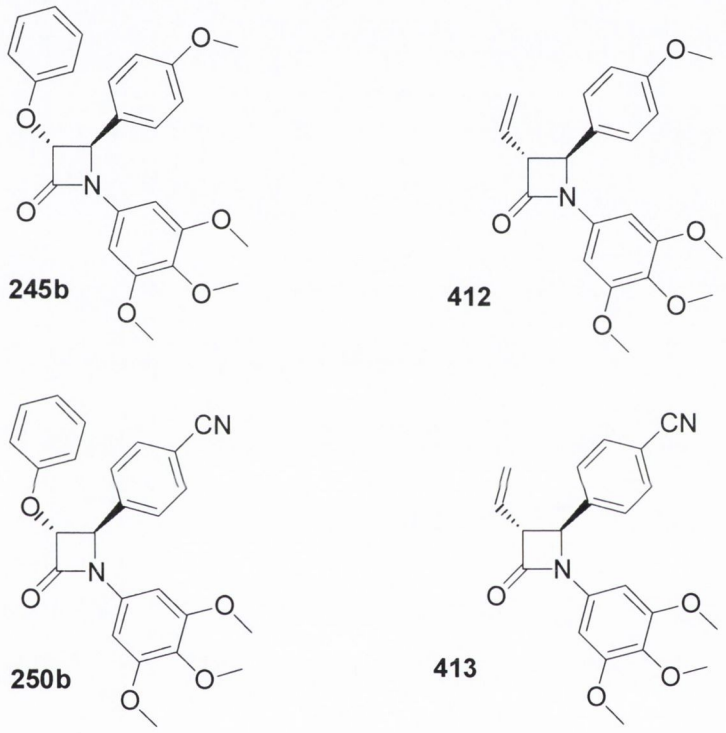

Fig 3.20 Investigating the introduction 3-vinyl group in combination with other substitution patterns in C_4 aryl ring

The compounds **412** and **413** were easily accessed via the Staundinger reaction (**scheme 3.23**), however in keeping with experience with other 3-vinyl compounds, the purification step with column chromatography proved difficult. In both cases only the *trans* isomer was observed in the reaction.

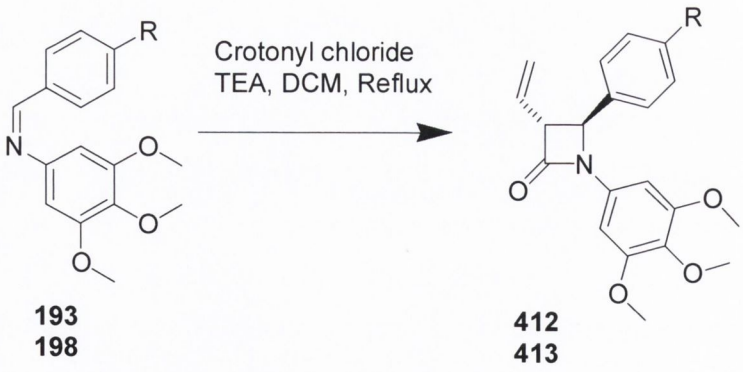

193
198

412
413

Scheme 3.23 Synthesis of 3-vinyl substituted β-lactams

Compound No.	R	IR	MP (°C)	Yield (%)
412	OMe	1738	Oil	22
413	CN	1744, 2312	Oil	17

Table 3.6 Melting point, yield, and IR data for compounds **412** and **413**

Summary

Chapter 3 presents the details of the synthesis of a series of β-lactams incorporating varying substituents at C_3 of the β-lactam ring. The substituted aryl ring was kept constant during these changes with the 3-hydroxy-4-methoxy substitution pattern that had been identified in Chapter 2. Initially structural diversity was incorporated onto C_3 by successful modification of the Staundinger reaction from which the 3-vinyl β-lactam was identified as a promising substitution. An aldol type addition of carbonyl compounds to 3-unsubstituted β-lactam was also carried out. From biochemical evaluation of the compounds, the 3-vinyl substituent was identified as leading to potent compounds. A number of chemical transformations were carried out on the vinyl containing β-lactams including an attempted epoxidation reaction, an OsO_4 oxidation to the corresponding diol, and the synthesis of a 3-ethylidene analogue. Having identified the 3-vinyl substituent at C_3 as being important, a 3-vinyl analogue also bearing the 3-amino-4-methoxy substitution pattern at the aryl ring attached to C_4 was also synthesised. To further investigate the role of the 3-vinyl substituent, further analogues with substituted aryl rings at C_4 previously identified as not possessing significant biochemical activity were also synthesised.

Chapter 4

Biochemical, Stability, and Molecular Modelling Studies of Novel Anticancer β-Lactams

4.1 Introduction

The results of *in vitro* biochemical testing of the analogues synthesised thus far are presented in this chapter. A number of factors were considered when deciding the most appropriate method to test the compounds such as assay cost, availability of biological specimens such as cells, purified tubulin protein etc., time, expertise needed to carry out the test, and waste disposal. The ability to draw comparisons between the method selected and the results presented in literature by other researchers was also a priority. The MTT antiproliferative, and LDH cytotoxiciy assays in MCF-7 cells, and inhibition of tubulin polymerisation were considered to be the most appropriate individual assays for these compounds. **Section 4.1.1** presents a brief overview of some of the more common *in vitro* assays available for evaluating test compounds both in terms of antiproliferative and cytotoxic effects as well as methods for determining antitubulin effects. The evaluation of any therapeutic compound agent *in vivo* is a natural progression from *in vitro* testing and a brief summary of the area is presented in **section 4.1.2**. *In vivo* testing typically involves a major investment in time and materials and requires expertise generally not found in a medicinal chemistry setting. For these reasons *in vivo* testing of compounds is only performed after identification of promising leads from an *in vitro* screen. In this thesis only *in vitro* testing was carried out, but it is intended to submit the more promising lead compounds for *in vivo* testing in the future in collaboration with Dr. D. Zisterer, School of Biochemistry, TCD.

4.1.1 Evaluating Combretastatin Analogues *In Vitro*

The antiproliferative and cytotoxic effects of the analogues synthesised as part of this thesis were evaluated using MTT and LDH based assays respectively. Both of these methods are quick, easy to use, relatively cheap and are therefore well suited for use as an initial screening method to identify promising analogues from the compound libraries synthesised thus far. Since the mechanism of action of combretastatin (and analogues there of) is that of a tubulin disrupting agent, there are a number of assays described in literature that examine the effects of such agents on tubulin. These tubulin assays fall into two categories: tubulin polymerisation assays and tubulin binding assays. Such tubulin assays are important since they evaluate directly the antitubulin effects of the compound of interest whereas the MTT/LDH method really only uses cell proliferation/cell death as a proxy for antitubulin activity. Later in Chapter 4 the use of a tubulin polymerisation assay is discussed in detail. This particular assay was only carried out on the most promising analogues identified by the MTT and LDH assays mainly due to the

monetary cost of the assay. A typical tubulin binding assay involves examining the competitive binding of a compound and a labelled colchicine derivative to the colchicine site of tubulin. Generally the colchicine is either fluorescently or radio labelled, but in both cases the principle is the same.

Since CA4 has a well characterised antivascular effect, assays using human umbilical vein endothelial cells (HUVEC cells) have been developed. HUVECs are in widespread use as a model for tumour vasculature endothelial cells for research in both antiangiogenesis and antivascular effects. The cytotoxicity of the the test compound to HUVECs has been determined by Dark *et al* [320].

The effect of CA4 on the organisation of the tubulin ctyoskeleton in HUVEC cells has also been demonstrated[321] (**fig 4.1**). Galbraith *et al* used a monoclonal antibody conjugated to cyanine 3 to selectively stain the tubulin protein in the cytoskeleton. Image (a) depicts the network prior to exposure to CA4 and (b) after exposure to 3μM CA4 for six hours, clearly showing the disruption of the cytoskeleton.

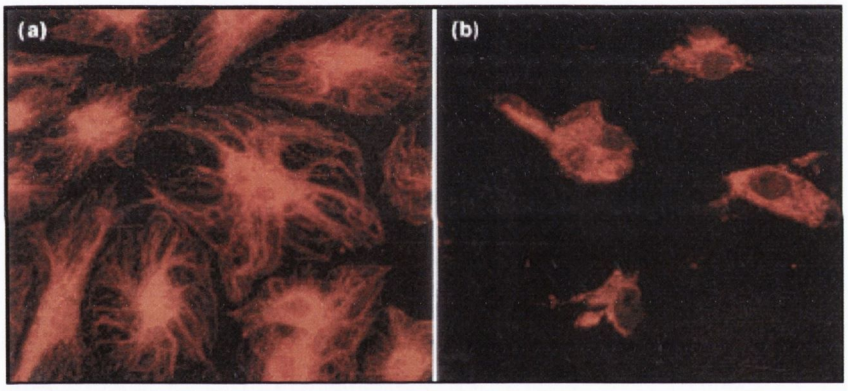

Fig 4.1 The effect of CA4 on the organisation of the cytoskeleton network in HUVEC cells (Galbraith *et al*)[321].

HUVECs grown on extracellular support can be used to determine the antivascular effects of combretastatin analogues[89]. Grosios *et al* used HUVEC cells grown in a collagen matrix to form HUVEC networks. Treatment with CA4 (0.31μM for 3 hours) resulted in the disruption of these networks.

In the present work, all of the compounds synthesised were initially evaluated for both antiproliferative and cytotoxic effects in the MCF-7 cell line. The most promising compounds identified were then screened for their effect on tubulin polymerisation.

4.1.2 Evaluating Combretastatin Analogues *In Vivo*

There are a number of reports on the effects of combretastatin in animal models of human cancer available. The simplest form of such a study is to examine the effects of the compound on the growth of an implanted tumour over a period of time as presented by Chaplin[93] (**fig 4.2**). The procedure used in this case involved initiating the growth of a murine adenocarcinoma in imunocompromised mice by injection of a suspension of the appropriate cancer cells. The growth of the tumour in the presence of the test compound can then be monitored by excision of the tumour and measurement of tumour mass and dimensions.

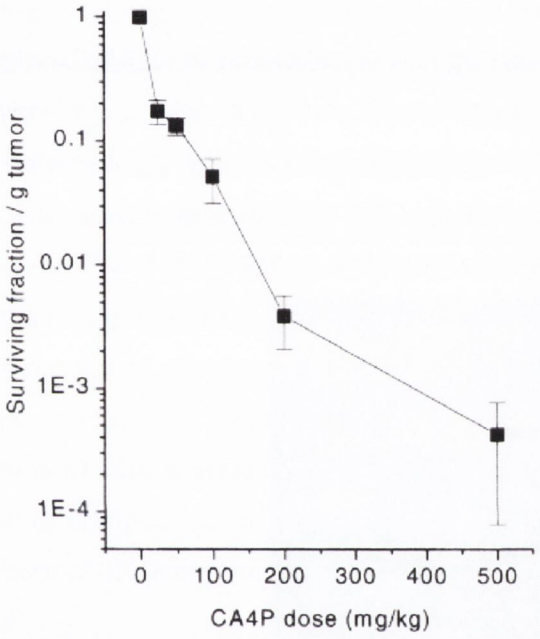

Fig 4.2 Surviving fraction of tumour 18-24 hours after treatment with various doses of CA4P (Chaplin *et al*)[93]

Chaplin also describes the use of a fluorescent dye to evaluate the perfusion of the tumour. The dye is injected followed by excision of the tumour. Examination of the tumour sections then allows an estimation of tumour perfusion. By this method Chaplin recorded a reduction of over 80% in tumour perfusion 24 hours after treatment. More interestingly a number of studies have been carried out that monitor directly the effect of combretastatin on tumour blood flow particularly by functional MRI[322] and by PET scanning[323]. PET scanning is particularly useful since it is non-invasive and is suited to measuring tumour and normal tissue perfusion. Anderson *et al* [324] have presented an excellent investigation of the effect of CA4P on tumour vasculature in a phase I trial of CA4P in patients with advanced solid tumours. The study used O^{15} radiolabelled water and carbon dioxide to measure the vascular effects of CA4P. A mean reduction of 49% in tumour perfusion was seen 30

minutes after treatment and tumour blood volume dropped by 15%. The change in blood flow to physiological tissue was also monitored with the spleen showing a reduction of 35% in perfusion after 30 minutes.

4.2 Materials and Methods Used

A full list of the materials used along with supplier details is provided in Chapter 5, along with detailed descriptions of the methods used.

4.2.1 Culture of the MCF-7 and MDA Cell Lines

Initially both the MCF-7 (estrogen receptor positive) and MDA-MB-231 (estrogen receptor negative) human breast cancer cell lines were used to screen for biochemical activity. The use of both of these cell lines arose as a consequence of previous work within the School of Pharmacy, TCD, that focussed on the synthesis of novel selective estrogen receptor modulators (SERMs) as anticancer agents. The use of both cell lines in screening was important since it illustrated that these novel agents may be working through the ER. Since the compounds presented in this work were expected to work through inhibition of tubulin polymerisation, it was decided only to use the MCF-7 cell line after testing of a number of compounds in both cell lines. The MCF-7 human breast tissue adenocarcinoma cell line was used to screen all of the compounds. The MCF-7 cell line has been extensively used as a model for estrogen receptor positive breast cancer both previously by our group and by various other groups[325]. It is also a member of the National Cancer Institute's 60 cell line panel which is used extensively in the evaluation of novel anticancer agents. A number of groups have included the MCF-7 cell line in the *in vitro* testing of combretastatin analogues[326].

The MCF-7 cell line (**fig 4.3**) was obtained by pleural effusion from a 69 year old female Caucasian and was supplied originally by the European Centre of Animal Cell Cultures. The cells were cultured in Eagles Minimum Essential Medium supplemented with 10% foetal bovine serum, 2mM *l*-glutamine, 1% non-essential amino acids, and 100ug/ml penicillin-streptomycin to prevent infections. For long term storage, a pellet of cells is stored in a mixture of EMEM with 10% DMSO acting as a cryopreservant is frozen in liquid nitrogen. The MDA cell line was cultured in Dulbecco's Modified Eagle's Medium supplemented with 10% v/v foetal bovine serum, 2mM l-glutamine, and 100µg/mL penicillin/stryptomycin To start the growth of a new culture of cells, this pellet is rapidly thawed out, diluted in 10mL of complete media, centrifuged, and the pellet resuspended in fresh media before being transferred to a flask. Generally the cells were grown in 14mL of the above media in a $75cm^3$ flask fitted with a filter cap in a moist incubator at 37°C with a 95% air / 5% CO_2 atmosphere, typically taking 5-7 days to reach confluency. A confluent $75cm^2$ flask can comfortably provide enough cells to carry out the assays and to seed a new flask. To guard against both infection of the cell culture and the risk of exposure of

lab workers to pathogens, all operations involving the culture of cells were carried out in laminar flow hoods under level 2 biological containment.

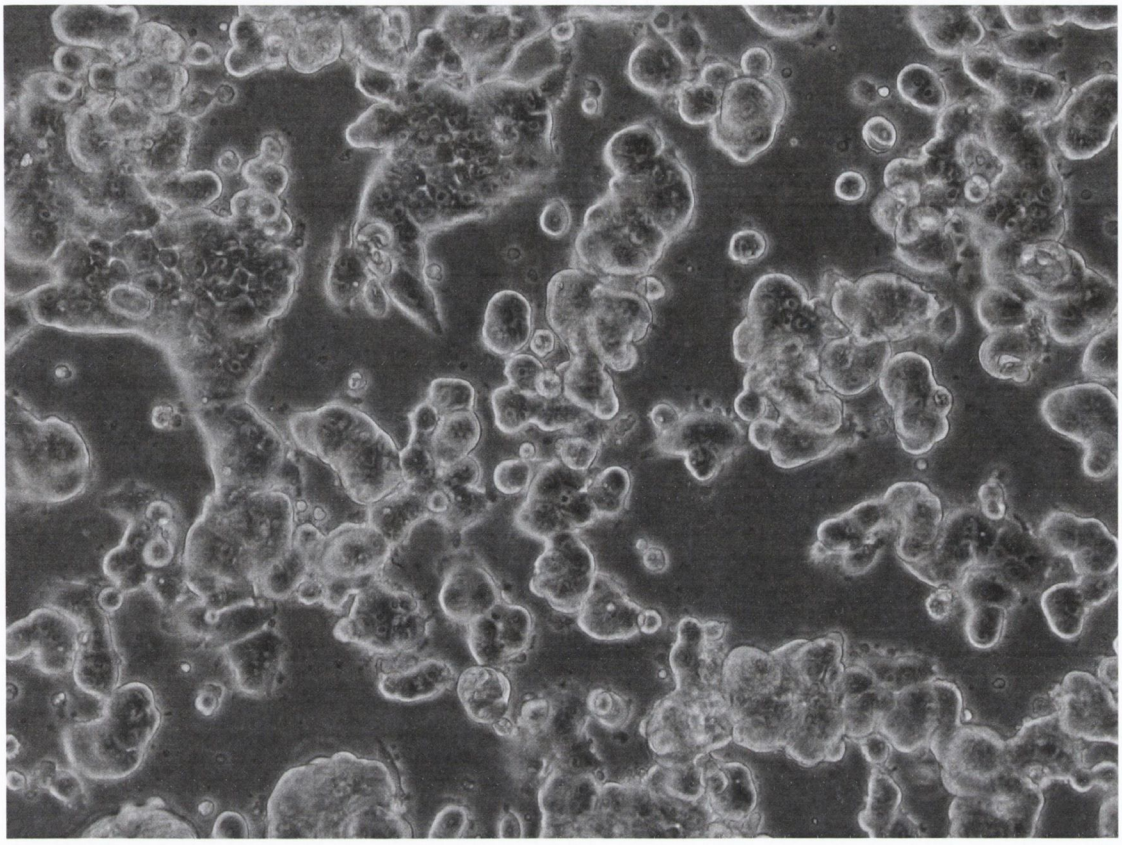

Fig 4.3 MCF-7 cells at 20X magnification. Image taken from the Berkely Lab website[327]

4.2.2 Sub-culturing and Seeding of Cells

Upon reaching confluency, the flask was removed from the incubator and carefully examined under the microscope to insure that a healthy biofilm of cells was present on the surface of the flask. Dead cells tend to float in the media while living cells remain stuck to the flask wall. This biofilm was gently washed with media to remove any loose dead cells and then treated with trypsin to break up the biofilm. The trypsin was allowed to work at 37°C for three minutes after which time the break up of the biofilm was apparent to the naked eye. The trypsin/cell suspension was then diluted with media and transferred to a centrifuge vial and centrifuged to yield a pellet of healthy MCF-7 cells. This dilution step is important since the large excess of media quickly denatures the trypsin protease before it has a chance to adversely affect the cells. The pellet was next diluted accurately to known volume and the actual number of cells in this volume was determined by counting on a haemocytometer. A small portion of this volume was transferred to a new flask with

fresh media to provide a new generation of cells for the next round of testing while the remaining volume was diluted with complete media to reach a working concentration of $2.5x10^5$ cells/mL. From this, a number of 96 well plates may be filled containing 200µL per well of the $2.5x10^5$ cells/mL suspension. The plates were then left to incubate for 24 hours to give the cells an opportunity to begin proliferating and adhere to the plate surface.

4.2.3 Treatment of 96 Well Plates

Each of the plates prepared was dosed with solutions of varying concentration of the compound of interest as described in Chapter 5. Ideally the test compounds should be prepared in either media or else water to minimize the effects of solvent on the assay. Failing this the compounds may be prepared in ethanol or DMSO. Of the two, ethanol has been found to be less toxic to the cells, but the test compounds are not soluble in 100% ethanol. For this reason the test solutions were prepared in 60%/40% DMSO/EtOH which provided a compromise between solubility and toxicity. The design of the treatment regime also aided in reducing solvent effect in the assay. Each plate contains a row of wells either dosed with the solvent (vehicle) or left blank. By comparison of the results from both these wells the solvent effect can be estimated and taken into account. For each compound a stock solution of 10mM was prepared and from this serial dilutions were carried out to give solutions of 5mM, 1mM, 0.5mM, 0.1mM, 10µM, 1µM, and 100nM. Since only 2µL of each was placed in the well this results in a final concentration ranging from 50µM to 1nM of the test compound in the well.

4.2.4 Cytotoxic Effects

The cytotoxic effects of the test compounds were evaluated using a commercially available kit available from Promega (CytoTox 96 non-radioactive assay). The assay exploits the release of lactate dehydrogenase from cells that have undergone lysis. The release of LDH is measured by the enzymatic conversion of tetrazolium salt to formazan (**fig 4.4**). The assay is straight forward and involves an initial step of treating the control well that had been set aside in treatment with a suitable lysis solution such as 10% Triton in PBS to induce complete cell lysis and thereby give a value that represents 100% cytoxicity. The wells that were treated with only the vehicle then represent 0% cell death. After incubation of the control wells with lysis solution for a minimum of 30 minutes, 30µL of cell media was removed from each well and transposed into a new 96 well plate. Since the LDH is

released into the cell media only the cell media needs to be sampled and care must be taken not to disturb the layer of cells adhered to the well wall as this will adversely affect the antiproliferative assay. 30µL of the freshly prepared substrate mix from the kit was then added into each well containing 30µL of media and the plate was then covered with tinfoil to exclude light and left at room temperature. After 20 minutes, 30µL of stop solution (NaOH solution) was added to each well and the absorbance at 490nm for each well was recorded on the plate reader. The cleavage of the tetrazolium salt is noticeable from the appearance of purple/navy crystals in the well

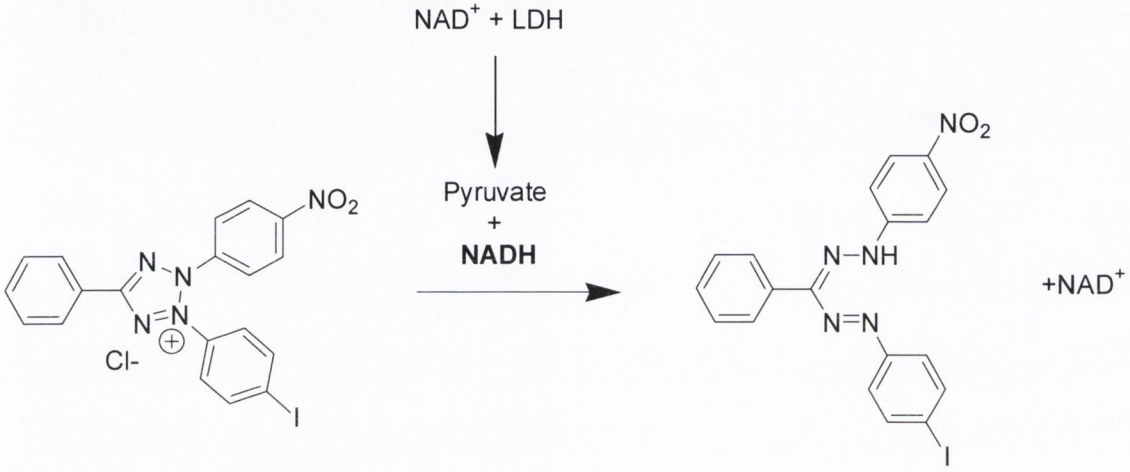

Fig 4.4 Enzymatic conversion of tetrazolium salt to formazan for the detection of LDH released from dead cells

4.2.5 Antiproliferative Effects

The antiproliferative effects of the test compounds were evaluated using the method described by Mosmann[328]. This involved the use of a MTT (3-(4,5-dimethylthiazol-2-yl)-2,5-diphenyltetrazolium) bromide) based assay. The principle behind this assay is relatively simple and involves the cleavage of MTT by mitochondrial dehydrogenase enzymes present within the MCF-7 cells. The cleavage of MTT results in the formation of formazan crystals and leads to an abrupt colour change from the pale yellow MTT to the navy/blue formazan which can be effectively monitored at 595nm on a plate reader. Only cells that are proliferating will take up the MTT and cleave it to formazan and the extent to which this occurs is directly proportional to the number of proliferating cells with in the well. In contrast to the cytotoxic assay, the antiproliferative assay requires the use of the cells present in the wells. The cell media was removed from the plate and the plate was gently washed with PBS solution to remove any remaining traces of media. Into each well 50µL of MTT solution was added and the plate was immediately covered to exclude light. Great care was taken to ensure that both the MTT solution and the plates were

not exposed to light because this can cause inadvertent cleavage of the MTT. The plate was left to incubate at 37°C for 2 hours which allows enough time for the cells to take up and cleave the MTT (**fig 4.5**). The cleavage of MTT results in the formation of purple crystals of formazan which are visible in the well. DMSO was used to solublise these crystals and the absorbance for each well was recorded at 595nm on a plate reader. For the antiproliferative assay the control wells provide a figure for 0% proliferation while the vehicle wells provide a figure for 100% proliferation.

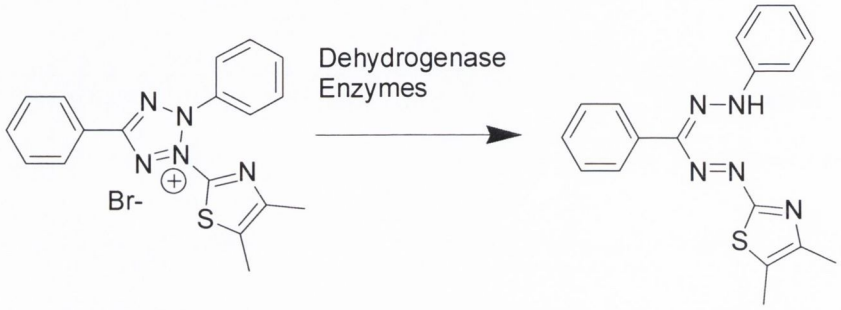

Fig 4.5 Ezymatic cleavage of MTT by dehydrogenase enzymes in the mitochondria of metabolically active cells

4.2.6 Cytotoxic/Antiproliferative effects of CA4

In order to ensure that the assays described above were working properly and yielding consistent results, CA4 was tested as a control. The reporting of values for a known compound like CA4 along with values for our novel compounds is important. It ensures that the protocols used for the determination of the cytotoxic/antiproliferative effects are yielding reasonable results and also allows direct comparisons between our novel compounds and CA4 to be made. The IC_{50} value for antiproliferative effects was determined as 4.2nM with a standard deviation of less than 0.1nM, while the percentage cell death at 10μM was found to be 11.8%. For comparison, the NCI quotes a value of 5.0nM in its MCF-7 cell line.

Results from library evaluation

4.3 Optimisation of the 4-Phenyl Ring

As has been discussed in Chapter 1, the "B" ring in combretastatin A4 (CA4) has been the subject of extensive modification in the search for improved CA4 analogues. In the case of the analogues presented here the C_4 phenyl ring of the β-lactam ring is comparable to the "B" ring of CA4. For this reason an initial library of compounds designed to identify the most promising substitution patterns for the C_4 position was synthesised. The results for this library are presented in **table 4.1**.

4.3.1 Effect of substitution on C_4 Aryl Ring

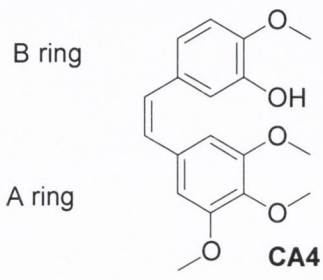

CA4

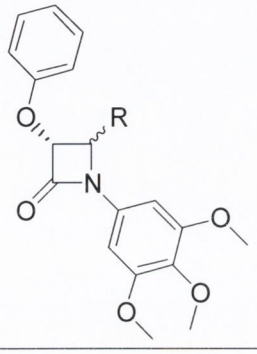

Compound No.	R	Isomer	MCF 7 Cell Line	
			IC_{50} µM (SEM)	% Cell Death @ 10µM
244	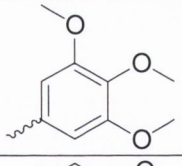	*Cis*	28.73 (19.57)	0
246	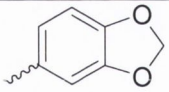	*Cis*	47.87 (8.50)	8.3
250	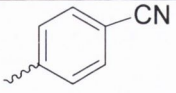	*Cis*	31.62 (17.19)	4.8
		Trans	168.4 (80.61)	2.1
253	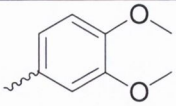	*Cis*	25.79 (10.33)	11.2
255	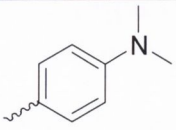	*Cis*	30.64 (20.94)	5.9

Table 4.1 Antiprolifferative and cytotoxic data for compounds **244 246 250 253 255**

Sun *et al* has demonstrated for a number of examples that the position of the trimethoxy substituted ring on the β-lactam ring is important (the trimethoxy phenyl substituent attached to N_1 seemed to be favoured), but no data on the effect of having a trimethoxy substituted ring at both C_1 and C_4 was presented. Previous work by Carr[203] also supports the finding that the trimethoxy phenyl ring at N_1 is favoured (**fig 4.6**). To further investigate this observation compound **244** was synthesised possessing an extra trimethoxy substituted phenyl ring at C_4. It displayed poor activity (IC_{50} = 28.73μM) indicating that the extra trimethoxy group is probably too bulky to sit comfortably in the colchicine binding site. The 3,4-dimethoxy pattern is found in ring B of CA5 but does not display significant activity in this case (IC_{50} for **253** = 25.79μM).

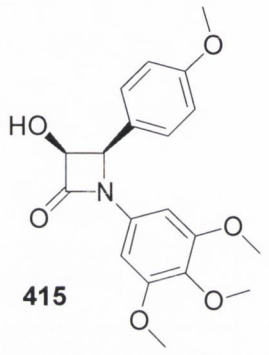

415

IC_{50} (IMR32) 33nM

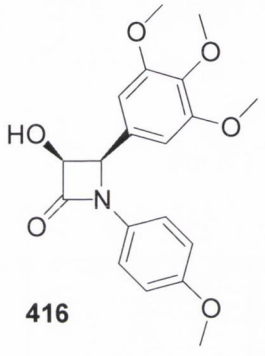

416

IC_{50} (IMR32) >1000nM

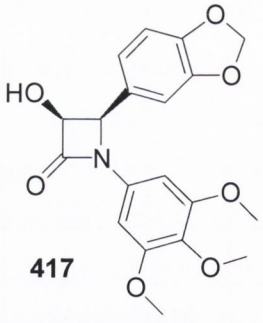

417

IC_{50} (IMR32) 473nM

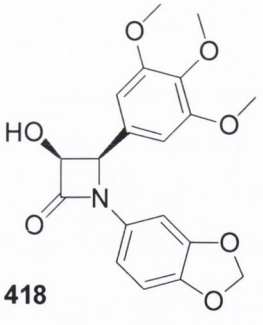

418

IC_{50} (IMR32) >1000nM

Fig 4.6 Effect of placement of the trimethoxy phenyl ring on the potency of selected analogues reported by Sun[162]

In the present work incorporation of the piperonal type substitution pattern for compound **246** was thought to be interesting since it is a structural feature of other antimitotic agents such as steganacin and podophyllotoxin, however compound only displayed an IC_{50} value of nearly 50μM making it 100 times less active than a similar structure (**417**) reported by Sun. This observation is further evidence for the importance of the substituent at C_3 for activity. The dimethylamino compound (**255**)

has an IC_{50} value of 30.6μM however it has been noted that the dimethylamino compound **72** also displays poor antiproliferative activity but that its antitubulin effects remain intact. A tubulin polymerisation assay was carried out on compound **255** to see if this was the case (**fig 4.15**). In the case of the cyano compound (**250**) both the *cis* and *trans* isomers were obtained in sufficient quantity to allow for testing. The *cis* isomer isomer was found to be the more active of the two but again only in the mid micromolar range(IC_{50} 17.19μM).

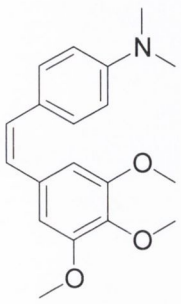

Fig 4.7 compound **72**

4.3.2 Halogen containing analogues

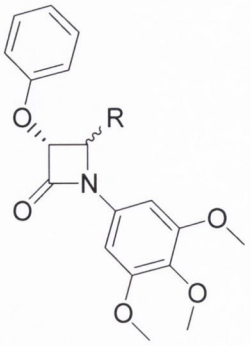

Compound No.	R	Isomer	MCF 7	
			IC_{50} µM (SEM)	%Cell Death @ 10µM
249	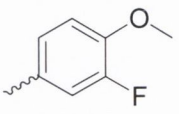	*Cis*	6.32 (4.28)	70
248	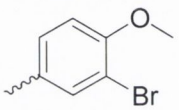	*Cis*	5.07 (1.77)	6.4
		Trans	30.71 (29.66)	3.9

Table 4.2 Antiproliferative and cytotoxicity data for the halogenated compounds

A number of analogues of CA4 containing halogens instead of the 3-hydroxy substitution on ring "B" have been reported. Replacement of the 3-hydroxy group of CA4 with a fluorine group led to only a small decrease in activity. The incorporation of a fluorine group into the phenyl ring is also important from a metabolism point of view, where the fluorine group should hinder the metabolism of the analogues by electrophillic substitutions and by conjugates. To further investigate the utility of this halogen substitution, **249** and **248** were synthesised. In both cases this led to compounds with low micromolar activity rather than the low nanomolar activity seen with CA4 (**table 4.2**). The bromine analogue **248** was found to be the more active of the two which is in contrast to the case with combretastatin analogues where the 3-fluoro compound is more active. For the 3-bromo analogue, it was found that the *cis* isomer was far more active than the *trans* isomer.

4.3.3 Nitrogen-containing analogues

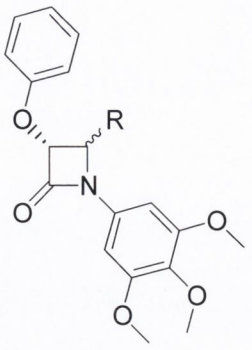

Compound No.	R	Isomer	MCF 7	
			IC_{50} µM (SEM)	Cell Death @ 10µM
251	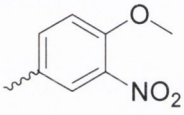	*Cis*	69.09 (25.12)	5.3
		Trans	4.15 (1.90)	*5.2*
264	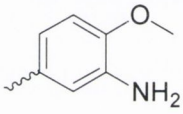	*Cis*	27.22 (10.15)	4.7
		Trans	0.1525 (0.1491)	10.2

Table 4.3 Antiproliferative and cytotoxicity data for nitrogen-containing compounds

It has been noted by a number of researchers that the replacement of the 3-hydroxy group of CA4 with an amino group leads to analogues displaying promising activity. The importance of this substitution pattern is underlined by the fact that a prodrug of such a compound has entered clinical trials in the form of AVE8062 (**48**). A number of other CA4 analogues where the olefin bridge has been replaced also display excellent *in vitro* activity, particularly in compounds where a five-membered ring is used such as oxazole, imidazole, benzothiophene, indole, dioxalane, tetrazole, thiazole, and furazan compounds (**91-98** and **420-422**). For these reasons compound **264** was synthesised. The nitro compound (**251**) was first formed and displayed low to mid micromolar activity (**table 4.3**). Interestingly the *trans* isomer proved to be more active than the *cis* isomer (in contrast to previous observations for **248**) displaying low micromolar activity but still 1000 times less active than CA4. Upon the reduction of the nitro to the amino group (**264**) a large increase in activity was observed in both isomers. The IC_{50} for the *cis* isomer decreased from 69µM to

27μM – a decrease of 60%. More impressively, the *trans* amino compound displayed an IC_{50} value of 153nM – a 27 fold decrease while still maintaining reasonable cell death at 10μM of 10.2%. This compound was then regarded as being a possible lead compound that warranted further investigation. A number of CA4 analogues containing NH_2 substituents are illustrated in **fig 4.8**.

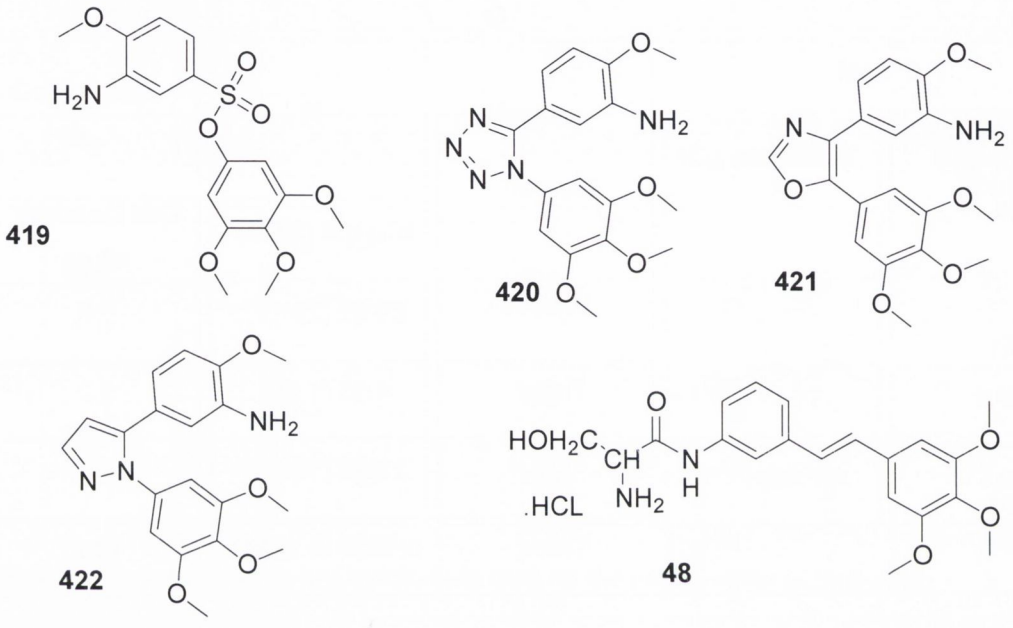

Fig 4.8 Selected amino containing combretastatin analogues

4.3.4 Sulphur containing analogues

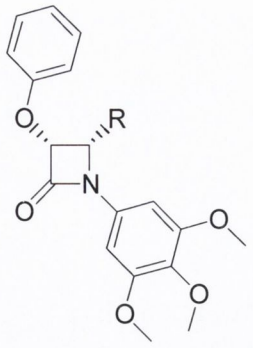

Compound No.	R	Isomer	MCF 7	
			IC_{50} µM (SEM)	%Cell Death @ 10µM
247	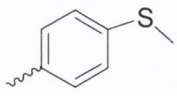	*Cis*	7.71 (6.05)	8.1
262	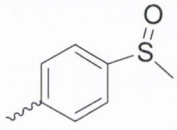	*Cis*	19.58 (4.98)	1.7
263	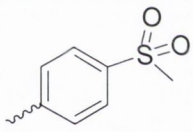	*Cis*	61.65 (13.95)	10.2

Table 4.4 Antiproliferative and cytotoxicity data for thio methyl compounds

For the above series of compounds, the 4-methoxy group was replaced with the more lipophilic thiol methyl group, which was subsequently oxidised to the corresponding sulphoxide and sulfone. The thio methyl group displayed reasonable activity which was lost upon conversion to the sulphoxide and sulphone (**table 4.4**). Cushman [117] formed a thio methyl analogue of CA4 and reported a 3-fold reduction in anti-tubulin activity and a 2-fold loss in potency compared to the corresponding 4-methoxy analogue.

4.3.5 Naphthyl containing analogues

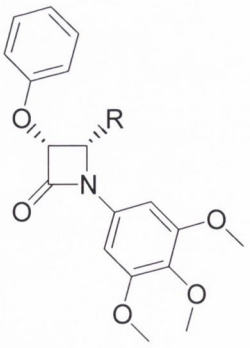

Compound No.	R	Isomer	MCF 7	
			IC_{50} µM (SEM)	Cell Death @ 10µM
254	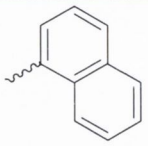	*Cis*	53.01 (27.32)	4.6
252	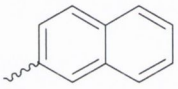	*Cis*	282.3 (187.96)	10.7

Table 4.5 Antiproliferative and cytotoxicity data for naphthyl containing compounds

The replacement of the substituted phenyl "B" ring with alternative polycyclic ring systems has shown some promise and is dealt with in detail by Medarde[127]. It was found that the naphthalene ring can act as an effective replacement for the 3-hydroxy-4-methoxy phenyl ring in CA4. Medarde reports that such compounds have a number of advantages over the traditional substituted phenyl ring compounds such as not requiring protecting group chemistry during synthesis, and having a large aromatic surface which could favourably interact with hydrophobic areas of the colchicine binding site in tubulin. To investigate if the inclusion of the naphthyl group at C_4 of the β-lactam ring would lead to active compounds, **254** and **252** were synthesised. Both displayed poor activity especially the 2-naphthyl compound with IC_{50} values in excess of 250µM (**table 4.5**).

4.3.6 Hydroxy containing anaolgues

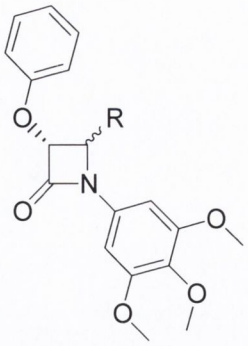

Compound No.	R	Isomer	MCF 7	
			IC_{50} µM (SEM)	%Cell Death @ 10µM
258	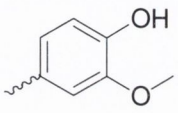	*Cis*	31.93 (19.76)	5.1
257	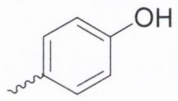	*Tested as 3:1 cis:trans*	47.76 (37.67)	0.1
259	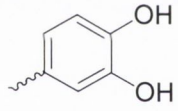	*Tested as 1:1 cis:trans*	4.52 (2.60)	6.0
256	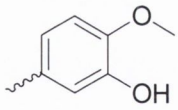	*Cis*	0.383 (0.1762)	2.8
		Trans	0.038 (0.0087)	28.7

Table 4.6 Antiproliferative and cytotoxicity data for hydroxy containing compounds

The synthesis of a number of analogues containing hydroxy groups at various positions on the phenyl "B" ring was carried out. Hydroxy substituted phenyl rings are a common feature in the "B" ring of the majority of members of the combretastatin family, with two of the more active members CA1 and CA4 both containing this feature (**fig 4.9**). Unfortunately the synthesis of the CA1 analogue was not successful, but the results obtained for a number of other analogues are presented above (**table 4.6**). The 4-hydroxy substituted phenyl group appears in two unnamed combretastatins **32** and **34**. The 3,4-dihydroxy substituted phenyl is a

feature of both CB3 and CB4, while the 3-hydroxy-4-methoxy substituted phenyl is a key feature of CA4.

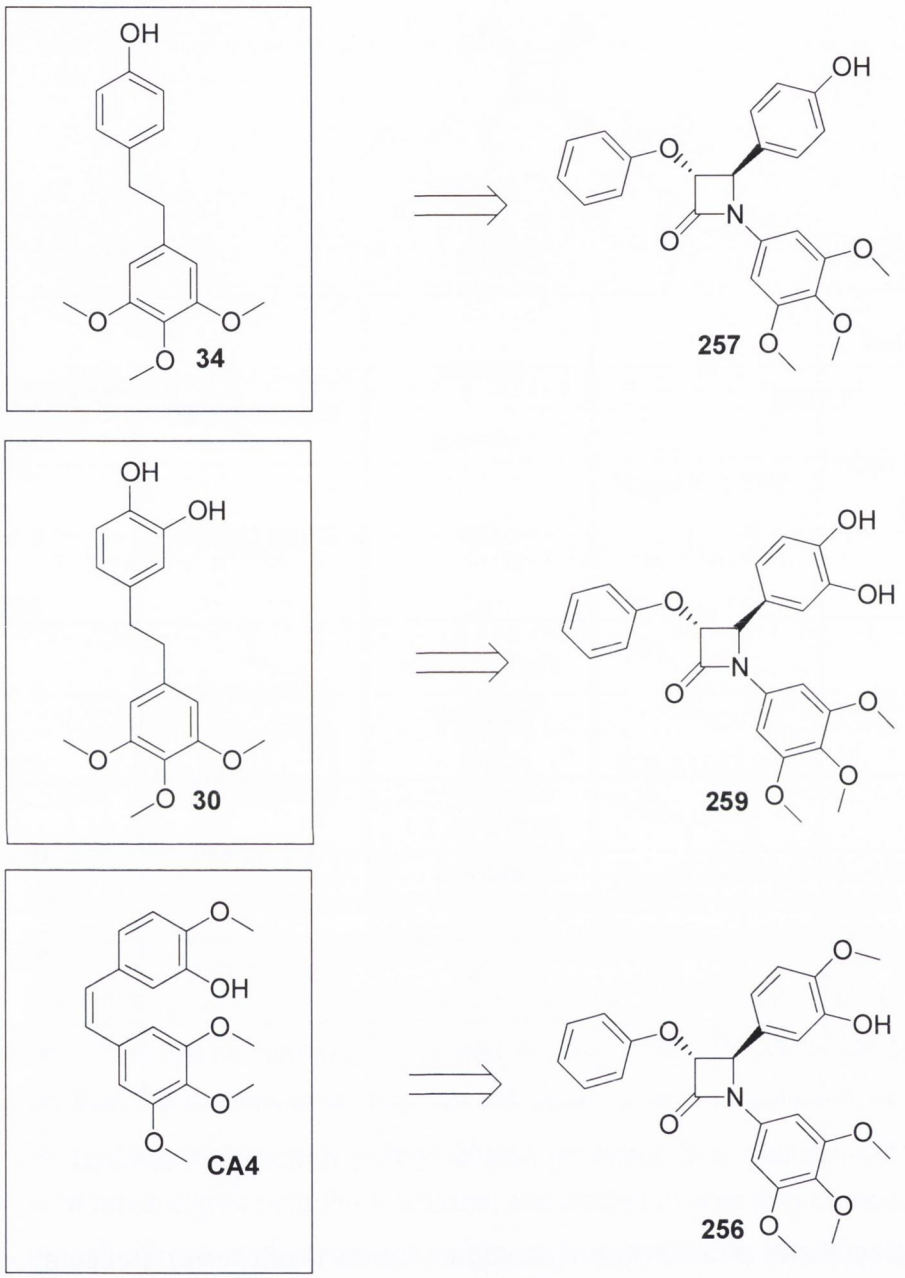

Fig 4.9 Illustration of various hydroxy containing combretastatins and their corresponding β-lactam analogues

For obvious reasons the 3-hydroxy-4-methoxy analogue (**256b**) proved to be the most potent in the MCF-7 cell line since it is a direct analogue of CA4. The *trans* isomer was found to be ten times more active than the *cis* isomer with an IC_{50} value of 38nM and 383nM respectively. The results for the MTT and LDH assays for **264b**

are presented in **fig 4.10**. The *trans* isomer also displays an increase in cell death at 10μM of 28.7% compared to 11.8% for CA4. Since the *trans* isomer is only ten times less active than CA4 it is therefore a promising lead compound along with the trans 3-amino compound (**264b**). The *cis* isomer also displayed good activity with an IC_{50} value of 383nM. Interchanging the positions of the hydroxy and methoxy groups appears to result in a decrease in activity and cell death to 31.93μM and 5.1%.

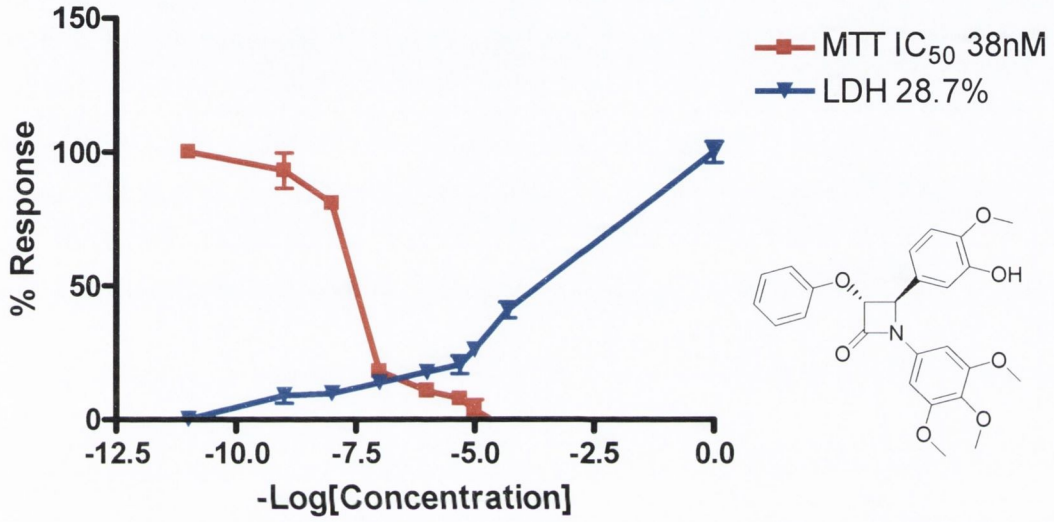

Fig 4.10 Antiproliferative and cytotoxicity dose response curves for **256b**. MCF-7 cells were seeded at a density of 2.5 x 10^4 cells/mL in 96 well plates and allowed to adhere to the well surfaces for 24 hours. The cells were then treated with the compound (1nM to 50μM final concentration) and incubated for 72 hours. Determination of cell proliferation was carried out using the MTT assay described in **section 4.2.5** and the cytotoxicity was evaluated using the LDH assay described in **section 4.2.4**

4.4 The role of the Carbonyl Group at C_2 on the β-Lactam Ring

The initial library of compounds screened focussed on optimising the structural features of the phenyl ring at C_4 of the β-lactam ring. In the course of the screen two particularly promising substitution patterns emerged (the 3-hydroxy-4-methoxy **256b** and the 3-amino-4-methoxy **264b**). A major question arising from these findings concerns the role of the β-lactam ring itself in the activity of these two lead compounds. In particular we were interested in the role of the carbonyl group at C_2. A major degradation pathway for the β-lactam ring in penicillins and monolactams is conversion to the ring opened form by hydrolysis. It was assumed then that the compounds in the present study would be subject to the same hydrolysis. Section 4.13 presents a stability study carried out the the β-lactam compounds in this work. If the C_2 area of the ring proved amenable to modification without affecting biochemical activity it may provide access to a series of compounds that would show increased stability *in vivo* for compounds **272** and **267**. Transformation of the carbonyl group of the β-lactam to a thione group (**267**) and also reduction to a azetidine (**272**) were investigated (**table 4.7**).

Compound No.	Structure	Isomer	MCF 7	
			IC_{50} µM (SEM)	%Cell Death @ 10µM
272	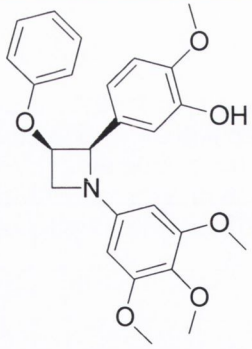	*Cis*	3.30 (2.35)	19.8
267	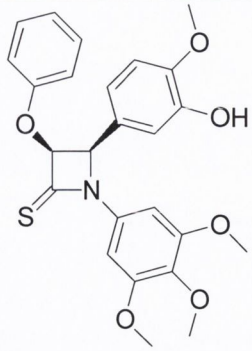	*Cis*	7.45 (0.63)	4.8

Table 4.7 Antiproliferative and cytotoxicity data for modified C_2 compounds **272** and **267**

In both transformations only the *cis* isomer was used as staring material resulting in only *cis* products obtained. This was due to the greater availability of the *cis* isomer starting material. This should still provide useful information on the importance of the carbonyl group for activity in the antiproliferative assay since the *cis* isomer displays sub micromolar activity. For both the complete removal of the carbonyl group by reduction and the conversion of the carbonyl group to the thione, a large decrease in activity was observed. The *cis* 3-hydroxy material had an IC_{50} of 383nM and exhibited 2.8% cell death at 10μM. In contrast the azetidine product displayed an IC_{50} value of 3.3μM with an increase in cell death at 10μM to nearly 20%. The thionation of C_3 resulted in a further decrease in activity to 7.45μM but with only a slight increase in cell death to 4.8%. It would appear that the carbonyl group at C_2 is crucial to antiproliferative biochemical activity. A later section (**section 4.14.5.3**) examines the relevance of the carbonyl group to binding of the compounds at the colchicine site of tubulin by *in silico* modeling. Also if additional activity observed in compounds **256b** and **264b** depends on the enzyme catalysed ring opening reaction, then this is not possible with **271** and **267**.

4.5 Chlorambucil coupled analgues

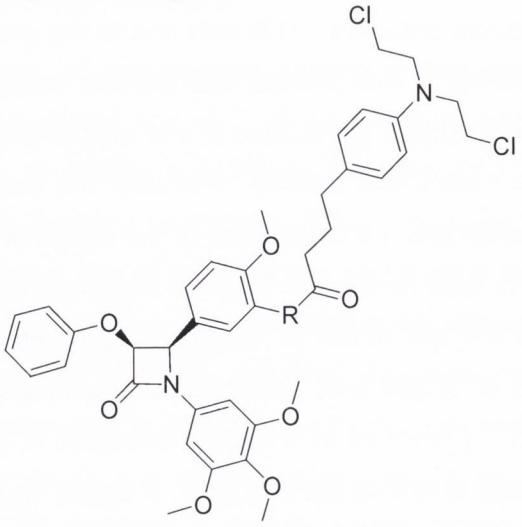

Compound No.	R	Isomer	MCF 7	
			IC_{50} µM (SEM)	%Cell Death @ 10µM
265	O	*Cis*	0.407 (0.421)	8.0
266	NH	*Cis*	145 (35.35)	3.2

Table 4.8 Antiproliferative and cytotoxicity data for chlorambucil analogues

A number of clinical trials involving CA4P in combination with an established chemotherapy agent are in progress. These combination therapies are discussed in detail in **section 1.5.5.3**. The above **table 4.8** presents data for two analogues where compounds **256a** and **264a** have been successfully coupled to chlorambucil via an ester/ amide linkage respectively. For the ester compound **265**, a similar IC_{50} value to the parent compound was observed of 407nm, but there was a marked increase in cell death to 8% from 2.8%. On its own the IC_{50} value for chlorambucil in the MCF-7 cell line has been reported as being 97µM[329]. One possible explanation for these observations was that the ester linkage was cleaved *in situ* during the assay yielding the free hydroxy compound and the chlorambucil compounds respectively. In contrast the amide compound **266** would not be subject to this hydrolysis to the same extent. The chorambucil side chain would have an obvious effect on **266** to bind in the colchicine site. Coggiola *et al*[250] examined the mechanism of action of chlorambucil-CA4 compounds and found that the conjugate compounds induced the same changes in the cell cycle namely G_2/M arrest, as the parent CA4 compound. It was also found that tubulin polymerisation was inhibited by the conjugates to the same extent as the parent CA4 compound. The presence of the free hydroxy

compound would account for the similar results to **256** found. The increase in the percentage cell death is most likely due to the presence of chlorambucil which is known to be toxic.

4.6 The role of the trimethoxy phenyl ring in antiproliferative activity

Compound No.		Isomer	MCF 7	
			IC_{50} µM (SEM)	%Cell Death @ 10µM
276	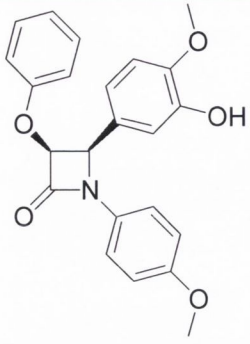	*Cis*	49.09 (21.6)	10.4

Table 4.9 Antiproliferative and cytotoxicity data *p*-methoxy β-lactam 2**76**

As part of an investigation into the synthesis of N-unsubstituted β-lactams, the compound **276** was produced. Although the planned dearylation reaction on this compound was unsuccessful (**section 2.4.5**), it is useful for illustrating the necessity of the trimethoxy substitution pattern for biochemical activity. Without the presence of the trimethoxy group there is a drop in activity from 383nM to 49.1µM compared to compound **256b** which does have the trimethoxy group present (**table 4.9**). This drastic reduction in activity hints at the important role that the trimethoxy subunit plays in the binding of compounds at the colchicine site. Most obviously the trimethoxy subunit is present in colchicine, but it is also present in other antimitotic agents such as steganacin and podophyllotoxin. The trimethoxy subunit is also present in a number of members of the combretastatin family most notably CA1 and CA4. CA3 and CA2 are notable since neither have the trimethoxy subunit but yet exhibit sub-micromolar activity in the L210 cell line (see **table 1.3** in **section 1.5.2.1**). In the case of CA3 the methoxy group at the 3-position is replaced with a hydroxy group resulting in a compound with an IC_{50} value of 26nM which favourably compares to the value of 3.4nM for CA4. It is likely then that the β-lactam compounds presented in this thesis possess a trimethoxy subunit that is a suitable mimic for the trimethoxy subunit found in colchicine.

4.7 Hydroxy & Nitrogen Containing modification of Ring "B"

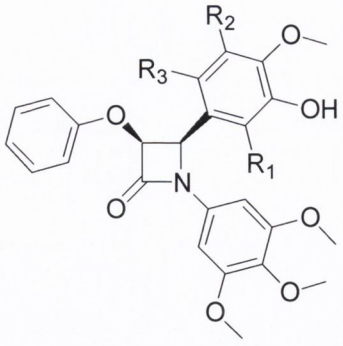

Compound No.	R_1	R_2	R_3	Isomer	MCF 7	
					IC_{50} µM (SEM)	%Cell Death @ 10µM
302	NO_2	H	H	*Cis*	88.50 (0.707)	12.7
303	H	NO_2	H	*Cis*	58.60 (6.93)	9.9
304	H	H	NO_2	*Cis*	69.13 (9.40)	12.1
305	NH_2	H	H	*Cis*	18.54 (19.45)	51.9
306	H	NH_2	H	*Cis*	20.09 (21.82)	70.1
307	H	H	NH_2	*Cis*	8.79 (2.31)	14.0

Table 4.10 Antiproliferative and cytotoxicity data for various N-containing compounds

So far it has been shown that the 3-hydroxy-4-methoxy (**256**) and 3-amino-4-methoxy (**264**) substituted phenyl group at C_4 is necessary for biochemical activity. Monk *et al*[74] synthesised a number of CA4 analogues containing the 3-hydroxy-4-methoxy function but also including an amino group substituted at the remaining free positions on the phenyl ring, leading to analogues with similar anti-tubulin effects to that of CA4. Data on a series of similarly substituted β-lactam type compounds is presented above (**table 4.10**). None of the compounds synthesised were active on a submicromolar level, but it can be clearly seen that the conversion of the nitro to the amino does lead to increases in activity. It is worth noting that the compounds **302-304** could only be synthesised as the *cis* isomer. Similar work with **251** and **264** has shown that the *trans* isomer can be the more active of the two by a factor of 27 and so the *trans* isomers of the above compounds could be more potent.

4.8 Ring "B" Azide Substituted CA4 Analogues

Compound No.		Isomer	MCF 7	
			IC_{50} µM (SEM)	%Cell Death @ 10µM
319	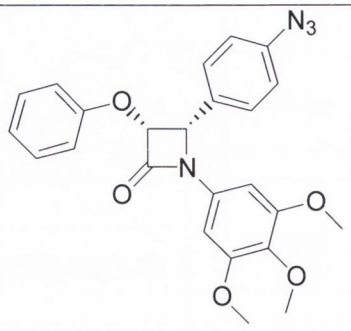	*Cis*	23.25 (0.354)	5.8

Table 4.11 Antiproliferative and cytotoxicity data for azide analogue

The 4-azido substituted compound (**319**) was synthesised in an effort to create a novel photoaffinity probe for the colchicine site. Given the amount of interest in agents that bind at the colchicine site of tubulin, any agent that could possibly provide information on the interaction of compounds with the colchicine site would prove useful The 4-azido compound displayed a poor IC_{50} value of 23.25µM (**table 4.11**). This calls into doubt its ability to function as a photoaffinity probe since such a low IC_{50} value would indicate that it does not bind efficiently at the colchicine site. It is possible that while the compound may not have antiproliferative effects, it may still bind efficiently to the tubulin site. Pinney *et al*[105] has demonstrated the introduction of the azide group into a 3-amino analogue of CA4 without affecting its antitubulin properties, but the attempted synthesis of the corresponding β-lactam analogue did not result in success (see **section 2.5.3**). The possibility of incorporating the azide functionality onto other parts of the β-lactam ring should be further explored in the future.

4.9 Optimisation of the 3'' and 4'' substituents required at ring "B"

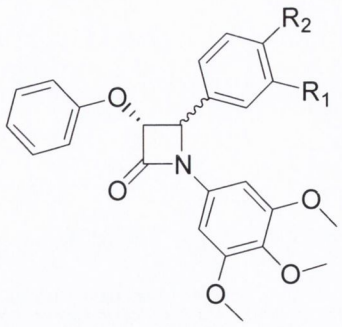

Compound No.	R_1	R_2	Isomer	MCF 7	
				IC_{50} µM (SEM)	%Cell Death @ 10µM
324	OH	H	*Cis*	54.0(7.07)	22.0
325	NO_2	H	*Cis*	30.15(6.55)	16.7
326	H	NO_2	*Cis*	63.1(39.74)	27.1
329	OMe	H	*Cis*	171.00(161.22)	22.0
327	NH_2	H	*Cis*	17.44(5.85)	48.4
328	H	NH_2	*Cis*	160(56.57)	14.7
264	NH_2	OMe	*Cis*	27.22 (10.15)	16.1
256	OH	OMe	*Cis*	0.383 (0.1762)	2.8
245	H	OMe	*Cis*	34.91 (9.77)	6.5
	H	OMe	*Trans*	*6.91*	7.3

Table 4.12 Antiproliferative and cytotoxicity data for compounds bearing substituents at C_3'' and C_4'' of the C_4 aryl ring

So far the most potent analogues synthesised in this study all contain a methoxy group at the 4-position of the phenyl ring alongside either an amino of hydroxy group at the 3-position **256b** and **264b**. The analogues presented in the above **table 4.12** were synthesised in an effort to establish the role that each of these substituents plays individually in moderating biochemical activity. Compound **245** was initially synthesised due to many reports that suggested for CA4 that the 4-methoxy group was necessary for activity while the 3-hydroxy group was not. This was found not to be the case in the β-lactam compound above, with the *trans* isomer showing increased IC_{50} values (34.91µM *cis* and 6.91µM *trans*) compared to the values recorded for **256** (383nM *cis*, 38nM *trans*) indicating that the substituent at the 3-position plays a role in the binding of molecules to tubulin at the colchicine site.

To investigate further the role of the 3-substituent, compounds **324** and **327** were synthesised which contain a hydroxy and an amino group at C_3" respectively. It would have been desirable to obtain **324** and **327** as *trans* products to allow for a direct comparison to be made to the more active *trans* compounds **256** and **264** but the reaction only yielded the *cis* isomer. Compound **324** with only a hydroxy group at the 3-position exhibited a large increase in its IC_{50} value to 54.0μM but also displayed an increase in cell death to 22% from 2.8% when compared to **256**. This would indicate that the 3-hydroxy group is not solely responsible for the biochemical activity of *256*. From **section 4.3.6** it can be seen that not only is the presence of both the methoxy and hydroxy groups required but also their relative positioning is important. The 3-amino compound **327** was also tested and displayed a slightly increased IC_{50} value of 17.44μM over the corresponding 3-amino-4-methoxy compound **264**. It is difficult to draw conclusions from this result in the same manner as for compounds **324** and **256** since the *cis* isomer **264** has been shown not to be active. The only effective way to evaluate the role of the 3-amino group in antiproliferative activity for these compounds would be to obtain a sample of the trans isomer of **327**. What is clear is that for the hydroxy compound it would appear that having both the hydroxy and the methoxy groups in their respective positions on ring "B" is neccessay for activity. It is likely then that the same could be said for the 3-amino-4-methoxy compounds **264** and **327**.

Placing a hydroxy (**257**) or amino (**328**) group on its own at the 4-position or placing a methoxy (**329**) group at the 3-postion of ring "B" all yield compounds with poor activity.

4.10 Optimisation of the 3-position substituents

4.10.1 Analogues by modification of the Staundinger route

The antiproliferative results for a number of analogues containing modifications at C_3 are presented below (**table 4.13**). These compounds were obtained by modification of the Staundinger reaction. The majority of the analogues were formed exclusively as the *trans* isomer which was fortuitous since earlier work has demonstrated that the *trans* isomer is more active than the *cis* isomer. It should be noted the compound **341** (prepared by TG) has previously been reported in Carr's thesis[203] (labelled as compound **275**) and was used in the present work as a reference material.

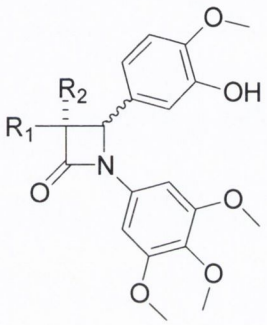

Compound No.	R_1	R_2	Isomer	MCF 7	
				IC_{50} µM (SEM)	%Cell Death @ 10µM
339	Cl	H	*Trans*	0.0175(0.0088)	16.7
340	Cl	Cl	*Trans*	0.3324(0.1589)	7.9
341	Ph	H	*Trans*	0.0214(0.0068)	22.8
342	$PhCH_2$-	H	*Trans*	0.2293(0.1535)	14.7
343	CH_2=CH-	H	*Trans*	0.0014(0.0008)	25.9
344	CH_2=C(CH_3)-	H	*Trans*	0.0376(0.00272)	32.1
355	Phth-	H	*Cis*	11.28(4.57)	41.0
361	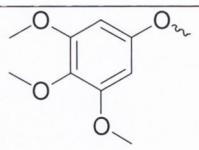	H	*Cis*	33.49(10.15)	10.9

Table 4.13 Antiproliferative and cytotoxicity data for various C_3 substituted β-lactams

Compound **342** examined the replacement of the oxygen of the phenoxy group with a methylene group. This led to a dramatic drop in activity from 38nM to 229nM. Indicating the the oxygen of the phenoxy group may be of importance for

antiproliferative activity. Sun and Carr both reported examples containing small groups at C_3 (such as hydroxy and methoxy groups) leading to compounds with good activity[162]. To this end, two chloro substituted compounds (**339** and **340**) were formed with the mono chloro compound **339** being the more active of the two displaying an IC_{50} value of 17.5nM. Interestingly **339** was slightly more potent than **341** while at the same time it displayed 6.1% less cell death. Unfortunately the bromo analogue which would have provided a useful comparison to the chloro compounds could not be synthesised by the usual method. Likewise a 3-amino analogue could not successfully be obtained from the cleavage of the 3-phthalimido compound **355**. Compound **355** was itself tested but showed little activity with an IC_{50} value of 11.28μM. Further evidence that the presence of a large bulky group at C_3 is not favoured came from the trimethoxyphenoxy substituted compound **361** which also displayed mid-micromolar IC_{50}.

Compound **343** containing the vinyl substitution at C_3 was by far the most active compound assayed with an IC_{50} value of 1.4nM. The initial assay suggested an IC_{50} of less than 1nM using the typical treatment regime of between 50μM and 1nM. On obtaining such an active result the treatment regime was changed with the two high doses of 10μM and 10μM being replaced with two lower doses of 100pM and 10pM, leading to the final IC_{50}value reported. Unfortunately **343** displayed a high value for cell death at 10μM of 25.9%. The antiproliferative and cytoxicity data for **343** is presented in **fig 4.11**. Because of the potent nature of **343** further investigation of this substitution pattern was carried out beginning with the synthesis of **344** containing the 3-isopropenyl substitution. The introduction of the extra methyl group led to a drop in activity to 37nM. A number of further analogues containing vinyl groups at C_3 were synthesised to further optimize activity and are discussed in the following sections.

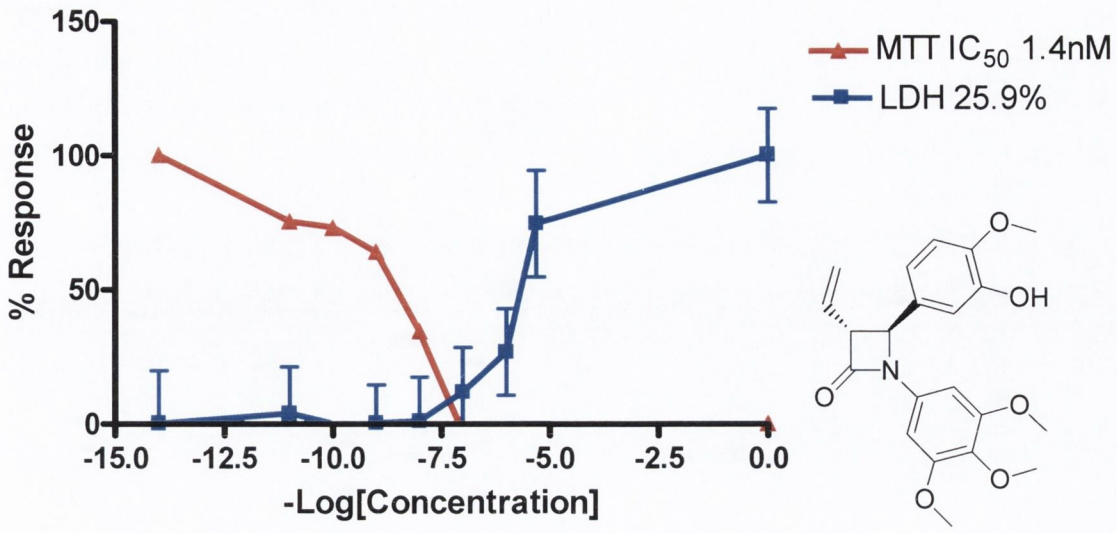

Fig 4.11 Antiproliferative and cytotoxicity dose response curves for **343**. MCF-7 cells were seeded at a density of 2.5 x 10^4 cells/mL in 96 well plates and allowed to adhere to the well surfaces for 24 hours. The cells were then treated with the compound (1nM to 50μM final concentration) and incubated for 72 hours. Determination of cell proliferation was carried out using the MTT assay described in **section 4.2.5** and the cytotoxicity was evaluated using the LDH assay described in **section 4.2.4**

4.10.2 C_3 alkyl substituted β-lactams

The initial starting material for the development fo C_3 alkyl and related products was the C_3 unsubstituted compound **380** which in its own right displayed impressive activity with an IC_{50} value of 56nM and had a cell death at 10μM value of 14.7%. The antiproliferative and cytotoxicity data for **380** is presented in **fig 4.12.**

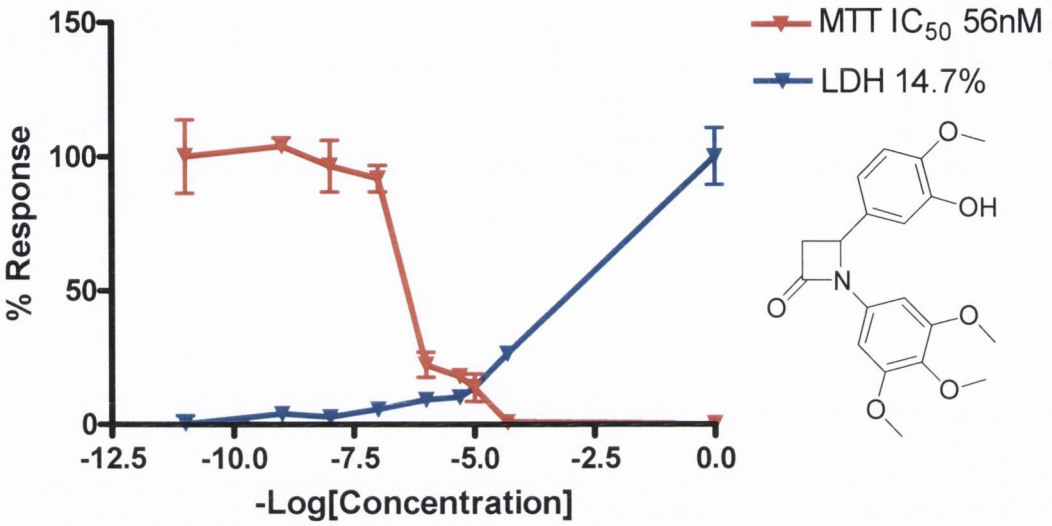

Fig 4.12 Antiproliferative and cytotoxicity dose response curves for **380**. MCF-7 cells were seeded at a density of 2.5 x 10^4 cells/mL in 96 well plates and allowed to adhere to the well surfaces for 24 hours. The cells were then treated with the compound (1nM to 50μM final concentration) and incubated for 72 hours. Determination of cell proliferation was carried out using the MTT assay described in **section 4.2.5** and the cytotoxicity was evaluated using the LDH assay described in **section 4.2.4**

Table 4.14 presents biochemical data for a number of 3-substituted β-lactams synthesised in the current work, including four analogues (**389, 391, 392, 393**) all containing various vinyl type substituents. Compounds **388** and **390** expand upon work carried out by Carr[203] that identified a number of analogues containing 3-methyl and 3,3-dimethyl groups that showed promising activity illustrated in **fig 4.13** below.

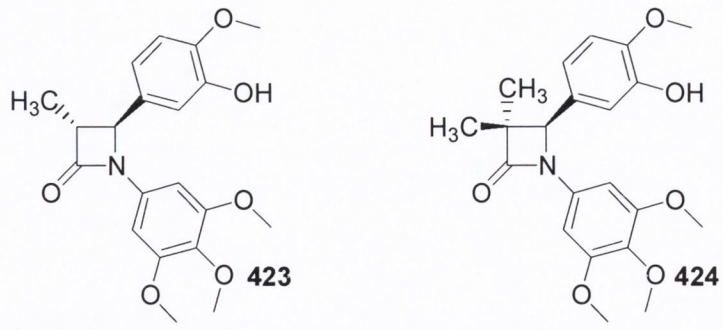

10nM
15%

250nM
12%

Fig 4.13 Antiproliferative and cytotoxicity data for selected analogues from Carr

Both **388** and **390** were less potent that **423** and **424** but still displayed reasonable sub-micromolar IC_{50} values. **395** was synthesised to examine the role of the C_5 hydroxy group in **388** by oxidation to the corresponding ketone (**395**). A decrease in activity from 65nM to 419nM was observed indicating that the C_5 hydroxy group does have a role to play in antiproliferative activity (**table 4.14**).

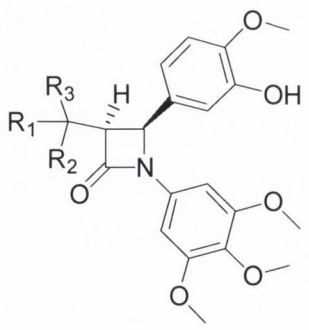

Compound No.	R_1	R_2	R_3	Isomer	MCF 7	
					IC_{50} µM (SEM)	% Cell Death @ 10µM
388	CH_3-	H	OH	*Trans*	0.0652(0.0158)	26.6
389	CH_3CH=CH-	H	OH	*Trans*	0.5701(0.246)	24.0
390	CH_3-	CH_3-	OH	*Trans*	0.5446(0.3101)	9.8
391	PhCH=CH-	H	OH	*Trans*	0.0468(0.041)	7.6
392	CH_2=CH-	H	OH	*Trans*	0.2888(0.076)	20.9
393	CH_2=CH-	CH_3-	OH	*Trans*	0.4679(0.2533)	49.9
395	CH_3-	H	O	*Trans*	0.4194(0.1321)	24.7

Table 4.14 Antiproliferative and cytotoxicity data for various compounds obtained from **73**

Compounds **389**, **391**, **392**, **393** were all synthesised to further investigate the role of the vinyl group in biochemical activity. None of the four compounds displayed activity approaching that of **343** although **391** did yield an IC_{50} value of 47nM, and an improved cell death of 7.6% compared to nearly 26% for **343**. While not as active as **343**, these compounds may prove valuable for identifying the structural characteristics of **343** that lead to its exceptional activity and may be developed as less toxic analogues of **343**.

4.11 Transformation of the 3-vinyl β-lactams

The 3-vinyl compound **343** was further modified to yield the ethylidene compounds **397** and the diol **398**. The placement of the double bond directly onto C_3 led to a drastic decrease in potency to 502nM. The transformation to the diol also led to a decrease in activity but not to the same extent. Despite being less active, **398** had a similar percentage cell death to **343** (**table 4.15**).

Compound No.		Isomer	MCF 7	
			IC_{50} µM (SEM)	% Cell Death @ 10µM
397	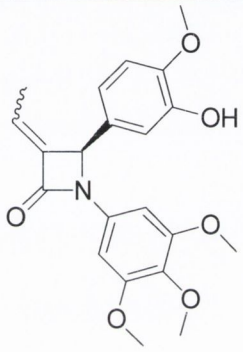	Tested as a 1:1 mixture of *E:Z* isomers	0.5021(0.2127)	8.4
398	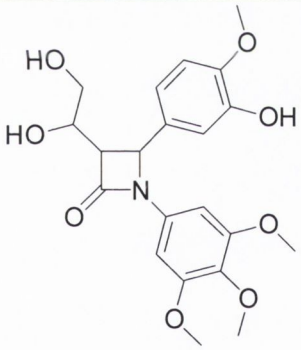	*Trans*	0.0697 (0.029)	29.3

Table 4.15 Antiproliferative and cytoxicity data for compounds **397** and **398**

4.11 Synthesis of further vinyl analogues

Compound **343** represents the combination of the most active substitution patterns identified for C_3 and C_4 e.g. the vinyl group at C_3 and the 3-hydroxy-4-methoxy substituted aryl ring at C_4. The 3-amino-4-methoxy phenyl group at C_4 was also identified as a promising substitution pattern and so it was decided to synthesise an analogue containing this pattern at C_4 and the vinyl group at C_3. The 3-nitro compound **410** was examined first and was found to have an IC_{50} value of 2.27μM, which is about twice as active as the corresponding phenoxy compound **251**. This points to the 3-vinyl group playing a role in activity even for compounds that have not been optimised at the C_4. Upon the reduction to the amino compound **399** there was a large increase in activity to 13.7nM. Despite not being as potent as **343**, **399** does display a more favourable cell death of 16.1% at 10μM and could act as a lead compound for further structural modification and formation of conjugates (**table 4.16**).

Compound No.		Isomer	MCF 7	
			IC_{50} μM (SEM)	Cell Death @ 10μM
410	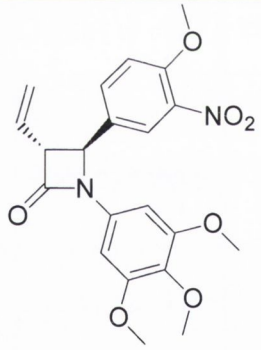	*Trans*	2.27 (1.42)	9.2
399	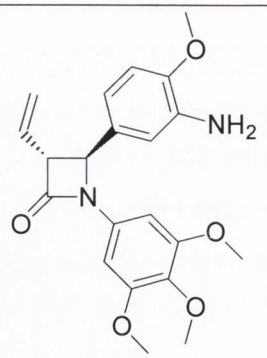	*Trans*	0.0137(0.0015)	16.1

Table 4.16 Antiproliferative and cytoxicity data for compounds **410** & **399**

Compounds **412** and **413** were synthesised to investigate the utility of the 3-vinyl group to improve the potency of otherwise inactive compounds. In the initial library synthesised, the 4-nitrile analogue **250** displayed an IC_{50} value of 168μM. Upon the replacement of the phenoxy group with the vinyl group in **412** the IC_{50} value fell to 6.25μM – nearly a 27 fold decrease (**table 4.17**). This clearly illustrates the important role that the 3 position plays. A number of CA4 analogues containing only a *para*-substituted methoxy group have been reported as being active[117], but within this thesis it was found the analogues containing only the methoxy group were not active. To further explore this, and to examine the effect of the vinyl group **413** was synthesised. An improvement in activity from 6.91μM in the phenoxy derivative **245** to 447nM in the vinyl **413** was observed. Despite this improvement, the activity of **413** still falls short of that of CA4. This indicates that for the particular structures presented here, the presence of the *p*-methoxy group only does not yield as potent compounds as those observed for CA4 analogues, while the combination of 3-vinyl and and 3"-hydroxy-4"-methoxy substitutions yield compounds with increased potency compared to CA4

Compound No.		Isomer	MCF 7	
			IC_{50} μM (SEM)	Cell Death @ 10μM
412	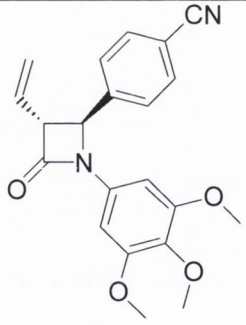	*Trans*	6.251 (5.08)	4.5
413	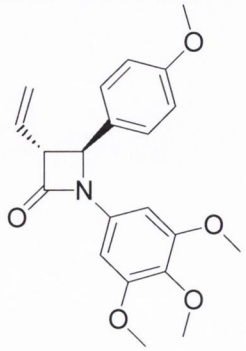	*Trans*	0.4469(0.256)	2.4

Table 4.17 Antiproliferative and cytotoxicity data for compounds **412** and **413**

4.12 Tubulin Polymerisation Assay

The biochemistry results presented so far have all dealt with the *in vitro* effects of CA4 analogues on the MCF-7 cell line. CA4 and its analogues act through a mechanism involving the tubulin protein found in cells. While it is useful to quantify the effects of these compounds on the cell, it is also necessary to examine their effects directly on tubulin/microtubules. A number of commercial assays that examine tubulin polymerisation, microtubule stablisation/destablisation, and competitive binding assays are available for this purpose.

In this thesis the most promising compounds were the subject of a tubulin polymerisation assay. The assay in question was purchased in kit form from Cytoskeleton (#BK006). The assay monitors the polymerisation of highly pure tubulin isolated from bovine brain tissue. Tubulin from bovine brain tissue is homologous to human tubulin since the tubulin protein is highly conserved throughout many mammalian species. The polymerisation of tubulin in the presence of various test compounds and controls is monitored by absorbance. Since the polymerisation of tubulin is highly dependent upon on temperature amongst other things, the absorbance measurements must be made at 37°C.

Cytoskeleton also supply a microtubule stablisation/destablisation assay. The assay monitors the depolymerisation of fluorescently labelled microtubules in the presence of the compound of interest. A competitive binding assay is also available using radiolabelled colchicine. This assay was not used to evaluate the compounds presented in this thesis due its use of a radiolabelled ligand.

The initial assay performed established the dose dependent effect of **343** on tubulin polymerisation (**fig 4.14**). DMSO and paclitaxel were used as controls. The DMSO curve clearly show the three stages of polymerisation – nucleation, growth, and steady state equilibrium. Paclitaxel eliminates the nucleation phase, increases V_{max} and increases the final polymer mass. An assay was also carried out on two other compounds **250b** and **255** and the results are shown in **fig 4.15**.

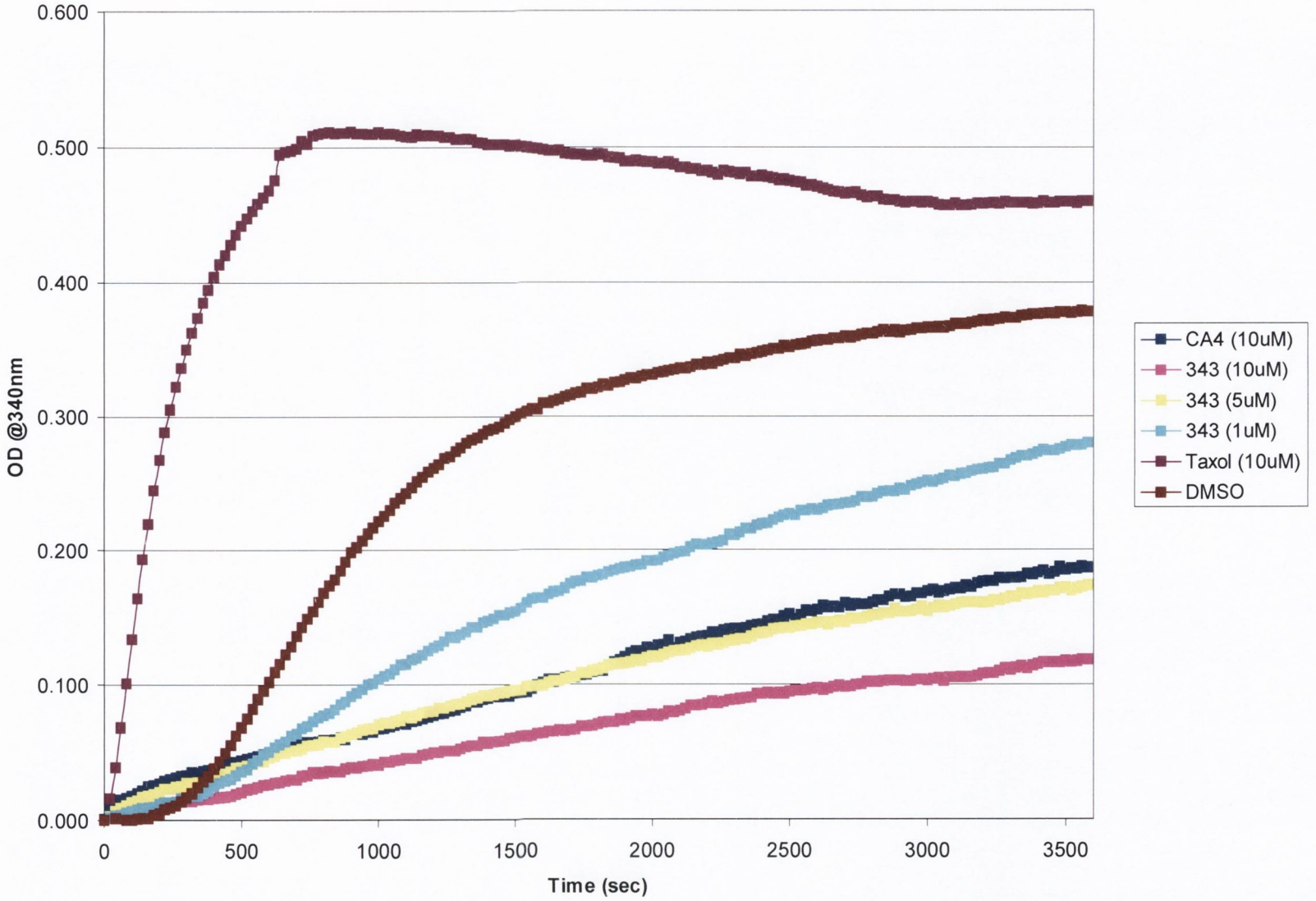

Fig 4.14: Tubulin polymerisation assay for compound **343** at 10μM, 5μM, and 1μM with DMSO, Taxol (10μM), and CA4 (10μM) controls.

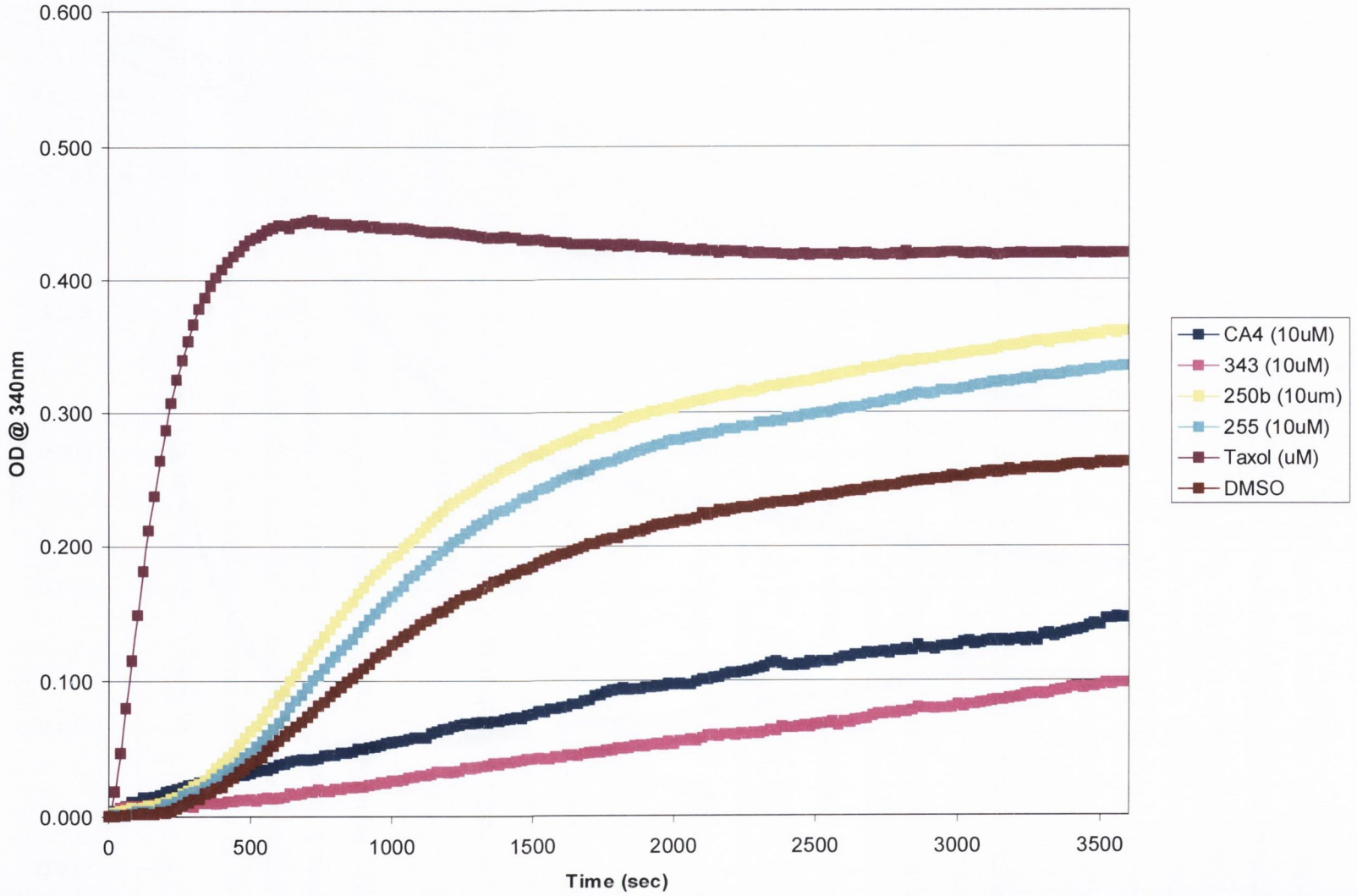
0.600
0.500
0.400
0.300
0.200
0.100
0.000
OD @ 340nm
0
500
1000
1500
2000
2500
3000
3500
Time (sec)
CA4 (10uM)
343 (10uM)
250b (10um)
255 (10uM)
Taxol (uM)
DMSO

The fold inhibition of each compound tested with respect to the DMSO control is presented in **table 4.18**. Exposure to 10μM CA4 brings about a 5.28 fold inhibition in the V_{max} observed for the polymerisation. Compound **343** compares very favourably to CA4 in this respect since exposure of the tubulin to 10μM **343** results in an 8.7 fold inhibition of the V_{max} observed for the polymerisation. These V_{max} results show good agreement with the antiproliferative data recorded for both CA4 (IC_{50} = 4.2nM and **343** (IC_{50} = 1.4nM) in the MCF-7 line.

It can also be clearly seen that the fold inhibition of V_{max} follows a dose response curve. Exposure of the tubulin to 5μM and 1μM of **343** resulted in fold inhibitions of V_{max} of 7.31 and 2.61 respectively. From the graph (**fig 4.14**) it can be seen that **343** also reduces the final polymer mass in a dose dependent manner.

Compound	Concentration (μM)	Fold Inhibition of tubulin polymerisation
DMSO	10	1
CA4	10	5.28
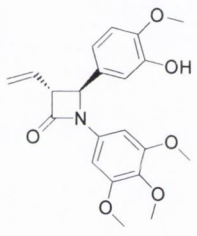	10	8.7
	5	7.31
	1	2.61

Table 4.18 fold inhibition data for compound **343** compared to CA4. The values represent the average values from two separate assays.

Fig 4.15 presents the tubulin polymerisation data for compounds **343**, **255**, and **250b**. The assay was performed on **250b** to demonstrate that a compound such as **250b** that was not active in the screen against MCF-7 cells (IC_{50}=168.4μM) would not posses significant tubulin polymerisation inhibition properties. Compound **255** was used in the assay due to reports that compounds that do not display activity in cancer cell lines may nonetheless possess tubulin polymerisation inhibition properties[123]. From **fig 4.15** it can be clearly seen that both **255** and **250b** do not exhibit any tubulin polymerisation inhibition properties. Indeed both compounds appear to increase the V_{max} rates of tubulin polymerisation and the final polymer mass but not to the same extent as the taxol control. V_{max} for the DMSO control was found to be 10.9 mOD/min, for **255** was found to be 14.14 mOD/min and for **250b** was found to be 14.7 mOD/min. For the taxol control the V_{max} was found to be 89.4

mOD/min. These results may then account for the poor *in vitro* activity of both compounds (IC_{50} values of 30.64μM and 168.4μM respectively).

Clearly it can be seen that for the β-lactam containing CA4 analogues presented in this work that activity against the MCF-7 cell line and inhibition of tubulin polymerisation are closely related. It has also been shown that the most active compound synthesised (**343**) inhibits tubulin polymerisation to a greater extent than CA4 and in a dose dependent manner.

4.13 HPLC Stability Studies

The stability of any pharmaceutical preparation is of enormous importance. At the very least degradation results in loss of potency of the product leading to a poor outcome for the patient, while at the worst the degradation products may be unsafe, untested, and lead to unwanted side effects and complications. Since the β-lactam ring is at the core of a number of medicinal products in current use, the degradation of the β-lactam ring has been extensively studied particularly by clinically important serine β-lactamases and metallo lactamases. It has been shown that monobactams such as aztreonam are not subject to hydrolysis by metallo β-lactamases and so the stability study presented here concentrates on evaluating the pH dependent hydrolysis of monocyclic β-lactams such as illustrated in **fig 4.16**.[330]

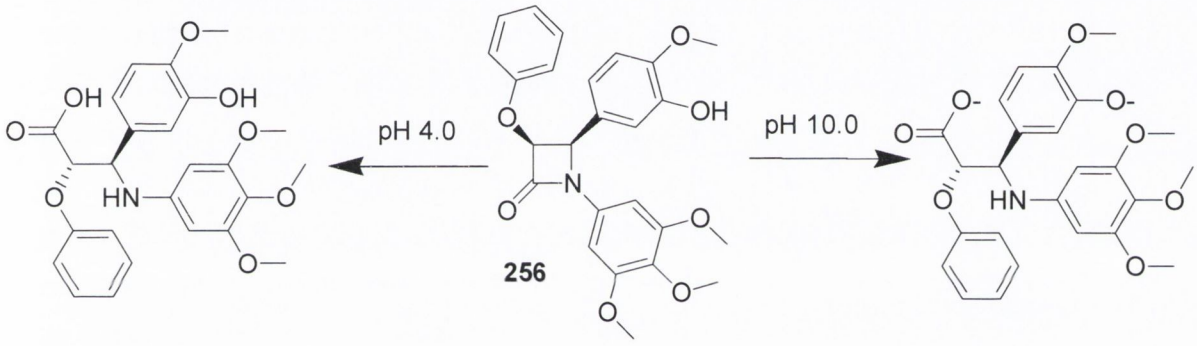

Fig 4.16 Compound **256** selected as a model compound for the stability study

The stability of compound **256** from the first library synthesised was evaluated in buffered solution and in blood plasma by HPLC. The HPLC method is described in detail in the experimental section, along with details on the preparation of the buffers and blood plasma. The separation was carried out on a Spherisorb column with a isocratic mobile phase consisting of 60:40 acetonitrile:water. The peak shape of the resulting chromatogram indicated a high degree of tailing. The symmetry factor for the peak was found to be 2.09 which lies well outside the BP specifications of between 0.8 and 1.5 (Appendix III BP 2008). Theorizing that the tailing of the analyte peak was due to the acidic phenol interacting with the column packing material, the mobile phase was modified with 0.1% *v/v* of trifluoroacetic acid. This resulted in an analyte peak with a symmetry factor of 1.19 which lies within the BP specifications. A linear response test was carried out on the system by the injection of serial dilutions of the analyte onto the system. The results are presented in **fig 4.17** and

show that a linear response was obtained over the concentration range depicted. To assess the reproducibility of the system, six injections at a single concentration of analyte were made. The relative standard deviation was found to be 0.72. The BP specifies a maximum RSD of 0.85. It was therefore concluded that the HPLC method developed was suitable for the determination of the analyte **256**.

The hydrolysis of the β-lactam ring under acidic/basic conditions is a major degradation pathway for any β-lactam ring containing molecule. Drug stability testing is an important part of the development of any new pharmaceutical prior to entry into the market. Guideline Q1A (R2) issued by the International Conference on Harmonisation (ICH) suggests that stress studies to determine the stability of a compound and the determination of its degradation products should be carried out [331]. Ezetimibe is a good example of a monocyclic β-lactam pharmaceutical whose stability under stress at various pH's has been determined by HPLC [332 333]. Singh *et al* carried out a study on the degradation of ezetimibe at 80°C at neutral pH and in 0.1M NaOH and HCl respectively. It was found that under basic conditions the ezetimibe completely degraded within one minute of contact with the basic solution. In a more dilute 0.01M NaOH solution complete degradation was observed after four hours. In neutral conditions complete degradation was observed after one hour. In acidic conditions, the ezetimibe degraded at a much slower rate than observed at neutral and basic pH's. This clearly indicates that while degradation of the β-lactam ring can occur at both acidic, neutral, basic pH's, the rates of degradation may not all be equal. The rate of hydrolysis at different pH's has implications for the selection of a route of administration and for the formulation of the product prior to delivery to the patient. It was found that the stability of the compound increased with increasing pH as can be clearly seen by the graphs presented below (**fig 4.18-4.20**). This trend is in good agreement with previous work carried out by Carr and O'Donoghue[334] on structurally similar compounds. Most promisingly the compound displays an average half life of 92 minutes at pH 7.5 (**table 4.19**) which indicates that the compound may be stable at the physiological pH of blood. At pH 4.0, there appears to be a rapid loss in analyte of approximately 20% in the first three minutes after contact with the buffer. There is then a plateau in degradation until 35 minutes after contact at which time the degradation of the analyte resumes in a linear fashion resulting in a half life of nearly 40 minutes at pH4.0. This pattern was initially thought to arise from loss of compound due to poor solubility in the aqueous buffer. Closer inspection revealed no visible precipitates formed in the test solution during the first 20 minutes of the experiment. Precipitate was observed after this time but was presumed to be a consequence of the hydrolysis of the β-lactam. Great care was also taken during the

experiment to ensure that the test solution was thoroughly mixed by vortex before the removal of sample to eliminate the possibility of the results being due to the presence of a heterogeneous solution. At pH 7.5 the degradation of analyte is almost linear throughout the timescale of the experiment resulting in a half life of approximately 90 minutes. At pH10 there is an initial loss of approximately 10% in the first minutes of contact with the buffer after which time no further degradation is observed up to 48 hours later at which point the study was terminated. This was a puzzling finding since some degree on hydrolysis over the long time scale should be observed.

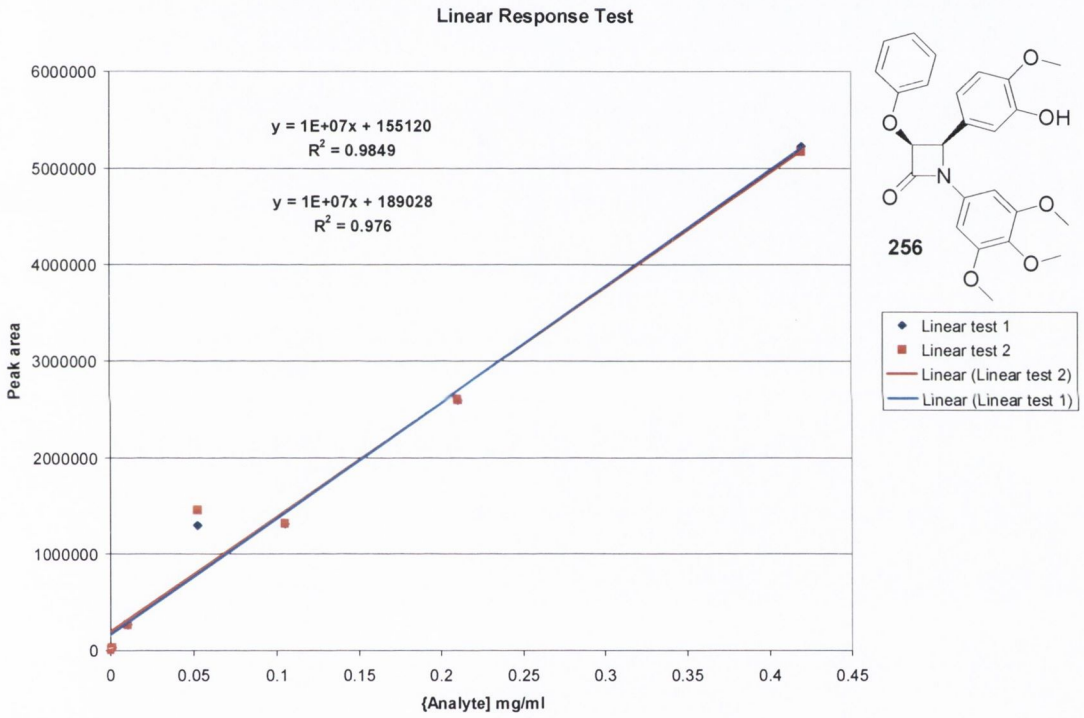

Fig 4.17 Linear response test for **256**

pH	R^2 value	$t_{1/2}$ (min)
4.0	0.90	39.88
4.0	0.94	40.45
7.5	0.95	96.63
7.5	0.96	85.31
10.0	na	91% remaining after 24 hours
10.0	na	95 % remaining after 24 hours

Table 4.19 Calculated half lives for **256** in pH buffers

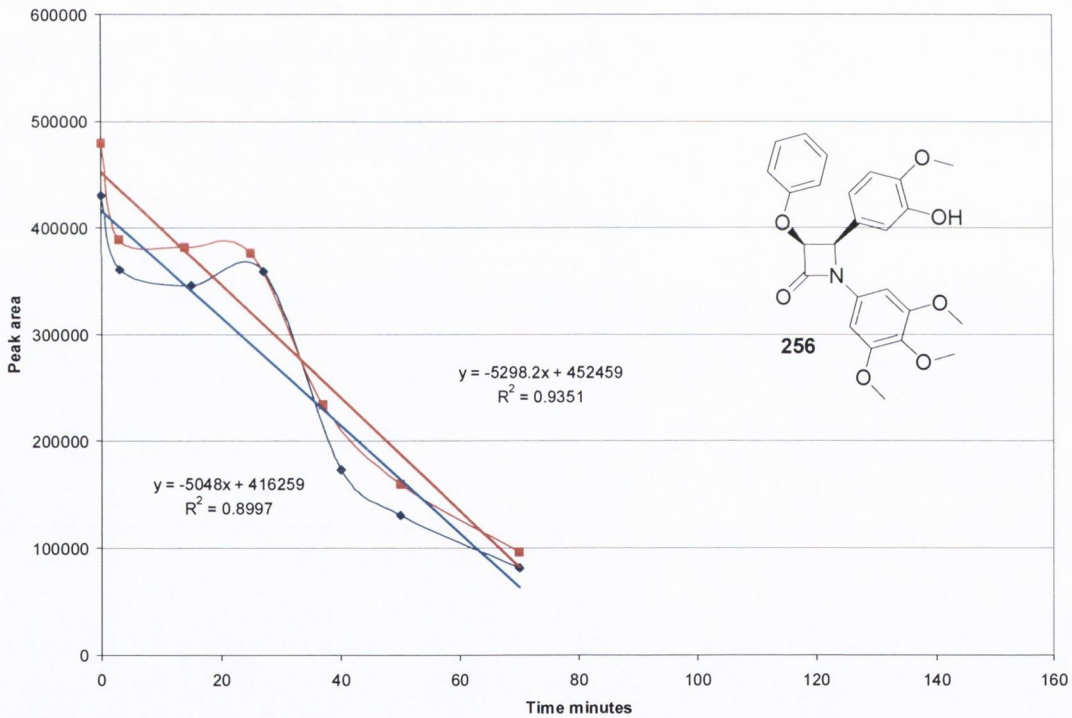

Fig 4.18 Degradation curve for **256** at ph 4.0

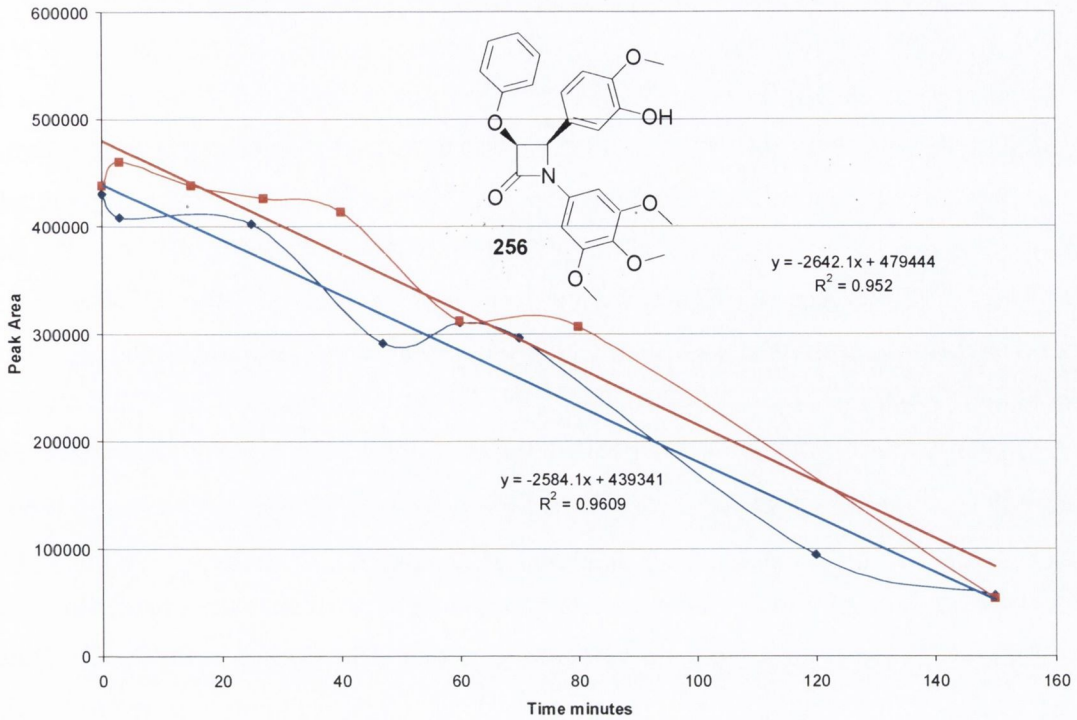

Fig 4.19 Degradation curve of **256** at pH 7.5

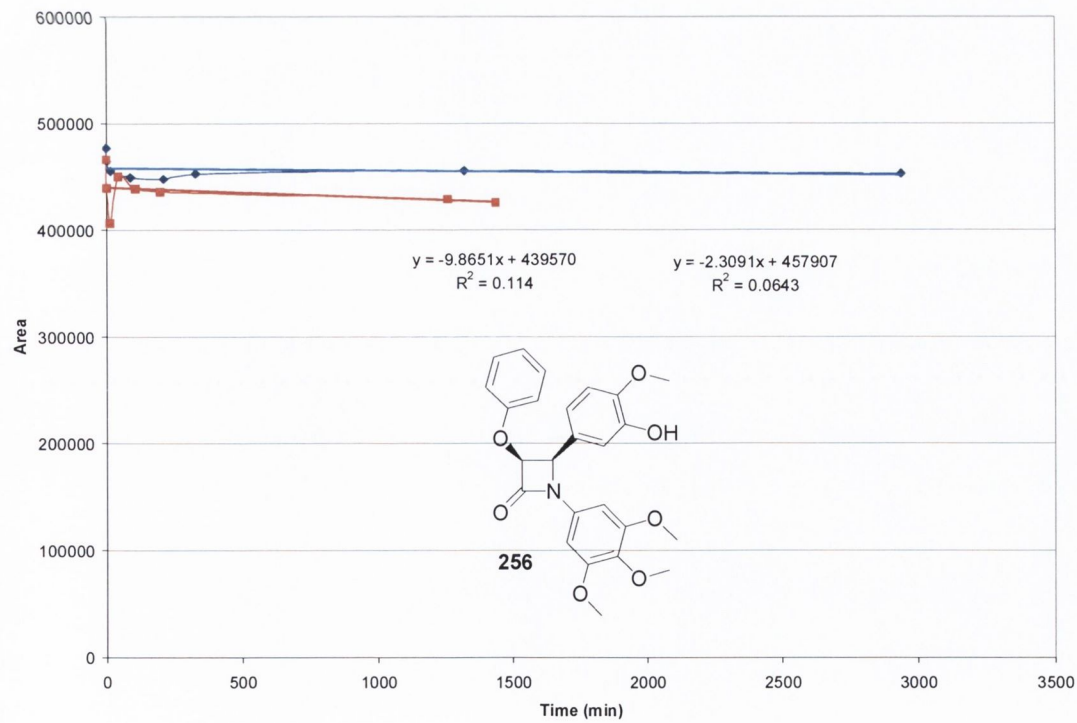

Fig 4.20 Degradation curve of **256** at pH 10.0

Numerous studies have been carried out on the *in vivo* stability of CA4P in both human and animal models[335] [336]. Kirwan *et al*[100] carried out a detailed study of the metabolism and pharmacokinetics of both CA4P and CA1P in an effort to establish a reason for the difference observed in tumour response between the two *in vivo*. Kirwan also suggests that the enhanced activity of CA1 over CA4 may be due to the formation of an active metabolite of CA1. It was found that CA4P and CA4 had half lives of 1.38 hours and 0.35 hours respectively in blood plasma. CA4 was also found to be reasonably stable in a MAC 29 tumour homogenate. Aprile *et al* has published a study on the stability of CA4 in rat and human liver microsomes monitored by HPLC-ESI. Aprile determined that CA4 in pH 7.4 phosphate buffer incubated with shaking at 37°C for 60 minutes resulted in only a small isomerisation (approximately 2%) of the *Z* to *E* isomer. When CA4 was incubated with rat and human liver microsomes, conversion from the *Z* to *E* isomer was observed (**fig 4.21**). A number of metabolites were also observed and are illustrated in **fig 4.22**. These metabolites include both *E* and *Z* isomers. Aromatic hydroxylation and demethylation appear to be the two main metabolic pathways for CA4.

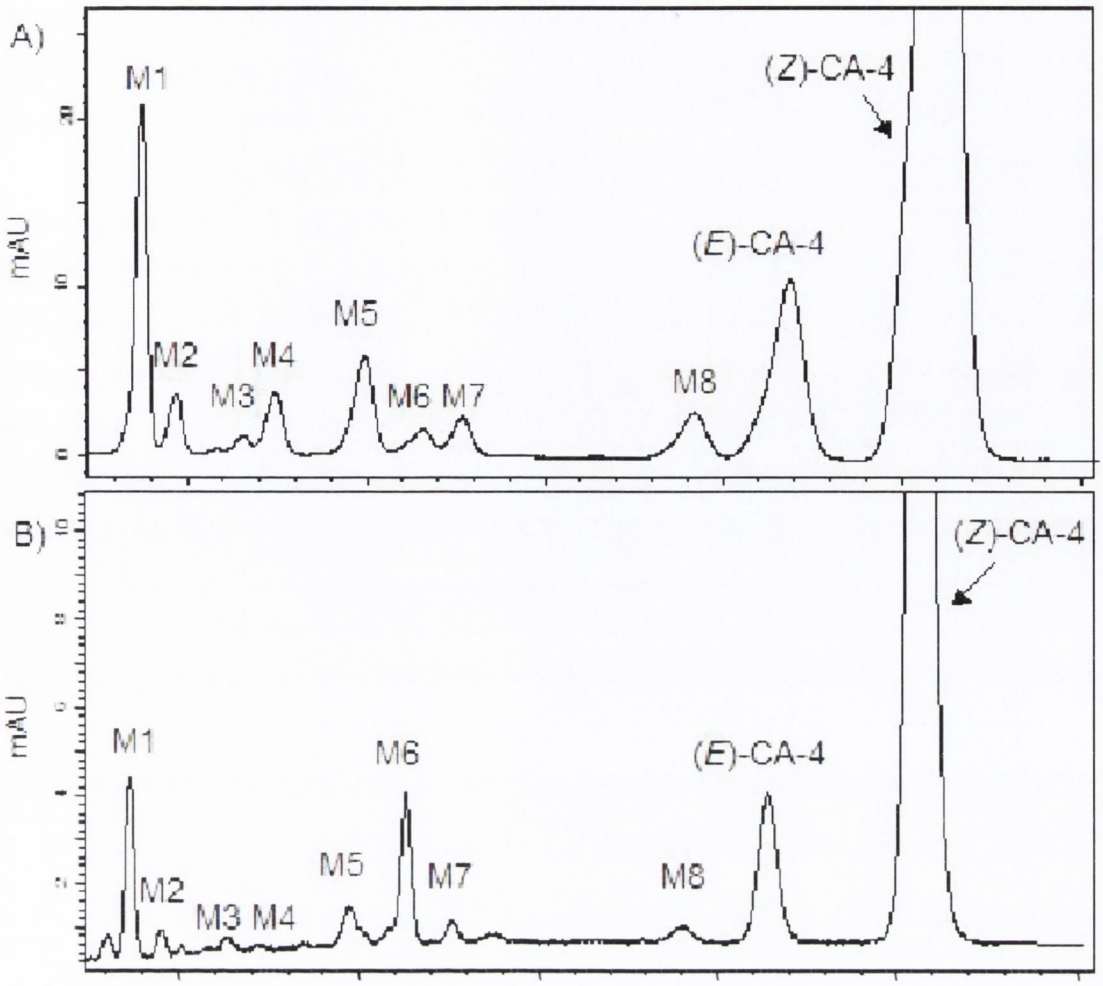

Fig 4.21 Chromatograph obtained from incubation of CA4 with rat (top) and human (bottom) liver microsomes carried out by Kirwan *et al.* The structures for the metabolites M1-M8 are presented in **fig 4.22**.

To compare the β-lactam compounds to CA4, a stability study on compound **256** in human blood plasma was carried out and the results are presented below, from which little information can be gained. From the graphs it can be seen that there is an initial drop in concentration as monitored by peak area followed by a lengthy period (up to 1500 minutes after contact with buffer) where the peak area is maintained (**fig 4.23** top graph) followed by degradation. This was a curious finding since the degradation study at pH 7.5 has shown that even without the influence of blood plasma the compound should still display a half life of approximately 91 minutes at pH 7.5. The final concentration of **256** in the test solution was 112μM which is more concentrated than that used by Aprile. Dowlati *et al* [91] suggests that a typical plasma concentration of CA4P is between 30μM and 46μM after a dose of between 52 mg/m^2 and 68 mg/m^2.

For this reason a second study was run using a final concentration of 58μM of **256** in blood plasma (**fig 4.23** bottom graph). The most likely explanation for this is that the compound under investigation is binding to plasma proteins and not being subjected to hydrolysis.

The use of the β-lactam ring as a scaffold for CA4 has both advantages and disadvantages in terms of stability. The use of the β-lactam ring results in product that are not labile to photo catalysed isomerisation but the β-lactam ring is subject to hydrolysis reaction *in vivo* that are not an issue for CA4. Further investigation into the stability of the β-lactam compounds *in vivo* is required. If possible the metabolites should be identified, synthesised and tested individually. It is possible that the metabolites particularly the ring opened β-lactam may possess biochemical activity in their own right.

It is intended in the future to carry out a more detailed study on the metabolism of these β-lactam compounds by using liver microsomes. This would provide a more accurate estimation of the effects of metabolism on the compound. If possible such a study should be carried out by LC-MS so that information about the nature of the metabolites can be ascertained.

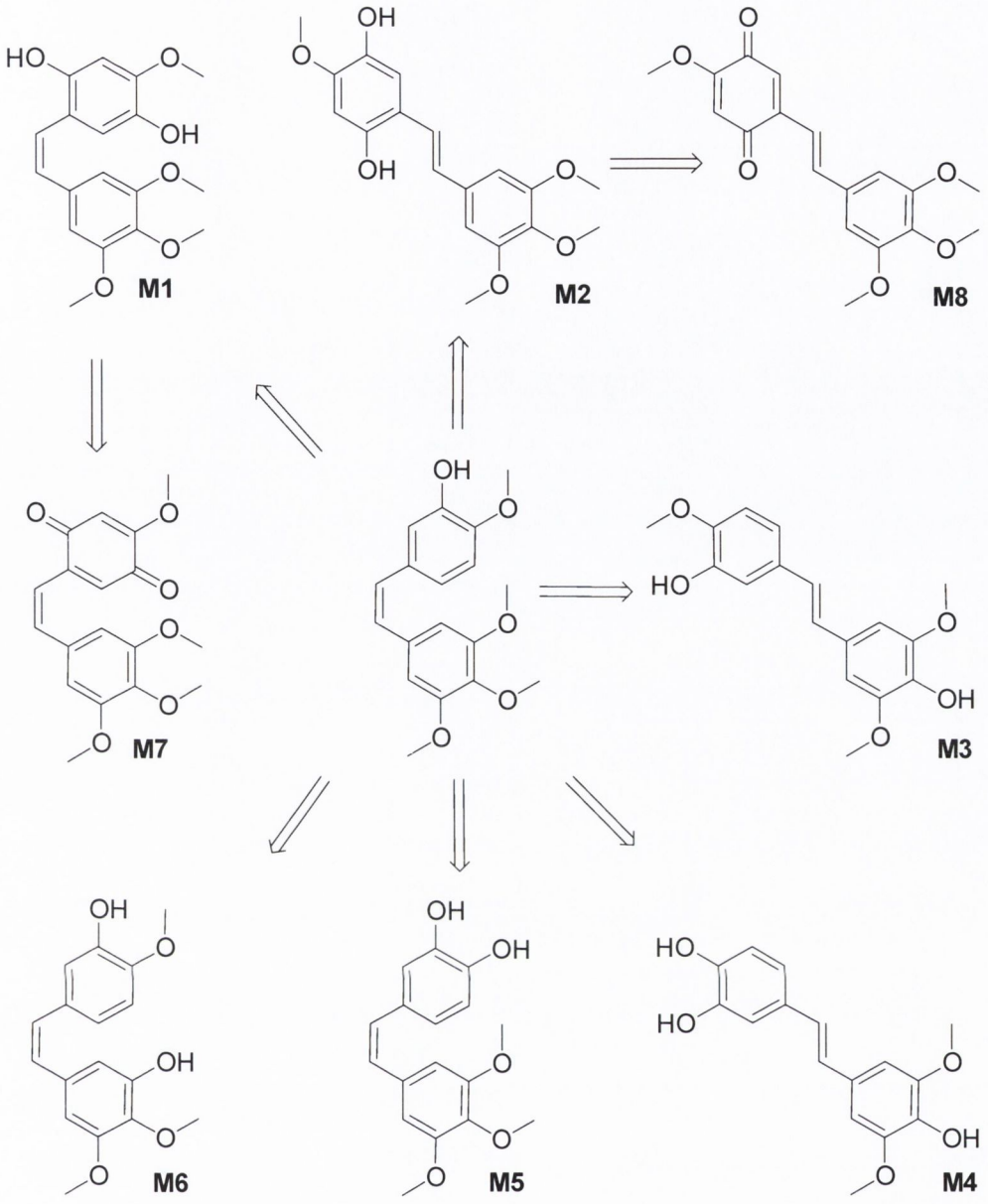

Fig 4.22 structures for metabolites of CA4

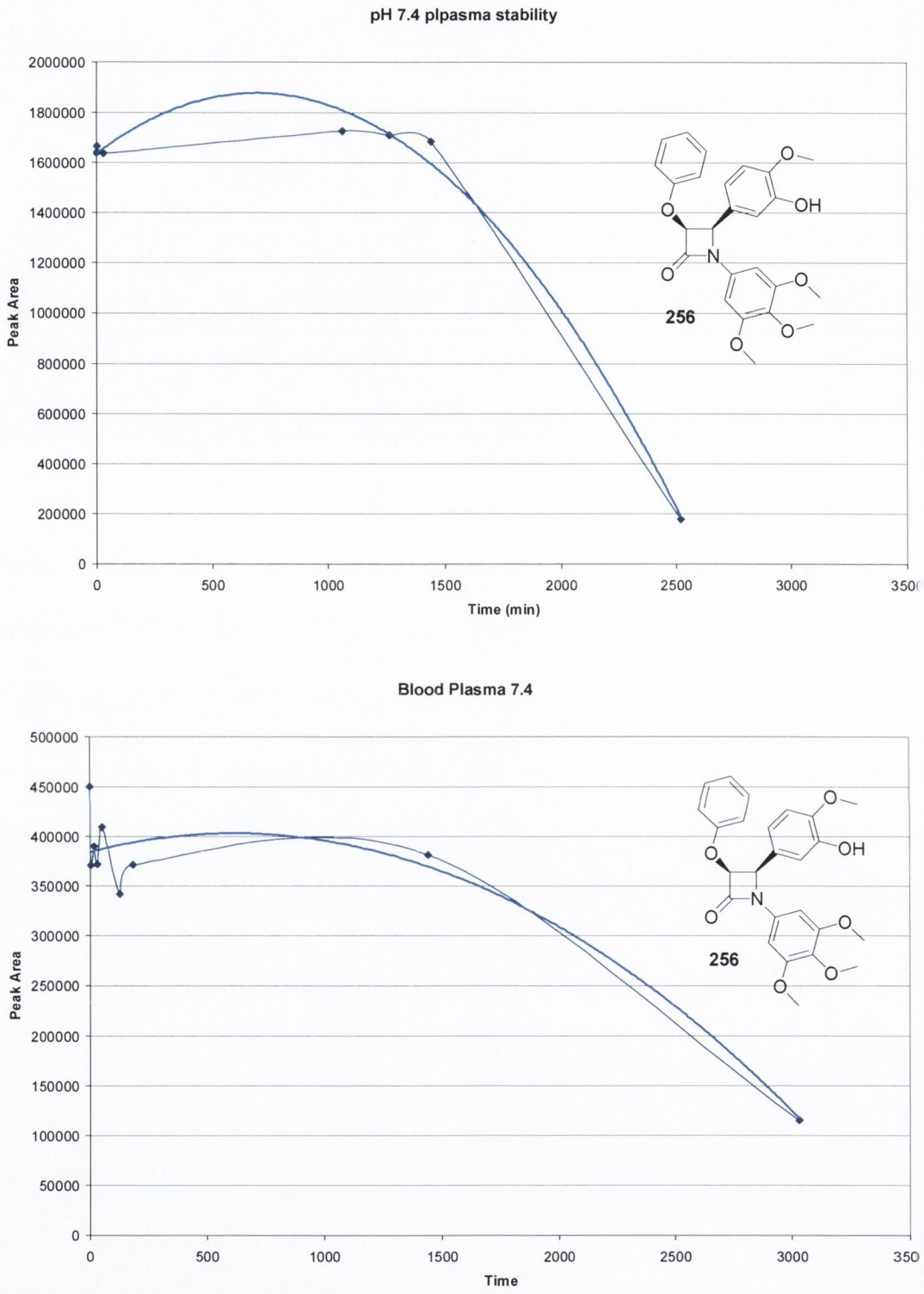

Fig 4.23 Degradation of compound **256** in human blood plasma. The top graph presents tle data obtained with a final concentration of **256** of 112μM. The bottom graph presents tle data obtained with a final concentration of **256** of 58μM.

4.14 Molecular Modelling Studies

A molecular modelling study was undertaken in an attempt to rationalise the biochemical results observed for the compounds synthesised within this thesis. The study was facilitated by the availability of a crystal structure of colchicine DMAA docked in the colchicine site of tubulin[17]. The study initially focussed on identifying a suitable method for producing energy minimised models of the compounds designed as CA4 analogues binding to the colchicine binding site of tubulin. Once produced these models were compared to the XRD structures obtained for a number of the β-lactam compounds to ensure that the energy minimised models were a realistic substitute for structures experimentally determined by XRD. When a database of such structures was established the next task was to dock the structures into the colchicine site of tubulin to examine if a correlation between the docked solution and biochemical activity could be established. Finally a structure activity relationship study was undertaken to screen the series of compounds *in silico* for rationlisations/predictions of biochemical activity prior to synthesis of future compounds.

It is important to note that for any molecular modelling study there exists a possibility that the study will not reflect accurately the molecular interactions occurring in nature. For instance there may be differences in protein structure when crystallised as a crystal suitable for XRD analysis compared to the conformations under physiological conditions. The same applies to energy minimised structures which may be calculated for molecules using programs such as *Macromobel.* assuming the molecule exists in ideal conditions. Despite these cautionary examples, molecular modelling is an important tool in medicinal chemistry and is mainly used to rationalise the biochemical activity of active compounds.

4.14.1 Generation of Energy Minimised Models

Previous work within our research group has utilised the *Macromodel* program supplied by Tripos[337] as a means for generating energy minimised models of low molecular weight molecules. In the present work a number of minimised structures of selected compounds were obtained using this program and the resulting structures were compared to the structures obtained by XRD. This comparison was deemed important since it is a means of evaluating how realistic and accurate the modelled structure is. The comparison between the energy minimised and XRD structures was made by superimposing both molecules using *MOE* [338]. This allowed for comparison both in terms of the RMS of the superimposition and by visual inspection. Close attention was paid to the trimethoxy substituted aryl ring of the

structure since it is well established as an important feature for binding at the colchicine site.

4.14.1.1 *Macromodel* as a source of energy minimised structures

Macromodel is capable of generating three dimensional energy minimised structures of compounds using force field methods. Force fields are used to examine the molecule as a function of the distance and angles between the individual atoms of the molecule. The MM3 forcefield was used to generate minimised models of the various β-lactams compounds. The MM3 forcefield uses a number of different descriptors including: bond stretching; angle bending; torsion; stretch-bend interaction; torsion-stretch interaction; torsion-bend interaction; bend-bend interaction; van der Waals interaction; electrostatics; and rotational barrier. Initially the minimizations were carried out on structures for which the XRD structure had been determined (e.g. compounds **244**, **245**, **254**, **256**, **262**, and **264**). The details of these XRD structures are presented in **Appendix I**. The accuracy of the energy minimized models from *Macromodel* was checked by comparison to the structures obtained by XRD. An example of this comparison is presented in **fig 4.24** where the *Macromodel* structure (blue) is superimposed with the XRD structure (light blue). It is apparent that while there are differences between the two structures, the *Macromodel* structure is similar to the XRD structure particularly in the trimethoxy aryl ring region. Therefore in the absence of an XRD structure, *Macromodel* can provide a suitable alternative. Fortunately compound **256** which displayed significant antiproliferative activity yielded an XRD structure. The crystal structure of CA4P as a dimer was kindly supplied by Prof. Del Herald (by private correspondence), Cancer Research Institute, Arizona State University[125]. This allowed a comparison between the structure of **256** and CA4P (**fig 4.25**). The similarity between the two structures especially in the trimethoxy aryl ring region is apparent.

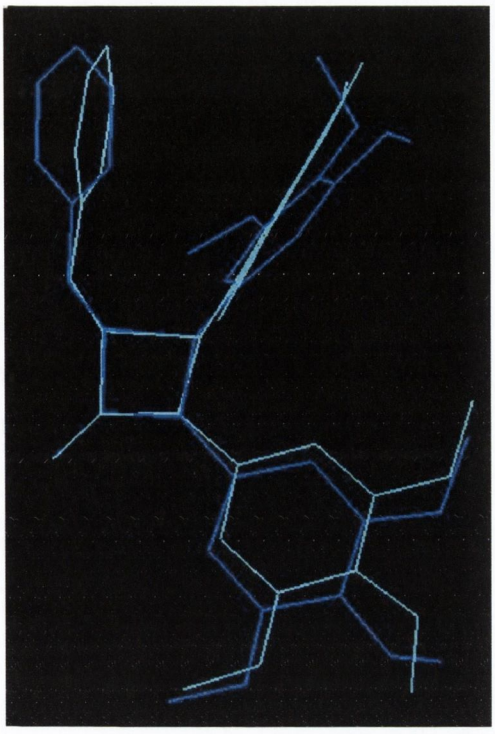

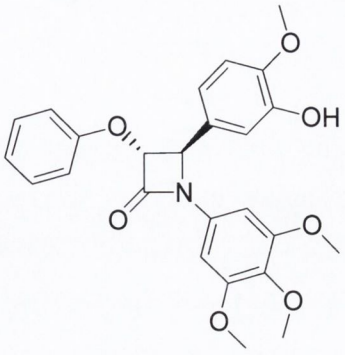

Fig 4.24 comparison of energy minimised model (blue) and XRD structure (light blue) of **256**

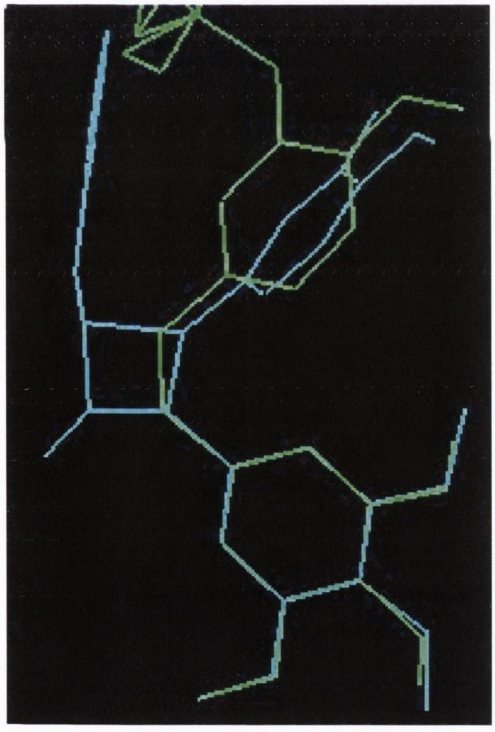

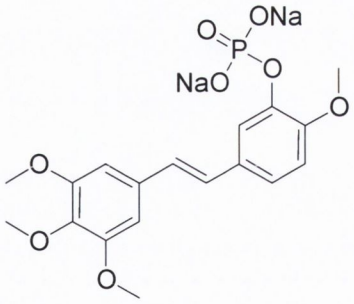

Fig 4.25 Comparison of the XRD structures of **256** (blue) and CA4P (green)

4.14.1.2 Energy Minimised structures using MOE

MOE was also used to generate energy minimised structures using the Merck molecular force field MMFF94s. MMFF94s is a modified version of MMFF94* that is tailored for use in energy minimisation[339]. In particular it provides better results for amines and amides and gives planar or near planar geometries for these compounds. To evaluate the effectiveness of *MOE* as a method for producing energy minimised models, the models obtained for **256** were compared to the structures obtained by XRD by superimposition in *MOE* (**fig 4.26**). As was the case with the *Macromodel* structures, there are differences between the structures, but there is good agreement in the crucial trimethoxy region.

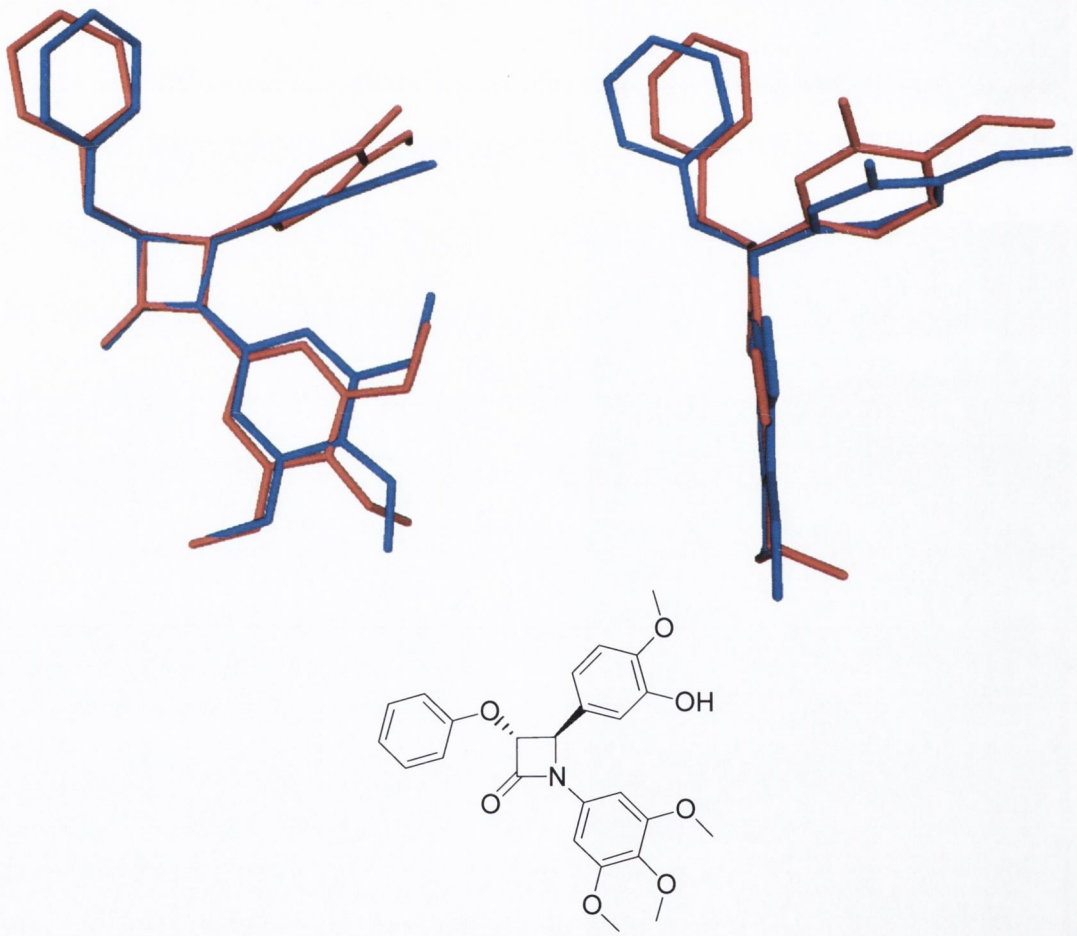

Fig 4.26 Comparison of *MOE* energy minimised model (blue) and XRD structure (red) for **256**

4.14.2 Preparation for docking studies

4.14.2.1 Tubulin crystal structure

A 3.58 Å resolution structure for tubulin-colchicine-stathmin like domain has been deposited in the RSCB protein databank (1SAO)[340]. The particular structure obtained contains a colchicine derivative in the colchicine site (**fig 4.27**).

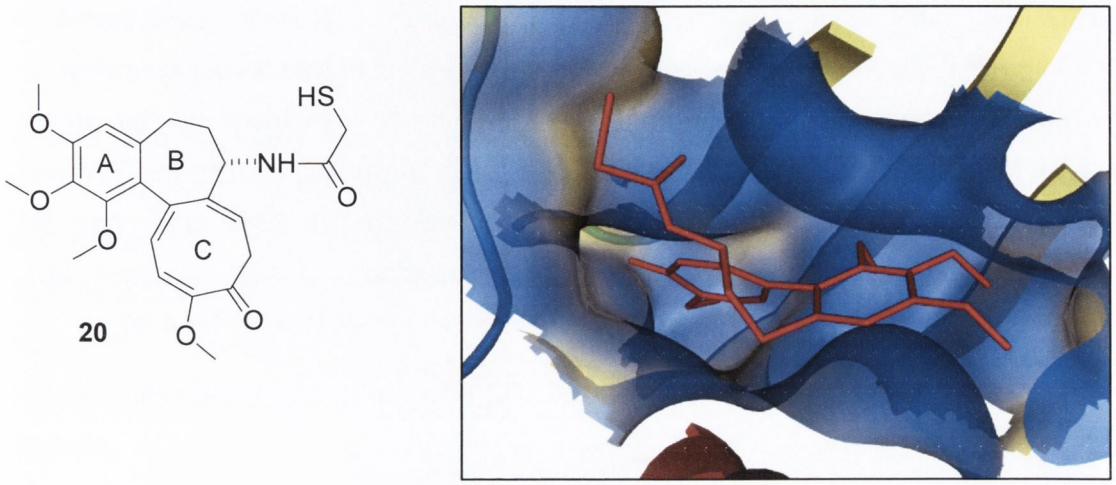

Fig 4.27 DAMA colchicine ligand (**20**) in the colchicine site of tubulin as determined by XRD. The blue surface represents the surface of the pocket with the α-tubulin subunit removed for clarity.

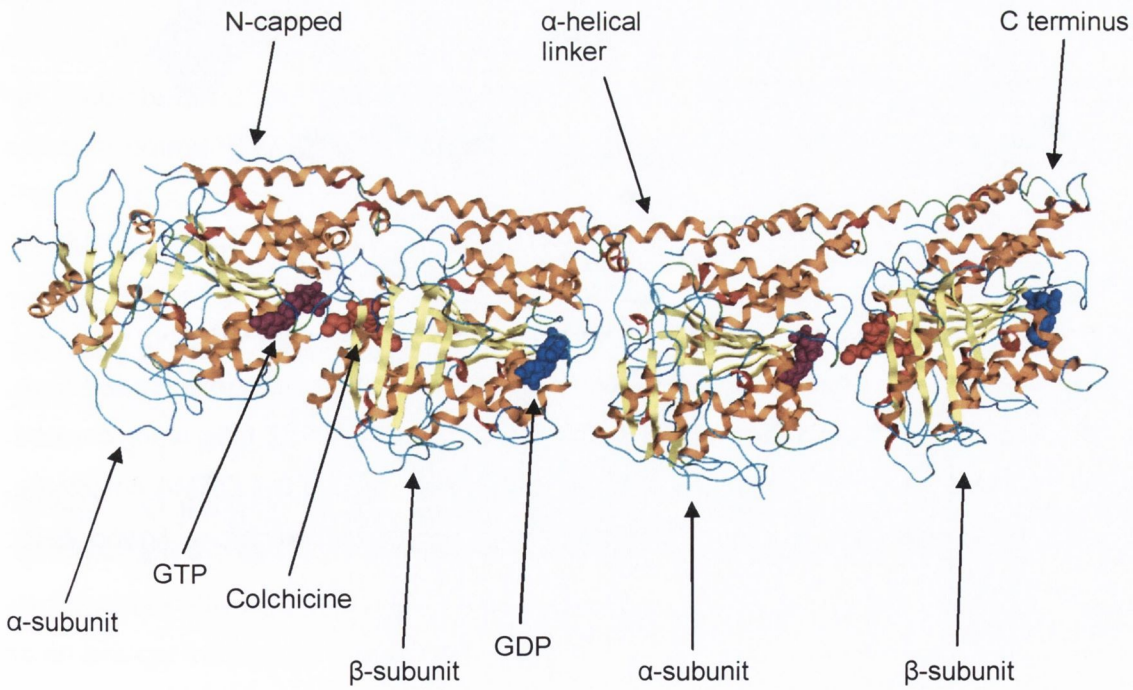

Fig 4.28 Tubulin hetereodimer on a stathmin like domain as determined by XRD[407]

The structure determined by XRD presents tubulin as a heterodimer of α and β subunits complexed with the stathmin like domain RB3 (**fig 4.28**). The RB3 domain is made up of an N-terminus and a C-terminus joined by a α-helical linker. A number of low molecular weight molecules are also depicted, GTP in purple, GDP in blue, and colchicine in red. The binding of colchicine DAMA to the colchicine site has already been discussed in **section 1.4.4.3**. The colchicine site is buried mostly in the β-subunit but with some interactions with the α-subunit. Ravelli notes that the presence of the colchicine derivative leads to the α-subunit of tubulin being unable to adopt its favoured straight conformation with β-tubulin. It does this by steric interference with residues Val α101 and ASN α181 in α-tubulin., forcing the T7 loop and H8 helix to clash with the α-tubulin, and forcing the Lys β352 side chain to interfere with the α-tubulin. A close up view of the position of DAMA colchicine (**20**) relative to the T7 and H8 protein structures in β-tubulin is presented in **fig 4.29**.

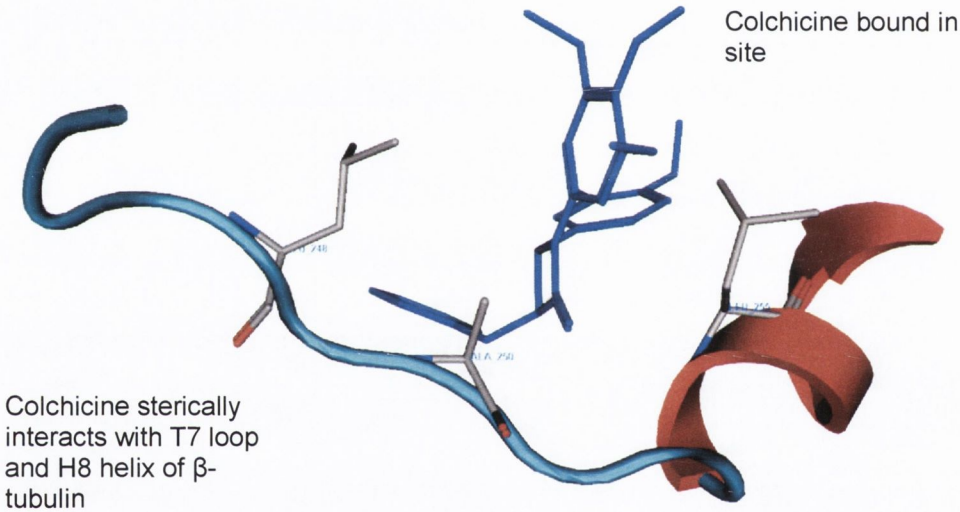

Fig 4.29 Representation of the DAMA colchicine ligand (blue) with the T7 loop (light blue) and H8 helix (red) of β-tubulin

In preparation for the docking study, the tubulin protein was downloaded from the RSCB database as a .pdb file (1SAO). Two separate .mol2 files were created with one containing the protein only and the second containing the DAMA colchicine ligand. MOE was used to ensure that the protein and DAMA colchicine ligand were correctly protonated.

4.14.2.2 Preparation of ligands for docking

As has previously been discussed, the generation of energy minimised structures in *Macromodel* can be useful for the creation of ligands with which to carry

out docking in *FRED* (Fast Rigid Exhaustive Docking program supplied by Openeye software). One major disadvantage of such an arrangement is that only a single conformation of the molecule is docked into the protein. This is particularly an issue where a program such as FRED is used because FRED docks the ligand rigidly. For FRED it is recommended that a number of conformations of the ligand are docked sequentially, and the highest scoring docked conformation outputted as the docked solution. *OMEGA* also supplied by OpenEye was used for conformer generation.

4.14.3 Use of FRED for docking studies

An initial attempt at docking was made using the Sybyl[341] program but failed. Sybyl has been previously used successfully within our research group to dock ligands into the estrogen receptor site. The failure may have been the result of the nature of the colchicine site in tubulin which is somewhat boxed in by the α-subunit of tubulin. A second piece of software (FRED) was able to successfully dock the ligands.

4.14.3.1 How FRED works

The Fast Rigid Exhaustive Docking (FRED) program was obtained from Openeye software. As the name implies FRED is capable of quickly docking a rigid ligand into an active site. The exhaustive part of the docking involves the program looking at all the possible orientations (poses) of the ligand in the active site. FRED has a number of useful attributes. It can be used in situations where there is data for a known bound ligand (such as is the case here) to improve on the docked results. FRED has a consensus structure function which examines the docked solution supplied by different scoring functions for each ligand which increases the likelihood that the docked solution is correct. It uses Chemgauss 3 to describe the shape and chemistry of the molecules of interest, and is very effective at determining the shape of the active site of the protein.

FRED accepts ligand inputs in the form of a number of commonly used file formats. In general it is recommended that the input file contains a number of conformers that have been previously generated by using *OMEGA*. However it is also capable attempting to dock ligand files containing only a single conformer such as an energy minimised structure or from a XRD structure. A second input file called a receptor file is also required. The receptor file specifies the structure of the protein, the location of the receptor site for docking, and also contains the shape potential grid of the receptor site which in essences describes the shape of the site. The

receptor site can also contain the known bound ligand. The receptor file can be generated either by an external program or by FRED internally which was the case here. To generate the receptor file internally, the known bound ligand must be specified.

Once the various inputs have been specified the process of exhaustive docking can commence. The first step is to establish all possible orientations (poses) that the ligand may adopt in the active site. This is done by rigid rotation and translation of the ligand in small steps typically of 1Å. This generates an ensemble of poses for the given ligand which must be filtered to insure that each pose obeys certain conditions within the active site. These conditions can be regarded as making sure that the ligand fits snugly into the site. The program specifies an inner and an outer contour level measuring roughly 50 and 1500 cubic Angstroms respectively. Each pose must have a minimum of one heavy atom within the inner contour and all the heavy atoms must fit within the outer contour. The entire ensemble is then filtered to ensure that no pose clashes with the surface of the protein. The user can also specify other constraints by which the ensemble can be filtered and can also set the maximum number of poses to be examined (typically 100 poses). The second step after the generation of the ensemble of poses is to score each pose ie to measure by a scoring function how well it fits into the active site. FRED contains a number of different scoring functions that may be used but only the PLP scoring function was selected for use. The PLP function was selected since its speed allows it to be used in exhaustive docking, and it takes into account ligand shape, hydrogen bonding, metal interactions and non-polar interactions. FRED ranks each pose in terms of the specified scoring function typically Chemgauss 3 or in our case PLP. Alternatively the consensus structure scoring can be used where the pose is ranked according to the sum of its scoring functions. The resulting top ranked pose is outputted as the docked solution. If neccessay the docked solution can be further optimised by subjecting all of the atoms of the top ranked pose to a force field optimisation.

4.14.3.2 Validation of docking protocol

To ensure that the docked solution obtained from FRED represents a realistic pose for the ligand in the site, the original known bound ligand was taken and redocked in the site (**fig 4.30**). In this way comparison between the known ligand and when it is redocked provides a way to evaluate the performance of the docking

program. In particular the redocked ligand should maintain the same ligand-protein interactions as the DAMA colchicine ligand (**20**).

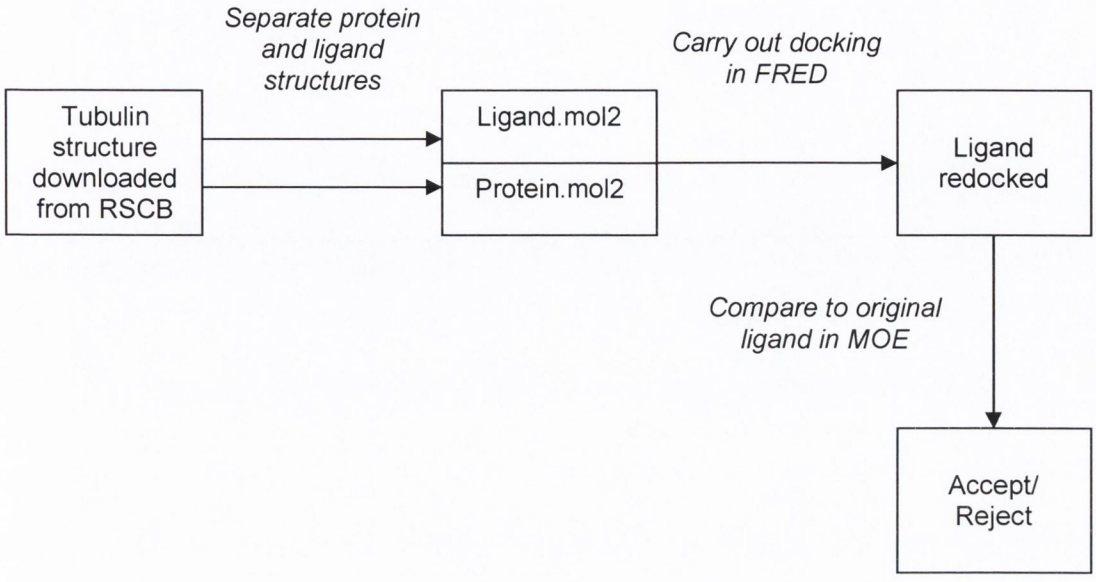

Fig 4.30 Procedure developed for validating the use of FRED in docking

Two important residues (Val β318 and Cys β241) in the site have been identified from biochemical data and both have been preserved in the docked solution. Modification of the Val β318 residue has been shown to reduce the sensitivity of tubulin to colchicine[62]. Colchicine derivatives with groups substituted at the methoxy positions can crosslink with Cys β241.[61] Upon visual inspection the success of the docking procedure can be seen. There is good agreement between the two trimethoxy regions and the two important Val β318 (hydrophobic interaction) and Cys β241 (polar contact) contacts are maintained in the docked solution. **Fig 4.31** illustrates the success of FRED at redocking the DAMA colchicine ligand (**20**) back into the colchicine site.

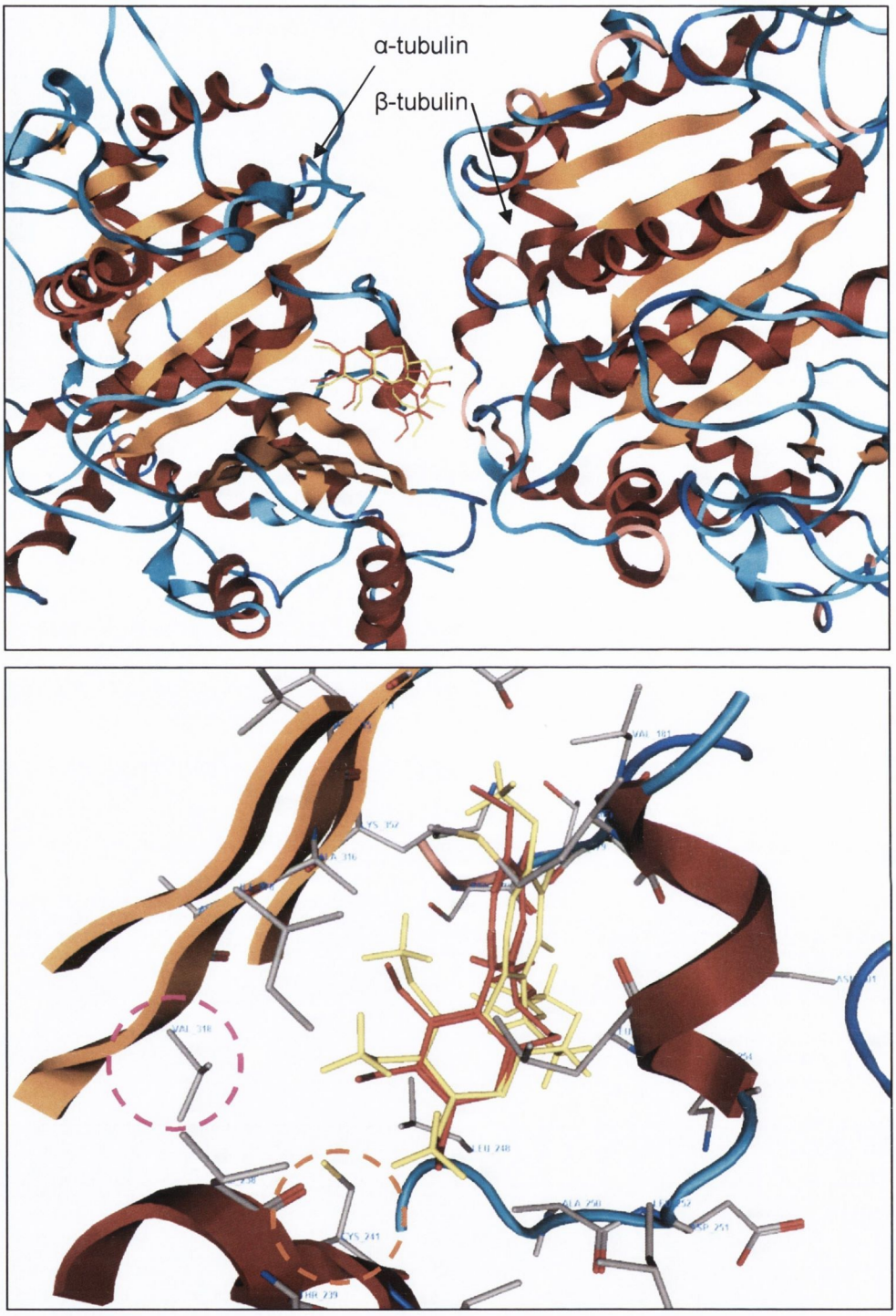

Fig 4.31 Validation of docking protocol. The original DAMA colchicine ligand (**20**) (red) and this ligand redocked (yellow) are shown in the colchince site at the interface of α and β tubulin (top). Two important contacts Val β318 (pink circle) and Cys β241 (orange circle) are maintained in the docked solution (bottom).

4.14.3.3 Finalised Procedure for Docking

The previous sections have demonstrated energy minimised compounds are realistic representations of the actual structures for the β-lactams presented in this work. It has also been seen that *FRED* has been validated for the docking of compounds into the colchicine site of tubulin. It is apparent from visual inspection that *FRED* can successfully carry out the docking. **Fig 4.32** outlines the finalised procedure for docking our database of β-lactam compounds into the colchicine site of tubulin. The database is made up of over seventy β-lactam compounds that have been synthesised and evaluated for antiproliferative activity in the MCF-7 cancer cell line. A MOE database of these compounds was created which was then subjected to energy minimisation to generate an energy minimised database. For each entry in the database a series of conformers were generated using OMEGA. This database of conformers was then docked into the colchicine site using FRED and the best conformer as identified by the scoring function taken as the docked solution. The docked solution was evaluated in terms of interactions with the protein and compared to the its XRD structure if available.

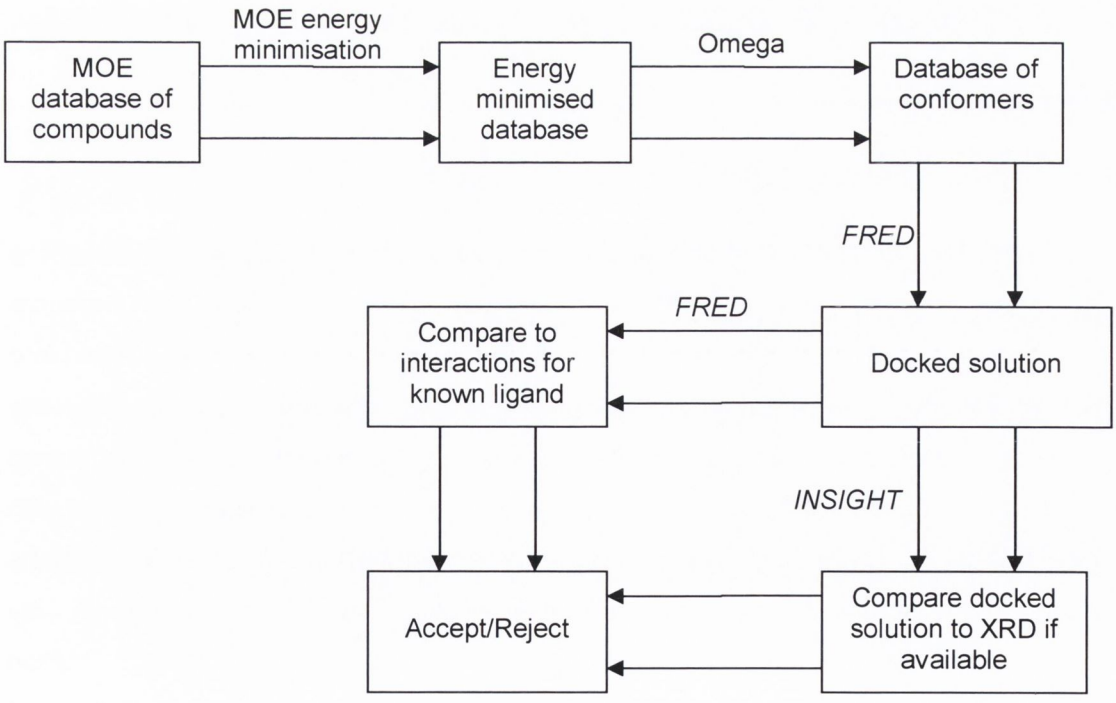

Fig 4.32 Finalised procedure for docking of energy minimised compounds

4.14.4 Evaluation of docked solutions

4.14.4.1 Scoring functions

The Piecewise Linear Potential (PLP) scoring function was selected to score the docked structures. The final PLP score is the sum of four components: nonpolar interactions; hydrogen bond interactions; sulphur interactions; heavy metal interactions. The function includes both steric and hydrogen bond components and is particularly useful where there are close contacts between the ligand and the protein. This is particularly useful for ligands in the colchicine site due to the tight confines of the pocket. The PLP function relies on dealing with only the heavy atoms present in the system, however it is still important to have properly protonated structures for both the ligand and the protein.

4.14.4.2 Ligand Interactions

The ligand-protein interactions for each docked solution were closely examined particularly in terms of the conservation of the two important Val β318 and Cys β241 contacts in the trimethoxy region. Ravelli[17] has also suggested that colchince exerts its effect through steric hindrance with α-subunit residues and by forcing some β-subunit structures to prevent α-tubulin adopting a straight chain confirmation. The presence/absence of these interactions in the docked solutions were also monitored.

4.14.5 Docked solutions

4.14.5.1 CA4 docked solution

Before discussing the outcome of the molecular modelling study of the β-lactam compounds, it is useful to examine the docked solution of CA4 and attempt to identify the important attributes that lead to its exceptional activity. **Fig 4.33** presents both the *cis* and *trans* isomers of CA4, and **fig 4.34** depicts both isomers docked into the colchicine site. It is clearly apparent that both adopt different positions within the active site particularly when the trimethoxy regions of the two isomers are compared to that of colchicine. Both the Z isomer and the DAMA colchicine ligand interact with the importat Val β318 and Cys 241 residues (hydrophobic and polar interactions respectively) while the E isomer only interacts with the Cys β241 residue which may account for the difference in activity seen between the Z and E isomers. Upon rendering the surface of the site it can be seen that the E isomer extends further out of the site than either the Z isomer or the DAMA colchicine ligand. This may result in the 3-hydroxy-4-methoxy phenyl ring clashing with some of the α-subunit residues

that cap the top of the colchicine site. In contrast the Z isomer places its 3-hydroxy-4-methoxy phenyl ring in the vicinity of the C ring of DAMA colchicine where it can interact with residues Lys β352 (basic interaction) and Val α101 (hydrophobic interaction). Ravelli[17] has noted the importance of these residues for colchicine to exert its effect on tubulin. Steric hindrance between colchicine and Val α101 prevents the α-subunit from adopting its desired straight conformation. Bound colchicine also causes the Lys β352 side chain to interfere with and prevent α-tubulin adopting this straight chain confirmation. Both of these interactions are absent from the E isomer again possibly explaining the large difference in potency between the two isomers.

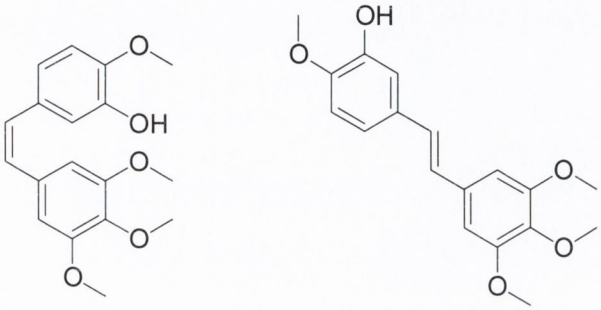

Z-CA4 **E-CA4**

Fig 4.33 CA4 E and Z isomers

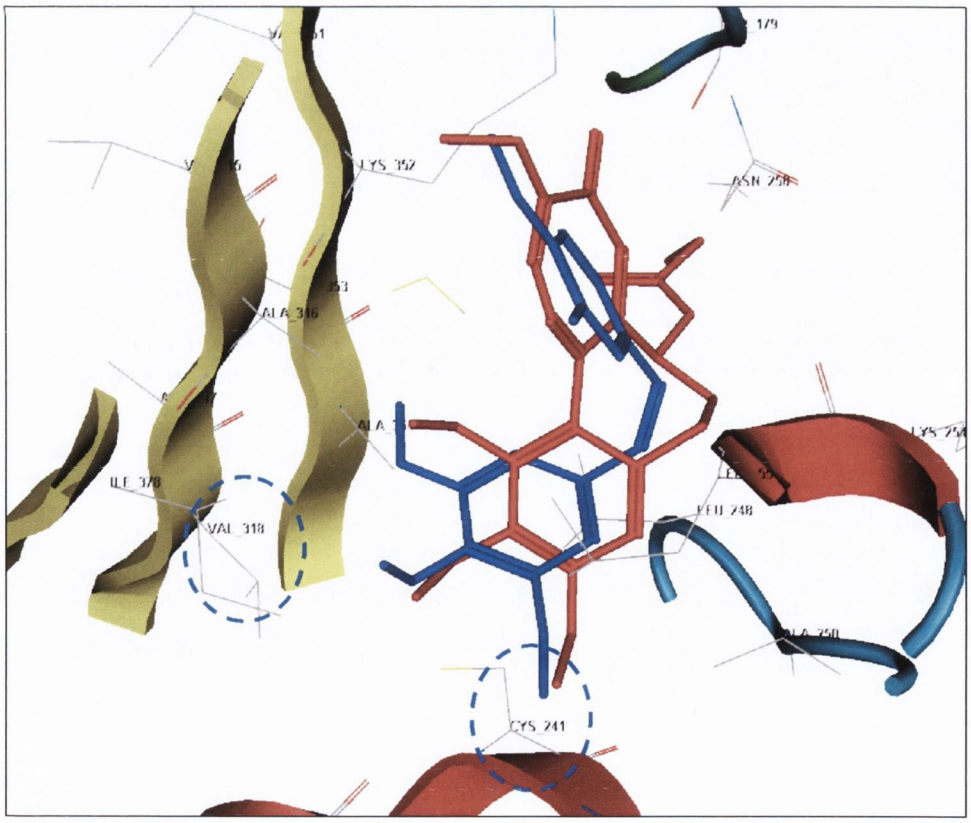

Fig 4.34 Docked solution of *Z*-CA4 (blue) with the original DAMA colchicine (**20**) (red)

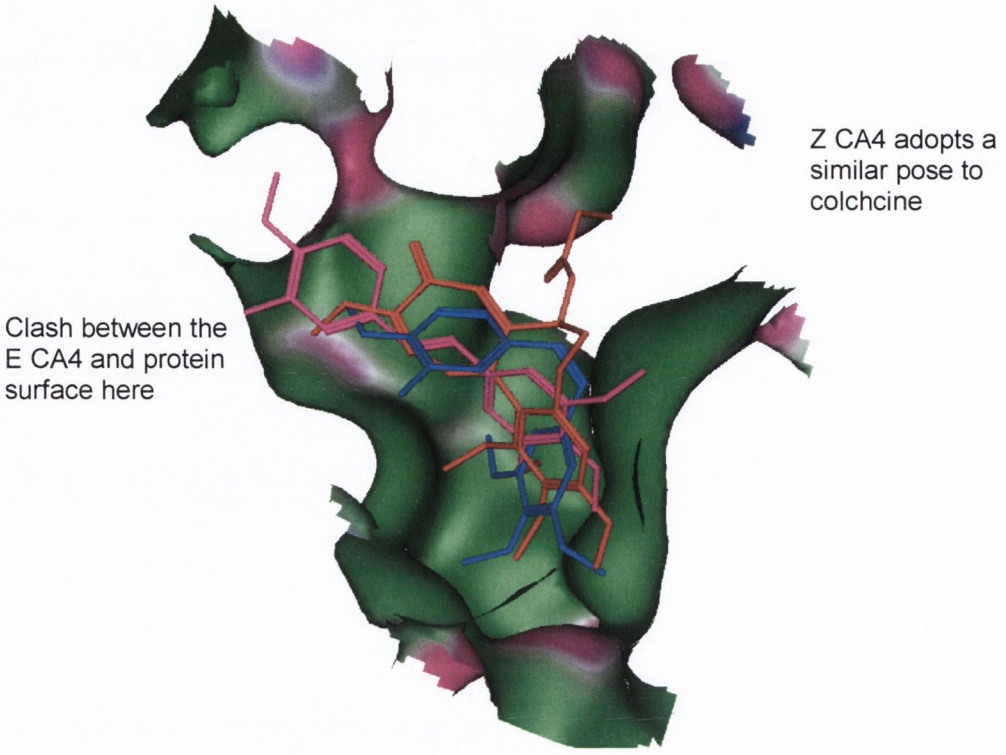

Fig 4.35 Docked solution of Z-CA4 (blue) and *E*-CA4 (pink) with the original DAMA colchicine ligand (red). The α-subunit was removed for clarity.

4.14.5.2 Modelling studies of 4-position analogues

The first library of compounds examined focussed on optimising the substitution pattern at C_4 of the β-lactam ring as described in Chapter 2. The majority of compounds in this library displayed poor activity (typically displaying IC_{50} values greater than 20μM) in the MCF-7 cell line and the docked solutions for these compounds reflect this. In the case where the compound was found to be very inactive (ie IC_{50} greater than 100μM) FRED could not find a reasonable docked solution. This is not unexpected since the high IC_{50} value would indicate that the compound is not binding at the colchicine site *in vitro* and so it is unreasonable to expect to obtain a docked solution. Even though the compounds are themselves not active, they may prove useful for constructing a structure activity relationship. A number of members of the first library were found to be active and so reasonable docked solutions were obtained for these. In particular the 3-halogen-4-methoxy compounds (**248** and **249**) displayed reasonable activity in the low micromolar range. From the biochemical results it can be seen that the *cis* isomer appears to be favoured over the *trans* isomer. By examining the ligand interactions for the docked compounds (**fig 4.36**) it becomes apparent that the *cis* 3-bromo (**248**) and *cis* 3-fluoro (**249**) both adopt a similar pose within the active site and maintain the important interactions with Cys β241 (polar), Val β318 (polar), Lys β352 (basic), and Val α181 (hydrophobic). The trans 3-bromo compound also maintains these interactions with the crucial exception of the Val β318. This may account for the drop in activity from approximately 5-6μM in the case of the *cis* fluoro and bromo compounds to nearly 31μM for the *trans* 3-bromo compound. What remains unexplained is why if all the important ligand interactions are maintained for **248** and **249** an IC_{50} value approaching that of combretastatin is not observed?

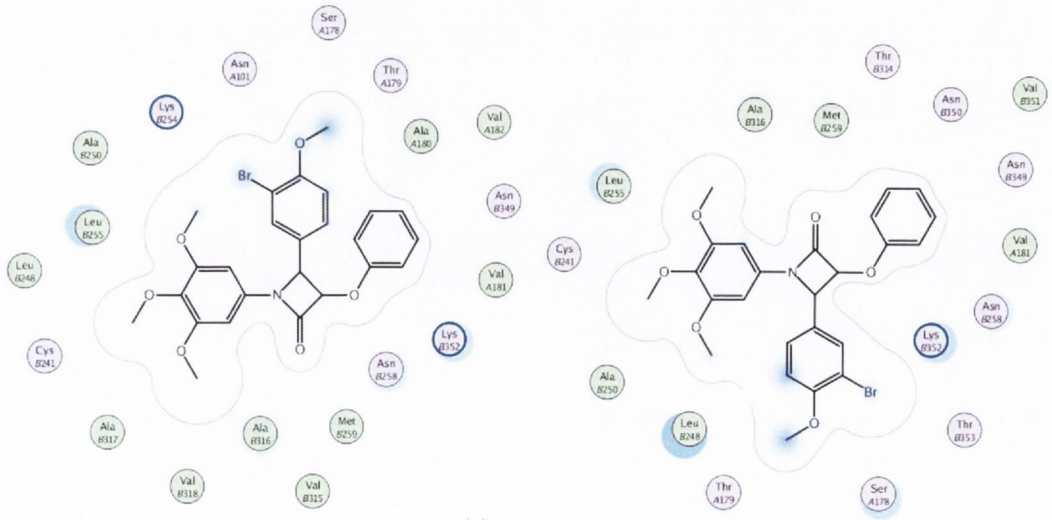

Fig 4.36 Protein-ligand interactions for *cis* (left) and *trans* (right) bromine compounds **248**

The most active compounds identified from the first library were the 3-amino and 3-hydroxy compounds **264** and **256** both of which displayed submicromolar activity. Interestingly the *trans* isomer was favoured in both cases rather than the *cis*, as was previously seen with the halogen analogues. For the hydroxy compound **256**, IC_{50} values of 383nM and 38nM were obtained for the *cis* and *trans* isomers respectively. Both isomers interact as expected with the residues reported by Ravelli, but there are small differences in the poses adopted by both isomers in the colchicine site (**fig 4.37**). In the trimethoxy region of the two isomers, the *trans* isomer more closely resembles the trimethoxy area of colchicine. The *trans* isomer is offset from colchicine by 1.25A compared to 2.13A for the *cis* isomer. Likewise the 3-hydroxy-4-methoxy group of the *trans* isomer is a better mimic of the C ring of the colchicine derivative particularly with respect to the placement of the respective methoxy groups. The *trans* isomers places its methoxy group 1.11Å from that of DAMA colchicine compared to 1.49 Å for the *cis* isomer. It has been noted that for many CA4 analogues, the para-methoxy group is essential for activity and the docked solution presented here would seem to indicate that the *p*-methoxy group plays a role in sterically interacting with the Lys β352.

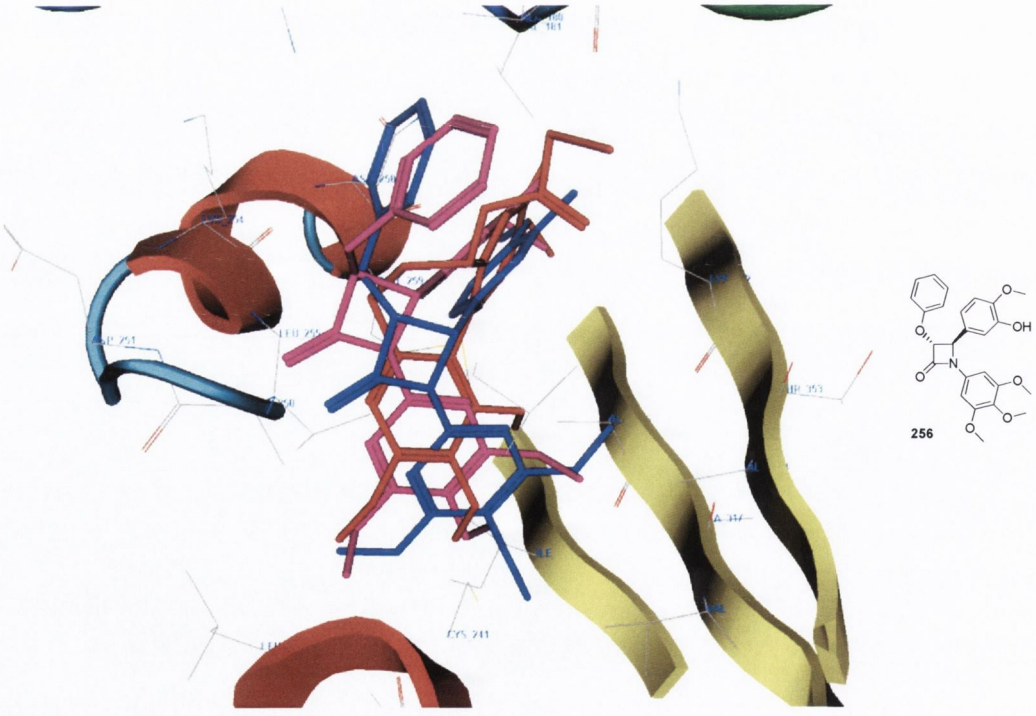

Fig 4.37 Docked solution of *trans* 3hydroxy (pink) (**256a**) and *cis* 3hydroxy (blue) (**256b**) with DAMA colchicine (red) (**20**).

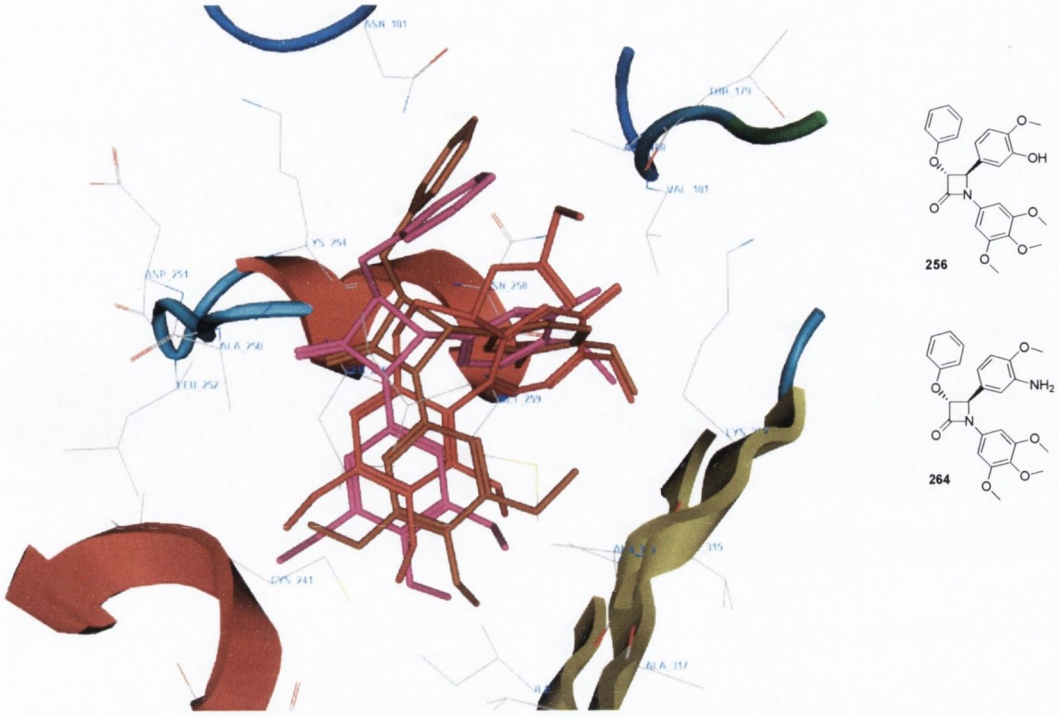

Fig 4.38 Docked solution of *trans* 3hydroxy (pink) (**256**) and *trans* 3amino (brown) (**264**) with DAMA colchicine (red) (**20**)

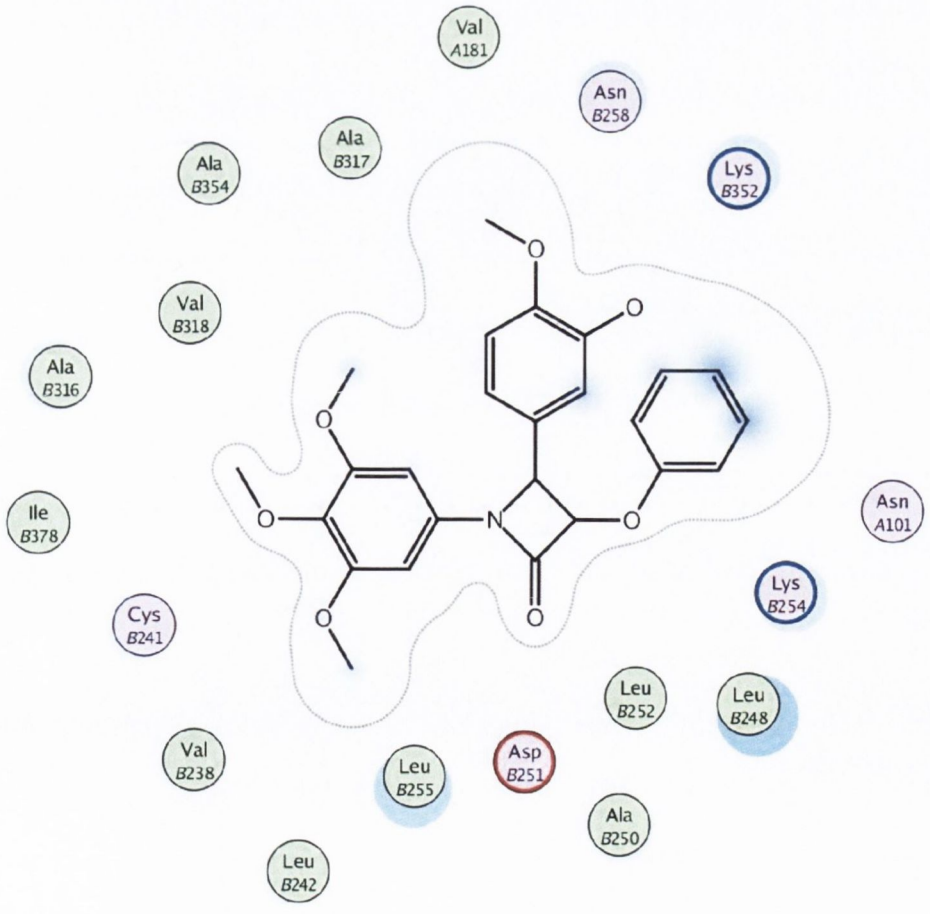

Fig 4.39 Protein-ligand interactions for the trans isomer of **256**

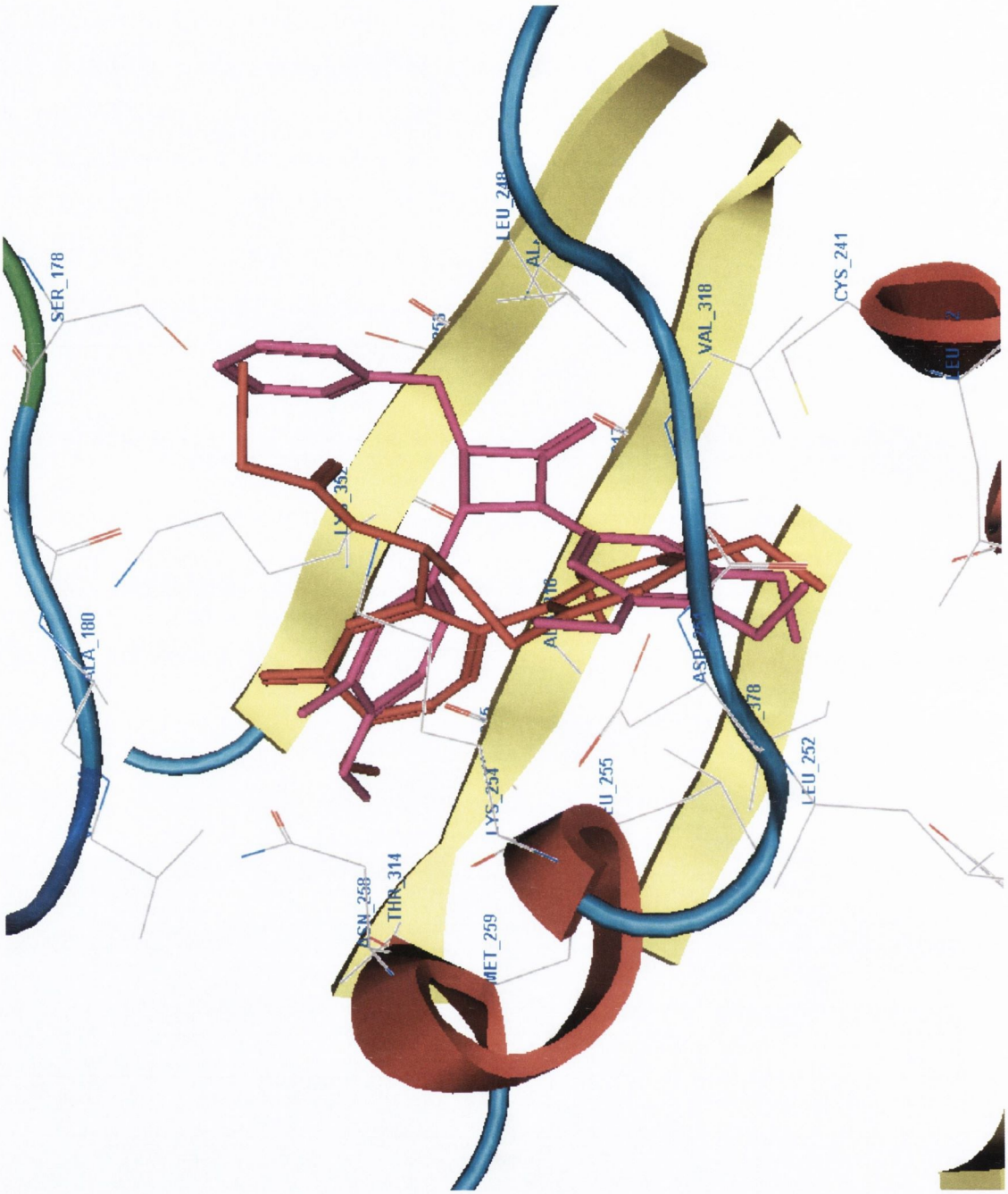

Fig 4.40 Enlarged view of the *trans* isomer of **256** (pink) docked in the colchicine site along with DAMA colchicine (red)

Fig 4.39 and **fig 4.40** present enhanced views of the ligand interactions and docked solutions of **256**.

For the amino compound (**264**), both isomers are far less active than their hydroxy (**256**) counterparts, although the *trans* isomer does display a respectable IC_{50} value of 153nM. The docked solution for the *trans* amino isomer shows that it maintains the same important contacts as the hydroxy compound, but adopts a slightly different pose in the colchicine site (**fig 4.38**). The trimethoxy region is offset by an average of 1.4Åcompared to 1.25Å for the hydroxy compound. This is still less than the offset of 2.13Å for the *cis* hydroxy compound. The biochemical results bear out this trend since the potency of the amino compound lies between that of the *trans* hydroxy (38nM) and the *cis* hydroxy (383nM).

4.14.5.3 Modelling studies of β-lactam analogues

Compound **267** (IC_{50}=3.3μM) and **272** (IC_{50}=7.45μM) clearly show that the carbonyl group at C_2 of the β-lactam ring is necessary for activity. Modelling shows that both compounds are no longer interacting with Val β318 which is one possible explanation for their poor biochemical activity. From the previous examples the β-lactam carbonyl appears to interact with three residues – Ala β250 (hydrophobic), Leu β255 (hydrophobic), and Leu β248 (hydrophobic) which are members of the T7 loop H8 helix. It may be important for a ligand to interact in this way, since colchicine also interacts with these residues resulting in T7loop and H8 helix moving to interfere with α-tubulin. Therefore removal of the carbonyl group may adversely affect biochemical activity by reducing these interactions

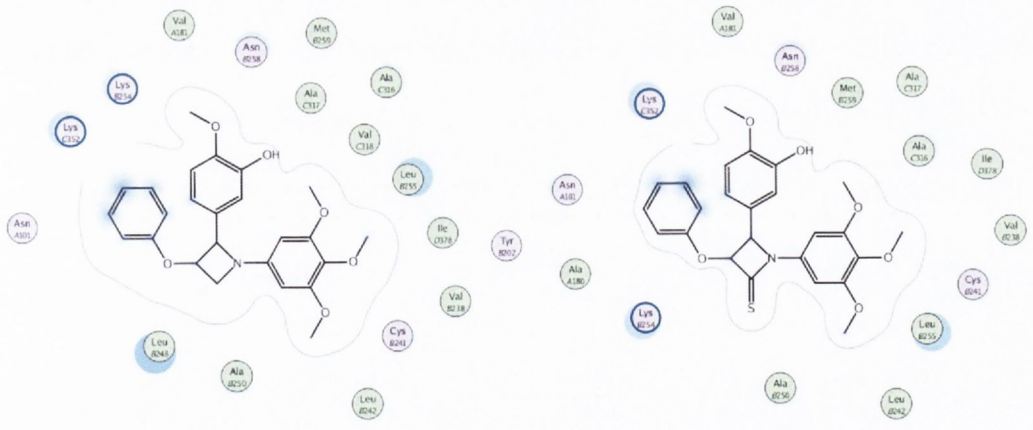

Fig 4.41 Protein-ligand interactions for the azetidine **272** and the thione **267**

4.14.5.4 Modelling studies thio-methyl ring substituents

Both the sulfoxide (**262**) and the sulfone (**263**) compounds were successfully docked in the colchicine site (**fig 4.42**). Both compounds displayed all of the

important ligand interactions identified however *in vitro* testing shows that neither compound is active against the MCF-7 cell line. One possible explanation for this is the presence of hydrogen bonding between Asn β258 of the H8 helix and the sulfoxide/sulfone group. This hydrogen bonding may block the movement of H8 into a position where it can interfere with the α-tubulin. The ligand-protein interactions are presented in greater detail in **fig 4.43**.

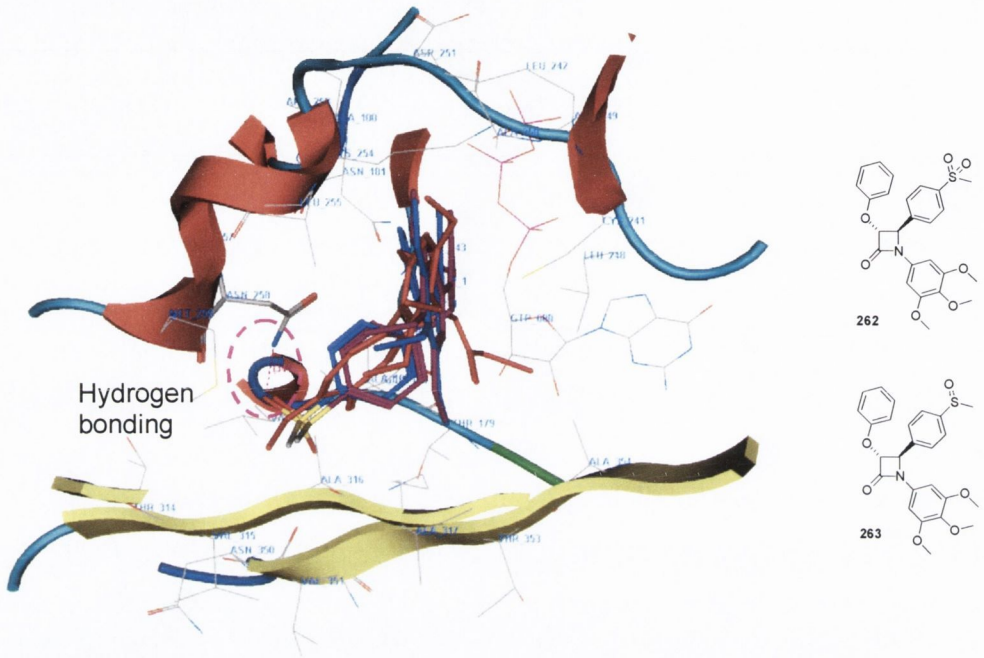

Fig 4.42 Docked solution of DAMA colchicine (**20**) (red), sulfoxide (**262**) (purple), and sulphone (**263**) (blue) illustrating the presence of hydrogen bonding (dashed line) between the ligands (**262** and **263**) and the Asn β258 residue

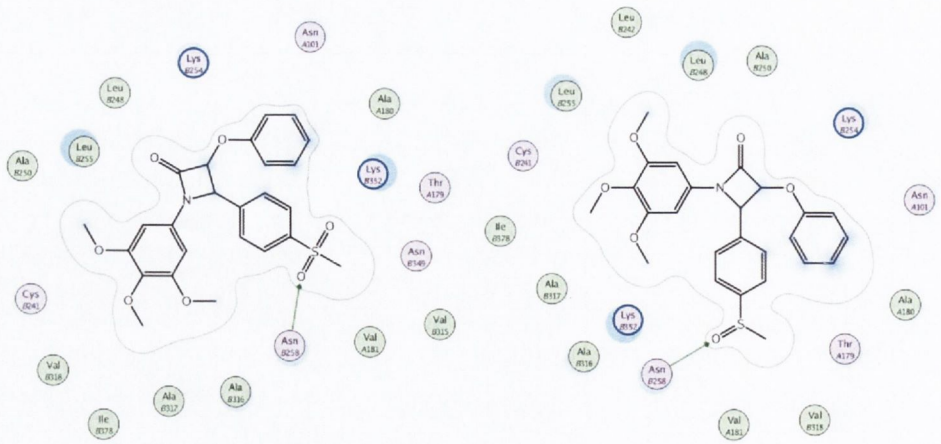

Fig 4.43 Ligand-protein interactions for the sulphosxide **262** and the sulfone **263**

4.14.5.5 Naphthyl analogues

Both of the naphthyl compounds (**252** and **254**) displayed poor activity and this is reflected in their respective docked solutions. The pose adopted by the compounds in the site is significantly affected by the naphthyl leading to a noticeable displacement of the trimethoxy phenyl ring from the position adopted by colchicine. This results in the loss of the crucial Val β318 contact thereby resulting in poor activity.

4.14.5.6 Azide analogue

The azide compound (**319**) was of particular interest as a starting point for the development of a photoaffinity probe. A prerequisite for any affinity probe is its ability to adopt a similar pose to the binding agent under investigation in the site. From the docked solution it can be seen that this is the case with the azide analogue, but yet it only displays an IC_{50} value of 23.25μM. The most likely explanation for this is the formation of hydrogen bonds between the azide group and the residues Lys β352 and Val α181. For bound colchicine, steric hindrance with Val α181 and Lys β352 forces the α-tubulin subunit into the curved chain arrangement with β-tubulin. For the azide compound the opposite seems to occur explaining the lack of sensitivity of the cells to the compound. The docked solution (**fig 4.44**) indicated that the azide **319** adopts a suitable pose that may allow it to act as a photolabel (as discussed in Chapter 2) particularly by reacting with the amino group of the Lys β353 residue to which its adjacent. The hydrogen bonds are shown in **fig 4.44**.

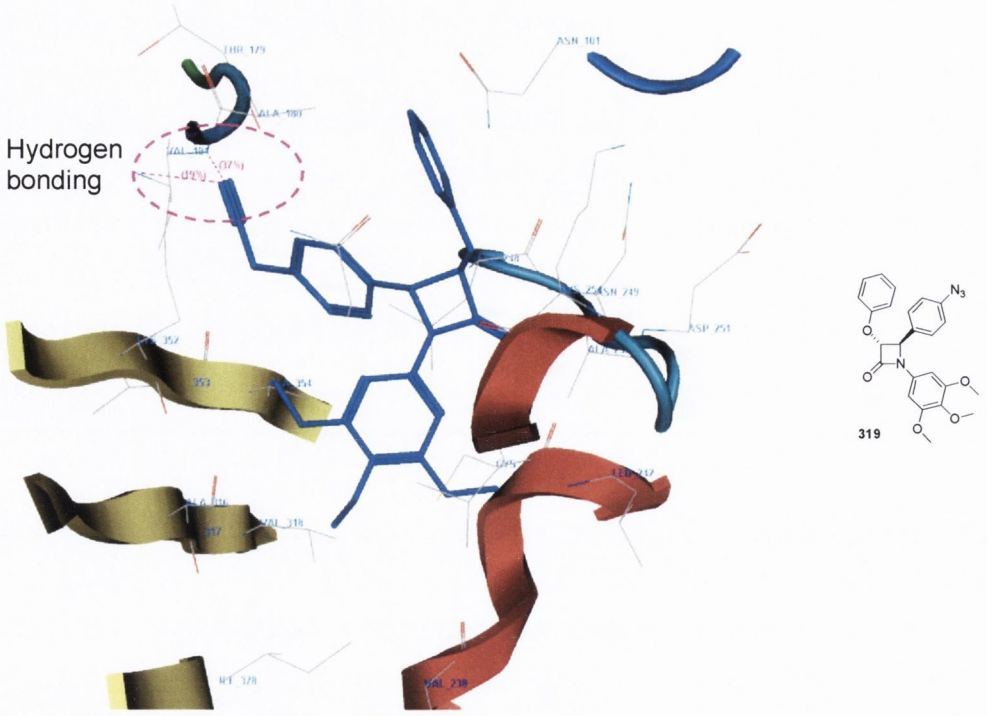

Fig 4.44 Docked solution of the azide compound (**319**) (blue) with hydrogen bonding (dashed lines) between the ligand and residues Val α181 and Lys β352

4.14.5.7 Optimisation of the substitution pattern on the C_4 aryl ring

From the molecular modelling and biochemical results obtained for the compounds discussed thus far it can be seen that the substituted phenyl ring at the C_4 of the β-lactam ring plays a crucial role in moderating biochemical activity. In particular the 3-hydroxy-4-methoxy and 3-amino-4-methoxy substituted phenyl rings yielded active compounds in the combretastatin series. In the present work a series of compounds were synthesised to further investigate this feature of the β-lactam ring with a focus on the position of the amino, hydroxy, and methoxy groups. The compounds in this library were only obtained as the *cis* isomer and so the role of the amino group could not be examined in as great detail as wished since its *cis* isomer is not potent. From the biochemical results it would appear that both the 4-methoxy and the 3-hydroxy groups are needed for activity. The modeling studies reveal that the removal of the methoxy group has a deleterious effect upon the pose adopted by the compound in the site. This is in good agreement with the biochemical data where the removal of the methoxy group results in a 140 fold loss in activity from IC_{50}= 383nM (**256**) to IC_{50}= 54μM (**324**). For the removal of hydroxy group there is a 91 fold decrease in potency observed from IC_{50} 383nM (**256**) to IC_{50} 35μM (**245**) . This is in contrast to the many reports of CA4 analogues containing only the 4-methoxy

group that are active. The docked solution supports the case for the 4-methoxy compound being active, so the observed drop in activity with our β-lactam analogues is puzzling. The 4-methoxy compound (**245**) maintains all the crucial ligand interactions and the 4-methoxy group appears to be a good mimic for the methoxy group of the C ring of DAMA colchicine.

The combination of the hydroxy and amino groups have led to CA4 analogues that are active in tumour cell lines and in tubulin polymerisation[74]. All of the compounds of this type presented in this thesis were inactive. To investigate this further, both compound **305** and the corresponding active CA4 analogue (**73**) were docked in the colchicine site and the differences between the two solutions examined (**fig 4.41**). The CA4 analogue (**73**) adopts a very similar pose to colchicine in the active site especially in the trimethoxy region, and maintains all of the crucial contacts described by Ravelli. The β-lactam compound is a poorer fit. The trimethoxy region is further offset from that of colchicine compared to the CA4 analogue, and the 4-phenyl ring is out of plane compared to the C ring of DAMA colchicine. This particular series of compounds clearly illustrates that not every substitution pattern reported as active for CA4 analogues will result in the corresponding activity for the β-lactam analogue.

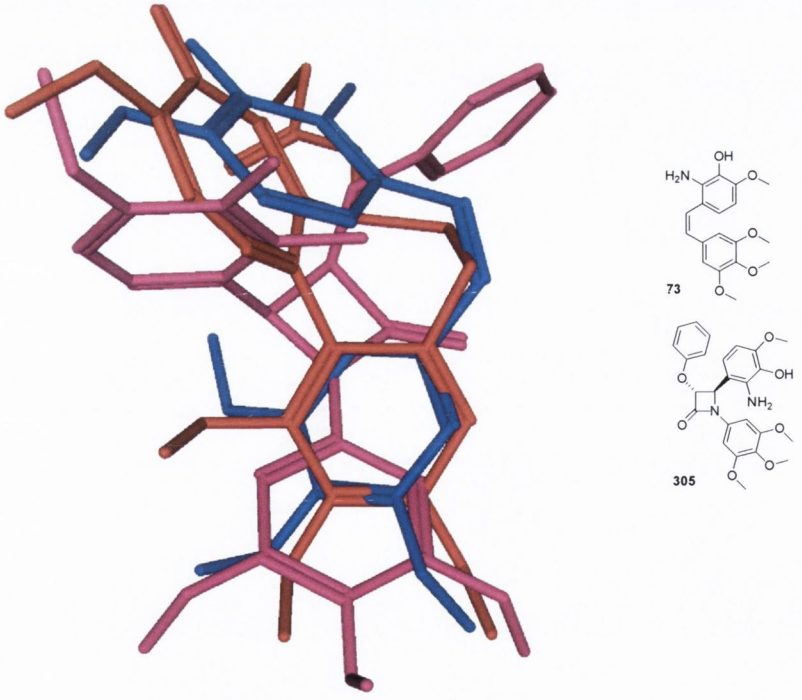

Fig 4.45 Pose adopted by the DAMA colchicine ligand (**20**) (red), 2-amino CA4 analogue (**73**) (blue), and the 2-amino compound (**305**) (purple). A clear difference between the positioning of the trimethoxy subunit for **73** and **305** can be seen resulting in the differences in biochemical activity observed for the two compounds. The protein pocket surrounding the compounds is omitted for clarity.

4.14.6 Investigation of β-lactam stereochemistry

Two chiral centres are present at C_3 and C_4 of the β-lactam ting for each of the compounds discussed thus far leading to two enantiomers for each *cis/trans* isomer. This can be clearly seen from the XRD crystal structures obtained for **256**. The two enantiomers can be assigned as 3S, 4S and 3R, 4R and both have the H_3 and H_4 protons arranged *trans* to one another. Likewise the *cis* version can be assigned as 3S, 4R and 3R, 4S. The molecular modelling studies undertaken thus far have only used the 3S, 4S and the 3R, 4S enantiomers. It may be instructive to examine the docked solutions for both enantiomers particularly for very active compounds such as **256**. The docked solution may suggest that one particular enantiomer is favoured in terms of both docking and biochemical activity (**fig 4.42**). The use of molecular modelling in this way is useful as a method for determining if it is worthwhile in carry out an asymmetric synthesis or separation to isolate a particular isomer. The docked solution for both enantiomers clearly shows that both isomers adopt a different pose within the colchicine site. The 3S,3S enantiomer interacts with all the expected residues, while the 3R,4R enantiomer fails to interact with the Val β318 residue. This would seem to indicate that there may be a substantial difference in the biochemical activity between the two enantiomers with the 3S,4S enantiomer being favoured. The independent biochemical activity of both enantiomers will be investigated in a future study either by chiral separation and/or stereoselective synthesis.

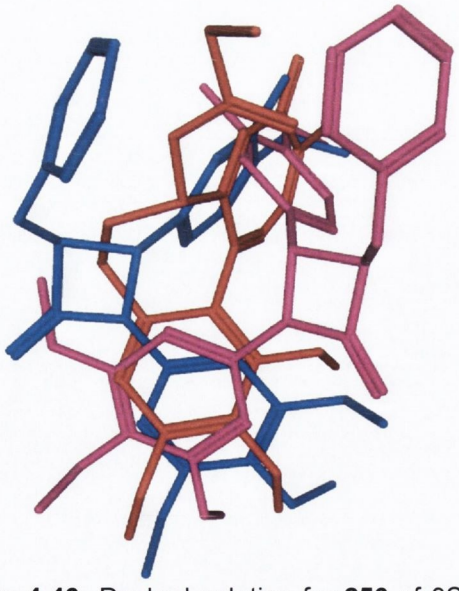

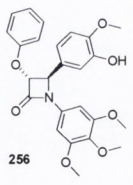

Fig 4.46 Docked solution for **256** of 3S 4S enantiomer (blue) and 3R 4R enantiomer (pink) along with DAMA colchicine (red) (**20**0 clearly showing the different poses adopted in the pocket by both enantiomers. The protein pocket surrounding the compounds is omitted for clarity

4.14.7 Molecular modelling studies on the C_3-position analogues

It is clear from biochemical results obtained that the substituent at C_3 of the β-lactam ring is important for biochemical activity. By comparison of the activeyy β-lactam compound (**256**) to DAMA colchicine it can be seen that the substituent attached at the C_3 position may be able to take up a similar position to the mercaptoacetyl group of the B ring of DAMA colchicine. The phthalimido (**355**) and trimethoxy (**361**) compounds both have large bulky groups at C_3 and both display IC_{50} values in excess of 10μM. From the docked solutions it can be clearly seen that the bulky groups are not easily incorporated into the site especially compared to the phenoxy group of **256** (**fig 4.43**). Neither compound maintains the hydrophobic contact with Val β318.

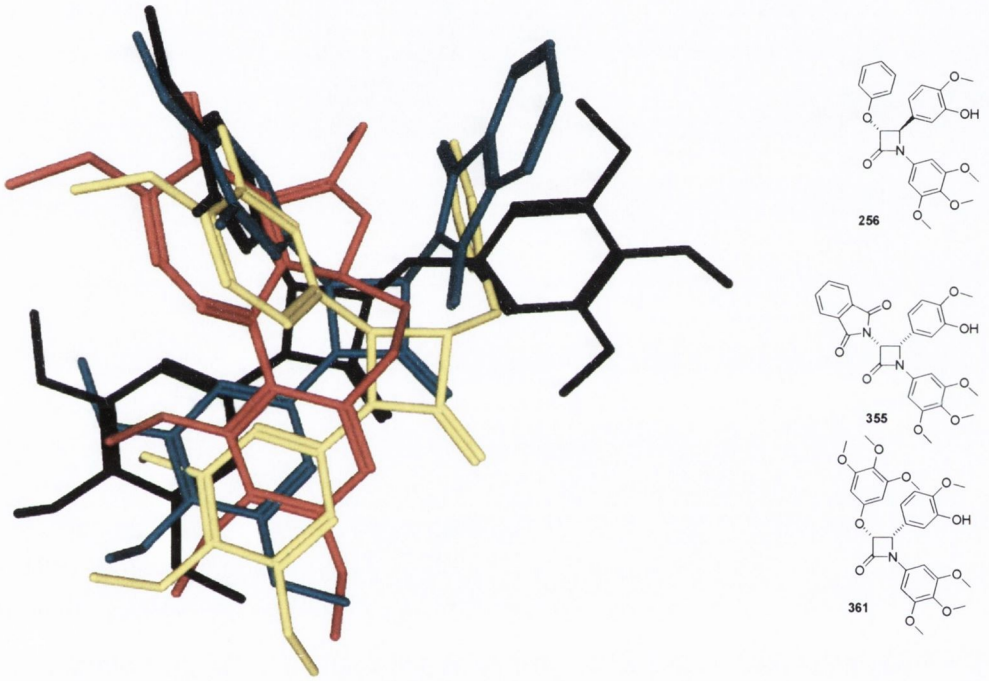

Fig 4.47 Docked solution of **256** trans isomer (yellow), phthalimido (**355**) (turquoise), trimethoxy (**361**) (black), and DAMA colchicine (**20**) (red). The protein pocket surrounding the compounds is omitted for clarity.

Compound **256** displays a potency (38nM) approaching that of CA4. To investigate the role of the oxygen in the phenoxy group attached at C_3 of the β-lactam ring in tubulin binding, the benzyl compound **342** was synthesised. Compound **342** displayed a decrease in activity to 229nM compared to 38nM for **256**. From the docked solution it can be seen that **342** adopts a different pose from that of **256** in the colchicine site resulting in the loss of the Val β318 contact. It can also be seen that the phenoxy group adopts a position closer to that of the Leu β248 residue of the T7 loop compared to the benzyl group of **342**. Given the previously discussed

importance of T7 loop in the activity of colchicine binding agents this may lead to the greater activity of **256** over **342**.

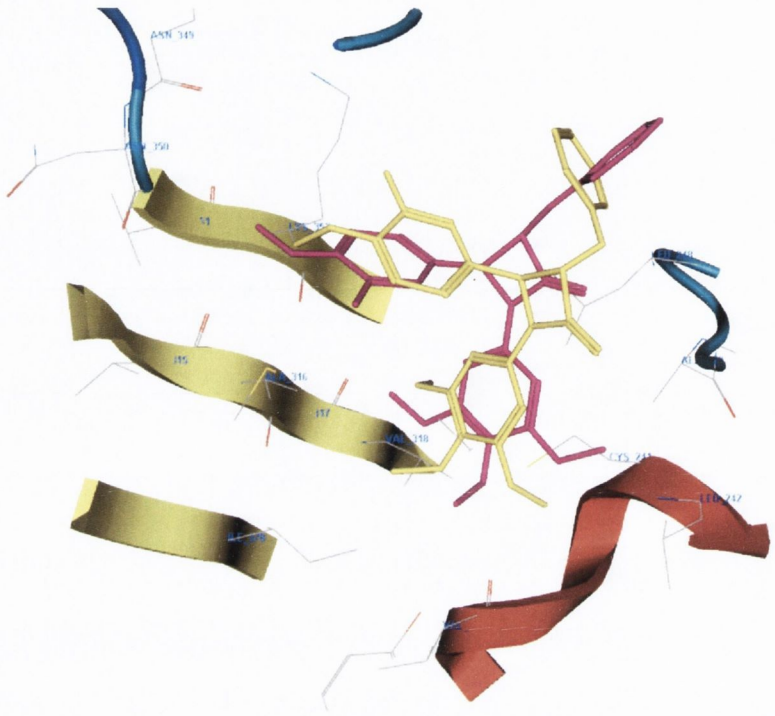

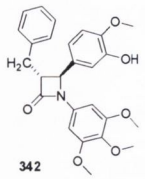

Fig 4.48 Docked solution of **342** (yellow) alongside **256b** (pink) for comparison

Both the dichloro (**340**) and Reformatsky (**380**) compounds were less potent than **256** with IC_{50} values of 332nM and 56nM respectively. From the docked solution (**fig 4.49**) the reason for this difference is not apparent. Both maintain the important ligand interactions in the trimethoxy region and with the T7 loop H8 helix. It is possible that without the presence of the a larger group such as the phenoxy group the interaction between the compounds and the T7 loop H8 helix is minimised leading to the drop in activity.

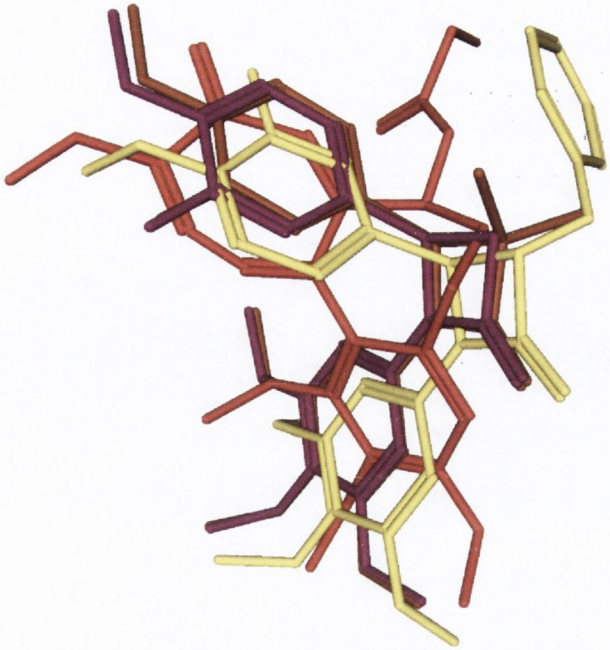

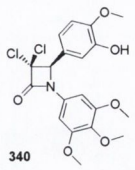

340

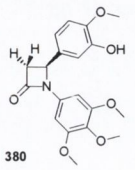

380

Fig 4.49 Docked solutions for the dichloro (**340**) (brown), Reformatsky (**380**) (purple), **256** (yellow), and DAMA colchicine (red). The protein pocket is omitted for clarity

The phenyl (**341**) (IC_{50} 21.4nM) and monochloro (IC_{50} 17.5nM) (**339**) compounds proved to be slightly more active than **256**. Both display good overlap in the trimethoxy region and maintain all the same important interactions (**fig 4.50**). It is interesting to note that the three compounds all display similar activity despite having differences in terms of the groups attached at C_3.

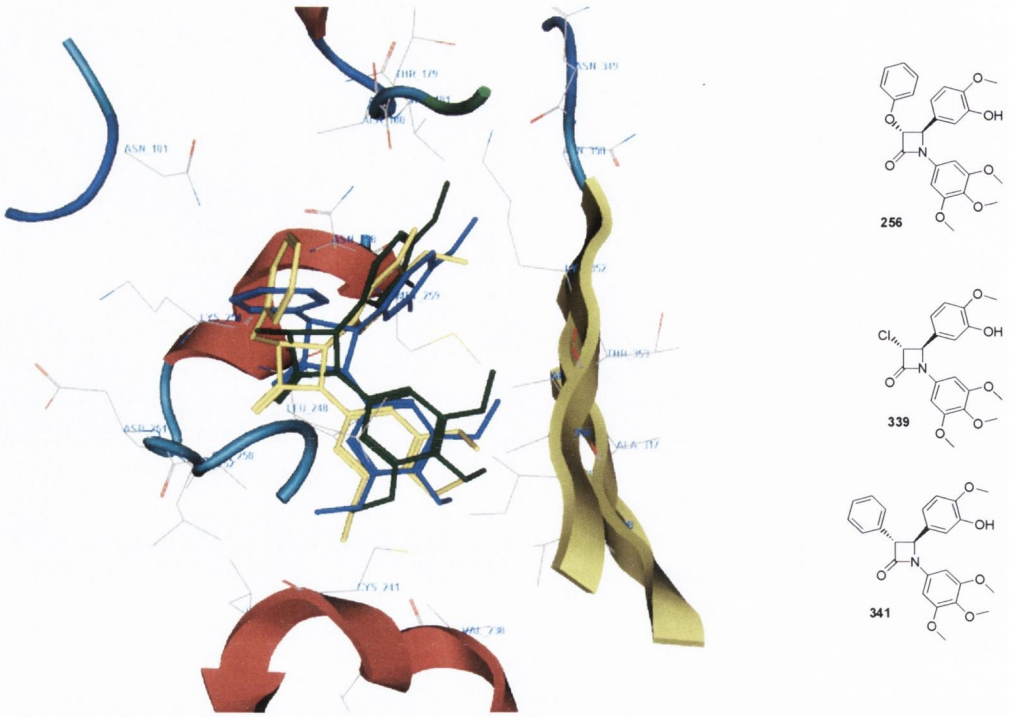

Fig 4.50 Docked solutions for **256** (yellow), chloro (**339**) (green), and phenyl (**341**) (blue)

4.14.8 Molecular modelling of 3-vinyl β-lactams and related compounds

The 3-vinyl compound **343** represents the most potent compound synthesised with and IC_{50} value of 1.4nM. **Fig 4.53** and **fig 4.54** present the protein-ligand interactions and the docked solution of **343**. Two analogues of this compound were synthesised to investigate the role of the vinyl group, the ethylidene analogue (**397**), and the diol analogue (**398**). Compound **343** (IC_{50} 1.6nM) and **397** (IC_{50} 502nM) adopted a very similar position in the colchicine site but yet differ in activity by over a factor of 350. Both maintain the important Cys β241 (polar) and Val β318 (hydrophobic) contacts in the trimethoxy region, as well as all the Ala β250 (basic), Leu β255 (basic), and Leu β248 (basic) residues which are members of the T7 loop H8 helix (**fig 4.51**). The only difference in the ligand interactions between the two is an Ala β354 basic interaction present for **343** but absent in **397**. This contact is present the docked solution for **398** which displays an activity (IC_{50} 70nM) intermediate to that of **343** and **397** and is also maintained in the docked solution for other active compounds such as **256**.

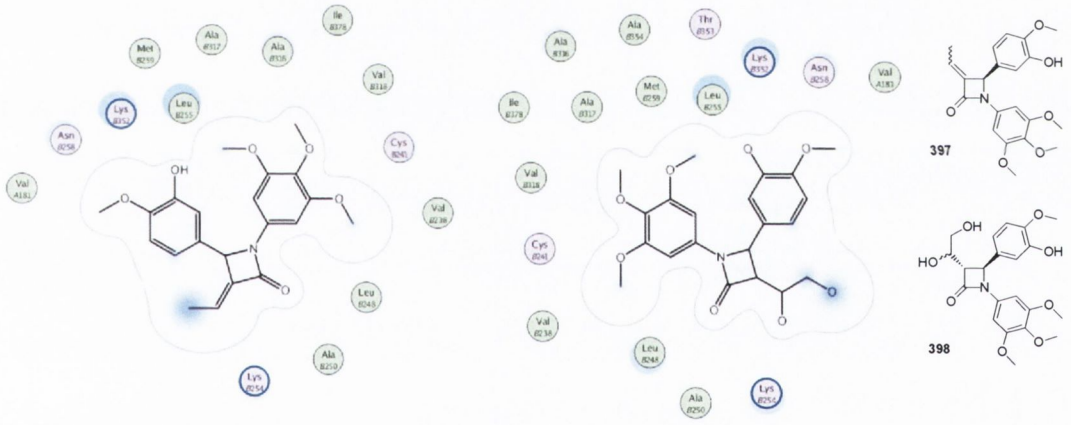

Fig 4.51 Protein-ligand interactions for the ethylidene compound (**397**) and the diol (**398**)

Compound **344** where the vinylic proton was replaced with a methyl group showed a decrease in activity (IC_{50} 468nM) compared to **343** (IC_{50} 1.6nM). In the docked solution **344** maintains many of the same protein interactions as **343** with the Leu β248 residue a notable exception (**fig 4.52**). Since this residue is part of the T7 loop, this may account for the drop in activity.

Fig 4.52 Docked solutions for isopropnyl (**344**) (turquoise), vinyl (**343**) (pink), and DAMA colchicine (**20**) (red)

Fig 4.53 and **fig 4.54** present enhanced views the ligand interactions and docked solutions of **343**.

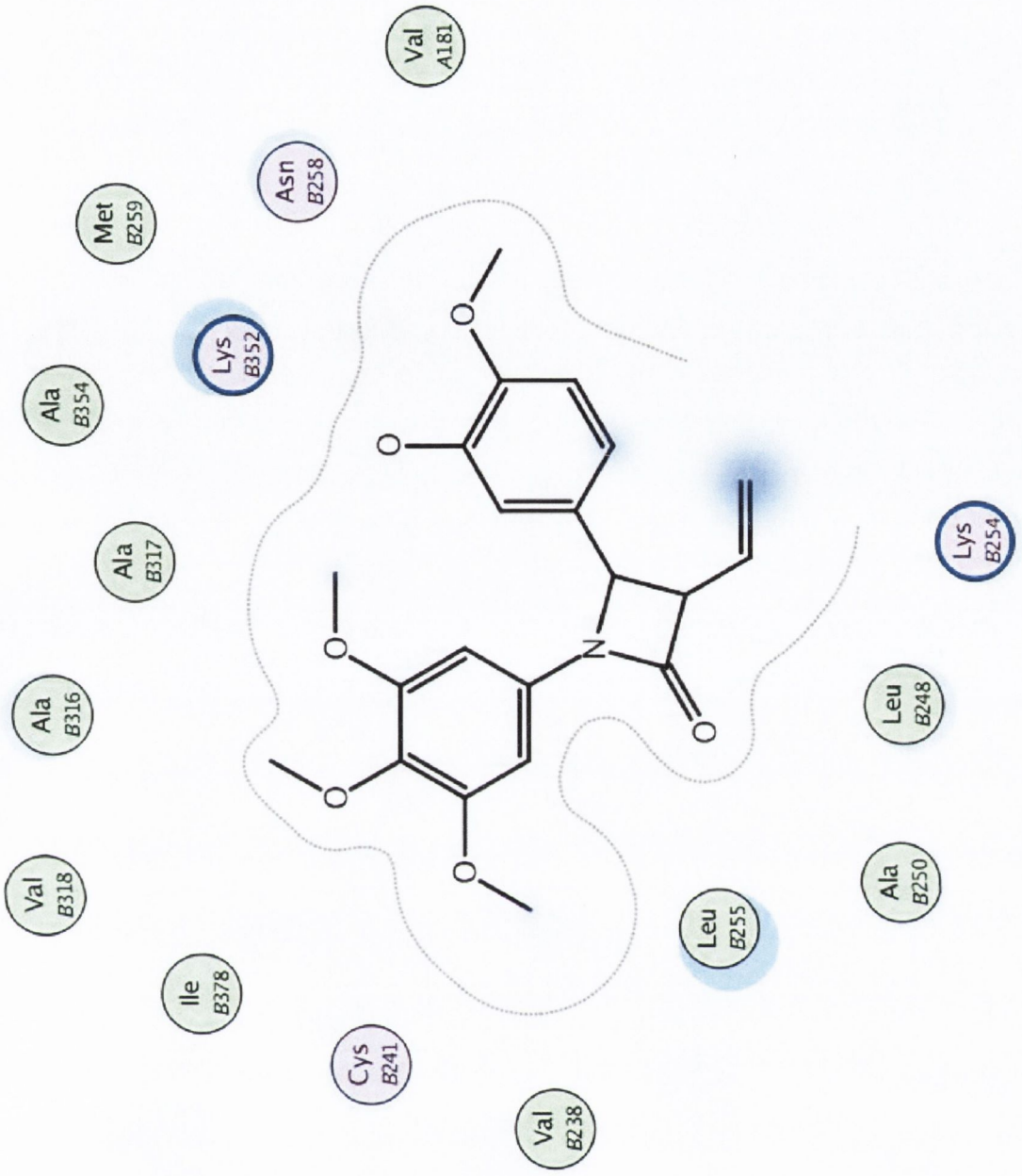

Fig 4.53 Protein-ligand interactions for the vinyl compound (**343**)

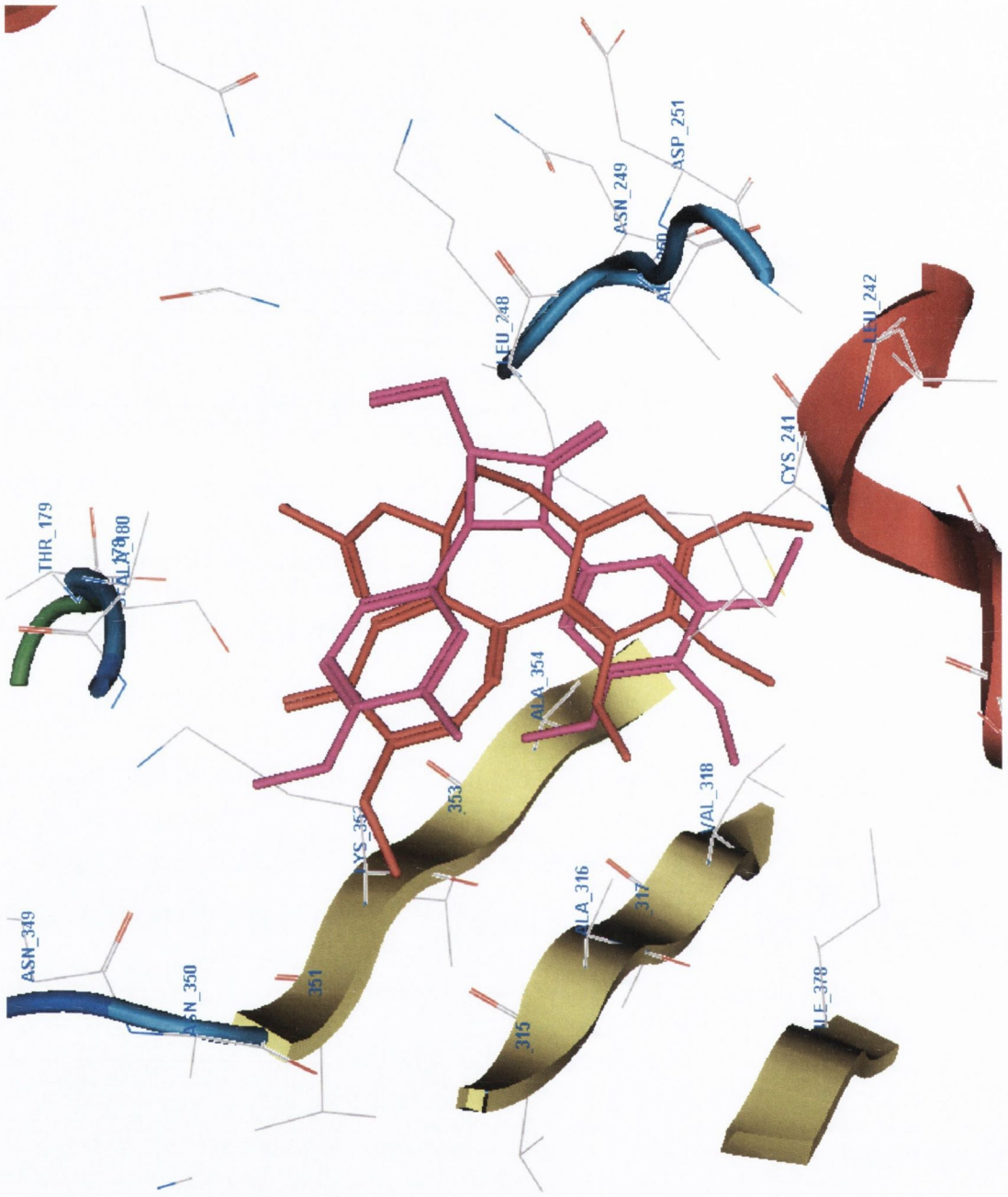

Fig 4.54 docked solution for the vinyl compound (**343**)

A further modelling study involving a number of related compounds (**388-395**) was carried out (**fig 4.55**). Of these compounds only **388** and **391** displayed activity approaching that of **343** with potencies of 65.2nM and 46.8nM respectively. Both retain the important contacts previously discussed except for the Ala β354 contact which is only present in **391**. Possibly the most interesting aspect of both of these

compounds is the diversity of substituents at C_3 while still allowing retention of activity. This clearly demonstrates that the C_3 position is open to the introduction of a variety of groups with a view to creating highly optimised β-lactam analogues of CA4.

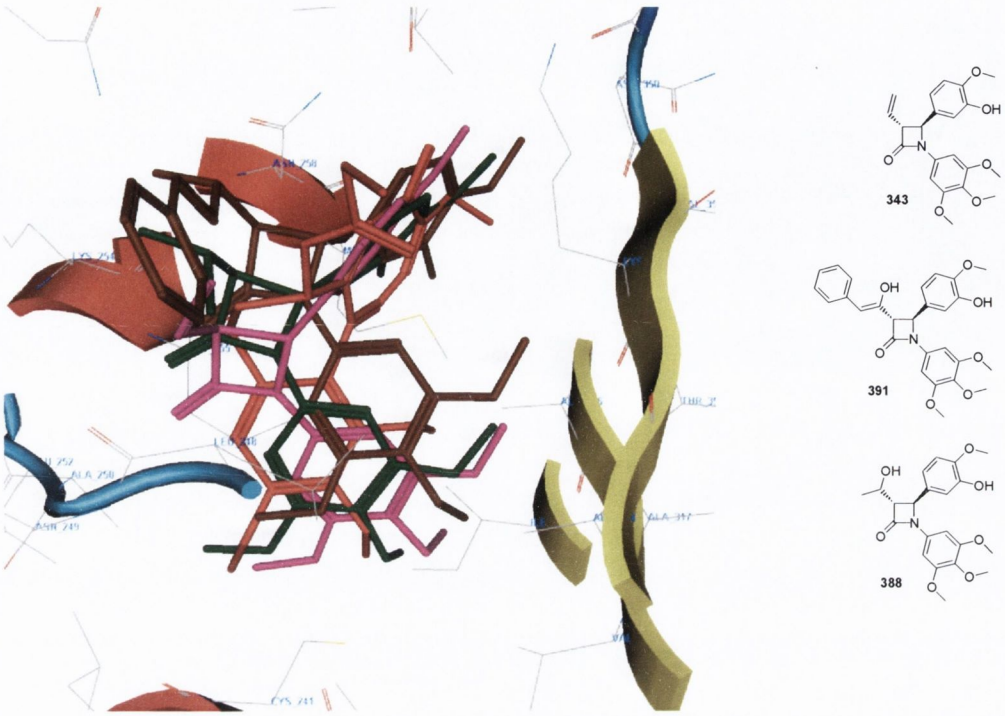

Fig 4.55 Docked solutions of **343** (pink), **391** (brown)and **388** (green) and colchicine (red) (**20**)

All of the above vinyl analogues contained the 3-hydroxy-4-methoxy phenyl ring at C_4. A further number of compounds were synthesised with a different substitution patterns at C_4. Of particular interest was the 3-amino-4-methoxy group which was identified as an active group in the initial library of compounds. The replacement of the phenoxy group (**264**) with the vinyl group (**399**) led to an increase in potency from 152.5nM to 13.7nM. Both compounds maintain all the important ligand-protein interactions, but yet adopt considerably different poses within the colchicine site (**fig 4.56**). Compound **399** adopts a pose more closely matching that of the DAMA colchicine ligand (**20**) especially in the placement of the 3-amino-4-methoxy phenyl ring. So despite maintaining the same protein interactions, subtle differences between the two poses adopted by the compounds may lead to the substantial difference in biochemical activity observed.

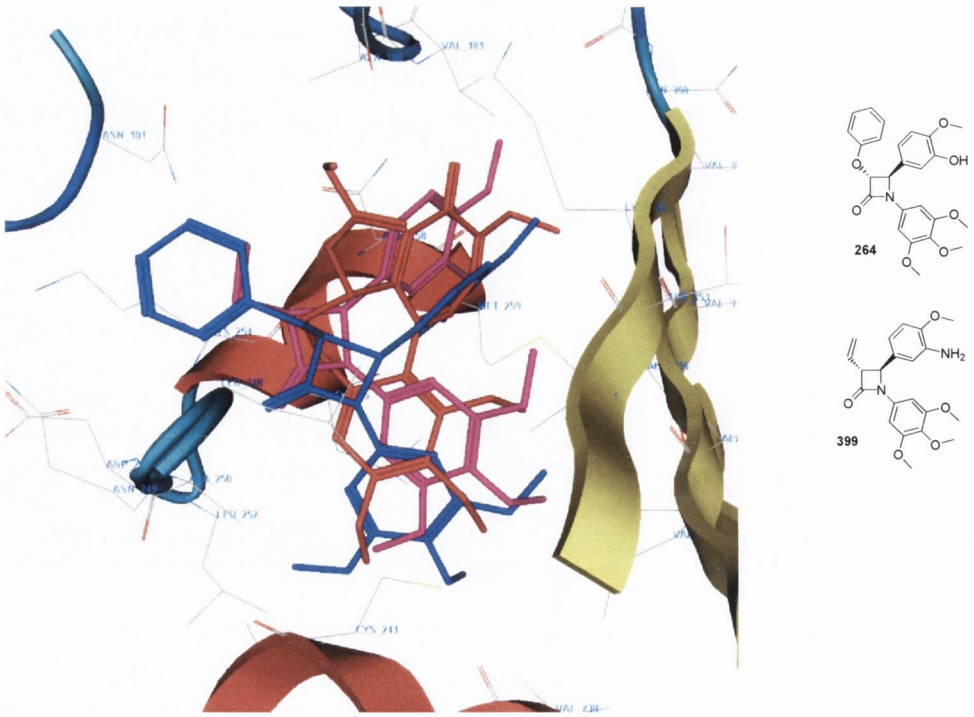

Fig 4.56 Docked solutions for **399** (pink), **264** (blue) and DAMA colchicine (red) (**20**)

The effect of replacing the phenoxy group at C_3 on the activity of analogues that were not previously active against the MCF-7 cell line was also evaluated. Compounds **250** and **245** displayed IC_{50} values of 168.4μM and 6.91μM respectively. Upon the replacement of the phenoxy group with the vinyl group there was a significant improvement in potency to 6.25μM (**413**) and 446.9nM (**412**) respectively. This clearly illustrates that the 3-position of the β-lactam ring has an important role to play in moderating biochemical activity independently of the substituents at the 4-position. The activities of the methoxy compounds **245** and **412** is interesting to note since the *p*-methoxy group is regarded as necessary for activity in a range of CA4 analogues. Both compounds **245** and **412** adopt a very similar pose in the active site except for the placement of their respective C_3 groups (**fig 4.57**). The vinyl group of **412** is placed much closer to the T7 loop than the phenoxy group of **245**, which may account for the increase in activity observed.

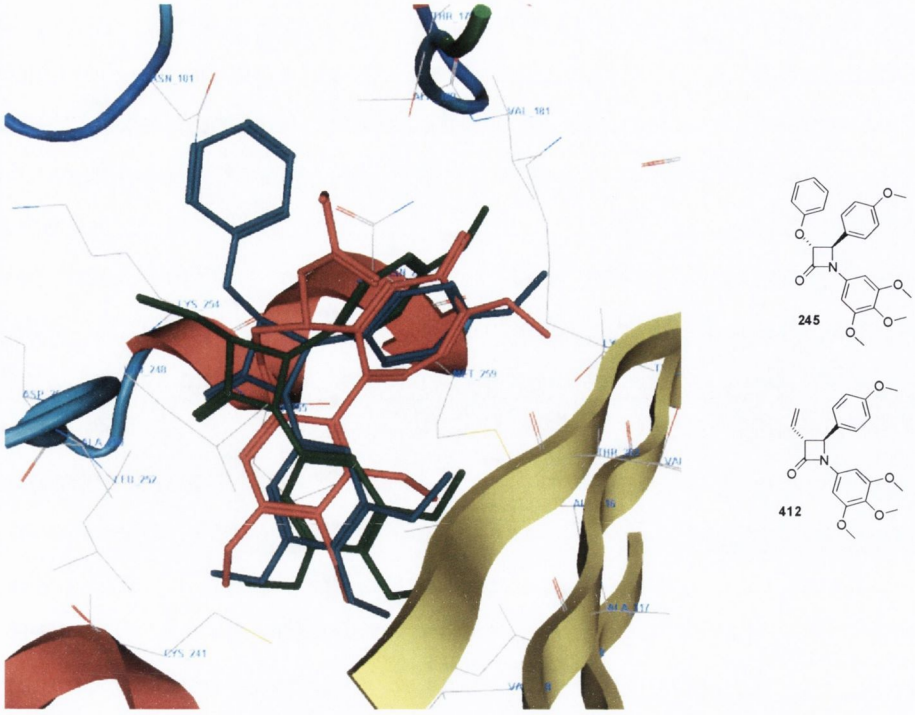

Fig 4.57 Docked solutions for **245** (turquoise), **412** (green), and DAMA colchicine (**20**) (red)

4.14.7 Structure Activity Relationship Study

The establishment of an accurate quantitative structure activity relationship (QSAR) for the compounds synthesised within this thesis was next attempted. QSAR involves the construction of a model that uses the physical parameters of molecules to predict the biological activity of those molecules. QSAR is particularly useful for the optimisation of lead compounds. Such a working QSAR would be helpful as a screening method for candidate compounds prior to synthesis. This would help in eliminating any inactive compounds while fasttracking the synthesis of potentially active compounds.

Prior to investigating the establishment of a QSAR study, an attempt to correlate the scoring function for each docked compound in the colchicine site of tubulin was made. Nearly 80 synthesised compounds were docked in the active site using the PLP scoring function of *FRED* as discussed in **section 4.4.3.1**. The PLP scoring function takes into account ligand shape, hydrogen bonding, metal interactions, and non-polar interactions. Despite successfully docking nearly 80 synthesised compounds in the colchicine site of tubulin, no definite correlation was established between the scoring function for the docked compound and its antiproliferative activity so instead MOE was used in an attempt to establish a working Quantitive Structure Activity Relationship for the dataset of β-lactam compounds.

A database containing all the biochemical data and energy minimised structures was created. From this the 2-D descriptors for each molecule were calculated in MOE. The QSAR was also performed in MOE using $-Log_{10}\{IC_{50}\}$ as the activity parameter and the auto QSAR function function was used. The top ranked linear model contained more than 11 descriptors (**fig 4.58**), but the second ranked model (**fig 4.58**) only contained four descriptors, and this was used as the basis for further study. Unfortunately the most active compound of the series the 3-vinyl compound **343** appeared as an outlier in this linear model as well as in the majority of other linear models used. The linear model was determined as:

$$-Log(IC_{50}) = 0.3338 + 0.672(PC+) - 0.828(PC-) - 0.00412(PEOE_VSA_POS) - 0.04602(Q_VSA_NEG)$$

where PC+ and PC- are the total positive and negative partial charges respectively, PEOE_VSA_POS is the total positive van der Waals surface area (calculated by partial equalisation of orbital electronegativities), and Q_VSA_NEG is the total negative van der Waals surface area (as found in the energy minimised model

calculated by MOE). The correlation coefficient was found to be only 0.66 compared to 0.77 for the top ranked model containing 11 descriptors. Cross validation was carried out under the leave-one-out method and resulted in a cross validated correlation coefficient of 0.62. While these correlation coefficients indicate that the model is far from a perfect fit for the data, the model is still useful from the point of view of screening potential compounds. To test this, an independent training set of compounds was obtained from O'Boyle[342] and the four descriptors used in the above equation were calculated for these compounds (**table 4.20**). The results obtained showed that the linear model did not correctly screen for all the active compounds reported by Boyle.

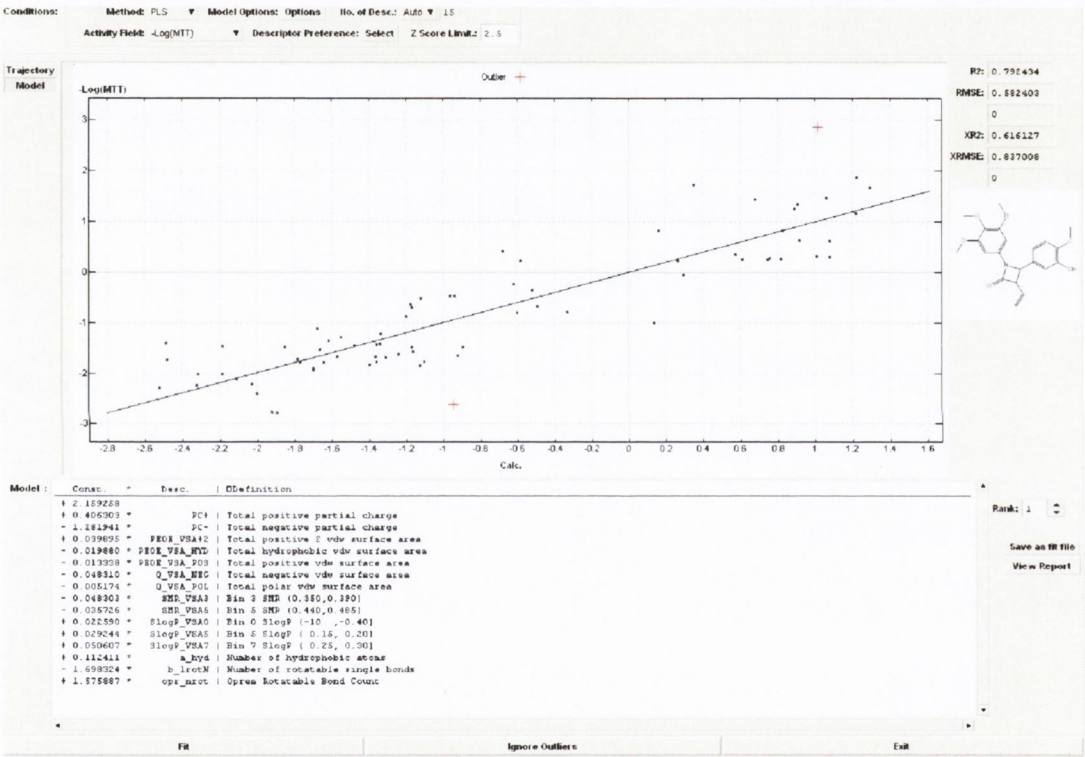

Fig 4.58 Top ranked QSAR model obtained

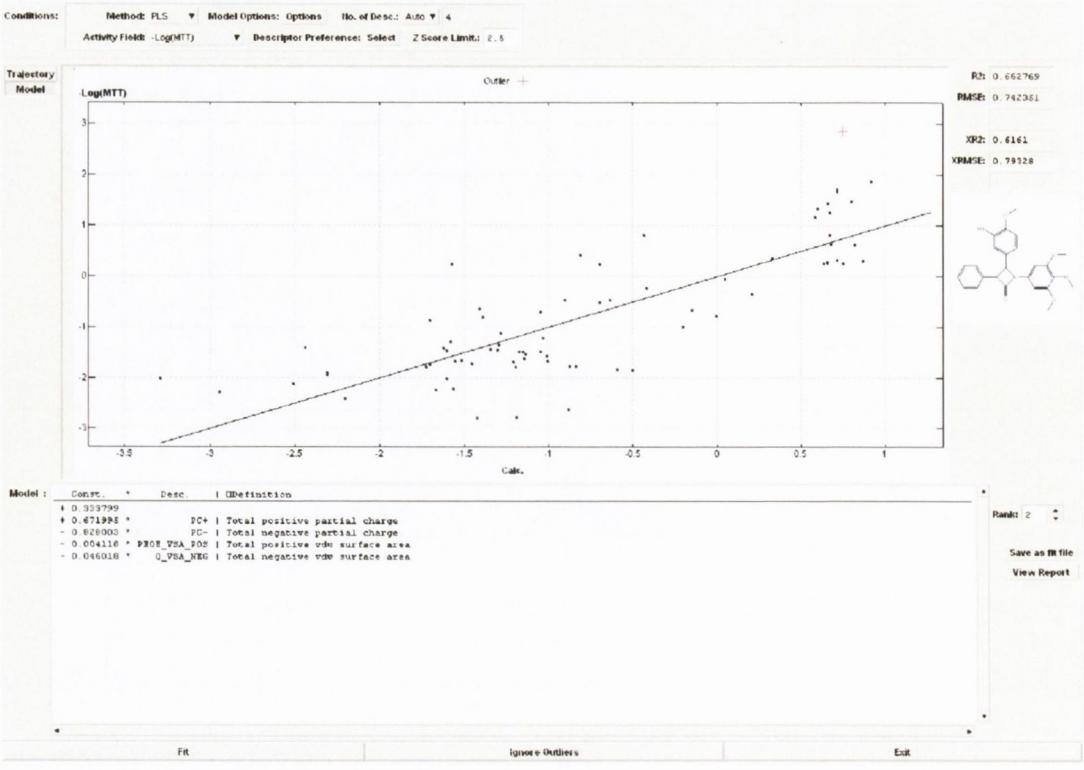

Fig 4.59 Second ranked QSAR model obtained.

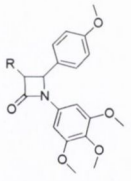

Compound number	PC+	PC-	VSA Pos	VSA Neg	Actual Activity IC_{50} MCF-7 (μM)	Predicted Activity IC_{50} MCF-7 (μM)
414	**4.796**	**-4.797**	**180.8455**	**178.5943**	**0.344**	**41.83571**
415	5.008	-5.01	222.8324	168.8432	6.994926	23.08453
416	5.008	-5.01	222.8324	168.8432	3.263124	23.08453
417	5.008	-5.01	222.8324	168.8432	1.820088	23.08453
418	5.22	-5.223	264.8194	159.092	2.227957	12.73776
419	5.432	-5.436	306.8063	149.3409	71.19233	7.02857
420	4.978	-4.979	193.5609	186.1	4.47983	47.39658
421	4.79	-4.791	189.3763	168.548	3.152151	27.53799
422	4.823	-4.824	181.0998	195.9214	3.051963	89.27229
423	4.823	-4.647	178.8323	166.3394	4.195804	26.24673
424	**4.836**	**-4.837**	**185.6009**	**178.248**	**0.422987**	**39.54368**
425	4.85	-4.851	181.3542	213.2484	33.60534	190.4953
426	4.876	-4.877	190.3564	177.9018	3.13894	37.3774
427	5.81	-5.811	187.8341	204.2739	16.57648	30.67103
428	5.546	-5.547	203.928	204.2739	4.855855	48.69738
429	5.546	-5.547	200.5177	192.6997	0.507979	28.18895
430	5.902	-5.904	238.3784	232.3262	79.8608	119.5458
431	**5.178**	**-5.179**	**195.3628**	**174.107**	**0.591014**	**20.36985**

Table 4.20 Descriptor values for set of β-lactam compounds used to test the QSAR model obtained. The QSAR model failed to predict the activity of three of the more active compounds (bold), and so its use as a screening method is doubtful.

4.15 The NCI 60 cell line panel

A screening program for novel anticancer agents has been run by the NCI since 1990 [343]. Approximately 12,000 synthetic and natural products are screened per year. The panel is a diverse collection of 60 cell lines representing lung, brain, colon, ovarian, breast, prostate, kidney, melanoma, and leukaemia cancers. The diversity of the panel allows for the use of pattern recognition software (COMPARE) to suggest a possible mechanism of action for the test compound. Enrolment of compounds into the program can only take place after the signing of a confidentially agreement between the NCI and the supplier. The first step in the process is the online submission of the compound structure along with any relevant information. The compound is then assessed before a sample of the compound is requested. Typically 20mg of test compound are supplied. The compound is screened for activity at 10μM in the full panel of 60 cell lines. The compound only enters dose response testing in the panel if sufficient activity is shown at 10μM. Data from the dose response testing is subject to review by the biological evaluation committee prior to the next stage of testing. The next stage of testing involves acute toxicity testing, hollow fibre assay, and lastly xenograft evaluation.

The dose response testing is carried out using 96 well plates. Typically a 100μL suspension of cancer cells in media is used to seed the plates. Seeding densities depend upon the type of cell and range from 5000 to 40000 cells/mL. The plates were incubated for 24 hours prior to treatment. The test compound is made up in DMSO to 400 times the final concentration and diluted down to the final working concentration with media. A treatment volume of 100μL is used giving a final concentration in the well of between 100μM and 10nM. T_0 was measured by fixing cells and reading prior to treatment. The plate is then incubated for a further 48 hours before the cells are fixed to the plate, washed, and dried. Sulforhodamine B (SRB) was added to each well, left for 10 minutes before the excess SRB was washed off. The bound SRB was solublised in trizma base before being read at 515nm to find the control growth (C) and growth in the presence of the test compound (T_i). The GI_{50} (the concentration of compound required to inhibit growth by 50%) was calculated from $[(T_i-T_0)/(C-T_0)] * 100 = 50\%$. Total growth inhibition (TGI) (the concentration of compound required to totally inhibit growth) is found from $T_i = T_0$. The TGI is effectively a measure of the cytostatic effect of the compound. The LC_{50} (concentration of test compound required for loss of 50% of total protein) was found from $[(T_i-T_0)/T_0]*100 = -50\%$. The LC_{50} therefore measures the cytotoxic effects of the compound. In cases where values cannot be accurately determined, the result is reported as being less than/greater than the upper/lower limit for the

variable. In this way the lower limit for GI_{50} is 10nM, meaning that compounds that may be more potent than this will be reported only as being less than 10nM. When calculating the average value for GI_{50} in cases where these limits have been exceeded, an approximation of the GI_{50} is used. Where a compound is significantly more potent that 10nM a second round of testing is carried out at a lower dose. CA4 has been screened in this way and yield an average GI_{50} value of 99.3nM. A subsequent screen where the treatment regime was changed to take into account the exceptional activity of CA4 yielded an average GI_{50} value of 7.68nM.

Four compounds (**256**, **264**, **342**, and **341**) displaying reasonable activity in the MCF-7 cell line were enrolled into the screening program. The more active compounds were not enrolled for intellectual property reasons. **Table 4.21** presents a summary of the results obtained from the screen. The full screening results for the four compounds in the 60 cell lines are presented in Appendix 1. Three individual values are reported for each compound in each cell line: GI_{50}, TGI, and LC_{50}. GI_{50} is the concentration of test compound required to inhibit the growth of 50% of the cells compared to prior to treatment with the test compound. TGI is the concentration of the test compound required to completely inhibit the growth of the cells and represents the cytostatic effect of the test compound. The LC_{50} is the concentration of test compound required to kill 50% of the cancer cells and represents the cytotoxic effect of the test compound.

From **table 4.21** it can be clearly seen that compounds **264** and **341** have superior average values for GI_{50} of 21.38nM and 23.99nM compared to 99.3nM for CA4. Both compounds are also slightly more cytotoxic than CA4 with average LC_{50} values of 55.88μM and 75.86μM compared to 85.5μM for CA4. In the majority of the cell lines in the panel both compounds display GI_{50} values of less than 10nM. Compound **264** returns values of less than 10nM in 32 of the 60 cell lines and **341** in 39 of the 60 cell lines. This indicates that the compounds should be retested in the panel using a lower concentration treatment regime so as to determine accurately the GI_{50} values. Only then can the true extent of the activity of the compounds be judged on equal terms with CA4.

Compound	GI_{50}	TGI	LC_{50}	NCI Ref. Number
CA4	99.3nM	10.3μM	85.5μM	
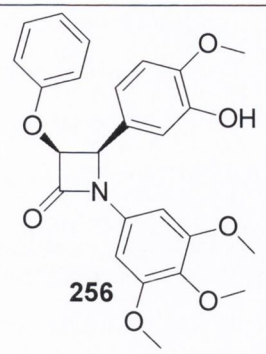 **256**	1.45μM	33.11μM	81.28μM	746998
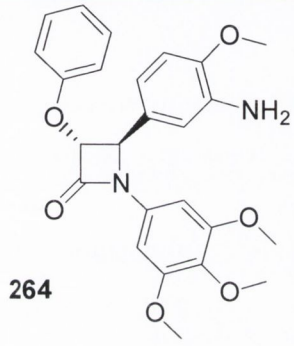 **264**	21.38nM	7.08μM	58.88μM	746999
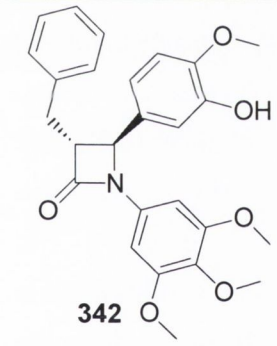 **342**	691.83nM	25.12μM	87.10μM	747000
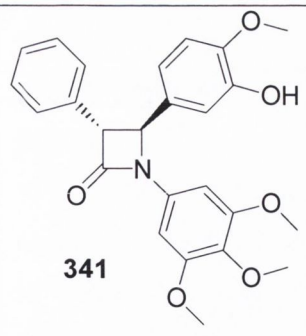 **341**	23.99nM	14.79μM	75.86μM	747001

Table 4.21 Summary of NCI 60 cell line screening results for compounds **256 264 342** and **341**. GI_{50} and LC_{50} are the concentrations required to inhibit the growth and kill 50% of the cells in the assay respectively. TGI is the concentration required to completely inhibit the growth of all cells

The diversity of the cell lines used in the screen coupled with the large number of synthetic and natural products screened, allows for the comparison of data obtained for the test compound to other entries in the database. This is carried out using the COMPARE program, which essentially searches the NCI database for compounds that display a similar pattern of activity to that of the test compound. Any such compounds found are then ranked according to their Pearson correlation factor. Compounds high in the ranking may possess a similar mechanism of action to the test compound. The database of NCI compounds is split into a number of subgroups. The three main groups are synthetic and natural products with a known structure, crude natural product extracts, and standard agents. The standard agent database is comprised of around 170 entries of standard chemotherapy agents of clinical importance, while the synthetic and natural products database contains details on members of the combretastatins including CA4 and CA1.

The amino compound (**264**) was subjected to this analysis. In the standard agent database vincristine sulphate was the top ranked hit with an R value of 0.518 although in general an R value in excess of 0.6 is defined as being significant. This is not unusual since vincristine also has a mechanism of action through involving tubulin. In the synthetic and natural products database, the top hit was a synthetic compound NCI-175636 with an R value of 0.955. This compound is a substituted dihydro quinazolinone (DHQZ) first synthesised by Yale and Kalkstein[344] who noted that the compound was capable of inhibiting the growth of cells in suspension. The mechanism for this inhibition was not understood until the compound was enrolled in the NCI screening program. Hamel *at al*[345] carried out a COMPARE analysis on the results from the 60 cell line panel, and noted that the hits obtained all belonged to compounds that were known to act through tubulin. For example vinblastine and CA4 displayed R values of 0.77 and 0.71 respectively. Hamel evaluated NCI-175636 in terms of its effect on tubulin polymerisation, colchicine and vinblastine binding. For tubulin polymerisation an IC_{50} value of 1.0μM was found while the percentage inhibition of colchicine and vinblastine binding was 34% and 15% respectively at 5μM. The effect on tubulin polymerization is comparable to that noted by the same authors for colchicine and CA4, but the inhibition of colchicine binding (34%) is much lower than that obtained for CA4 (92%) although it does suggest that the compound may act through the colchicine site.

The remaining hits are made up of other structurally related compounds enrolled in the screening program by our group. Podophylotoxin and CA4 also

appear as hits with R values of 0.627 and 0.611 respectively. These three hits in the COMPARE analysis are strong evidence that the β-lactam compounds presented in this thesis are inhibitors of tubulin polymerisation acting through the colchicine site.

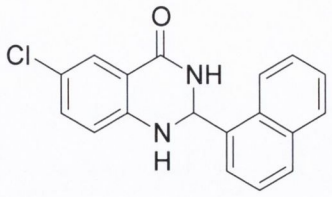

Fig 4.60 Structure of NCI-175636

Conclusions
&
Future Work

The aim of the work presented in this thesis was to synthesise a series of novel β-lactam containing analogues of the natural product combretastatin A4. From the initial library (chapter 2), two promising substitution patterns for the C_4 substituted aryl ring were identified, namely the 3-hydroxy-4-methoxy compound **256b**, and the 3-amino-4-methoxy compound **264b**. Both of these analogues possessed sub-micromolar activity against the MCF-7 breast cancer line, and appear to represent an optimised substitution pattern for the C_4 position. Biological evaluation of the corresponding thione and azetidine indicate that the carbonyl of the β-lactam at C_2 is crucial to the activity of this series of compounds. A stability study of **256** revealed that the β-lactam ring was subject to hydrolysis at acidic ($t_{1/2}$ 40 minutes) and neutral ($t_{1/2}$ 90 minutes) pH's but remained stable at pH10.

Chapter 3 presents the synthesis of a series of compounds varying only at the C_3 position of the β-lactam while maintaining the 3-hydroxy-4-methoxy substituted aryl ring at C_4. Initially these compounds were synthesised by successfully modifying the Staundinger by using a variety of acids/acid chlorides. Evaluation of this library of compounds in the MCF-7 cell line identified **343** containing a vinyl group at C_3 as a potent analogue displaying superior activity to that of CA4. Further vinyl analogues were synthesised by the aldol type addition of carbonyl containing compounds to 3-unsubstitutes β-lactams. While some compounds displayed promising activity, none approached the activity of **343**. Compound **343** was subjected to further transformations, all of which led to a reduction in observed activity. As a result the 3-vinyl substituent was identified as being highly optimised for antiproliferative activity. The replacement of the phenoxy substituent in previously inactive compounds led to large increases in the potencies observed again highlighting the role of the 3-vinyl group. **343** was found to inhibit tubulin polymerisation to a greater extent than that of CA4 possibly explaining the superior potency of **343** observed in the MCF-7 cell line. It was also demonstrated that compounds found to be inactive in the cell line were not efficient inhibitors of tubulin polymerisation. A number of analogues displaying mid-nanomolar activity were screened in the NCI 60 cell line panel and found to be on average four times more potent across the 60 cell lines.

The results obtained for the β-lactam containing CA4 analogues were rationalised by carrying out a detailed molecular modelling study in the colchicine site of tubulin. The importance of the Valβ318 and Cysβ241 contacts in the colchicine site was highlighted with all of the active compounds synthesised maintaining these two contacts. The observation that the substituent at C_3 moderates biochemical activity was explained by the interaction of the C_3 substituent with the T7 loop and H_8 helix of tubulin. By comparison of **343** to less active analogues, it was found that the

Ala β354 and Leu β248 contacts may play important roles, and should be the subject of further investigation.

Clearly the present work highlights the usefulness of the β-lactam ring as a scaffold for CA4 analogues. Through a process of synthesis of a diverse range of compounds and biochemical evaluation, a highly optimised compound (**343**) emerged.

Future work should focus on the role of C_3 on biochemical activity. In particular the epoxidation of the 3-vinyl group and subsequent ring opening should be carried out. The choice of substituents at C_3 should be made on the basis of maximising the interaction between the compound and the T7 H8 loop of tubulin.

A blood plasma metabolism study carried out was not successful and should be attempted again. The major metabolite of these compounds is expected to be the ring opened β-lactam. These ring opened compounds should be synthesised and evaluated for anticancer activity in their own right.

All of the compounds presented in this work were synthesised as racemic mixtures, but molecular modelling has demonstrated that key differences exist between the docked solutions of the component enantiomers. To this end optically pure compounds should be obtained by either chiral separation or asymmetric synthesis.

The presence of hydroxy and amino substituents on a number of the more active compounds opens up the possibility of forming prodrugs of the compounds similar to CA4P.

The more potent compounds should be screened in a commercially available competitive binding assay with a radiolableled colchicine ligand in the colchicine site. The effect of these compounds on the cell cycle should also be examined. Ultimately the antivascular effects of the most promising compounds should be demonstrated in animal models of solid tumours.

Chapter 5

Experimental

5.1 Materials & Methods

Chemicals were purchased from Sigma Aldrich and Lancaster Synthesis with a minimum assay of 98% unless otherwise stated. Solvents were either purchased dry or purified by distillation in accordance with literature methods.

H^1 and C^{13} NMR spectra were collected on a Bruker DPX 400 spectrometer, and analysed with Bruker WIN-NMR software. H^1 at 400.13 MHz and C^{13} at 100.61MHz. Experiments were run in deuterated chloroform ($CDCl_3$) with tetramethylsilane (TMS) as the internal standard, unless other wise stated. The spectra were analysed with Bruker WIN-NMR, MestREC and Bruker TopSpin. Coupling constants were reported in Hertz (Hz). Abbreviations used in the assigning of the spectra include s = singlet, br s = broad singlet, d = doublet, t = triplet, q = quartet, qn = quintet and m = multiplet.

The crystal structure of compounds was determined by X-ray diffraction on a Bruker SMART APEX (2001) diffractometer using MoK α radiation from a fine focus sealed source and a graphite monochromator. The structure solution was found using SHELXS-97 and the structure refinement was carried out using SHELXL-97.

IR spectra were obtained on a Perkin Elmer Spectrum 100 FTIR spectrometer using either potassium bromide (KBr) disks or thin film on sodium chloride plates (NaCl).

High resolution mass spectrometry (HRMS) was carried out using a Micromass LCT electrospray mass spectrometer.

Melting points were determined on a Gallenkamp melting point apparatus using a mercury 300°C thermometer and are uncorrected.

Thin layer chromatography was carried out using Merck F-254 plates visualised with UV at 254nm. Separation by flash chromatography was carried out using Merck Kiesegel 60 silica with a particle size of 0.040 mm to 0.063 mm. Alternatively flash chromatography using a Biotage SP1 ™ separation system was carried out using 12+M and 40+M silica cartridges and detection at 280nm. A typical separation employed a gradient elution with hexane/ethyl acetate over the course of 15 column volumes with fractions of 12mL collected from the 12+M columns and 24mL form the 40+M columns.

Determination of purity was determined by HPLC using a Waters HPLC system fitted with a Spherisorb column (2-5μm particle size, 4.5x250mm) supplied by Alltech Associates Incorporated. A mobile phase of 60/40

acetonitrile/water with 0.1% (v/v) TFA added to prevent peak tailing was used throughout. The mobile phase was only prepared from HPLC grade solvents and degassed by sonication prior to use. Flow rate was maintained at 1mL per minute with a pressure of approximately 1300 psi on a Waters 1525 binary pump equipped with an in line degasser. Where samples were run over a protracted period of time, the mobile phase was recycled back to the reservoir without any detriment to separation. Elution was detected at 280nm with a Waters 2487 dual wavelength detector. Multiple injections were carried out using a Waters 717 autosampler. All samples were filtered via a syringe filter (Pall, 0.45μM) prior to injection. The system was flushed with 2-propanol before shutting down for protracted periods of time.

Nomenclature was determined using Chemdraw 2004.

5.2 Synthesis of Imines

The appropriately substituted benzaldehyde (10mmol) and corresponding substituted aniline (10mmol) starting materials were refluxed together in ethanol (40mL) for five hours with a catalytic amount of concentrated H_2SO_4. The reaction volume was then reduced to approximately 10mL by removal of solvent under reduced pressure. The Schiff base was seen to precipitate out from solution upon standing at room temperature. The precipitate was removed by vacuum filtration and the solid obtained purified by recrystalistion from hot ethanol before being dried on filter paper.

(3,4,5-Trimethoxy-benzylidene)-(3,4,5-trimethoxy-phenyl)-amine **(192)**

Yield: 75%, 2.71g, white solid

MP: 174°C

IR (KBr ν max): 1626 cm^{-1} (C=N)

^{1}H NMR (400MHz, $CDCl_3$): δ3.88 (s, 3H, -OMe), δ3.92 (s, 6H, -OMe), δ3.94 (s, 3H, -OMe), δ3.97 (s, 6H, -OMe), δ6.50 (s, 2H, H_2' H_6'), δ7.28 (s, 2H, H_2'' H_6''), δ8.39 (s, 1H, Imine)

^{13}C NMR (100 MHz, $CDCl_3$): δ55.65, δ55.78, δ60.54, δ60.57 (-OMe), δ97.67 (C_2'&C_6'), δ105.21 (C_2''&C_6''), δ131.11 (C_1''), δ135.86 (C_4'), δ140.47 (C_4''), δ147.36 (C_3'&C_5'), δ153.06 (C_3''&C_5''), δ153.11 (C_1''), δ158.74 (Imine)

HRMS $C_{19}H_{23}NO_6$ M^++1 requires (m/e) 362.1604, found (m/e) 362.1602 (-0.6ppm)

(4-Methoxy-benzylidene)-(3,4,5-trimethoxy-phenyl)-amine **(193)**

Yield: 79%, 2.38g, pale yellow solid

MP: 114 °C

IR (KBr ν max): 1607 cm^{-1} (C=N)

^{1}H NMR (400MHz, $CDCl_3$): δ3.86 (s, 6H, -OMe), δ3.89 (s, 6H, -OMe), δ6.47 (s, 2H, H_2' H_6'), δ6.99 (d, J=8.52 2H, H_3'' H_5''), δ7.83 (d, J=8.52, 2H, H_2' H_6'), δ8.40 (s, 1H, Imine)

^{13}C NMR (100 MHz, $CDCl_3$): δ54.96, δ55.62, δ60.54 (-OMe), δ97.62 (C_2'&C_6'), δ113.75 (C_3''&C_5''), δ128.58 (C_1''), δ130.02 (C_2''&C_6''), δ135.58 (C_4'), δ147.83 (C_1'), δ153.06 (C_3'&C_5'), δ158.64 (Imine), δ161.81 (C_4'')

HRMS $C_{17}H_{19}NO_4$ M^++1 requires 302.1392, found 302.1400 (2.5ppm)

Benzo[1,3]dioxol-5-methylene-(3,4,5-trimethoxy-phenyl)-amine **(194)**

Yield: 68%

MP: 101 °C

IR (KBr ν max): 1629 cm^{-1} (C=N)

^{1}H NMR (400MHz, $CDCl_3$): δ3.86, (s, 3H, -OMe), δ3.89, (s, 6H, -OMe), δ5.93, (s, 2H, -$C\underline{H}_2$), δ6.05-7.42, (m, 5H, H_2' H_6' H_2'' H_5'' H_6''), δ8.35, (s, 1H, Imine)

^{13}C NMR (100 MHz, $CDCl_3$): δ55.41 δ55.64 δ60.55 (-OMe), δ97.63 (C_2'&C_6'), δ101.20 (-$\underline{C}H_2$), δ106.26 (C_5''), δ107.79 (C_2''), δ125.29 (C_5), δ130.54 (C_1''), δ135.70 (C_4'), δ147.49 (C_1'), δ148.01 (C_3'&C_5'), δ150.11 (C_3''), δ153.39 (C_4''), δ158.35 (Imine)

HRMS $C_{17}H_{17}NO_5$ M^++1 requires (m/e) 316.1185, found 316.1186 (0.3ppm)

(4-Methylsulfanyl-benzylidene)-(3,4,5-trimethoxy-phenyl)-amine **(195)**

Yield: 88%, 2.79g, yellow soild

MP: 96 °C

IR (KBr ν max): 1628 cm^{-1} (C=N)

^{1}H NMR (400MHz, $CDCl_3$): δ2.52 (s, 3H, -SCH3), δ3.87 (s, 3H, -OMe), δ3.89 (s, 6H, -OMe), δ6.48-7.80 (m, 6H, H_2' H_6' H_2'' H_3'' H_5'' H_6''), δ8.41 (s, 1H, Imine)

^{13}C NMR (100 MHz, $CDCl_3$): δ14.57 (SCH3), δ55.65 (-OMe), δ60.55 (-OMe), δ97.69 (C2'&C6'), δ125.16 (C3''&C5''), δ132.19 (C1''), δ135.83 (C4'), δ142.87 (C4''), δ147.51 (C1'), δ153.09 (C3'&C5'), δ158.51 (Imine)

HRMS $C_{17}H_{19}NO_3S$ M^++1 requires 318.1164, found 318.1162 (-0.6ppm)

(3-Bromo-4-methoxy-benzylidene)-(3,4,5-trimethoxy-phenyl)-amine **(196)**

Yield: 84%, 3.19g, off white solid

MP: 126 °C

IR (KBr ν max): 1585 cm^{-1} (C=N)

^{1}H NMR (400MHz, $CDCl_3$): δ3.88 (s, 3H, -OMe), δ3.92 (s, 6H, -OMe), δ3.99 (s, 3H, -OMe), δ6.49, s, 2H, H_2' H_6'), δ7.21-8.18 (m, 3H, H_2'' H_5'' H_6''), δ8.37 (s, 1H, Imine)

^{13}C NMR (100 MHz, $CDCl_3$): δ55.65, δ55.97, δ60.56 (-OMe), δ97.66 (C_2&C_6'), δ111.12 (C_5'), δ111.91 (C_3''), δ129.25 (C_6''), δ129.78 (C_1''), δ132.74 (C_2''), δ135.87 (C_4'), δ147.21 (C_1'), δ153.09 (C_3'&C_5'), δ156.98 (C_4''), δ157.76 (Imine)

HRMS: $C_{17}H_{18}BrNO_4$ M^++Na requires (m/e) 402.0317, found (m/e) 402.0320 (0.7ppm)

3-Fluoro-4-methoxy-benzylidene)-(3,4,5-trimethoxy-phenyl)-amine **(197)**

Yield: 84%, 2.68g, white solid

MP: 100 °C

IR (KBr ν max): 1609 cm^{-1} (C=N)

^{1}H NMR (400MHz, $CDCl_3$): δ3.82, (s 3H –OMe), δ3.91, (s 6H –OMe), δ3.97, (s 3H –OMe), δ6.48, (s, 2H, H_2' H_6'), δ7.62-7.75, (m H_2'' H_5'' H_6''), δ8.39 (s 1H Imine)

^{13}C NMR (100 MHz, $CDCl_3$): δ55.41 δ55.64 δ60.55 (-OMe), δ97.65 (C_2'&C_6'), δ112.27 (C_5''), δ114.65 (C_2''), δ125.75 (C_6''), δ129.17 (C_1''), δ135.86 (C_4'), δ147.24 (C_1'), δ149.43 (C_3''), δ150.84 (C_4''), δ153.30 (C_3'&C_5'), δ157.41 (Imine)

HRMS $C_{17}H_{18}FNO_4$ M^++1 requires 320.1298 found 320.1284 (-4.4ppm)

4-[(3,4,5-Trimethoxy-phenylimino)-methyl]-benzonitrile **(198)**

Yield: 92%, 2.72g, pale yellow solid

MP: 134 °C

IR (KBr ν max): 1580 cm^{-1} (C=N), 2223 cm^{-1} (C≡N)

^{1}H NMR (400MHz, $CDCl_3$): δ3.88 (s, 3H, -OMe), δ3.92 (s, 6H, -OMe), δ6.55-8.02 (m, 6H, H_2' H_6' H_2'' H_3'' H_5'' H_6''), δ8.53 (s, 1H, Imine)

^{13}C NMR (100 MHz, $CDCl_3$): δ56.18, δ61.05 (-OMe), δ98.36 (C_2'&C_6'), δ114.34 (C_4''), δ118.48 (Nitrile), δ129.05, (C_2''&C_6''), δ132.58 (C_3''&C_5''), δ137.20 (C_4'), δ139.85 (C_1''), δ146.76 (C_1'), δ153.68 (C_3'&C_5'), δ157.07 (Imine)

HRMS $C_{17}H_{16}N_2O_3$ M^++Na requires 297.1239, found 297.1250 (3.6ppm)

(4-Methoxy-3-nitro-benzylidene)-(3,4,5-trimethoxy-phenyl)-amine **(199)**

Yield: 94%, 2.97g, bright yellow solid

MP: 156 °C

IR (KBr ν max): 1618 cm^{-1} (C=N)

^{1}H NMR (400MHz, $CDCl_3$): δ3.88 (s, 3H, –OMe), δ3.91 (s, 6H, –OMe), δ4.06 (s, 3H –OMe), δ6.51, (s, 2H, H_2' H_6'), δ7.18-8.39 (m, 3H, H_2'' H_5'' H_6''), δ8.44 (s 1H Imine)

^{13}C NMR (100 MHz, $CDCl_3$): δ55.68 δ56.38 δ60.57 (-OMe), δ97.73 (C_2'&C_6'), δ113.20 (C_5''), δ125.50 (C_2''), δ128.49 (C_1''), δ133.35 (C_6''), δ136.28 (C_4'), δ139.36 (C_3''), δ146.55 (C_1'), δ153.16 (C_3'&C_5'), δ154.38 (C_4''), δ155.66 (Imine)

HRMS $C_{17}H_{18}N_2O_6$ M^++1 requires (m/e) 347.1243, found (m/e) 347.1240 (-0.9ppm)

Naphthalen-2-ylmethylene-(3,4,5-trimethoxy-phenyl)-amine **(200)**

Yield: 94%, 3.02g, pale yellow solid

MP: 128 °C

IR (KBr ν max): 1580 cm^{-1} (C=N)

^{1}H NMR (400MHz, $CDCl_3$): δ3.91 (s, 3H, -OMe), δ3.95 (s, 6H, -OMe), δ6.58-8.24 (m, 9H, Ar-H), δ8.67 (s, 1H, Imine)

^{13}C NMR (100 MHz, $CDCl_3$): δ55.44, δ55.74, δ60.63 (-OMe), δ97.75 (C_2'&C_6'), δ123.76 (C_8"&C_7"), δ124.44 (C_3"), δ124.88 (C_2"), δ128.39 (C_4"), δ129.47 (C_6"&C_9"), δ130.99 (C_{10}'), δ131.59 (C_5"), δ133.58 (C_1"), δ135.93 (C_4'), δ148.14 (C_1'), δ153.20 (C_3'&C_5'), δ159.05 (Imine)

HRMS $C_{20}H_{19}NO_3$ M^++Na requires (m/e) 322.1419, found (m/e) 322.1438 (5.9ppm)

(3,4-Dimethoxy-benzylidene)-(3,4,5-trimethoxy-phenyl)-amine **(201)**

Yield: 54%, 1.79g, off white solid

MP: 131 °C

IR (KBr ν max): 1626 cm^{-1} (C=N)

^{1}H NMR (400MHz, $CDCl_3$): δ3.87 (s, 3H, -OMe), δ3.92 (s, 6H, -OMe), δ3.97 (s, 3H, -OMe), δ4.00 (s, 3H, -OMe), δ5.94 (s, 2H, H_2' H_6') δ7.11-7.61 (m, 3H, H_2" H_5" H_6"), δ8.40 (s, 1H, Imine)

^{13}C NMR (100 MHz, $CDCl_3$): δ55.44, δ60.58 (OMe), δ97.63 (C_2'&C_6'), δ108.32 (C_5"), δ110.00 (C_1"), δ123.99 (C_6"), δ128.92 (C_1"), δ147.72 (C_1'), δ149.02 (C_3"), δ151.60 (C_3"&C_5"), δ153.09 (C_4"), δ158.81 (C=N)

HRMS $C_{18}H_{21}NO_5$ M^++1 requires (m/e) 332.1498, found (m/e) 332.1485 (-3.9ppm)

Naphthalen-1-ylmethylene-(3,4,5-trimethoxy-phenyl)-amine **(202)**

Yield: 81%, 2.60g, yellow solid

MP: 108 °C

IR (KBr ν max): 1584 cm^{-1} (C=N)

^{1}H NMR (400MHz, $CDCl_3$): δ3.83 (s, 3H, -OMe), δ3.89 (s, 6H, -OMe), δ6.58-9.11 (m, 9H, φ-H), δ9.17 (s, 1H, Imine)

^{13}C NMR (100 MHz, $CDCl_3$): δ55.44 δ60.63 (OMe), δ97.75 (C_2'&C_6'), δ123.76 (C_8"&C_7"), δ124.44 (C_3"), δ125.84 (C_2"), δ127.09 (C_4"), δ129.47 (C_6"&C_9"), δ130.85 (C_{10}"), δ131.59 (C_5"), δ133.48 (C_1"), δ135.95 (C_4'), δ148.14 (C_1'), δ153.20 (C_3'&C_5'), δ159.05 (Imine)

HRMS $C_{20}H_{19}NO_3$ M^++1 requires 322.1443, found 322.1436 (-2.2ppm)

(4-Dimethylamino)-(3,4,5-trimethoxy-phenyl)-amine **(203)**

Yield: 71%, 2.23g, white solid

MP: 83 °C

IR (KBr ϒ max): 1607 cm^{-1} (C=N)

^{1}H NMR (400MHz, $CDCl_3$): δ3.11 (s, 6H, –OMe), δ3.91 (s, 3H, –OMe), δ6.47 (s, 2H, (H_2' H_6'), δ 7.18-7.79 (m 4H H_2'' H_3'' H_5'' H_6''), δ8.35 (s 1H Imine)

^{13}C NMR (100 MHz, $CDCl_3$): δ40.23 & δ40.25 ($N(CH_3)_2$), δ56.1 & δ61.04 (OMe), δ97.75 (C_2'&C_6'), δ111.5 (C_3''&C_5''), δ124.14 (C_1''), δ130.05 (C_2''&C_6''), δ135.63 (C_4'), δ148.97 (C_4''), δ152.53 (C_1'), δ153.49 (C_3'&C_5'), δ159.70 (Imine)

HRMS $C_{18}H_{22}N_2O_3$ M^++1 requires (m/e) 315.1709, found (m/e) 315.1721 (3.8ppm)

5.3 Synthesis of Hydroxy Containing Imines

Compounds **204-207** were syntheised according to the procedure previously described in **section 5.2**.

2-Methoxy-5-[(3,4,5-trimethoxy-phenylimino)-methyl]-phenol **(204)**

Yield: 89%, 2.82g, pale yellow solid

MP: 134 °C

IR (KBr ν max): 1613 cm^{-1} (C=N), 3347 (OH)

^{1}H NMR (400MHz, $CDCl_3$): δ3.64 (s, 3H, -OMe), δ3.82 (s, 6H, -OMe), δ3.84 (s, 3H, -OMe), δ6.58 (s, 2H, H_2' & H_6'), δ6.95 (d, J=8.52Hz, H_5''), δ7.29 (dd, J=1.48, 8.28, H_6''), δ7.42 (d, J=1.48, H_2''), δ8.49 (s, 1H, Imine), δ9.35 (s, 1H, OH).

^{13}C NMR (100 MHz, $CDCl_3$): δ55.61, δ55.67, δ60.58 (-OMe), δ97.96 (C_2&C_6), δ109.87 (C_5''), δ113.31 (C_2''), δ121.85 (C_6''), δ129.49 (C_1''), δ136 (C_4'), δ145.51 (C_3''), δ147.71 (C_1'), δ153.08 (C_4'') & (C_3'&C_5'), δ158.72 (Imine)

HRMS $C_{17}H_{19}NO_5$ M^++1 requires (m/e) 318.1341, found (m/e) 318.1353 (3.8ppm)

4-[(3,4,5-Trimethoxy-phenylimino)-methyl]-phenol **(205)**

Yield: 69%, 1.98g, pale yellow solid

MP: 158 °C

IR (KBr ν max): 1624 cm^{-1} (C=N), 3398 (OH)

^{1}H NMR (400MHz, $CDCl_3$): δ3.87 (s 3H –OMe), δ3.89 (s 6H –OMe), δ6.48, (s, 2H, H_2' H_6'), δ7.26-7.76 (m 4H H_2'' H_3'' H_5'' H_6''), δ8.39 (s 1H Imine)

^{13}C NMR (100 MHz, $CDCl_3$): δ55.56, δ55.64, δ60.57 (-OMe), δ97.66 (C_2'&C_6'), δ108.02 (C_2''), δ113.90 (C_5''), δ124.82 (C_6''), δ128.38 (C_1''), δ135.63 (C_4'), δ146.80 (C_4''), δ147.64 (C_1'), δ148.75 (C_3'&C_5'), δ153.53 (C_3''), δ159.15 (Imine)

HRMS $C_{16}H_{17}NO_4$ M^++1 requires (m/e) 288.1236, found 288.1235 (-0.3ppm)

4-[(3,4,5-Trimethoxy-phenylimino)-methyl]-benzene-1,2-diol **(206)**

Yield: 82%, 2.49g, white solid

MP: 58 °C

IR (KBr ν max): 1645 cm^{-1} (C=N), 3401 (OH)

^{1}H NMR (400MHz, $CDCl_3$): δ3.78 (s, 3H, -OMe), δ3.88 (s, 6H, -OMe), δ4.9 (s broad, 1H, -OH), δ6.55 (s, 2H, H_2' H_6'), δ7.31-7.42 (m 3H H_2'' H_5'' H_6''), δ8.38 (s 1H Imine)

^{13}C NMR (100 MHz, $CDCl_3$): δ54.40, δ54.72, δ59.44 (-OMe), δ97.59 (C_2'&C_6'), δ112.92 (C_1''), δ114.44 (C_5''), δ117.58 (C_6''), δ122.63 (C_1''), δ127.45 (C_4'), δ135.33 (C_1'), δ142.05 (C_3''), δ135.65 (C_4''), δ153.04 (C_3'&C_5'), δ160.56 (Imine)

HRMS $C_{16}H_{17}NO_5$ M^++1 requires (m/e) 304.1185, found (m/e) 304.1181 (-1.3ppm)

2-Methoxy-4-[(3,4,5-trimethoxy-phenylimino)-methyl]-phenol **(207)**

Yield: 61%, 1.94g, pale yellow solid

MP: 140 °C

IR (KBr ν max): 1613 cm^{-1} (C=N), 3403cm^{-1} (OH)

^{1}H NMR (400MHz, $CDCl_3$): δ3.87 (s, 6H, -OMe), δ3.91 (s 6H –OMe), δ3.07, (s, 3H, -OMe), δ6.48-7.61 (m 5H H_2' H_6' H_2'' H_5'' H_6''), δ6.36, (broad s, 1H –OH), δ8.37 (s, 1H, Imine)

^{13}C NMR (100 MHz, $CDCl_3$): δ56.00 & δ61.03 (OMe), δ98.14 (C_2'&C_6'), δ108.52 (C_2''), δ114.39 (C_5''), δ125.30 (C_6''), δ128.80 (C_1''), δ136.09 (C_4'), δ147.30 (C_4''), δ148.09 (C_1'), δ149.25 (C_3''), δ153.56 (C_3'&C_5'), δ159.65 (Imine)

HRMS $C_{16}H_{17}NO_4$ M^++1 requires (m/e) 318.1331, found 318.1341 (3.1ppm)

Synthesis of silyl ether imines

Method 1 (Route A)

To a solution of the appropriately substituted Schiff base (**204-207**) (5mmol) and *t*-butyldimethylsilylchloride (6mmol) in anhydrous DCM (40mL) under a nitrogen atmosphere, DBU (8mmol) was added dropwise via syringe. Stirring under nitrogen was continued until starting material had disappeared as monitored by TLC in 50:50 hexane/ethyl acetate (2 - 4 hours). Upon completion the reaction was diluted with 50mL of dichloromethane and transferred to a separating funnel. The reaction was washed with water (2 x 100mL), 0.1M HClaq (2 x 50mL), and saturated $NaHCO_3$ aqueous solution (2 x 50mL), retaining the organic layer each time, before drying over Na_2SO_4. The solvent was removed under reduced pressure to yield the protected Schiff base. The product was used as starting material for β-lactam synthesis without further purification.

Method 2 (Route B)

To a solution of the appropriately substituted benzaldehyde (**212-215**) (5mmol) and *t*-butyldimethylsilylchloride (6mmol) in anhydrous DCM (40mL) under a nitrogen atmosphere, DBU (8mmol) was added dropwise via syringe. Stirring under nitrogen was continued until starting material had disappeared as monitored by TLC in 50:50 hexane/ethyl acetate (2 - 4 hours). Upon completion the reaction was diluted with 50mL of dichloromethane and transferred to a separating funnel. The reaction was washed with water (2 x 100mL), 0.1M HCl_{aq} (2 x 50mL), and saturated $NaHCO_3$ aqueous solution (2 x 50mL), retaining the organic layer each time, before drying over Na_2SO_4. The solvent was removed under reduced pressure to yield the protected benzaldehyde, which served as starting material without further purification for the synthesis of protected Schiff bases (**208-211**) as described above.

3-(*t*-Butyl-dimethyl-silanyloxy)-4-methoxy-benzaldehyde **(216)**

Yield: 94%, 1.25g, colourless oil

MP: Oil

IR (NaCl ν max): 1689 cm^{-1} (C=N)

^{1}H NMR (400MHz, $CDCl_3$): δ0.11 (6H, s, $Si(CH_3)_2$, $C(CH_3)_3$), δ0.93 (9H, s, $Si(CH_3)_2C(CH_3)_3$), δ3.81 (3H, s, -OMe), δ6.88 (1H, d, J=8.52, H_5), δ7.32 (1H, s, H_2), δ7.48 (1H, d, J=2Hz, H_6)

^{13}C NMR (100 MHz, $CDCl_3$): δ-5.19, δ17.86, δ25.15 (TBDMS), δ54.95 (OMe), δ110.69 (C_5), δ119.31 (C_2), δ125.90 (C_6), δ129.66 (C_1), δ145.02 (C_3), δ156.07 (C_4), δ190.27 (CHO)

HRMS: $C_{14}H_{22}O_3Si$ M^+ calculated 266.1338, found 266.1349 (4.1ppm)

4-(*t*-Butyl-dimethyl-silanyloxy)-benzaldehyde **(217)**

Yield: 92%, 1.09, amber oil

MP: 97°C

IR (KBr ν max): 1693 cm^{-1} (C=N)

^{1}H NMR (400MHz, $CDCl_3$): δ0.20 (s, 6H, TBDMS), δ0.94 (s, 9H, TBDMS), δ6.89 (d, J=8.56Hz, 2H, H_3 H_5), δ7.73 (d J=8.52, 2H, H_2 H_6), δ9.81 (s, 1H, CHO)

^{13}C NMR (100 MHz, $CDCl_3$): δ-4.63, δ17.53, δ25.29 (TBDMS), δ119.96 (C_3&C_5), δ129.86 (C_1), δ131.43 (C_2&C_6), δ161.02 (C_4), δ190.38 (CHO).

HRMS: $C_{13}H_{20}O_2Si$ M+ calculated 236.1233 found 236.1227 (-2.5ppm)

3,4-Bis-(*t*-butyl-dimethyl-silanyloxy)-benzaldehyde **(218)**

Yield: 89%, 1.63g, amber oil

MP: Oil

IR (NaCl ν max): 1694 cm^{-1} (C=N)

^{1}H NMR (400MHz, $CDCl_3$): δ0.22 (s, 6H, TBDMS), δ0.25 (s, 6H, TBDMS), δ0.88 (s, 9H, TBDMS), δ0.98 (s, 9H, TBDMS), δ6.92-7.35 (m, 3H, H_2 H_5 H_6), δ9.75 (s, 1H, CHO)

^{13}C NMR (100 MHz, $CDCl_3$): δ-4.64, δ-4.06, δ17.52, δ17.90, δ25.13, δ25.41 (TBDMS), δ120.07 (C_2), δ120.31 (C_6), δ124.97 (C_5), δ130.11 (C_1), δ147.18 (C_3), δ152.96 (C_4), δ190.53 (CHO)

HRMS: $C_{19}H_{34}O_3Si_2$ calculated 366.2046, found 366.2039 (-1.9ppm)

4-(*t*-Butyl-dimethyl-silanyloxy)-3-methoxy-benzaldehyde **(219)**

Yield: 97%, 1.29g, amber oil

MP: Oil

IR (NaCl ν max): 1687 cm^{-1} (C=N)

^{1}H NMR (400MHz, $CDCl_3$): δ0.15 (s, 6H, TBDMS), δ0.96 (s 9H TBDMS), δ3.81 (s 3H OMe),δ 6.90-7.16 (m 3H, H_2 H_5 H_6), δ9.77 (s 1H CHO)

^{13}C NMR (100 MHz, $CDCl_3$): δ-4.92, δ17.53, δ25.20 (TBDMS), δ54.84 (OMe), δ109.70 (C_2), δ120.20 (C_5), δ125.73 (C_6), δ130.37 (C_1), δ150.86 (C_4), δ151.09 (C_5), δ190.33 (CHO)

HRMS: $C_{14}H_{22}O_3Si$ calculated 266.1338, found 266.1345 (2.6ppm)

[3-(*t*-Butyl-dimethyl-silanyloxy)-4-methoxy-benzylidene]-(3,4,5-trimethoxy-phenyl)-amine **(208)**

Yield: Route A 78% 1.68g, amber oil, Route B 76%, 1.64g, amber oil

MP: Oil

IR (NaCl ν max): 1585 cm^{-1} (C=N)

^{1}H NMR (400MHz, $CDCl_3$): δ0.20 (s, 6H, -tBDMSi), δ1.03 (s, 9H, -tBDMSi), δ3.77 (s, 3H, -OMe), δ3.81 (s, 6H, -OMe), δ3.89 (s, 3H, -OMe), δ5.94 (s, 2H, H_2' H_6'),δ 6.48 (s, 1H, H_5''), δ6.92 (1H, d, H_2''), δ7.46 (1H, d, H_6''), δ8.35 (1H, s, imine)

^{13}C NMR (100 MHz, $CDCl_3$): δ-5.67, δ18.07, δ25.26 (–tBDMSi), δ54.99, δ55.64 δ60.62 (–OMe), δ92.12 (C_2'&C_6'), δ110.96 (C_5''), δ119.74 (C_2''), δ123.42 (C_6''), δ128.95 (C_1''), δ144.50 (C_4'), δ144.87 (C_3''), δ147.94 (C_1'), δ153.06 (C_3'&C_5'), δ153.40 (C_4''), δ158.82 (imine)

HRMS: $C_{23}H_{33}NO_5Si$, calculated 431.2128, found 431.2127 (-0.2ppm)

[4-(*t*-Butyl-dimethyl-silanyloxy)-benzylidene]-(3,4,5-trimethoxy-phenyl)- amine **(209)**

Yield: Route A 91% 1.83g, amber oil, Route B 93% 1.87g, amber oil

MP: Oil

IR (NaCl ν max): 1581 cm^{-1} (C=N)

^{1}H NMR (400MHz, $CDCl_3$): : δ0.21 (6H, s, -tBDMSi), δ1.01 (9H, s, -tBDMSi), δ3.88 (3H, s, -OMe), δ3.91 (6H, s, -OMe),δ 6.48 (2H, s, H_2' H_6'), δ6.94 (2H, d, H_3'' H_5''), δ7.79 (2H, d, H_2'' H_6''), δ8.41 (1H, s, imine)

^{13}C NMR (100 MHz, $CDCl_3$): δ-5.92, δ18.10, δ25.32 (-OTBDMS) δ55.12, δ56.00 δ61.03 (OMe), δ98.14 (C_2'&C_6'), δ108.52 (C_2''), δ114.39 (C_5''), δ125.30 (C_6''), δ128.80 (C_1''), δ136.09 (C_4'), δ147.30 (C_4''), δ148.09 (C_1'), δ149.25 (C_3''), δ153.56 (C_3'&C_5'), δ159.65 (Imine)

HRMS: $C_{22}H_{31}NO_4Si$, calculated 401.2022, found 401.2031 (2.2ppm)

[3,4-Bis-(*t*-butyl-dimethyl-silanyloxy)-benzylidene]-(3,4,5-trimethoxy-phenyl)-amine**(210)**

Yield: Route A 88%, 2.27g, colourless oil, Route B 87%, 2.25g, colourless oil

MP: oil

IR (NaCl ν max): 1598 cm^{-1} (C=N)

^{1}H NMR (400MHz, $CDCl_3$): : δ0.25 (12H, s, -tBDMSi), δ1.05 (18H, s, -tBDMSi), δ3.87 (3H, s, -OMe), δ3.92 (6H, s, -OMe), δ6.47 (2H, s, H_2' H_6'), δ7.28 (1H, s, H_5''), δ7.40 (2H, m, H_2'' H_6''), δ8.32 (1H, s, imine)

^{13}C NMR (100 MHz, $CDCl_3$): δ-5.96, δ-5.99, δ18.02, δ18.07, δ25.26 (–tBDMSi), δ54.89, δ55.37, δ60.61 (–OMe), δ91.98 (C_2'&C_6'), δ111.21 (C_5''), δ120.02 (C_2''), δ123.67 (C_6''), δ129.02 (C_1''), δ137.62 (C_4'), δ142.37 (C_3''), δ147.01 (C_1'), δ151.48 (C_4''), δ154.55 (C_3'&C_5'), δ158.82 (imine)

HRMS: $C_{28}H_{45}NO_5Si_2$ M^+ requires 531.2836, found 531.2839 (0.6ppm)

[4-(*t*-Butyl-dimethyl-silanyloxy)-3-methoxy-benzylidene]-(3,4,5-trimethoxy-phenyl)-amine **(211)**

Yield: Route A 75%, 1.62g, amber oil, Route 77%, 1.66g, amber oil

MP: Oil

IR (NaCl ν max): 1574 cm^{-1} (C=N)

^{1}H NMR (400MHz, $CDCl_3$): δ0.20 (6H, s, -tBDMSi), δ1.02 (9H, s, -tBDMSi), δ3.87 (3H, s, -OMe), δ3.91 (6H, s, -OMe), δ3.97 (3H, s, -OMe), δ6.48 (2H, s, H_2'' H_6''), δ6.93 (1H, d, J=8.21Hz, H_5''), δ7.28 (1H, d, J=8.11Hz, H_6''), δ7.38 (1H, s, H_2''), δ8.39 (1H, s, imine)

^{13}C NMR (100 MHz, $CDCl_3$): δ5.97, δ18.11, δ25.34 (-OTBDMS), δ56.03, δ60.59 (OMe), δ101.19 (C_2'&C_6'), δ122.3 (C_3''&C_5''), δ125.11 (C_1''), δ130.08 (C_2''&C_6''), δ131.71 (C_4'), δ148.95 (C_1'), δ152.46 (C_3'&C_5'), δ150.68 (C_4''), δ159.34 (Imine)

HRMS: $C_{23}H_{33}NO_5Si$ M^+ requires 431.2128, found 431.2135 (1.6ppm)

5.4 Synthesis of β-Lactams

Method A Thermal Heating Method

To a stirring, refluxing solution of the imine (**192-203**) (5mmol) and triethylamine (6mmol) in anhydrous dichloromethane (40mL), a solution of the appropiate acid chloride (6mmol) in anhydrous dichloromethane (10mL) was added over 45 minutes under nitrogen. The reaction was kept at reflux during the day (5 hours) and at room temperature overnight (16 hours), continuously under nitrogen, until the starting material had disappeared as monitored by TLC in 50:50 hexane/ethyl acetate. A characteristic darkening of the reaction to an amber colour over time was observed.

The reaction was transferred to a separating funnel and washed with water (2 x 100mL), with the organic layer being retained each time. The reaction was dried over Na_2SO_4 before the solvent was removed under reduced pressure. The crude product was purified by flash chromatography over silica gel in 1:1 *n*-hexane: ethyl acetate.

Method B Microwave Heating Method

A stirring solution of the imine (**193**) (1mmol) and triethylamine (1.2mmol) in dichloroethane (10mL) was heated to 40 °C by microwave irradiation at atmospheric pressure and under a nitrogen atmosphere. To this solution, the acid chloride (1.2mmol) in dichloroethane (5mL) was added dropwise over 45 minutes. Upon completion of the addition, the reaction temperature was maintained at 40°C by continous microwave irradiation, while maintaining the nitrogen atmosphere. A characteristic darkening of the reaction was noticed upon completion of the reaction.

The reaction was transferred to a separating funnel and washed with water (2 x 100mL), with the organic layer being retained each time. The reaction was dried over Na_2SO_4 before the solvent was removed under reduced pressure. The crude product was purified by flash chromatography over silica gel eulted with 1:1 n-hexane: ethyl acetate.

Method C Triphosgene Activation

A solution of phenoxyacetic acid (150mg, 1mmol) and triphosgene (149mg, 0.5mmol) in dry DCM (10mL) was brought to reflux under N_2. After 30 minutes TEA (0.21mL, 1.5mmol) was added, followed by the dropwise addition of the appropriate imine (**208**) (0.5mmol) dissolved in dry DCM (15mL) over the course of 30 minutes. The reaction was left to reflux for a further 6 hours before being allowed to cool. The reaction was washed with H_2O (20mL), saturated $NaHCO_3$ (2x20mL), and brine (10mL), before being dried over $MgSO_4$, filtered, and solvent removed under reduced pressure.

Method D Mukaiyama Reagent

A solution of Mukaiyama's reagent (0.617g, 2.4mmol), phenoxyacetic acid (0.369g, 2.4mmol), and TPA (1.14mL, 6mmol) in dry DCM (30mL) was refluxed under N_2 for 30minutes. The appropriate imine (**208**) (2mmol) in DCM (10mL) was added dropwise to this refluxing solution over 30 minutes. The reaction was left to reflux for a further 8 hours and at room temperature overnight, before being washed with H_2O (100mL), 2%HCl (50mL), and H_2O (100mL), dried over $MgSO_4$, filtered and solvent removed under reduced pressure.

3-Phenoxy-1,4-bis-(3,4,5-trimethoxy-phenyl)-azetidin-2-one **(244)**

Yield: 32%, 790mg, white solid

MP: 132-134 °C

IR (KBr ν max): 1762 cm^{-1} (C=O)

^{1}H NMR (400MHz, $CDCl_3$): : δ3.75 (s 12H –OMe), δ3.79 (s 6H –OMe), δ5.20 (d 1H C_3 J=5.00Hz), δ5.6 (d 1H C_3 J=5.00Hz), δ6.57, (s, 2H, H_2' H_6'), δ6.98 - 7.19 (m 7H, H_2'' H_3'' H_4'' H_5'' H_6'' H_2''' H_6''').

^{13}C: δ55.0, δ55.5, δ60.5 (OMe), δ62.0 (H_4), δ80.5 (H_3), δ95.0 (C_2'&C_6'), δ102.5 (C_2'''&C_6'''), δ115 (C_2''&C_6''), δ122 (C_4''), δ127.5 (C_4'), δ129 (C_3''&C_5''), δ132.5 (C_4'''), δ134.53 (C), δ138.19 (C_1'''), δ152.5 (C_3'&C_5'), δ153.14 (C_3'''&C_5'''), δ156.04 (C_1''), δ162.73 (C_2)

HRMS: $C_{27}H_{29}NO_8$ M^++Na requires (m/e) 518.1792, found 518.1786 (-1.2ppm)

4-(4-Methoxy-phenyl)-3-phenoxy-(3,4,5-trimethoxy-phenyl)-azetidin-2-one **(245)**

Yield: *Trans* 21%, 0.46g, white solid, *Cis* 33%, 0.72g, white solid

MP: 155 °C (*cis*), 112-114 °C (*trans*)

IR (KBr ν max): 1740 cm^{-1} *trans* (C=O), 1741 cm^{-1} *cis* (C=O)

^{1}H NMR (400MHz, $CDCl_3$): : *Trans isomer* δ3.72 (s, 6H –OMe), δ3.79 (s, 3H –OMe), δ3.87 (s, 3H –OMe), δ4.95 (d, 1H, C_4 J= 2.19Hz), δ5.13 (d, 1H, C_3 J= 2.19Hz), δ6.58-7.28 (m, 11H, H_2' H_6' H_2'' H_3'' H_4'' H_5'' H_6'' H_2''' H_3''' H_5''' H_6''')
Cis isomer δ3.74 (s, 6H –OMe), δ3.78 (s, 3H –OMe), δ3.79 (s, 3H –OMe), δ5.34 (d, 1H, H_4, J=5.02Hz), δ5.54 (d, 1H, H_3, J=5.02Hz), δ6.58-7.28 (m ,11H, H_2' H_6' H_2'' H_3'' H_4'' H_5'' H_6'' H_2''' H_3''' H_5''' H_6''')

^{13}C NMR (100 MHz, $CDCl_3$): *Trans isomer* δ54.93, δ55.55, δ63.61 (OMe), δ60.50 (C_4), δ86.74 (C_3), δ94.85 (C_2'&C_6'), δ114.37 (C_3'''&C_5'''), δ114.93 (C_2''&C_6''), δ121.83 (C_4''), δ126.94 (C_4'), δ127.40 (C_2'''&C_6'''), δ129.21 (C_3''&C_5''), δ132.66 (C_1'''), δ134.41 (C_1'), δ153.01 (C_3'&C_5'), δ156.54 (C_1''), δ159.82 (C_4'''), δ162.14 (C_2)
Cis isomer δ55.23,δ56.06, δ60.96 (OMe), δ62.09 (C_4), δ81.11 (C_3), δ95.31 (C_2'&C_6'), δ113.94 (C_3'''&C_5'''), δ115.70 (C_2''&C_6''), δ122.22 (C_4''), δ124.42 (C_4'), δ129.32 (C_2'''&C_6'''), δ129.49 (C_3''&C_5''), δ133.14 (C_1'''), δ134.90 (C_1'), δ153.52 (C_3'&C_5'), δ156.99 (C_1''), δ159.95 (C_4'''), δ163.04 (C_3)

HRMS: $C_{25}H_{25}NO_6$
Trans isomer M^++Na requires (m/e) 458.1580, found (m/e) 458.1580 (0ppm)
Cis isomer M^++Na requires 458.1580, found 458.1576 (-0.9ppm)

4-Benzo[1,3]dioxol-5-yl-3-phenoxy-1-(3,4,5-trimethoxy-phenyl)-azetidin-2-one **(246)**

Yield: 71%, 1.60g, pale yellow soild

MP: 156 °C

IR (KBr ν max): 1747 cm^{-1} (C=O)

^{1}H NMR (400MHz, $CDCl_3$): δ3.75 (s 6H –OMe), δ3.79 (s 3H –OMe), δ5.32 (d 1H H_4 Jcis=5.00Hz), δ5.51 (d 1H H_3 Jcis=5.00Hz), δ5.95 (d 2H CH_2), δ6.64-7.28 (m 10H H_2' H_6' H_2'' H_3'' H_4'' H_5'' H_6'' H_2''' H_5''' H_6''').

^{13}C: δ56.03, δ60.51, δ62.09 (H4), δ80.55 (H3), δ95.40 (C-(O)2), δ101.69 (C2'&C6'), δ107.53 (C2'''&C5'''), δ115.83 (C2''&C6'''), δ121.49 (C4''), δ122.29 (C6'''), δ126.39 (C4'), δ129.59 (C3''&C5''), δ132.72 (C1'), δ134.85 (C1'''), δ147.41 (C3'''&C4'''), δ153.42 9C3'&C5'), δ156.72 (C1''), δ162.83 (C2)

HRMS: $C_{25}H_{23}NO_7$
$2M^+$+Na requires (m/e) 921.2847, found (m/e) 921.2844 (-0.3ppm)

4-(4-Methylsulfanyl-phenyl)-3-phenoxy-1-(3,4,5-trimethoxy-phenyl)-azetidin-2-one **(247)**

Yield: 77%, 1.74g, pale yellow solid

MP: 130 °C

IR (KBr ν max): 1744 cm^{-1} (C=O)

^{1}H NMR (400MHz, $CDCl_3$): δ2.45 (s, 3H, SCH3), δ3.74 (s, 1H, -OMe), δ3.79 (s, 1H -OMe), δ5.34 (d, 1H, H4), δ5.55 (d, 1H, H3), δ6.57-7.17 (m, 11H, φ-H)

^{13}C NMR (100 MHz, $CDCl_3$): δ15.74 (SCH3), δ55.74, δ60.39 (OMe), δ61.47 (C4), δ80.33 (C3), δ94.55 (C2'&C6'), δ115.11 (C2''&C6''), δ121.56 (C4''), δ125.62 (C3'''&C5'''), δ128.36 (C2'''&C6'''), δ128.19 (C3''&C5''), δ132.75 (C4'''), δ134.18 (C1'), δ139.62 (C1'''), δ153.93 (C3'&C5'), δ156.27 (C1''), δ162.15 (C2)

HRMS: $C_{25}H_{25}NO_5S$ $2M^+$+Na requires (m/e) 925.2805, found 925.2841 (3.9ppm)

4-(3-Bromo-4-methoxy-phenyl)-3-phenoxy-1-(3,4,5-trimethoxy-phenyl)-azetidin-2one **(248)**

Yield: 61% *cis*, 1.56g, white solid, 31% *trans,* 0.80g, white solid

MP: 158°C 170°C

IR (KBr ν max): 1753 cm^{-1} *trans* (C=O), 1756 cm^{-1} *cis* (C=O)

^{1}H NMR (400MHz, $CDCl_3$): : *Cis isomer* δ3.76 (s, 6H, -OMe), δ3.80 (s, 3H, -OMe), δ3.87, (s, 3H, -OMe), δ5.29 (d, J=5.22Hz, 1H, H_4), δ5.55 (d, J= 5.23Hz, 1H, H_3), δ6.62-7.35, (m, 10H, H_2' H_6' H_2'' H_3'' H_4'' H_5'' H_6'' H_2''' H_5''' H_6'''). *Trans isomer* δ3.73, (s, 6H, -OMe), δ3.79 (s, 3H, -OMe), δ3.94 (s, 3H, -OMe), δ4.92 (d, J=2.03Hz, 1H, H_4), δ5.12 (d, J=2.03Hz, 1H, H_3), δ6.57-7.64 (m, 11H, H_2' H_6' H_2'' H_3'' H_4'' H_5'' H_6'' H_2''' H_5''' H_6''')

^{13}C NMR (100 MHz, $CDCl_3$): *Cis isomer*: δ55.68, δ55.76, δ60.52 (OMe), δ60.89 (C4), δ80.54 (C3), δ94.78 (C2'&C6'), δ111.13 (C3'''), δ111.20 (C5'''), δ115.17 (C2''&C6''), δ121.95 (C4''), δ125.62 (C6'''), δ127.94 (C4'), δ128.95 (C3''&C5''), δ132.43 (C2'''), δ132.62 (C1'''), δ134.62 (C1'), δ153.14 (C3'&C5'), δ155.73 (C1''), δ156.31 (C4'''), δ162.33 (C2). *Trans isomer*: δ55.63, δ55.93, δ60.50 (OMe), δ62.78 (C4), δ86.68 (C3), δ94.85 (C2'&C6'), δ111.99 (C3'''), δ112.26 (C5'''), δ114.95 (C2''&C6''), δ120.01 (C4''), δ126.29 (C6'''), δ128.55 (C4'), δ129.27 (C3''&C5''), δ131.02 (C2'''), δ132.40 (C1'''), δ134.67 (C1'), δ153.11 (C3'&C5'), δ156.13 (C1''), δ156.45 (C4'''), δ161.88 (C2)

HRMS: $C_{25}H_{24}BrNO_6$

Cis isomer requires M^+Na (m/e) 536.0685, found (m/e) 536.0701 (3.0ppm)

Trans isomer requires M^+Na (m/e) 536.0685, found (m/e) 536.0676 (-1.6ppm)

4-(3-Fluoro-4-methoxy-phenyl)-3-phenoxy-1-(3,4,5-trimethoxy-phenyl)-azetidin-2-one **(249)**

Yield: 56%, 1.27g, white solid

MP: 120 °C

IR (KBr ν max): 1752 cm^{-1} (C=O)

^{1}H NMR (400MHz, $CDCl_3$): δ3.75 (s, 6H –OMe), δ3.86 (s, 3H –OMe), δ3.86 (s, 3H –OMe), δ5.30 (d, 1H, H_4 J=5.01Hz), δ5.52 (d, 1H, H_3, Jcis=5.01Hz), δ6.6-7.1 (m ,10H, H_2' H_6' H_2'' H_3'' H_4'' H_5'' H_6'' H_2''' H_5''' H_6''')

^{13}C NMR (100 MHz, $CDCl_3$): δ55.49 δ60.28 (OMe), δ61.49 (C4), δ80.29 (C3), δ94.52 (C2'&C5'), δ112.73 (C2''&C5''), δ115.83 (C2'''), δ115.49 (C5'''), δ121.19 (C4''), δ113.25 (C6'''), δ125.66 (C4'), δ129.57 (C3''&C5'', δ132.59 (C1'''), δ134.83 (C1'), δ147.21 (C3'''&C5'''), δ153.85 (C3'&C5'), δ156.59 (C1''), δ162.01 (C2)

HRMS: $C_{25}H_{24}FNO_6$ $2M^+$+Na requires (m/e) 929.3057, found 929.3073 (1.7ppm)

4-[4-Oxo-3-phenoxy-1-(3,4,5-trimethoxy-phenyl)-azetidin-2-yl]-benzonitrile **(250)**

Yield: 37% *cis*, 0.80g, off white solid, 24% *trans*, 0.52g, off white solid

MP: 174 °C cis, 162 °C trans

IR (KBr ν max): 1765 cm^{-1} (C=O), 2237 cm^{-1} (CN) *Trans* 1760 cm^{-1} (C=O), 2227 cm^{-1} (CN)

^{1}H NMR (400MHz, $CDCl_3$): : *Cis isomer* δ3.75 (s, 6H, -OMe), δ3.80 (s, 3H, -OMe), δ5.44 (d, J =5.01, 1H, H4), δ5.64 (d, J = 5.01 , 1H, H3), δ6.56-7.63 (m, 11H, φ-H) *Trans isomer* δ3.72 (s, 6H, -OMe), δ3.79 (s, 3H, -OMe), δ5.08 (d, J=1.52Hz, 1H, H_4), δ5.12 (d, J=1.52, 1H, H_3), δ6.50 (s, 2H, H_2'&H_6'), δ6.88-7.76 (m, 9H, H_2'' H_3'' H_4'' H_5'' H_6'' H_2''' H_3''' H_5''' H_6''')

^{13}C NMR (100 MHz, $CDCl_3$): *Cis isomer:* δ55.69, δ60.52 (OMe), δ61.03 (C_4), δ80.52 (C_3), δ94.68 (C_2'&C_6'), δ112.31 (C_4''), δ114.95 (C_2'&C_6'), δ117.86 (CN), δ122.21 (C_4''), δ128.29 (C_2'''&C_6'''), δ129.05 (C_3''&C_5''), δ131.78 (C_3'''&C_5'''), δ132.11 (C_4'), δ135.05 (C_1'), δ137.93 (C_1'''), δ153.27 (C_3'&C_5'), δ155.95 (C_1''), δ161.89 (C_2). *Trans Isomer:* δ55.65, δ60.52 (OMe), δ63.03 (C_4), δ86.64 (C_3), δ94.78 (C_2'&C_6'), δ112.86 (C_4'''), δ115.01 (C_2''&C_6''), δ117.57 (CN), δ122.37 (C_4''), δ126.71 (C_2'''&C_6'''), δ129.36 (C_3''&C_5''), δ132.02 (C_4'), δ132.82 (C_3'''&C_5'''), δ134.91 (C_1'), δ140.56 (C_1'''), δ153.25 (C_3'&C_5'), δ156.27 (C_1''), δ161.45 (C_2)

HRMS: $C_{25}H_{22}N_2O_5$

Trans isomer M^++Na requires (m/e) 453.1426, found (m/e) 453.1435

Cis isomer M^++Na requires (m/e) 453.1426, found (m/e) 453.1427 (0.2ppm).

4-(4-Methoxy-3-nitro-phenyl)-3-phenoxy-1-(3,4,5-trimethoxy-phenyl)-azetidin-2-one **(251)**

Yield: 52% *cis*, 1.25g, pale brown solid, 26% *trans*, 0.62g, pale brown solid

MP: *Cis* 136-138 °C, *trans* 160°C

IR (KBr ν max): *Cis* 1758 cm^{-1} (C=O) *Trans* 1753 cm^{-1} (C=O)

^{1}H NMR (400MHz, $CDCl_3$): *Cis isomer* δ3.76 (s, 3H –OMe), δ3.79 6H (s –OMe), δ3.93 (s, 3H –OMe), δ5.41 (d, 1H, H_4, J=5.06Hz), δ5.60 (d, 1H, H_3 J=5.06), δ6.59 (s, 2H, H_2' H_6'), δ7.23 -7.92 (m, 8H, H_2'' H_3'' H_4'' H_5'' H_6'' H_2'' H_5'' H_6'') *Trans isomer* δ3.76 (s, 6H –OMe), δ3.80 (3H, s –OMe), δ4.02 (s, 3H –OMe), δ5.03 (d, 1H, H_4, J=1.40Hz), δ5.14 (d, 1H, H_3 J=1.50Hz), δ6.61 (s, 2H, H_2' H_6'), δ7.28-7.92 (m, 8H, H_2'' H_3'' H_4'' H_5'' H_6'' H_2''' H_5''' H_6''').

^{13}C NMR (100 MHz, $CDCl_3$): *Cis isomer* δ55.72, δ56.15, δ60.30 (OMe), δ60.30 (C4), δ80.38 (C3), δ94.73 C2'&C6'), δ113.28 (C5'''), δ114.95 (C2''&C6''), δ122.16 (C4''), δ124.72 (C2''), δ125.34 (C4'), δ129.08 (C3''&C5'), δ132.17 (C5'''), δ133.17 (C3'''), δ134.80 (C1'''), δ138.68 (C1'), δ152.83 (C3'&C5'), δ153.24 (C1''), δ156.00 (C4'''), δ162.05 (C2)

Trans isomer δ55.69, δ56.33, δ60.51 (OMe), δ62.26 (C4), δ86.61 (C3), δ94.87 (C2'&C6'), δ114.25 (C5'''), δ114.97 (C2''&C6''), δ122.26 (C4''), δ123.60 (C2''), δ127.49 (C4'), δ129.37 (C3''&C5'), δ131.30 (C5'''), δ132.01 (C3'''), δ134.85 (C1'''), δ139.48 (C1'), δ152.97 (C3'&C5'), δ153.24 (C1''), δ156.31 (C4'''), δ161.64 (C2)

HRMS: $C_{25}H_{24}N_2O_8$

Cis isomer: M^++Na requires (m/e) 503.1430, found (m/e) 503.1433 (0.6ppm).

Trans isomer: M^++Na requires (m/e) 503.1430, found (m/e) 503.1418 (-2.4ppm)

4-Naphthalen-2-yl-3-phenoxy-1-(3,4,5-trimethoxy-phenyl)-azetidin-2-one **(252)**

Yield: 42%, 0.96g, white solid

MP: 162 °C

IR (KBr ν max): 1746 cm^{-1}(C=O)

^{1}H NMR (400MHz, $CDCl_3$): δ3.71 (s, 6H, -OMe), δ3.78 (s, 3H, -OMe), δ5.57 (d, J=5.23Hz, 1H, H_4), δ5.67 (d, J=5.23Hz 1H, H_3), δ6.68-7.81 (m, 14H, Ar-H)

^{13}C NMR (100 MHz, $CDCl_3$): δ55.51 (OMe), δ60.49 (OMe), δ62.09 (C4), δ80.88 (C3), δ94.82 (C2'&C6'), δ115.26 (C2''&C5''), δ121.85 (C4''), δ124.80 (C6'''), δ125.92 (C5'''), δ127.32 (C4'), δ127.40 (C2'''), δ127.87 (C4'''), δ128.85 (C10'''&C9'''&C7'''), δ129.96 (C3''&C5''), δ132.57 (C3'''&C8'''), δ132.70 (C1'''), δ134.52 (C1'), δ153.11 (C3'&C5'), δ156.52 (C1''), δ162.70 (C2)

HRMS: $C_{28}H_{25}NO_5$ M^++Na requires (m/e) 478.1630, found (m/e) 478.1647 (3.6ppm)

4-(3,4-Dimethoxy-phenyl)-3-phenoxy-1-(3,4,5-trimethoxy-phenyl)-azetidin-2-one **(253)**

Yield: 56%, 1.30g, white solid

MP: 152 °C

IR (KBr ν max): 1751 cm^{-1} (C=O)

^{1}H NMR (400MHz, $CDCl_3$): δ3.75 (s, 6H –OMe), δ3.79 (s, 6H –OMe), δ3.85 (s, 3H–OMe), δ5.33 (d, 1H, H_4, J=5.00Hz), δ5.58 (d, 1H, H_3, J= 4.52Hz), δ6.66-6.99 (10H, H_2' H_6' H_2'' H_3'' H_4'' H_5'' H_6'' H_2''' H_5''' H_6''')

^{13}C: δ55.07, δ55.94, δ60.28 (OMe), δ62.55 (C4), δ80.24 (C3), δ95.94 (C2'&C6'), δ110.88 (C2'''&C5'''), δ115.38 (C2''&C6''), δ120.12 (C4''), δ122.42 (C6'''), δ124.74 C4'), δ129.67 (C3''&C5''), δ133.25 (C1'''), δ134.16 (C1'), δ148.92 (C3'&C5'), δ156.43 (C1''), δ162.07 (C2)

HRMS: $C_{26}H_{27}NO_7$

M^++Na requires (m/e) 488.1685, found (m/e) 488.1697 (2.5ppm)

4-Naphthalen-1-yl-3-phenoxy-1-(3,4,5-trimethoxy-phenyl)-azetidin-2-one **(254)**

Yield: 98%, 2.23g, off white solid

MP: 182-186 °C

IR (KBr ν max):1757 cm^{-1} (C=O)

^{1}H NMR (400MHz, $CDCl_3$): : δ3.70 (s, 6H, -OMe), δ3.84 (s, 3H, -OMe), δ5.77 (d, 1H, H4), δ6.17 (d, 1H, H3), δ6.68-7.85, (m, 14H, Ar-H)

^{13}C NMR (100 MHz, $CDCl_3$): δ55.69 (OMe), δ60.55 (C4) δ81.67 (C3), δ94.83 (C2'&C6'), δ116.09 (C2''&C6''), δ121.92 (C4'), δ124.89 (C4'''&C5'''), δ125.35 (C2'''), δ125.97 (C10'''&C9'''&C8'''), δ127.67 (C4'), δ127.76 (C6'''&C3'''), δ128.64 (C3''&C5''), δ130.85 (C2'''), δ132.92 132.92 (C7'''), δ133.17 (C1'''), δ134.25 (C1'), δ153.20 (C3'&C5'), δ156.98 (C1''), δ163.28 (C2)

HRMS: $C_{28}H_{25}NO_5$ M^++Na requires (m/e) 478.1630, found (m/e) 478.1631 (0.2ppm).

4-(4-Dimethylamino-phenyl)-3-phenoxy-1-(3,4,5-trimehtoxy-phenyl)-azetidin-2-one (**255**)

Yield: 34%, 0.76g, pale brown solid

MP: 166 °C

IR (KBr ν max): 1744 cm^{-1} (C=O)

^{1}H NMR (400MHz, $CDCl_3$): δ2.92 (s, 6H, N-(CH_3)$_2$), δ3.72 (s, 6H –OMe), δ3.74 (s, 3H –OMe), δ5.32 (d, 1H, H_4, J=5.11), δ5.51 (d, 1H, H_3, J=5.11), δ6.62 (s, 2H, H_2' H_6'), δ6.87-7.11 (9H, m, H_2'' H_3'' H_4'' H_5'' H_6'' H_2''' H_3''' H_5''' H_6''')

^{13}C NMR (100 MHz, $CDCl_3$): δ40.45 (N-(CH3)2), δ55.06 δ60.94 (OMe), δ62.71 (C4), δ81.74 (C3), δ97.93 (C2'&C6'), δ111.37 (C3'''&C5'''), δ114.86 (C2''&C6''), δ119.37 (C4''), δ121.65 (C4'), δ128.11 (C3''&C5''), δ129.31 (C2''&C6''), δ132.53 (C1'''), δ134.71 (C1'), δ150.51 (C3'&C5'), δ152.39 (C4'''), δ156.59 (C1''), δ162.99 (C2).

HRMS: $C_{26}H_{28}N_2O_5$ M^+ requires (m/e) 449.2096, found (m/e) 449.2076 (-4.5ppm)

5.5 Synthesis of Silyl Ether Protected β-Lactams

To a stirring, refluxing solution of the protected imine (**208-211**) (5mmol) and triethylamine (6mmol) in anhydrous dichloromethane (40mL), a solution of the appropiate acid chloride (6mmol) in anhydrous dichloromethane (10mL) was added over 45 minutes under nitrogen. The reaction was kept at reflux during the day (8 hours) and at room temperature overnight (16 hours), continuously under nitrogen, until the starting material had disappeared as monitored by TLC in 50:50 hexane:ethyl acetate (total reaction time of 48–96 hours). A characteristic darkening of the reaction over time was observed. The reaction was transferred to a separating funnel and washed with water (2 x 100mL), with the organic layer being retained each time. The reaction was dried over Na_2SO_4 before the solvent was removed under reduced pressure and the silyl ether β-lactam isolated by flash chromatography over silica gel eluted with 1:1 *n*-hexane:ethyl acetate. The first silyl ether was characterised fully and subsequent silyl ether β-lactams were directly deprotected to yield the free phenols as follows. To a stirring solution of the sily ether β-lactam (2mmol) under N_2 and at 0^0C in dry THF was added dropwise 1.0 M t-BAF solution in hexanes (2mL, 2mmol). The resulting solution was left to stir at 0^0C until reaction was complete as seen on TLC. Reaction was diluted with ethyl acetate (75mL) and washed with 0.1M HCL_{aq} (100mL). The aqueous layer was further extracted with ethyl acetate (2x25mL). All the organic layers were collected and washed with H_2O (100mL), and saturated brine (100mL) before being dried over Na_2SO_4. Solvent was removed under reduced pressure to yield the free phenol.

4-[3-(t-Butyl-dimethyl-silanyloxy)-4-methoxy-phenyl]-3-phenoxy-1-(3,4,5-trimethoxy-phenyl)-azetidin-2-one

Yield: *Cis* 61%, 1.73g, white resin *Trans* 21%, 0.59g white resin

IR (KBr ν max): 1729 cm^{-1}(C=O)

MP: Resin

^{1}H: *Cis isomer* δ0.04 (6H, s, -tBDMSi), δ0.91 (9H, s, -tBDMSi), δ3.72 (3H, s, -OMe), δ3.74 (6H, s, -OMe), δ3.91 (3H, s, -OMe), δ5.28 (1H, d J=4.52 Hz, H_4), δ5.52 (1H, d, J=5Hz, H_3), δ6.64-6.89 (10H, m, φ-H)

Trans isomer δ0.02 (6H, s, -tBDMSi), δ1.02 (9H, s, -tBDMSi), δ3.75 (3H, s, -OMe), δ3.77 (6H, s, -OMe), δ3.92 (3H, s, -OMe), δ4.89 (1H, d J=1.52Hz, H_4), δ5.10 (1H, d J=1.5Hz, H_3), δ6.58-6.87 (10H, m, φ-H)

^{13}C NMR (100 MHz, $CDCl_3$): *Cis isomer* δ-4.20, δ-4.16, δ17.88, δ23.48 (OtBDMS) δ55.43, δ55.73, δ60.59 (OMe), δ61.89 (C_4), δ81.06 (C_3), δ94.87 (C_2'&C_6'), δ113.59(C_5'''), δ114.51 (C_2''&C_6''), δ117.44 (C_2'''), δ119.41 (C_4''), δ120.27 (C_6'''), δ125.12 (C_3'' C_5''), δ128.02 (C_4'), δ132.39 (C_1'), δ137.83 (C_1'''), δ142.02 (C_3'''), δ148.27(C_3'C_5'), δ151.15 (C_4'''), δ156.69 (C_1''), δ162.67 (C_2)

Trans isomer δ-4.22, δ-4.18, δ17.56, δ24.09, δ54.82, δ54.95, δ59.22 (OMe), δ62.32 (C_4), δ82.56 (C_3), δ95.17 (C_2'&C_6'), δ111.38 (C_2''&C_6''), δ114.18 (C_5'''), δ117.58 (C_2'''), δ119.79 (C_4''), δ120.39 (C_6'''), δ128.22 (C_4'), δ131.35 (C_3''&C_5''), δ132.29 (C_1'), δ138.28 (C_1'''), δ143.11 (C_3'''), δ149.67 (C_4'''), δ149.99 (C_3'&C_5'), δ157.32 (C_1''), δ161.07 (C_2)

HRMS: $C_{31}H_{39}NO_7Si$ M^++Na requires 588.2393, found 588.2402 (1.5ppm)

4-(3-Hydroxy-4-methoxy-phenyl)-3-phenoxy-1-(3,4,5-trimethoxy-phenyl)-azetidin-2-one (**256**)

Yield: Method A 73%, 1.65g, Method C 53%, 0.13g Method D 0% Method B 32%, 0.14g white solid

MP: 176-180 °C

IR (KBr ν max): 1739 cm^{-1} (C=O), 3401 cm^{-1} (-OH) 1737 cm^{-1}(C=O), 3498 cm^{-1}(OH)

^{1}H NMR (400MHz, $CDCl_3$): *Trans* δ3.65 (s, 3H, OMe), δ3.70 (s, 6H, OMe), δ3.88 (s, 3H, OMe), δ5.10 (d, J=1.52Hz, 1H, H_4), δ5.35 (d, J=1.52, 1H, H_3), δ6.70 (s, 2H, C_2'&C_6'), δ6.92-7.31 (m, 8H, Ar-H), δ7.87 (s, 1H, OH)

Cis δ3.74 (s, 6H, OMe), δ3.79 (s, 3H, OMe), δ3.86 (s, 3H, OMe), δ5.29 (d, J=5.0Hz, 1H, H_4), δ5.53 (d, J=5.0Hz, 1H, H_3), δ6.65 (s, 2H, H_2'&H_6'), δ6.78-7.21 (m, 8H, H_2'' H_3'' H_4'' H_5'' H_6'' H_2''' H_5''' H_6''')

^{13}C: *Cis isomer* δ55.40, δ55.64, δ60.50 (OMe), δ61.64 (C_4), δ80.72 (C_3), δ94.84 (C_2'&C_6'), δ109.94 (C_2''&C_6''), δ113.90 (C_2'''), δ115.34 (C_5'''), δ119.68 (C_4''), δ121.75 (C_6'''), δ125.12 (C_4'), δ128.84 (C_3''&C_5''), δ132.67 (C_1'), δ145.10 (C_1'), δ145.12 (C_1'''), δ146.42 (C_4'''), δ153.05 (C_3'&C_5'), δ156.64 (C_1''), δ162.54 (C_2)

Trans isomer δ54.88, δ54.94, δ59.21 (OMe), δ63.01 (C_4), δ86.47 (C_3), δ95.15 (C_2'&C_6'), δ111.31 (C_2''&C_6''), δ112.93 (C_2'''), δ114.90 (C_5'''), δ118.29 (C_4''), δ121.61 (C_6'''), δ128.23 (C_4'), δ129.13 (C_3''&C_5''), δ132.73 (C_1'), δ134.23 (C_1'''), δ146.81 (C_3'''), δ147.74 (C_4'''), δ153.26 (C_3'&C_5'), δ156.85 (C_1''), δ161.61 (C_2)

HRMS: $C_{25}H_{25}NO_7$

Cis isomer M^++Na requires (m/e) 474.1529, found (m/e) 474.1529 (0ppm)

Trans isomer M^++Na requires 474.1526, found 474.1533 (0.9ppm)

4-(4-Hydroxy-phenyl)-3-phenoxy-1-(3,4,5-trimethoxy-phenyl-azetidin-2-one **(257)**

Yield: 40%, 0.84g, white solid

MP: 142 °C

IR (KBr ν max): 1741 cm^{-1} (C=O), 3287 cm^{-1} (-OH)

^{1}H NMR (400MHz, $CDCl_3$): δ3.72 (s, 6H, OMe), δ3.80 (s, 3H, OMe), δ5.27 (d, J=4.76Hz, 1H, H_4), δ5.54,(d, J=5.0Hz, 1H, H_3), δ6.66 (s, 2H, H_2'&H_6'), δ6.73-7.18 (9H, H_2'' H_3'' H_4'' H_5'' H_6'' H_2''' H_3''' H_5''' H_6''')

^{13}C NMR (100 MHz, $CDCl_3$): δ56.07, δ60.98 (OMe), δ62.44 (C_4), δ81.17 (C_3), δ95.30 (C_2'&C_6'), δ114.30 (C_2''&C_6''), δ115.75 (C_3'''&C_5'''), δ118.69 (C_4''), δ122.28 (C_2'''&C_6'''), δ129.30 (C_3''&C_5''), δ133.17 (C_4'), δ133.78 (C_1'), δ134.90 (C_1'''), δ146.57 (C_3'&C_5'), δ153.53 (C_4'''), δ157.12 (C_1''), δ163.07 (C_2)

HRMS: $C_{24}H_{23}NO_6$ M^++Na requires (m/e) 444.1423, found (m/e) 444.1432 (2.0ppm)

4-(4-Hydroxy-3-methoxy-phenyl)-3-phenoxy-1-(3,4,5-trimethoxy-phenyl)-azetidin-2-one **(258)**

Obtained as an inseperable mixture of isomers in 2:1 trans: cis ratio

Yield: 57%, 1.29g, white solid

MP: 158 °C

IR (KBr ν max): 1757 cm^{-1} (C=O), 3415 cm^{-1} (-OH)

^{1}H NMR (400MHz, $CDCl_3$): δ3.75 (s, 6H, OMe), δ3.80 (s, 3H, OMe), δ3.85 (s, 3H, OMe), δ4.64 (d, J=1.8Hz, 0.66H, H_4), δ4.87 (d, J=1.8Hz, 0.66H, H_3), δ5.40 (d, J=5.0Hz, 0.33H, H_4), δ5.60 (d, J=5.0Hz, 0.33H, H_3), δ6.61-7.42 (m, 10H, Ar-H)

^{13}C NMR (100 MHz, $CDCl_3$): δ56.11, δ56.20, δ61.7 (OMe), δ60.99 (C_4), δ81.07 (C_3), δ95.30, δ97.88 (C_2'&C_6'), δ114.71 & δ114.91 (C_2''&C_6''), δ115.66 (C_2'''), δ121.48 (C_5'''), δ122.11 (C_4''), δ122.44 & δ122.57 (C_6'''), δ129.34 (C_3''&C_5''), δ130.73 (C_4'), δ132.86 & δ132.89 (C_1'), δ134.8 (C_1'''), δ153.42, δ153.62 (C_4'''), δ156.76, δ156.99 (C_3'''), δ157.81 (C_3''&C_5''), δ162.80 (C_1''), δ166.27, δ167.24 (C_2)

HRMS: $C_{25}H_{25}NO_7$ M^++Na requires (m/e) 474.1529, found (m/e) 474.1528 (-0.2ppm)

4-(3,4-Dihdroxy-phenyl)-3-phenoxy-1-(3,4,5-trimethoxy-phenyl)-azetidin-2- one

(259)

Yield: 26%, 0.57g, off white solid

MP: 180-182 °C

IR (KBr ν max): 1749 cm^{-1} (C=O), 3426 cm^{-1} (-OH)

^{1}H NMR (400MHz, $CDCl_3$): δ3.67 (overlapping singlets, 9H, OMe), δ3.71 (overlapping singlets, 6H, OMe), δ4.88 (d, J= 2.0Hz, 0.65H, H_4), δ5.09 (d, J=2.0Hz, 0.65H, H_3), δ5.28 (d, J=4.92, 0.35H, H_4), δ5.52 (d, J=4.92Hz, 0.35H, H_3), δ5.69 (br, s, 0.4H, OH), δ5.88 (br, s, 0.6H, OH), δ6.53-7.24 (m, 10H, Ar-H)

^{13}C: δ55.51, δ55.57, δ60.53, δ63.85 (OMe), δ62.18 (C_4), δ80.78 (C_3), δ94.90, δ94,95 (C_2'&C_6'), δ112.14 (C_2''&C_6''), δ114.06, δ114.61 (C_2'''), δ115.835, δ115.39 (C_5'''), δ119.32 (C_4''), δ120.95, δ121.91 (C_6'''), δ127.32 (C_4'), δ128.89, δ129.23 (C_3''&C_5''), δ132.44, δ132.55 (C_1'''), δ134.40 (C_1'), δ143.46 (C_4'''), δ144.34, δ144.43 (C_3'''), δ152.98, δ153.05 (C_3'&C_5'), δ156.41, δ156.49 (C_1''), δ162.45 (C_2)

HRMS: $C_{24}H_{23}NO_7$ M^++Na requires (m/e) 460.1372, found (m/e) 460.1367 (-1.1ppm)

5.6 MCPBA Oxidation of Sulphur

Oxidation to the Sulfoxide

To a stirring solution of the *cis* β-lactam (**247**) (0.25mmol) in 10mL dry DCM was added *m*CPBA (0.25mmol) in 10mL dry DCM dropwise under N2 and left to stir for 2 hours. The reaction was washed with 50mL each of 5% NaHCO3 aq and H_2O, organic layer collected, dried over Na2SO4, filtered, and solvent removed under reduced pressure. Chromatography on silica gel eluted with 9:1 ethyl acetate: *n*-hexane) yielded the title compound.

4-(4-Methanesulfinyl-phenyl)-3-phenoxy-1-(3,4,5-trimethoxy-phenyl-azetidin-2-one **(262)**

Yield: 63%, 74mg, pale brown solid

MP: 156 °C

IR (KBr ϒ max): 1749 cm^{-1} (C=O) 1051cm^{-1} (S-O)

^{1}H NMR (400MHz, $CDCl_3$): ($CDCl_3$): δ2.65 (pair of singlets, 3H, S(O)CH_3), δ3.71 (s, 6H, -OMe), δ3.77 (s, 3H, -OMe), δ5.44 (d, J=5.11 1H, H_4), δ5.62 (dd, J=5.11HZ, 5.01Hz 1H, H_3), δ6.57 (s, 2H, H_2' H_6'), δ6.74 (m, 2H, H_2'' H_6''), δ6.89 (t, J=2.14Hz, 8.18Hz, 1H, H_4''), δ7.13 (t, J=1.98Hz, δ7.97Hz, 2H, H_3'' H_5''), δ7.55 (m, 4H, H_2''' H_3''' H_5''' H_6''')

^{1}H NMR (400MHz, DMSO) δ2.65 & 2.66 (pair of singlets, 3H, S(O)CH_3), δ3.60 (s, 6H, OMe), δ3.66 (s, 3H, OMe), δ5.84 (d, J=4.74Hz, 1H, H_4), δ5.97 (d, J=4.74Hz, H_3), δ6.62 (s, 2H, H_2'&H_6') δ6.82 (dd, J=2.15, 9.10Hz, 2H, H_2''&H_6''), δ6.91-6.94 (m, 1H, H_4''), δ7.19-7.21 (m, 2H, H_3''&H_5''), δ7.60 (d, J=8.32Hz, 2H H_2''' H_6'''), δ7.89 (d, J=8.29, 2H, H_3''' H_5''')

^{13}C NMR (100 MHz, $CDCl_3$): ($CDCL_3$): δ43.37, δ43.79 (S(O)-CH3), δ56.10 (OMe), δ60.89 (OMe), δ60.89, δ61.58 (C4), δ80.89, δ80.94 (C3), δ95.28, δ95.32 (C2'&C6'), δ115.45, δ115.46 (C2''&C6''), δ122.43, δ122.45 (C4''), δ123.59 (C3'''&C5'''), δ129.04 (C2'''&C6'''), δ128.92 (C3''&C5''), δ132.68 (C4'), δ135.32 (C1'), δ136.18 (C4'''), δ146.55, δ146.57 (C1'''), δ153.65 (C3'&C5'), δ156.50 (C1''), δ162.45

162.49 (C2)

^{13}C NMR (100 MHz, $CDCl_3$): (DMSO): δ43.35 & δ43.37 (S(O)$\underline{C}H_3$), δ56.20 (OMe), δ60.45 (OMe), δ60.84 (C4), δ80.72 (C3), δ95.60 (C2'&C6'), δ115.46 (C2''&C6''), δ122.30 (C4''), δ123.75 (C3'''&C5'''), δ129.35 (C2'''&C6'''), δ129.70 (C3''&C5''), δ132.87 (C4'), δ134.83 (C1'), δ136.46 (C4'''), δ146.82 (C1'''), δ153.61 (C3'&C5'), δ156.54 (C1''), δ162.86 (C_2)

HRMS $C_{25}H_{25}NO_6$ M^++Na requires 490.1300, found 490.1280 (-4.1ppm)

Oxidation to the Sulfone

To a stirring solution of the β-lactam (**247**) (0.25mmol) in 10mL dry DCM was added MCPBA (0.66mmol) as a solid under N_2 and left to stir for 30 minutes. The reaction was washed with 50mL each of 5% $NaHCO_3$ aq and H2O, organic layer collected, dried over Na_2SO_4, filtered, and solvent removed under reduced pressure. Chromatography over silica gel (7:3 ethyl acetate:*n*-hexane) yielded the title compound.

4-(4-Methanesulfonyl-phenyl)-3-phenoxy-1-(3,4,5-trimethoxy-phenyl)-azetidin-2-one **(263)**

Yield: 66%, 80mg, pale brown solid

MP: 160-162 °C

IR (KBr ν max): 1750 cm^{-1} (C=O) 1307 cm^{-1} 1221 cm^{-1} (S-O)

^{1}H NMR (400MHz, $CDCl_3$): δ3.04 (s, 3H, S(O2)CH3), δ3.77 (s, 6H, -OMe), δ3.81 (s, 3H, -OMe), δ5.49 (d, 1H, H_4), δ5.67 (d, 1H, H_3), δ6.59 (s, 2H, H_2' H_6'), δ6.81 (d, J=8.25Hz, H_2'' H_6''), δ6.96 (t, J=8.15Hz 2.10Hz, 1H, H_4''), δ7.20 (t, J=8.07Hz, 1.96Hz, 2H, H_3'' H_5''), δ7.62 (d, J=7.98Hz, 2H H_2''' H_6'''), δ7.92 (d, J=8.03Hz, 2H, H_3''' H_5''')

^{13}C: δ43.92 (S(O2)CH3), δ57.75 (OMe), δ60.54 (OMe), δ60.89 (C_4), δ80.55 (C_3), δ94.75 (C_2'&C_6'), δ115.03 (C_2''&C_6''), δ122.20 (C_4''), δ127.06 (C_3'''&C_5'''), δ128.58 (C_2'''&C_6'''), δ129.01 (C_3'''&C_5'''), δ132.01 (C_4'), δ134.92 (C_1'), δ138.89 (C_4'''), δ140.45 (C_1'''), δ153.29 (C_3'&C_5'), δ155.99 (C_1''), δ161.94 (C_2)

HRMS: $C_{25}H_{25}NO_7S$ M^++Na requires (m/e) 506.1249, found (m/e) 506.1262 (2.6ppm)

5.7 Reduction of Nitro Derivatives

To a flask containing the *cis* (**264a**) or *trans* (**264b**) β-lactam (0.25mmol, 123mg) and zinc powder 10μm (2.5mmol 165mg) was added 15mL of acetic acid at room temperature under N_2 and reaction left to stir for 7 days. The reaction was filtered through a celite pad and the filtrate collected. Solvent was removed under reduced pressure and purified by flash chromatography over silica gel eluted with 1:1 ethyl acetate:*n*-hexane carried out to yield the title compound.

4-(3-Amino-4-methoxy-phenyl)-3-phenoxy-1-(3,4,5-trimethoxy-phenyl)-azetidin-2-one **(264)**

Yield: 83% cis, 93mg, pale brown solid 94%trans, 106mg, pale brown solid

MP: 158 °C cis, 128-130 °C trans

IR (KBr ϒ max): *Cis* 1754 cm^{-1} (C=O) 3368 cm^{-1} (NH_2), *trans* 1756 cm^{-1} (C=O), 3465 cm^{-1} (NH_2)

^{1}H NMR (400MHz, $CDCl_3$): *Cis isomer* δ3.74 (s, 6H, -OMe), δ3.78 (s, 3H, -OMe), δ3.81 (s, 3H, -OMe), δ5.23 (d, J=5.12Hz, 1H, H_4), δ5.49 (d, J=4.40., 1H, H_3), δ6.65- δ6.98 (m, 8H, H_2' H_6' H_2'' H_4'' H_6'' H_2''' H_5''' H_6'''), δ7.22-7.27 (m, 2H, H_3'' H_5'')

Trans isomer δ3.73 (s, 6H, -OMe), δ3.78, (s, 3H, -OMe), δ3.90 (s, 3H, -OMe), δ3.93 (br s, 2H, -NH_2), δ4.85 (d, J=1.52 Hz., 1H, H_4), δ5.12 (d, J=1.48., 1H, H_3), δ6.62 (s, 2H, H_2' H_6') δ6.71- 6.81 (m, 5H, H_2'' H_6'' H_2''' H_5''' H_6'''), δ7.08 (t, J=2.12Hz, 8.19Hz, 1H, H_4''), δ7.24- 7.29 (m, 2H, H_3'' H_5'')

^{13}C: Trans isomer: δ55.12, δ55.57, δ60.49 (OMe), δ63.91 (C4), δ86.64 (C3), δ94.84 (C2'&C6'), δ110.07 (C2''), δ111.34 (C5''), δ114.96 (C2''&C6''), δ116.52 (C6'''), δ121.72 (C4''), δ127.53 (C3'''), δ129.17 (C3''&C5''), δ132.86 (C4'), δ134.34 (C1'''), δ136.73 (C1'), δ147.40 (C3'&C5'), δ152.98 (C4'''), δ156.60 (C1''), δ162.22 (C2)

Cis isomer: δ54.94, δ55.61, δ60.49 (OMe), δ61.92 (C4), δ80.79 (C3), δ94.85 (C2'&C6'), δ109.43 (C2''), δ113.74 (C5''), δ115.47 (C2''&C6''), δ118.25 (C6'''), δ121.72 (C4''), δ124.49 (C3'''), δ128.81 (C3''&C5''), δ132.79 (C4'), δ134.53 (C1'''), δ135.76 (C1'), δ147.23 (C3'&C5'), δ153.02 (C4'''), δ156.76 (C1''), δ162.73 (C2)

HRMS: $C_{25}H_{26}N_2O_6$ (Cis isomer) M^++Na calculated 473.1689, found 473.1685 (-0.8ppm)

Trans isomer M^++Na requires 473.1689, found 473.1681, (-1.6ppm)

5.8 Chlorambucil Coupling

Chlorambucil (0.5 mmol), EDCL (0.7 mmol), and DMAP (0.07) were dissolved together in 35 mL dry DCM under N2 and stirred at room temperature for 10 minutes. To this stirring solution the β-lactam (**256a** or **264a**) (0.5mmol) in 6 mL dry DCM was added dropwise under N_2 via syringe and the reaction left to stir under N2 overnight. The reaction was diluted with 50 mL DCM washed with H_2O (100mL), saturated $NaHCO_3$ aq (100mL) and H2O (100mL), organic layer was collected and dried over Na_2SO_4, filtered and solvent removed under reduced pressure. Chromatography over silica gel eluted with 1:1 ethyl acetate:*n*-hexane) yielded the title compound.

4-{4-[Bis-(2-chloro-ethyl)-amino]-phenyl}-butyric acid 2-methoxy-4-[4-oxo-3-phenoxy-1-(3,4,5-trimethoxy-phenyl)-azetidin-2-yl]-phenyl ester **(265)**

Yield: 53%, 195mg, amber oil

MP: Oil

IR (NaCl ν max): 1003 cm^{-1} 1270 cm^{-1} (C-O stretch), 1760 cm^{-1} (C=O)

^{1}H NMR (400MHz, $CDCl_3$): δ2.00-2.07 (qt, J=7.51, 2H, H_6), δ2.56-2.60 (t, J=7.73, 2H, H_5), δ2.65-2.67 (t, J=7.73, 2H, H_7), δ3.63,-3.67 (overlapping triplets, 4H, H_{10} &H_{11}), δ3.71-3.76 (m, 10H, OMe & H_8 & H_9), δ3.80, (s, 3H, OMe), δ3.82 (s, 3H, OMe), δ5.31-5.32, (d, J=5.74Hz, 1H, H_4), δ5.56-5.57 (d, J=5.45Hz, H_3), δ6.64-7.28 (m, 14H, Ar-H)

^{13}C NMR (100 MHz, $CDCl_3$): δ26.42, δ32.77, δ33.32 (C_7, C_6, C_8), δ40.06 (C_{11}&C_{12}), δ53.01 & δ53.14 (C_9&C_{10}), δ55.41, δ55.65, δ60.50 (OMe), δ61.29 (C_4), δ80.65 (C_3), δ94.81 (C_2'&C_6'), δ111.71 (C_3'''' & C_5''''), δ115.39 (C_2''&C_6''), δ121.90 (C_1''''), δ122.56 (C_5'''), δ124.60 (C_4''), δ126.10 (C_2'''), δ128.93 (C_6'''), δ129.31 (C_2''''&C_6''''), δ129.33 (C_3''&C_5''), δ130.04 (C_4'), δ132.55 (C_1''), δ134.51 (C_1'), δ139.32 (C_3'''), δ143.91 (C_4''''), δ151.11 (C_3'&C_5'), δ153.11 (C_4'''), δ156.47 (C_1''), δ162.50 (C_5), δ170.75 (C_3)

HRMS $C_{39}H_{42}N_2O_8Cl_2$ M^+Na requires 759.2216, found 759.2203 (-1.7ppm)

4-{4-[Bis-(2-chloro-ethyl)-amino]-phenyl}-N-{2-methoxy-5-[4-oxo-3-phenoxy-1-(3,4,5-trimethoxy-phenyl)-azetidin-2-yl]-phenyl}-butyramide **(266)**

Yield: 38, 140mg, amber oil

MP: oil

IR (NaCl ν max): 1686 cm^{-1} (amide) 1755 cm^{-1} (β-lactam carbonyl)

^{1}H NMR (400MHz, $CDCl_3$): : δ2.04 (qn, J=6.31, 13.71Hz, 2H, H_6), δ2.41 (t, 2H, J=7.48, 15.21Hz, 2H, H_5), δ2.64 (t, J=7.64, 14.78, 2H, H_7), δ3.63-3.77 (m, 10H, H_7, H_8 -OMe), δ3.79 (s, 3H, OMe), δ3.88 (s, 3H, OMe), δ5.38 (d, J=4.99, 1H, H_4), δ5.54 (d, J=4.56, 1H, H_3), δ6.66-6.85 (m, 8H, H_2' H_6' H_2'' H_6'' H_5''' H_6''' H_3'''' H_5''''), δ7.11-7.20 (m, 5H, H_3'' H_4'' H_5'' H_2'''' H_6''''), δ7.72 (s, 1H, H_2'''), δ8.59 (s, 1H, N<u>H</u>-C=O)

^{13}C NMR (100 MHz, $CDCl_3$): δ26.65, δ33.46, δ36.65 (C_7, C_6, C_8), δ40.04 (C_{11}&C_{12}), δ53.11 & δ53.14 (C_9&C_{10}), δ55.26, δ55.70, δ60.49 (OMe), δ61.73 (C_4), δ80.75 (C_3), δ94.85 (C_2'&C_6'), δ109.52 (C_3'''' & C_5''''), δ111.72 (C_5'''), δ115.36 (C_2''&C_6''), δ119.75 (C_4''), δ121.69 (C_2'''), δ127.04 (C_6'''), δ128.86 (C_3'''), δ129.27 (C_4'), δ130.03 (C_1''''), δ132.47 (C_1''), δ132.64 (C_3''&C_5''), δ134.37 (C_2''''&C_6''''), δ143.91 (C_1'), δ144.09 (C_4''''), δ147.17 (C_1'''), δ151.23 (C_3'&C_5'), δ153.78 (C_4'''), δ156.81 (C_1''), δ162.59 (C_3), δ170.54 (C_5)

HRMS: $C_{39}H_{43}N_3O_7Cl_2$ M^++Na requires 758.2376, found 758.2350 (-3.4ppm)

5.9 Sulphurisation of β-Lactam Carbonyl

The *cis* β-lactam (**256a**) (0.25 mmol) and Lawesson's Reagent (112mg, 0.275mmol) were dissolved in dry toluene (3mL) under N_2, and the resulting solution brought to reflux for 12 hrs and left to stir at room temperature under N_2 overnight. Solvent was removed from the flask using N_2 and gentle heating. The resulting solid was purified by flash chromatography over silica gel eluted with 1:1 *n*-hexane/ethyl acetate), and product washed with *n*-hexane to remove the last traces of odour from the Lawesson's reagent.

4-(3-Hydroxy-4-methoxy-phenyl)-3-phenoxy-1-(3,4,5-trimethoxy-phenyl)-azetidine-2-thione **(267)**

Yield: 63%, 74mg, pale yellow solid

MP: 110 °C

IR (KBr ν max): 3336 cm^{-1} (OH)

H NMR (400MHz, $CDCl_3$): δ3.76 (s, 6H, OMe), δ3.81 (s, 3H, OMe), δ3.86 (s, 3H, OMe), δ5.32 (d, J=4.01Hz, 1H, H_4), δ5.61 (br, s, 1H, OH), δ5.78 (d, J=4.01Hz, 1H, H_3), δ6.77 (s, 2H, H_2' H_6') δ6.91-7.28 (m, 8H, H_2'' H_3'' H_4'' H_5'' H_6'' H_2''' H_5''' H_6''')

^{13}C NMR (100 MHz, $CDCl_3$): δ53.23, δ54.56, δ59.98 (OMe), δ69.78 (C_4), δ97.49 (C_3), δ99.67 (C_2'&C_6'), δ111.74 (C_2''&C_6''), δ114.98 (C_2'''), δ115.65 (C_5'''), δ119.75 (C_4''), δ121.04 (C_6'''), δ128.38 (C_3''&C_5''), δ131.25 (C_4'), δ133.45 (C_1'), δ137.67 (C_1'''), δ141.26 (C_3'''), δ146.8 (C_4'''), δ149.68 (C_3'&C_5'), δ157.80 (C_1''), δ198.90 (C_2)

HRMS: $C_{25}H_{25}NO_6S$ M^++Na requires 490.1300, found 490.1293 (-1.5ppm)

5.10 DIBAL-H Reductions

To a solution of the *cis* β-lactam (**256a**) (0.25mmol) in dry THF (3mL) was added 1.0M DIBAL-H (1.0mL 1.0mmol) dropwise under N_2 and the reaction brought to reflux. After 2 hours the reaction was extracted between DCM (20mL) and H_2O (20mL) and the aqueous layer further extracted with 10 ml DCM. The organic layers were combined and dried over Na2SO4, filtered, and solvent removed under reduced pressure. Flash chromatography over silica gel eluted with 1:1 ethyl acetate:*n*-hexane yielded the title compound.

2-Methoxy-5-[3-phenoxy-1-(3,4,5-trimethoxy-phenyl)-azetidin-2-yl]-phenol **(272)**

Yield: 27%, 30mg, brown oil

MP: oil

IR (NaCl ν max): 1508 cm^{-1}, 1598 cm^{-1}, 3412 cm^{-1} (OH)

^{1}H NMR (400MHz, $CDCl_3$): δ3.52 (m, 2H, CH_2), δ3.72 (s, 6H, OMe), δ3.78 (s, 3H, OMe), δ3.83 (s, 3H, OMe), δ4.79 (d, J=5.40, 1H, H_4), δ5.29 (m, 1H, H_3), δ6.02 (s, 2H, H_2' H_6'), δ6.88-6.98 (m, 6H, H_2'' H_4'' H_6'' H_2''' H_5''' H_6'''), δ7.22-7.27 (m, 1H, H_3'' H_5'')

^{13}C NMR (100 MHz, $CDCl_3$): δ53.10 (C_2), δ55.34, δ56.05, δ61.23 (OMe) δ69.45 (C_4), δ76.39 (C_3), δ98,73 (C_2'&C_6'), δ113.79 (C_2''&C_6''), δ115.23 (C_5'''), δ116.34 (C_2'''), δ119.98 (C_4''), δ120.85 (C_6'''), δ125.06 (C_4'), δ129.13 (C_3''&C_5''), δ131.25 (C_1'''), δ141.33 (C_1'), δ142.35 (C_3'''), δ143.56 (C_4'''), δ150.58 (C_3'&C_5'), δ156.78 (C_1'')

HRMS $C_{25}H_{27}NO_6$ M^++Na requires 460.1736, found 460.1721 (-3.3ppm)

5.11 Dearylated Analogues

Imine Synthesis

The appropriately substituted benzaldehyde (10mmol) and p-anisidine (10mmol) starting materials were refluxed together in ethanol (40mL) for five hours with a catalytic amount of H_2SO_4. The reaction volume was then reduced to approximately 10mL by removal of solvent under reduced pressure. The Schiff base was seen to precipitate out from solution upon standing at room temperature. The precipitate was removed by vacuum filtration and the solid obtained purified by recrystalistion from hot ethanol before being dried on filter paper.

2-Methoxy-5-[(4-methoxy-phenylimino)-methyl]-phenol **(273)**

Yield: 95%, 2.44g, pale yellow solid

MP: 112-114 °C

IR (KBr ν max): 1576 cm^{-1}(C=N)

^{1}H NMR (400MHz, $CDCl_3$): δ3.81 (s, 3H, OMe), δ3.91 (s, 3H, OMe), δ5.86, (br s, 1H, OH), δ6.92-7.51 (m, 7H, H_2' H_3' H_5' H_6' H_2'' H_5'' H_6''), δ8.38, (s, 1H, Imine)

^{13}C NMR (100 MHz, $CDCl_3$): δ55.05 & δ55.56 (OMe), δ109.90 (C_3'&C_5'), δ113.31 (C_5''), δ113.89 (C_2''), δ121.54 (C_6''), δ121.69 (C_1'&C_6'), δ129.84 (C_1''), δ144.62 (C_3''), δ145.48 (C_1'), δ148.74 (C_4''), δ157.57 (C_6'), δ157.56 (Imine)

HRMS: $C_{15}H_{15}NO_3$ M^++Na caluculated 258.1130 found 258.1122 (-3.1ppm)

Protected Imine Synthesis

The Schiff base (**273**) (5mmol) and *t*-butyldimethylsilylchloride (6mmol) were mixed together in anhydrous dichloromethane (40mL) under a nitrogen atmosphere. To this stirring solution, DBU (8mmol) was added dropwise under nitrogen via syringe. Stirring under nitrogen was continued until starting material had disappeared as monitored by TLC in 50:50 hexane/ethyl acetate (2 - 4 hours).

Upon completion the reaction was diluted with 50mL of dichloromethane and transferred to a separating funnel. The reaction was washed with water (2 x 100mL), 0.1M HCl_{aq} (2 x 50mL), and saturated $NaHCO_3$ aqueous solution (2 x 50mL), retaining the organic layer each time, before drying over Na_2SO_4. The solvent was removed under reduced pressure to yield the protected Schiff base (**274**). The product was used as starting material for β-lactam synthesis without further purification.

[3-(tBDMSi)-4-methoxy-benzylidene]-(4-methoxy-phenyl)-amine **(274)**

Yield: 83%, 1.54g, clear oil

MP: oil

IR (NaCl ν max): 1574 cm^{-1}(C=N)

^{1}H NMR (400MHz, $CDCl_3$): δ0.22 (s, 6H, OtBDMS), δ1.05 (s, 9H, OtBDMS), δ3.85 (s, 3H, OMe), δ3.91 (s, 3H. OMe), δ6.93-7.45 (m, 7H, H_2' H_3' H_5' H_6' H_2'' H_5'' H_6''), δ8.39 (s, 1H, Imine)

^{13}C NMR (100 MHz, $CDCl_3$): δ-4.5, δ18.52, δ27.72 (OtBDMS), δ55.45 & δ55.50 (OMe), δ111.44 (C_5''), δ114.32 (C_3'&C_5'), δ120.17 (C_2''), δ122.13 (C_6''), δ123.67 (C_2'&C_6'), δ129.77 (C_1''), δ145.23 (C_3''), δ153.79 (C_4''&C_1''), δ153.79 (C_4'), δ157.94 (Imine)

β-Lactam Synthesis

To a stirring, refluxing solution of the imine (**274**) (5mmol) and triethylamine (6mmol) in anhydrous dichloromethane (40mL), a solution of the appropiate acid chloride (6mmol) in anhydrous dichloromethane (10mL) was added over 45 minutes under nitrogen. The reaction was kept at reflux during the day (5 hours) and at room temperature overnight (16 hours), continuously under nitrogen, until the starting material had disappeared as monitored by TLC in 50:50 hexane/ethyl acetate. A characteristic darkening of the reaction to an amber colour over time was observed.

The reaction was transferred to a separating funnel and washed with water (2 x 100mL), with the organic layer being retained each time. The reaction was dried over Na_2SO_4 before the solvent was removed under reduced pressure. The crude product was purified by flash chromatography over silica gel eluted with 1:1 *n*-hexane:ethyl acetate.

4-[3-(*t*-Butyl-dimethyl-silanyloxy)-4-methoxy-phenyl]-1-(4-methoxy-phenyl)-3-phenoxy-azetidin-2-one **(275)**

Yield: 87%, 2.198g, white resin

MP: resin

IR (NaCl ν max): 1743cm^{-1} (C=O)

^{1}H NMR (400MHz, $CDCl_3$): δ0.05 (s, 6H, OtBDMS), δ0.95 (s, 9H, OtBDMS), δ3.75 (s, 3H, OMe), δ3.77 (s, 3H, OMe), δ5.26 (d, J=5.0Hz, 1H, H_4), δ5.52 (d, J=5.0Hz, 1H, H_3), δ6.74-6.92 (m, 12H, Ar-H)

^{13}C NMR (100 MHz, $CDCl_3$): δ-5.34, δ-5.20, δ17.94, δ25.23 (OtBDMS), δ54.87, δ54.99 (OMe), δ61.40 (C_4), δ80.61 (C_3), δ111.21(C_2''&C_6''), δ113.86 (C_3'&C_5'), δ115.05 (C_5'''), δ118.55 (C_2'''), δ120.50 (C_4''), δ121.41 (C_6'''), δ121.55 (C_2'&C_6'), δ124.37 (C_3''&C_5''), δ128.79 (C_1'), δ130.04 (C_1'''), δ144.39 (C_3'''), δ150.91 (C_4'''), δ155.99 (C_4'), δ156.51 (C_1''), δ161.98 (C_2)

HRMS: $C_{29}H_{35}NO_5Si$ M^++Na requires 528.2182, found, 528.2193 (2.1ppm)

β-Lactam Deprotection

To a stirring solution of the protected β-lactam (**275**) (5mmol) under N_2 and at 0^{0}C in dry THF was added dropwise 1.0 M t-BAF solution in hexanes (5mL, 5mmol). The resulting solution was left to stir at 0^{0}C until reaction was complete as seen on TLC. Reaction was diluted with ethyl acetate (75mL) and washed with 0.1M HCL_{aq} (100mL). The aqueous layer was further extracted with ethyl acetate (2x25mL). All the organic layers were collected and washed with H_2O (100mL), and saturated brine (100mL) before being dried over Na_2SO_4. Solvent was removed under reduced pressure to yield the free phenol (**276**) which was further purified from recrystallisation from hot ethanol.

4-(3-Hydroxy-4-methoxy-phenyl)-1-(4-methoxy-phenyl)-3-phenoxy-azetidin-2-one **(276)**

Yield: 46%, 900mg, white solid

MP: 136-138 °C

IR (KBr ν max):1743 cm^{-1}(C=O), 3379 cm^{-1}(OH)

^{1}H NMR (400MHz, $CDCl_3$): δ3.77 (s, 3H, OMe), δ3.86 (s, 3H, OMe), δ5.28 (d, J=5.0Hz, 1H H_4), δ5.52 (d, J=5.0Hz, 1H, H_3), δ6.76-6.98 (m, 8H H_3' H_5' H_2'' H_4'' H_6'' H_2''' H_5''' H_6'''), δ7.18-7.32 (m, 4H, H_2' H_6' H_3'' H_5'')

^{13}C NMR (100 MHz, $CDCl_3$): δ54.78, δ54.97 (OMe), δ61.32 (C_4), δ80.63 (C_3), δ111.19 (C_2''&C_6''), δ113.58 (C_3'&C_5'), δ114.78 (C_5'''), δ116.29 (C_2'''), δ120.57 (C_4''), δ121.02 (C_6'''), δ121.53 (C_2'&C_6'), δ124.33 (C_3''&C_5''), δ129.00 (C_1'),

δ129.38 (C_1'''), δ144.08 (C_3'''), δ148.59 (C_4'''), δ155.94 (C_4'), δ156.59 (C_1''), δ162.02 (C_2)

HRMS $C_{23}H_{21}NO_5$ M^++Na requires 414.1317, found 414.1313 (-1.1ppm)

Attempted synthesis of 4-(3-Hydroxy-4-methoxy-phenyl)-3-phenoxy-azetidin-2-one (**277**)

To a stirring solution of the β-lactam (**276**) (1mmol) in ACN (25mL), cooled to 0°C over ice water, was added cerium ammonium nitrate (0.906g, 1.65mmol) in H_2O (5mL), dropwise over 2 minutes. The resulting solution was left to stir for 30 minutes at 0°C. The reaction was diluted with 50mL H_2O, and extracted with ethyl acetate (3x75mL). The organic layers were collected and washed with 5% $NaHCO_3$ (150mL). The aqueous layer was further extracted with ethyl acetate (50mL). The recombined organic layers were washed with 10% Na_2SO_3 in 50mL portions until the aqueous layer was clear in colour (5x50mL), 5% $NaHCO_3$ (100mL), and saturated brine (100mL). The organic layer was stirred over charcoal for 1 hour, dried over $NaSO_4$, filtered through celite and the solvent removed under reduced pressure. ^1H NMR indicated the destruction of the β-lactam

5.12 Combretastatin A1 Analogues

Demethylation Reaction

To a solution of 2,3,4-trimethoxy benzaldehyde (**279**) (3.924g, 20 mmol) in dry DCM (60mL) under N_2 was added 1.0M BCl_3 (20mL, 20mmol) via syringe and the reaction left to stir for a further 2 hours at room temperature, after which a further charge of 1.0M BCl_3 (20mL, 20mmol) was added. The reaction was then left to stir at room temperature under N_2 overnight. 10% $NaHCO_{3\ aq}$ (100mL) was added to destroy any remaining BCl_3, and the resulting organic layer was transferred to a separating funnel and washed with 5% NaOH (2x100mL). All three aqueous layers were combined and acidified with $H_2SO_{4\ conc}$ to pH 1 (by Litmus paper), resulting in the formation of a precipitate. This slurry was washed with portions of diethyl ether (4x150mL) until the organic layer remained clear. Organic layers combined, dried over Na_2SO_4, filtered, and solvent removed under reduced pressure. The solid produced was recrystallised from hot ethanol to yield **280**.

2,3-Dihydroxy-4-methoxy-benzaldehyde **(280)**

Yield: 67%, 2.25g off white solid

MP: 98°C

IR (KBr ν max): 3072cm^{-1}(OH) 1640 cm^{-1}(C=O)

^{1}H NMR (400MHz, $CDCl_3$): δ3.98 (s, 3H, -OMe), δ5.72 (s, 1H, -OH), δ6.63 (d, 1H, H_5), δ7.15 (d, 1H, H_6), δ9.74 (s, 1H, -OH), δ11.12 (s, 1H -CHO)

^{13}C NMR (100 MHz, $CDCl_3$): δ55.93 (OMe), δ103.2 (C5), δ115.6 (C1), δ125.73 (C6), δ132.54 (C3), δ148.59 (C2), δ155.32 (C4), δ194.86 (CHO)

HRMS: $C_8H_8O_4$ M^+ requires 168.0423, found 168.0415 (-4.8ppm)

CA1 Imine Formation

The benzaldehyde (**280**) (20mmol) and trimethoxyaniline were refluxed together in ethanol (50mL) for 6 hours in the presence of a catalytic amount of H_2SO_4. The reaction was reduced in volume by half and cooled to room temperature then to 0°C over ice water until precipitate was seen to crash out. The precipitate was removed by filtration and allowed to dry on filter paper overnight to yield the imine (**281**).

3-Methoxy-6-[(3,4,5-trimethoxy-phenylimino)-methyl]-benzene-1,2-diol **(281)**

Yield: 62%, 4.133g, bright red solid

MP: 174 °C

IR (KBr ν max): 1622 cm^{-1}, 3270 cm^{-1}

^{1}H NMR (400MHz, $CDCl_3$): δ3.87 (s, 3H -OMe), δ3.93 (s, 6H OMe), δ3.96 (s, 3H OMe), δ6.52-6.97 (m, 4H, H_2' H_6' H_2'' H_5'' H_6''), δ8.51 (s, 1H, Imine)

^{13}C NMR (100 MHz, $CDCl_3$): δ55.75, δ60.59 (OMe), δ97.71 (C_2'&C_6'), δ102.69 (C_5''), δ113.10 (C_1''), δ123.26 (C_6''), δ133.04 (C_3''), δ136.43 (C_4'), δ143.10 (C_2''), δ149.83 (C_1'), δ150.03 (C_3'&C_5'), δ153.33 (C_4''), δ160.45 (Imine)

HRMS: $C_{17}H_{19}NO_6$ M^++Na requires 356.1110, found 356.1119 (2.5ppm)

Attempted Diol Protection

Method A. To a stirring solution of the benzaldeyhde (**280**) (106mg, 0.63mmol) and *t*BDMSiCl (228mg, 1.512mmol) in dry DCM (3mL) under N_2 was added dropwise 1.0 M DBU in hexanes (0.3mL, 2.1mmol) and the resulting mixture left to stir for 2.5 hours. The reaction was diluted with DCM (20mL), and washed with H_2O (25mL), 0.1M HCl_{aq} (25mL) and saturated $NaHCO_{3\ aq}$ (25mL). The organic layer was collected, dried over Na_2SO_4, filtered, and the removed under reduced pressure to yield the monoprotected benzaldehyde (**284**).

Method B. To a stirring solution of the benzaldehyde (**280**) (563 mg, 3.35mmol) and diisopropylethyl amine (1.8mL, 1.75 mmol) in dry DMF (5mL) was added tBDMSCl (1.155g, 7.47mmol) under a nitrogen blanket. The resulting solution was left to stir at room temperature under N_2 for 20 minutes, then poured onto crushed ice (10g), before being extracted with diethyl ether (3 x 20mL). The ether solution was washed with H_2O (20mL), saturated $NaHCO_3$ (2x20mL), and H_2O (20ml), dried over Na_2SO_4, filtered and the solvent removed under reduced pressure to yield the monoprotected benzaldehyde as a yellow oil (**284**).

Method C. To a stirring solution of the imine or benzaldeyde (**280**) (2.5mmol) and TMS (6mmol) in dry DCM (5mL) at room temperature under N_2 was added dropwise 1.0M DBU (9mmol, 9mL) and the resulting reaction was left to stir for 2 hours. The reaction was diluted with DCM (20mL), and washed with H_2O (25mL), 0.1M HCl_{aq} (25mL) and saturated $NaHCO_{3\ aq}$ (25mL). The organic layer was collected, dried over Na_2SO_4, filtered, and the removed under reduced pressure to yield the monoprotected product (**284**).

3-(*t*-Butyl-dimethyl-silanyloxy)-2-hydroxy-4-methoxy-benzaldehyde **(284)**

Yield: 87% method A, 84% method B, 63% method C.

MP: oil

IR (NaCl ν max): 1637 cm^{-1}(C=O)

^{1}H NMR (400MHz, $CDCl_3$): δ0.21 (6H, s, -tBDMSi), δ1.11 (9H, s, -tBDMSi), δ3.89 (3H, s, -OMe), δ6.55 (d, J=8.33, 1H, (H_5), δ6.98 (1H, d, J=8.27, H_6), δ8.49 (1H, s, imine)

^{13}C NMR (100 MHz, $CDCl_3$): δ-4.97 δ18.17 δ25.41 (OTBDMS), δ56.34 (OMe), δ105.87 (C_5), δ118.37 (C_1), δ124.23 (C_6), δ131.45 (C_3), δ149.03 (C_2), δ158.78(C_4), δ192.32 (CHO)

HRMS: $C_{14}H_{22}O_4Si$ M^+ requires 282.1287, found 282.1277 (-3.5ppm)

Further protection of monoprotected benzaldehyde

To a stirring solution of the monoprotected benzaldeyhde (**284**) (1mmol) and t-BDMSiCl (4.8mmol) in dry DCM (6mL) under N_2 was added dropwise 1.0M DBU in hexanes (6.6mL) and the resulting mixture left to stir for 90 minutes at room temperature. The reaction was diluted with DCM (20mL), and washed with H_2O (25mL), 0.1M HCl_{aq} (25mL) and saturated $NaHCO_{3\ aq}$ (25mL). The organic layer was collected, dried over Na_2SO_4, filtered, and the removed under reduced pressure to yield the monoprotected product spectroscopically identical to the monoprotected product above (**284**).

CA1 Imine Protection

Method A. To a solution of the appropriately substituted imine (**281**) (5mmol) and *t*-butyldimethylsilylchloride (6mmol) in anhydrous DCM (40mL) under a nitrogen atmosphere, DBU (8mmol) was added dropwise via syringe. Stirring under nitrogen was continued until starting material had disappeared as monitored by TLC in 50:50 hexane/ethyl acetate (2 - 4 hours). Upon completion the reaction was diluted with 50mL of dichloromethane and transferred to a separating funnel. The reaction was washed with water (2 x 100mL), 0.1M HClaq (2 x 50mL), and saturated $NaHCO_3$ aqueous solution (2 x 50mL), retaining the organic layer each time, before drying over Na_2SO_4. The solvent was removed under reduced pressure to yield the monoprotected imine (**282**)

Method B. To a stirring solution of the imine (**281**) (5mmol) and diisopropylethylamine (2.5mmol) in dry DMF (10mL) stirring at room temperature under N_2 was added *t*BDMSCl (10mmol). The resulting solution was left to stir at room temperature under N_2 for 20 minutes, then poured onto crushed ice (10g), before being extracted with diethyl ether (3 x 40mL). The ether solution was washed with H_2O (50mL), saturated $NaHCO_3$ (2x40mL), and H_2O (40ml), dried over Na_2SO_4, filtered and the solvent removed under reduced pressure to yield the monoprotected imine as a brown oil (**282**).

Yielded the monoprotected imine by both method A and method B

2-(tert-Butyl-dimethyl-silanyloxy)-3-methoxy-6-[(3,4,5-trimethoxy-phenylimino)-methyl]-phenol **(282)**

Yield: 78% method A, 71% method B

MP: Oil

IR (NaCl ν max): 1624 cm^{-1} (C=N), 3421 cm^{-1} (OH)

^{1}H NMR (400MHz, $CDCl_3$): δ0.02 (s, 6H, OtBDMS), δ1.08 (s, 9H, OtBDMS), δ3.88 (s, 3H, OMe), δ3.89 (s, 3H, OMe), δ3.93 (s, 6H, OMe), δ6.53 (m, 3H, H_2' H_6' H_5''), δ7.01 (d, J=8.65, 1H, H_6''), δ8.39 (s, 1H, Imine)

^{13}C NMR (100 MHz, $CDCl_3$): δ-4.93, δ18.29, δ25.40, δ25.47 (OtBDMS), δ55.05 δ57.73 δ60.59 (OMe), δ97.85 (C_2'&C_6'), δ102.40 (C_5''), δ113.88 (C_1''), δ125.03 (C_6''), δ132.21 (C_3''), δ136.17 (C_4'), δ144.34 (C_2''), δ153.20 (C_1'), δ153.23 (C_3'&C_5'), δ154.46 (C_4''), δ161.18 (Imine)

HRMS: $C_{23}H_{33}NO_6Si$ M^++1 requires 448.2077, found 448.2089 (2.7ppm)

Attempted Acetal protection

Method A. The benzaldehyde (0.07mL, 0.673mmol) in DMSO (2mL) was added and the reaction was left to stir at room temperature under N_2 for 26 hours. TLC in 1:1 hexane:ethyl acetate was carried out and indicated the presence of a new product. IR indicated the presence of a hydroxy peak and ^{1}H NMR showed that the protection had not been successful

Method B. To a stirring solution of the benzaldehyde (165mg, 0.98mmol) in DCM at room temperature under N_2 was added pyridine (0.15mL, 2mmol), followed by the dropwise addition of a solution of triphosgene (101mg, 0.33mmol) in DCM (5mL) over the course of 3 minutes. The reaction was left to stir for a further 15 minutes at which time TLC in 1:1 hexane:ethyl acetate indicated that no new product had been formed. The reaction was left for a total of 2 hours after which time the reaction was diluted with ethyl acetate (30mL), washed with 50mL H_2O, the organic layer collected, dried over Na_2SO_4, filtered and the solvent removed under reduced pressure. ^1H NMR and IR of the crude reaction mixture indicated that the diol remained unprotected.

5.13 Nitrated Isovanillin Derivatives

Isovanillin Nitration at 2 & 6 Positions

To a stirring solution of isovanillin (10mmol) in acetone (40mL) at room temperature was added HNO_3 conc. (12 mmol, 0.5mL) and left to stir for 30 minutes, poured onto 200cm^3 of ice water and resulting precipitate filtered off via a sinter glass funnel and vacuum. Filter cake found to contain the 6 nitro isomer. Filtrate collected, reduced in volume under reduced pressure, left to cool to room temperature, then left to stand over ice water. Precipitate formed was collected on sinter glass. Found to contain 4:1 mixtures of the 2-nitro (**292**):6-nitro (**293**) isomers.

3-Hydroxy-4-methoxy-2-nitro-benzaldehyde **(292)**

Yield: 42%, 828mg, bright yellow solid

MP: 186 °C

IR (KBr ν max): 1671 cm^{-1}(C=O), 3326 cm^{-1} (OH)

^{1}H NMR (400MHz, $CDCl_3$): δ4.09 (s, 3H, -OMe), δ7.15 (d, J=8.58 1H, H_5), δ7.51 (d, J=8.52Hz 1H, H_6), δ10.10 (s, 1H, -CHO)

^{13}C NMR (100 MHz, $CDCl_3$): δ59.01 (OMe), δ119.07 (C_5), δ123.58 (C_6), δ129.82 (C_1), δ139.79 (C_2), δ141.29 (C_3), δ153.32 (C_4), δ187.24 (C=O)

HRMS:$C_8H_7NO_5$ M^++Na requires 220.0222, found 220.0209 (-5.9ppm)

5-Hydroxy-4-methoxy-2-nitro-benzaldehyde **(293)**

Yield: 31%, 611mg, brown solid

MP: 142

IR (KBr ν max): 1694 cm^{-1}(C=O), 3332 cm^{-1} (OH)

^{1}H: δ4.10 (s, 3H, -OMe), δ6.25 (s, 1H, -OH), δ7.49 (s, 1H, H_2), δ7.68,(s, 1H, H_5), δ10.44 (s, 1H, -CHO)

^{13}C NMR (100 MHz, $CDCl_3$): δ58.34 (OMe), δ109.45 (C_5), δ119.08 (C_2), δ123.45 (C_1), δ144.26 (C_6), δ150.01 (C_3), δ158.56 (C_4), δ188.67 (C=O)

HRMS:$C_8H_7NO_5$ M^++Na requires 220.0222, found 220.0231 (4.1ppm)

Isovanillin Nitration at 5-Position

Isovanillin Acetate Formation

To a solution of isovanillin (6.112g, 40mmol), and KOH (2.318g, 40mmol) in 195mL water at 0 ^{0}C was added acetic anhydride (3.8mL, 40mmol) in 40mL diethyl ether dropwise with stirring. Upon completion of the addition the reaction was observed to turn milky white. Reaction left to stir at 0°C for a further 30 minutes before resulting precipitate was filtered off through sinter glass. Yielded a white powder (7.21g)

Acetic acid 5-formyl-2-methoxy-phenyl ester **(298)**

Yield: 93%, 7.21g, white powder

MP: 73 °C

IR (KBr ν max): 1684 cm^{-1} (benzaldehyde), 1769 cm^{-1} (ester)

^{1}H NMR (400MHz, $CDCl_3$): δ2.33 (3H, s, -CH3), δ3.91 (3H, s, -OMe), δ4.82 (1H s br, -OH), δ7.06 (1H, d, J=8.52 H_5), δ7.58-7.76 (2H, m, H_2 H_6), δ9.82, (s, 1H, CHO)

^{13}C NMR (100 MHz, $CDCl_3$): δ20.11 (CH_3), δ55.77 (OMe), δ111.57 (C5), δ122.90 (C2), δ129.81 (C6), δ139.73 (C1), δ155.89 (C3), δ168.28 (C4), δ189.68 (CHO)

5-Nitro Isovanillin Acetate

To a stirring solution of conc. HNO_3 (15mL, 360mmol) at -18°C, acetic acid 5-formyl-2-methoxy-phenyl ester (**298**) (6.977g, 36mmol) was added in portions over 10 minutes, and the resulting solution left to stir at -18°C for 2 minutes then at -5°C for a further 20 minutes, before being poured onto 150cm^3 of crushed ice. Resulting slurry was left at 5°C overnight, then filtered through a sinter glass funnel. Filter cake was washed with water (five 10mL portions), then left to dry on filter paper. (5.802g)

Acetic acid 5-formyl-2-methoxy-3-nitro-phenyl ester **(299)**

Yield: 82%, 7.056g, pale yellow solid

MP: 65 °C

IR (KBr ν max): 1698 cm^{-1} (benzaldehyde), 1778 cm^{-1} (ester)

^{1}H NMR (400MHz, $CDCl_3$): δ2.41 (3H, s, -CH3), δ4.02 (3H, s, -OMe), δ7.85 (1H, d, J=2.0Hz H_2), δ8.20 (1H, d, J=2.0Hz, H_6), δ9.93 (1H, s, -CHO)

^{13}C NMR (100 MHz, $CDCl_3$): δ20.17 (CH_3), δ62.53 (OMe), δ123.61 (C_6), δ127.39 (C_2), δ130.75 (C_1), δ145.11 (C_5), δ150.28 (C_3), δ167.66 (C_4), δ187.83 (CHO)

5-Nitro isovanillin

Acetic acid 5-formyl-2-methoxy-3-nitro-phenyl ester (**299**) (5.638g, 23.5mmol) was taken up into warm 5% $NaOH_{aq}$. Upon complete dissolution the reaction took on a dark red colour. The solution was allowed to cool to room temperature then acidified with conc. HCl to pH 1 by litmus paper, which resulted in loss of colour and the formation of a precipitate. This mixture was left to stir at room temperature, then at 0°C , before the precipitate was removed through a sinter glass. The solid collected was dried between filter paper (2.137g)

3-Hydroxy-4-methoxy-5-nitro-benzaldehyde **(300)**

Yield: 8%, 370mg, off white solid

MP: 52-56 °C

IR (KBr ν max): 1690cm^{-1} (C=O) 4415 cm^{-1} (OH)

^{1}H: δ4.08 (3H, s, -OMe), δ6.59 (1H, s br, -OH), δ7.74 (1H, d, J=2.0Hz, H_2), δ7.98 (1H, d, J=1.52 H_6), δ9.94 (1H, s, -CHO)

^{13}C NMR (100 MHz, $CDCl_3$): δ62.34 (OMe), δ118.53, (C6), δ118.83 (C2), δ131.30 (C1), δ142.34 (C3), δ145.54 (C5), δ150.94 (C4), δ188.90 (CHO)

HRMS: $C_8H_7NO_5$ M^++Na requires 220.0222, found 220.0217 (-2.3ppm)

Nitrated Isovanillin Protection

The nitrated benzaldehyde (**292 293 300**) (5mmol) and *t*-butyldimethylsilylchloride (6mmol) were mixed together in anhydrous dichloromethane (40mL) under a nitrogen atmosphere. To this stirring solution, DBU (8mmol) was added dropwise under nitrogen via syringe. Stirring under nitrogen was continued until starting material had disappeared as monitored by TLC in 50:50 hexane/ethyl acetate (2 - 4 hours).

Upon completion the reaction was diluted with 50mL of dichloromethane and transferred to a separating funnel. The reaction was washed with water (2 x 100mL), 0.1M HCl_{aq} (2 x 50mL), and saturated $NaHCO_3$ aqueous solution (2 x 50mL), retaining the organic layer each time, before drying over Na_2SO_4.

3-(t-Butyl-dimethyl-silanyloxy)-4-methoxy-2-nitro-benzaldehyde **(292)**

Yield: 83%, 1.291g, amber oil

MP: Oil

IR (NaCl ν max): 1693cm^{-1} (C=O)

^{1}H NMR (400MHz, $CDCl_3$): δ0.22 (6H, s, -tBDMSi), δ0.97 (9H, s, -tBDMSi), δ3.97 (3H, s, -OMe), δ7.04 (1H, d, J=8Hz, H_5), δ7.50 (1H, d, J=8.6Hz, H_6), δ9.80 (1H, s, -CHO)

^{13}C NMR (100 MHz, $CDCl_3$): δ-4.52, δ18.05, & δ25.06 (tBDMSi), δ55.47 (OMe), δ111.19 (C5), δ116.45 (C1), δ120.44 (C3), δ124.59 (C6), δ142.32 (C2), δ155.67 (C4), δ185.71 (C=O)

5-(t-Butyl-dimethyl-silanyloxy)-4-methoxy-2-nitro-benzaldehyde **(293)**

Yield: 91%, 1.416g, amber oil

MP: Oil

IR (NaCl ν max): 1689cm^{-1} (C=O)

^{1}H NMR (400MHz, $CDCl_3$): δ0.21 (6H, s, -tBDMSi), δ1.00 (9H, s, -tBDMSi), δ3.97 (3H, s, -OMe), δ7.36 (1H, s, H_2), δ7.61 (1H, s, H_5), δ10.37 (1H, s, -CHO)

^{13}C NMR (100 MHz, $CDCl_3$): δ-4.07, δ17.87, δ25.17 (OtBDMS), δ59.94 (OMe), δ107.48 (C_5), δ119.38 (C_2), δ125.18 (C_1), δ143.62 (C_6), δ149.73 (C_3), δ153.93 (C_4), δ170.72 (C=O)

3-(t-Butyl-dimethyl-silanyloxy)-4-methoxy-5-nitro-benzaldehyde **(300)**

Yield: 77%, 1.198g, amber oil

MP: Oil

IR (NaCl ν max): 1690 cm^{-1} (C=O)

^{1}H NMR (400MHz, $CDCl_3$): δ0.21 (6H, s, -tBDMSi), δ1.00 (9H, s, -tBDMSi), δ3.97 (3H, s, -OMe), δ6.59 (1H, s br, -OH), δ7.71 (1H, d, J=2Hz, H_2), δ7.88 (1H, d, J=1.52 H_6), δ9.81 (1H, s, -CHO)

^{13}C NMR (100 MHz, $CDCl_3$): δ-5.07, δ17.99, δ25.37 (OtBDMS), δ56.37 (OMe), δ119.45 (C_6), δ127.49 (C_2), δ131.25 (C_1), δ136.78 (C_5), δ141.47 (C_3), δ158.28 (C_4), δ188.38 (C=O)

Nitrated Isovanillin Imine Formation

The appropriately substituted benzaldehyde (**292 293 300**) (10mmol) and corresponding substituted aniline (10mmol) starting materials were refluxed together in ethanol (40mL) for five hours. The reaction volume was then reduced to approximately 10mL by removal of solvent under reduced pressure. The Schiff base was seen to precipitate out from solution upon standing at room temperature. The precipitate was removed by vacuum filtration and the solid obtained purified by recrystalistion from hot ethanol before being dried on filter paper.

6-Methoxy-2-nitro-3-[(3,4,5-trimethoxy-phenylimino)-methyl]-phenol **(294)**

Yield: 23%, 833mg, yellow solid

MP: 136 °C

IR (KBr ν max): 1578 cm^{-1} (C=N), 3275 cm^{-1}(OH)

^{1}H NMR (400MHz, $CDCl_3$): δ1.73 (1H, s broad, -OH), δ3.87 (3H, s, -OMe), δ3.91 (6H, s, -OMe), δ4.01 (3H, s, -OMe), δ6.51 (2H, s, H_2' H_6'), δ7.11 (1H, d, J=8.5, H_5), δ7.66 (1H, d, J=8.53, H_6), δ8.61 (1H, s, imine)

^{13}C NMR (100 MHz, $CDCl_3$): δ55.44 (OMe), δ56.49 (OMe), δ60.63 (OMe), δ97.96 (C2'&C6'), δ113.83 (C5''), δ120.44 (C6''), δ122.92 (C1'), δ135.80 (C2''), δ136.39 (C3''), δ142.31 (C4'), δ146.57 (C1'), δ150.37 (C3'&C5'), δ153.39 (C4''), δ154.29 (Imine)

HRMS: $C_{17}H_{18}N_2O_7$ M^++1 calculated 363.1192 found 363.1180 (-3.3ppm)

2-Methoxy-3-nitro-5-[(3,4,5-trimethoxy-phenylimino)-methyl]-phenol **(301)**

Yield: 47%, 1.702g, yellow solid

MP: 105 °C

IR (KBr ν max): 1592 cm^{-1}(C=N) 3420 cm^{-1} (OH)

^{1}H NMR (400MHz, $CDCl_3$): : δ3.83 (s, 3H, OMe), δ3.90 (s, 6H, OMe), δ4.05 (s, 3H, OMe), δ6.53 (s, 2H, H_2'&H_6'), δ7.82 (d, J=1.70Hz, 1H H_2''), δ7.99 (d, J=1.70Hz, 1H, H_6''), δ8.42 (s, 1H, Imine)

^{13}C NMR (100 MHz, $CDCl_3$): δ55.46, δ55.71, δ60.60, δ62.37 (OMe), δ97.85 (C_2'&C_6'), δ117.04 (C_6''), δ118.64 (C_2''), δ131.98 (C_1''), δ136.57 (C_4'), δ142.33 (C_5''), δ142.82 (C_3''), δ146.15 (C_4''), δ150.50 (C_1'), δ153.20 (C_3'&C_5'), δ155.50 (Imine)

HRMS: $C_{17}H_{18}N_2O_7$ M^+ calculated 363.1192 found 363.1184 (-2.3ppm)

2-Methoxy-4-nitro-5-[(3,4,5-trimethoxy-phenylimino)-methyl]-phenol **(295)**

Yield: 10%, 362mg, yellow solid

MP: 188 °C

IR (KBr ν max): 1583 cm^{-1} (C=N) 3428 cm^{-1} (OH)

^{1}H NMR (400MHz, $CDCl_3$): δ3.88 (3H, s, -OMe), δ3.92 (6H, s, -OMe), δ4.03 (3H, s, -OMe), δ6.56 (2H, s, H_2'&H_6'), δ7.67 (1H, s, H_2''), δ7.76 (1H, s, H_5''), δ9.01 (1H, s, imine)

^{13}C NMR (100 MHz, $CDCl_3$): δ55.45 (OMe), δ55.69 (OMe), δ60.58 (OMe), δ98.10 (C2'&C6'), δ106.91 (C5''), δ113.96 (C2''), δ126.46 (C1''), δ136.49 (C4'), δ141.38 (C6''), δ146.51 (C1'), δ147.48 (C3''), δ150.12 (C3'&C5'), δ153.14 (C4''), δ155.15 (Imine)

HRMS: $C_{17}H_{18}N_2O_7$ M^++1 calculated 363.1192 found 363.1178 (-3.9ppm)

Protected Nitrated Isovanillin Imine Formation

Method A. The appropitaed nitrated imine (**294 295 301**) (5mmol) and *t*-butyldimethylsilylchloride (6mmol) were mixed together in anhydrous dichloromethane (40mL) under a nitrogen atmosphere. To this stirring solution, DBU (8mmol) was added dropwise under nitrogen via syringe. Stirring under nitrogen was continued until starting material had disappeared as monitored by TLC in 1:1 hexane/ethyl acetate (2 - 4 hours). Upon completion the reaction was diluted with 50mL of dichloromethane and transferred to a separating funnel. The reaction was washed with water (2 x 100mL), 0.1M HClaq (2 x 50mL), and saturated NaHCO3 aqueous solution (2 x 50mL), retaining the organic layer each time, before drying over Na_2SO4. The solvent was removed to yield the title compound which was used in the Staundinger reaction without further purification.

Method B. The appropriately silyl ether nitrated benzaldehyde (**292 293 300**) ((10mmol) and corresponding substituted aniline (10mmol) starting materials were refluxed together in ethanol (40mL) for five hours. The reaction volume was then reduced to approximately 10mL by removal of solvent under reduced pressure. No precipitate was observed in the reaction and so the reaction was evaporated to dryness to yield the sily ether protected imines which were used in the Staundinger reaction without further purification.

[3-(*t*-Butyl-dimethyl-silanyloxy)-4-methoxy-5-nitro-benzylidene]-(3,4,5-trimethoxy-phenyl)-amine **(302)**

Yield: 91%, 2.167g, amber oil

MP: oil

IR (NaCl ν max): 1596 cm^{-1}(C=N)

^{1}H NMR (400MHz, $CDCl_3$): δ0.23 (s, 6H, OtBDMS), δ0.96 (s, 9H, OtBDMS), δ3.86 (s, 3H, OMe), δ3.93 (s, 6H, OMe), δ4.03 (s, 3H, OMe), δ6.52 (s, 2H, H_2'&H_6'), δ7.04 (d, J=1.70Hz, 1H H_2''), δ7.68 (d, J=1.70Hz, 1H, H_6''), δ8.27 (s, 1H, Imine)

^{13}C NMR (100 MHz, $CDCl_3$): δ-4.60, δ-4.04, δ18.06, δ25.11 (OtBDMS), δ55.25, δ55.44, δ56.37, δ60.56 (OMe), δ97.78 (C_2'&C_6'), δ120.12 (C_6''), δ121,17 (C_2''), δ131.98 (C_1''), δ137.67 (C_4'), δ146.67 (C_5''), δ151.08 (C_3''), δ152.32 (C_1'), δ153.07 (C_3'&C_5'), δ154.22 (C_4''), δ161.29 (Imine)

[3-(*t*-Butyl-dimethyl-silanyloxy)-4-methoxy-2-nitro-benzylidene]-(3,4,5-trimethoxy-phenyl)-amine **(296)**

Yield: 88%, 2.095g, amber oil

MP: oil

IR (NaCl ν max): 1579 cm^{-1}(C=N)

^{1}H NMR (400MHz, $CDCl_3$): δ0.26 (6H, s, -tBDMSi), δ1.04 (9H, s, -tBDMSi), δ3.89 (3H, s, -OMe), δ3.93 (6H, s, -OMe), δ3.97 (3H, s, -OMe), δ6.56 (2H, s, H_5''), δ7.64 (2H, d J=22Hz, H_6''), δ8.99 (1H, s, imine)

^{13}C NMR (100 MHz, $CDCl_3$): δ-4.88, δ17.34 & δ25.11 (tBDMSi), δ55.53, δ55.70, δ60.59 (OMe), δ98.08 (C2'&C6'), δ107.65 (C5''), δ119.62 (C2''), δ123.35 (C1''), δ136.40 (C4'), δ142.53 (C6''), δ146.85 (C3''), δ149.78 (C1'), δ152.10 (C3'&C5'), δ153.14 (C4'), δ154.99 (N=CH)

[5-(*t*-Butyl-dimethyl-silanyloxy)-4-methoxy-2-nitro-benzylidene]-(3,4,5-trimethoxy-phenyl)-amine **(297)**

Yield: 87%, 2.071g, amber oil

MP: oil

IR (NaCl ν max): 1583 cm^{-1}(C=N)

^{1}H NMR (400MHz, $CDCl_3$): δ0.25 (6H, s, -tBDMSi), δ1.06 (9H, s, -tBDMSi), δ3.86 (3H, s, -OMe), δ3.94 (6H, s, -OMe), δ4.08 (3H, s, -OMe), δ6.59 (2H, s, H_2'&H_6'), δ7.64 (1H, s, H_2''), δ7.81 (1H, s, H_5''), δ8.11 (1H, s, imine)

^{13}C NMR (100 MHz, $CDCl_3$): δ-4.76, δ17.44 & δ25.18 (–tBDMSi) δ55.52, δ55.77, δ60.89 (OMe), δ98.03 (C2'&C6'), δ119.93 (C_6''), δ122.99 (C1''), δ128.35 (C_2''), δ133.78 (C4'), δ137.28 (C_5''), δ147.55 (C3''), δ149.73 (C1'), δ151.09 (C3'&C5'), δ153.99 (C4'), δ158.78 (Imine)

Nitrated β-Lactam Formation

To a stirring, refluxing solution of the silyl ether imine (**296 297 302**) (5mmol) and triethylamine (6mmol) in anhydrous dichloromethane (40mL), a solution of the appropiate acid chloride (6mmol) in anhydrous dichloromethane (10mL) was added over 45 minutes under nitrogen. The reaction was kept at reflux during the day (5 hours) and at room temperature overnight (16 hours), continuously under nitrogen, until the starting material had disappeared as monitored by TLC in 1:1 hexane/ethyl acetate. A characteristic darkening of the reaction to an amber colour over time was observed. The reaction was transferred to a separating funnel and washed with water (2 x 100mL), with the organic layer being retained each time. The reaction was dried over Na_2SO_4 before the solvent was removed under reduced pressure. The crude product was purified by chromatography using a Biotage ™ SP1 system with a +40M cartridge, detection at 280nm, 24mL fraction collection, and a gradient eleution from 2% ethyl acetate in hexaxe to 80% ethyl acetate in hexane over the course of 10 column volumes.

4-[5-(*t*-Butyl-dimethyl-silanyloxy)-4-methoxy-2-nitro-phenyl]-3-phenoxy-1-(3,4,5-trimethoxy-phenyl)-azetidin-2-one

Yield: 61%, 1.861g, amber oil

MP: Oil

IR (NaCl ν max): 1758 cm^{-1}(C=O)

^{1}H NMR (400MHz, $CDCl_3$): δ0.01 (s, 3H, OtBDMS), δ0.03 (s, 3H, OtBDMS), δ0.87 (s, 9H, OtBDMS), δ3.81 (s, 6H, OMe), δ3.82 (s, 3H, OMe), δ3.93 (s, 3H, OMe), δ5.40 (d, J=5.73, 1H, H_4), δ5.71 (d, J=5.40Hz, 1H, H_3), δ6.68 (s, 2H, H_2'&H_6'), δ6.90-6.96 (m, 4H, H_2'' H_6'' H_4'' H_2'''), δ7.22-7.28 (m, 2H, H_3''&H_5''), δ7.82 (s, 1H, H_5''')

^{13}C NMR (100 MHz, $CDCl_3$): δ-5.34, δ-5.27, δ17.91, δ24.87 (OtBDMS), δ55.60, δ55.81, δ60.54 (OMe), δ58.70 (C_4), δ81.68 (C_3), δ94.70 (C_2'&C_6'), δ108.86 (C_5'''), δ115.94 (C_2''&C_6''), δ119.85 (C_4''), δ122.25 (C_2'''), δ123.65 (C_4') δ129.00 (C_3''&C_5''), δ132.43 (C_1'''), δ134.84 (C_1'), δ140.75 (C_6'''), δ150.29 (C_3'''), δ150.32 (C_3'&C_5'), δ153.45 (C_4'''), δ156.84 (C_1''), δ163.22 (C_2)

HRMS: $C_{31}H_{38}N_2O_9Si$ M^++Na requires 633.2244, found 633.2232 (-1.9ppm)

4-[3-(*t*-Butyl-dimethyl-silanyloxy)-4-methoxy-2-nitro-phenyl]-3-phenoxy-1-(3,4,5-trimethoxy-phenyl)-azetidin-2-one

Yield: 58%, 1.77g, amber oil

MP: oil

IR (NaCl ν max): 1759cm^{-1} (C=O)

^{1}H NMR (400MHz, $CDCl_3$): δ0.12 (s, 3H, OtBDMS), δ0.15 (s, 3H, OtBDMS), δ0.96 (s, 9H, OtBDMS), δ3.79 (s, 3H, OMe), δ3.82 (s, 3H, OMe), δ3.84 (s, 6H, OtBDMS), δ5.27 (d, J=4.77Hz, 1H, H_4), δ5.54 (d, J=4.77Hz, 1H, H_3), δ6.70 (s, 2H, H_2'&H_6'), δ6.84-6.96 (m, 4H, H_2'' H_6'' H_4'' H_6'''), δ7.12-7.25 (m, 3H, H_5''' H_3'' H_5'')

^{13}C NMR (100 MHz, $CDCl_3$): δ-4.79, δ-4.76, δ18.01, δ25.09 (OtBDMS), δ55.00, δ55.68, δ60.49 (OMe), δ55.95 (C_4), δ80.78 (C_3), δ94.33 (C_2'&C_6'), δ112.12 (C_2''&C_6''), δ115.14 (C_4''), δ115.84 (C_5'''), δ120.67 (C_6'''), δ122.04 (C_4'), δ129.00 (C_3''&C_5''), δ132.02 (C_1'''), δ134.49 (C_1'), δ136.51, (C_3'''), δ144.34 (C_2'''), δ150.74 (C_3'&C_5'), δ153.22 (C_4'''), δ156.12 (C_1''), δ162.04 (C_2)

HRMS: $C_{31}H_{38}N_2O_9Si$ M^++Na requires 633.2244, found 633.2231 (-2.1ppm)

4-(3-(*t*-Butyl-dimethyl-silanyloxy))-4-methoxy-5-nitro-phenyl)-3-phenoxy-1-(3,4,5-trimethoxy-phenyl)-azetidin-2-one

Yield: 73%, 2.277g, amber oil

MP: Oil

IR (NaCl ν max): 1753cm^{-1} (C=O)

^{1}H NMR (400MHz, $CDCl_3$): δ0.23 (s, 6H, OtBDMS), δ0.96 (s, 9H, OtBDMS), δ3.75 (s, 9H, OMe), δ3.77 (s, 3H, OMe), δ3.82 (s, 3H, OMe), δ5.28 (d, J=5.04Hz, 1H, H_4), δ5.51 (d, J=5.04Hz, 1H, H_3), δ6.20 (broad s, 1H, OH) δ6.64 (s, 2H, H_2'&H_6'), δ6.71-6.78 (m, 3H, H_2' H_6' H_4'), δ7.11-7.19 (m, 3H, H_2''' H_3'' H_5''), δ7.47 (d, J=2.07Hz, 1H, H_6''')

^{13}C NMR (100 MHz, $CDCl_3$): δ55.79, δ60.46, δ62.09 (OMe), δ60.54 (C_3), δ80.39 (C_4), δ94.80 (C_2'&C_6'), δ115.09 (C_2''&C_6''), δ116.09 (C_6'''), δ119.28 (C_4''), δ122.24 (C_2'''), δ129.05 (C_3''&C_5''), δ129.27 (C_4'), δ132.04 (C_1'), δ141.06 (C_5'''), δ141.78 (C_1'''), δ150.39 (C_4'''), δ151.07 (C_3'&C_5'), δ153.29 (C_3'''), δ155.97 (C_4''), δ161.96 (C_3)

HRMS: $C_{31}H_{38}N_2O_9Si$ M^++Na requires 633.2244, found 633.2245 (0.2ppm)

Nitrated β-lactams deprotection

To a stirring solution of the sily ether β-lactam (2.5mmol) in THF (10mL) under N_2 at 0°C was added dropwise 1.0M *t*BAF solution (2.5ml, 2.5mmol). The reaction was left to stir at 0°C for 60 minutes before being diluted with ethyl acetate (25mL), and washed with H_2O (25mL), 0.1M HCl_{aq} (25mL) and

saturated $NaHCO_3$ (25mL). The organic layers were collected and dried over $MgSO_4$ and the solvent removed to yield the free phenol β-lactam. The β-lactam was subsequently purifed by recrystallisation from hot ethanol.

4-(3-Hydroxy-4-methoxy-5-nitro-phenyl)-3-phenoxy-1-(3,4,5-trimethoxy-phenyl)-azetidin-2-one **(304)**

Yield: 39% overall, 484mg, pale brown solid

MP: 105 °C

IR (KBr ν max): 1756 cm^{-1} (C=O), 3355 cm^{-1} (OH)

^{1}H NMR (400MHz, $CDCl_3$): : δ3.77 (s, 9H, OMe), δ3.79 (s, 3H, OMe), δ4.02 (s, 3H, OMe), δ5.36 (d, J=5.04Hz, 1H, H_4), δ5.61 (d, J=5.04Hz, 1H, H_3), δ6.26 (broad s, 1H, OH) δ6.61 (s, 2H, H_2'&H_6'), δ6.82-6.99 (m, 3H, H_2' H_6' H_4'), δ7.20-7.30 (m, 3H, H_2''' H_3'' H_5''), δ7.50 (d, J=2.07Hz, 1H, H_6''')

^{13}C NMR (100 MHz, $CDCl_3$): δ55.79, δ60.46, δ62.09 (OMe), δ60.54 (C_3), δ80.39 (C_4), δ94.80 (C_2'&C_6'), δ115.09 (C_2''&C_6''), δ116.09 (C_6'''), δ119.28 (C_4''), δ122.24 (C_2'''), δ129.05 (C_3''&C_5''), δ129.27 (C_4'), δ132.04 (C_1'), δ141.06 (C_5'''), δ141.78 (C_1'''), δ150.39 (C_4'''), δ151.07 (C_3'&C_5'), δ153.29 (C_3'''), δ155.97 (C_4''), δ161.96 (C_3)

HRMS: $C_{25}H_{24}N_2O_9$ requires 519.1380, found 519.1387 (1.4ppm)

4-(3-Hydroxy-4-methoxy-2-nitro-phenyl)-3-phenoxy-1-(3,4,5-trimethoxy-phenyl)-azetidin-2-one **(302)**

Yield: 22% overall, 273mg, off white solid

MP: 136 °C

IR (KBr ν max): 1748 cm^{-1} (C=O), 3274 cm^{-1} (OH)

^{1}H NMR (400MHz, DMSO): δ3.61 (s, 3H, OMe), δ3.71 (s, 6H, OMe), δ3.81 (s, 3H, OMe), δ5.52 (d, J=5.12Hz, 1H, H_4), δ5.83 (d, J=5.12Hz, 1H, H_3), δ6.64 (s, 2H, H_2'&H_6'), δ6.82-6.91 (m, 4H, H_2' H_6' H_4' H_6'), δ7.14-7.26 (m, 3H, H_5''' H_3'' H_5'')

^{13}C NMR (100 MHz, $CDCl_3$): (DMSO) δ55.80, δ55.92, δ60.13 (OMe), δ56.24 (C_4), δ80.79 (C_3), δ94.72 (C_2'&C_6'), δ113.10 (C_2''&C_6''), δ115.50 (C_4''), δ118.60 (C_5''), δ122.19 (C_6'''), δ129.48 (C_4'), δ132.39 (C_3'' & C_5''), δ134.38 (C_1'''), δ136.36 (C_3'''), δ138.68 (C_1'), δ140.85 (C_2'''), δ147.09 (C_4'''), δ148.82 (C_3'&C_5'), δ155.33 (C_1''), δ162.53 (C_2)

HRMS: $C_{25}H_{26}N_2O_7$ M^+Na requires 519.1380, found 519.1369 (-2.1ppm)

4-(5-Hydroxy-4-methoxy-2-nitro-phenyl)-3-phenoxy-1-(3,4,5-trimethoxy-phenyl)-azetidin-2-one **(303)**

Yield: 23% overall, 285mg, white solid

MP: 188 °C

IR (KBr ν max): 1757 cm^{-1} (C=O), 3355 cm^{-1}(OH)

^{1}H NMR (400MHz, DMSO): δ3.65 (s, 3H, OMe), δ3.72 (s, 6H, OMe), δ3.89 (s, 3H, OMe), δ6.02 (d, J=5.33Hz, 1H, H_4), δ6.27 (d, J=5.33Hz, 1H, H_3), δ6.79 (s, 2H, H_2'&H_6'), δ6.84-7.01 (m, 4H, H_2'' H_6'' H_2'''), δ7.26 (t, J=7.75, 2H, H_3'' H_5''), δ7.80 (s, 1H, H_5''')

^{13}C NMR (100 MHz, DMSO): δ56.00, δ56.07, δ60.15 (OMe), δ59.44 (C_4), δ81.83 (C_3), δ95.30 (C_2'&C_6'), δ109.26 (C_5'''), δ114.06 (C_2''&C_6''), δ116.00 (C_2'''), δ122.34 (C_4''), δ125.69 (C_4'), δ129.49 (C_3''&C_5''), δ133.08 (C_1'''), δ134.47 (C_1'), δ139.11 (C_6'''), δ146.88 (C_3'&C_5'), δ152.44 (C_4'''), δ153.40 (C_3'''), δ157.21 (C_1''), δ164.12 (C_2)

HRMS: $C_{25}H_{24}N_2O_9$, M^++Na requires 519.1380, found 519.1388 (1.6ppm)

Reduction of Nitro Derivatives

To a flask containing the β-lactam (**302 303 304**) (0.25mmol) and zinc powder 10μm (2.5mmol 165mg) was added 15mL of acetic acid at room temperature under N and reaction left to stir for 7 days. The reaction was filtered through a celite pad and the filtrate collected. Solvent was removed under reduced pressure and the resulting residue was eluted through a short pad of silica with DCM. The resulting product was recrystallised with hot ethanol to yield the title compounds

4-(2-Amino-5-hydroxy-4-methoxy-phenyl)-3-phenoxy-1-(3,4,5-trimethoxy-phenyl)-azetidin-2-one **(306)**

Yield: 73%, 85mg, brown solid

MP: 210 °C

IR (KBr ν max): 1756 cm^{-1} (C=O), 3447 cm^{-1} (OH)

^{1}H NMR (400MHz, $CDCl_3$): δ3.71 (s, 3H, OMe), δ3.74 (s, 6H, OMe), δ3.81 (s, 3H, OMe), δ5.21 (d, J=4.88Hz, 1H, H_4), δ5.57 (d, J=4.88Hz, 1H, H_4), δ5.63 (s, 1H, H_5'''), δ6.61 (s, 2H, H_2'H_6'), δ6.72-6.81 (m, 4H, H_2'' H_4'' H_6'' H_2'''), δ7.21-7.27 (m, 2H, H_3'' H_5'')

^{13}C NMR (100 MHz, $CDCl_3$): δ56.02, δ56.11, δ60.03 (OMe), δ58.76 (C_4), δ80.24 (C_3), δ95.37 (C_2'&C_6'), δ99.49 (C_5'''), δ113.84 (C_2''&C_6''), δ117.20(C_2'''), δ122.21 (C_4''), δ125.23 (C_1'''), δ125.98 (C_4'), δ128.91 (C_3''&C_5''), δ136.29 (C_1'), δ137.17 (C_6'''), δ141.35 (C_3'''), δ146.06 (C_3'&C_5'), δ151.34 (C_4'''), δ157.56 (C_1''), δ164.85 (C_2) **HRMS:** $C_{25}H_{26}N_2O_7$ M^+Na requires 489.1638, found 489.1646 (1.7ppm)

4-(3-Amino-5-hydroxy-4-methoxy-phenyl)-3-phenoxy-1-(3,4,5-trimethoxy-phenyl)-azetidin-2-one **(307)**

Yield: 91%, 106mg, brown solid

MP: 182 °C

IR (KBr ν max): 1752 cm^{-1}(C=O), 3468 cm^{-1}(OH)

^{1}H NMR (400MHz, $CDCl_3$): δ2.77 (br s, 2H, NH_2), δ3.74 (s, 6H, OMe), δ3.76 (s, 3H, (OMe), δ3.80 (s, 3H, OMe), δ5.17 (d, J=5.30Hz, 1H, H_3), δ5.52 (d, J=5.30, 1H, H_4), δ6.39 (d, J=1.98Hz, 1H, H_6'''), δ6.43 (d, J=2.08, 1H, H_2'''), δ6.66 (s, 2H, H_2' H_6'), δ6.86-7.21 (m, 5H, H_2'' H_3'' H_4'' H_5'' H_6'')

^{13}C NMR (100 MHz, $CDCl_3$): δ55.32, δ58.49, δ59.98, (OMe), δ60.18 (C_3), δ80.02 (C_4), δ94.86 (C_2'&C_6'), δ106.98 (C_6'''), δ107.62 (C_2'''), δ114.89

(C_2''&C_6''), δ118.96 (C_4''), δ127.27 (C_3''&C_5''), δ128.23 (C_1'''), δ128.47 (C_4'''), δ129.46 (C_4'), δ131.26 (C_1'), δ137.27 (C_5'''), δ151.01 (C_3'&C_5'), δ154.12 (C_3'''), δ154.27 (C_4''), δ161.54(C_3)

HRMS: $C_{25}H_{26}N_2O_7$ M^++Na requires 489.1638, found 489.1622 (-3.3ppm)

4-(2-Amino-3-hydroxy-4-methoxy-phenyl)-3-phenoxy-1-(3,4,5-trimethoxy-phenyl)-azetidin-2-one **(305)**

Yield: 88%, 103mg, brown solid

MP: 188 °C

IR (KBr ν max): 1756 cm^{-1}(C=O), 3359 cm^{-1}(OH)

^{1}H NMR (400MHz, $CDCl_3$): δ2.56 (br s, 2H, NH_2) δ3.74 (s, 9H, OMe), δ3.78 (s, 3H, OMe), δ4.91 (s, 3H, OMe), δ5.24 (d, J=5.04Hz, 1H, H_4), δ5.54 (d, J=5.04Hz, 1H, H_3), δ6.59 (s, 2H, H_2'&H_6'), δ6.79-6.84 (m, 3H, H_2'' H_6'' H_4''), δ7.19-7.28 (m, 4H H_3'' H_5'' H_5''' H_6''')

C^{13}: δ55.52, δ55.78, δ59.12 (OMe), δ56.17 (C_4), δ80.05 (C_3), δ94.76 (C_2'&C_6'), δ113.15 (C_2''&C_6''), δ115.27 (C_4''), δ118.16 (C_5'''), δ121.38 (C_6'''), δ129.28 (C_4'), δ131.23 (C_3'' & C_5''), δ120.94 (C_1'''), δ128.82 (C_3'''), δ138.02 (C_1'), δ138.17 (C_2'''), δ147.16 (C_4'''), δ149.02 (C_3'&C_5'), δ156.34 (C_1''), δ163.03 (C_2)

HRMS: $C_{25}H_{26}N_2O_7$ M^+Na requires 489.1623, found 489.1646 (-3.0ppm)

5.14 Azide Analogues

Azide Formation

To a stirring suspension of 4-(amino-benzyl)-alcohol (**315**) (616mg, 5mmol) in 2M H_2SO_4 (6mL) at 0°C was added $NaNO_2$ (519mg, 7.5mmol) in water (4mL) dropwise. After the addition the reaction became clear and colourless. Reaction was left to stir for 15 minutes before NaN_3 (488mg, 7.5mmol) in water (4mL) was added very carefully dropwise over 5 minutes, resulting in the evolution of gas bubbles.

The reaction was left to stir at room temperature for a further hour at which point a brown oil had formed at the bottom of the reaction vessel. The reaction was extracted with DEE (2x10mL), organic layer dried over Na_2SO_4, filtered, and solvent removed under reduced pressure to yield the title compound.

4-(Azido-phenyl)-methanol **(316)**

Yield: 90%, 671mg, clear oil

MP: Oil Litt. 27-28°C

IR (NaCl ν max): 3321 cm^{-1}(OH), 2117cm^{-1}

^{1}H NMR (400MHz, $CDCl_3$): δ2.32 (1H, s, broad, -OH), δ4.64 (2H, s, -CH_2OH), δ7.00 (2H, d, J=8.44Hz, H_2' H_6'), δ7.32 (2H, d, J=8.61Hz, H_3' H_5')

^{13}C NMR (100 MHz, $CDCl_3$): δ64.11 (CH_2OH), δ118.63 (C_2&C_6), δ128.08 (C_3&C_5), δ137.11 (C_4), δ138.85 (C_1)

PCC oxidation

To a stirring solution of the 4-(azido-phenyl)-methanol (**316**) (668mg, 4.47mmol) in dry DCM (20mL) under N_2, was added PCC (1.64g, 7.6mmol), and the resulting solution allowed to stir together at room temperature for 1 hour. The reaction was diluted with DCM (20mL), and the reaction filtered through a 1cm pad of silica and the solvent removed under reduced pressure to yield an orange oil.

4-Azido-benzaldehyde **(317)**

Yield: 78%, 513mg, orange oil

MP: Oil

IR (NaCl ν max): 2110 cm^{-1} (Azide) , 1694 cm^{-1} (C=O)

^{1}H NMR (400MHz, $CDCl_3$): δ7.10 (2H, d, J=8.29Hz H_3 H_5), δ7.83 (2H, d, J=8.29Hz H_2 H_6), δ9.89 (1H, s, -CHO)

^{13}C NMR (100 MHz, $CDCl_3$): δ119.03 (C3&C5), δ131.12 (C2&C6), δ132.74 (C4), δ190.23 (CHO)

Imine Synthesis

4-Azido-benzaldehyde (**317**) (658mg, 4.47mmol) and 3,4,5-trimethoxy aniline (823mg, 4.47mmol) were refluxed together in ethanol for 1.5 hours. The imine was seen to precipitate out upon reducing the reaction volume by half and allowing to stand at room temperature. The precipitate was filtered off by vacuum and allowed to dry overnight between filter paper.

(4-Azido-benzylidene)-(3,4,5-trimethoxy-phenyl)-amine **(318)**

Yield: 18%, 251mg, yellow solid

MP: 74 °C

IR (KBr ν max): 2120 cm^{-1}(azide), 1584 cm^{-1}(C=N)

^{1}H NMR (400MHz, $CDCl_3$): δ3.89 (s, 3H, OMe), δ3.92 (s, 6H, OMe), δ6.51 (s, 2H, C_2'&C_6'), δ7.14 (d, J=8.27Hz, 2H, H_3'' H_5''), δ7.91 (d, J=8.65, 2H, H_2'' H_6''), δ8.45 (s, 1H, Imine)

^{13}C NMR (100 MHz, $CDCl_3$): 55.87, 57.23 (OMe), 98.10 (C_2' C_6'), 122.56 (C_2'' C_6''), 127.39 (C_3'' C_5''), 128.39 (C_1'), 129.89 (C_1''), 133.28 (C_4''), 135.38 (C_4'), 151.49 (C_3' C_5'), 161.14 (imine)

HRMS $C_{16}H_{16}N_4O_3$ M^++1 requires 313.1222 found 313.1225 (1.0ppm)

β-Lactam formation

To a stirring, refluxing solution of the imine (**318**) (5mmol) and triethylamine (6mmol) in anhydrous dichloromethane (40mL), a solution of the phenoxy acetyl chloride (6mmol) in anhydrous dichloromethane (10mL) was added over 45 minutes under nitrogen. The reaction was kept at reflux during the day (5 hours) and at room temperature overnight (16 hours), continuously under nitrogen, until the starting material had disappeared as monitored by TLC in 1:1 hexane/ethyl acetate. A characteristic darkening of the reaction to an amber colour over time was observed. The reaction was transferred to a separating funnel and washed with water (2 x 100mL), with the organic layer being retained each time. The reaction was dried over Na_2SO_4 before the solvent was removed under reduced pressure. The crude product was purified by flash chromatography over silica gel using 1:1 *n*-hexane:ethyl acetate to yield the title compound.

4-(4-Azido-phenyl)-3-phenoxy-1-(3,4,5-trimethoxy-phenyl)-azetidin-2-one **(319)**

Yield: 64%, 1.428g, grey solid

MP: 134-138°C

IR (KBr ν max): 1761 cm^{-1}(C=O), 2136 cm^{-1}(azide)

^{1}H NMR (400MHz, $CDCl_3$): δ3.75 (s, 6H, OMe), δ3.80 (s, 3H. OMe), δ5.37 (d, J=4.80Hz, 1H, H_4), δ5.57 (d, J=4.80Hz, 1H, H_3), δ6.61 (s, 2H, H_2'&H_6'), δ6.82 (d, J=7.86, 2H, H_2''&H_6''), δ6.97 (m, 3H, H_4'' & H_3''' & H_5'''), δ7.20 (d, J=8.35, 8.85, 2H, H_3''&H_5''), δ7.40 (d, J=8.23, 2H, H_2'''&H_6''')

^{13}C NMR (100 MHz, $CDCl_3$): δ55.63, δ55.67, δ60.51 (OMe), δ61.32 (C_4), δ80.52 (C_3), δ94.76 (C_2'&C_6'), δ115.07 (C_2''&C_6''), δ118.68 (C_2'''&C_6'''), δ121.92 (C_4''), δ128.85 (C_3''' &C_5'''), δ128.94 (C_3''&C_5''), δ129.18 (C_4''), δ132.45 (C_4'), δ134.57 (C_1'), δ140.15 (C_1'''), δ153.13 (C_3'&C_5'), δ156.29 (C_1''), δ162.34 (C_2)

HRMS: $C_{24}H_{22}N_4O_5$ M^++Na requires 469.1488, found 469.1500 (2.6ppm)

5.15 3''' and 4''' aryl ring substitutions

Imine synthesis

The appropriately substituted benzaldehyde (10mmol) and corresponding substituted aniline (10mmol) starting materials were refluxed together in ethanol (40mL) for five hours with a catalytic amount of $H_2SO_{4\ (conc)}$. The reaction volume was then reduced to approximately 10mL by removal of solvent under reduced pressure. The Schiff base was seen to precipitate out from solution upon standing at room temperature. The precipitate was removed by vacuum filtration and the solid obtained purified by recrystalistion from hot ethanol before being dried on filter paper.

3-[(3,4,5-Trimethoxy-phenylimino)-methyl]-phenol **(320)**

Yield: 73%, 2.097g, white solid

MP: 121 °C

IR (KBr ν max): 1583 cm^{-1} (C=N), 3327 cm^{-1} (OH)

^{1}H NMR (400MHz, $CDCl_3$): δ3.76 (s, 3H, OMe), δ3.88 (s, 6H, -OMe), δ6.50 (s, 2H, H_2'H_6') δ7.33-7.42 (m, 4H, H_2'' H_4'' H_5'' H_6''), δ7.00 (s br, 1H, -OH)

^{13}C NMR (100 MHz, $CDCl_3$): δ55.68 & δ60.60 (-OMe), δ97.81 (C_2'&C_6'), δ114.10 (C_2''), δ118.75 (C_4''), δ121.50 (C_6''), δ129.64 (C_5''), δ136.10 (C_4'), δ136.72 (C_1''), δ147.09 (C_1'), δ153.09 (C_3'&C_5'), δ156.03 (C_3''), δ159.78 (Imine)

HRMS $C_{16}H_{17}NO_4$ M^++1 requires 288.1236, found 288.1249

(3-Nitro-benzylidene)-(3,4,5-trimethoxy-phenyl)-amine **(321)**

Yield: 93%, 2.940g, yellow solid

MP: 160 °C

IR (KBr ν max): 1588 cm^{-1}(C=N)

^{1}H NMR (400MHz, $CDCl_3$): δ3.89 (s, 3H, -OMe), δ3.93 (s, 6H, -OMe), δ6.56 (s, 2H, H_2'H_6'), δ6.66-6.72 (m, 4H, H_2''H_4''H_5''H_6''), δ8.76 (s, 1H, Imine)

^{13}C NMR (100 MHz, $CDCl_3$): δ55.70 & δ60.58 (-OMe), δ97.90 (C_2'&C_6'), δ122.96 (C_2''), δ125.10 (C_4''), δ129.39 (C_5''), δ133.56 (C_6''), δ136.69 (C_4'), δ137.32 (C_1''), δ146.13 (C_1'), δ148.23 (C_3'&C_5'), δ153.22 (C_3''), δ155.92 (Imine)

HRMS $C_{16}H_{16}N_2O_5$, M^++1 requires 317.1137, found 317.11434 (1.7ppm)

(4-Nitro-benzylidene)-(3,4,5-trimethoxy-phenyl)-amine **(322)**

Yield: 82%, 2.592g, yellow solid

MP: 158°C

IR (KBr ν max): 1587 cm^{-1}(C=N)

^{1}H NMR (400MHz, $CDCl_3$): δ3.90 (s, 3H, OMe), δ3.94 (s, 6H, OMe), δ6.57 (s, 2H, H_2' H_6'), δ8.09 (d, J=8.04, 2H, H_2'' H_6''), δ8.34 (d, J=8.04, 2H, H_3'' H_5''), δ8.59 (s, 1H, Imine)

^{13}C NMR (100 MHz, $CDCl_3$): δ56.19, δ61.06 (OMe), δ98.45 (C_2'&C_6'), δ124.06 (C_3''&C_5''), δ129.34 (C_2''&C_6''), δ137.38 (C_4'), δ141.50 (C_1''), δ146.65 (C_3'&C_5'), δ149.23 (C_3'&C_5'), δ153.70 (C_4''), δ156.50 (Imine)

HRMS $C_{16}H_{16}N_2O_5$ M^++1 requires 317.1137, found 317.1124 (-4.2ppm)

(3-Methoxy-benzylidene)-(3,4,5-trimethoxy-phenyl)-amine **(323)**

Yield: 88%, 2.65g, white solid

MP: 59 °C

IR (KBr ν max): 1587 cm^{-1}(C=N)

^{1}H NMR (400MHz, $CDCl_3$): δ3.88 (s, 3H, -OMe), δ3.90 (s, 6H, -OMe), δ3.92 (s, 3H, -OMe), δ6.51 (s, 2H, H_2'H_6'), δ7.32-7.52 (m, 4H, H_2'' H_4'' H_5'' H_6''), δ8.46 (s, 1H, Imine)

^{13}C NMR (100 MHz, $CDCl_3$): δ54.98, δ55.67, δ60.57 (-OMe), δ97.71 (C_2'&C_6'), δ111.33 (C_2''), δ117.87 (C_4''), δ121.84 (C_6''), δ129.32 (C_5''), δ135.95 (C_4'), δ137.02 (C_1''), δ147.40 (C_1'), δ153.11 (C_3'&C_5'), δ159.19 (Imine), δ159.56 (C_3'')

HRMS $C_{17}H_{19}NO_4$ M^++1 requires 302.1392, found 302.1403 (3.5ppm)

Imine Protection

The appropriate imine (**320**) (5mmol) and *t*-BDMSCl (6mmol) were mixed together in anhydrous dichloromethane (40mL) under a nitrogen atmosphere. To this stirring solution, DBU (8mmol) was added dropwise under nitrogen via syringe. Stirring under nitrogen was continued until starting material had disappeared as monitored by TLC in 1:1 hexane/ethyl acetate (2 - 4 hours). Upon completion the reaction was diluted with 50mL of dichloromethane and transferred to a separating funnel. The reaction was washed with water (2 x 100mL), 0.1M HClaq (2 x 50mL), and saturated NaHCO3 aqueous solution (2 x 50mL), retaining the organic layer each time, before drying over Na_2SO4. The solvent was removed to yield the title compound which was used in the Staundinger reaction without further purification.

[3-(*t*-Butyl-dimethyl-silanyloxy)-benzylidene]-(3,4,5-trimethoxy-phenyl)- amine

Yield: 92%, 1.847g, amber oil

MP: Oil

IR (NaCl ν max): 1597 cm^{-1}(C=N)

^{1}H NMR (400MHz, $CDCl_3$): δ0.23 (s, 3H, OtBDMS), δ0.24 (s, 3H, OtBDMS), δ1.00 (s, 9H, OtBDMS), δ3.87 (s, 3H, OMe), δ3.90 (s, 6H, OMe), δ6.50 (s, 2H, H_2'&H_6'), δ6.97 (1H, q, J=2.24Hz, 7.73Hz, H_4''), δ7.34-7.41 (m, 3H, H_2'' H_5'' H_6''), δ8.42 (s, 1H, imine)

^{13}C NMR (100 MHz, $CDCl_3$): δ-4.91, δ-4.84, δ17.73, δ25.17 (OtBDMS), δ53.01, δ55.63, δ60.53 (OMe), δ97.71 (C_2'&C_6'), δ119.26 (C_2''), δ121.87 (C_6''), δ122.89 (C_4''), δ129.32 (C_5''), δ135.87 (C_4'), δ137.07 (C_1''), δ147.47 (C_1'), δ153.08 (C_3' C_5') δ155.67 (C_3'') δ159.24 (Imine)

HRMS: $C_{16}H_{17}NO_4$ M^++1 requires 287.1158, found 287.1164 (2.1ppm)

β-Lactam formation

To a stirring, refluxing solution of the silyl ether imine or the imine (**320-323**) (5mmol) and triethylamine (6mmol) in anhydrous dichloromethane (40mL), a solution of the appropiate acid chloride (6mmol) in anhydrous dichloromethane (10mL) was added over 45 minutes under nitrogen. The reaction was kept at reflux during the day (5 hours) and at room temperature overnight (16 hours), continuously under nitrogen, until the starting material had disappeared as monitored by TLC in 1:1 hexane/ethyl acetate. A characteristic darkening of the reaction to an amber colour over time was observed. The reaction was transferred to a separating funnel and washed with water (2 x 100mL), with the organic layer being retained each time. The reaction was dried over Na_2SO_4 before the solvent was removed under reduced pressure. The crude product was purified by flash chromatography over silica gel in 1:1 *n*-hexane:ethyl acetate to yield the title compounds.

4-(4-Nitro-phenyl)-3-phenoxy-1-(3,4,5-trimethoxy-phenyl)-azetidin-2-one **(325)**

Yield: 39%, 896mg, white solid

MP: 154 °C

IR (KBr ν max): 1765 cm^{-1}(C=O)

^{1}H NMR (400MHz, $CDCl_3$): δ3.75 (s, 3H, OMe), δ3.80 (s, 6H OMe), δ5.51 (d, J= 5.04Hz 1H, H_4), δ5.66 (d, J=5.6Hz, 1H, H_3), δ6.57-8.20 (m, 11H, Ar-H)

^{13}C NMR (100 MHz, $CDCl_3$): δ55.71, δ60.53 (OMe), δ60.79 (C_4), δ80.61 (C_3), δ94.66 (C_2'&C_6'), δ114.94 (C_2''&C_6''), δ122.27 (C_4''), δ123.22 (C_3'''&C_5'''), δ128.51 (C_2'''&C_6''), δ129.08 (C_3''&C_5''), δ132.07 (C_4'), δ139.93 (C_4''), δ147.70 (C_1'''), δ153.30 (C_3'&C_5'), δ155.95 (C_1'), δ161.87 (C_2)

HRMS: M^++Na requires 473.1325, found 473.1335 (2.2ppm)

4-(3-Methoxy-phenyl)-3-phenoxy-1-(3,4,5-trimethoxy-phenyl)-azetidin-2-one **(329)**

Yield: 34%740mg, white solid

MP: 158 °C

IR (KBr ν max): 1749cm^{-1} (C=O)

^{1}H NMR (400MHz, $CDCl_3$): δ3.76 (s, 6H, OMe), δ3.81 (s, 6H, OMe), δ5.32 (d, J=5.1Hz, 1H, H_4), δ5.57 (d, J=5.1Hz, 1H, H_3), δ6.67 (s, 2H, H_2' H_6'), δ6.82-7.29 (m, 9H, Ar-H)

^{13}C NMR (100 MHz, $CDCl_3$): δ56.08, δ60.98 (OMe), δ62.50 (C_4), δ81.03 (C_3), δ95.26 (C_2'&C_6'), δ110.26 (C_4'''), δ114.20 (C_2'''), δ115.59 (C_2''&C_6''), δ121.93 (C_6'''), δ122.26 (C_4''), δ124.42 (C_5'''), δ129.35 (C_2''&C_5''), δ133.22 (C_4'), δ134.95 (C_1'), δ146.24 (C_1'''), δ146.72 (C_3'&C_5'), δ153.53 (C_1''), δ156.93 (C_3'''), δ163.02 (C_3)

HRMS: M^++Na requires 458.1580, found 458.1574 (-1.0ppm)

4-(3-Nitro-phenyl)-3-phenoxy-1-(3,4,5-trimethoxy-phenyl)-azetidin-2-one **(325)**

Yield: 47%, 1.059g, brown solid

MP: 170-174 °C

IR (KBr ν max): 1762 cm^{-1} (C=O)

^{1}H NMR (400MHz, $CDCl_3$): δ3.76 (s, 3H, -OMe), δ3.80 (s, 6H, -OMe), δ5.53 (d J=5Hz, 1H, H_4), δ5.68 (d J=5Hz, 1H, H_3), δ6.60 (s, 2H, H_2' H_6'), δ7.34-8.27 (m, 9H, H_2'' H_3'' H_4'' H_5'' H_6'' H_2''' H_4''' H_5''' H_6''')

^{13}C NMR (100 MHz, $CDCl_3$): δ55.74, δ60.53 (-OMe), δ60.72 (H_4), δ80.41 (H_3), δ94.73 (C_2'&C_6'), δ114.91 (C_2''&$C_{6''}$), δ122.23 (C_4''), δ122.72 (C_3'''&C_5'''), δ123.49 (C_2'''&C_6'''), δ129.17 (C_3''&C_5''), δ132.06 (C_4'), δ133.41 (C_4'''), δ134.79 (C_1'), δ134.85 (C_1''), δ147.70 (C_1'''), δ153.31 (C_3'&C_5'), δ155.84 (C_1''), δ161.85 (C_2)

HRMS: M^++Na requires 473.1325, found 473.1325 (4.1ppm)

4-(3-Hydroxy-phenyl)-3-phenoxy-1-(3,4,5-trimethoxy-phenyl)-azetidin-2-one **(324)**

Yield: 43%, 905mg, white solid

MP: 218-220 °C

IR (KBr ν max): 1749 cm^{-1}(C=O), 3380 cm^{-1}(OH)

^{13}C NMR (100 MHz, $CDCl_3$): δ55.75 & δ60.14 (-OMe), δ61.11 (C_4), δ80.36 (C_3), δ95.05 (C_2'&C_6'), δ114.58 (C_4'''), δ115.16 (C_2''&C_6''), δ115.53 (C_2'''), δ119.22 (C_6'''), δ121.88 (C_4''), δ129.24 (C_5'''), δ132.81 (C_4'), δ134.27 (C_1'), δ134.62 (C_1'''), δ153.22 (C_3'&C_5'), δ156.56 (C_3'''), δ157.05 (C_1''), δ162.72 (C_2)

^{1}H NMR (400MHz, $CDCl_3$): δ3.59 (s, 3H, -OMe), δ3.66 (s, 6H, -OMe), δ5.64 (d, J=4.5Hz, 1H, H_4), δ5.86 (d, J=5Hz, 1H, H_3), δ6.60 (s, 2H, H_2' H_6'), δ6.97.23 (m, 9H, H_2'' H_3'' H_4'' H_5'' H_6'' H_2''' H_4''' H_5''' H_6'''), δ9.41 (s, 1H, -OH)

HRMS: M^++Na requires 444.1423, found 444.1414 (-2.0)

Reduction of nitro compounds

To a flask containing the β-lactam (**325-326**) (0.25mmol) and zinc powder 10μm (2.5mmol 165mg) was added 15mL of acetic acid at room temperature under N and reaction left to stir for 7 days. The reaction was filtered through a celite pad and the filtrate collected. Solvent was removed under reduced pressure and the resulting residue was eluted through a short pad of silica with DCM. The resulting product was recrystallised with hot ethanol to yield the title compounds

4-(4-Amino-phenyl)-3-phenoxy-1-(3,4,5-trimethoxy-phenyl)-azetidin-2-one **(328)**

Yield: 79%, 166mg, brown solid

MP: 172 °C

IR (KBr ν max): 1753 cm^{-1}(C=O), 3362 cm^{-1}(OH)

^{1}H NMR (400MHz, $CDCl_3$): δ1.7 (br s, 2H, NH_2), δ3.75 (s, 3H, OMe), δ3.79 (s, 3H, OMe), δ5.28 (d, J=5.0Hz, 1H, H_4), δ5.52 (d, J=5.0Hz, 1H, H_3), δ6.61 (s, 2H, H_2' H_6') δ7.07-7.21 (m, 9H, H_2'' H_3'' H_4'' H_5'' H_6'' H_2''' H_3''' H_5''' H_6''')

^{13}C NMR (100 MHz, $CDCl_3$): δ55.27,δ56.04, δ60.76 (OMe), δ61.09 (C_4), δ81.83 (C_3), δ94.27 (C_2'&C_6'), δ112.67 (C_3'''&C_5'''), δ114.99 (C_2''&C_6''), δ123.45 (C_4''), δ124.27 (C_4'), δ119.37 (C_2'''&C_6'''), δ129.51 (C_3''&C_5''), δ133.79 (C_1'''), δ134.92 (C_1'), δ153.47 (C_3'&C_5'), δ157.29 (C_1''), δ160.01 (C_4'''), δ164.04 (C_3)

HRMS: $C_{24}H_{24}N_2O_5$ M^++Na requires 443.1583, found 443.1576 (-1.6ppm)

4-(3-Amino-phenyl)-3-phenoxy-1-(3,4,5-trimethoxy-phenyl)-azetidin-2-one **(327)**

Yield: 87%, 183mg, brown solid

MP: 184 °C

IR (KBr ϒ max): 1752 cm^{-1}(C=O), 3453 cm^{-1}(OH)

^{1}H NMR (400MHz, $CDCl_3$): δ3.74 (s, 9H, OMe), δ3.80 (s, 3H, OMe), δ5.32 (d, J=5.04Hz, 1H, H_4), δ5.58 (d, J=5.04Hz, 1H, H_3), δ6.64 (2, 2H, H_2' H_6'), δ6.82-7.23 (m, 9H, H_2'' H_3'' H_4'' H_5'' H_6'' H_2''' H_3''' H_5''' H_6''')

^{13}C NMR (100 MHz, $CDCl_3$): δ55.31, δ56.07, δ60.96 (OMe), δ62.31 (C_4), δ81.06 (C_3), δ95.26 (C_2'&C_6'), δ113.71 (C_4'''), δ114.39 (C_2'''), δ115.72 (C_2''&C_6''), δ120.62 (C_6'''), δ122.26 (C_4''), δ129.32 (C_5'''), δ129.53 (C_3''&C_5''), δ133.14 (C_4'), δ134.27 (C_3''&C_5''), δ134.96 (C_1'''), δ153.55 (C_3'''), δ156.97 (C_3'&C_5'), δ159.64 (C_1''), 162.93 (C_2)

HRMS: $C_{24}H_{24}N_2O_5$ M^++Na requires 443.1583, found 443.1597 (3.2ppm)

5.16 3-Position Analogues

To the silyl ether imine **208** (5mmol) in DCM (25mL), and (TEA 6mmol) stirring at reflux under N_2 was added a solution of the appropriate acid chloride (6mmol) in DCM (10mL) dropwise over the course of 25 minutes. The reaction was then left to reflux under N_2 for 6 hours and at room temperatures overnight. The reaction was diluted with DCM and washed with H_2O (2x100mL). The organic layer was collected and dried over $MgSO_4$ before the solvent was removed under reduced pressure. The deprotection of the β-lactam product was carried out by treatment with tBAF in dry THF at 0°C under N_2 as previously described.

3-Chloro-4-(3-hydroxy-4-methoxy-phenyl)-1-(3,4,5-trimethoxy-phenyl)-azetidin-2-one **(339)**

Yield: 34%, 668mg, brown oil

MP: oil

IR (NaCl ν max): 1770 cm^{-1}(C=O), 3417 cm^{-1}(OH)

^{1}H NMR (400MHz, $CDCl_3$): δ3.74 (s, 6H OMe), δ3.78 (s, 3H OMe), δ3.92 (s, 3H OMe), δ4.61 (d, J=2.04Hz 1H H_3), δ4.89 (d, J=1.52Hz 1H H_3), δ5.81 (s, 1H OH), δ6.56 (s, 2H H_2'H_6'), δ6.87-6.95 (m, 3H H_2'' H_5'' H_6'')

^{13}C NMR (100 MHz, $CDCl_3$): δ55.59, δ55.63, δ60.51 (OMe), δ62.67 (C_3), δ65.63 (C_4), δ94.81 (C_2'&C_6'), δ110.61 (C_2''), δ111.58 (C_5''), δ117.72 (C_6''), δ127.52 (C_4'), δ132.50 (C_1'), δ134.63 (C_1''), δ146.04 (C_3''), δ147.00 (C_4''), δ153.08 (C_3'&C_5'), δ160.22 (C_2)

HRMS: M^+Na calculated 416.0877, found 416.0897, (4.8ppm)

3,3-Dichloro-4-(3-hydroxy-4-methoxy-phenyl)-1-(3,4,5-trimethoxy-phenyl)-azetidin-2-one **(340)**

Yield:28%, 600mg, brown oil

MP: oil

IR (NaCl ν max): 1777 cm^{-1}(C=O), 3420 cm^{-1}(OH)

^{1}H NMR (400MHz, $CDCl_3$): δ3.74 (s, 6H, OMe), δ3.80 (s, 3H, OMe), δ3.93 (s, 3H, OMe), δ5.40 (s, 1H, H_4), δ5.85 (br s, 1H, OH), δ6.57-7.00 (m, 5H, H_2' H_6' H_2'' H_5'' H_6'')

^{13}C NMR (100 MHz, $CDCl_3$): δ55.52, δ55.75, δ60.52 (OMe), δ73.54 (C_4), δ95.42 (C_2'&C_6'), δ110.18 (C_2''), δ113.33 (C_5''), δ119.44 (C_6''), δ124.00 (C_4'), δ124.16 (C_1'), δ145.49 (C_3''), δ147.31 (C_4''), δ153.16 (C_3'&C_5'), δ157.91 (C_2)

HRMS: M^+ requires 428.0668, found 428.0663 (-1.1ppm)

4-(3-Hydroxy-4-methoxy-phenyl)-3-phenyl-1-(3,4,5-trimethoxy-phenyl)-azetidin-2-one **(341)**

Yield: 22%, 479mg, brown oil

MP: oil

IR (NaCl ν max): 1746 cm^{-1}(C=O), 3418 cm^{-1}(OH)

^{1}H NMR (400MHz, $CDCl_3$): δ3.75 (s, 6H, OMe), δ3.80 (s, 3H, OMe), δ3.93 (s, 3H, OMe), δ4.29 (d, J=2.52Hz, 1H, H_4), δ4.82 (d, J=2.52, 1H, H_3), δ6.63 (s, 2H, H_2'H_6'), δ6.88-7.38 (m, 8H, H_2'' H_3'' H_4'' H_5'' H_6'' H_2''' H_5''' H_6''')

^{13}C NMR (100 MHz, $CDCl_3$): δ55.58, δ55.60, δ60.51 (OMe), δ63.35 (C_3), δ64.49 (C_4), δ94.41 (C_2'&C_6'), δ110.57 (C_2''), δ111.55 (C_5'''), δ117.39 (C_6'''), δ126.96 (C_4''), δ127.43 (C_3''&C_5''), δ128.57 (C_2''&C_6''), δ130.47 (C_4'), δ133.02 (C_1'), δ134.31 (C_1''), δ144.65 (C_1'''), δ145.88 (C_3'''), δ146.33 (C_4'''), δ153.05 (C_3'&C_5'), δ157.81 (C_2)

HRMS M^++Na requires 458.1580, found 458.1568 (-2.5ppm)

3-Benzyl-4-(3-hydroxy-4-methoxy-phenyl)-1-(3,4,5-trimethoxy-phenyl)-azetidin-2-one (**342**)

Yield: 36%, 809mg, brown oil

MP: oil

IR (NaCl ν max): 1744 cm^{-1}(C=O), 3346 cm^{-1}(OH)

^{1}H NMR (400MHz, $CDCl_3$): δ2.81 (dd, J=2.1Hz, 6.8Hz, 2H, CH_2), δ3.71-3.89 (m, 13H, H_3 & OMe), δ4.60 (d, J=2.0Hz, 1H, H_4), δ5.69 (br, s, 1H, OH), δ6.48 (s, 2H, H_2'H_6'), δ7.08-7.33 (m, 8H, H_2'' H_3'' H_4'' H_5'' H_6'' H_2''' H_5''' H_6''')

^{13}C NMR (100 MHz, $CDCl_3$): δ34.10 (CH_2), δ55.48, δ55.56, δ55.61 (OMe), δ60.37 (C_3), δ60.50 (C_4), δ94.24 (C_2'&C_6'), δ97.06 (C_5'''), δ103.03 (C_2'''), δ110.35 (C_6'''), δ111.47 (C_4''), δ117.18 (C_2''&C_6''), δ125.83 (C_4'), δ127.7 (C_3''&C_5''), δ130.21 (C_1'''), δ133.46 (C_1'), δ137.39 (C_1''), δ145.60 (C_3'''), δ146.06 (C_4'''), δ152.98 (C_3'&C_5'), δ166.66 (C_2)

HRMS: M^++Na calculated 472.1736, found 472.1727, -1.9ppm,

4-(3-Hydroxy-4-methoxy-phenyl)-1-(3,4,5-trimethoxy-phenyl)-3-vinyl-azetidin-2-one **(343)**

Yield: 18%, 347mg, brown oil

MP: oil

IR (NaCl ν max): 1732 cm^{-1}(C=O), 3408 cm^{-1}(OH)

^{1}H NMR (400MHz, $CDCl_3$): δ3.75 (m, 7H, OMe & H_3), δ3.78 (s, 3H, OMe), δ3.91 (s, 3H, OMe), δ4.69 (d, J=2.04Hz, 1H, H_4), δ5.34 (t, J=8Hz,10.56, 2H, CHCH_2), δ5.78 (s, 1H, OH), δ5.98-6.38 (m, 1H, CHCH_2), δ6.57-6.94 (m, 5H, H_2' H_6' H_2'' H_5'' H_6'')

^{13}C NMR (100 MHz, $CDCl_3$): δ55.56, δ55.59, δ60.86 (OMe), δ60.50 (C_3), δ63.37 (C_4), δ94.27 (C_2'&C_6'), δ110.51 (C_1''), δ111.54 (C_2''), δ111.57 (C_5''), δ117.31 (C_6''), δ119.42 (CHCH_2), δ129.91 (C_4'), δ130.09 (CHCH_2), δ133.38 (C_1'), δ134.12 (C_1''), δ145.84 (C_3''), δ146.37 (C_4''), δ153.01 (C_3'&C_5'), δ164.85 (C_2)

HRMS M^+Na requires 408.1423, found 408.1420 (-0.8ppm)

4-(3-Hydroxy-4-methoxy-phenyl)-3-isopropenyl-1-(3,4,5-trimethoxy-phenyl)-azetidin-2-one **(344)**

Yield: 22%, 439mg, brown oil

MP: oil

IR (NaCl ν max): 1717 cm^{-1}(C=O), 3532 cm^{-1}(OH)

^{1}H NMR (400MHz, $CDCl_3$): δ1.84 (s, 3H, CH_3), δ3.72 (d, J=1.78, 1H, H_3), δ3.74 (s, 6H, OMe), δ3.78 (s, 3H, OMe), δ3.91 (s, 3H, OMe), δ4.72 (d, J=1.78, 1H, H_4), δ5.01 (d, J=14.3Hz, 1H, CH_2), δ5.08 (d, J=14.38Hz, 1H, CH_2), δ5.79 (br, s, 1H, OH), δ6.59 (s, 2H, H_2'&H_6'), δ6.86-6.90 (m, 3H, H_2'' H_5'' H_6'')

^{13}C NMR (100 MHz, $CDCl_3$): δ20.10 (C_7), δ55.86, δ55.90, δ60.22 (OMe), δ60.76 (C_3), δ66.68 (C_4), δ94.70 (C_2'&C_6'), δ110.90 (C_2''), δ111.98 (C_5''), δ114.15 (C_6), δ117.58 (C_6''), δ130.67 (C_4'), δ133.63 (C_1'&C_1''), δ134.35 (C_2''), δ138.03 (C_3''), δ146.19 (C_5), δ146.67 (C_4''),δδ153.35 (C_3'&C_5'), δ165.04 (C_2)

HRMS: M^++Na requires 422.1580, found 422.1596 (3.9ppm)

5.17 Phthalimido Route to 3-NH_2 β-Lactam

To a stirring solution of glycine (10mmol 2.05g) in dichloroethane (50mL) and DMF (0.5 mL) was added $SOCl_2$ (30mmol 2.18mL) under N2 and reaction brought to reflux for 90 minutes. Solvent and excess SOCl2 were removed under reduced pressure to yield the title compound. Used immediately without further purification. The acid chloride (6mmol) in DCM (10mL) was added to a solution of the silyl ether imine (5mmol) and TEA (6mmol) in DCM (40mL) and the resulting solution was stirred under N_2 at reflux for eight hours followed by room temperature for 18hours. The reaction was diluted with DCM (50mL) and washed with H_2O (100mL), 0.1M HCl (100mL), and saturated $NaHCO_3$ (100mL) and the organic layer collected, dried over $MgSO_4$, filtered and the solvent removed under reduced pressure. The product was isolated by flash chromatography over silica gel in 1:1 *n*-hexane:ethyl acetate.

2-[2-[3-(*t*-Butyl-dimethyl-silanyloxy)-4-methoxy-phenyl]-4-oxo-1-(3,4,5-trimethoxy-phenyl)-azetidin-3-yl]-isoindole-1,3-dione **(354)**

Yield: 71%, 2.197g, amber oil

MP: oil

IR (NaCl ν max): 1719 cm^{-1}(C=O), 1762 cm^{-1}(C=O)

^{1}H NMR (400MHz, $CDCl_3$): δ0.09 (s, 6H, OtBDMS), δ0.21 (s, 9H, OtBDMS), δ3.64 (s, 3H, OMe), δ3.72 (s, 3H, OMe), δ3.79 (s, 3H, OMe), δ5.99 (d, J=5.43Hz, 1H, H_4), δ6.07 (d, J=5.44Hz, 1H, H_3), δ6.67 (s, 2H, H_2'&H_6'), δ6.69-6.74 (m, 3H, H_2''' H_5''' H_6'''), δ7.51-7.54 (m, 2H, H_3'' H_5''), δ8.13-8.15 (m, 2H, H_2'' H_6'')

^{13}C NMR (100 MHz, $CDCl_3$): δ-4.14, δ-4.07, δ17.68, δ24.15 (OtBDMS), δ55.57, δ55.73, δ59.28, δ60.26 (OMe), δ60.19 (C_3), δ65.69 (C_4), δ94.91 (C_2'C_6'), δ112.59 (C_2'''), δ114.71 (C_5'''), δ119.67 (C_6'''), δ126.19 (C_3'' C_6''), δ128.49 (C_4'), 1δ30.53 (C_4''C_5''), δ131.29 (C_2''&C_7''), δ133.21 (C_1'), δ133.45 (C_1'''), δ141.29 (C_3'''), δ149.54 (C_4'''), δ159.19 (C_3' C_5'), δ162.59 (C_1'' C_8''), δ166.81 (C_2)

HRMS: $C_{33}H_{38}N_2O_8Si$ M^++1 requires 619.2397, found 619.2385 (1.9ppm)

To a stirring solution of the sily ether β-lactam (**354**) (3mmol) under N_2 and at 0^0C in dry THF was added dropwise 1.0 M t-BAF solution in hexanes (3mL, 3mmol). The resulting solution was left to stir at 0^0C until reaction was complete as seen on TLC. Reaction was diluted with ethyl acetate (75mL) and washed with 0.1M HCL_{aq} (100mL). The aqueous layer was further extracted with ethyl acetate (2x25mL). All the organic layers were collected and washed with H_2O (100mL), and saturated brine (100mL) before being dried over Na_2SO_4. Solvent was removed under reduced pressure to yield the free phenol.

2-[2-(3-Hydroxy-4-methoxy-phenyl)-4-oxo-1-(3,4,5-trimethoxy-phenyl)-azetidin-3-yl]-isoindole-1,3-dione **(355)**

Yield: 64%, 1.614g, amber oil

MP: oil

IR (NaCl ν max): 1721 cm^{-1}(C=O), 1762 cm^{-1}(C=O), 3423 cm^{-1}(OH)

^{1}H NMR (400MHz, $CDCl_3$): δ3.69 (s, 3H, OMe), δ3.78 (s, 3H, OMe), δ3.86 (s, 3H, OMe), δ6.02 (d, J=5.55Hz, 1H, H_4), δ6.13 (d, J=5.55Hz, 1H, H_3), δ6.68 (s, 2H, H_2'&H_6'), δ6.73-6.78 (m, 3H, H_2''' H_5''' H_6'''), δ7.54-7.58 (m, 2H, H_3'' H_5''), δ8.12-8.15 (m, 2H, H_2'' H_6'')

^{13}C NMR (100 MHz, $CDCl_3$): δ55.63, δ55.83, δ59.24, δ61.89 (OMe), δ60.59 (C_3), δ66.36 (C_4), δ94.77 (C_2'C_6'), δ113.84 (C_2'''), δ116.72 (C_5'''), δ121.19 (C_6'''), δ126.17 (C_3'' C_6''), δ128.42 (C_4'), δ130.47 (C_4''C_5''), δ131.20 (C_2''&C_7''), δ133.29 (C_1'), δ134.32 (C_1'''), δ143.70 (C_3'''), δ152.37 (C_4'''), δ159.06 (C_3' C_5'), δ162.35 (C_1'' C_8''), δ166.71 (C_2)

HRMS: $C_{27}H_{24}N_2O_8$ M^++Na requires 527.1430, found 527.1442 (2.2ppm)

Attempted cleavage of **355**

To a stirring solution of the β-lactam (**355**) (210mg, 0.413mmol) in ethylene glycol dimethyl ether (15mL) at 0°C under N_2 was added methyl hydrazine (0.09mL, 1.702mmol). The reaction was allowed to stir at 0°C for five minutes before being left to stir at room temperature for a further 90 minutes, after which the solvent was removed under reduced pressure. The resulting residue wa reconstituted in DCM (5mL) and allowed to stand overnight before any insoluble materials were removed by filtration. The filtrate was evaporated to dryness under reduced pressure before being reconstituted in ethyl acetate (25mL). Any insolubles were filtered off and the filtrate was washed with 0.05M HCl (3 x 25mL). The aqueous layers were combined and basified to pH 8 with 5% $NaHCO_3$ and extracted with chloroform (3 x 25mL). The organic layers were combined and washed with saturated brine (100mL), dried over Na_2SO_4, filtered and the solvent removed under reduced pressure. ^1H NMR indicated that no product had formed and that the starting material had degraded

5.18 Substituted Acid Formation

To a stirring solution of the appropriately substituted phenol (4.606g, 25mmol), and chloroacetic acid (2.367g, 25mmol) in dry DMF at 0°C under N_2 was added 60% NaH (2.206g, 55mmol) in 6 equal portions. Upon completion of the addition the reaction was left to stir at room temperature for 2 days, before the solvent was removed under reduced pressure. The resulting residue was reconstituted with water (50mL), and washed with DEE (60mL). The aqueous layer was acidified to pH1 with conc. HCl, before being extracted with DEE (4x50mL). The extracts were combined, dried over Na_2SO_4, filtered, and solvent removed under reduced pressure to yield a brown solid.

(3,4,5-Trimethoxy –phenoxy)-acetic acid **(359)**

Yield: 48%, 2.905, brown solid

MP:

IR (KBr ν max): 3522 cm^{-1}(OH), 1758 cm^{-1}(C=O)

^{1}H NMR (400MHz, $CDCl_3$): δ3.79 (s, 3H –OMe), δ3.87 (s, 6H –OMe), δ4.66 (s, 2H –OCH2-), δ6.19 (s, 2H, H_2, H_6) δ7.28 (s, br, 1H –OH)

^{13}C NMR (100 MHz, $CDCl_3$): δ55.68, δ60.56, δ64.82 (OMe), δ77.01 ($\underline{C}H_2$) δ92.11 (C_2 C_6) δ132.54 (C_4) δ153.27 (C_3 C_5) δ153.68 (C_1) δ173.01 (C=O)

HRMS: M^+ calculated 243.0869 found 243.0873 (1.8ppm)

β-lactam formation

A solution of the acid (**359**) (1mmol) and triphosgene (0.5mmol) in dry DCM (10mL) was brought to reflux under N_2. After 30 minutes TEA (0.21mL, 1.5mmol) was added, followed by the dropwise addition of the appropriate imine (0.5mmol) dissolved in dry DCM (15mL) over the course of 30 minutes. The reaction was left to reflux for a further 6 hours before being allowed to cool. The reaction was washed with H_2O (20mL), saturated $NaHCO_3$ (2x20mL), and brine (10mL), before being dried over $MgSO_4$, filtered, and solvent removed under reduced pressure. The silyl ether β-lactam was isolated by flash chromatography over silica gel eluted with 1:1 *n*-hexane:ethyl acetate. To a stirring solution of the silyl ether β-lactam (2mmol) in dry THF (10mL) was added a solution of 1.0M tBAF in hexanes (2mL, 2mmol) under N_2 at 0^0C. The reaction was stirred for a further 90 minutes. Reaction was diluted with ethyl acetate (75mL) and washed with 0.1M HCL_{aq} (100mL). The aqueous layer was further extracted with ethyl acetate (2x25mL). All the organic layers were collected and washed with H_2O (100mL), and saturated brine (100mL) before being dried over Na_2SO_4. Solvent was removed under reduced pressure to yield the free phenol.

4-(3-Hydroxy-4-methoxy-phenyl)-3-(3,4,5-trimethoxy-phenoxy)-1-(3,4,5-trimethoxy-phenyl)-azetidin-2-one **(361)**

Yield: 36%, 390mg, off white solid

MP: 134-136 °C

IR (KBr ν max): 1745 cm^{-1}(C=O), 3431 cm^{-1}(OH)

^{1}H NMR (400MHz, $CDCl_3$): δ3.71-3.91 (m, 21H, OMe), δ5.28 (d, J=5.55Hz, 1H, H_4), δ5.56 (d, J=5.55Hz, 1H, H_3), δ5.77 (s, 2H, H_2'' H_6'') δ6.01 (s, 2H, H_2' H_6'), δ6.32-6.39 (m, 3H, H_2''' H_5''' H_6''')

^{13}C NMR (100 MHz, $CDCl_3$): δ55.65, δ56.01, δ60.52, δ60.67, δ61.99 δ64.82 (OMe), δ61.38 (C_4), δ81.46 (C_3), δ92.34 (C_2'' C_6''), δ97.46 (C_2' C_6'), δ113.28 (C_2'''), δ114.56 (C_4'''), δ119.93 (C_6'''), δ122.29 (C_4''), δ127.38 (C_4'), δ129.94 (C_1'), δ133.94 (C_1'''), δ139.83 (C_3'''), δ141.59 (C_4'''), δ146.38 (C_3'&C_5'), δ152.59 (C_3'' C_5''), δ158.52 (C_1''), δ168.94 (C_2)

HRMS: $C_{28}H_{31}NO_{10}$ M^++Na requires 564.1846, found 564.1859 (2.3ppm)

5.19 Formation of 3-unsubstituted β-lactams by the Reformatsky reaction

Zinc powder (458mg, 7mmol (method A) or 21mmol (method B)) and TMSC (0.32mL, 2.5mmol) were refluxed for 3 minutes in anhydrous benzene (10mL) under N_2 and then allowed to cool. To the cooled stirring solution, the appropriately substituted imine (**208**) (5mmol) and ethylbromoacetate (0.66mL, 6mmol) were added and refluxed for 7 hours. The reaction was cooled to 0°C and poured onto NH_4Cl_{sat} (10mL) and 30% NH_4OH (10mL). The resulting solution was extracted with DCM (2x20mL) and the organic layer further washed with 0.1N HCl (20mL) and H_2O (20mL) before being dried over Na_2SO_4, filtered and the solvent removed under reduced pressure.

4-[3-(*t*-Butyl-dimethyl-silanyloxy)-4-methoxy-phenyl]-1-(3,4,5-trimethoxy-phenyl)-azetidin-2-one (**379**)

Yield: 37%, 876mg (method A), 77%, 1.823g (method B), pale brown resin

MP: Resin

IR (NaCl ν max): 1749cm^{-1}(C=O)

^{1}H NMR (400MHz, $CDCl_3$): δ0.07 (s, 3H, OtBDMS), δ0.09 (s, 3H, OtBDMS), δ2.91-2.95 (dd, J=2.47Hz, 15.04, 1H, H_3), δ3.48-3.53 (dd, J= 5.52Hz, 15.55Hz, 1H, H_3), δ3.71 (s, 6H, OMe), δ3.76 (s, 3H, OMe), δ3.80 (s, 3H, OMe), δ4.86-4.88 (dd, J=2.52Hz, 5.52, 1H, H_4), δ6.54 (s, 2H, H_2'&H_6'), δ6.83-6.94 (m, 3H, H_2'' H_5'' H_6'')

^{13}C NMR (100 MHz, $CDCl_3$): δ-5.19, δ-5.17, δ17.98, δ25.02 (OtBDMS), δ46.41 (C_3), δ53.59, δ55.03 δ60.46 (OMe), δ55.49 (C_4), δ94.04 (C_2'&C_6'), δ111.82 (C_2''), δ117.99 (C_5''), δ119.05 (C_6''), δ129.98 (C_4'), δ133.57 (C_1'), δ133.74 (C_1''), δ145.15 (C_3''), δ150.74 (C_4''), δ152.95 (C_3'&C_5'), δ164.14 (C_2)

HRMS: $C_{19}H_{21}NO_6$ M^++Na requires 382.1267 found 382.1251 (-4.1ppm)

β-lactam deprotection

To a stirring solution of the silyl ether β-lactam (**379**) (4mmol) in dry THF (30mL) was added a solution of 1.0M tBAF in hexanes (4mL, 4mmol) under N_2 at 0^0C. The reaction was stirred for a further 90 minutes. Reaction was diluted with ethyl acetate (150mL) and washed with 0.1M HCL_{aq} (200mL). The aqueous layer was further extracted with ethyl acetate (2x50mL). All the organic layers were collected and washed with H_2O (200L), and saturated brine (200mL) before being dried over Na_2SO_4. Solvent was removed under reduced pressure and the free phenol was isolated by flash chromatography over silica gel eluted with 1:1 hexane:ethyl actetate.

4-(3-Hydroxy-4-methoxy-phenyl)-1-(3,4,5-trimethoxy-phenyl)-azetidin-2-one (**380**)

Yield: 73%, 1.049g, brown resin

MP: Resin

IR (NaCl ν max): 1741 cm^{-1}, 3443 cm^{-1}, 2937 cm^{-1}

^{1}H NMR (400MHz, $CDCl_3$): δ2.88-2.93 (dd, J=2.48Hz, 15.06Hz, 1H, H_3), δ3.45-3.50 (dd, J= 5.52Hz, 15.56Hz, 1H, H_3), δ3.67 (s, 6H, OMe), δ3.72 (s, 3H, OMe), δ3.84 (s, 3H, OMe), δ4.84-4.86 (dd, J=2.52Hz, 5.52Hz, 1H, H_4), δ6.14 (s, 1H, OH), δ6.53 (s, 2H, H_2'&H_6'), δ6.81-6.93 (m, 3H, H_2'' H_5'' H_6'')

^{13}C NMR (100 MHz, $CDCl_3$): δ46.27 (C_3), δ53.68, δ60.44 (OMe), δ55.52 (C_4), δ94.04 (C_2'&C_6'), δ110.57 (C_2''), δ111.63 (C_5''), δ117.36 (C_6''), δ130.61 (C_4'), δ133.56 (C_1'), δ133.75 (C_1''), δ145.90 (C_3''), δ146.48 (C_4''), δ152.94 (C_3'&C_5'), δ164.27 (C_2)

HRMS: $C_{19}H_{21}NO_6$ M^++Na requires 382.1267, found 382.1251 (-4.1ppm)

5.20 Reaction of 3-unsubstituted β-lactams

To a solution of the 3-unsubstituted β-lactam (**379**) (125mg, 0.264mmol) in dry THF (3mL) under N_2 at -78°C (dry ice and acetone) was added 2.0M LDA solution (0.264mL, 0.528mmol). The resulting solution was left to stir for 5 minutes before a solution of the appropriately substituted aldehyde (49mg, 0.396mmol) in dry THF (1.5mL) was added. The reaction was left to stir for 30 minutes at -78°C, then poured onto $NaCl_{sat}$ (25mL). The resulting solution was extracted with ethyl acetate (50mL), and the solvent was dried over Na_2SO_4 before being removed under reduced pressure. Gross impurities were removed from the resulting residue by passage through a short pad (5cm) of silica with DCM to yield addition product.

To a stirring solution of the addition product (2mmol) in dry THF (10mL) was added a solution of 1.0M tBAF in hexanes (2mL, 2mmol) under N_2 at 0°C. The reaction was stirred for a further 90 minutes. Reaction was diluted with ethyl acetate (75mL) and washed with 0.1M HCL_{aq} (100mL). The aqueous layer was further extracted with ethyl acetate (2x25mL). All the organic layers were collected and washed with H_2O (100mL), and saturated brine (100mL) before being dried over Na_2SO_4 and solvent was removed under reduced pressure. Purification was carried out by chromatography using a Biotage ™ SP1 chromatography system using a +12M column and detection set at 280nM and a fraction volume of 12mL. A gradient elution of 2% ethyl acetate in *n*-hexane to 100% ethyl acetate over 15 column volumes was used.

3-(1-Hydroxy-ethyl)-4-(3-hydroxy-4-methoxy-phenyl)-1-(3,4,5-trimethoxy-phenyl)-azetidin-2-one **(388)**

Yield: 17%, 36mg, brown oil

MP: Oil

IR (NaCl ν max): 1738 cm^{-1}(C=O), 3427 cm^{-1}(OH)

^{1}H NMR (400MHz, $CDCl_3$): δ1.33 (d, J=6.28Hz, 1H, CH_3), δ1.40 (d, J=6.52Hz, 2H, CH_3), δ2.58 (br s, 1H, OH), δ3.14 (m, 1H, H_3), 3δ.72 (s, 6H, OMe), δ3.76 (s, 3H, OMe), δ3.89 (s, 3H, OMe), δ4.24 (q, J=6.04Hz, 4.24Hz, 0.66H, H_5), δ4.36 (q, J=5.76Hz, 4.01Hz, 0.33H, H_5), δ4.77 (d, J=2.28Hz, 0.6H,H_4), δ4.99 (d, J=2.28, 0.4H, H_4), δ5.95 (s, 0.6H, OH), δ5.96 (s, 0.4H, OH), δ6.54 (s, 2H, H_2'&H_6'), δ6.83-7.01 (m, 3H, H_2" H_5" H_6")

^{13}C NMR (100 MHz, $CDCl_3$): δ21.34, δ21.52 (CH_3), δ55.99, δ56.06 (C_4), δ57.64 δ57.68 (C_3), δ56.68, δ60.93, δ64.94 (OMe), δ66.05 δ66.10 (C_5), δ94.70, δ94.75 (C_2'&C_6'), δ111.05 (C_5''), δ112.16, δ112.22 (C_2''), δ117.88 (C_6''), δ130.50 (C_4'), δ130.97 (C_1'), δ133.67, δ134.32 (C_1''), δ146.25, δ146.32 (C_3''), δ146.88 (C_3'&C_5'), δ153.43 (C_4''), δ165.89, δ166.06 (C_2)

HRMS: M^++Na calculated 426.1529, found 426.1540 2.6ppm

3-(1-Hydroxy-but-2-enyl)-4-(3-hydroxy-4-methoxy-phenyl)-1-(3,4,5-trimethoxy-phenyl)-azetidin-2-one **(389)**

Yield: 32%, 73mg, broen oil

MP: Oil

IR (NaCl ν max): 1732 cm^{-1}(C=O), 3427 cm^{-1}(OH)

^{1}H NMR (400MHz, $CDCl_3$): δ1.72 (d, J=7Hz, 1.8H, CH_3), δ1.74 (d, J=1Hz, 1.2H, CH_3), δ2.50 (br, s, 1 H, OH), δ3.24 (m, 1H, H_3), δ3.73-3.79 (overlapping singlets, 9H, OMe), δ3.89 (s, 3H, OMe), δ4.51 (t, J=6.53Hz, 7.8Hz, 0.4H, H_5), δ4.67 (t, J=5.02, 6.8, 0.6H, H_5), δ4.76 (d, J=2.48Hz, 0.4H, H_4), δ4.96 (d, J=2.0Hz, 0.6H, H_4), δ5.78-5.85 (m, 2H, H_6&H_7)

^{13}C NMR (100 MHz, $CDCl_3$): δ17.25 (CH_3), δ55.53, δ55.84, δ64.38 (OMe), δ60.47 (C_3), δ64.65 (C_4), δ68.42, δ70.60 (C_5), δ94.26 (C_2'&C_6'), δ110.50 (C_5''), δ111.75, δ111.82 (C_2''), δ117.42, δ117.48 (C_6''), δ127.62 (C_7), δ129.22 (C_1''), δ129.78 (C_6), δ130.47 (C_4'), δ133.25 δ133.27 (C_1'), δ146.17 (C_4'') δ146.32 (C_3''), δ152.93 (C_3'&C_5'), δ165.21 (C_2)

HRMS: M^++Na calculated 452.1685, found 452.1707 4.8ppm

4-(3-Hydroxy-4-methoxy-phenyl)-3-(1-hydroxy-1-methyl-ethyl)-1-(3,4,5-trimethoxy-phenyl)-azetidin-2-one (**390**)

Yield: 23%, 51mg, brown oil

MP: Oil

IR (NaCl ν max): 1732 cm^{-1} (C=O), 3429 cm^{-1}(OH)

^{1}H NMR (400MHz, $CDCl_3$): δ1.35 (s, 3H, CH_3), δ1.48 (s, 3H, CH_3), δ1.91 (br, s, 1H, OH), δ3.13 (d, J=2.52Hz, 1H, H_3), δ3.72 (s, 6H, OMe), δ3.76 (s, 3H, OMe), δ3.89 (s, 3H, OMe), δ4.89 (d, J=2.52, 1H, H_4), δ5.90 (br, s, 1H, OH), δ6.56 (s, 2H, H_2'&H_6'), δ6.83-6.96 (m, 3H, H_2'' H_5'' H_6'')

^{13}C NMR (100 MHz, $CDCl_3$): δ27.36, δ27.62 (CH_3), δ55.50, δ55.53 (OMe), δ56.73 (C_4), δ60.47 (C_5), δ69.50 (C_3), δ94.27 (C_2'&C_6'), δ110.57 (C_5''), δ111.78 (C_2''), δ117.48 (C_6''), δ130.51 (C_4'), δ133.18 (C_1''), δ133.79 (C_1'), δ145.80 (C_3''), δ146.25 (C_4''), δ152.93 (C_3'&C_5'), δ165.29 (C_2)

HRMS: M^++Na calculated 440.1685, found 440.1671, -3.2 ppm,

4-(3-Hydroxy-4-methoxy-phenyl)-3-(1-hydroxy-3-phenyl-allyl)-1-(3,4,5-trimethoxy-phenyl)-azetidin-2-one (**391**)

Yield: 38%, 99mg, brown oil

MP: Oil

IR (NaCl ν max): 1732cm^{-1} (C=O) 3418 cm^{-1}(OH)

^{1}H NMR (400MHz, $CDCl_3$): δ3.21 (br, s, 1H, OH), δ3.34 (dd, J=2.55 5.63Hz, 0.53H, H_3), δ3.37 (dd, J=2.55, 5.62 Hz, 0.57H, H_3), δ3.69 (s, 6H, OMe), δ3.76 (s, 3H, OMe), δ3.85 (s, 3H, OMe), δ4.75 (t, J=6.13Hz, 12.40Hz, 0.43H, H_5), δ4.86 (d, J=2.45Hz, 0.43H, H_4), δ4.91 (t, J=3.82 7.63Hz, 0.57H, H_5), δ5.03 (d, J=2.45Hz, 0.53H, H_4), δ5.81-5.98 (m, 1H, H_6), δ6.24 (dd, J=5.54, 16.28Hz, 0.57H, H_7), δ6.41 (dd, J=5.54, 16.28, 0.43H, H_7), δ6.58 (s, 2H, H_2' H_6'), δ6.72-6.96 (m, 3H, H_2''' H_5''' H_6'''), δ7.35-7.39 (m, 5H, H_2'' H_3'' H_4'' H_5'' H_6'')

^{13}C NMR (100 MHz, $CDCl_3$): δ53.32, δ55.84, δ56.17, δ60.75 (OMe) δ57.35, δ57.41(C_4) δ64.81, δ68.41 (C_3) δ70.77 (C_5) δ94.81 (C_3'C_5') δ94.86, δ95.12, δ110.61 (C_5''') δ110.95, δ110.98 (C_2''') δ117.84, δ117.91 (C_6''') δ126.37, δ126.61 (C_6) δ128.03, δ128.46 (C_7) δ129.49 (C_4') δ130.33 (C_2''C_6'') δ131.45 (C_4') δ133.12 (C_1') δ134.48 (C_1'') δ136.20 (C_4') δ146.16 (C_3'' C_5'') δ146.61 (C_4''') δ148.29 (C_3''') δ153.29, δ153.31 (C_1''') δ165.48, δ165.48 (C_2)

HRMS: $C_{28}H_{29}NO_7$ M^++Na requires 514.1842, found 514.1826 (-3.1ppm)

3-(1-Hydroxy-allyl)-4-(3-hydroxy-4-methoxy-phenyl)-1-(3,4,5-trimethoxy-phenyl)-azetidin-2-one (**392**)

Yield: 22%, 48mg, brown oil

MP: Oil

IR (NaCl ν max): 1732 cm^{-1}(C=O), 3428 cm^{-1}(OH)

^{1}H NMR (400MHz, $CDCl_3$): δ1.78 (br, s, 1H, OH), δ2.42 (br, s, 1H, OH), δ3.24-3.30 (m, 1H, H_3), δ3.73 (s, 6H, OMe), δ3.77 (s, 3H, OMe), δ3.91 (s, 3H, OMe), δ6.60 (t, J=6.4Hz, 6.6Hz, 0.58H, H_5), δ4.74 (t, J=6.4Hz, 6.5Hz, 0.32H, H_5), δ4.80 (d, J=2.3Hz, 0.58H, H_4), δ4.96 (d, J=2.7Hz, 0.32H, H_4), δ5.28-5.44 (m, 2H, H_7), δ5.78 (br, s, 1H, OH), δ5.90-5.98 (m, 0.32H, H_6), δ6.02-6.10 (m, 0.68H, H_6), δ6.56 (s, 2H, H_2'&H_6'), δ6.84-7.28 (m, 3H, H_2'' H_5'' H_6'')

^{13}C NMR (100 MHz, $CDCl_3$): δ55.53, δ55.55, δ55.62, δ60.48 (OMe) δ56.85 (C_3), δ63.99 (C_4), δ68.28 δ70.76 (C_5), δ94.34 (C_2' C_6'), δ110.47 δ110.52 (C_7), δ111.74 δ111.81 (C_5''), δ115.56 (C_2''), δ117.47 δ117.51 (C_6''), δ129.93 (C_4'),

δ130.20 (C_1''), δ133.20 (C_1'), δ136.59 δ136.80 (C_6), δ145.79 (C_4''), δ146.14 δ146.33 (C_3''), δ152.96 (C_3'C_5'), δ164.89 (C_2)

HRMS: $C_{22}H_{25}NO_7$ M^++Na requires 438.1529, found 438.1547 (4.2ppm)

4-(3-Hydroxy-4-methoxy-phenyl)-3-(1-hydroxy-1-methyl-allyl)-1-(3,4,5-trimethoxy-phenyl)-azetidin-2-one (**393**)

Yield: 18%, 41mg, brown oil

MP: Oil

IR (NaCl ϒ max): 1734 cm^{-1}(C=O), 3433 cm^{-1}(OH)

^{1}H NMR (400MHz, $CDCl_3$): δ1.46 (s, 1.53H, CH_3), δ1.56 (s, 1.34H, CH_3), δ1.8 (br, s, 1H, OH), δ3.17 (d, J=2.40Hz, 0.45H, H_3), δ3.25 (d, J=2.42Hz, 0.42H, H_3), δ3.71 (s, 6H, OMe), δ3.76 (s, 3H, OMe), δ3.88 (s, 3H, OMe), δ4.81 (d, J=2.40, 0.47H, H_4), δ4.86 (d, J=2.41Hz, 0.44H, H_4), δ5.17-5.23 (1H, H_7), δ5.31-5.42 (1H, H_7), δ5.81-6.81 (m, 1H, H_6), δ5.81-5.83 (overlapping singlets, 1H, OH), δ6.54 (s, 2H, H_2'&H_6'), δ6.83-6.96 (m, 3H, Ar-H)

^{13}C NMR (100 MHz, $CDCl_3$): δ26.06, δ26.19 (CH_3), δ53.00, δ56.01, δ60.46 (OMe), δ55.51, δ55.54 (C_4), δ67.47, δ68.46 (C_3), δ71.70, δ71.76 (C_5), δ94.28 (C_2'&C_6'), δ110.46, δ110.54 (C_2''), δ111.84, δ111.92 (C_7), δ117.51, δ117.60 (C_5''), δ130.35 (C_4'), δ133.17 (C_1''), δ133.81 (C_1'), δ140.73 (C_6''), δ141.39, δ141.46 (C_6), δ145.66 (C_4''), δ146.13 (C_2''), δ152.94 (C_3'C_5'), δ164.45, δ164.91 (C_2)

HRMS: M^+Na calculated 452.1685, found 452.1691 (1.3ppm)

5.21 Oxidation of the Hydroxy Group

PCC Route (Method A)

To a stirring solution of PCC (132mg, 0.57mmol) in dry DCM (2mL) under N_2 at room temperature was added quickly a solution of the silyl protected β-lactam (**382**) (195mg, 0.38mmol). The reaction was left to stir at room temperature for 18hrs before being diluted with DEE (25mL) and the resulting suspension allowed to settle and the DEE layer decanted off. The remaining solid was washed and decanted twice with two 25mL portions of DEE.. The organic extracts were combined and dried over $MgSO_4$, fil*t*ed, and the solvent removed under reduced pressure. The ^1H NMR and IR of the crude material indicated the hydroxy group had been oxidised to yield the titlt compound in reduced yield of 7% due to difficulty in extracting the PCC residue from PCC residue.

.

Low Temperature Addition Route (Method B)

The 3-unsubstituted β-lactam (**379**) (378mg, 0.80mmol) was dissolved up in THF (7mL) in a clean dry flask well inerted with N_2 and cooled to -78°C. To this stirring solution LDA 1.0M solution (0.8mL, 0.8mmol) was added all at once and the reaction left to stir for 5 minutes prior to the dropwise addition of acetyl chloride (0.085mL, 1.2mmol), in THF (2mL). The reaction was allowed to stir at -78°C for 30 minutes then allowed to stir at room temperature for 5 minutes before being poured into saturated brine (50mL). The brine solution was extracted with ethyl acetate (2x50mL), and the organic layers combined, dried over $MgSO_4$, filtered, and the solvent removed under reduced pressure. IR spectroscopy indicated the formation of the both the hydroxy and ketone products. The title compound was isolated by flash column chromatography over silica gel eluted with 1:1 *n*-hexane:ethyl acetate and the *t*BDMS ether was removed by treatment with tBAF as previously described.

3-Acetyl-4-(3-hydroxy-4-methoxy-phenyl)-1-(3,4,5-trimethoxy-phenyl)-azetidin-2-one (**395**)

Yield: 7%, 11mg (method A), 11%, 35mg (method B)

MP: Oil

IR (NaCl ν max): 1731 cm^{-1}(C=O), 1739, cm^{-1}(C=O) 3434 cm^{-1}(OH)

^{1}H NMR (400MHz, $CDCl_3$): δ1.99 (s, 3H, OMe), δ3.73 (s, 6H, OMe), δ3.75 (s, 3H, OMe), δ3.81 (s, 3H, OMe), δ4.23 (d, J=1.98Hz, 1H, H_3), δ5.12 (d, J=1.99Hz, 1H, H_4), δ6.08 (s, 2H, C_2'&C_6'), δ6.37-6.57 (m, 3H, H_2'' H_5'' H_6'')

^{13}C NMR (100 MHz, $CDCl_3$): δ23.14 (CH_3), δ53.93 (C_4), δ55.71, δ60.87, δ65.03 (OMe), δ61.71 (C_3), δ93.81 (C_2'&C_6'), δ111.21 (C_5''), δ113.02 (C_2''), δ118.21 (C_6''), δ130..98(C_4'), δ131.02 (C_1'), δ134.27 (C_1''), δ147.12 (C_3''), δ147.34 (C_3'&C_5'), δ153.27 (C_4''), δ164.45 (C_2), δ181.23 (C_5)

HRMS: $C_{21}H_{23}NO_7$ M^++1 requires 402.1475, found 402.1463 (-3.0ppm)

5.21 Epoxidation Reaction

The β-lactam (**337**) (0.18mmol, 1eq) was stirred with mCPBA (3eq) in DCM (4mL) for 24 hours at room temperature. The reaction was diluted with DCM (10mL) and washed with 50mL each of saturated $NaHCO_3$ and H_2O. The organic layer was collected and dried over Na_2SO_4, and the solvent removed under reduced pressure. ^1H NMR spectroscopy indicated the destruction of the starting material and no formation of products

5.22 OsO_4 Mediated Transformation

To a solution of the silyl ether protected beta lactam (**337**) (156mg, 0.312mmol) in pyridine (0.5mL) stirring under N_2 at room temperature was added OsO_4 (80mg, 0.312mmol). The reaction darkened in colour and became hot to the touch upon completion of the addition. The flask was immersed in ice water for one minute, then left to stir at room temperature under N_2 for 22 hours. A solution of $Na_2(SO_3)_2$ (1.343g, 6.8mmol) in a 1:4 mixture of pyridine/water (20mL) was added and the reaction left to stir at room temperature for a further 7 hours. The reaction was extracted with warm ethyl acetate (100mL). The formation of hydroxy groups was confirmed by IR . The organic layer was collected and washed with 0.1M HCl_{aq} (100mL), saturated $NaHCO_3$ (100mL), and water (100mL). The organic layer was collected and dried over $MgSO_4$, filtered and the solvent removed under reduced pressure. The gross impurities were removed by passage through a pad of silica (5cm) eluted with DCM. The tBDMS group was cleaved by treatment with tBAF

3-(1,2-Dihydroxy-ethyl)-4-(3-hydroxy-4-methoxy-phenyl)-1-(3,4,5-trimethoxy-phenyl)-azetidin-2-one (**398**)

Yield: 39%, 51mg, white resin

MP: resin

IR (NaCl ν max): 1727 cm^{-1}(C=O), 3454 cm^{-1}(OH)

^{1}H NMR (400MHz, $CDCl_3$): δ2.72 (br s, 1H, OH), δ3.16 (dd, 0.72H, J=2.42Hz, 5.55Hz, H_3), δ3.19 (dd, 0.29H, J=2.46Hz, 4.56Hz, H_3), δ3.60-3.67 (m, 8H, H_6 & OMe), δ3.74 (s, 3H, OMe), δ3.83 (s, 3H, OMe), δ4.10 (q, J=4.05Hz, 0.26H, H_5), δ4.19 (q, J=5.50hz, 0.75H, H_5), δ4.25 (br s, 0.5H, OH), δ4.90 (d, J=2.37, 0.31H, H_4), δ5.00 (d, J=2.36, 0.69H, H_4), δ6.25 (br, s, 0.30H, OH), δ6.46 (br, s, 0.70H, OH), δ6.53 (s, 2H, H_2' H_6'), δ6.77-6.94 (m, 3H, H_2'' H_5'' H_6'')

^{13}C NMR (100 MHz, $CDCl_3$): δ55.79, δ55.85 (C_4), δ56.80, δ56.97, δ60.73 (OMe), δ62.18 (C_3), δ64.46, δ64.76 (C_6), δ68.54, δ69.30 (C_5), δ94.92 (C_2'C_6'), δ111.06, δ111.11 (C_5''), δ112.23, δ112.43 (C_2''), δ117.76, δ117.90 (C_6''), δ129.92 (C_4'), δ130.29 (C_1'), δ133.17, δ133.33 (C_1''), δ146.07, δ146.22 (C_3''), δ146.85, δ146.98 (C_4''), δ153.27 (C_3'&C_5'), δ165.76, δ165.96 (C_2)

HRMS: $C_{21}H_{25}NO_8$ M^++Na requires 442.1478, found 442.1490 (2.7ppm)

5.23 Ethylidene Compounds

Alkyl Chloride Route

Attempted synthesis of **408**. To a stirring solution of the protected β-lactam (466mg, 0.90mmol), in dry chloroform (20mL), was added thionyl chloride (0.07mL, 0.90mmol) under N_2. The reaction was left to stir at room temperature for 2 hours at which time TLC in 1:1 hexane:ethyl acetate indicated that the reaction had not gone to completion and IR confirmed this. A further equivalent of thionyl chloride (0.07mL, 0.90mmol) was charged to the reaction and stirring at room temperature continued for a further 2 hours, after which the excess thionyl chloride and solvent were removed under reduced pressure. ^{1}H NMR of the crude reaction mixture indicated no product present and that the starting material has been destroyed.

Mitsunobu Route

To a solution of the silyl ether protected β-lactam **337** (1mmol) in DCM (10 mL) stirring at 0°C under N_2 was added PPh_3 (1mmol) and DEAD (1.2mmol). Stirring at 0°C was continued for a further 3 minutes before the reaction was allowed to warm to room temperature. Diethyl ether (30 mL) was added to the reaction to precipitate out the triphenyl oxide side product which was removed by filtration. The filtrate was collected and evaporated to dryness under reduced pressure to yield the product in a mixture of isomers. Seperation of the isomers was carried out on a Biotage SP1 system using a gradient elution from 2% ethyl acetate in hexane to 100% ethyl acetate over 20 column volumes and detection at 280 nm.

3-Ethylidene-4-(3-hydroxy-4-methoxy-phenyl)-1-(3,4,5-trimethoxy-phenyl)-azetidin-2-one (**397**)

Yield: 52%, 87mg, white resin

MP: resin

IR (NaCl ν max): 1738 cm^{-1}(C=O), 2935 cm^{-1} (CH), 3327 cm^{-1}(OH)

^{1}H NMR (400MHz, $CDCl_3$): : *E isomer,* δ1.60 (d, J=4.4Hz, 3H, CH_3), δ3.76 (s, 6H, OMe), δ3.78 (s, 3H, OMe), δ3.92 (s, 3H, OMe), δ5.32 (s, 1H, H_4), δ5.68, s, 1H, OH), δ6.32 (m, 1H, H_5), δ6.61 (s, 2H, H_2'&H_6'), δ6.86 (d, J=8.2, 1H, H_5''), δ7.03 (d, J=1.96Hz, 1H, H_2''), δ6.99 (m, 1H, H_6'')

Z isomer, δ2.10 (d, J=4.16Hz, 3H, CH_3), δ3.76 (s, 6H, OMe), δ3.79 (s, 3H, OMe), δ3.92 (s, 3H, OMe), δ5.19 (s, 1H, H_4), δ5.65-5.66 (m, 2H, OH & H_5), δ6.63 (s, 2H, H_2'&H_6'), δ6.85-6.90 (m, 3H, H_2'' H_5'' H_6'')

^{13}C NMR (100 MHz, $CDCl_3$): *E isomer* δ13.26 (CH_3), δ55.80, δ55.88, δ60.76 (OMe), δ62.72 (C_4), δ94.47 (C_2'&C_6'), δ110.68 (C_2''), δ113.04 (C_5''), δ118.87 (C_6''), δ123.32 (C_5), δ129.72 (C_4'), δ133.94 (C_1'), δ134.20 (C_1''), δ142.32 (C_3), δ146.04 (C_3''), δ146.74 (C_4''), δ153.33 (C_3'&C_5'), δ161.19 (C_2)

Z isomer δ14.30 (CH_3), δ55.81, δ55.82, δ60.81 (OMe), δ62.80 (C_4), δ94.57 (C_2'&C_6'), δ110.61 (C_2''), δ112.73 (C_5''), δ118.48 (C_6''), δ126.89 (C_5), δ130.37 (C_4'), δ133.93 (C_1'), δ134.15 (C_1''), δ141.71 (C_3), δ146.11 (C_3''), δ146.72 (C_4''), δ153.38 (C_3'&C_5'), δ161.79 (C_2)

HRMS: $C_{21}H_{23}NO_6$ M^++Na requires 408.1423, found 408.1411 (-2.9ppm)

5.24 Synthesis of 3-vinyl amino containing compounds

To a stirring, refluxing solution of the imine (**199**) (5mmol) and triethylamine (6mmol) in anhydrous dichloromethane (40mL), a solution of crotonyl chloride (6mmol) in anhydrous dichloromethane (10mL) was added over 45 minutes under nitrogen. The reaction was kept at reflux during the day (5 hours) and at room temperature overnight (16 hours), continuously under nitrogen, until the starting material had disappeared as monitored by TLC in 50:50 hexane/ethyl acetate. A characteristic darkening of the reaction to an amber colour over time was observed. The reaction was transferred to a separating funnel and washed with water (2 x 100mL), with the organic layer being retained each time. The reaction was dried over Na_2SO_4 before the solvent was removed under reduced pressure. The crude product was purified by flash chromatography in 1:1 hexane:ethyl acetate.

4-(4-Methoxy-3-nitro-phenyl)-1-(3,4,5-trimethoxy-phenyl)-3-vinyl-azetidin-2-one (**410**)

Yield: 37%, 766mg, brown oil

MP: oil

IR (NaCl ν max): 1754 cm^{-1}(C=O)

^{1}H NMR (400MHz, $CDCl_3$): δ3.74 (s, 6H, -OMe), δ3.78 (s, 3H, -OMe), δ3.99 (m, 4H, -OMe & H_3), δ4.81 (d, J=2.5Hz, 1H, H_4), δ5.39 (t, J=18.56, 9.28, 2H, CH_2CH), δ5.95-6.07 (m, 1H, CH_2CH), δ6.51 (d, J=3.76, 2H, H_2' H_6'), δ7.14-7.29 (m, 1H, H_5''), δ7.56 (dd, J=2.24Hz, 8.76Hz, 1H, H_6''), δ7.90 (d, J=2Hz, H_2'')

^{13}C NMR (100 MHz, $CDCl_3$): δ56.15, δ56.74, δ60.97 (δOMe), δ60.11 (C_3), δ63.90 (C_4), δ94.7 (C_2'&C_6'), δ114.60 ($CHCH_2$), δ120.63 ($CHCH_2$), δ123.63 (C_5''), δ129.86 (C_1''), δ131.22 (C_6''), δ133.27 (C_4'), δ134.01 (C_1''), δ135.09 (C_1'), δ139.80 (C_3''), δ153.10 (C_3'&C_5'), δ153.69 (C_4''), δ164.65 (C_2)

HRMS M^+ + Na calculated 437.1325 found 437.1339 (3.3ppm)

Nitro group reduction

To a flask containing the β-lactam (**410**) (0.50 mmoll) and zinc powder (10μm mesh) (5.0mmol) was added 30mL of acetic acid at room temperature under N_2 and reaction left to stir for 7 days. The reaction was filtered through a celite pad and the filtrate collected. Solvent was removed under reduced pressure and chromatography (1:1 ethyl acetate:hexane) carried out to yield the title compound.

4-(3-Amino-4-methoxy-phenyl)-1-(3,4,5-trimethoxy-phenyl)-3-vinyl-azetidin-2-one (**399**)

Yield: 37%, 711mg, brown oil

MP: oil

IR (NaCl ν max): 1746 cm^{-1}(C=O) 3470 cm^{-1}(NH_2)

^{1}H NMR (400MHz, $CDCl_3$): δ3.76 (s, 7H, OMe & H_3), δ3.79 (s, 3H, OMe), δ3.87 (s, 3H, OMe), δ4.65 (d, J=2Hz, 1H, H_4), δ5.34 (m, 2H, $CHCH_2$), δ6.02 (m, 1H, $CHCH_2$), δ6.60 (s, 2H, C_2'&C_6'), δ6.76 (m, 3H, H_2'' H_5'' H_6'')

^{13}C NMR (100 MHz, $CDCl_3$): δ55.57, δ55.91, δ60.95 (OMe), δ61.62 (C_3), δ63.80 (C_4), δ94.71 (C_2'&C_6'), δ110.37 (C_2''), δ116.39 (C_5''), δ119.76 (C_6''), δ129.69 (C_4'), δ130.73 (C_6'), δ134.00 (C_3''), δ134.31 (C_1'), δ134.33 (C_1''), δ153.45 (C_4''), δ153.49 (C_3'&C_5'), δ165.56 (Imine)

HRMS $C_{21}H_{24}N_2O_5$ M^++Na requires 407.1583, found 407.1571 (-2.9ppm)

5.25 Further 3-vinyl compounds

To a stirring, refluxing solution of the imine (**193 198**) (5mmol) and triethylamine (6mmol) in anhydrous dichloromethane (40mL), a solution of crotonyl chloride (6mmol) in anhydrous dichloromethane (10mL) was added over 45 minutes under nitrogen. The reaction was kept at reflux during the day (5 hours) and at room temperature overnight (16 hours), continuously under nitrogen, until the starting material had disappeared as monitored by TLC in 50:50 hexane/ethyl acetate. A characteristic darkening of the reaction to an amber colour over time was observed. The reaction was transferred to a separating funnel and washed with water (2 x 100mL), with the organic layer being retained each time. The reaction was dried over Na_2SO_4 before the solvent was removed under reduced pressure. The crude product was purified by flash chromatography over silica gel eluted with 1:1 *n*-hexane:ethyl acetate.

4-(4-Methoxy-phenyl)-1-(3,4,5-trimethoxy-phenyl)-3-vinyl-azetidin-2-one (**412**)

Yield: 22%, 436mg, brown oil

MP: Oil

IR (NaCl ν max): 1738 cm^{-1}(C=O)

^{1}H NMR (400MHz, $CDCl_3$): δ3.71 (s, 9H, OMe), δ3.76 (s, 3H, OMe), δ3.83-3.88 (m, 1H, H_3), δ4.85 (d, J=2.67Hz, 1H, H_4), δ5.37 (d, J=Hz, 2H, H_6), δ6.01 (m, 1H, H_5), δ6.48 (s, 2H, H_2'H_6'), δ7.48 (d, J=8.20Hz, 2H, H_3'' H_5''), δ7.71 (d, 2H, J=8.32Hz, 2H, H_2''H_6'')

^{13}C NMR (100 MHz, $CDCl_3$): δ55.59, δ55.63, δ60.26 (OMe), δ59.93 (C_3), δ63.43 (C_4), δ94.17 (C_2' C_6'), δ112.19 (C_3'' C_5'') δ117.76 (C_6), δ126.12 (C_2'' C_6''), δ129.33 (C_4'), δ131.72 (C_1''), δ132.66 (C_1'), δ132.79(C_5), δ142.34(C_3' C_5'), δ153.22 (C_4''), δ163.92 (C_2)

HRMS: $C_{21}H_{23}NO_5$ M^++Na requires 392.1474, found 392.1468 (-1.5ppm)

4-(4-Methylsulfanyl-phenyl)-1-(3,4,5-trimethoxy-phenyl)-3-vinyl-azetidin-2-one (**413**)

Yield: 17%, 328mg, brown oil

MP: Oil

IR (NaCl ν max): 1744 cm^{-1}(C=O)

^{1}H NMR (400MHz, $CDCl_3$): δ2.48 (s, 3H, SCH_3), δ3.72-3.76 (m, 10H, OMe & H_3), δ4.75 (d, J=2.33Hz, 1H, H_4), δ5.31-5.40 (m, 2H, H_6), δ5.98-6.05 (m, 1H, H_5), δ6.54 (s, 2H, H_2' H_6'), δ7.25-7.31 (m, 4H, H_2'' H_3'' H_5'' H_6'')

^{13}C NMR (100 MHz, $CDCl_3$): δ15.55 (SCH_3), δ55.88, δ55.61, δ60.77 (OMe), δ60.47 (C_3), δ63.39 (C_4), δ94.23 (C_2' C_6'), δ119.59 (C_6), δ125.98 (C_3''C_5''), δ126.09 (C_4'), δ129.96 (C_2'' C_6''), δ133.25(C_4''), δ133.49 (C_1'), δ139.00 (C_5), δ141.19 (C_1''), δ153.05 (C_3' C_5'), δ164.70 (C_2)

HRMS: $C_{21}H_{23}NO_4S$, M^++Na requires 408.1245, found 408.1230 (-3.7ppm)

5.26 XRD Studies

A saturated solution of the test compound (**242, 245b, 254,256b, 262, 264b,328**) was prepared in ethanol. This solution was transferred to a 5mL test tube and an equal quantity of ethanol was added leading to a 50% saturated solution. The tube was then stoppered and a needle used to punch a small hole in the stopper to allow for the slow evaporation of the solvent. The tubes were placed in the dark at room temperature until they had evaporated to dryness (approximately 6 months). The crystals thus obtained were checked under the microscope for defects before being mounted for XRD analysis.

The crystal structure of compounds was determined by X-ray diffraction on a Bruker SMART APEX (2001) diffractometer using MoKa radiation from a fine focus sealed source and a graphite monochromator. The structure solution was found using SHELXS-97 and the structure refinement was carried out using SHELXL-97.

The crystal structure data is presented in appendix 1

5.27 Biochemical Testing

Cell Media

Complete growth medium for the MCF-7 cell line was prepared as follows: 10% foetal calf serum, 1% L-glutamine, 1% non-essential amino acids, 1% penicillin streptomycin and 87% MEME.

Cell Growth

Cells from the MCF-7 cell line were obtained as pellets in a mixture of 10% DMSO and 90% cell medium, frozen in liquid nitrogen. Pellet was warmed to room temperature in a water bath at 37^0C, then immediately added to a centrifuge vial containing complete growth medium (final volume of 10mL). Vial was centrifuged at 175g for 5 minutes. Supernatant liquid was poured off and pellet resuspended in complete growth medium (9mL), then transferred to a 25 cm^2 tissue culture flask fitted with a filter screw cap. Plate was incubated at 37^0C in a humid atmosphere with 5% CO_2. Once cells reached 80% confluencey (3-5 days) they were transferred to a larger 75 cm^2 flask with complete growth medium (14mL).

Plate Seeding

Upon reaching 80% confluence, the cell medium was poured off and the biofilm remaining in the flask was rinsed with medium (10mL), and this rinse was discarded. Trypsin (2-3mL depending on confluency of cells) was added and the flask returned to the incubator for 3 minutes. Upon removal from the incubator, the biofilm was seen to have dissolved. Complete growth medium (10mL) was added to the flask and this suspension was then centrifuged at 175g for 5 minutes. The supernatant liquid was poured off and the remaining pellet was resuspended in complete growth medium (1mL, 2mL, 3mL depending on size of pellet).

The density of cells present in the suspension prepared above was determined by counting a 12µL sample with a haemocytometer under a microscope. A serial dilution was carried out to produce a suspension with a density of $2.5x10^4$ cells/mL. Sterile 96 well plates were seeded with this suspension (200µL per well) with the wells around the outside of the plate remaining empty. Plates were then incubated for 24 hours prior to dosing

Treatment

A 10mM solution of the compound to be tested was prepared in 60% DMSO/40% ethanol. The combination of DMSO and ethanol was used because of the cytotoxic effects of DMSO. From this stock solution, a serial dilution was carried out producing solutions of 5mM, 1mM, 0.5mM, 0.1mM, 10μM, 1μM, and 100nM. The plate was treated as illustrated in Fig1. Two compounds were tested per plate – one in the top three rows and one in the bottom three rows. Each well was treated with 2μL of test compound which represented a 1 in 100 dilution factor. The columns marked "C" and "B" were for the control and blank used in the assays. The column marked "V" was the vehicle i.e. dosed with 2μL of the solvent used to dissolve the test compound. The plates were then incubated for a further 72 hours before the assays were carried out.

	C	V	B	100nM	1μM	10μM	0.1mM	0.5mM	1mM	5mM	
	C	V	B	100nM	1μM	10μM	0.1mM	0.5mM	1mM	5mM	
	C	V	B	100nM	1μM	10μM	0.1mM	0.5mM	1mM	5mM	
	C	V	B	100nM	1μM	10μM	0.1mM	0.5mM	1mM	5mM	
	C	V	B	100nM	1μM	10μM	0.1mM	0.5mM	1mM	5mM	
	C	V	B	100nM	1μM	10μM	0.1mM	0.5mM	1mM	5mM	

Fig 5.1 Treatment regime for 96-well plates seeded with MCF-7 cells

Assays

The cytotoxity and antiproliferative effects of each compound were determined by the LDH and MTT assay respectively. Cell lysis solution (30µL) was added to each control well in the plates. This served as the 100% cell death control, with the blank well serving as the 0% cell death controls. From each well 30µL of the medium was withdrawn and transferred to a non-sterile 96 well plate along with 30µL of LDH solution. These plates were wrapped in tinfoil and left at room temperature for 20 minutes. Stop solution (30µL per well) was added to each plate after 20 minutes, the plate placed in a plate reader and read at 490nm.

The remaining medium in the sterile plates was poured off and the plate washed twice with phosphate buffered saline before being dried. MTT solution (50µL per well) was added to each plate. The plates were wrapped immediately in tinfoil and placed in the incubator for a further 2 hours. After incubation, DMSO (200µL per well) was added to each plate and any purple crystals fully dissolved up before the plate was placed in a plate reader and read at 595nm.

Data manipulation

The crude data obtained from the plate reader was analysed using GraphPad Prism software.

5.28 Stability Studies

System

Stability studies were carried out using a Waters HPLC system fitted with a Spherisorb column (2-5µm particle size, 4.5x250mm) supplied by Alltech Associates Incorporated. A mobile phase of 60/40 acetonitrile/water with 0.1% (v/v) TFA added to prevent peak tailing was used throughout. The mobile phase was only prepared from HPLC grade solvents and degassed by sonication prior to use. Flow rate was maintained at 1mL per minute with a pressure of approximately 1300 psi on a Waters 1525 binary pump equipped with an in line degasser. Where samples were run over a protracted period of time, the mobile phase was recycled back to the reservoir without any detriment to separation. Elution was detected at 280nm with a Waters 2487 dual wavelength detector. Multiple injections were carried out using a Waters 717 autosampler. All samples were filtered via a syringe filter (Pall, 0.45µM) prior to injection. The system was flushed with 2-propanol before shutting down for protracted periods of time.

Buffers

Phosphate Buffers at the desired pH (4.0, 7.5, 10) were prepared in accordance with the BP monograph (A139). The only deviation was a reduction by a factor of four in the volume of buffer prepared at any one time. Buffers were freshly prepared just prior to use. pH meter used for pH determinations was calibrated once per day prior to use as per the manufacturers specifications.

Stock Solutions

Stock solutions were prepared by dissolving approx 11mg of compound in 25mL acetonitrile by sonication for 20 minutes before filtering through a syringe filter resulting in an appromiately 1.1mM solution. Minimum purity of stock solution was 98% by peak area in all cases. Stock solution was able to be stored at -20°C without affecting purity as determined by HPLC.

System Performance

A linear calibration curve was obtained by preparing serial dilutions of the stock solution and injecting in triplicate. A data point in the middle of this calibration was selected and injected six times as a measure of reproducibility.

Blood Plasma

Whole blood (50mL) was withdrawn from a healthy 25 year old male with 5mL 2% sodium citrate. Plasma was obtained by centrifuging at 1957g for 10 minutes and drawing off the supernatant layer of plasma to obtain approx 20mL of plasma from each 50mL of whole blood. The plasma was aliquoted (1mL) into 1.5mL epfendorfs and stored at -20°C until needed. Assays using plasma were carried out within 6 weeks of obtaining the plasma. All waste that came into contact with the plasma was disposed of in accordance with School of Pharmacy, TCD, guidelines.

pH Stability Studies

The appropriate phosphate buffer was prepared as described above and warmed to 37°C in a water bath for at least 30 minutes prior to use. The stock solution was removed from the fridge and allowed to warm to room temperature. T_0 was determined by taking the stock solution (50µL) and mixing by vortex with acetonitrile (900µL). Three separate injections (10µL) of this solution were made and the average peak area taken as T_0. The test solution was prepared by mixing the stock solution (500µL) in the prewarmed buffer (9000µL) by vortex. This dilution results in a final concentration of 58µM of the analyte in the buffer. The moment of contact of the stock solution with the buffer was recorded. The test solution was maintained at 37°C by immersion in a water bath. Samples were withdrawn from the test solution at predetermined intervals as follows. The test solution was thoroughly mixed by vortexing before 1.2mL of sample was withdrawn by syringe, filtered, and injected (10µL) onto the system.

Blood Plasma Studies

pH 7.5 phosphate buffer was prepared as described above and warmed to 37°C in a water bath for at least 30 minutes prior to use. The blood plasma was removed from the freezer and quickly warmed to 37°C in the water bath. The plasma (2.5mL) was added to prewarmed buffer (10mL) and mixed together by vortexing and placed back in the water bath to ensure the mixture had equilibrated to 37°C. To this mixture, stock solution (1.4mL) was added and mixed well by vortexing resulting in a final concentration of 112µM. The moment of contact of the stock solution with the buffer was recorded. The test solution was maintained at 37°C by immersion in a water bath. Samples were

withdrawn from the test solution at predetermined intervals as follows. The test solution was thoroughly mixed by vortexing before 1000 µL of sample was withdrawn and added to 1000µL of 2% (w/v) $ZnSo_4$, and the resulting mixture was centrifuged at 1252g for 5 minutes, before the supernatant was filtered and injected (10µL) onto the system. T_0 was determined by adding the stock solution (700 µL) to acetonitrile (6.25mL) and mixing well by vortex before filtering and injecting onto the system. Three separate injections (10µL) of this solution were made and the average peak area was taken as T_0. All waste that came into contact with the plasma was disposed of in accordance with School of Pharmacy TCD guidelines. The blood plasma study was carried out a second time using a final concentration of 58µM of β-lactam.

References

Chapter 1

---

[1] Hanahan, D.; Folkman J. *Cell* **1996**, 86, 353–64.
[2] Alberts, B. Molecular biology of the cell. **2002**, 4th edt., Garland Science.
[3] All Ireland Cancer Statistics Second Report 1998-2000 retrieved from the National Cancer Registry website at www.ncri.ie/pubs//pubs.shtml.
[4] Hanrahan, D.; Weinburg, J. *Cell*, **2000**, 100, 57-70.
[5] Murray, A.; Hunt, T.; The Cell Cycle – an introduction. **1993**, Oxford University Press.
[6] Zarnecka, A. M.; Gammazza, A .M.; Di Felice, V.; Zummo, G.; Cappello, F. *Journal of Cancer Molecules* **2007**, 3(3), 71-79.
[7] Murray, P.G.; Young, L.S.; Viral and Immunological Malignancies, **2006**.
[8] Adachi, S.; Shibuya, A.; Miura, Y.; Takeuchi, A.; Nakazawa, T.; Saigenji, K. *Scandinavian Journal of Gastroenterology* **2008**, 43(7), 849-856.
[9] Campeau, P.M.; Foulkes, W.D.; Tischkowitz, M.D. *Human Genetics* **2008**, 124(1), 31-42.
[10] Halliwell, B. *Biochemical Journal* **2007**, 401(1), 1-11
[11] Cancer in Ireland 1994-2001: Incidence, Mortality and Treatment retrieved from the Cancer Registry Ireland website at www.ncri.ie/pubs//pubs.shtml
[12] Lacassagne, A.; *The American Journal of Cancer* **1996**, 27, 217-225
[13] Groleau, S.; Nault, J.; Lepage, M.; Couture, M.; Dallaire, N.; Berube, G.; Gauderault, R.C.; *Bioorganic Chemistry* **1999**, 27, 383-394
[14] Kent O.C. *The New England Journal of Medicine* **1998**, 339, 1609-1618
[15] Dhingra, K. *Investigational New Drugs* **1999**, 17, 285-311
[16] Attard, G.; Greystoke, A.; Kaye, S.; De Bono, J. *Pathologie Biologie* **2006**, 54(2), 72-84.
[17] Ravelli R.B.G.; Gigant B.; Curmi P.A.; Jourdain I.; Lachkar S.; Sobel A.; Knossow M. *Nature* **2004**, 428(6979), 198-202.
[18] Wade, R.H. *Methods in Molecular Medicine* **2007**, 137(Microtubule Protocols), 1-16
[19] Downing, K.H.; Nogales, E. *Current Opinion in Structural Biology* **1998**, 8(6), 785-791.
[20] Elie-Caille, C.; Severin, F.; Helenius, J.; Howard, J.; Muller, D.J.; Hyman, A.A. *Current Biology* **2007**, 17(20), 1765-1770
[21] Fanara, P.; Turner, S.; Busch, R.; Killion, S.; Awada, M.; Turner, H.; Mahsut, A.; LaPrade, K.L.; Stark, J.M.; Hellerstein, M.K. *Journal of Biological Chemistry* **2004**, 279 (48), 49940-49947
[22] Keskin, O.; Durell, S.R.; Bahar, I.; Jernigan, R.L.; Covell, D.G. *Biophysical Journal* **2002**, 83(2), 663-680
[23] Gamblin, C.T; Nachmanoff, K.; Halpain, S.; Williams, R.C.; *Biochemistry* **1996**, 35(38), 12576-12586.
[24] Hyman, A. A.; Salser, S.; Drechsel, D. N.; Unwin, N.; Mitchison, T. J. *Molecular Biology of the Cell* **1992**, 3(10), 1155-67
[25] Tito, A, (ed.) The role of microtubules in cell biology, neurobiology and oncology, Humana Press, **2008**
[26] Jordan, M.A.; Wilson, L.; *Nature Reviews* **2004**, 4, 253-265
[27] Cragg, D.M.; Newman, D.J.; *Journal of Ethnopharmacology* **2005**, 100, 72-79
[28] Thurston, D.E.; Chemistry and Pharmacology of Anticancer Drugs, **2007**, pg88, CRC Press
[29] Jordan, M.A.; Thrower, D.; Wilson, L.; *Cancer Research* **1991**, 51, 2212
[30] Bai, R.B.; Pettit, G. R.; Hamel, E.; *Journal of Biological Chemistry* ***1990***, 265, 17141-17149
[31] Wilson, L.; Jordan, M.A.; Morse, A.; Margolis, R.L.; *Journal of Molecular Biology* **1982**, 159, 129-149
[32] Jordan, M. A. *Current Medicinal Chemistry Anti-Cancer Agents* **2002**, 2, 1–17.
[33] Jordan, M.A.; Margolis, R.L.; Himes, R.H.; Wilson, L. *Journal of Molecular Biology* **1986**, 187, 61–73.
[34] Singer, W.D.; Jordan, M.A.; Wilson, L.; Himes, R.H. *Molecular Pharmacology* **1989**, 36, 366–370.
[35] Gigant B.; Wang C.; Ravelli R.B.G.; Roussi F.; Steinmetz M.O.; Curmi P.A.; Sobel A.; Knossow M. *Nature* **2005**, 435(7041), 519-522.
[36] Rai, S.; Wolff, J.; *Journal of Biological Chemistry* **1996**, 271, 14707-14711
[37] Trimurtulu, G.; Ohtani, I.; Patterson, G.M.L.; Moore, R.E.; Corbett, T.H.; Valeriote, F.A.; Demchik, L. *Journal of the American Chemical Society* **1994**, 116(11), 4729-37.
[38] Hamel, E. *Pharmacology & Therapeutics* **1992**, 55(1), 31-51.

[39] Pettit, G.R.; Kamano, Y; Herald, C.L.; Tuinman, A.A.; Boettner, F.E.; Kizu, H.; Schmidt, J.M.; Baczynskyj, L.; Tomer, K.B.; Bontems, R.J. *Journal of the American Chemical Society* **1987**, 109(22), 6883-6885.
[40] Kerksiek, K.; Mejillano, M.R.; Schwartz, R.E.; Georg, G.I.; Himes, R.H. *FEBS letters* **1995**, 377(1), 59-61.
[41] Liduena, R.F.; *Biochemical. Pharmacology* **1993**, 45, 421.
[42] Wani, M.C.; Taylor, H.L.; Wall, M.E.; Coggon, P.; McPhail, A.T. *Journal of the American Chemical Society* **1971**, 93(9), 2325-2327.
[43] Denis, J.N., *Journal of the American Chemical Society* **1998,** 110, 5917.
[44] www.bms.com/static/ehs/report/data/s03p25 retrieved from the BMS website August 2008
[45] Holton, R.A.; Kim, H.B.; Somoza, C.; Liang, F.; Biediger, R.J.; Boatman, P.D.; Shindo, M.; Smith, C.C.; Kim, S. *Journal of the American Chemical Society* **1994**, 116(4), 1599-1600
[46] Holton, R.A.; Somoza, C.; Kim, H.B.; Liang, F.; Biediger, R.J.; Boatman, P. D.; Shindo, M.; Smith, C.C.; Kim, S. *Journal of the American Chemical Society* **1994**, 116(4), 1597-8.
[47] Schiff, P.B.; Fant, J.; Horwitz, S.B. *Nature* **1979**, 277, 665–667
[48] Schiff, P.B., Horwitz, S.B., *Proceedings National Academy Sciences USA* **1980**, 77, 1561
[49] Jordan, M.A.; Toso, R.J.; Thrower, D.; Wilson, L. *Proceedings of the National Academy of Sciences of the United States of America* **1993**, 90(20), 9552-6.
[50] Nogales, E.; Wolf, S.G.; Khan, I.A.; Luduena, R.F.; Downing, K.A. *Nature* **1995**, 375, 424–427.
[51] Bollag, D.M.; McQueney, P.A.; Zhu, J.; Hensens, O.; Koupal, L.; Liesch, J.; Goetz, M.; Lazarides, E.; Woods, C.M. *Cancer Research* **1995**, 55(11), 2325-2333.
[52] ter Haar, E.; Kowalski, R.J.; Hamel, E.; Lin, Chii M.; Longley, R.E.; Gunasekera, S.P.; Rosenkranz, H.S.; Day, B.W. *Biochemistry* **1996**, 35(1), 243-50.
[53] Lindel, T. *Journal of the American Chemical Scoiety* **1997**, 119, 8744.
[54] Cragg, G.M.; Kingston, D.G.I.; Newman, D.J.; Anticancer agents from natural products CRC Press, **2005**, pg181
[55] Bhattacharyya, B.; Panda, D.; Gupta, S.; Banerjee, M. *Medicinal Research Reviews* **2008**, 28(1), 155-183.
Deery W.J.; Weisenberg R.C. *Biochemistry* **1981**, 20(8), 2316-2324.
[56] Sherline P.; Leung J.T.; Kipnis D.M. *The Journal of Biological Chemistry* **1975**, 250 (14), 5481-5486.
[57] Margolis, R.L.; Wilson, L. *Proceedings of the National Academy of Sciences of the United States of America* **1977**, 74(8), 3466-3470
[58] Deery W.J.; Weisenberg, R.C. *Biochemistry* **1981**, 20 (8), 2316-2324.
[59] Baguley, B.C.; Holdaway, K.M.; Thomsen, L.L.; Zhuang, L.; Zwi, L.J. *European Journal of Cancer* **1991**, 27(4), 482-487.
[60] Morris I.; Varughese G.; Mattingly P. *British Medical Journal* (Clinical research ed.) **2003**, 327(7426), 1275-1276
[61] Bai, R.; Covell, D.G.; Pei, X.F; Ewell, J.B.; Nguyen, N.Y.; Brossi, A.; Hamel, E. *Journal of Biological Chemistry* **2000**, 275(51), 40443-40452.
[62] Burns, R.G.; *FEBS Letters* **1992**, 297, 205–208.
[63] Skoufias, D.A.; Wilson, L.; *Biochemistry* **1992**, 31, 738-746.
[64] Cragg, G.M.; Kingston, D.G.I.; Newman, D.J.; Anticancer agents from natural products CRC Press, **2005**, pg 23.
[65] Hamel, E.; Lin, C.M.; Ho, H.H.; Pettit, G.R. *Biochemistry* **1989**, 28, 6984.
[66] Wang, L.; Woods, K.W.; Li, Q.; Barr, K.J.; McCroskey, R.W.; Hannick, S.M.; Gherke, L.; Credo, R.B.; Hui, Y.H.; Marsh, K.; Warner, R.; Lee, J.Y.; Zielinski-Mozng, N.; Frost, D.; Rosenberg, S.H.; Sham, H.L.; *Journal of Medicinal Chemistry* **2002**, 45, 1697.
[67] Pettit, G.R.; Singh, S.B.; Hamel, E.; Lin, C.M.; Alberts, D.S.; Garcia-Kendall, D.; *Experientia*, **1989**, 45, 209.
[68] Pettit, G.R.; Cragg, G.M.; Herald, D.L.; Schmidt, J.M.; Lohavanijaya, P. *Canadian Journal of Chemistry* **1982**, 60(11), 1374-1376.
[69] Lin, C.M.; Singh, S.B.; Chu, P.S.; Dempcy, R.O.; Schmidt, J.M.; Pettit, G.R.; Hamel, E. *Molecular Pharmacology* **1988**, 34(2), 200-208.
[70] Pettit, G.R.; Singh, S.B. *Canadian Journal of Chemistry* **1987**, 65, 2390.
[71] Pettit, G.R.; Singh, S.B.; Boyd, M.R.; Hamel, E.; Pettit, R.K.; Schmidt, J.M.; Hogan, F. *Journal of Medicinal Chemistry* **1995**, 38, 1666.
[72] Alessandra C.; Mann *Journal of Natural Products Rep.*, **2003**, 20, 558–564
[73] Kelland, L.R.; Abel, G. *Cancer Chemotherapies Pharmacology* **1992**, 30(6), 444-450.

[74] Monk, K.A.; Siles, R.; Hadimani, M.B.; Mugabe, B.E.; Ackley, J.F.; Studerus, S.W.; Edvardsen, K.; Trawick, M.L.; Garner, C.M.; Rhodes, M.R.; Pettit, G.R.; Pinney, K.G. *Bioorganic & Medicinal Chemistry* **2006**, 14(9), 3231-3244

[75] Cragg, G.M.; Kingston, D.G.I.; Newman, D.J.; Anticancer agents from natural products CRC Press, **2005**, pg28-30

[76] Pettit, G.R.; Singh, S.B.; Niven, M.L. *Journal of the American Chemical Society* **1988**, 110, 8539.

[77] Singh, S.B.; Pettit, G.R., *Journal of Organic Chemistry* **1990**, 55, 2797.

[78] Tron, G.C.; Pirali, T.; Sorba, G.; Pagliai, F.; Busacca, S.; Genazzani, A.A. *Journal of Medicinal Chem*istry **2006**, 49, 11.

[79] Griggs, J., *The Lancet Oncology* **2001**, 2, 82-87

[80] Tozer, G.M.; Kanthou, C.; Baguley, B.C., *Nature Reviews Cancer* **2005**, 5, 423-435

[81] Jain, R.K., *Cancer Metastasis Rev.* **1987**, 6, 559-593

[82] Vaupel, P.; Hockel, M., *International Journal of Oncology* **2000**, 17, 869-879

[83] Sevick, E.M.; Jain, R.K., *Cancer Research* **1989**, 49, 3506-3512

[84] Tozer G.M.; Prise V.E., *Journal of Cancer Research* **1999**, 59, 1626-1634

[85] Galbraith, S.M.; Chaplin, D.J.; Lee, F.; Stratford, M.R.L.; Locke, R.J.; Vojnovic, B.; Tozer, G.M., *Anticancer Research* (**2001**), 21(1A), 93-102

[86] Tozer, G.M.; Kanthou, K.; Parkins, C.S.; Hill, S.A., *International Journal of Experimental Pathology* **2002**, 83, 21-38

[87] ter Haar, E.; Rosenkranz, H.S.; Hamel, E.; Day, B.W. *Bioorganic & Medicinal Chemistry* (**1996**), 4(10), 1659-1671

[88] Nam, N.H., *Current Medicinal Chemistry* (**2003**), 10(17), 1697-1722

[89] West, C.M.L.; Price, P., *Anti-Cancer Drugs* (**2004**), 15(3), 179-187
Grosios, K.; Holwell, S. E.; McGown, A. T.; Pettit, G. R.; Bibby, M. C., *British Journal of Cancer* (**1999**), 81(8), 1318-1327

[90] Bedford, S.B.; Quarterman, C.P.; Rathbone, D.L.; Slack, J.A.; Griffin, R.J.; Stevens, M.F.G., *Bioorganic & Medicinal Chemistry Letters* (**1996**), 6(2), 157-60

[91] Dowlati, A.; Robertson, K.; Cooney, M.; Petros, W.P.; Stratford, M.; Jesberger, J.; Rafie, N.; Overmoyer, B.; Makkar, V.; Stambler, B.; Taylor, A.; Waas, J.; Lewin, J.S.; McCrae, K.R.; Remick, S.C., *Cancer Research* (**2002**), 62(12), 3408-3416

[92] Szakacs, G., *Nature Reviews Drug Discovery.* **2006**, 5, 219-234

[93] Chaplin, D.J.; Hill, S.A., *International Journal Radiation Oncology Biology Physics* **2002**, 54, 5, 1491–1496

[94] Pettit, G.R.; Temple, C.; Narayanan, V.L.; Varma, R.; Simpson, M.J.; Boyd, M.R.; Rener, G.A.; Bansal, N., *Anti-Cancer Drug Design*, **1995**, 10, 299.

[95] Chaplin, D.J.; Pettit, G.R.; Hill, S.A., *Anticancer Research.*, **1999**, 19, 189.

[96] Li, L.; Rojiani, A.; Siemann, D.; *International Journal Radiation Oncology Biology Physics* **1998**, 42, 899.

[97] Grosios, K.; Loadman, M.P.; Swaine, D.J.; Pettit, G.R.; Bibby, C.M., *Anticancer Research.*, **2000**, 20, 229.

[98] Pettit, G.R.; Lippert, J.W.; *Anticancer Drug Design,* **2000**, 15, 203-216

[99] Chaplin, D.J.; Pettit, G.R.; Parkins, C.S.; Hill, A.S., *British Journal of Cancer* **1996**, 74, 86.

[100] Kirwan, I.G.; Loadman, P.M.; Swaine, D.J.; Anthoney, D.A.; Pettit, G.R.; Lippert, J.R.; Shnyder, S.; Cooper, P.A.; Bibby, M.C., *Clinical Cancer Research*, 10, 1446–1453

[101] Holwell, S.E.; Cooper, P.A.; Grosios, K.; Lippert, J.W.; Pettit, G.R.; Shnyder, S.D., *Anticancer Research* **2002**, 22, 707–711.

[102] Hill, S.A.; Tozer, G.M.; Pettit, G.R.; Chaplin, D.J., *Anticancer Research* **2002**, 22, 1453–1458.

[103] Kanthou, C.; Tozer, G.M., *Blood* **2002**, 99, 6, 2060-2069.

[104] Ohsumi, K.; Hatanaka, T.; Nakagawa, R.; Fukuda, Y.; Morinaga, Y.; Suga, Y.; Nihei, Y.; Ohishi, K.; Akiyama, Y.; Tsuji, T., *Anti-cancer drug design* **1999**, 14, 6, 539-548

[105] Pinney, K.G.; Mejia, M.P.; Villalobos, V.M.; Rosenquist, B.E.; Pettit, G.R.; Verdier-Pinard, P.; Hamel, E., *Bioorganic Medicinal Chemistry* **2000**, 8, 2417.

[106] Ohsumi, K.; Nakagawa, R.; Fukuda, Y.; Hatanaka, T.; Morinaga, Y.; Nihei, Y.; Ohishi, K.; Suga, Y.; Akiyama, Y.; Tsuji, T., *Journal of Medicinal Chemistry* **1998**, 41, 3022.

[107] Ohsumi, K.; Tsuji, T.; Morinaga, Y.; Ohishi, K., *U.S.Patent 5,525,632,* **1996**.

[108] Gaukroger, K.; Hadfield, J.A.; Hepworth, L.A.; Lawrence, N.J.; McGown, A.T., *Journal of Organic Chemistry* **2001**, 66, 24, 8135-8138

[109] Pettit, G.R., Rhodes, M.R., *Anti-cancer Drug Design*, **1998**, 13, 183.

[110] Beauregard, D.A.; Thelwall, P.E.; Chaplin D.J., *British Journal of Cancer* **1998**, 77, 1761–1167.
[111] Bilenker, J.H.; Flaherty, K.T.; Rosen, M.; Davis, L.; Gallagher, M.; Stevenson, J.P.; Sun, W.; Vaughn, D.; Giantonio, B.; Zimmer, R.; Schnall, M.; O'Dwyer, P.J., *Clinical Cancer Research* **2005**, 11, 4, 1527-1533.
[112] Chaplin, D.J.; Pettit, G.R.; *Anticancer Research* **1999**, 19, 189-196.
[113] Nguyen-Hai, N, *Current Medicinal Chemistry* **2003**, 10, 1697-1722
[114] Tron, G.C.; Pirali, T.; Sorba, G.; Pagliai, F.; Busacca, S.; Genazzani, A.A., *Journal of Medicinal Chem*istry **2006**, 49, 11, 3033-3044.
[115] Nam, N., *Current Medicinal Chem*istry **2003**, 10, 1697–1722.
[116] Hsieh, H.P.; Liou, J.P.; Mahindroo, N. *Current Pharm. Design* **2005**, 11, 1655–1677.
[117] Cushman, M.; Nagarathnam, D.; Gopal, D.; He, H.M.; Lin, C.M.; Hamel, E.; *Journal of Medicinal Chemistry* **1992**, 35, 2293.
[118] Aleksandrzak, K.; McGown, A.T.; Hadeld, J.A., *Anti-Cancer Drugs*, **1998**, 9, 545.
[119] Andreu, J.M.; Perez-Ramirez, B.; Gorbuno, M.J.; Ayala, D.; Timashe, S.N.; *Biochemistry* **1998**, 37, 8356.
[120] Gaukroger K.; Hadfield, J.A.; Lawrence, N.J.; Nolan, S.; McGown, N.T.; *Organic and Biomolecular Chemistry* **2003**, 1, 3033-3037
[121] Pettit, G.R.; Minardi, M.D.; Rosenberg, H.J.; Hamel, E.; Bibby, M.C., *Journal of Natural Products* **2005**, *68*, 1450-1458.
[122] Hai, N.N., *Current Medicinal Chemistry* **2003**, 10, 1697-1722
[123] Cushman, M.; Nagarathnam, D.; Gopal, D.; Chakraborti, A.K.; Lin, C.M.; Hamel, E., *Journal of Medicinal Chemistry* **1991**, 34, 8, 2579-2588
[124] Lawrence, N.J.; Hepworth, L.A.; Rennison, D.; McGown, A.T.; Hadfield, J.A. *Journal of Fluorine Chemistry* **2003**, 123, 101-108.
[125]Pettit, G.R.; Rhodes, M.R.; Herald, D.L.; Hamel, E.; Schmidt, J.M., *Journal of Medicinal Chemistry* **2005**, 48, 4087-4099.
[126] Kong, Y.; Grembecka, J.; Edler, M.C.; Hamel, E.; Mooberry, S.L.; Sabat, M.; Rieger, J.; Brown, M.L.; *Chemistry & Biology* **2005**, 12, 1007–1014.
[127] Maya, A.B.S.; Perez-Melero, C.; Mateo, C.; Alonso, D.; Fernandez, J.L.; Gajate, C.; Mollinedo, F.; Pelaez, R.; Caballero, E.; Medarde, M., *Journal of Medicinal Chemistry* **2005**, 48, 2, 556-568.
[128] Hatanaka, T.; Fujita, K.; Ohsumi, K.; Nakagawa, R.; Fukuda, Y., *Bioorganic Medicinal Chemistry Letters* **1998**, *8*, 3371-3374.
[129] Lawrence, N.J.; Rennison, D.; Woo, M.; McGown, A.T.; Hadfield, J.A., *Bioorganic & Medicinal Chemistry Letters* (**2001**), 11(1), 51-54.
[130] Getahun, Z.; Jurd, L.; Chu, P.S.; Lin, C.M.; Hamel E., *Journal of Medicinal Chemistry* **1992**, 35, 6, 1058-1067.
[131] Gwaltney, S.L.; Imade, H.M.; Barr, K.J.; Li, Q.; Gehrke, L.; Credo, R.B.; Warner, R.B.; Lee, J.Y.; Kovar, P.; Wang, J.; Nukkala, M.A.; Zielinski, N.A.; Frost, D.; Ng, S.C.; Sham, H.L. *Bioorganic & Medicinal Chemistry Letters* **2001**, 11, 7, 871-874.
[132] Ducki, S.; Forrest, R.; Hadfield, J.A.; Kendall, A.; Lawrence, N.J.; McGown, A.T.; Rennison, D., *Bioorganic & medicinal chemistry letters* **1998**, 8, 9, 1051-1056
[133] Pettit, G.R.; Toki, B.; Herald, D.L.; Verdier-Pinard, P.; Boyd, M.R.; Hamel, E.; Pettit, R.K., *Journal of Medicinal Chemistry* **1998**, 41, 10, 1688-95.
[134] Flynn, B.L.; Flynn, G.P.; Hamel, E.; Jung, M.K., *Bioorganic Medicinal Chemistry Letters* **2001**, 11, 2341.
[135] Shirai, R.; Okabe, T.; Iwasaki, S.; *Heterocycles* **1997**, 46, 145
[136] Ohsumi, K.; Hatanaka, T.; Fujita, K.; Nakagawa, R.; Fukuda, Y.; Niher, Y.; Suga, Y.; Morinaga, Y.; Akiyama, Y.; Tsuji, T., *Bioorganic Medicinal Chemistry Letters* **1998**, 8, 3153.
[137] Tron, G.C.; Pagliai, F.; Del Grosso, E.; Genazzani, A.A; Sorba, G., *Journal of Medicinal Chemistry* **2005**, 48, 9, 3260-8
[138] Medarde, M.; Ramos, A.C.; Caballero, E.; Pelaez-Lamamie de Clairac, R.; Lopez, J.L.; Gravalos, D.G.; Feliciano, A.S., *Bioorganic & Medicinal Chemistry Letters* **1999**, 9, 16, 2303-2308
[139] Pinney, K.G.; Bounds, A.D.; Dingeman, K.M.; Mocharla, V.P.; Pettit, G.R.; Bai, R.; Hamel, E., *Bioorganic & Medicinal Chemistry Letters* **1999**, 9, 8, 1081-1086.
[140] Flynn, B.L.; Hamel, E.; Jung, M.K., *Journal of Medicinal Chemistry* ***2002***, 45, 2670.

[142] Tron, G.C.; Pirali, T.; Sorba, G.; Pagliai, F.; Busacca, S.; Genazzani, A.A; *Journal of Medicinal Chemistry* **2006**, 49, 11, 3033-3044
[143] Deshmukha, A.R.A.S.; Bhawalb, B.M.; Krishnaswamya, D.; Govandea, V.V.; Shinkrea, B.A.; Jayanthia, A.; *Current Medicinal Chemistry* **2004**, 11, 1889-1920
[144] Rosenblum, S.B.; Huynh, T.; Afonso, A.; Davis, H.R.; Yumibe, N.; Clader, J.W.; Burnett, D.A., *Journal of Medicinal Chemistry* **1998**, 41, 973–980
[145] Clader, J.W., *Journal of Medicinal Chem*istry **2004**, 47, 1–9
[146] Burnett, D.A., *Current Medicinal Chemistry*, **2004**, 11, 1873-1887
[147]Kosoglou, T.; Meyer, I.; Veltri, E.P.; Statkevich, P.; Yang, B.; Zhu, Y.; Mellars, L.; Maxwell, S.E.; Patrick, J.E.; Cutler, D.L.; Batra, V.K.; Afrime, M.B. *British Journal of Clinical Pharm.,* **2002**, 54, 309-
319.
[148] Lopez-Otin, C.; Overall, C.M., *Nature Reviews Molecular Cell Biology* **2002,** 3, 509–519.
[149] Turk, B., *Nature Reviews Drug Discovery* **2006**, 5, 785–799.
[150] Han, W.T.; Trehan, A.K.; Wright, J.J.; Federici, M.E.; Seiler, S.M.; Meanwell, N.A.; *Bioorganic Medicinal Chemistry Letters* **1995**, 3, 1123-1143
[151] Adlington, R.M.; Baldwin, J.E.; Chen, B.; Cooper, S.L.; McCoull, W.; Pritchard, G.J.; Howe, T.J., *Bioorganic Medicinal Chemistry Letters* **1997**, 7, 1689-1694.
[152] López-Otín, C.; Matrisian, L.M.; *Nature Reviews* **2007**, 7, 800-808
[153] Koblinski, J.E.; Ahram, M.; Sloane, B.F;. *Clinical Chimica Acta.* **2000**, 291, 113–135.
[154] Teitz, T.; Wei, T.; Valentine, M.B.; Vanin, E.F.; Grenet, J.; Valentine, V.A.; Behm, F.G.; Look, A.T.; Lahti, J.M.; Kidd, V.J., *Nature Medicine* **2000**, 6, 5, 529-535.
[155] Egeblad, M.; Werb, Z., NatureReviews Cancer **2002,** 2, 161–174.
[156] Montel, V.; Kleeman, J.; Agarwal, D.; Spinella, D.; Kawai, K.; Tarin, D,. *Cancer Research* **2004**, 64, 5, 1687-94.
[157] Coussens, L.M.; Fingleton, B.; Matrisian, L.M., *Science* **2002**, 295, 2387–2392.
[158] Joyce, J.A.; Baruch, A.; Chehade, K.; Meyer-Morse, N.; Giraudo, E.; Tsai, F.Y.; Greenbaum, D.C.; Hager, J.H.; Bogyo, M.; Hanahan, D., *Cancer Cell* **2004**, 5,
[159] Smith, D.M.; Aslamuzzaman, K.; Smith, L.; Long, T.E.; Heldreth, B.; Turos, E.; Q. Ping D., *Molecular Pharmacology* 2002, 61, 1348–1358
[160] Banik, B.K.; Banik, I.; Becker, F.F., *Bioorganic & Medicinal Chemistry* **2005**, 13, 3611–3622
[161] Banik, B.K.; Banik, I.; Becker, F.F., *Bioorganic & Medicinal Chemistry* **2004**, 12, 2523–2528
[162] Sun, L.; Vasilevich, N.I.; Fuselier, J.A.; Hocart, S.J.; Coy, D.H. *Bioorganic Medicinal Chemistry Letters* **2004**, 14, 9, 2041-2046
[163] Greewood, B.; Mutabingwa, T., *Nature* **2002**, 415, 670–672
[164] Nivsarkar, M.; Thavaselvam, D.; Prasanna, S.; Sharma, M., Kaushik, M.P.; *Bioorganic and Medicinal Chemistry Letters* **2005**, 15, 1371–1373
[165] Ojima, I.; Fenoglio, I.; Park, Y.H.; Sun, C.M.; Appendino, G.; Bernacki, R.J.; Pera, P., *Journal of Organic Chemistry* **1994**, 59, 3, 515-17.
[166] Singh, G.S., *Tetrahedron* **2003**, 59, 7631–7649
[167] Georg, G.I., The organic chemistry of ß-lactams. VCH Publishers 1992, Chapter 1
[168] Sheehan, J.C.; Hennery-Logan, K.R., *Journal of the American Chemical Society* **1962**, 84, 2983.
[169] Huang, H.; Iwasawa, N.; Mukaiyama, T.; *Chemistry Letters* **1984**, 1465
[170] Staudinger, H., *Liebigs Annalen der Chemie* **1907**, 356, 51.
Escalante, J.; Gonzalez-Tototzin, M. A.; Avina, J.; Munoz-Muniz, O.; Juaristi, E. *Tetrahedron* **2001**, 57, 1883.
[171] Palomo, C.; Aizpurua, J.M.; Ganboa, I.; Oiarbide, M., *European Journal of Organic Chemistry* **1999**, 3232-3235
[172] Palomo, C.; Cosslo, F.P.; Arrieta, A.; Odriozola, J.M.; Oiarbide, M.; Ontoria, J.M.; *Journal of Organic Chem*istry **1989**, 54, 5736-5745
[173] Gilman, H.; Speeter, H., *Journal of the American Chemical Society* **1943**, 65, 2250.
[174] Ferocia, M.; Orsinia, M.; Palombib, L.; Rossic, L.; Inesic, A., *Electrochimica Acta* **2005**, 50 2029–2036
[175] Kambara, T.; Nomura, Y.; Kanai, M.; Koga, K. Chem. Lee, K.I.; Yoon, T.H.; Shim, Y.K.; Kim, W.*J., Bulletin of the Chemical Society of Korea* **2000**, 22, 935.
[176] Chmielewski, M.; Kaluza, Z.; Furman, B.; *Chemical Communications* **1996**, 2689-2696
[177] Takahashi, E.; Fujisawa, H.; Yanai, T.Y., Mukaiyama, T.; *Chemistry Lett*ers **2005**, 34 (2), 216-217

[178] Troisi, L.; De Vitis, L.; Granito, C.; Pilatib, T.; Pindinellia, E., *Tetrahedron* **2004**, 60, 6895–6900
[179] Tanaka, H., *Journal of Organic Chemistry* **1994**, 59, 3040-3046
[180] Lindler, M. R.; Frey, W. U.; Podlech, J., *Journal of the Chemical Society Perkin Transactions.* 1 **2001**, 2566.
[181] Griesbeck, A. G.; Heckroth, H. *Synthesis Letters* **2002**, 131.
[182] Sierra, M. A.; Mancheno, M. J.; Vicente, R.; Gomez-Gallego, M., *Journal of Organic Chemistry* **2001**, 66, 8920.
[183] Wu, G.; Wong, Y.S.; Chen, X.; Ding, Z., *Journal of Organic Chemistry* **1999**, 64, 10, 3714-3718.
[184] Cerreti, A.; D'Annibale, A.; Trogolo, C.; Umani, F. *Tetrahedron Letters* **2000**, 41, 3261.
[185] Thiagarajan, K.; Puranik, V. G.; Deshmukh, A. R. A. S.; Bhawal, B. M. *Tetrahedron* **2000**, 56, 39, 7811-7816
[186] Evans, D.A.; Kleinbeck, F.; Ruping, M., *Asymmetric Synthesis* **2007**, 72-77
Coyne, A.G.; Mueller-Bunz, H.; Guiry, P.J. *Tetrahedron: Asymmetry* **2007**, 18, 2, 199-207.
Lu, H.; Li, C. *Organic Letters* **2006**, 8, 23, 5365-5367.
[187] Fu, G.C.; Lo, M.M., Journal of the American Chemical Society **2002**, 124, 4572-4573
[188] Clark, A.J.; Battlea, G.M.; Bridge, A., *Tetrahedron Letters* **2001**, 42, 4409–4412
[189] Boiteau, L.; Boivinb, J.; Quiclet-Sire, C.; Zarday, S.Z.; Sauniera,Samir, J.B.; Zard, Z., *Tetrahedron* **1998**, 54, 2087-2098
[190] Ishibashi, H.; Kameoka, C.; Kodama, K.; Ikeda, M., *Tetrahedron* **1996**, 52, 2, 489-502,
[191] Quiclet-Sirea, B.; Sauniera, J.B.; Zarda, S.Z.; *Tetrahedron Letters,* **1996** 31, 9, 1397-1400.
[192] De Risi, C.; Pollini, G. P.; Veroneze, A. C.; Bertolasi, V., *Tetrahedron* **2001**, 57, 10155.
[193] Veronese, A.C.; Gandolfi, V., *Journal of Molecular Catal*ysis **1989**, 54, 73
[194] Salzmann, T.N., *et al Journal of the American Chemical Society* **1980**, 102, 6161-6163
[195] Gluchowski, C.; Cooper, L.; Bergbreiter, D.E.; Newcomb, M., *Journal of Organic Chemistry* **1980**, 45, 17, 3413-3416
[196] Hart, D.J.; Deok-Chan, H.; *Chemical Reviews*, **1989**, 89, 1447-1465
[197] Gluchowski, C.; Cooper, L.; Bergbreiter, D.E.; Newcomb, M., *Journal of Organic Chem*istry **1980**, 45, 3413-3416
[198] Hart, D.J.; Lee, C.S.; Pirkle, W.H.; Hyon, M.H.; Tsipouras, A., *Journal of the American Chemical Soc*iety **1986**, 108, 6054.
[199] van der SteeHenk Kleijn, F.H; George, J.P.; Britovsek, J.; Jastrzebski, T.B.H.; van Koten, G., *Journal of Organic Chemistry* **1992**, 57, 3906-3916,
[200] Singh, R.; Nuss, J.M.; *Tetrahedron Letters* **1999**, 40, 1249-1252
[201] Donati, D.; Morelli, C.; Porcheddu, A.; Taddei, M.; *Journal of Organic Chemistry* **2004**, 69, 9316-9318
[202] Schunk, S.; Enders, D.; *Organic Letters* **2000**, 2, 7, 907-910.

---

[203] Carr, M., Development of the β-lactam structure as a scaffold for biologically active compounds. Ph.D. Thesis, Trinity College Dublin, **2006.**
[204] Cessio, F.P.; Ugalde, J.M.; Lopez, X.; Lecea, B.; Palomot, C. *Journal of the American Chemical Society* **1993**, *115, 995-1004*
[205] Jennings, W.B.; Wilson, V.E.; Boyd, D.R.; Coulter, P.B.; *Organic Magnetic Resonance* ***1983***, 21, 4
[206] Lynch, J.E.; Riseman, S.M.; Laswell, W.L.; Volante, R.P.; Smith, G.B.; Shinkai, I.; Tschaen, D.M. *Journal of Organic Chemistry* **1989**, 54, 16, 3792-3796
[207] Liang, Y.; Jiao, L.; Zhang, S.; Xu, J.. *Journal of Organic Chemistry* **2005**, 70, 1, 334-337.
[209] Arrieta, A.; Cossıo, F.P.; *Journal of Organic Chemistry* **2000**, 65, 8458-8464
[210] Hegedus, L. S.; Montgomery, J.; Narukawa, Y.; Snustad, D. C., *Journal of the American Chemical Soc*iety **1991**, 113, 5784- 5791.
[211] Cossio, F. P.; Ugalde, J. M.; Lopez, X.; Lecea, B.; Palomo, C., *Journal of the American Chemical Society* **1993**, 115, 995-1004.
[212] Arrieta, A.; Ugalde, J. M.; Cossio, F. P., *Tetrahedron Lett*ers **1994**, 35, 4465-4468.
[213] Georg, G. I.; He, P.; Kant, J.; Wu, Z. J. *Journal of Organic Chem*istry **1993**, 58, 5771-5778.
[214] Jiao, L.; Liang, Y.; Xu, J.; *Journal of the American Chemical Soc*iety **2006**, 128, 6060-6069
[215] Palomo, C.; Aizpurua, J.M.; Ganboa, I.; Oiarbide, M.; *European Journal of Organic Chemistry* **1999**, 3223-3235
[216] Panunzio, M.; Bacchi, S., *Tettrahedron Lett*ers, **1999**, 40, 8495-8498
[217] Bose, A.K.; Manhas, M.S.; van der Veen, J.M.; Bari, S.S.; Wagle, D.R.; *Tetrahedron* **1992**, 48, 4831-4844.
[218] Aruna, M.; Joshi, S.N.; Puranik, V.G.; Bhawalc, B.M.; Deshmukha, A.R.A.S., *Tetrahedron* **2003**, 59, 2309–2316
[219] Evans, D. A.; Sjögren, E. B., *Tetrahedron Lett*ers, **1985**, 27, 3783.
[220] Ruhlan, B.; Bhandari, A.; Gordon, E.M.; Gallop, M.A.; *Journal of the American Chemical Society* **1996**, 118, 253-254
[221] Hodous, B.L.; Fu, G.C., Journal of the American Chemical Society **2002**, 124, 8
[222] Just, G.; Ugolini, A.; Zamboni, R.. *Synthetic Communications* **1979**, 9, 2, 117-121
[223] Arrieta, A.; Lecea, B.; Cossı, F.P., *Journal of Organic Chem*istry **1998**, 63, 5869-5876
[224] Browne, M.; Burnett, D.A.; Caplen, M.A.; Chen, L.Y.; Clader, J.W.; Domalski, M.; Dugar, S.; Pushpavanam, P.; Sher, R.; *et al. Tetrahedron Letters* **1995**, 36, 15, 2555-8.
[225] Barbaro, G.; Bataglia, A.; Bruno, C.; Giorgianni, P.; Guerrini, A. *Journal of Organic Chem*istry **1996**, 61, 8480.
[226] Georg, G.I.; Mashava, P.M.; Xiangming G.; *Tetrahedron Letters* **1991**, 32, 5, 581-584
[227] Tidwell, T.T., Ketenes, 2nd Edt, Wiley Interscience, New Jersey, **2006**
[228] Tidwell, T.T., *European Journal of Organic Chem*istry **2006**, 563–576
[229] Abaecherli, C.; Miller, R.J.; Othmer, K., *Encyclopedia of Chemical Technology* Wiley Interscience (available online)
[230] Wolff, L., *Justus Liebigs Annalen der Chem*ie **1902**, 325, 129–195
[231] Kirmse, W. *European Journal of Organic Chemistry* **2002**, 2193–2256
[232] Martinez, R.; Huff, M.C.; Barteau, M.A.; *Applied Catalysis A* **2000**, 200, 1-2, , 79-88
[233] Becerraa, A.J.; Martineza, R.; Huff, M.C.; Barteau, M.A., Catalysis Today **2005**, 107-108, 244-249
[234] Calter, M.A.; Orr, R.K.; Song, W.; *Organic Lett*ers **2003**, 5, 4745–4748
[236] Mascitti, V.; Corey, E.J.; *Journal of the American Chemical Society* **2004**, *126*, 15664–15665
[237] Nicolaou, K.C.; Baran, P.S.; Zhong, Y.L.; Fong, K.C.; He, Y.; Yoon, W.H.; Choi, H.S.; *Angewandte Chemie International Ed*ition **1999**, 38, 1676–1678
[238] Tidwell, T.T., Ketenes, 2nd Edt, Wiley Interscience, New Jersey, **2006**, pg 94-95
[239] Linder, M. R.; Podlech, J., *Organic Letters* **2001**, 3, 1849-1851.
[240] Liang, Y.; Jiao, L.; Zhang, S.; Xu, J.; Journal of Organic Chemistry (Notes) **2005**, 70, 1, 334-337
[241] Podlech, J., *Synthesis Letters* **1996**, 5822-5824.
[242] Zamboni, R.; Just, J., *Canadian Journal of Chemistry* **1979**, 57, 1945
[243] de Faria, A.R.; Salvador, E.L.; Correia, C.R.D., *Journal of Organic Chemistry* **2002**, 3651-3661

[244] Krishnaswamy, D.; Bhawal, B.M.; Deshmukh, A.R.A.S., *Tetrahedron Letters* **2000**, 41, 417–419
[245] Amin, S. G.; Glazer, R. D.; Manhas, M. S., Synthesis **1979**, 210.
[246] Tidwell, T.T.; Ketenes, 2nd edn, Wiley Interscience, New Jersey **2006** pg 57-75
[247] Hayes B.L.; Microwave synthesis – chemistry at the speed of light. CEM publishing **2002**
[248] Manhas, M.S.; Banik, B.K.; Mathur, A.; Vincent, J.E.; Bose, A.K., *Tetrahedron* **2000**, 56, 5587-5601
[249] Bose, A.K.; Banik, B.K.; Manhas, M.S., *Tettrahedron Letters* **1995**, 36, 2, 213-216
[250] Coggiola, B.; Pagliai F.; Allegrone G.; Genazzani A.A.; Tron G.C., *Bioorganic & medicinal chemistry letters* **2005**, 15, 15, 3551-3554
[251] Zhao, D.; Jiang, L.; Hahn, E.W.; Mason, R.P., *International Journal of Radiation Oncology, Biology, Physics* **2005**, 62, 3, 872-880
[252] http://www.nlm.nih.gov/medlineplus/druginfo/medmaster/a682899.html Retrieved May 2008
[253] Jesberger, M.; Davis, T.P.; Barner, L.; *Synthesis*, **2003**, 13, 1929-1958
[254] Zacharie, B.; Lagraoui, M.; Dimarco, M.; Penney, C.M.; Gagnon, L., *Journal of Medicinal Chemistry* **1999**, 42, 2046-2052
[255] Kitajima, M.; Kogure, N.; Yamaguchi, K.; Takayama, H.; Aimi N.; *Organic Letters* **2003**, 5, 12, 2075-2078
[256] Isono, K.; Asahi, K.; Suzuki, S., *Journal of the American Chemical Society* **1969**, 91, 26, 7490-7505
[257] Ojima, I.; Zhao, M.; Yamato, T.; Nakahash, K., *Journal of Organic Chemistry* **1991**, 56, 5263-5277
[258] Georg, G.I.; Kant, J.; Gill, H.S., *Journal of the American Chemical Society* **1987**, 109, 1129-1135
[259] Kronenthal, D.R.; C. Y. Han; Taylor, M.K., *Journal of Organic Chemistry* **1982**, 47, 2765-2768
[260] Kaisalo, L.; Latvala, A.; Hase, T., *Synthetic Communications* **1986**, 16(6), 645-648
[261] Pettit, G.R.; Singh, S.B; Niven, M.L; Hamel, E.; Schmidt, J.M., *Journal of Natural Products* **1987**, 50, 1, 119-131
[262] Greene, T.W.; Wutts, P.G.M., *Protective groups in organic synthesis.* **1999**, Wiley & Sons
[263] Harayama, T.; Katsuno, K.; Nishita, Y., *Heterocycles* **2001**, 54, 1, 319-328
[264] Grossa, M.; Wessely, F., *Monatshefte fuer Chemie* **1966**, 97, 1384-1390
[265] McDonald, S., *Journal of Chemical Society Perkin 1*, **1978**, 440-445
[266] Hazlet, B., *Journal of Organic Chemistry* **1962**, 27, 3253-3255
[267] Spletstoser, J.T.; Flaherty, P.T.; Himes, R.H.; Georg, G.I., *Journal of Medicinal Chemistry* **2004**, 47, 6459-6465
[268] Pinney, K.G.; Mejia, M.P.; Villalobos, V.M.; Rosenquist, B.E.; Pettit, G.R.; Verdier-Pinardc, P.; Hamelc, E., *Bioorganic & Medicinal Chemistry* **2000**, 8, 2417-2425.
[269] Schwartz, M.A., *Photochem.Probes.Biochem.* **1989**, 272, 157-168
[270] Csaszar, J.; Balog, J., *Acta Chimica Academiae Scientiarum Hungaricae* **1975**, 86, 1, 3-8.

[271]Georg, G.I., *The organic chemistry of β-lactams*. VCH Publishers **1992,** Chapter 6
[272] Bose, A.K.; Chiang, Y.H.; Manhas, M.S., *Tetrahedron Letters* **1972**, 40, 4091-4094
[273] Bose, A.K.; Krishnan, L.; Wagle, D.R.; Manhas, M.S., *Tetrahedron Letters* **1986**, 27, 49, 5955-5958.
[274] Manhas, M.S.; Ghosh, M.; Bose, A.K., *Journal of Organic Chemistry* **1990**, 55, 2, 575-580.
[276] Duran, F.; Ghosez, L., *Tetrahedron Letters* **1970**, 3, 245-8
[277] Jiao, L.; Liang, Y.; Xu, J., *Journal of the American Chemical Society* **2006**, 128, 18, 6060-6069
[278] Casadei, M.A.; Moracci, F.M.; Inesi, A., *Journal of the Chemical Society Perkin Transactions 2 Physical Organic Chemistry* **1986**, 3, 419-423
[279] Sunagawa, M.; Matsumura, H.; Sasaki, A.; Yamaga, H.; Kitamura, Y.; Sumita, Y.; Nouda, H., *The Journal of Antibiotics* **1997**, 50, 7, 621-627
[280] *Chemistry of Heterocyclic Compounds* **1998**, 34 (11), 1319-1323
[281] Senring, H. P.; Hofheinz, W., *Tetrahedron* **1983**, 39, 15, 2591-2597.
[282] Maruyama, H.; Hiraoka, T., *Journal of Organic Chemistry* **1986**, 51,3, 399-402
[283] Chen, Y.L.; Hedberg, K.; Barrett, J.F.; Retsema, J.A., *The Journal of Antibiotics* **1988**, 41, 1, 134-138.
[284] Hanessian, S.; Alpegiani, M., *Tetrahedron* **1989**, 45, 4, 941-950
[285] Palomo, C.; Aizpurua, J.M., *Chemistry of Heterocyclic Compounds* **1998**, 34, 11, 1222-1236.
[286] Palomo, C.; Aizpurua, J.M.; Galarza, R.; Benito, A.; Khamrai, U.K.; Eikeseth, U.; Linden, A., *Tetrahedron* **2000**, 56, 31, 5563-5570.
[287] Palomo, C.; Aizpurua, J.M.; Legido, M.; Mielgo, A.; Galarza, R., *Chemistry a European Journal* **1997**, 3, 9, 1432-1441
[288] Fujisawa, T.; Shibuya, A.; Sato, D.; Shimizu, M., *Synthesis Letters* **1995**, 10, 1067-1068.
[289] Schmincke, H.; Hoppe, D., *Tetrahedron* **1989**, 45, 3, 701-707
[290] Dugat, D.; Just, G.; Sahoo, S., *Canadian Journal of Chemistry* **1987**, 65, 1, 88-93.
[291] Prodan, K.A.; Hershenson, F.M., *Chemical & Engineering News* **1981**, 59, 14, 59.
[292] Sheehan, J.C.; Ryan, J.J., Journal of the American Chemical Society **1951**, 73, 4367
[293] Yoshioka, K.; Miyawaki, T.; Kishimoto, S.; Matsuo, T.; Ochiai, M., *Journal of Organic Chemistry* **1984**, 49, 8, 1427-1430.
[294] Barton, D.H.R.; GateaOleSker, A.; Anaya-Mateos, J.; Cleophax, J.; Angel, S.D.; Riche, C.C., *Journal of the Chemical Society Perkin Transactions 1* **1990**, 3211-3213
[295] Hart, D.J.; HA, D.C.; *Chemical Rev*iews **1989**, 89, 1447-1465
[296] Techamber, T.J., *Tetrahedron Lett*ers **1980**, 4503.
[297] Picotin, G.; Miginiac, P., *Journal of Organic Chemistry* **1987**, 52, 21, 4796-4798
[298] Repic, O.; Vogt, S., *Tetrahedron Letters* **1982**, 23, 27, 2729-2732
[299] Bose, A.K.; Gupta, K.; Manhas, M.S., *Journal of the Chemical Society Chemical Communications* **1984**, 2, 86-87.
[300] Han, B.H.; Boudjouk, P., *Journal of Organic Chemistry* **1982**, 47, 25, 5030-5032.
[301] Martellia, G.; Spuntaa, G.; Panunziob, M., *Tetrahedron Letters* **1998**, 39, 6257-6260
[302] Tierney, J.P.; Lidstrom, P., *Micorwave Assisted Organic Synthesis*, **2005**, CRC Press
[303] Bose, A.K.; Manhas, M.S.; Ghosh, M.; Shah, M.; Raju, V.S.; Bari, S.S.; Newaz, S.N.; Banik, B.K.; Chaudhary, A.G.; Barakat, K.J.; *Journal of Organic Chemistry* **1991**, 56, 25
[304] Maryhofer, R.; Otto, H., *Synthesis,* **1980**, 247-248
[305] Smith, M.B., March, J., *March's advanced organic chemistry.* **2001.** Wiley Interscience pg 1136
[306] Palomo, C.; Cossio, F.P.; Ontoria, J.M.; Odriozola, J.M., *Journal of Organic Chemistry* **1991**, 56, 5948-5951
[307] Pastor, I.M.; Yus, M., *Current Organic Chemistry* **2005**, 9, 1-29
[308] Cuerva, J.M.; Justicia, J.; Oller-López, J.L.; Bazdi, B.; Oltra, J.E., *Mini-Reviews in Organic Chemistry* **2006**, 3, 23-35
[309] Pineschi, M., *European Journal of Organic Chemistry* **2006**, 4979–4988
[310] Cardillo, G.; Benfatti, F.; Gentilucci, L.; Perciaccante, R.; Tolomelli, A.; Catapano, A., *Journal of Organic Chemistry* **2006**, 71, 9229-9232

[311] Palomo, C.; Aizpurua, J.M.; Ganboa, I.; Oiarbide, M., *European Journal of Organic Chemistry* **1999**, 12, 3223-3235.
[312] Burke, C.M., Synthesis of Intermediates for Carbapenem antibiotics and synthesis analogues of DHEA, Ph.D. Thesis Trinity College Dublin. **1999**
[313] Rastetter, W.H.; Richard, T.J.; Lewis, M.D. *Journal of Organic Chemistry* **1978**, 43, 16, 3163-3166
[314] Emmons, W.D.; Pagano, A.S. *Journal of the American Chemical Society* **1955**, 77, 89-92
[315] Smith, M.B., March, J., *March's advanced organic chemistry*. **2001.** Wiley Interscience. pg 1169
[316] Neary, A.D., Studies in the synthesis of 3-vinylcarbapenems. PhD thesis, Trinity College Dublin **1997**
[317] O' Leary, A, Studies in the synthesis and chemistry of 3-vinylazetidin-2-ones and related compounds. Ph.D. thesis Trinity College Dublin **1991**
[318] Kano, S.; Ebata, T.; Funaki, K.; Shibuya, S., *Synthesis* **1978**, 10, 746-747.
[319] Plantan, I.; Selic, L.; Mesar, T.; Anderluh, P.S.; Oblak, M.; Prezelj, A.; Hesse, L.; Andrejasic, M.; Vilar, M.; Turk, D.; Kocijan, A.; Prevec, T.; Vilfan, G.; Kocjan, D.; Copar, A.; Urleb, U.; Solmajer, T.; *Journal of Medicinal Chemistry* **2007**, 50, 4113-4121

[320] Dark, G.G.; Hill, S.A.; Prise, V.E.; *Cancer Research* **1997**, 57, 1829–1834.
[321] Galbraith, S.M.; Lee, F.; Vojnovic, B., Clinical Cancer Research **1999**, 5, 399.
[322] Hori, K.; Saito, S.; Nihei, Y., *Japanese Journal of Cancer Research* **1999**, 90, 1026–1038.
[323] Zhao, S.; Moore, J.V.; Waller, M.L., et al. *European Journal of Nuclear Medicine* **1999**, 26, 231–238.
[324] Helen, L.; Anderson, J.T.; Yap, M.P.; Miller, A.R.; Jones, T.; Price, P.M.; Journal of Clinical Oncology **2003,** 21, 15, 2823-2830
[325] Meegan, M.J.; Barrett, I.; Zimmermann, J.; Knox, A.J.S.; Zisterer, D.M.; Lloyd, D.G. *Journal of Enzyme Inhibition and Medicinal Chemistry* **2007**, 22, 5, 655-666.
[326] Kerr, D.J.; Hamel, E.; Jung, M.K.; Flynn, B.L., *Bioorganic & Medicinal Chemistry* **2007**, 15, 9, 3290-3298
[327] Image taken directly from the Berkely Lab website www.icbp.lbl.gov/breastcancer/viewline.php?id=40
[328] Mosmann, T., *Journal of immunological methods* **1983**, 65, 1-2, 55-63.
[329] Bielawska, A.; Bielawska, K.; Muskynska, A., *Il Farmaco* **2004**, 59, 2, 111-117
[330] Rossolini, G.M., *Biochemical* Journal **1998**, 332, 145-152
[331] ICH, Stability Testing of New Drug Substances and Products Q1A (R2), International Conference on Harmonization, IFPMA, Geneva, **2003**.
[332] Singh, S.; Singh, B.; Bahuguna, R.; Wadhwa, L.; Saxena, R.; *Journal of Pharmaceutical and Biomedical Analysis* **2006**, 41, 1037–1040
[333] Doshi, A.S.; Kachhadia, P.K.; Joshi, H.S., *Chromatographia* **2008**, 67, 1/2, 137-142
[334] O'Donohoe, C.A., *Synthesis, SAR, and in vitro antitumour activity evaluation of heterocycle-based combretastatin A4 analogues.* M.Sc. thesis, Trinity College Dublin. **2004**
[335] Stratford, M.R,L.; Dennis, M.F., *Journal of Chromatography B* **1999**, 721, 77–85
[336] Rustin, G.J.S.; Galbraith, S.M.; Anderson, H.; Stratford, M.; Folkes, L.K.; Sena, L.; Gumbrell, L.; Price, P.M.; *Journal of Clinical Oncology* **2003**, 21, 15, 2815-2822
[337] Details on the *Macromodel* program are available from the TRIPOS website www.tripos.com
[338] Details on the *MOE* software package are available from the Chemical Computing Group website www.chemcorp.com
[339] Halgren, T.A., *Journal of Computational Chemistry* **1999**, 20, 7, 720-729.
[340] The protein databank can be accessed via the website www.rscb.org
[341] Details on the *Sybyl* program are available from the TRIPOS website www.tripos.com
[342] Ongoing research within the School of Pharmacy, TCD, obtained by private communication
[343] Information on the NCI screening program including details of submitting compounds is available from the NCI website www.dtp.nci.nih..gov/branches/btb/ivclsp.html
[344] Yale, H.L.; Kalkstein, M., *Journal of Medicinal Chem*istry **1967**, 10, 334-336,
[345] Hamel, E., *Biochemical Pharmacology* **1996**, 51, 53-59,

Appendix 1

Determination of crystal structures by XRD

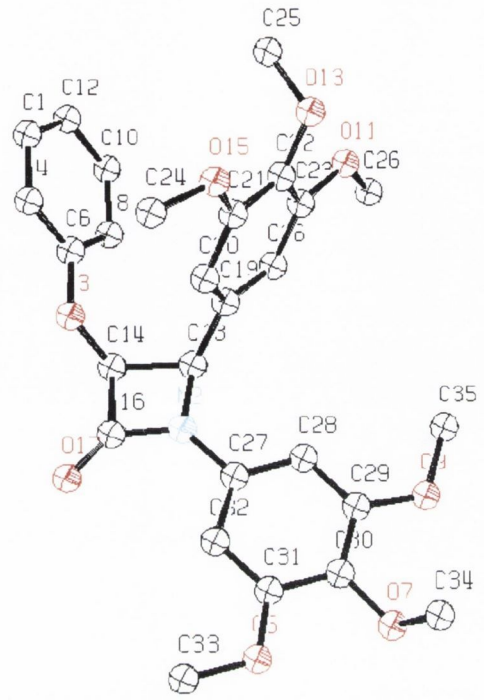

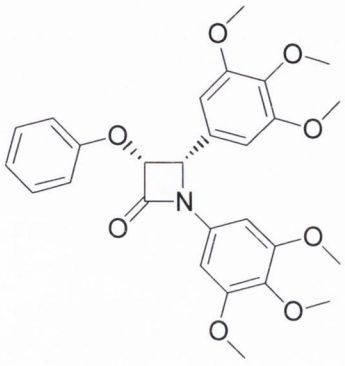

```
data_mjmtg00m

_audit_creation_method            SHELXL-97
_chemical_name_systematic
;
 ?
;
_chemical_name_common             ?
_chemical_melting_point           ?
_chemical_formula_moiety          ?
_chemical_formula_sum
 'C27 H29 N O8'
_chemical_formula_weight          495.51

loop_
 _atom_type_symbol
 _atom_type_description
 _atom_type_scat_dispersion_real
 _atom_type_scat_dispersion_imag
 _atom_type_scat_source
 'C'  'C'   0.0033   0.0016
 'International Tables Vol C Tables 4.2.6.8 and 6.1.1.4'
 'H'  'H'   0.0000   0.0000
 'International Tables Vol C Tables 4.2.6.8 and 6.1.1.4'
 'N'  'N'   0.0061   0.0033
 'International Tables Vol C Tables 4.2.6.8 and 6.1.1.4'
 'O'  'O'   0.0106   0.0060
 'International Tables Vol C Tables 4.2.6.8 and 6.1.1.4'

_symmetry_cell_setting            ?
```

```
_symmetry_space_group_name_H-M    ?

loop_
 _symmetry_equiv_pos_as_xyz
 'x, y, z'
 '-x, -y, -z'

_cell_length_a                    8.9118(5)
_cell_length_b                    11.7367(7)
_cell_length_c                    12.2126(7)
_cell_angle_alpha                 90.8580(10)
_cell_angle_beta                  90.4980(10)
_cell_angle_gamma                 100.6200(10)
_cell_volume                      1255.27(13)
_cell_formula_units_Z             2
_cell_measurement_temperature     571(2)
_cell_measurement_reflns_used     ?
_cell_measurement_theta_min       ?
_cell_measurement_theta_max       ?

_exptl_crystal_description        ?
_exptl_crystal_colour             ?
_exptl_crystal_size_max           ?
_exptl_crystal_size_mid           ?
_exptl_crystal_size_min           ?
_exptl_crystal_density_meas       ?
_exptl_crystal_density_diffrn     1.311
_exptl_crystal_density_method     'not measured'
_exptl_crystal_F_000              524
_exptl_absorpt_coefficient_mu     0.097
_exptl_absorpt_correction_type    ?
_exptl_absorpt_correction_T_min   ?
_exptl_absorpt_correction_T_max   ?
_exptl_absorpt_process_details    ?

_exptl_special_details
;
 ?
;

_diffrn_ambient_temperature       571(2)
_diffrn_radiation_wavelength      0.71073
_diffrn_radiation_type            MoK\a
_diffrn_radiation_source          'fine-focus sealed tube'
_diffrn_radiation_monochromator   graphite
_diffrn_measurement_device_type   ?
_diffrn_measurement_method        ?
_diffrn_detector_area_resol_mean  ?
_diffrn_standards_number          ?
_diffrn_standards_interval_count  ?
_diffrn_standards_interval_time   ?
_diffrn_standards_decay_%         ?
_diffrn_reflns_number             9230
_diffrn_reflns_av_R_equivalents   0.0196
_diffrn_reflns_av_sigmaI/netI     0.0264
_diffrn_reflns_limit_h_min        -10
_diffrn_reflns_limit_h_max        10
_diffrn_reflns_limit_k_min        -13
_diffrn_reflns_limit_k_max        12
_diffrn_reflns_limit_l_min        -13
_diffrn_reflns_limit_l_max        13
```

```
_diffrn_reflns_theta_min          1.67
_diffrn_reflns_theta_max          24.00
_reflns_number_total              3950
_reflns_number_gt                 3575
_reflns_threshold_expression      >2sigma(I)

_computing_data_collection        ?
_computing_cell_refinement        ?
_computing_data_reduction         ?
_computing_structure_solution     'SHELXS-97 (Sheldrick, 1990)'
_computing_structure_refinement   'SHELXL-97 (Sheldrick, 1997)'
_computing_molecular_graphics     ?
_computing_publication_material   ?

_refine_special_details
;
 Refinement of F^2^ against ALL reflections.  The weighted R-factor
wR and
 goodness of fit S are based on F^2^, conventional R-factors R are
based
 on F, with F set to zero for negative F^2^. The threshold expression
of
 F^2^ > 2sigma(F^2^) is used only for calculating R-factors(gt) etc.
and is
 not relevant to the choice of reflections for refinement.  R-factors
based
 on F^2^ are statistically about twice as large as those based on F,
and R-
 factors based on ALL data will be even larger.
;

_refine_ls_structure_factor_coef  Fsqd
_refine_ls_matrix_type            full
_refine_ls_weighting_scheme       calc
_refine_ls_weighting_details
 'calc w=1/[\s^2^(Fo^2^)+(0.0416P)^2^+0.6930P] where
P=(Fo^2^+2Fc^2^)/3'
_atom_sites_solution_primary      direct
_atom_sites_solution_secondary    difmap
_atom_sites_solution_hydrogens    geom
_refine_ls_hydrogen_treatment     mixed
_refine_ls_extinction_method      none
_refine_ls_extinction_coef        ?
_refine_ls_number_reflns          3950
_refine_ls_number_parameters      331
_refine_ls_number_restraints      0
_refine_ls_R_factor_all           0.0509
_refine_ls_R_factor_gt            0.0453
_refine_ls_wR_factor_ref          0.1091
_refine_ls_wR_factor_gt           0.1060
_refine_ls_goodness_of_fit_ref    1.120
_refine_ls_restrained_S_all       1.120
_refine_ls_shift/su_max           0.002
_refine_ls_shift/su_mean          0.000
```

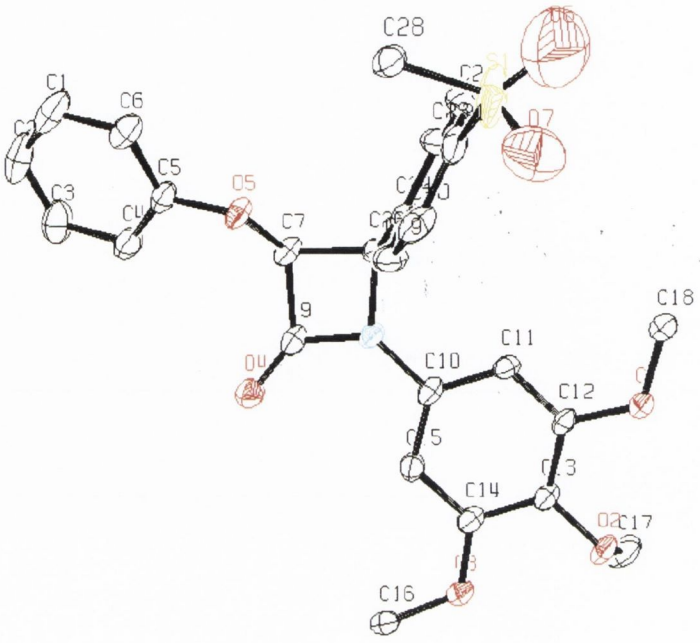

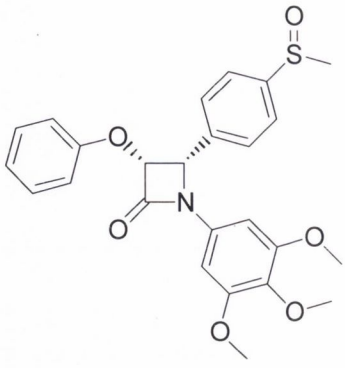

```
data_mjmtg003m in P-1
_symmetry_cell_setting              triclinic
_symmetry_space_group_name_H-M      'P -1'
_symmetry_Int_Tables_number         2
loop_
_symmetry_equiv_pos_site_id
_symmetry_equiv_pos_as_xyz
1 x,y,z
2 -x,-y,-z
_cell_length_a                      9.5683(19)
_cell_length_b                      11.422(2)
_cell_length_c                      11.892(2)
_cell_angle_alpha                   114.97(3)
_cell_angle_beta                    101.24(3)
_cell_angle_gamma                   93.60(3)
_cell_volume                        1140.01
loop_
_atom_site_label
_atom_site_type_symbol
_atom_site_fract_x
_atom_site_fract_y
_atom_site_fract_z
'C'  'C'   0.0033   0.0016
 'International Tables Vol C Tables 4.2.6.8 and 6.1.1.4'
 'H'  'H'   0.0000   0.0000
 'International Tables Vol C Tables 4.2.6.8 and 6.1.1.4'
 'N'  'N'   0.0061   0.0033
 'International Tables Vol C Tables 4.2.6.8 and 6.1.1.4'
 'O'  'O'   0.0106   0.0060
 'International Tables Vol C Tables 4.2.6.8 and 6.1.1.4'
```

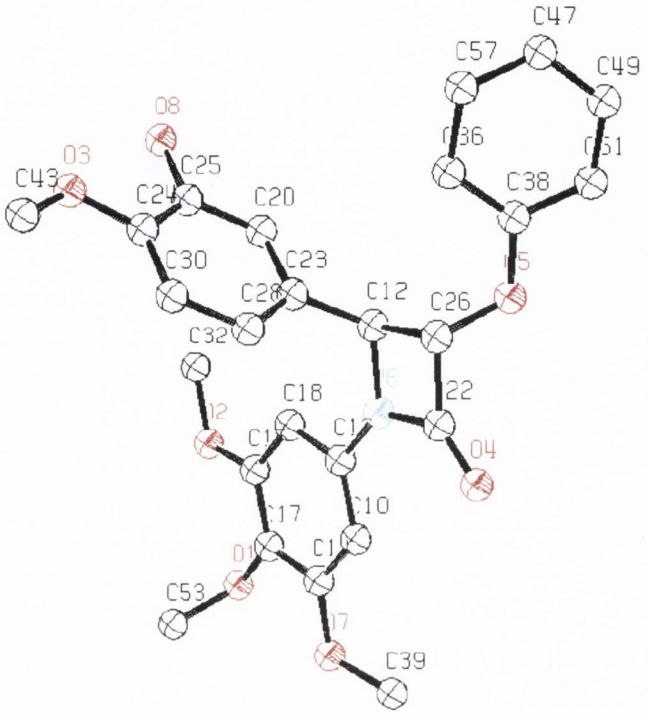

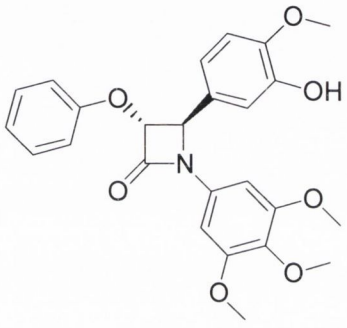


```
data_mjmtg00m

_audit_creation_method            SHELXL-97
_chemical_name_systematic
;
 ?
;
_chemical_name_common             ?
_chemical_melting_point           ?
_chemical_formula_moiety          ?
_chemical_formula_sum
 'C25 H25 N O7'
_chemical_formula_weight          451.46

loop_
 _atom_type_symbol
 _atom_type_description
 _atom_type_scat_dispersion_real
 _atom_type_scat_dispersion_imag
 _atom_type_scat_source
 'C'  'C'   0.0033   0.0016
 'International Tables Vol C Tables 4.2.6.8 and 6.1.1.4'
 'H'  'H'   0.0000   0.0000
 'International Tables Vol C Tables 4.2.6.8 and 6.1.1.4'
 'N'  'N'   0.0061   0.0033
 'International Tables Vol C Tables 4.2.6.8 and 6.1.1.4'
 'O'  'O'   0.0106   0.0060
```

```
 'International Tables Vol C Tables 4.2.6.8 and 6.1.1.4'

_symmetry_cell_setting            ?
_symmetry_space_group_name_H-M    ?

loop_
 _symmetry_equiv_pos_as_xyz
 'x, y, z'
 '-x, -y, -z'

_cell_length_a                    10.1929(11)
_cell_length_b                    10.4180(11)
_cell_length_c                    12.6792(14)
_cell_angle_alpha                 90.803(2)
_cell_angle_beta                  110.232(2)
_cell_angle_gamma                 117.556(2)
_cell_volume                      1095.2(2)
_cell_formula_units_Z             2
_cell_measurement_temperature     571(2)
_cell_measurement_reflns_used     ?
_cell_measurement_theta_min       ?
_cell_measurement_theta_max       ?

_exptl_crystal_description        ?
_exptl_crystal_colour             ?
_exptl_crystal_size_max           ?
_exptl_crystal_size_mid           ?
_exptl_crystal_size_min           ?
_exptl_crystal_density_meas       ?
_exptl_crystal_density_diffrn     1.369
_exptl_crystal_density_method     'not measured'
_exptl_crystal_F_000              476
_exptl_absorpt_coefficient_mu     0.100
_exptl_absorpt_correction_type    ?
_exptl_absorpt_correction_T_min   ?
_exptl_absorpt_correction_T_max   ?
_exptl_absorpt_process_details    ?

_exptl_special_details
;
 ?
;

_diffrn_ambient_temperature       571(2)
_diffrn_radiation_wavelength      0.71073
_diffrn_radiation_type            MoK\a
_diffrn_radiation_source          'fine-focus sealed tube'
_diffrn_radiation_monochromator   graphite
_diffrn_measurement_device_type   ?
_diffrn_measurement_method        ?
_diffrn_detector_area_resol_mean  ?
_diffrn_standards_number          ?
_diffrn_standards_interval_count  ?
_diffrn_standards_interval_time   ?
_diffrn_standards_decay_%         ?
_diffrn_reflns_number             11079
_diffrn_reflns_av_R_equivalents   0.0161
_diffrn_reflns_av_sigmaI/netI     0.0251
_diffrn_reflns_limit_h_min        -13
_diffrn_reflns_limit_h_max        13
_diffrn_reflns_limit_k_min        -13
```

```
_diffrn_reflns_limit_k_max        13
_diffrn_reflns_limit_l_min        -16
_diffrn_reflns_limit_l_max        16
_diffrn_reflns_theta_min          1.75
_diffrn_reflns_theta_max          28.19
_reflns_number_total              5336
_reflns_number_gt                 4679
_reflns_threshold_expression      >2sigma(I)

_computing_data_collection        ?
_computing_cell_refinement        ?
_computing_data_reduction         ?
_computing_structure_solution     'SHELXS-97 (Sheldrick, 1990)'
_computing_structure_refinement   'SHELXL-97 (Sheldrick, 1997)'
_computing_molecular_graphics     ?
_computing_publication_material   ?

_refine_special_details
;
 Refinement of F^2^ against ALL reflections.  The weighted R-factor
wR and
 goodness of fit S are based on F^2^, conventional R-factors R are
based
 on F, with F set to zero for negative F^2^. The threshold expression
of
 F^2^ > 2sigma(F^2^) is used only for calculating R-factors(gt) etc.
and is
 not relevant to the choice of reflections for refinement.  R-factors
based
 on F^2^ are statistically about twice as large as those based on F,
and R-
 factors based on ALL data will be even larger.
;

_refine_ls_structure_factor_coef  Fsqd
_refine_ls_matrix_type            full
_refine_ls_weighting_scheme       calc
_refine_ls_weighting_details
 'calc w=1/[\s^2^(Fo^2^)+(0.0836P)^2^+1.0152P] where
P=(Fo^2^+2Fc^2^)/3'
_atom_sites_solution_primary      direct
_atom_sites_solution_secondary    difmap
_atom_sites_solution_hydrogens    geom
_refine_ls_hydrogen_treatment     mixed
_refine_ls_extinction_method      none
_refine_ls_extinction_coef        ?
_refine_ls_number_reflns          5336
_refine_ls_number_parameters      303
_refine_ls_number_restraints      0
_refine_ls_R_factor_all           0.0695
_refine_ls_R_factor_gt            0.0623
_refine_ls_wR_factor_ref          0.1680
_refine_ls_wR_factor_gt           0.1620
_refine_ls_goodness_of_fit_ref    1.027
_refine_ls_restrained_S_all       1.027
_refine_ls_shift/su_max           0.004
_refine_ls_shift/su_mean          0.001

_audit_creation_method            SHELXL-97
_chemical_name_systematic
;
```

```
 ?
;
_chemical_name_common              ?
_chemical_melting_point            ?
_chemical_formula_moiety           ?
_chemical_formula_sum
 'C50 H52 N2 O13'
_chemical_formula_weight           888.94

loop_
 _atom_type_symbol
 _atom_type_description
 _atom_type_scat_dispersion_real
 _atom_type_scat_dispersion_imag
 _atom_type_scat_source
 'C'  'C'   0.0033   0.0016
 'International Tables Vol C Tables 4.2.6.8 and 6.1.1.4'
 'H'  'H'   0.0000   0.0000
 'International Tables Vol C Tables 4.2.6.8 and 6.1.1.4'
 'N'  'N'   0.0061   0.0033
 'International Tables Vol C Tables 4.2.6.8 and 6.1.1.4'
 'O'  'O'   0.0106   0.0060
 'International Tables Vol C Tables 4.2.6.8 and 6.1.1.4'

_symmetry_cell_setting             ?
_symmetry_space_group_name_H-M     ?

loop_
 _symmetry_equiv_pos_as_xyz
 'x, y, z'
 '-x, y, -z+1/2'
 'x+1/2, y+1/2, z'
 '-x+1/2, y+1/2, -z+1/2'
 '-x, -y, -z'
 'x, -y, z-1/2'
 '-x+1/2, -y+1/2, -z'
 'x+1/2, -y+1/2, z-1/2'

_cell_length_a                     19.4658(13)
_cell_length_b                     13.4807(9)
_cell_length_c                     17.5627(12)
_cell_angle_alpha                  90.00
_cell_angle_beta                   106.5660(10)
_cell_angle_gamma                  90.00
_cell_volume                       4417.4(5)
_cell_formula_units_Z              4
_cell_measurement_temperature      396(2)
_cell_measurement_reflns_used      ?
_cell_measurement_theta_min        ?
_cell_measurement_theta_max        ?

_exptl_crystal_description         ?
_exptl_crystal_colour              ?
_exptl_crystal_size_max            ?
_exptl_crystal_size_mid            ?
_exptl_crystal_size_min            ?
_exptl_crystal_density_meas        ?
_exptl_crystal_density_diffrn      1.337
_exptl_crystal_density_method      'not measured'
_exptl_crystal_F_000               1880
_exptl_absorpt_coefficient_mu      0.097
```

```
_exptl_absorpt_correction_type    ?
_exptl_absorpt_correction_T_min   ?
_exptl_absorpt_correction_T_max   ?
_exptl_absorpt_process_details    ?

_exptl_special_details
;
 ?
;

_diffrn_ambient_temperature       396(2)
_diffrn_radiation_wavelength      0.71073
_diffrn_radiation_type            MoK\a
_diffrn_radiation_source          'fine-focus sealed tube'
_diffrn_radiation_monochromator   graphite
_diffrn_measurement_device_type   ?
_diffrn_measurement_method        ?
_diffrn_detector_area_resol_mean  ?
_diffrn_standards_number          ?
_diffrn_standards_interval_count  ?
_diffrn_standards_interval_time   ?
_diffrn_standards_decay_%         ?
_diffrn_reflns_number             21975
_diffrn_reflns_av_R_equivalents   0.0291
_diffrn_reflns_av_sigmaI/netI     0.0293
_diffrn_reflns_limit_h_min        -25
_diffrn_reflns_limit_h_max        24
_diffrn_reflns_limit_k_min        -17
_diffrn_reflns_limit_k_max        17
_diffrn_reflns_limit_l_min        -21
_diffrn_reflns_limit_l_max        23
_diffrn_reflns_theta_min          1.86
_diffrn_reflns_theta_max          28.29
_reflns_number_total              5466
_reflns_number_gt                 4647
_reflns_threshold_expression      >2sigma(I)

_computing_data_collection        ?
_computing_cell_refinement        ?
_computing_data_reduction         ?
_computing_structure_solution     'SHELXS-97 (Sheldrick, 1990)'
_computing_structure_refinement   'SHELXL-97 (Sheldrick, 1997)'
_computing_molecular_graphics     ?
_computing_publication_material   ?

_refine_special_details
;
 Refinement of F^2^ against ALL reflections.  The weighted R-factor
wR and
 goodness of fit S are based on F^2^, conventional R-factors R are
based
 on F, with F set to zero for negative F^2^. The threshold expression
of
 F^2^ > 2sigma(F^2^) is used only for calculating R-factors(gt) etc.
and is
 not relevant to the choice of reflections for refinement.  R-factors
based
 on F^2^ are statistically about twice as large as those based on F,
and R-
 factors based on ALL data will be even larger.
;
```

```
_refine_ls_structure_factor_coef  Fsqd
_refine_ls_matrix_type            full
_refine_ls_weighting_scheme       calc
_refine_ls_weighting_details
 'calc w=1/[\s^2^(Fo^2^)+(0.0606P)^2^+3.8757P] where
P=(Fo^2^+2Fc^2^)/3'
_atom_sites_solution_primary      direct
_atom_sites_solution_secondary    difmap
_atom_sites_solution_hydrogens    geom
_refine_ls_hydrogen_treatment     mixed
_refine_ls_extinction_method      none
_refine_ls_extinction_coef        ?
_refine_ls_number_reflns          5466
_refine_ls_number_parameters      302
_refine_ls_number_restraints      0
_refine_ls_R_factor_all           0.0583
_refine_ls_R_factor_gt            0.0499
_refine_ls_wR_factor_ref          0.1265
_refine_ls_wR_factor_gt           0.1210
_refine_ls_goodness_of_fit_ref    1.038
_refine_ls_restrained_S_all       1.038
_refine_ls_shift/su_max           0.001
_refine_ls_shift/su_mean          0.000
```

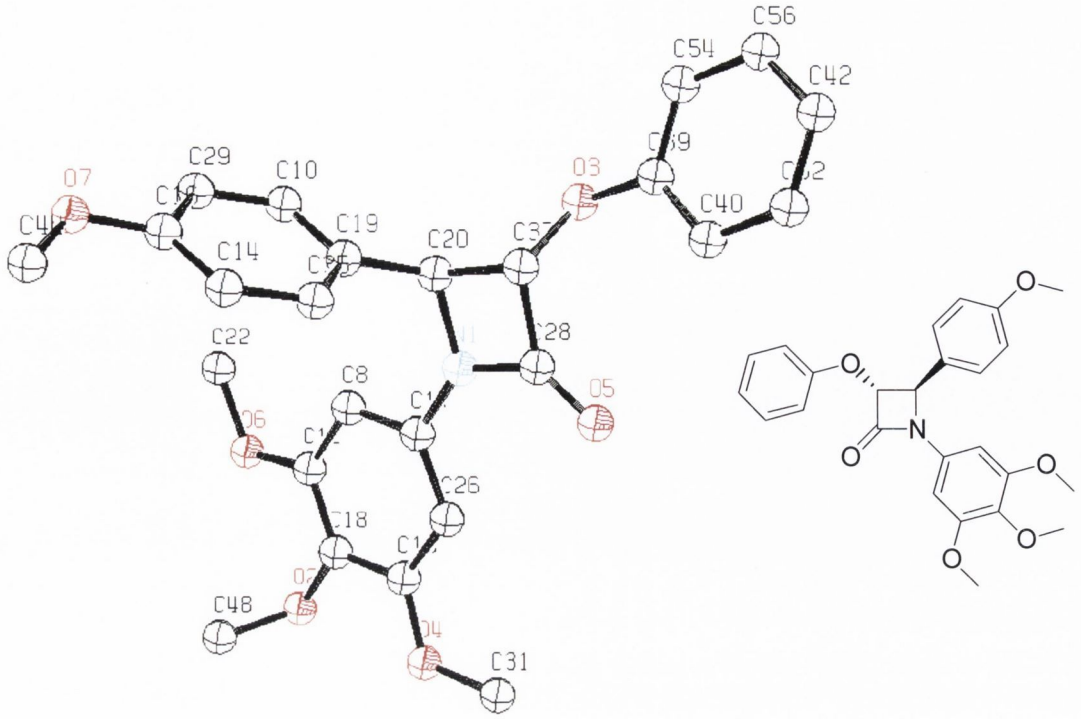


```
_audit_creation_method            SHELXL-97
_chemical_name_systematic
;
 ?
;
_chemical_name_common             ?
_chemical_melting_point           ?
_chemical_formula_moiety          ?
_chemical_formula_sum
 'C50 H52 N2 O13'
_chemical_formula_weight          888.94

loop_
 _atom_type_symbol
 _atom_type_description
 _atom_type_scat_dispersion_real
 _atom_type_scat_dispersion_imag
 _atom_type_scat_source
 'C'  'C'   0.0033   0.0016
 'International Tables Vol C Tables 4.2.6.8 and 6.1.1.4'
 'H'  'H'   0.0000   0.0000
 'International Tables Vol C Tables 4.2.6.8 and 6.1.1.4'
 'N'  'N'   0.0061   0.0033
 'International Tables Vol C Tables 4.2.6.8 and 6.1.1.4'
 'O'  'O'   0.0106   0.0060
 'International Tables Vol C Tables 4.2.6.8 and 6.1.1.4'

_symmetry_cell_setting            ?
_symmetry_space_group_name_H-M    ?

loop_
 _symmetry_equiv_pos_as_xyz
```

```
 'x, y, z'
 '-x, y, -z+1/2'
 'x+1/2, y+1/2, z'
 '-x+1/2, y+1/2, -z+1/2'
 '-x, -y, -z'
 'x, -y, z-1/2'
 '-x+1/2, -y+1/2, -z'
 'x+1/2, -y+1/2, z-1/2'

_cell_length_a                    19.4658(13)
_cell_length_b                    13.4807(9)
_cell_length_c                    17.5627(12)
_cell_angle_alpha                 90.00
_cell_angle_beta                  106.5660(10)
_cell_angle_gamma                 90.00
_cell_volume                      4417.4(5)
_cell_formula_units_Z             4
_cell_measurement_temperature     396(2)
_cell_measurement_reflns_used     ?
_cell_measurement_theta_min       ?
_cell_measurement_theta_max       ?

_exptl_crystal_description        ?
_exptl_crystal_colour             ?
_exptl_crystal_size_max           ?
_exptl_crystal_size_mid           ?
_exptl_crystal_size_min           ?
_exptl_crystal_density_meas       ?
_exptl_crystal_density_diffrn     1.337
_exptl_crystal_density_method     'not measured'
_exptl_crystal_F_000              1880
_exptl_absorpt_coefficient_mu     0.097
_exptl_absorpt_correction_type    ?
_exptl_absorpt_correction_T_min   ?
_exptl_absorpt_correction_T_max   ?
_exptl_absorpt_process_details    ?

_exptl_special_details
;
 ?
;

_diffrn_ambient_temperature       396(2)
_diffrn_radiation_wavelength      0.71073
_diffrn_radiation_type            MoK\a
_diffrn_radiation_source          'fine-focus sealed tube'
_diffrn_radiation_monochromator   graphite
_diffrn_measurement_device_type   ?
_diffrn_measurement_method        ?
_diffrn_detector_area_resol_mean  ?
_diffrn_standards_number          ?
_diffrn_standards_interval_count  ?
_diffrn_standards_interval_time   ?
_diffrn_standards_decay_%         ?
_diffrn_reflns_number             21975
_diffrn_reflns_av_R_equivalents   0.0291
_diffrn_reflns_av_sigmaI/netI     0.0293
_diffrn_reflns_limit_h_min        -25
_diffrn_reflns_limit_h_max        24
_diffrn_reflns_limit_k_min        -17
_diffrn_reflns_limit_k_max        17
```

```
_diffrn_reflns_limit_l_min        -21
_diffrn_reflns_limit_l_max        23
_diffrn_reflns_theta_min          1.86
_diffrn_reflns_theta_max          28.29
_reflns_number_total              5466
_reflns_number_gt                 4647
_reflns_threshold_expression      >2sigma(I)

_computing_data_collection        ?
_computing_cell_refinement        ?
_computing_data_reduction         ?
_computing_structure_solution     'SHELXS-97 (Sheldrick, 1990)'
_computing_structure_refinement   'SHELXL-97 (Sheldrick, 1997)'
_computing_molecular_graphics     ?
_computing_publication_material   ?

_refine_special_details
;
 Refinement of F^2^ against ALL reflections.  The weighted R-factor
wR and
 goodness of fit S are based on F^2^, conventional R-factors R are
based
 on F, with F set to zero for negative F^2^. The threshold expression
of
 F^2^ > 2sigma(F^2^) is used only for calculating R-factors(gt) etc.
and is
 not relevant to the choice of reflections for refinement.  R-factors
based
 on F^2^ are statistically about twice as large as those based on F,
and R-
 factors based on ALL data will be even larger.
;

_refine_ls_structure_factor_coef  Fsqd
_refine_ls_matrix_type            full
_refine_ls_weighting_scheme       calc
_refine_ls_weighting_details
 'calc w=1/[\s^2^(Fo^2^)+(0.0606P)^2^+3.8757P] where
P=(Fo^2^+2Fc^2^)/3'
_atom_sites_solution_primary      direct
_atom_sites_solution_secondary    difmap
_atom_sites_solution_hydrogens    geom
_refine_ls_hydrogen_treatment     mixed
_refine_ls_extinction_method      none
_refine_ls_extinction_coef        ?
_refine_ls_number_reflns          5466
_refine_ls_number_parameters      302
_refine_ls_number_restraints      0
_refine_ls_R_factor_all           0.0583
_refine_ls_R_factor_gt            0.0499
_refine_ls_wR_factor_ref          0.1265
_refine_ls_wR_factor_gt           0.1210
_refine_ls_goodness_of_fit_ref    1.038
_refine_ls_restrained_S_all       1.038
_refine_ls_shift/su_max           0.001
_refine_ls_shift/su_mean          0.000
```

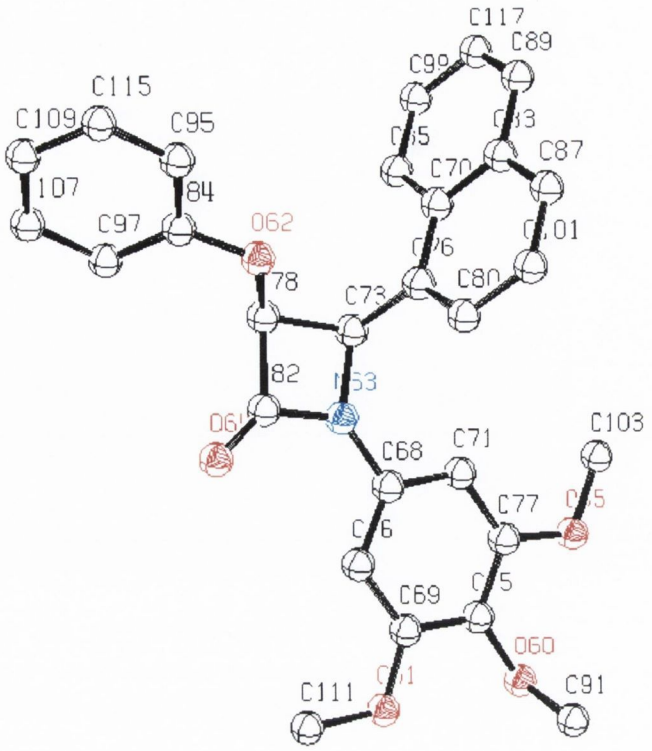

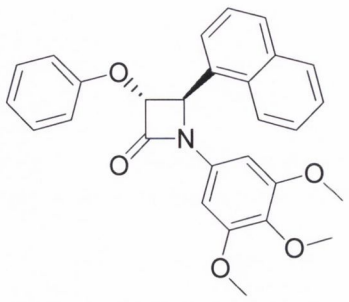


```
data_mjmtg10m

_audit_creation_method            SHELXL-97
_chemical_name_systematic
;
 ?
;
_chemical_name_common             ?
_chemical_melting_point           ?
_chemical_formula_moiety          ?
_chemical_formula_sum
 'C28 H25 N O5'
_chemical_formula_weight          455.49

loop_
 _atom_type_symbol
 _atom_type_description
 _atom_type_scat_dispersion_real
 _atom_type_scat_dispersion_imag
 _atom_type_scat_source
 'C'  'C'   0.0033   0.0016
 'International Tables Vol C Tables 4.2.6.8 and 6.1.1.4'
 'H'  'H'   0.0000   0.0000
 'International Tables Vol C Tables 4.2.6.8 and 6.1.1.4'
 'N'  'N'   0.0061   0.0033
 'International Tables Vol C Tables 4.2.6.8 and 6.1.1.4'
 'O'  'O'   0.0106   0.0060
 'International Tables Vol C Tables 4.2.6.8 and 6.1.1.4'

_symmetry_cell_setting            ?
_symmetry_space_group_name_H-M    ?

loop_
 _symmetry_equiv_pos_as_xyz
```

```
 'x, y, z'
 '-x, -y, -z'

_cell_length_a                    10.1226(5)
_cell_length_b                    14.7272(7)
_cell_length_c                    17.3808(8)
_cell_angle_alpha                 74.9040(10)
_cell_angle_beta                  75.6960(10)
_cell_angle_gamma                 74.3650(10)
_cell_volume                      2365.1(2)
_cell_formula_units_Z             4
_cell_measurement_temperature     396(2)
_cell_measurement_reflns_used     ?
_cell_measurement_theta_min       ?
_cell_measurement_theta_max       ?

_exptl_crystal_description        ?
_exptl_crystal_colour             ?
_exptl_crystal_size_max           ?
_exptl_crystal_size_mid           ?
_exptl_crystal_size_min           ?
_exptl_crystal_density_meas       ?
_exptl_crystal_density_diffrn     1.279
_exptl_crystal_density_method     'not measured'
_exptl_crystal_F_000              960
_exptl_absorpt_coefficient_mu     0.088
_exptl_absorpt_correction_type    ?
_exptl_absorpt_correction_T_min   ?
_exptl_absorpt_correction_T_max   ?
_exptl_absorpt_process_details    ?

_exptl_special_details
;
 ?
;

_diffrn_ambient_temperature       396(2)
_diffrn_radiation_wavelength      0.71073
_diffrn_radiation_type            MoK\a
_diffrn_radiation_source          'fine-focus sealed tube'
_diffrn_radiation_monochromator   graphite
_diffrn_measurement_device_type   ?
_diffrn_measurement_method        ?
_diffrn_detector_area_resol_mean  ?
_diffrn_standards_number          ?
_diffrn_standards_interval_count  ?
_diffrn_standards_interval_time   ?
_diffrn_standards_decay_%         ?
_diffrn_reflns_number             18923
_diffrn_reflns_av_R_equivalents   0.0242
_diffrn_reflns_av_sigmaI/netI     0.0330
_diffrn_reflns_limit_h_min        -12
_diffrn_reflns_limit_h_max        12
_diffrn_reflns_limit_k_min        -17
_diffrn_reflns_limit_k_max        17
_diffrn_reflns_limit_l_min        -20
_diffrn_reflns_limit_l_max        20
_diffrn_reflns_theta_min          1.24
_diffrn_reflns_theta_max          25.00
_reflns_number_total              8330
_reflns_number_gt                 6630
```

```
_reflns_threshold_expression      >2sigma(I)

_computing_data_collection        ?
_computing_cell_refinement        ?
_computing_data_reduction         ?
_computing_structure_solution     'SHELXS-97 (Sheldrick, 1990)'
_computing_structure_refinement   'SHELXL-97 (Sheldrick, 1997)'
_computing_molecular_graphics     ?
_computing_publication_material   ?

_refine_special_details
;
 Refinement of F^2^ against ALL reflections.  The weighted R-factor
wR and
 goodness of fit S are based on F^2^, conventional R-factors R are
based
 on F, with F set to zero for negative F^2^. The threshold expression
of
 F^2^ > 2sigma(F^2^) is used only for calculating R-factors(gt) etc.
and is
 not relevant to the choice of reflections for refinement.  R-factors
based
 on F^2^ are statistically about twice as large as those based on F,
and R-
 factors based on ALL data will be even larger.
;

_refine_ls_structure_factor_coef  Fsqd
_refine_ls_matrix_type            full
_refine_ls_weighting_scheme       calc
_refine_ls_weighting_details
 'calc w=1/[\s^2^(Fo^2^)+(0.0592P)^2^+0.5023P] where
P=(Fo^2^+2Fc^2^)/3'
_atom_sites_solution_primary      direct
_atom_sites_solution_secondary    difmap
_atom_sites_solution_hydrogens    geom
_refine_ls_hydrogen_treatment     mixed
_refine_ls_extinction_method      none
_refine_ls_extinction_coef        ?
_refine_ls_number_reflns          8330
_refine_ls_number_parameters      619
_refine_ls_number_restraints      0
_refine_ls_R_factor_all           0.0551
_refine_ls_R_factor_gt            0.0420
_refine_ls_wR_factor_ref          0.1170
_refine_ls_wR_factor_gt           0.1059
_refine_ls_goodness_of_fit_ref    1.039
_refine_ls_restrained_S_all       1.039
_refine_ls_shift/su_max           0.002
_refine_ls_shift/su_mean          0.000
```

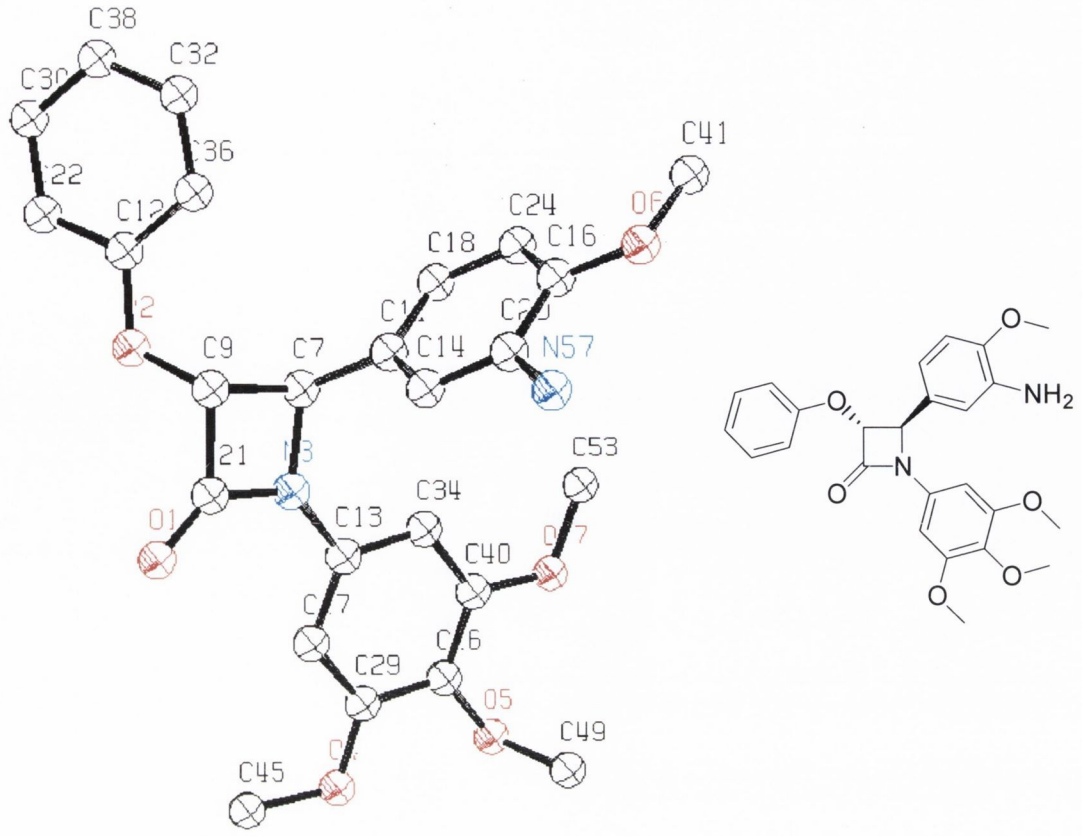


```
_audit_creation_method            SHELXL-97
_chemical_name_systematic
;
 ?
;
_chemical_name_common             ?
_chemical_melting_point           ?
_chemical_formula_moiety          ?
_chemical_formula_sum
 'C27 H29 N O8'
_chemical_formula_weight          495.51

loop_
 _atom_type_symbol
 _atom_type_description
 _atom_type_scat_dispersion_real
 _atom_type_scat_dispersion_imag
 _atom_type_scat_source
 'C'  'C'   0.0033   0.0016
 'International Tables Vol C Tables 4.2.6.8 and 6.1.1.4'
 'H'  'H'   0.0000   0.0000
 'International Tables Vol C Tables 4.2.6.8 and 6.1.1.4'
 'N'  'N'   0.0061   0.0033
 'International Tables Vol C Tables 4.2.6.8 and 6.1.1.4'
 'O'  'O'   0.0106   0.0060
 'International Tables Vol C Tables 4.2.6.8 and 6.1.1.4'

_symmetry_cell_setting            ?
_symmetry_space_group_name_H-M    ?

loop_
 _symmetry_equiv_pos_as_xyz
```

```
 'x, y, z'
 '-x, -y, -z'

_cell_length_a                    8.9118(5)
_cell_length_b                    11.7367(7)
_cell_length_c                    12.2126(7)
_cell_angle_alpha                 90.8580(10)
_cell_angle_beta                  90.4980(10)
_cell_angle_gamma                 100.6200(10)
_cell_volume                      1255.27(13)
_cell_formula_units_Z             2
_cell_measurement_temperature     571(2)
_cell_measurement_reflns_used     ?
_cell_measurement_theta_min       ?
_cell_measurement_theta_max       ?

_exptl_crystal_description        ?
_exptl_crystal_colour             ?
_exptl_crystal_size_max           ?
_exptl_crystal_size_mid           ?
_exptl_crystal_size_min           ?
_exptl_crystal_density_meas       ?
_exptl_crystal_density_diffrn     1.311
_exptl_crystal_density_method     'not measured'
_exptl_crystal_F_000              524
_exptl_absorpt_coefficient_mu     0.097
_exptl_absorpt_correction_type    ?
_exptl_absorpt_correction_T_min   ?
_exptl_absorpt_correction_T_max   ?
_exptl_absorpt_process_details    ?

_exptl_special_details
;
 ?
;

_diffrn_ambient_temperature       571(2)
_diffrn_radiation_wavelength      0.71073
_diffrn_radiation_type            MoK\a
_diffrn_radiation_source          'fine-focus sealed tube'
_diffrn_radiation_monochromator   graphite
_diffrn_measurement_device_type   ?
_diffrn_measurement_method        ?
_diffrn_detector_area_resol_mean  ?
_diffrn_standards_number          ?
_diffrn_standards_interval_count  ?
_diffrn_standards_interval_time   ?
_diffrn_standards_decay_%         ?
_diffrn_reflns_number             9230
_diffrn_reflns_av_R_equivalents   0.0196
_diffrn_reflns_av_sigmaI/netI     0.0264
_diffrn_reflns_limit_h_min        -10
_diffrn_reflns_limit_h_max        10
_diffrn_reflns_limit_k_min        -13
_diffrn_reflns_limit_k_max        12
_diffrn_reflns_limit_l_min        -13
_diffrn_reflns_limit_l_max        13
_diffrn_reflns_theta_min          1.67
_diffrn_reflns_theta_max          24.00
_reflns_number_total              3950
_reflns_number_gt                 3575
```

```
_reflns_threshold_expression      >2sigma(I)

_computing_data_collection        ?
_computing_cell_refinement        ?
_computing_data_reduction         ?
_computing_structure_solution     'SHELXS-97 (Sheldrick, 1990)'
_computing_structure_refinement   'SHELXL-97 (Sheldrick, 1997)'
_computing_molecular_graphics     ?
_computing_publication_material   ?

_refine_special_details
;
 Refinement of F^2^ against ALL reflections.  The weighted R-factor
wR and
 goodness of fit S are based on F^2^, conventional R-factors R are
based
 on F, with F set to zero for negative F^2^. The threshold expression
of
 F^2^ > 2sigma(F^2^) is used only for calculating R-factors(gt) etc.
and is
 not relevant to the choice of reflections for refinement.  R-factors
based
 on F^2^ are statistically about twice as large as those based on F,
and R-
 factors based on ALL data will be even larger.
;

_refine_ls_structure_factor_coef  Fsqd
_refine_ls_matrix_type            full
_refine_ls_weighting_scheme       calc
_refine_ls_weighting_details
 'calc w=1/[\s^2^(Fo^2^)+(0.0416P)^2^+0.6930P] where
P=(Fo^2^+2Fc^2^)/3'
_atom_sites_solution_primary      direct
_atom_sites_solution_secondary    difmap
_atom_sites_solution_hydrogens    geom
_refine_ls_hydrogen_treatment     mixed
_refine_ls_extinction_method      none
_refine_ls_extinction_coef        ?
_refine_ls_number_reflns          3950
_refine_ls_number_parameters      331
_refine_ls_number_restraints      0
_refine_ls_R_factor_all           0.0509
_refine_ls_R_factor_gt            0.0453
_refine_ls_wR_factor_ref          0.1091
_refine_ls_wR_factor_gt           0.1060
_refine_ls_goodness_of_fit_ref    1.120
_refine_ls_restrained_S_all       1.120
_refine_ls_shift/su_max           0.002
_refine_ls_shift/su_mean          0.000
```

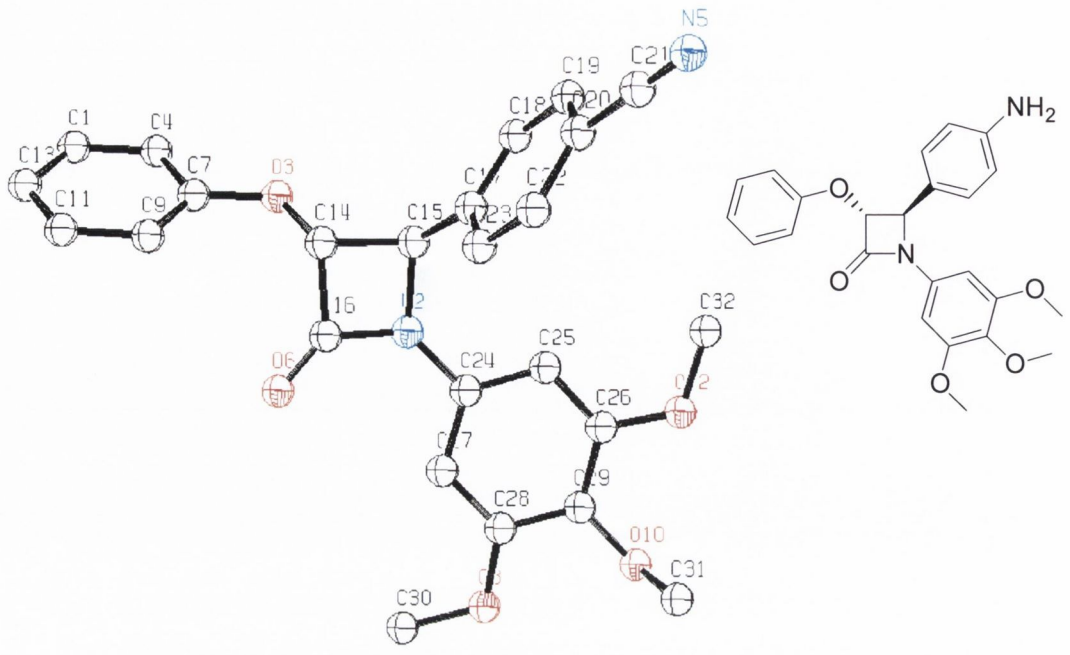


```
data_mjmtg15m

_audit_creation_method            SHELXL-97
_chemical_name_systematic
;
 ?
;
_chemical_name_common             ?
_chemical_melting_point           ?
_chemical_formula_moiety          ?
_chemical_formula_sum
 'C25 H22 N2 O5'
_chemical_formula_weight          430.45

loop_
 _atom_type_symbol
 _atom_type_description
 _atom_type_scat_dispersion_real
 _atom_type_scat_dispersion_imag
 _atom_type_scat_source
 'C'  'C'   0.0033   0.0016
 'International Tables Vol C Tables 4.2.6.8 and 6.1.1.4'
 'H'  'H'   0.0000   0.0000
 'International Tables Vol C Tables 4.2.6.8 and 6.1.1.4'
 'N'  'N'   0.0061   0.0033
 'International Tables Vol C Tables 4.2.6.8 and 6.1.1.4'
 'O'  'O'   0.0106   0.0060
 'International Tables Vol C Tables 4.2.6.8 and 6.1.1.4'

_symmetry_cell_setting            ?
_symmetry_space_group_name_H-M    ?

loop_
 _symmetry_equiv_pos_as_xyz
 'x, y, z'
 '-x, y+1/2, -z+1/2'
 '-x, -y, -z'
```

```
 'x, -y-1/2, z-1/2'

_cell_length_a                    14.9002(9)
_cell_length_b                    14.0903(8)
_cell_length_c                    21.0318(12)
_cell_angle_alpha                 90.00
_cell_angle_beta                  94.6700(10)
_cell_angle_gamma                 90.00
_cell_volume                      4400.9(4)
_cell_formula_units_Z             8
_cell_measurement_temperature     396(2)
_cell_measurement_reflns_used     ?
_cell_measurement_theta_min       ?
_cell_measurement_theta_max       ?

_exptl_crystal_description        ?
_exptl_crystal_colour             ?
_exptl_crystal_size_max           ?
_exptl_crystal_size_mid           ?
_exptl_crystal_size_min           ?
_exptl_crystal_density_meas       ?
_exptl_crystal_density_diffrn     1.299
_exptl_crystal_density_method     'not measured'
_exptl_crystal_F_000              1808
_exptl_absorpt_coefficient_mu     0.091
_exptl_absorpt_correction_type    ?
_exptl_absorpt_correction_T_min   ?
_exptl_absorpt_correction_T_max   ?
_exptl_absorpt_process_details    ?

_exptl_special_details
;
 ?
;

_diffrn_ambient_temperature       396(2)
_diffrn_radiation_wavelength      0.71073
_diffrn_radiation_type            MoK\a
_diffrn_radiation_source          'fine-focus sealed tube'
_diffrn_radiation_monochromator   graphite
_diffrn_measurement_device_type   ?
_diffrn_measurement_method        ?
_diffrn_detector_area_resol_mean  ?
_diffrn_standards_number          ?
_diffrn_standards_interval_count  ?
_diffrn_standards_interval_time   ?
_diffrn_standards_decay_%         ?
_diffrn_reflns_number             44037
_diffrn_reflns_av_R_equivalents   0.0245
_diffrn_reflns_av_sigmaI/netI     0.0229
_diffrn_reflns_limit_h_min        -19
_diffrn_reflns_limit_h_max        19
_diffrn_reflns_limit_k_min        -18
_diffrn_reflns_limit_k_max        18
_diffrn_reflns_limit_l_min        -28
_diffrn_reflns_limit_l_max        26
_diffrn_reflns_theta_min          1.74
_diffrn_reflns_theta_max          28.26
_reflns_number_total              10853
_reflns_number_gt                 9281
_reflns_threshold_expression      >2sigma(I)
```

```
_computing_data_collection          ?
_computing_cell_refinement          ?
_computing_data_reduction           ?
_computing_structure_solution       'SHELXS-97 (Sheldrick, 1990)'
_computing_structure_refinement     'SHELXL-97 (Sheldrick, 1997)'
_computing_molecular_graphics       ?
_computing_publication_material     ?

_refine_special_details
;
 Refinement of F^2^ against ALL reflections.  The weighted R-factor
wR and
 goodness of fit S are based on F^2^, conventional R-factors R are
based
 on F, with F set to zero for negative F^2^. The threshold expression
of
 F^2^ > 2sigma(F^2^) is used only for calculating R-factors(gt) etc.
and is
 not relevant to the choice of reflections for refinement.  R-factors
based
 on F^2^ are statistically about twice as large as those based on F,
and R-
 factors based on ALL data will be even larger.
;

_refine_ls_structure_factor_coef  Fsqd
_refine_ls_matrix_type            full
_refine_ls_weighting_scheme       calc
_refine_ls_weighting_details
 'calc w=1/[\s^2^(Fo^2^)+(0.0651P)^2^+1.1360P] where
P=(Fo^2^+2Fc^2^)/3'
_atom_sites_solution_primary      direct
_atom_sites_solution_secondary    difmap
_atom_sites_solution_hydrogens    geom
_refine_ls_hydrogen_treatment     mixed
_refine_ls_extinction_method      none
_refine_ls_extinction_coef        ?
_refine_ls_number_reflns          10853
_refine_ls_number_parameters      611
_refine_ls_number_restraints      0
_refine_ls_R_factor_all           0.0497
_refine_ls_R_factor_gt            0.0424
_refine_ls_wR_factor_ref          0.1169
_refine_ls_wR_factor_gt           0.1111
_refine_ls_goodness_of_fit_ref    1.027
_refine_ls_restrained_S_all       1.027
_refine_ls_shift/su_max           0.001
_refine_ls_shift/su_mean          0.000
```

Appendix 2

Data from the testing of compounds by the National Cancer Institute

National Cancer Institute Developmental Therapeutics Program Dose Response Curves	NSC : D - 746998 / 1	SSPL: 0X0S	EXP. ID: 0805NS99
	Report Date: June 10, 2008	Test Date: May 05, 2008	

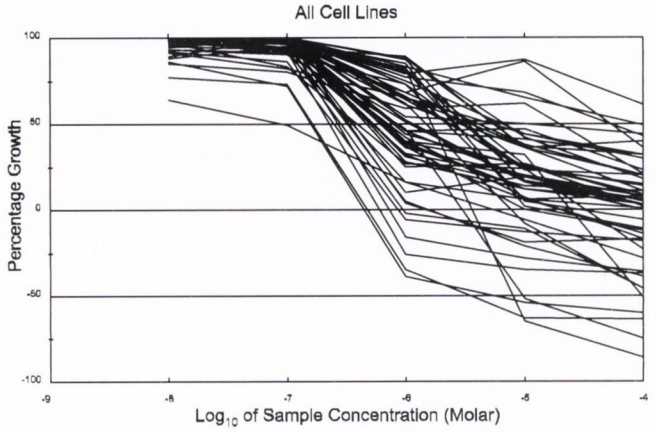

National Cancer Institute Developmental Therapeutics Program Dose Response Curves	NSC: D - 746998 / 1	SSPL: 0X0S	EXP. ID: 0805NS99
	Report Date: June 10, 2008	Test Date: May 05, 2008	

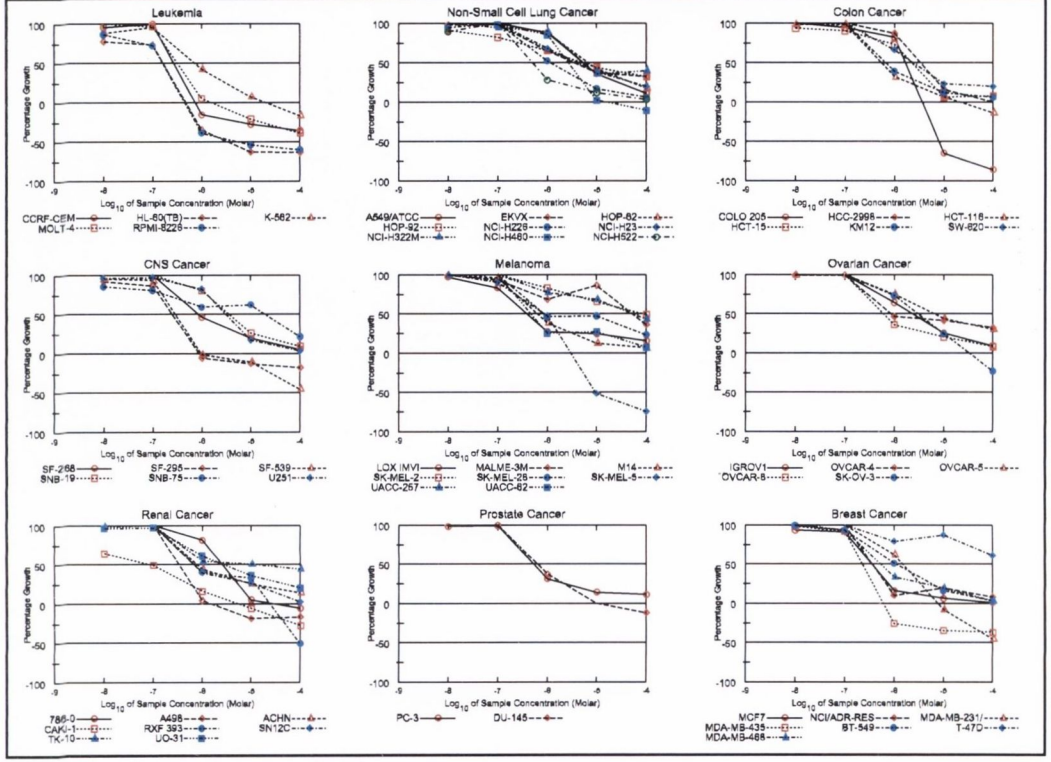

National Cancer Institute Developmental Therapeutics Program
In-Vitro Testing Results

NSC : D - 746998 / 1	Experiment ID : 0805NS99	Test Type : 08	Units : Molar
Report Date : June 10, 2008	Test Date : May 05, 2008	QNS :	MC :
COMI : mjmtg001 (70760)	Stain Reagent : SRB Dual-Pass Related	SSPL : 0X0S	

Panel/Cell Line	Time Zero	Ctrl	Mean Optical Densities Log10 Concentration -8.0	-7.0	-6.0	-5.0	-4.0	Percent Growth -8.0	-7.0	-6.0	-5.0	-4.0	GI50	TGI	LC50
Leukemia															
CCRF-CEM	0.246	0.761	0.736	0.758	0.207	0.176	0.159	95	99	-16	-28	-36	2.88E-7	7.26E-7	> 1.00E-4
HL-60(TB)	0.415	1.127	0.983	0.935	0.268	0.156	0.148	77	73	-35	-63	-64	1.83E-7	4.71E-7	3.45E-6
K-562	0.147	0.889	0.797	0.854	0.455	0.198	0.122	88	95	42	7	-17	6.96E-7	1.94E-5	> 1.00E-4
MOLT-4	0.193	0.701	0.705	0.683	0.217	0.152	0.118	101	96	5	-21	-39	3.21E-7	1.51E-6	> 1.00E-4
RPMI-8226	0.269	0.460	0.433	0.406	0.165	0.125	0.109	86	72	-39	-54	-60	1.57E-7	4.45E-7	5.62E-6
Non-Small Cell Lung Cancer															
A549/ATCC	0.217	1.137	1.158	1.220	1.023	0.546	0.318	102	109	88	36	11	5.32E-6	> 1.00E-4	> 1.00E-4
EKVX	0.731	1.716	1.693	1.693	1.374	1.100	1.050	98	98	65	37	32	3.53E-6	> 1.00E-4	> 1.00E-4
HOP-62	0.637	1.617	1.723	1.761	1.502	1.049	0.812	111	115	88	42	18	6.71E-6	> 1.00E-4	> 1.00E-4
HOP-92	0.650	1.066	1.030	0.990	0.922	0.834	0.785	91	82	65	44	32	5.29E-6	> 1.00E-4	> 1.00E-4
NCI-H226	0.752	1.339	1.303	1.387	1.060	0.850	0.787	94	105	52	17	6	1.17E-6	> 1.00E-4	> 1.00E-4
NCI-H23	0.420	1.261	1.307	1.292	0.998	0.739	0.591	105	104	68	38	20	4.03E-6	> 1.00E-4	> 1.00E-4
NCI-H322M	0.460	1.067	1.084	1.033	0.998	0.680	0.703	103	94	89	36	40	5.44E-6	> 1.00E-4	> 1.00E-4
NCI-H460	0.238	2.162	2.244	2.115	1.869	0.273	0.212	104	98	85	2	-11	2.62E-6	1.39E-5	> 1.00E-4
NCI-H522	1.113	2.200	2.080	2.223	1.414	1.247	1.141	89	102	28	12	3	5.01E-7	> 1.00E-4	> 1.00E-4
Colon Cancer															
COLO 205	0.171	0.618	0.667	0.592	0.537	0.061	0.024	111	94	82	-65	-86	1.65E-6	3.62E-6	7.95E-6
HCC-2998	0.706	1.678	1.787	1.731	1.555	0.857	0.706	111	105	87	16	.	3.31E-6	9.90E-5	> 1.00E-4
HCT-116	0.162	1.319	1.298	1.301	0.531	0.227	0.140	98	98	32	6	-14	5.34E-7	1.95E-5	> 1.00E-4
HCT-15	0.303	1.546	1.459	1.416	1.215	0.373	0.404	93	90	73	6	8	2.21E-6	> 1.00E-4	> 1.00E-4
KM12	0.470	1.887	1.966	1.972	1.016	0.639	0.552	106	106	39	12	6	6.76E-7	> 1.00E-4	> 1.00E-4
SW-620	0.236	1.399	1.402	1.395	1.000	0.506	0.467	100	100	66	23	20	2.34E-6	> 1.00E-4	> 1.00E-4
CNS Cancer															
SF-268	1.045	2.468	2.522	2.567	1.706	1.321	1.118	104	107	46	19	5	8.74E-7	> 1.00E-4	> 1.00E-4
SF-295	0.548	1.355	1.289	1.239	0.517	0.476	0.452	92	86	-6	-13	-18	2.48E-7	8.65E-7	> 1.00E-4
SF-539	0.574	1.856	1.795	1.772	0.563	0.514	0.313	95	93	-2	-11	-46	2.85E-7	9.55E-7	> 1.00E-4
SNB-19	0.302	1.094	1.149	1.115	0.939	0.510	0.372	107	103	80	26	9	3.84E-6	> 1.00E-4	> 1.00E-4
SNB-75	0.581	1.337	1.226	1.187	1.027	1.053	0.738	85	80	59	62	21	1.99E-5	> 1.00E-4	> 1.00E-4
U251	0.290	1.351	1.312	1.321	1.159	0.466	0.323	96	97	82	17	3	3.08E-6	> 1.00E-4	> 1.00E-4
Melanoma															
LOX IMVI	0.311	1.781	1.740	1.531	0.704	0.657	0.626	97	83	27	24	15	3.85E-7	> 1.00E-4	> 1.00E-4
MALME-3M	0.620	0.977	0.975	0.951	0.863	0.927	0.750	99	93	68	86	36	5.32E-6	> 1.00E-4	> 1.00E-4
M14	0.332	1.393	1.387	1.355	0.735	0.462	0.394	99	96	38	12	6	6.21E-7	> 1.00E-4	> 1.00E-4
SK-MEL-2	0.475	0.945	0.977	1.008	0.868	0.779	0.704	107	113	83	65	49	8.17E-5	> 1.00E-4	> 1.00E-4
SK-MEL-28	0.433	1.117	1.133	1.142	0.747	0.753	0.589	102	104	46	47	23	8.50E-7	> 1.00E-4	> 1.00E-4
SK-MEL-5	0.429	2.307	2.362	2.122	1.308	0.205	0.108	103	90	47	-52	-75	8.43E-7	2.97E-6	9.50E-6
UACC-257	0.897	1.942	1.928	1.973	1.703	1.608	1.350	99	103	77	68	43	5.35E-5	> 1.00E-4	> 1.00E-4
UACC-62	0.506	1.726	1.721	1.728	0.806	0.837	0.596	100	100	25	27	7	4.60E-7	> 1.00E-4	> 1.00E-4
Ovarian Cancer															
IGROV1	0.454	1.343	1.377	1.419	1.027	0.678	0.537	104	109	64	25	9	2.34E-6	> 1.00E-4	> 1.00E-4
OVCAR-4	0.522	1.782	1.775	1.787	1.108	1.033	0.924	99	99	46	41	32	8.56E-7	> 1.00E-4	> 1.00E-4
OVCAR-5	0.514	1.301	1.293	1.335	1.108	0.859	0.751	99	104	75	44	30	6.35E-6	> 1.00E-4	> 1.00E-4
OVCAR-8	0.433	1.695	1.776	1.769	0.886	0.688	0.537	106	106	36	20	8	6.29E-7	> 1.00E-4	> 1.00E-4
SK-OV-3	0.509	1.374	1.453	1.394	1.145	0.721	0.394	109	102	73	24	-23	3.01E-6	3.30E-5	> 1.00E-4
Renal Cancer															
786-0	0.765	2.421	2.498	2.588	2.098	0.852	0.717	105	109	81	5	-6	2.54E-6	2.86E-5	> 1.00E-4
A498	0.944	1.652	1.694	1.656	0.970	0.762	0.779	106	101	4	-19	-17	3.32E-7	1.44E-6	> 1.00E-4
ACHN	0.392	1.608	1.643	1.627	0.923	0.702	0.566	103	102	44	25	14	7.78E-7	> 1.00E-4	> 1.00E-4
CAKI-1	0.535	0.660	0.616	0.597	0.555	0.503	0.387	64	49	16	-6	-28	8.86E-8	5.24E-6	> 1.00E-4
RXF 393	0.535	1.102	1.141	1.179	0.762	0.718	0.262	107	114	40	32	-51	7.33E-7	2.44E-5	9.72E-5
SN12C	0.319	1.273	1.317	1.319	0.687	0.566	0.335	105	105	39	26	2	6.73E-7	> 1.00E-4	> 1.00E-4
TK-10	0.497	1.011	1.001	1.023	0.773	0.754	0.725	98	102	54	50	44	9.29E-6	> 1.00E-4	> 1.00E-4
UO-31	0.426	1.334	1.296	1.305	0.978	0.751	0.608	96	97	61	36	20	2.70E-6	> 1.00E-4	> 1.00E-4
Prostate Cancer															
PC-3	0.217	0.645	0.638	0.640	0.350	0.275	0.266	98	99	31	14	11	5.25E-7	> 1.00E-4	> 1.00E-4
DU-145	0.145	0.511	0.539	0.555	0.279	0.145	0.127	108	112	37	.	-12	6.64E-7	9.79E-6	> 1.00E-4
Breast Cancer															
MCF7	0.266	1.459	1.381	1.356	0.460	0.334	0.280	93	91	16	6	1	3.55E-7	> 1.00E-4	> 1.00E-4
NCI/ADR-RES	0.497	1.602	1.746	1.717	0.608	0.709	0.590	113	110	10	19	8	4.00E-7	> 1.00E-4	> 1.00E-4
MDA-MB-231/ATCC	0.346	0.874	0.902	0.950	0.671	0.317	0.188	105	114	62	-8	-46	1.48E-6	7.59E-6	> 1.00E-4
MDA-MB-435	0.439	1.568	1.548	1.477	0.327	0.284	0.276	98	92	-26	-35	-37	2.27E-7	8.05E-7	> 1.00E-4
BT-549	0.865	1.703	1.693	1.648	1.289	0.995	0.887	99	93	51	16	3	1.04E-6	> 1.00E-4	> 1.00E-4
T-47D	0.310	0.748	0.792	0.768	0.655	0.693	0.579	110	104	79	87	61	> 1.00E-4	> 1.00E-4	> 1.00E-4
MDA-MB-468	0.239	0.944	0.944	0.893	0.472	0.375	0.257	100	93	33	19	3	5.20E-7	> 1.00E-4	> 1.00E-4

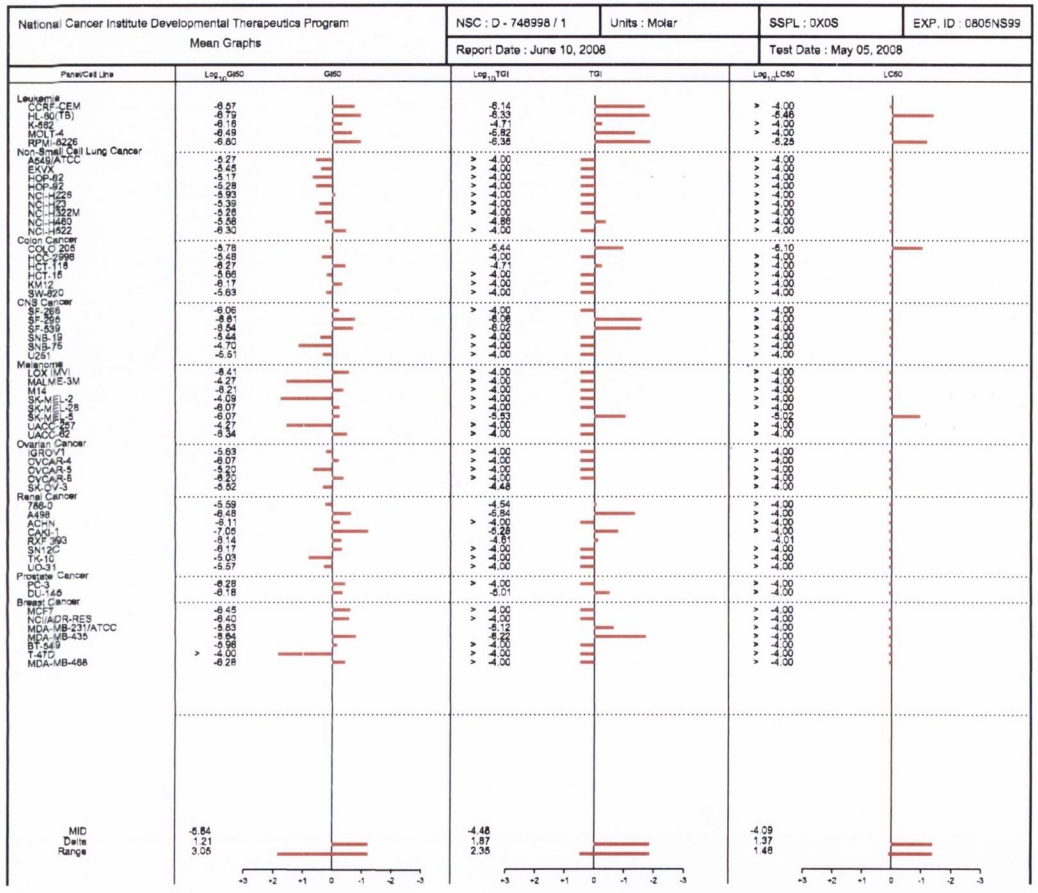

National Cancer Institute Developmental Therapeutics Program Dose Response Curves	NSC : D - 746999 / 1	SSPL: 0X0S	EXP. ID: 0805NS99
	Report Date: June 10, 2008	Test Date: May 05, 2008	

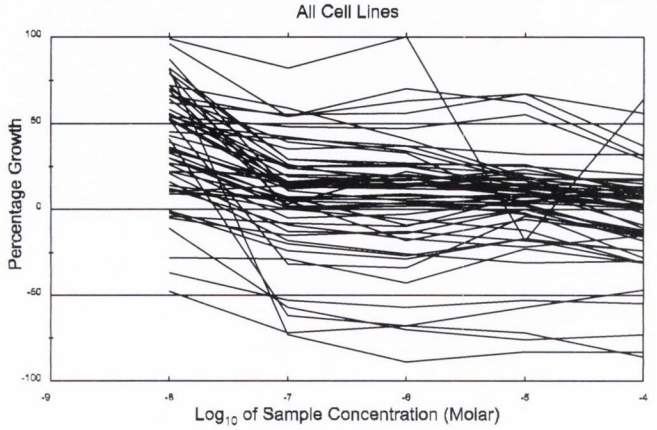

National Cancer Institute Developmental Therapeutics Program Dose Response Curves	NSC: D - 746999 / 1	SSPL: 0X0S	EXP. ID: 0805NS99
	Report Date: June 10, 2008	Test Date: May 05, 2008	

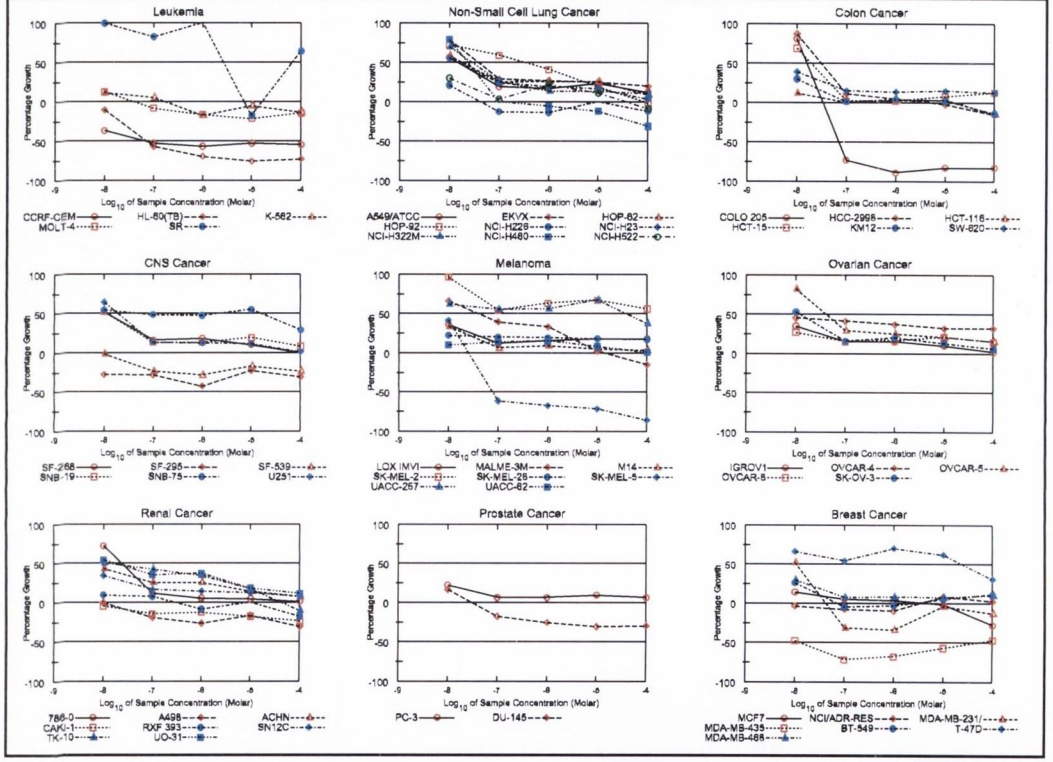

National Cancer Institute Developmental Therapeutics Program
In-Vitro Testing Results

NSC : D - 746999 / 1	Experiment ID : 0805NS99	Test Type : 08	Units : Molar
Report Date : June 10, 2008	Test Date : May 05, 2008	QNS :	MC :
COMI : mjmtg002 (71090)	Stain Reagent : SRB Dual-Pass Related	SSPL : 0X0S	

			Log10 Concentration												
	Time		Mean Optical Densities					Percent Growth							
Panel/Cell Line	Zero	Ctrl	-8.0	-7.0	-6.0	-5.0	-4.0	-8.0	-7.0	-6.0	-5.0	-4.0	GI50	TGI	LC50
Leukemia															
CCRF-CEM	0.246	0.670	0.155	0.115	0.107	0.116	0.111	-37	-53	-57	-53	-55	< 1.00E-8	< 1.00E-8	6.31E-8
HL-60(TB)	0.415	0.925	0.370	0.180	0.126	0.100	0.110	-11	-57	-70	-76	-73	< 1.00E-8	< 1.00E-8	7.13E-8
K-562	0.147	0.793	0.216	0.181	0.120	0.138	0.127	11	5	-18	-6	-14	< 1.00E-8	1.66E-7	> 1.00E-4
MOLT-4	0.193	0.628	0.247	0.176	0.160	0.150	0.165	12	-9	-17	-22	-15	< 1.00E-8	3.83E-8	> 1.00E-4
SR	0.185	0.658	0.654	0.574	0.726	0.152	0.488	99	82	114	-18	64	.	.	> 1.00E-4
Non-Small Cell Lung Cancer															
A549/ATCC	0.217	1.198	0.770	0.405	0.382	0.445	0.338	56	19	17	23	12	1.48E-8	> 1.00E-4	> 1.00E-4
EKVX	0.731	1.779	1.555	1.040	1.017	0.992	0.942	79	29	27	25	20	3.82E-8	> 1.00E-4	> 1.00E-4
HOP-62	0.637	1.662	1.227	0.894	0.901	0.906	0.733	58	25	26	26	9	1.71E-8	> 1.00E-4	> 1.00E-4
HOP-92	0.650	1.058	0.942	0.893	0.817	0.727	0.640	72	59	41	19	-2	3.25E-7	8.40E-5	> 1.00E-4
NCI-H226	0.752	1.247	0.855	0.653	0.649	0.752	0.659	21	-13	-14	.	-12	< 1.00E-8	1.00E-5	> 1.00E-4
NCI-H23	0.420	1.313	0.909	0.832	0.588	0.574	0.443	55	24	19	17	3	1.42E-8	> 1.00E-4	> 1.00E-4
NCI-H322M	0.460	1.059	0.877	0.616	0.542	0.544	0.519	70	26	14	14	10	2.83E-8	> 1.00E-4	> 1.00E-4
NCI-H460	0.238	2.228	1.813	0.243	0.223	0.209	0.165	79	.	-6	-12	-31	2.34E-8	1.09E-7	> 1.00E-4
NCI-H522	1.113	1.973	1.370	1.137	1.300	1.205	1.011	30	3	22	11	-9	< 1.00E-8	3.44E-5	> 1.00E-4
Colon Cancer															
COLO 205	0.171	0.596	0.516	0.046	0.018	0.029	0.030	81	-73	-89	-83	-83	1.59E-8	3.36E-8	7.08E-8
HCC-2998	0.706	1.933	1.774	0.840	0.770	0.685	0.596	87	11	5	-3	-16	3.07E-8	4.33E-6	> 1.00E-4
HCT-116	0.162	1.339	0.299	0.165	0.187	0.193	0.138	12	.	2	3	-15	< 1.00E-8	1.42E-5	> 1.00E-4
HCT-15	0.303	1.508	1.138	0.324	0.325	0.402	0.464	69	2	2	8	13	1.93E-8	> 1.00E-4	> 1.00E-4
KM12	0.470	1.830	0.876	0.478	0.525	0.493	0.404	30	1	4	2	-14	< 1.00E-8	1.27E-5	> 1.00E-4
SW-620	0.236	1.426	0.704	0.413	0.408	0.413	0.392	39	15	14	15	13	< 1.00E-8	> 1.00E-4	> 1.00E-4
CNS Cancer															
SF-268	1.045	2.467	1.782	1.274	1.297	1.188	1.040	52	16	18	10	.	1.12E-8	9.00E-5	> 1.00E-4
SF-295	0.548	1.268	0.393	0.392	0.315	0.421	0.376	-28	-29	-43	-23	-31	< 1.00E-8	< 1.00E-8	> 1.00E-4
SF-539	0.574	1.921	0.584	0.435	0.410	0.477	0.439	-2	-24	-29	-17	-24	< 1.00E-8	< 1.00E-8	> 1.00E-4
SNB-19	0.302	1.080	0.704	0.407	0.406	0.453	0.361	52	13	13	19	8	1.11E-8	> 1.00E-4	> 1.00E-4
SNB-75	0.581	1.409	1.028	0.982	0.973	1.038	0.823	54	46	47	55	29	.	> 1.00E-4	> 1.00E-4
U251	0.290	1.371	0.979	0.428	0.415	0.410	0.299	64	13	12	11	1	1.86E-8	> 1.00E-4	> 1.00E-4
Melanoma															
LOX IMVI	0.311	1.856	0.871	0.492	0.549	0.588	0.595	36	12	15	18	18	< 1.00E-8	> 1.00E-4	> 1.00E-4
MALME-3M	0.620	0.955	0.840	0.752	0.730	0.628	0.530	88	39	33	2	-15	3.98E-8	1.39E-5	> 1.00E-4
M14	0.332	1.454	0.697	0.402	0.435	0.393	0.365	33	6	9	5	3	< 1.00E-8	> 1.00E-4	> 1.00E-4
SK-MEL-2	0.475	0.890	0.873	0.699	0.738	0.753	0.708	96	54	63	67	56	> 1.00E-4	> 1.00E-4	> 1.00E-4
SK-MEL-28	0.433	1.199	0.803	0.585	0.576	0.572	0.562	22	20	19	18	17	< 1.00E-8	> 1.00E-4	> 1.00E-4
SK-MEL-5	0.429	2.404	1.239	0.164	0.137	0.120	0.062	41	-62	-68	-72	-86	< 1.00E-8	2.50E-8	7.66E-8
UACC-257	0.897	1.903	1.522	1.453	1.458	1.568	1.265	62	55	56	67	37	3.58E-5	> 1.00E-4	> 1.00E-4
UACC-62	0.506	1.630	0.618	0.668	0.678	0.592	0.517	10	14	15	8	1	< 1.00E-8	> 1.00E-4	> 1.00E-4
Ovarian Cancer															
IGROV1	0.454	1.455	0.803	0.602	0.608	0.552	0.473	35	15	15	10	2	< 1.00E-8	> 1.00E-4	> 1.00E-4
OVCAR-4	0.522	1.824	1.112	1.052	0.998	0.937	0.934	45	41	37	32	32	< 1.00E-8	> 1.00E-4	> 1.00E-4
OVCAR-5	0.514	1.351	1.197	0.760	0.720	0.690	0.642	82	29	25	21	15	4.03E-8	> 1.00E-4	> 1.00E-4
OVCAR-8	0.433	1.735	0.787	0.822	0.648	0.701	0.629	27	15	17	21	15	< 1.00E-8	> 1.00E-4	> 1.00E-4
SK-OV-3	0.509	1.277	0.915	0.634	0.660	0.605	0.555	53	18	20	13	6	1.19E-8	> 1.00E-4	> 1.00E-4
Renal Cancer															
786-0	0.765	2.541	2.048	0.983	0.855	0.839	0.778	72	11	5	4	1	2.31E-8	> 1.00E-4	> 1.00E-4
A498	0.944	1.664	0.939	0.752	0.688	0.784	0.650	-1	-20	-27	-17	-31	< 1.00E-8	< 1.00E-8	> 1.00E-4
ACHN	0.392	1.592	0.906	0.691	0.697	0.566	0.481	43	25	25	14	7	< 1.00E-8	> 1.00E-4	> 1.00E-4
CAKI-1	0.535	0.643	0.511	0.456	0.466	0.439	0.409	-5	-15	-13	-18	-24	< 1.00E-8	< 1.00E-8	> 1.00E-4
RXF 393	0.535	1.080	0.587	0.575	0.486	0.534	0.440	9	7	-9	.	-18	< 1.00E-8	2.75E-7	> 1.00E-4
SN12C	0.319	1.192	0.614	0.462	0.444	0.421	0.378	34	16	14	12	7	< 1.00E-8	> 1.00E-4	> 1.00E-4
TK-10	0.497	1.028	0.760	0.722	0.680	0.585	0.443	50	42	34	17	-11	< 1.00E-8	4.02E-5	> 1.00E-4
UO-31	0.426	1.375	0.935	0.761	0.774	0.596	0.531	54	35	37	18	11	1.57E-8	> 1.00E-4	> 1.00E-4
Prostate Cancer															
PC-3	0.217	0.650	0.313	0.242	0.242	0.256	0.242	22	8	8	9	8	< 1.00E-8	> 1.00E-4	> 1.00E-4
DU-145	0.145	0.522	0.205	0.119	0.107	0.101	0.102	16	-16	-26	-31	-30	< 1.00E-8	2.92E-8	> 1.00E-4
Breast Cancer															
MCF7	0.266	1.462	0.438	0.330	0.297	0.260	0.191	14	5	3	-2	-28	< 1.00E-8	3.24E-6	> 1.00E-4
NCI/ADR-RES	0.497	1.751	0.475	0.456	0.447	0.593	0.520	-4	-8	-10	8	2	< 1.00E-8	.	> 1.00E-4
MDA-MB-231/ATCC	0.346	0.833	0.598	0.234	0.230	0.332	0.300	52	-32	-34	-4	-13	1.05E-8	4.12E-8	> 1.00E-4
MDA-MB-436	0.439	1.641	0.228	0.123	0.140	0.188	0.231	-48	-72	-68	-57	-47	< 1.00E-8	< 1.00E-8	.
BT-549	0.865	1.611	1.057	0.826	0.842	0.903	0.951	26	-5	-3	5	11	< 1.00E-8	.	> 1.00E-4
T-47D	0.310	0.752	0.601	0.549	0.619	0.586	0.445	66	54	70	62	31	2.46E-5	> 1.00E-4	> 1.00E-4
MDA-MB-468	0.239	1.020	0.471	0.293	0.304	0.291	0.317	30	7	8	7	10	< 1.00E-8	> 1.00E-4	> 1.00E-4

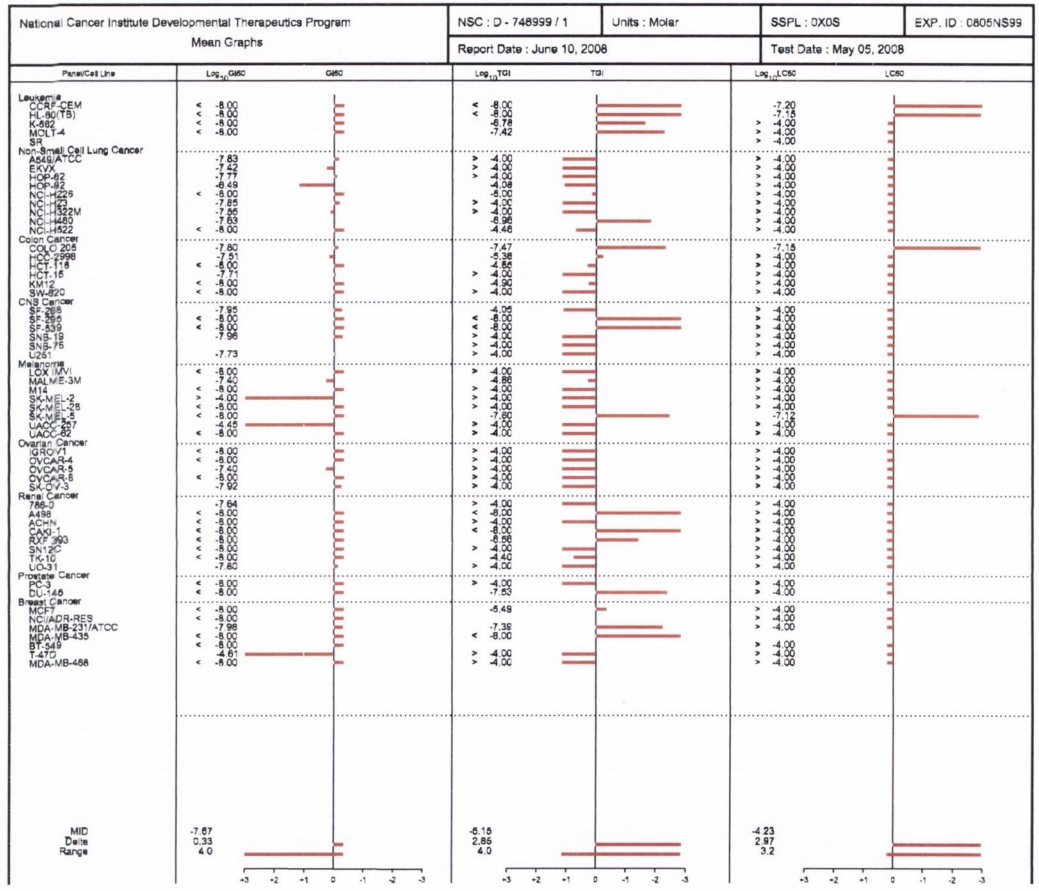

National Cancer Institute Developmental Therapeutics Program Dose Response Curves	NSC : D - 747000 / 1	SSPL: 0X0S	EXP. ID: 0805NS99
	Report Date: June 10, 2008	Test Date: May 05, 2008	

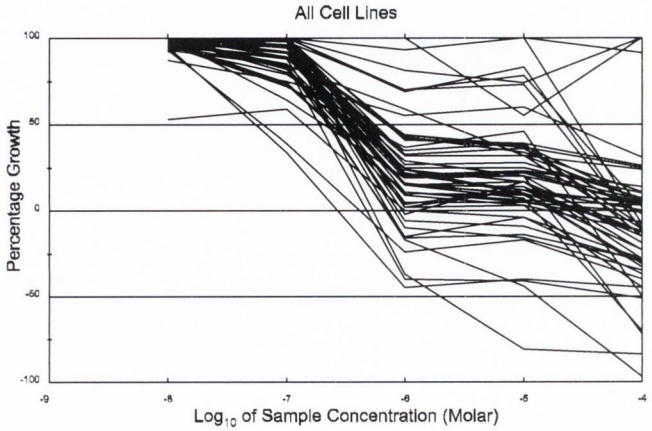

National Cancer Institute Developmental Therapeutics Program Dose Response Curves	NSC: D - 747000 / 1	SSPL: 0X0S	EXP. ID: 0805NS99
	Report Date: June 10, 2008	Test Date: May 05, 2008	

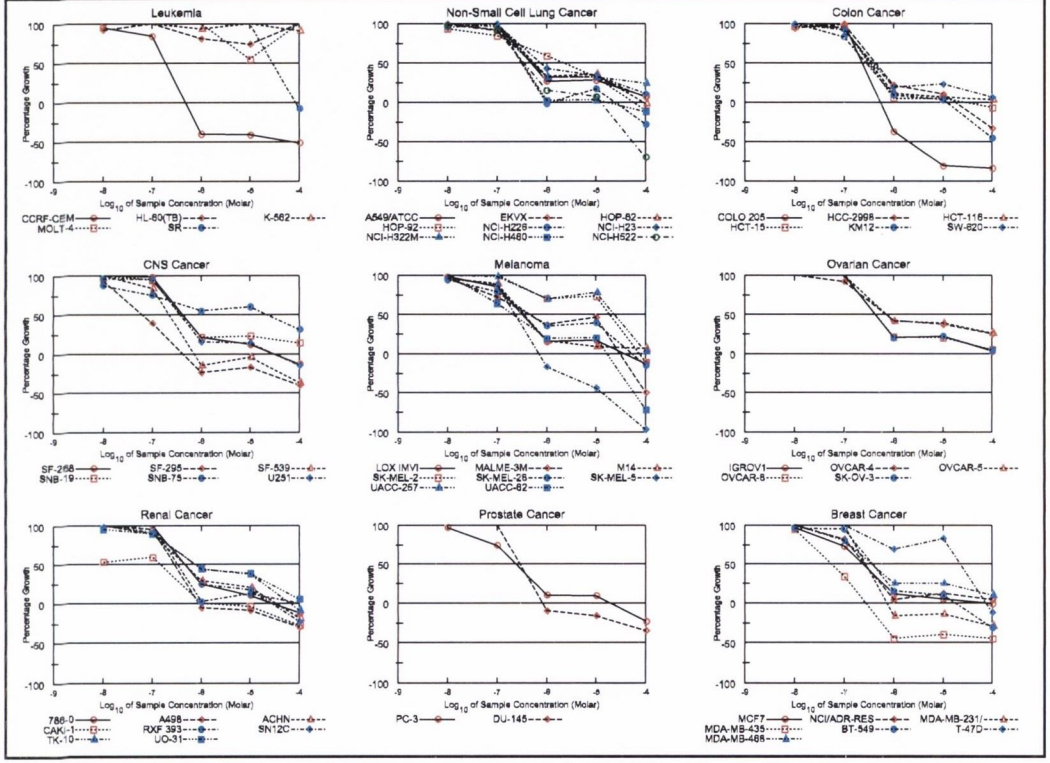

National Cancer Institute Developmental Therapeutics Program
In-Vitro Testing Results

NSC : D - 747000 / 1	Experiment ID : 0805NS99	Test Type : 08	Units : Molar
Report Date : June 10, 2008	Test Date : May 05, 2008	QNS :	MC :
COMI : mjmtg003 (71091)	Stain Reagent : SRB Dual-Pass Related	SSPL : 0X0S	

Panel/Cell Line	Time Zero	Ctrl	Mean Optical Densities -8.0	-7.0	-6.0	-5.0	-4.0	Percent Growth -8.0	-7.0	-6.0	-5.0	-4.0	GI50	TGI	LC50
Leukemia															
CCRF-CEM	0.246	0.670	0.847	0.604	0.148	0.145	0.122	95	84	-40	-41	-51	1.89E-7	4.78E-7	8.63E-5
HL-60(TB)	0.415	0.925	0.885	1.280	0.826	0.792	0.999	92	169	81	74	114	> 1.00E-4	> 1.00E-4	> 1.00E-4
K-562	0.147	0.793	0.803	1.184	0.745	0.938	0.732	102	161	93	122	91	> 1.00E-4	> 1.00E-4	> 1.00E-4
MOLT-4	0.193	0.628	0.661	1.177	0.706	0.434	0.958	108	226	118	55	176	> 1.00E-4	> 1.00E-4	> 1.00E-4
SR	0.185	0.658	0.727	0.926	0.937	0.681	0.171	115	157	159	105	-8	3.08E-5	8.56E-5	> 1.00E-4
Non-Small Cell Lung Cancer															
A549/ATCC	0.217	1.198	1.273	1.314	0.479	0.491	0.291	108	112	27	28	7	5.32E-7	> 1.00E-4	> 1.00E-4
EKVX	0.731	1.779	1.773	1.697	1.069	1.067	0.790	99	92	32	32	6	5.05E-7	> 1.00E-4	> 1.00E-4
HOP-62	0.637	1.662	1.700	1.686	0.971	1.003	0.624	104	102	33	36	-2	5.63E-7	8.83E-5	> 1.00E-4
HOP-92	0.650	1.058	1.028	0.992	0.889	0.782	0.577	93	84	59	32	-11	2.12E-6	5.52E-5	> 1.00E-4
NCI-H226	0.752	1.247	1.270	1.304	0.735	0.838	0.539	105	112	-2	17	-28	3.47E-7	.	> 1.00E-4
NCI-H23	0.420	1.313	1.271	1.307	0.802	0.728	0.522	95	99	43	34	11	7.43E-7	> 1.00E-4	> 1.00E-4
NCI-H322M	0.460	1.059	1.078	1.035	0.651	0.654	0.601	103	98	32	32	24	5.21E-7	> 1.00E-4	> 1.00E-4
NCI-H460	0.236	2.228	2.375	2.230	0.286	0.298	0.211	107	100	2	3	-12	3.26E-7	1.61E-5	> 1.00E-4
NCI-H522	1.113	1.973	1.957	1.897	1.243	1.174	0.336	98	91	15	7	-70	3.48E-7	1.24E-5	6.53E-5
Colon Cancer															
COLO 205	0.171	0.696	0.830	0.595	0.108	0.033	0.028	108	101	-37	-81	-84	2.33E-7	5.37E-7	1.96E-6
HCC-2998	0.706	1.933	1.864	1.923	0.977	0.823	0.471	94	99	22	10	-33	4.34E-7	1.67E-5	> 1.00E-4
HCT-116	0.162	1.339	1.387	1.271	0.292	0.230	0.199	104	94	11	6	3	3.40E-7	> 1.00E-4	> 1.00E-4
HCT-15	0.303	1.508	1.462	1.445	0.361	0.359	0.282	96	95	5	5	-7	3.15E-7	2.51E-5	> 1.00E-4
KM12	0.470	1.830	1.845	1.603	0.592	0.506	0.259	101	83	9	3	-45	2.81E-7	1.14E-5	> 1.00E-4
SW-620	0.236	1.426	1.419	1.335	0.457	0.507	0.310	99	92	19	23	6	3.75E-7	> 1.00E-4	> 1.00E-4
CNS Cancer															
SF-268	1.045	2.467	2.468	2.440	1.346	1.223	0.906	100	98	21	12	-13	4.22E-7	3.05E-5	> 1.00E-4
SF-295	0.548	1.268	1.216	0.826	0.419	0.457	0.329	93	39	-24	-17	-40	6.16E-8	4.18E-7	> 1.00E-4
SF-539	0.574	1.921	1.919	1.712	0.486	0.549	0.362	100	94	-15	-4	-37	2.21E-7	7.01E-7	> 1.00E-4
SNB-19	0.302	1.080	1.088	1.037	0.467	0.482	0.410	101	94	21	23	14	4.05E-7	> 1.00E-4	> 1.00E-4
SNB-75	0.581	1.409	1.301	1.203	1.038	1.078	0.840	87	75	55	60	31	2.23E-5	> 1.00E-4	> 1.00E-4
U251	0.290	1.371	1.330	1.322	0.448	0.446	0.247	96	95	15	14	-15	3.84E-7	3.09E-5	> 1.00E-4
Melanoma															
LOX IMVI	0.311	1.856	1.833	1.623	0.545	0.579	0.270	98	85	15	17	-13	3.16E-7	3.70E-5	> 1.00E-4
MALME-3M	0.620	0.955	0.940	0.882	0.745	0.775	0.313	96	72	37	46	-60	4.31E-7	3.04E-5	> 1.00E-4
M14	0.332	1.454	1.407	1.330	0.511	0.439	0.400	96	89	16	9	6	3.42E-7	> 1.00E-4	> 1.00E-4
SK-MEL-2	0.475	0.890	1.035	0.945	0.766	0.780	0.424	135	113	70	73	-11	1.90E-5	7.46E-5	> 1.00E-4
SK-MEL-28	0.433	1.199	1.150	1.039	0.704	0.734	0.370	94	79	35	39	-15	4.62E-7	5.37E-5	> 1.00E-4
SK-MEL-5	0.429	2.404	2.323	2.160	0.354	0.240	0.013	96	88	-17	-44	-97	2.28E-7	6.82E-7	1.29E-5
UACC-257	0.897	1.903	1.927	1.886	1.597	1.679	0.914	102	98	70	78	2	2.31E-5	> 1.00E-4	> 1.00E-4
UACC-62	0.506	1.630	1.684	1.229	0.719	0.730	0.144	105	64	19	20	-72	2.07E-7	1.65E-5	5.81E-5
Ovarian Cancer															
IGROV1	0.454	1.455	1.456	1.482	0.658	0.675	0.485	100	103	20	22	3	4.36E-7	> 1.00E-4	> 1.00E-4
OVCAR-4	0.522	1.824	1.903	1.726	1.071	1.007	0.845	108	92	42	37	25	6.99E-7	> 1.00E-4	> 1.00E-4
OVCAR-5	0.514	1.351	1.350	1.401	0.861	0.839	0.731	100	108	41	39	26	7.37E-7	> 1.00E-4	> 1.00E-4
OVCAR-8	0.433	1.735	1.609	1.823	0.703	0.698	0.493	108	107	21	20	5	4.57E-7	> 1.00E-4	> 1.00E-4
SK-OV-3	0.509	1.277	1.340	1.297	0.662	0.678	0.538	108	103	20	22	4	4.32E-7	> 1.00E-4	> 1.00E-4
Renal Cancer															
786-0	0.765	2.541	2.667	2.623	1.185	0.951	0.674	107	105	24	10	-12	4.73E-7	2.93E-5	> 1.00E-4
A498	0.944	1.664	1.708	1.629	0.886	0.861	0.658	106	95	-6	-9	-30	2.79E-7	8.69E-7	> 1.00E-4
ACHN	0.392	1.592	1.660	1.459	0.738	0.636	0.319	106	89	29	20	-19	4.44E-7	3.31E-5	> 1.00E-4
CAKI-1	0.535	0.643	0.592	0.598	0.536	0.516	0.386	53	59	.	-4	-28	1.41E-7	1.31E-6	> 1.00E-4
RXF 393	0.535	1.080	1.130	1.089	0.544	0.601	0.533	109	102	2	12	.	3.28E-7	9.17E-5	> 1.00E-4
SN12C	0.319	1.192	1.175	1.268	0.527	0.467	0.245	98	109	24	17	-23	4.92E-7	2.64E-5	> 1.00E-4
TK-10	0.497	1.028	1.035	0.982	0.733	0.695	0.451	101	91	44	37	-9	7.62E-7	6.30E-5	> 1.00E-4
UO-31	0.426	1.375	1.327	1.271	0.841	0.787	0.473	95	89	44	38	5	7.25E-7	> 1.00E-4	> 1.00E-4
Prostate Cancer															
PC-3	0.217	0.650	0.637	0.538	0.262	0.258	0.188	97	74	10	9	-23	2.40E-7	1.97E-5	> 1.00E-4
DU-145	0.145	0.522	0.539	0.551	0.131	0.122	0.095	105	108	-10	-16	-35	3.09E-7	8.22E-7	> 1.00E-4
Breast Cancer															
MCF7	0.266	1.462	1.431	1.141	0.394	0.323	0.263	97	73	11	5	-1	2.35E-7	8.44E-5	> 1.00E-4
NCI/ADR-RES	0.497	1.751	1.846	1.531	0.542	0.646	0.543	108	82	4	12	4	2.58E-7	> 1.00E-4	> 1.00E-4
MDA-MB-231/ATCC	0.346	0.833	0.866	0.879	0.290	0.299	0.244	107	109	-16	-14	-29	2.97E-7	7.43E-7	> 1.00E-4
MDA-MB-435	0.439	1.641	1.578	0.843	0.244	0.264	0.241	95	34	-45	-40	-45	5.39E-8	2.69E-7	> 1.00E-4
BT-549	0.865	1.611	1.581	1.573	0.978	0.940	0.593	96	95	15	10	-31	3.85E-7	1.75E-5	> 1.00E-4
T-47D	0.310	0.752	0.755	0.772	0.617	0.675	0.273	101	104	69	83	-12	2.21E-5	7.45E-5	> 1.00E-4
MDA-MB-468	0.239	1.020	1.042	0.865	0.433	0.435	0.318	103	80	25	25	10	3.50E-7	> 1.00E-4	> 1.00E-4

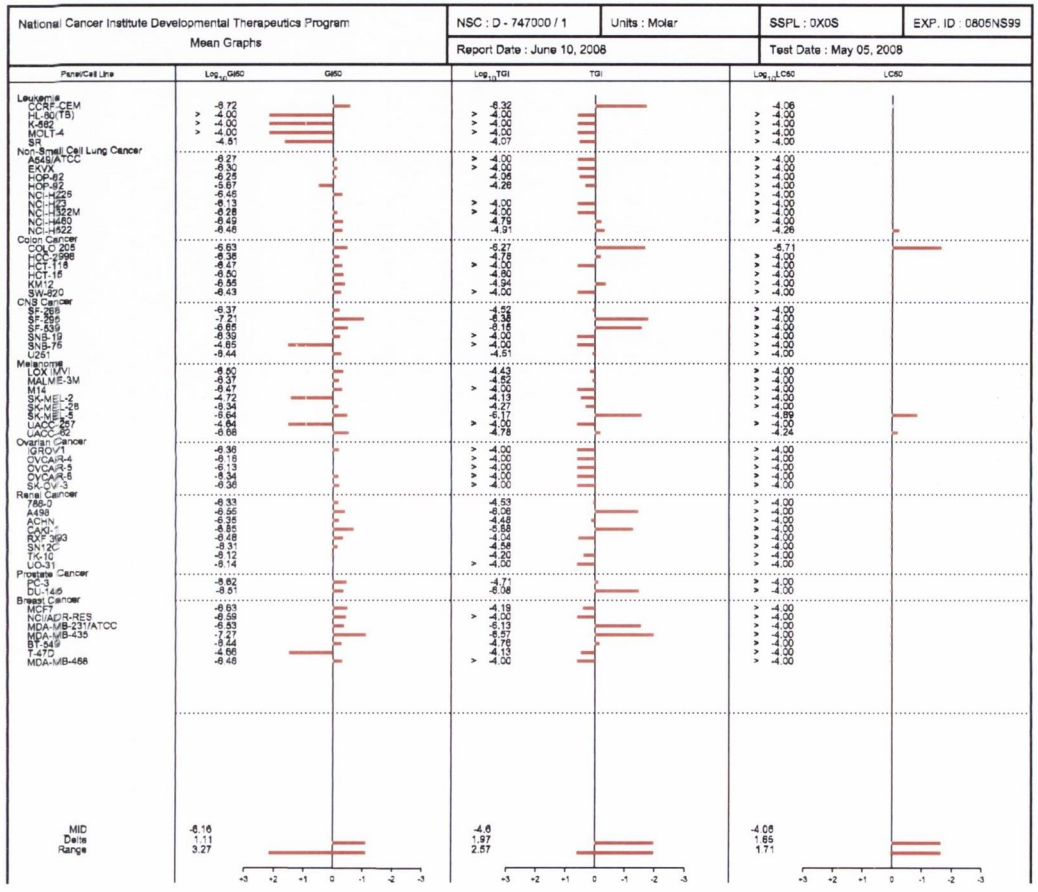

National Cancer Institute Developmental Therapeutics Program Dose Response Curves	NSC : D - 747001 / 1	SSPL: 0X0S	EXP. ID: 0805NS99
	Report Date: June 10, 2008	Test Date: May 05, 2008	

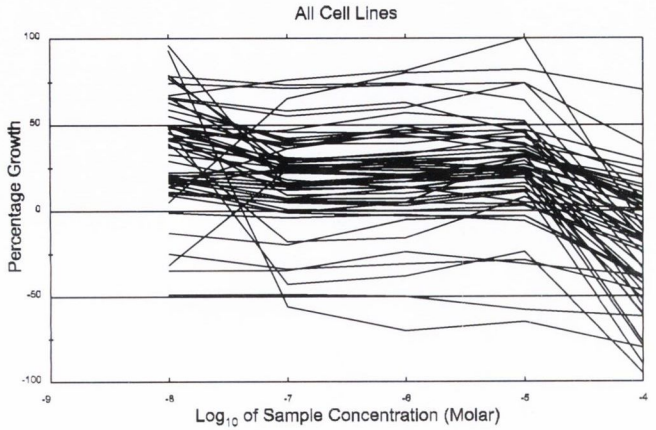

National Cancer Institute Developmental Therapeutics Program Dose Response Curves	NSC: D - 747001 / 1	SSPL: 0X0S	EXP. ID: 0805NS99
	Report Date: June 10, 2008	Test Date: May 05, 2008	

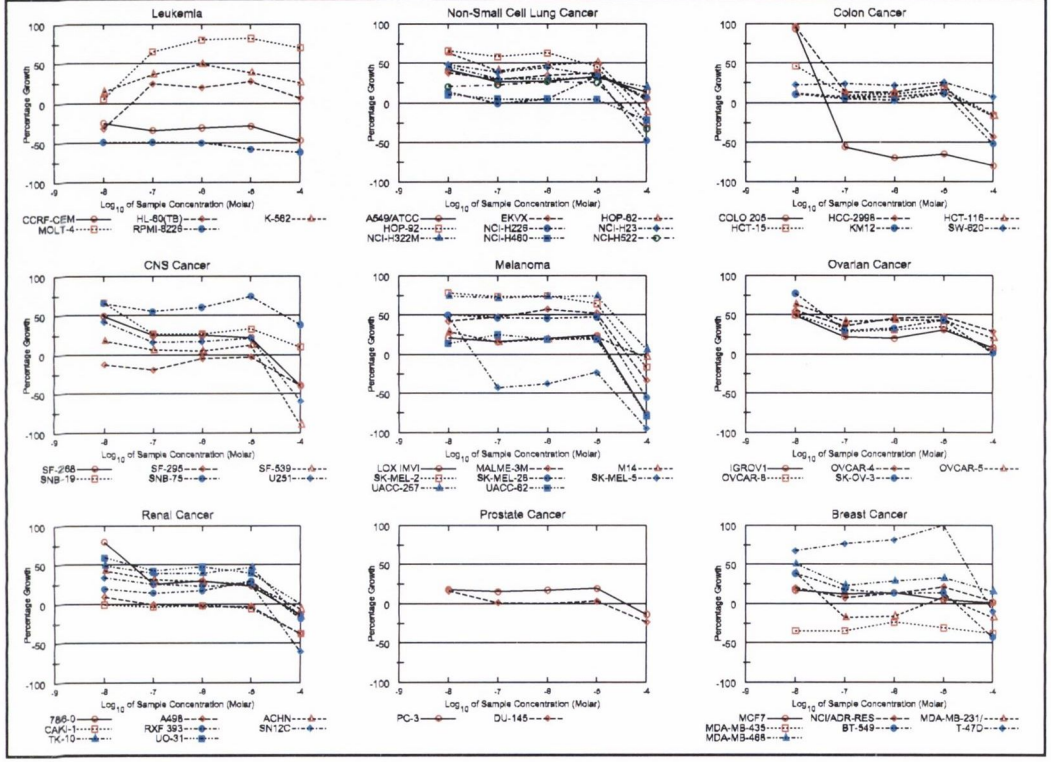

National Cancer Institute Developmental Therapeutics Program
In-Vitro Testing Results

NSC : D - 747001 / 1	Experiment ID : 0805NS99	Test Type : 08	Units : Molar
Report Date : June 10, 2008	Test Date : May 05, 2008	QNS :	MC :
COMI : mjmtg004 (71120)	Stain Reagent : SRB Dual-Pass Related	SSPL : 0X0S	

Log10 Concentration
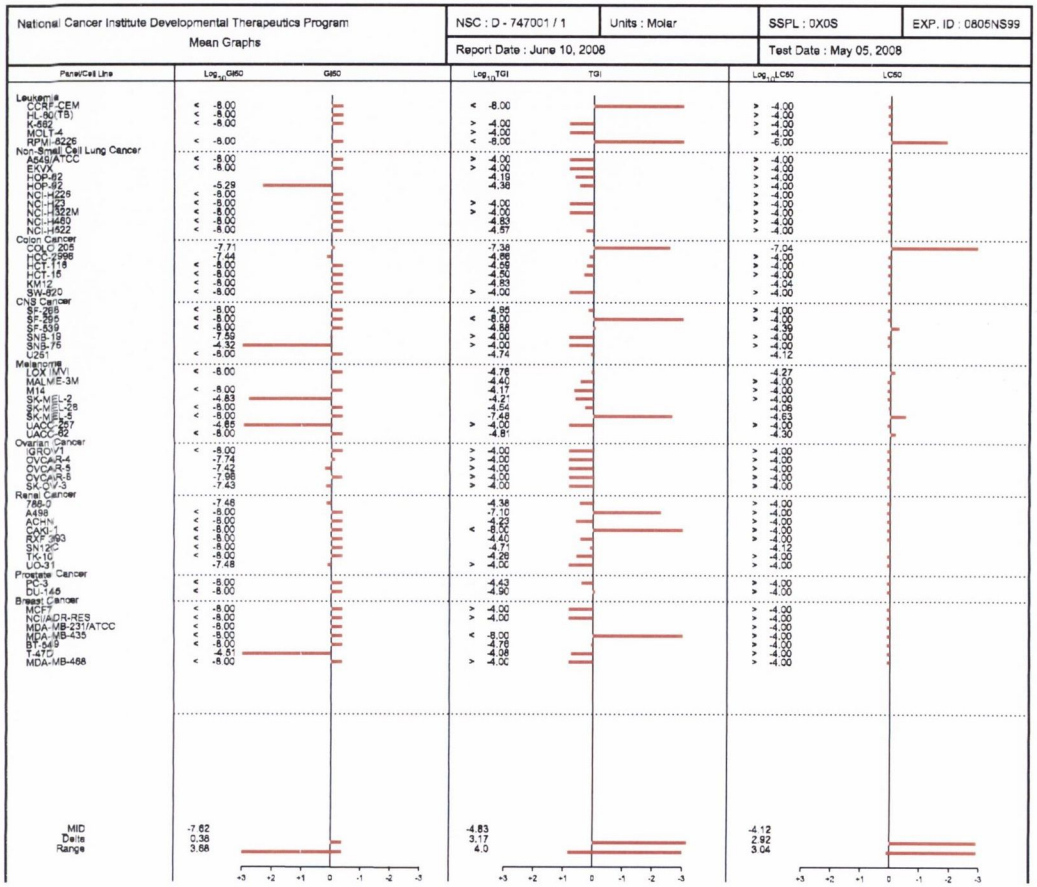
Panel/Cell Line	Time Zero	Ctrl	Mean Optical Densities -8.0	-7.0	-6.0	-5.0	-4.0	Percent Growth -8.0	-7.0	-6.0	-5.0	-4.0	GI50	TGI	LC50
Leukemia															
CCRF-CEM	0.246	0.747	0.185	0.183	0.171	0.175	0.131	-25	-34	-31	-29	-47	< 1.00E-8	< 1.00E-8	> 1.00E-4
HL-60(TB)	0.415	1.193	0.282	0.599	0.565	0.622	0.466	-32	24	19	27	6	< 1.00E-8	.	> 1.00E-4
K-562	0.147	0.910	0.257	0.424	0.519	0.434	0.341	14	36	49	38	25	< 1.00E-8	> 1.00E-4	> 1.00E-4
MOLT-4	0.193	0.702	0.219	0.524	0.601	0.613	0.551	5	65	80	82	70	.	> 1.00E-4	> 1.00E-4
RPMI-8226	0.269	0.481	0.138	0.137	0.135	0.114	0.101	-49	-49	-50	-58	-62	< 1.00E-8	< 1.00E-8	1.00E-6
Non-Small Cell Lung Cancer															
A549/ATCC	0.217	1.265	0.647	0.493	0.496	0.551	0.353	41	26	27	32	13	< 1.00E-8	> 1.00E-4	> 1.00E-4
EKVX	0.731	1.836	1.142	1.052	1.110	1.137	0.780	37	29	34	37	4	< 1.00E-8	> 1.00E-4	> 1.00E-4
HOP-62	0.637	1.823	1.388	1.107	1.193	1.239	0.564	63	40	47	51	-12	.	6.53E-5	> 1.00E-4
HOP-92	0.650	1.105	0.949	0.914	0.936	0.854	0.490	66	58	63	45	-25	5.15E-6	4.41E-5	> 1.00E-4
NCI-H226	0.752	1.268	0.826	0.743	0.778	0.917	0.394	14	-1	5	32	-48	< 1.00E-8	.	> 1.00E-4
NCI-H23	0.420	1.318	0.854	0.782	0.817	0.728	0.487	48	38	44	34	7	< 1.00E-8	> 1.00E-4	> 1.00E-4
NCI-H322M	0.460	1.082	0.740	0.649	0.645	0.655	0.576	45	30	30	31	19	< 1.00E-8	> 1.00E-4	> 1.00E-4
NCI-H460	0.238	2.337	0.448	0.334	0.336	0.331	0.186	10	5	5	4	-22	< 1.00E-8	1.47E-5	> 1.00E-4
NCI-H522	1.113	2.353	1.385	1.390	1.431	1.426	0.746	20	22	26	25	-33	< 1.00E-8	2.71E-5	> 1.00E-4
Colon Cancer															
COLO 205	0.171	0.841	0.809	0.075	0.052	0.081	0.035	93	-56	-70	-65	-80	1.94E-8	4.19E-8	9.08E-8
HCC-2998	0.706	1.925	1.873	0.870	0.866	0.970	0.404	96	13	13	22	-43	3.59E-8	2.17E-5	> 1.00E-4
HCT-116	0.162	1.423	0.301	0.255	0.245	0.308	0.135	11	7	7	12	-17	< 1.00E-8	2.57E-5	> 1.00E-4
HCT-15	0.303	1.655	0.924	0.431	0.437	0.520	0.255	46	9	10	16	-16	< 1.00E-8	3.18E-5	> 1.00E-4
KM12	0.470	1.858	0.608	0.541	0.518	0.617	0.225	10	5	3	11	-52	< 1.00E-8	1.47E-5	9.21E-5
SW-620	0.236	1.497	0.509	0.520	0.500	0.545	0.328	22	23	21	25	7	< 1.00E-8	> 1.00E-4	> 1.00E-4
CNS Cancer															
SF-268	1.045	2.626	1.816	1.446	1.447	1.388	0.632	49	25	25	22	-40	< 1.00E-8	2.26E-5	> 1.00E-4
SF-295	0.548	1.259	0.475	0.438	0.519	0.533	0.327	-13	-20	-5	-3	-40	< 1.00E-8	< 1.00E-8	> 1.00E-4
SF-539	0.574	1.963	0.827	0.654	0.650	0.742	0.055	18	6	5	12	-90	< 1.00E-8	1.31E-5	4.03E-5
SNB-19	0.302	1.130	0.849	0.527	0.530	0.575	0.384	86	27	27	33	10	2.58E-8	> 1.00E-4	> 1.00E-4
SNB-75	0.581	1.496	1.175	1.089	1.128	1.263	0.933	85	55	60	74	38	4.77E-5	> 1.00E-4	> 1.00E-4
U251	0.290	1.436	0.770	0.479	0.480	0.534	0.117	42	16	17	21	-60	< 1.00E-8	1.83E-5	7.60E-5
Melanoma															
LOX IMVI	0.311	1.969	0.859	0.577	0.637	0.712	0.070	21	18	20	24	-77	< 1.00E-8	1.73E-5	5.36E-5
MALME-3M	0.620	0.935	0.763	0.798	0.800	0.782	0.409	42	47	57	52	-34	.	4.00E-5	> 1.00E-4
M14	0.332	1.444	0.651	0.501	0.547	0.574	0.318	29	15	19	22	-4	< 1.00E-8	6.80E-5	> 1.00E-4
SK-MEL-2	0.475	0.970	0.863	0.837	0.842	0.792	0.394	78	73	74	64	-17	1.49E-5	6.16E-5	> 1.00E-4
SK-MEL-28	0.433	1.192	0.812	0.782	0.773	0.790	0.192	50	46	45	47	-56	< 1.00E-8	2.87E-5	8.81E-5
SK-MEL-5	0.429	2.436	1.390	0.243	0.267	0.327	0.023	48	-43	-38	-24	-95	< 1.00E-8	3.35E-8	2.34E-5
UACC-257	0.897	1.952	1.683	1.650	1.667	1.675	0.961	74	71	73	74	6	2.24E-5	> 1.00E-4	> 1.00E-4
UACC-62	0.506	1.612	0.662	0.780	0.712	0.713	0.105	14	25	19	19	-79	< 1.00E-8	1.55E-5	5.02E-5
Ovarian Cancer															
IGROV1	0.454	1.538	0.988	0.694	0.668	0.792	0.542	49	22	20	31	8	< 1.00E-8	> 1.00E-4	> 1.00E-4
OVCAR-4	0.522	1.891	1.276	1.008	1.134	1.172	0.925	55	36	45	47	29	1.82E-8	> 1.00E-4	> 1.00E-4
OVCAR-5	0.514	1.390	1.062	0.874	0.889	0.894	0.690	63	41	43	43	20	3.84E-8	> 1.00E-4	> 1.00E-4
OVCAR-8	0.433	1.750	1.097	0.808	0.842	0.889	0.490	50	28	31	35	4	1.04E-8	> 1.00E-4	> 1.00E-4
SK-OV-3	0.509	1.316	1.129	0.750	0.775	0.859	0.516	77	30	33	43	1	3.73E-8	> 1.00E-4	> 1.00E-4
Renal Cancer															
786-0	0.765	2.608	2.225	1.230	1.300	1.191	0.669	79	25	29	23	-14	3.47E-8	4.22E-5	> 1.00E-4
A498	0.944	1.687	1.008	0.935	0.914	0.918	0.584	9	-1	-3	-3	-38	< 1.00E-8	7.95E-8	> 1.00E-4
ACHN	0.392	1.627	0.914	0.781	0.739	0.702	0.363	42	31	28	25	-7	< 1.00E-8	5.92E-5	> 1.00E-4
CAKI-1	0.535	0.660	0.528	0.516	0.525	0.504	0.332	-1	-4	-2	-5	-38	< 1.00E-8	< 1.00E-8	> 1.00E-4
RXF 393	0.535	1.136	0.651	0.618	0.640	0.711	0.432	19	14	17	29	-19	< 1.00E-8	4.01E-5	> 1.00E-4
SN12C	0.319	1.151	0.596	0.531	0.514	0.520	0.126	33	25	23	24	-61	< 1.00E-8	1.93E-5	7.52E-5
TK-10	0.497	1.053	0.768	0.713	0.714	0.753	0.416	49	39	39	46	-16	< 1.00E-8	5.47E-5	> 1.00E-4
UO-31	0.426	1.418	1.010	0.840	0.895	0.811	0.427	59	42	47	39	.	3.28E-8	> 1.00E-4	> 1.00E-4
Prostate Cancer															
PC-3	0.217	0.693	0.304	0.288	0.299	0.307	0.187	18	15	17	19	-14	< 1.00E-8	3.73E-5	> 1.00E-4
DU-145	0.145	0.542	0.208	0.147	0.145	0.156	0.110	16	1	.	3	-24	< 1.00E-8	1.27E-5	> 1.00E-4
Breast Cancer															
MCF7	0.266	1.452	0.472	0.412	0.429	0.330	0.273	17	12	14	5	1	< 1.00E-8	> 1.00E-4	> 1.00E-4
NCI/ADR-RES	0.497	1.723	0.737	0.586	0.655	0.759	0.537	20	7	13	21	3	< 1.00E-8	> 1.00E-4	> 1.00E-4
MDA-MB-231/ATCC	0.346	0.857	0.546	0.283	0.292	0.387	0.286	39	-16	-16	8	-18	< 1.00E-8	.	> 1.00E-4
MDA-MB-435	0.439	1.639	0.286	0.284	0.332	0.301	0.272	-35	-35	-24	-31	-38	< 1.00E-8	< 1.00E-8	> 1.00E-4
BT-549	0.865	1.673	1.189	1.008	0.971	0.977	0.495	38	18	13	14	-43	< 1.00E-8	1.75E-5	> 1.00E-4
T-47D	0.310	0.765	0.616	0.654	0.680	0.803	0.281	67	76	81	108	-10	3.12E-5	8.30E-5	> 1.00E-4
MDA-MB-468	0.239	1.072	0.653	0.430	0.471	0.505	0.362	50	23	28	32	15	< 1.00E-8	> 1.00E-4	> 1.00E-4